

Serial No: 09-525
Docket No. 50-423

ENCLOSURE 10

Westinghouse Electric Company LLC, WCAP-17071-NP, "H*: Alternate Repair Criteria for the Tubesheet Expansion Region in Steam Generators with Hydraulically Expanded Tubes (Model F)," Revision 0, dated April 2009.

NON-PROPRIETARY

**DOMINION NUCLEAR CONNECTICUT, INC.
MILLSTONE POWER STATION UNIT 3**

**H*: Alternate Repair Criteria for
the Tubesheet Expansion Region
in Steam Generators with
Hydraulically Expanded Tubes
(Model F)**

WCAP-17071-NP

Revision 0

**H*: Alternate Repair Criteria for the Tubesheet Expansion
Region in Steam Generators with Hydraulically Expanded
Tubes (Model F)**

April 2009

Author: *
C. D. Cassino
Steam Generator Management Programs

Author: *
H. O. Lagally
Steam Generator Management Programs

Author: *
G. W. Whiteman
Regulatory Compliance and Plant Licensing

Reviewer: *
J. T. Kandra
Steam Generator Management Programs

Approved: *
D. A. Testa, Manager
Steam Generator Management Programs

* Electronically Approved Records Are Authenticated in the Electronic Document Management System

Westinghouse Electric Company LLC
P.O. Box 355
Pittsburgh, PA 15230-0355

© 2009 Westinghouse Electric Company LLC
All Rights Reserved

TABLE OF CONTENTS

1.0.	INTRODUCTION	1-1
1.1	H*/B* Background Information	1-1
1.2	Discussion of the Calculation Processes	1-2
1.2.1	Structural Integrity Analysis	1-3
1.2.2	Leakage Integrity Approach	1-4
1.3	Summary of Changes from Prior H* Submittals	1-4
1.3.1	Structural Integrity Analysis	1-4
1.3.2	Leakage Integrity Analysis	1-6
1.3.3	Probabilistic Analysis	1-7
1.4	Conservatism in the H* Analysis	1-7
1.5	Report Overview	1-8
1.6	References	1-8
2.0	RESOLUTION OF TECHNICAL ISSUES AND NRC REQUEST FOR ADDITIONAL INFORMATION (RAI) FROM PRIOR H* SUBMITTALS	2-1
2.1	Categorization of Technical Issues and Resolution Road Map	2-1
2.2	Review of Prior NRC Requests for Information	2-1
2.3	References	2-2
3.0	TEST PROGRAM IN SUPPORT OF H*	3-1
3.1	Coefficient of Thermal Expansion (CTE) of Alloy 600 and SA508 Steel	3-1
3.1.1	Review of Industry Data	3-2
3.2	CTE Tests	3-2
3.2.1	Description of the CTE Tests	3-2
3.2.2	CTE Tests	3-3
3.3	CTE Test Results	3-5
3.4	Discussion	3-5
3.5	Conclusions	3-6
3.6	References	3-7
4.0	STRUCTURAL AND LEAKAGE INTEGRITY ACCEPTANCE CRITERIA	4-1
4.1	Structural Integrity Acceptance Criteria	4-2
4.2	Primary-to-Secondary Leakage Acceptance Criteria	4-3
4.3	References	4-5

5.0	PLANT OPERATING CONDITIONS AND LOADINGS (MODEL F).....	5-1
5.1	Normal Operating Conditions and Loadings	5-1
5.2	Faulted Conditions.....	5-1
5.2.1	Feedwater Line Break and Steam Line Break	5-1
5.2.2	Locked Rotor	5-2
5.2.3	Control Rod Ejection	5-2
5.3	Calculation of Applied End Cap Loads	5-3
5.4	References.....	5-4
6.0	STRUCTURAL ANALYSIS OF THE TUBE-TO-TUBESHEET JOINT	6-1
6.1	Results Summary	6-1
6.1.1	Introduction.....	6-2
6.1.2	Evolution and Development of the H* Structural Model	6-3
6.2	3D Finite Element Tubesheet Displacement Analysis.....	6-8
6.2.1	Description of the Tubesheet Complex Model	6-8
6.2.2	Inputs to the Model and Their Variability.....	6-16
6.2.3	Bounding Sector Analysis	6-38
6.2.4	Radius Dependent Tubesheet Stiffness Analysis.....	6-41
6.2.5	Tubesheet Tube Bore Dilation.....	6-62
6.2.6	Divider Plate Modeling.....	6-82
6.3	Tubesheet Rotation Effects.....	6-83
6.4	Calculation of Tube-to-Tubesheet Contact Pressure	6-85
6.4.1	Calculation of Local Effects Due to Interaction of the Tube and Tubesheet Hole.....	6-85
6.4.2	General Description of 3D FEA Model Results	6-90
6.4.3	General Description of 3D FEA Post-Processing.....	6-95
6.4.4	Determination of Limiting Model F SG Plant in the H* Fleet	6-95
6.4.5	Sample Mean H* and Contact Pressure Calculation	6-98
6.4.6	Validation of Calculated Contact Pressures and Supporting Models	6-100
6.4.7	Distribution of Tube-to-Tubesheet Contact Pressure as a Function of Tubesheet Elevation.....	6-102
6.4.8	Effect of Excluding Specimen 7 Crevice Pressure Data on Contact Pressure Results.....	6-106
6.5	Conclusions.....	6-108

6.6	References.....	6-112
7.0	RESIDUAL CONTACT PRESSURE.....	7-1
7.1	Pull out Test Program.....	7-2
7.2	Analysis for Uncertainties in RCP.....	7-2
7.2.1	Variables that Affect the Value of RCP.....	7-2
7.2.2	Structural Analysis Model.....	7-3
7.2.3	Structural Analysis Results.....	7-4
7.2.4	RCP Uncertainty Evaluation.....	7-4
7.2.5	Application to H* Calculation.....	7-5
7.3	References.....	7-6
8.0	DETERMINATION OF H* AT THE REQUIRED PROBABILITY AND CONFIDENCE.....	8-1
8.1	Process.....	8-1
8.1.1	Effect of Crevice Pressure on H*.....	8-1
8.1.2	Definition of Variables and Their Variability.....	8-2
8.1.3	Interaction Among the Applicable Variables.....	8-3
8.1.4	Influence Factor Distributions.....	8-5
8.2	Calculation of Probabilistic H*.....	8-18
8.2.1	Square Root of the Sum of the Squares (SRSS) Approach.....	8-18
8.2.2	Monte Carlo Sampling Approach to Calculating the Probabilistic Value of H*.....	8-20
8.3	Summary and Conclusions.....	8-23
8.4	References.....	8-24
9.0	LEAK RATE ANALYSIS OF CRACKED TUBE-TO-TUBESHEET JOINTS.....	9-1
9.1	Leakage Analysis Methodology.....	9-1
9.1.1	Development of Overall Leakage Factor.....	9-1
9.1.2	Viscosity Subfactor.....	9-3
9.1.3	Discussion on Porous Medium.....	9-3
9.2	Determination of Limiting Conditions for H* Leakage Calculation.....	9-4
9.2.1	Background.....	9-4
9.2.2	Pressure-Time Histories for Accidents that Model Primary-to-Secondary Leakage.....	9-4
9.2.3	Limiting Temperature Conditions.....	9-5

9.3	Leak Rate Testing	9-7
9.3.1	Description of Testing	9-7
9.3.2	Leak Test Results.....	9-10
9.3.3	Loss Coefficient Evaluation.....	9-11
9.4	Development of Final Leakage Factors	9-12
9.5	Condition Monitoring/Operational Assessment Impact	9-13
9.6	Final Leakage Factor Determination	9-14
9.7	Ligament Tearing Discussion	9-14
9.7.1	Circumferential Cracks	9-14
9.7.2	Axial Cracks	9-15
9.8	Review of Leak Rate Susceptibility to Tube Slippage	9-19
9.8.1	Background.....	9-19
9.8.2	Assessment of the Potential for Tube Slippage	9-19
9.8.3	Assessment of of Leakage Potential Under Postulated Tube Slippage.....	9-20
9.8.4	Conclusions Regarding Tube Slippage.....	9-21
9.9	References.....	9-22
10.0	SUMMARY AND CONCLUSIONS	10-1
10.1	Recommended Value of H^*	10-1
10.2	H^* Concept and Evolution.....	10-1
10.3	Design Requirements	10-2
10.4	Design Conditions.....	10-2
10.5	Material Properties.....	10-3
10.6	Residual Contact Pressure	10-3
10.7	Structural Analysis.....	10-3
10.8	Leakage Analysis.....	10-4
10.9	Probabilistic Analysis	10-5
10.10	Tube Slippage	10-6
APPENDIX A	Tube Pull Out Testing Data	A-1
APPENDIX B	An Evaluation of the Statistical Variability in Coefficient of Thermal Expansion Properties of SA-508 and Alloy-600	B-1

LIST OF TABLES

Table 1-1	List of Conservatism in the H* Structural and Leakage Analysis.....	1-11
Table 2-1	NRC Technical Issue Response Road Map	2-3
Table 2-2	List of NRC RAI on H* and Resolution Status	2-4
Table 3-1	Chemical Certifications (in Weight Percent) for A508 Pressure Vessel Steel Used in the CTE Test Program	3-9
Table 3-2	Mechanical Certifications for A508 Pressure Vessel Steel in the CTE Test Program	3-9
Table 3-3	Summary of the A600 Tubes Used in the CTE Test Program	3-10
Table 3-4	Chemical Certifications (in Weight Percent) of the A600 Tubes Used in the CTE Test Program	3-10
Table 3-5	Mechanical Certifications of the A600 Tubes Used in the CTE Test Program	3-11
Table 3-6	Matrix for Coefficient of Thermal Expansion Tests	3-12
Table 3-7	Listing of the Test Results and Their Corresponding Figure Numbers	3-13
Table 5-1	Operating Conditions – Model F H* Plant	5-5
Table 5-2	Steam Line Break Conditions	5-6
Table 5-3	Feedwater Line Break Conditions	5-7
Table 5-4	Locked Rotor Event Conditions	5-8
Table 5-5	Control Rod Ejection	5-9
Table 5-6	Design End Cap Loads for Normal Operating Plant Conditions, Locked Rotor and Control Rod Ejection for Model F Plants	5-10
Table 6-1	List of Lower SG Complex Materials	6-16
Table 6-2	Summary of Material Properties for Alloy 600 Tube and Divider Plate Material	6-19
Table 6-3	Summary of Material Properties for SA-508 Class 2a Tubesheet Material	6-19
Table 6-4	Summary of Material Properties for SA-533 Grade A Class 2 Shell Material	6-20
Table 6-5	Summary of Material Properties for SA-216 Grade WCC Channelhead Material	6-20
Table 6-6	Summary of H* Millstone Unit 3 Analysis Mean Input Properties	6-21
Table 6-7	List of SG Models and H* Plants With Tubesheet Support Ring Structures	6-22
Table 6-8	Conservative Generic NOP Pressures and Temperatures for 4-Loop Model F	6-29
Table 6-9	Generic NOP Low T_{avg} Pressures and Temperatures for 4-Loop Model F	6-29
Table 6-10	Generic NOP High T_{avg} Pressures and Temperatures for 4-Loop Model F	6-29
Table 6-11	Generic SLB Pressures and Temperatures for 4-Loop Model F	6-30
Table 6-12	Generic FLB Pressures and Temperatures for 4-Loop Model F	6-30
Table 6-13	Conservative Generic SLB Pressures and Temperatures for 4-Loop Model F	6-30
Table 6-14	Analysis Results of Model 1 Inside Hole Deflection for Multiple Pressure Load Combinations	6-57
Table 6-15	Comparison of FEA Results and Thick Shell Results	6-60
Table 6-16	Calculation of Adjusted d	6-60
Table 6-17	Comparison of Thick Shell Results for Initial d and Adjusted d Values	6-61
Table 6-18	Contact Pressure for Square Displacement Model	6-70
Table 6-19	Contact Pressure for Diagonal Displacement Model	6-71
Table 6-20	Scale Factor as a Function of Initial Eccentricity	6-85
Table 6-21	Initial Mean H* Values	6-98
Table 6-22	Mean H* Values Adjusted for Thermal Distribution Effect	6-99
Table 6-23	Mean H* Values Including BET Offset	6-99
Table 6-24	Final Mean H* Values	6-100
Table 6-25	Mean Contact Pressure Distributions for NOP, Low T_{avg} Condition	6-109
Table 6-26	Mean Contact Pressure Distributions for SLB Condition	6-110
Table 6-27	Mean Contact Pressure Distributions for FLB Condition	6-111
Table 7-1	Variables That Affect Residual Contact Pressure	7-7
Table 7-2	Residual Contact Stress Model F Steam Generator	7-7

Table 7-3	Residual Contact Stress Model D5 Steam Generator	7-8
Table 7-4	Residual Contact Mode 44F Steam Generator.....	7-9
Table 7-5	Weibull Parameters for Residual Contact Pressure Variation	7-10
Table 8-1	H* Input Variables and Their Applications	8-7
Table 8-2	H* Variables and Influence Factors.....	8-8
Table 8-3	Matrix of Variable Interaction Study for H*	8-8
Table 8-4	Summary of Probabilistic Analysis	8-25
Table 9-1	Reactor Coolant System Temperature Increase Above Normal Operating Temperature Associated With Design Basis Accidents.....	9-24
Table 9-2	Reactor Coolant Systems Peak Pressures During Design Basis Accidents	9-25
Table 9-3	Model F Room Temperature Leak Rate Test Data.....	9-26
Table 9-4	Model F Elevated Temperature Leak Rate Test Data.....	9-27
Table 9-5	H* Plants Operating Conditions Summary.....	9-28
Table 9-6	H* Plant Maximum Pressure Differentials During Transients that Model Primary-to- Secondary Leakage	9-29
Table 9-7	Final H* Leakage Analysis Leak Rate Factors.....	9-30
Table A-1	Model F Test Specimen Pull Out Data (1 1/16 Inch Diameter Tubes).....	A-2
Table A-2	Model 44F and 51F Test Specimen Pull Out Data (7/8 Inch Diameter Table).....	A-3
Table A-3	Model D5 Test Specimen Pull Out Data (3/4 Inch Diameter Tubes)	A-4

TABLE OF FIGURES

Figure 1-1	Analysis Process for H*.....	1-10
Figure 3-1	Model F Steam Generator Split Collar Used to Strain Harden A600 Tubing	3-14
Figure 3-2	Model D5 Steam Generator Split Collar Used to Strain Harden A600 Tubing.....	3-15
Figure 3-3	Model 44F Steam Generator Split Collar Used to Strain Harden A600 Tubing	3-16
Figure 3-4	Heat-Up Test on A508 Gr. 3 Cl. 1 Material	3-17
Figure 3-5	Heat-Up Test on A508 Gr. 3 Cl. 2 Material	3-17
Figure 3-6	Heat-Up Test on A508 Gr. 3 Cl. 2 Material	3-18
Figure 3-7	Heat-Up Test on A508 Gr. 3 Cl. 2 Material	3-18
Figure 3-8	A508 Mean Curves Versus the ASME Code Curves	3-19
Figure 3-9	Heat-Up Test on A600, Model F Tube, Heat NX9749.....	3-19
Figure 3-10	Heat-Up Test on A600, Model F Tube, Heat NX0419.....	3-20
Figure 3-11	Heat-Up Test on A600, Model F Tube, Heat NX9821.....	3-20
Figure 3-12	Summary of Heat-Up Testing of All Heats of A600 Model F Tube	3-21
Figure 3-13	Mean Curves of Heats of A600 Model F Tube Versus the ASME Code Curve	3-21
Figure 3-14	Heat-Up Test of A600, Model D5 Tube, Heat NX1002.....	3-22
Figure 3-15	Heat-Up Test of A600, Model D5 Tube, Heat NX1019.....	3-22
Figure 3-16	Heat-Up Test of A600, Model D5 Tube, Heat NX1145.....	3-23
Figure 3-17	Summary of Heat-Up Testing of All Heats of A600 Model D5 Tube.....	3-23
Figure 3-18	Mean Curves of Heats of A600 Model D5 Tube Versus the ASME Code Curve.....	3-24
Figure 3-19	Heat-Up Tests of A600, Model 44F Tube, Heat NX9180.....	3-24
Figure 3-20	Heat-Up Tests of A600, Model 44F Tube, Heat NX9292.....	3-25
Figure 3-21	Heat-Up Tests of A600, Model 44F Tube, Heat NX1518.....	3-25
Figure 3-22	Summary of Heat-Up Testing of All Heats of A600 Model 44F Tube	3-26
Figure 3-23	Mean Curves of Heats of A600 Model 44F Tube Versus the ASME Code Curve.....	3-26
Figure 3-24	Mean Curves of All A600 Steam Generator Model Data Versus the ASME Code Curve.....	3-27
Figure 3-25	A508, Heat 97D258-1-1, Sample 8 Multiple Testing.....	3-27
Figure 3-26	A600, Heat NX1019, Sample 3 Multiple Testing.....	3-28
Figure 3-27	Heat-Up Tests of Strain Hardened A600 Model F Tubing, Heat NX9749.....	3-28
Figure 3-28	Heat-Up Tests of Strain Hardened A600 Model F Tubing, Heat NX0419.....	3-29
Figure 3-29	Heat-Up Tests of Strain Hardened A600 Model F Tubing, Heat NX9821.....	3-29
Figure 3-30	Heat-Up Tests of Strain Hardened A600 Model D5 Tubing, Heat NX1002.....	3-30
Figure 3-31	Heat-Up Tests of Strain Hardened A600 Model D5 Tubing, Heat NX1019.....	3-30
Figure 3-32	Heat-Up Tests of Strain Hardened A600 Model D5 Tubing, Heat NX1145.....	3-31
Figure 3-33	Heat-Up Tests of Strain Hardened A600 Model 44F Tubing, Heat NX9180.....	3-31
Figure 3-34	Heat-Up Tests of Strain Hardened A600 Model 44F Tubing, Heat NX9292.....	3-32
Figure 3-35	Heat-Up Tests of Strain Hardened A600 Model 44F Tubing, Heat NX1518.....	3-32
Figure 3-36	A600 Model F Tube, Heat NX0419, Repeat Test.....	3-33
Figure 3-37	A600 Model D5 Tube, Heat NX1019, Repeat Test.....	3-33
Figure 3-38	A600 Model 44F Tube, Heat NX9180, Repeat Test.....	3-34
Figure 3-39	A600 Model D5 Tube, Heat NX1145, Repeat Test.....	3-34
Figure 6-1	Mean H* Values for the Limiting Model F Plant.....	6-2
Figure 6-2	Solid 3D Model of a Typical SG With a Tubesheet Support Ring.....	6-11
Figure 6-3	Solid 3D Model of a Typical SG Without a TS Support Ring	6-11
Figure 6-4	3D Model Mesh Screen Shot.....	6-12
Figure 6-5	Close-Up of Tubesheet Junction Mesh in a Model Without a TS Support Ring.....	6-12
Figure 6-6	Typical Finite Element Mesh for a Prior Axisymmetric Tubesheet-Channelhead-Stub Barrel Model.....	6-13
Figure 6-7	3D Tubesheet Mesh Close-Up Screen Shot.....	6-14

Figure 6-8	Top Plane View of Perforated Tubesheet Mesh	6-15
Figure 6-9	Rear View of 3D Model Mesh	6-15
Figure 6-10	Important Structures in the Lower SG Complex	6-17
Figure 6-11	Top View of Tubesheet Showing Different Tubesheet Structures	6-17
Figure 6-12	Surface Groups for a Typical SG FEM	6-24
Figure 6-13	Important Edges in a Typical SG FEM With a Tubesheet Support Ring	6-24
Figure 6-14	Important Edges in a Typical SG FEM Without a Tubesheet Support Ring	6-25
Figure 6-15	Typical Structural Model Applied Loads	6-26
Figure 6-16	Typical Thermal Model Applied Loads	6-26
Figure 6-17	Typical Thermal Model Tubesheet Boundary Conditions Shown on Top View SG	6-27
Figure 6-18	Typical Structural Model Tubesheet Boundary Conditions Shown on Top View of Model F	6-27
Figure 6-19	Comparison of the Tubesheet Deflection for the Centerline Fixed and Tubesheet Support Ring Fixed Boundary Conditions for the Bottom of the Tubesheet (BTS) Surface and the Top of the Tubesheet (TTS) Surface for Both the HL and the CL of the SG	6-31
Figure 6-20	Comparison of Different Temperature Distributions Through the Tubesheet due to Varying Boundary Conditions	6-34
Figure 6-21	Radial Tubesheet Expansion due to Temperature	6-35
Figure 6-22	Graph Comparing the Radial Tubesheet Expansion of the Modified Thermal Distribution and the Scaled Linear Thermal Distribution Results	6-35
Figure 6-23	Graph of Difference in H^* Values at the Limiting TS Radius (Max H^*) for the NOP $Hi-T_{avg}$ Condition Using the Linear and Modified Thermal Distributions	6-36
Figure 6-24	Top View of Model F Tubesheet Showing Sector Regions for Displacement Analysis	6-38
Figure 6-25	Radial TS Displacement due to Pressure at TTS and BTS for TS Radius = 60 in. During NOP	6-39
Figure 6-26	Relative Change in Tubesheet Displacement as a Function of Sector Angle During NOP	6-40
Figure 6-27	FEA Model Orientations as Shown From a Top View of a Typical Tubesheet	6-44
Figure 6-28	Model 1 Geometry, Region of Tubesheet Perpendicular to Tube Lane	6-45
Figure 6-29	Model 2 Geometry, Region of Tubesheet Parallel to Tube Lane	6-45
Figure 6-30	Model 1 Applied Boundary Conditions - Perpendicular to Divider Lane	6-46
Figure 6-31	Model 2 Applied Boundary Conditions - Parallel to Divider Lane	6-46
Figure 6-32	Relative Location of the Three Tube Holes of Interest in Model 1 and Model 2	6-47
Figure 6-33	Close-Up of Inside Hole Location	6-47
Figure 6-34	Close-Up of Middle Hole Location	6-47
Figure 6-35	Close-Up of Outside Hole Location	6-48
Figure 6-36	Reference Configuration for Tube Bore Deflection Plots	6-50
Figure 6-37	Inside Hole Results for NOP Conditions, $P_{pri} = 2250$ psi, for Model 1	6-50
Figure 6-38	Middle Hole Results for NOP Conditions, $P_{pri} = 2250$ psi, for Model 1	6-51
Figure 6-39	Outside Hole Results for NOP Conditions, $P_{pri} = 2250$ psi, for Model 1	6-51
Figure 6-40	Inside Hole Results for SLB Conditions, $P_{pri} = 2560$ psi, for Model 1	6-52
Figure 6-41	Middle Hole Results for SLB Conditions, $P_{pri} = 2560$ psi, for Model 1	6-52
Figure 6-42	Outside Hole Results for SLB Conditions, $P_{pri} = 2560$ psi, for Model 1	6-53
Figure 6-43	Comparison of FEA Results and Thick Shell Equations for NOP and SLB Using Equations (6-1) and (6-2)	6-54
Figure 6-44	Typical Result for Including the Tube Cross Section Within the Tube Bore, for the Outside Hole, When All of the Tube Bores are Pressurized	6-54
Figure 6-45	Graphic of Applied Pressure Regions in Separate Pressure Combination Study	6-56

Figure 6-46	Tube Bore ID Deflection due to a Constant Applied Internal Pressure as a Function of Outer Collar Radius	6-58
Figure 6-47	Linear Relationships Between Applied Effective Outer Radius (d) and TS Radius for the NOP and SLB Conditions	6-61
Figure 6-48	Finite Element Model	6-72
Figure 6-49	Boundary Conditions for Square Displacement Model	6-72
Figure 6-50	Displaced Shape for S.1.1 Through S.1.6 Computer Runs	6-73
Figure 6-51	Displaced Shape for S.2.1 Through S.2.6 Computer Runs	6-73
Figure 6-52	Boundary Conditions for Diagonal Displacement Model	6-74
Figure 6-53	Displaced Shape for D.1.1 Through D.1.6 Computer Runs	6-74
Figure 6-54	Displaced Shape for D.2.1 Through D.2.6 Computer Runs	6-75
Figure 6-55	Computer Run S.1.5, Step 1, Stress Intensity	6-75
Figure 6-56	Computer Run S.1.5, Step 2, Stress Intensity	6-76
Figure 6-57	Computer Run S.1.5, Step 2, Contact Pressure	6-76
Figure 6-58	Computer Run S.1.5, Step 3, Stress Intensity	6-77
Figure 6-59	Computer Run S.1.5, Step 3, Contact Pressure	6-77
Figure 6-60	Computer Run S.1.5, Step 4, Stress Intensity	6-78
Figure 6-61	Computer Run S.1.5, Step 4, Contact Pressure	6-78
Figure 6-62	Computer Run S.1.5, Step 5, Stress Intensity	6-79
Figure 6-63	Computer Run S.1.5, Step 5, Contact Pressure	6-79
Figure 6-64	Computer Run S.1.5, Step 6, Stress Intensity	6-80
Figure 6-65	Computer Run S.1.5, Step 6, Contact Pressure	6-80
Figure 6-66	Computer Run S.1.5, Step 7, Stress Intensity	6-81
Figure 6-67	Computer Run S.1.5, Step 7, Contact Pressure	6-81
Figure 6-68	Comparison Between H^* Values for a Degraded Divider Plate ($DPF = [\quad]^{a,c,e}$) and an Intact Divider Plate ($DPF = [\quad]^{a,c,e}$)	6-83
Figure 6-69	Typical Combined Displacement for 3D Model During NOP	6-92
Figure 6-70	Typical Combined Displacement for 3D Model During SLB	6-92
Figure 6-71	Combined Thermal and Pressure Tubesheet Radial Displacement for Millstone Unit 3 at the Bottom of the Tubesheet, $DPF = [\quad]^{a,c,e}$	6-93
Figure 6-72	Combined Thermal and Pressure Tubesheet Radial Displacement for Millstone Unit 3 at the Neutral Axis of the Tubesheet, $DPF = [\quad]^{a,c,e}$	6-93
Figure 6-73	Combined Thermal and Pressure Tubesheet Radial Displacement for Millstone Unit 3 at the Top of the Tubesheet, $DPF = [\quad]^{a,c,e}$	6-94
Figure 6-74	Comparison of Tube-to-Tubesheet Contact Pressure for Millstone Unit 3 at the Limiting Tubesheet Radius of $[\quad]^{a,c,e}$ inches	6-94
Figure 6-75	Comparison of Contact Pressures for Model F Fleet Including All Crevice Pressure Data At Limiting TS Radius $[\quad]^{a,c,e}$	6-97
Figure 6-76	Tube-to-Tubesheet Contact Pressure for the Limiting Model F Plant (Millstone Unit 3) at the Limiting TS Radius Using Only the Specimen 8 Crevice Pressure Data	6-97
Figure 6-77	TS Radial Displacement Under Combined Thermal and Pressure Loads During SLB TTS = TS Elevation 21.0 in, BTS = TS Elevation 0.0 in.	6-103
Figure 6-78	TS Radial Displacement Under Combined Thermal and Pressure Loads for NOP TTS = TS Elevation 21.0 in, BTS = TS Elevation 0.0 in.	6-103
Figure 6-79	Combined Thermal And Pressure Load Tubesheet Radial Displacements for NOP TTS = TS Elevation 21.0 in, BTS = TS Elevation 0.0 in.	6-104
Figure 6-80	Combined Thermal and Pressure Load Tubesheet Radial Displacements for SLB TTS = TS Elevation 21.0 in, BTS = TS Elevation 0.0 in.	6-105

Figure 6-81	Mean Contact Pressure Distribution Case for Millstone Unit 3 Conditions at a TS Radius of [] ^{a,c} inches TTS = TS Elevation 0.0 in, BTS = TS Elevation 21.03 in.	6-106
Figure 6-82	Comparison of the Average Crevice Pressure Data as a Function of Depth Ratio for the Entire Crevice Pressure Data Set and the Data Set When Only Specimen 8 is Considered.....	6-107
Figure 6-83	Comparison of H* for Different Crevice Pressure Data Input.....	6-107
Figure 7-1	Finite Element Model – Overall View.....	7-11
Figure 7-2	Finite Element Model – Node Constraints.....	7-12
Figure 7-3	Cumulative Distribution Functions of RCP Variables Factors.....	7-13
Figure 7-4	Compositive Variability of Residual Contact Pressure.....	7-14
Figure 7-5	Illustration of Adjustment to H* for Positive RCP.....	7-14
Figure 8-1	Adjustment to H* for Distributed Crevice Pressure Referenced to Initial Prediction of H*.....	8-9
Figure 8-2	H* Variation of H* with Individual Input Variables.....	8-10
Figure 8-3	Variability of H* with All Relevant Parameters.....	8-11
Figure 8-4	Expected Variation of H* When Both α_T and α_{TS} are Varied and are Independent.....	8-12
Figure 8-5	Interaction Between α_{TS} and α_T	8-13
Figure 8-6	Interaction Between α_{TS} and E_{TS}	8-14
Figure 8-7	Interaction Between α_{TS} and E_T	8-14
Figure 8-8	Interaction Between α_T and E_T	8-15
Figure 8-9	Interaction Between α_T and E_{TS}	8-15
Figure 8-10	Interaction Between E_{TS} and E_T	8-16
Figure 8-11	Illustration of Biased Influence Factors.....	8-17
Figure 8-12	Single Tube Required Reliability, Expressed as Number of Standard Deviations from the Mean to Meet a Whole-Bundle (5626 Tubes) Reliability of 95%.....	8-26
Figure 9-1	Dynamic Viscosity as a Function of Temperature.....	9-31
Figure 9-2	Plot of Model D and Model F Total Data Set for 70°F and 600°F.....	9-32
Figure 9-3	Generic Model F SLB RCS Pressure-Time History Plot (4-Loop Plant).....	9-33
Figure 9-4	Model F SLB RCS Temperature-Time History Plot (4-Loop Plant).....	9-34
Figure 9-5	Model F FLB RCS Pressure-Time History Plot.....	9-35
Figure 9-6	Model F/44F/51F FLB SG HL Temperature-Time History Plot.....	9-36
Figure 9-7	Model F/44F/51F FLB SG CL Temperature-Time History.....	9-37
Figure 9-8	Example Leakage Test Schematic (Model F Testing Only).....	9-38
Figure 9-9	Schematic for the Test Autoclave Systems for Leak Rate Testing (Model D5 Testing Only).....	9-39
Figure 9-10	Example Tube Joint Leakage Test Configuration.....	9-40
Figure 9-11	Model F Room Temperature Leak Rate Test Results.....	9-41
Figure 9-12	Model F Elevated Temperature Leak Rate Test Results.....	9-42
Figure 9-13	Model F Room Temperature Leak Rate Ratio Versus Differential Pressure Ratio Comparison.....	9-43
Figure 9-14	Model F Elevated Temperature Leak Rate Ratio Versus ΔP Ratio Comparison (600°F).....	9-44
Figure 9-15	Results of Test-by-Test Loss Coefficient (K) Regression on Contact Pressure for Model D5 Test Specimens.....	9-45
Figure 9-16	Results of Test-by-Test Loss Coefficient (K) Regression on Contact Pressure for Model F Test Specimens.....	9-46
Figure 9-17	Typical Reactor Coolant Pump Locked Rotor and Control Rod Ejection Delta P for Model F SGs.....	9-47

1.0 INTRODUCTION

1.1 H*/B* BACKGROUND INFORMATION

In response to the detection of crack-like indications within the tube expansion region of steam generators (SGs) with Alloy 600 thermally-treated (A600TT) tubing, the NRC issued GL-2004-01 (Reference 1-14) which reiterated the requirement to inspect the full length of the tubes with probes capable of detecting potential degradation in all the areas of the steam generator (SG) unless a technical argument was available to demonstrate that specific types of degradation are not expected. Indications interpreted as primary water system stress corrosion cracking (PWSCC) were reported from the nondestructive, eddy current examination of the SG tubes during the fall 2004 outage at the Catawba Unit 2 Nuclear Power Plant (References 1-1, 1-2, and 1-3). The indications at Catawba Unit 2 were reported about 7.6 inches from the top of the tubesheet in one tube, and just above the tube-to-tubesheet welds in a region of the tube known as the tack expansion (TE) in several other tubes. The Catawba Unit 2 plant has Westinghouse designed, Model D5 SGs fabricated with A600TT tubes of 3/4 inch outside diameter. Subsequently, one indication was reported in each of two SG tubes at the Vogtle Unit 1 Plant (Reference 1-4). The Vogtle Unit 1 SGs are of the Westinghouse Model F design with 11/16 inch outside diameter A600TT tubes. The indication locations in both Catawba Unit 2 and Vogtle Unit 1 were coincident with geometric variations, termed "bulges" (BLG), in the expansion region. It was concluded from those observations that there is the potential for similar tube indications to be reported during future inspections of all SGs with hydraulically expanded A600TT tubes since geometric variations in the tubesheet expansion region are common. Since that time, several plants that have inspected through the entire thickness of the tubesheet with rotating pancake coil (RPC) have reported indications near the tube-to-tubesheet welds, in the tack expansion region.

The findings in the Catawba Unit 2 and Vogtle Unit 1 SG tubes present two distinct issues with regard to future inspections of A600TT SG tubes which have been hydraulically expanded into the tubesheet:

1. Indications may occur at internal bulges (BLG) or overexpansions (OXF) in the tubes within the tubesheet that were created as an artifact of the manufacturing process.
2. Indications may occur at the elevation of the tack expansion transition because it represents a stress riser in the tube.

Although some of the indications at Catawba were reported to be in the tube end weld, subsequent studies using a prototypic tube end test section concluded that the eddy current techniques were not capable of distinguishing the interface between the tube and weld, and further, that the indications likely were in the tube material. However, it could not be ruled out that the indications may extend into the weld. The indications were located within the tack expansion length, which, at Catawba, was made using a hard-rolling process. Thus, it was concluded that the indications that were observed all occurred in areas of potentially elevated residual stress in the tube material.

A technical evaluation is presented in this report that considers the requirements of the American Society of Mechanical Engineers (ASME) Code, Regulatory Guides, NRC Generic Letters, NRC Information Notices, the Code of Federal Regulations, NEI 97-06, and responses to NRC Request for Additional Information (RAI). The two major conclusions of the technical evaluation are that:

1. The structural integrity of the primary-to-secondary pressure boundary is unaffected by tube degradation of any magnitude below a specific depth of 11.2 inches, designated as H^* , and,
2. The accident condition leak rate integrity is bounded by an overall leakage increase of 2.03 during the limiting design basis accident (DBA) relative to normal operating plant conditions. This is known as the leakage factor. Although an increase in contact pressure at accident conditions relative to normal operating conditions is not a basis for the leakage evaluation, for conservatism, it is shown that the contact pressure between the tube and the tubesheet is greater at accident conditions than at normal operating conditions (NOP) for all relevant accidents.

The determination of the required engagement depth is based on the use of finite element model structural analyses and of a bounding leak rate evaluation for normal operation and postulated accident conditions. The results provide the technical rationale to exempt inspection of the region of the tube below the calculated H^* elevation. Such an approach is interpreted as a redefinition of the primary-to-secondary pressure boundary relative to the original design of the SG, which requires the approval of a license amendment by the NRC Staff.

The H^* values are determined to assure meeting the structural performance criteria for the operating SG tubes as delineated in NEI 97-06, Revision 2 (Reference 1-5). The leakage factors are determined based on meeting the accident condition leak rate performance criteria for all DBA that model primary-to-secondary leakage. The leakage analysis is based on a first principles application of the Darcy model for leakage through a porous medium, supported by empirical test results that show that there is no correlation between loss coefficient and contact pressure for the conditions of interest. The leakage analysis is supported by the structural analysis (Section 6.0) that shows that the contact pressure between the tubes and tubesheet is always greater at accident conditions than at normal operating conditions.

Tests have shown that all full-depth expanded tube-to-tubesheet joints in Westinghouse-designed SGs have a residual radial preload interface pressure between the tube and the tubesheet. Residual contact pressure is not an essential element for determining a value of H^* for hydraulically expanded tubes. The reference approach in this document is to assume zero contribution from residual contact pressure; however, when the existing residual contact pressure is more firmly established through additional testing, the value of H^* presented in this report will be significantly smaller. Thus, the assumption of zero residual contact pressure is a conservative assumption.

1.2 DISCUSSION OF THE CALCULATION PROCESSES

The current candidate plants for H^* are those plants whose SGs have Alloy 600TT tubes that are hydraulically expanded into the tubesheet. Among these are plants with Model F SGs, Model D5 SGs, Model 44F SGs and Model 51F SGs. Except for the Model 51F SGs, there are multiple plants with each of the other models of SGs. To reduce the analysis burden, a bounding plant was determined for each model of SG as discussed in Section 6.0. The value of H^* determined for each of the bounding plants is the recommended H^* for each of the models of SG, respectively.

This report is specifically based on the properties of the Model F SGs. Separate reports will be provided for the other models of SGs. While specific geometric and operating conditions are different among the various models of SGs, the methodology for the H* calculations are common to all models of SGs represented among the population of H* candidate plants.

1.2.1 Structural Integrity Analysis

The H* technical analysis consists of two essentially independent processes; the structural evaluation to define the value of H*, and the leakage analysis for the tubesheet expansion region. The structural analysis for H* is a complex analysis that involves the use of four different models as shown on the flowchart on Figure 1-1.

- A finite element structural model is used to calculate the deflections and rotations of the tubesheet complex components which include the tubesheet, channelhead, stub barrel and divider plate. The finite element model is a three-dimensional finite element model (3D FEA) using the ANSYS computer code. This model is described in detail in Section 6.0.
- An Excel[®](¹) (Reference 1-6) spreadsheet model utilizes the deflection and rotation output from the 3D FEA model (Reference 1-7) and a crevice pressure input based on test data to calculate the radially and axially distributed contact pressures between the tube and tubesheet for the various operating conditions. The spreadsheet also axially integrates the forces resisting tube pull out based on the contact pressures and a conservative value of coefficient of friction to define the mean value of H*. H* is defined as the distance from the top of the tubesheet at which the integrated pull out resisting force equals the applied end cap loads. The Excel[®] model is described in Section 6.0. The end cap force calculation applied to the tubes is described in Section 5.0.
- The third model is an Excel[®] spreadsheet that calculates the mean residual contact pressure based on pull out test data, and provides the residual contact pressure to the H* integrating spreadsheet discussed above. Residual contact pressure is defined as the contact pressure between the tube and the tubesheet at room temperature that results from the hydraulic expansion process. The use of this model is optional for the justification of H*; the reference calculation in this report assumes that residual contact pressure is zero.
- The variability of the residual contact pressure, also an input to the probabilistic analysis, is determined from a two-dimensional finite element model (2D FEA) (Reference 1-9). The variability of the inputs used to calculate the residual contact pressures are determined individually using an influence factor approach and combined into a single residual contact pressure variability distribution using different approaches including a Monte Carlo sampling technique. This is discussed in Section 7.0.

(1) Microsoft, MSN, and Windows Vista are trademarks of the Microsoft group of companies.

1.2.2 Leakage Integrity Approach

As discussed in Section 9.0 of this report, the expression used to predict the leak rate from tube cracks through the tube-to-tubesheet crevice is the Darcy expression for flow rate, Q , through porous media, i.e.,

$$Q = \frac{\Delta p}{12\mu Kl}$$

where

- μ = the viscosity of the fluid
- Δp = the driving pressure differential
- l = the physical dimension in the direction of the flow (effective crevice length)
- K = the leakage "loss coefficient" which can also be termed the flow resistance.

The leakage analysis utilizes a ratio approach, based on the Darcy equation, to determine the ratio of leakage at accident conditions to that at normal operating conditions. It is shown in Section 9.0 that the loss coefficient is not a function of contact pressure; therefore, the loss coefficient ratio has a value of 1. It is also shown that the tube and the tubesheet are in contact for the total length of the tubesheet thickness. Therefore, the ratio of the length of the porous medium also has a value of 1. The ratio of the viscosity at accident conditions to that at normal operating conditions is also conservatively shown to be 1. Consequently, the leakage ratio is a function of only the ratio of the driving heads, that is, the ratio of the accident condition Δp to that at normal operating conditions.

1.3 SUMMARY OF CHANGES FROM PRIOR H* SUBMITTALS

1.3.1 Structural Integrity Analysis

All prior submittals of the H* technical justification (e.g., Reference 1-9) utilized the same analysis approach summarized in Section 1.2.1. However, since the last submittal by Wolf Creek Nuclear Operating Corporation (Reference 1-8, with Reference 1-9 enclosed) significant changes have been made in the structural models. The original structural model utilized a two-dimensional (2D) axisymmetric model for the tubesheet complex. A number of RAIs were issued by the NRC (see Section 2.1) that questioned the details of the application of this model. Further, questions were raised regarding the efficacy of the superpositioning approach employed with this model because it was noted that different results were obtained when the model input was condition-specific compared to the superposition results based on temperature and pressure. The process of benchmarking the 2D model utilized state-of-the-art three-dimensional (3D) finite element capabilities inherent to the ANSYS computer code. Ultimately, a new 3D model of the tubesheet complex was developed and adopted as the reference model for the structural analysis. The 2D axisymmetric model is no longer used in the current tubesheet deflection calculations supporting the analysis of H*.

Prior calculations assumed that contact pressure from the tube would expand the tubesheet bore uniformly without considering the restoring forces from adjacent pressurized tubesheet bores. In the structural model, a tubesheet radius dependent stiffness effect is applied by modifying the representative collar thickness (see Section 6.2.4) of the tubesheet material surrounding a tube based on the position of the tube in the bundle. The basis for the radius dependent tubesheet stiffness effect is similar to the previously mentioned “beta factor” approach. The “beta factor” was a coefficient applied to reduce the crevice pressure to reflect the expected crevice pressure during normal operating conditions in some prior H* calculations and is no longer used in the structural analysis of the tube-to-tubesheet joint. The current structural analysis consistently includes a radius dependent stiffness calculation described in detail in Section 6.2.4. The application of the radius dependent stiffness factor has only a small effect on the ultimate value of H* but rationalizes the sensitivity of H* to uncertainties throughout the tubesheet.

The contact pressure analysis methodology has not changed since 2007 (Reference 1-9). However, the inputs to the contact pressure analysis and how H* is calculated have changed in that period of time. The details describing the inputs to the contact pressure analysis are discussed in Section 6.0.

The calculation for H* includes the summation of axial pull out resistance due to local interactions between the tube bore and the tube. Although tube bending is a direct effect of tubesheet displacement, the calculation for H* conservatively ignores any additional pull out resistance due to tube bending within the tubesheet or Poisson expansion effects acting on the severed tube end. In previous submittals, the force resisting pull out acting on a length of a tube between any two elevations *h1* and *h2* was defined in Equation (1-1):

$$\left[\dots \right]^{a,c,e} \tag{1-1}$$

where:

- F_{HE} = Resistance per length to pull out due to the installation hydraulic expansion,
- d = Expanded tube outer diameter,
- P = Contact pressure acting over the incremental length segment dh , and,
- μ = Coefficient of friction between the tube and tubesheet, conservatively assumed to be 0.2 for the pull out analysis to determine H*.

The current H* analysis generally uses the following equation to determine the axial pull out resistance of a tube between any two elevations *h1* and *h2*:

$$\left[\dots \right]^{a,c,e} \tag{1-2}$$

Where the other parameters in Equation (1-2) are the same as in Equation (1-1) and [

]^{a,c,e}. A detailed explanation of the

revised axial pull out equation are included in Section 6.0 of this report. However, the reference basis for the H* analysis is the assumption that residual contact pressure contributes zero additional resistance to tube pull out. Therefore, the equation to calculate the pull out resistance in the H* analysis is:

$$\left[\quad \quad \quad \right]^{a,c,e} \quad (1-3)$$

1.3.2 Leakage Integrity Analysis

Prior submittals of the technical justification of H* (Reference 1-9) argued that K was a function of the contact pressure, P_c , and, therefore, that resistance was a function of the location within the tubesheet. The total resistance was found as the average value of the quantity μK , the resistance per unit length, multiplied by L , or by integrating the incremental resistance, $dR = \mu K dL$ over the length L , i.e.,

$$R = \mu \bar{K} (L_2 - L_1) = \mu \int_{L_1}^{L_2} K dL \quad (1-4)$$

Interpretation of the results from multiple leak rate testing programs suggested that the logarithm of the loss coefficient was a linear function of the contact pressure, i.e.,

$$\ln K = a_0 + a_1 P_c, \quad (1-5)$$

where the coefficients, a_0 and a_1 of the linear relation were based on a regression analysis of the test data; both coefficients are greater than zero. Simply put, the loss coefficient was determined to be greater than zero at the point where the contact pressure is zero and it was determined that the loss coefficient increases with increasing contact pressure. Thus,

$$K = e^{a_0 + a_1 P_c}, \quad (1-6)$$

and the loss coefficient was an exponential function of the contact pressure.

The B* distance (LB) was defined as the depth at which the resistance to leak during SLB was the same as that during normal operating conditions (NOP) (using Equation 1-4, the B* distance was calculated setting $R_{SLB} = R_{NOP}$ and solving for LB). Therefore, when calculating the ratio of the leak rate during the design basis accident condition to the leak rate during normal operating conditions, the change in magnitude of leakage was solely a function of the ratio of the pressure differential between the design basis accident and normal operating plant conditions.

The NRC Staff raised several concerns relative to the credibility of the existence of the loss coefficient versus contact pressure relationship used in support of the development of the B* criterion:

1. The Model F SG loss coefficient versus contact pressure plot exhibits a higher slope than the case for the Model D5 SG (Reference 1-10).
2. Although the mean of the regression fits for the loss coefficient data for the Model F and the Model D5 SGs are within a factor of three (3) of each other, the slope and intercept properties remain highly divergent (Reference 1-11).
3. The Model D5 loss coefficient data is spread out in range and results in a slightly negative log-linear correlation (Reference 1-11).

The current approach to the leakage analysis shows that there is no significant correlation between loss coefficient and contact pressure based on the available test data. A ratio approach, using the Darcy formulation as noted above and as described in detail in Section 9.0, is the current reference basis for leakage ratio calculations.

1.3.3 Probabilistic Analysis

At a meeting in July 2008, the NRC requested a probabilistic evaluation of H^* . Probabilistic evaluations of H^* had not been performed. Previously, a limiting worst-case analysis was provided (Reference 1-11) that was based on an H^* variability study on individual inputs parameters. The worst-case values of the variables were then combined into an integrated case that resulted in a high probability value of H^* . This approach was not accepted as noted in the remaining technical concerns issued in Reference 1-12.

Because of the complexity of the H^* calculations (see Section 1.2.1) that involve the combined use of four different models, a pure Monte Carlo approach was not possible. The current analysis of H^* is based principally on the semi-statistical approach outlined in the EPRI Integrity Assessment Guidelines (Reference 1-13), in which the uncertainties are combined using a square root of sum of squares (SRSS) approach. Further, to support the SRSS approach, a Monte Carlo approach to the H^* calculation was developed that utilized influence factors. For the influence factor approach, a distribution of H^* in a single input variable is determined while maintaining all other input variables at their nominal values. This process is completed for each input variable, resulting in H^* distributions in every input variable. Monte Carlo sampling is performed from these distributions to develop the integrated variability of H^* in all variables. The probabilistic analysis for H^* is included in Section 8.0 of this report.

In response to the residual technical issues identified by the Staff, the capability to provide residual contact pressure variability as an input to the H^* integration model was developed. The mean value of residual contact pressure is based on test data, and the variability around the mean value is determined for each relevant input variable based on analysis. The individual variability distribution for residual contact pressure is combined in the same manner as discussed above for the probabilistic H^* determination. It is noted that the reference H^* calculation provided in this report assumes residual contact pressure to be zero. Any positive value of residual contact pressure will decrease the final value of H^* .

1.4 CONSERVATISMS IN THE H^* ANALYSIS

A conservative approach was taken for the calculation of H^* . Notwithstanding that the underlying structural integrity and leakage requirements are inherently conservative, e.g., application of a factor of

three (3) on expected normal operating pressure differentials, other conservative assumptions were made that provide significant confidence in the predicted value of H^* and the leakage factors. Table 1-1 summarizes the significant conservative assumptions and approaches included in the calculations for H^* .

1.5 REPORT OVERVIEW

Section 1.0 provides an introduction to WCAP-17071-P. Section 2.0 provides information on the resolution of all technical issues and NRC requests for additional information on this topic. Section 3.0 addresses the test programs in support of the technical justification of H^* . Section 4.0 addresses the structural and leakage analysis acceptance criteria. Section 5.0 discusses the plant operating conditions at the H^* plants with Model F SGs. Section 6.0 discusses the structural analyses of the tube-to-tubesheet joint. Section 7.0 addresses residual contact pressure and its variability. Section 8.0 uses the results provided in Section 6.0 and Section 7.0 to define the H^* values as a function of tubesheet radial location for each of the H^* plants for normal operating, postulated steam line break, and feedwater line break conditions to provide a probabilistic assessment of the H^* value. Section 9.0 discusses the details of the leakage analysis. Finally, Section 10.0 provides the conclusion of this report.

1.6 REFERENCES

- 1-1 OE19662 (Restricted & Confidential), "Steam Generators (Catawba Nuclear Power Station)," Institute of Nuclear Power Operations (INPO), Atlanta, GA, USA, December 13, 2004.
- 1-2 IN 2005-09, "Indications in Thermally-Treated Alloy 600 Steam Generator Tubes and Tube-to-Tubesheet Welds," United States Nuclear Regulatory Commission, Washington, DC, April 7, 2005.
- 1-3 SGMP-IL-05-01, "Catawba Unit 2 Tubesheet Degradation Issues," EPRI, Palo Alto, CA, March 4, 2005.
- 1-4 OE20339, "Vogtle Unit 1 Steam Generator Tube Crack Indications," Institute of Nuclear Power Operations (INPO), Atlanta, GA, USA, April 4, 2005.
- 1-5 NEI 97-06, Rev. 2, "Steam Generator Program Guidelines," Nuclear Energy Institute, Washington, DC, May 2005.
- 1-6 LTR-SST-05-19, Rev. 1, "System State Equivalency Testing Not Required for Windows XP SP-2," June 20, 2005.
- 1-7 LTR-SST-08-16, "ANSYS 10.0 for HP-UX 11.23i Release Letter," March 28, 2009.
- 1-8 WCNOG Letter ET-06-0004, "Revision to Technical Specification 5.5.9, Steam Generator Tube Surveillance Program," February 21, 2006.

-
- 1-9 LTR-CDME-05-209-P, "Steam Generator Tube Alternate Repair Criteria for the Portion of Tube Within the Tubesheet at the Wolf Creek Generating Station," January 2006.
 - 1-10 LTR-CDME-07-72, "Response to NRC Request for Additional Information Relating to LTR-CDME-05-209-P of the Wolf Creek Generating Station (WCGS) Permanent B* License Amendment Request," April 24, 2007 (Enclosure to WCNO Letter WO 07-0012, dated May 3, 2007).
 - 1-11 LTR-CDME-07-198, "Response to NRC Request for Additional Information Relating to LTR-CDME-07-72 P-Attachment and LTR-CDME-05-209-P of the Wolf Creek Generating Station (WCGS) Permanent B* License Amendment Request," September 24, 2007 (Enclosure to WCNO Letter ET-07-0043, dated September 27, 2007).
 - 1-12 NRC Letter, "Wolf Creek Generating Station – Withdrawal of License Amendment Request on Steam Generator Tube Inspections (TAC No. MD1097)," February 28, 2008.
 - 1-13 Steam Generator Integrity Assessment Guidelines, Revision 2, EPRI, Palo Alto, CA, July 2006, 1012987.
 - 1-14 NRC Generic Letter 2004-01, "Requirements for Steam Generator Tube Inspections," August 30, 2004.

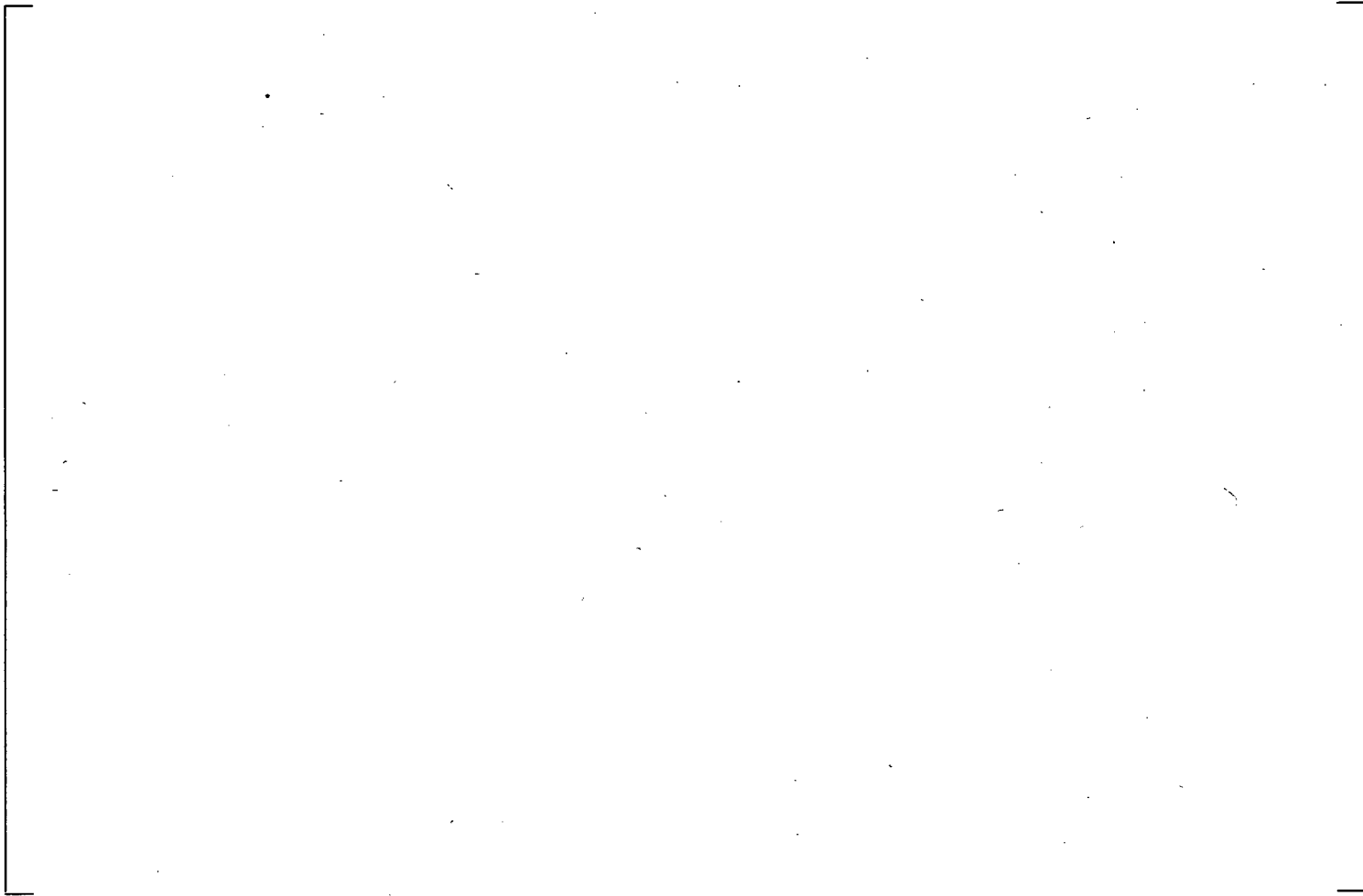


Figure 1-1 Analysis Process for H*

Table 1-1 List of Conservatisms in the H* Structural and Leakage Analysis

Assumption/Approach	Why Conservative?
The NEI 97-06 performance criteria, which address tube burst, are applied by equating failure to meet the H* distance with tube burst.	Tube burst cannot occur within the tubesheet (see Section 4.1), thus application of the same criteria designed to prevent tube burst in an area where tube burst cannot occur is inherently conservative. Prevention of tube burst is a necessity for preventing excessive leakage, and accident-induced leakage in the tubesheet expansion region is shown to be limited, independent of the H* distance. Therefore, equating failure to meet H* with tube burst, and application of the same criteria to prevent tube burst to H*, is inherently conservative.
H* distances are based on analysis of the worst tube in the bundle.	The distribution of the contact pressure between the tube and the tubesheet varies as a function of radial position in the tubesheet; <i>the worst-case tube location is used to establish the H* distance</i> (see Section 6.2.3). All other tubes have lower H* values.
Structural support from the divider plate is ignored.	The H* distances for a severely degraded divider plate (no connection between the tubesheet and the divider plate) bound the H* distances for a non-degraded divider plate (see Section 6.2.6).
Residual Contact Pressure Assumed to be Zero.	All pull out tests to date have shown that there is residual contact pressure from the hydraulic expansion; any non-zero value will decrease H* (see Section 7.0 and Appendix A).
Calculation of Pull out Force.	Assumes mean plus 2 sigma tubesheet bore diameter as basis for tube cross-sectional area (see Section 5.3).
Coefficient of Thermal Expansion.	Use of ASME Code mean is conservative relative to test data for both tubesheet and tubing material (see Section 3.5 and Appendix B).
Coefficient of Friction.	Lower bound value of [] ^{a,c,e} is used in the determination of the H* distance (see Section 6.2.2.3.3). Standard reference values suggest a reasonable value of coefficient of friction is [] ^{a,c,e} .
Darcy equation used to model leakage analysis.	The assumed linear relationship between leak rate and differential pressure is conservative relative to alternate models such as Bernoulli or orifice models which assume the leak rate to be proportional to the square root of the pressure differential (see Section 9.1.1 and Reference 9-5 of Section 9.0).

Table 1-1 List of Conservatisms in the H* Structural and Leakage Analysis (Continued)

Assumption/Approach	Why Conservative?
Use of different plant temperature and pressure conditions for structural and leakage calculations.	<p>The conditions that maximize H* are different from those that maximize leakage conditions. Separate maximizing assumptions are made for structural and leakage analysis (see Section 6.4.5 for the structural analysis assumptions and Section 9.4 for the leakage analysis assumptions).</p> <p>Bounding limit values for the most limiting plant operating pressure and temperatures which include maximum licensed steam generator tube plugging levels (i.e., in numbers of tubes plugged) are used to establish the H* distances for the Model F SGs (see Section 5.0).</p> <p>A combination of []^{a,c,e} are used for the structural evaluation (see Section 6.2.2.2 and Section 6.2.2.5).</p> <p>[]^{a,c,e} conditions are used for evaluating the overall leakage factors (to maximize the pressure difference ratio between design basis accident conditions and normal operating conditions) (see Section 9.4).</p>
H* distances based on hot leg temperatures and pressure.	The results described in this report conservatively bound the requirements for both the hot leg and the cold leg in any Model F SG (see Section 6.2.2.3).
Stiffening effect of the presence of tubes ignored in the structural analysis.	Equivalent properties of the tubesheet are calculated without taking credit for the stiffening effect in the tubes, which results in a conservatism in the calculations regarding tubesheet deflection (see Section 6.2.1).
Some local interactions between the tube bore and the tube are ignored.	Additional pull out resistance due to tube bending within the tubesheet or Poisson expansion effects on the severed tube end are ignored (see Section 1.3.1).
Peak reactor coolant system pressures and temperatures are assumed to exist during the entire design basis accidents.	Time varying, or transient pressures and temperatures would reduce the pressure and thermal loads on the tube and the tubesheet (see Section 6.2.2).

Table 1-1 List of Conservatisms in the H* Structural and Leakage Analysis (Continued)

Assumption/Approach	Why Conservative?
A [] ^{a,c,e}	This is conservative because it reduces the stiffness of the solid and perforated regions of the tubesheet to the lowest level for each operating condition (see Section 6.2.2.2).
Pressure is not applied to the [] ^{a,c,e}	Applying pressure to the [] ^{a,c,e} (see Section 6.2.2.4).
The radius dependent stiffness analysis ignores the presence of the [] ^{a,c,e}	Including these structures in the analysis would reduce the tubesheet displacement and limit the local deformation of the tubesheet hole ID (see Section 6.2.4.4).
The tubesheet bore dilation [] ^{a,c,e}	Thermal expansions under operating loads were [] ^{a,c,e} (see Section 6.2.5).

2.0 RESOLUTION OF TECHNICAL ISSUES AND NRC REQUEST FOR ADDITIONAL INFORMATION (RAI) FROM PRIOR H* SUBMITTALS

2.1 CATEGORIZATION OF TECHNICAL ISSUES AND RESOLUTION ROAD MAP

The open technical issues identified by the NRC Staff are included in Reference 2-1. Generally, the significant remaining technical issues are in the following categories:

1. Determination of residual contact pressures and variability of residual contact pressure.
2. Adequacy of the existing tube pull out data to justify residual contact pressure when potentially larger values of H* may be determined.
3. Justification of the mean values and variability of the coefficient of thermal expansion for the tubesheet material (SA508) and the tubing material (A600).
4. Leakage loss coefficient as a function of tube-to-tubesheet contact pressure.
5. Consideration of the potential for incremental tube slippage during pressure and temperature cycles.

Table 2-1 provides a listing of the remaining technical issues related to steam generator (SG) tube inspections based on the H*/B* methodology that were identified in Reference 2-1 and a road map to where these issues are addressed within this report. Since the issuance of Reference 2-1, four additional issues have been identified during NRC/Industry meetings. These issues are labeled as A**, B**, C**, and D** and are also resolved in this report.

2.2 REVIEW OF PRIOR NRC REQUESTS FOR INFORMATION

Wolf Creek Nuclear Operating Corporation (WCNOC) submitted a license amendment request on February 21, 2006 (Reference 2-4) proposing changes to the Technical Specifications for the Wolf Creek Generating Station. The proposed changes were to revise the Technical Specification to exclude portions of the SG tube for a distance from the top of the tubesheet in the SGs from periodic tube inspections based on the application of structural analysis and leak rate evaluation results to re-define the primary-to-secondary pressure boundary. The NRC Staff provided an initial Request for Additional Information (RAI) on June 27, 2006 (Reference 2-5). Subsequently, a second NRC Staff RAI was received by WCNOC via electronic mail on June 22, 2007. The second NRC Staff RAI was documented in Reference 2-6. Responses to these two sets of NRC RAI are included in References 2-2 and 2-3.

All previously issued NRC RAI are identified in Table 2-2 below along with a summary of either the resolution of the issues or identification of where the previous NRC RAI are addressed in this report.

2.3 REFERENCES

- 2-1 NRC Letter, "Wolf Creek Generating Station – Withdrawal of License Amendment Request on Steam Generator Tube Inspections (TAC No. MD0197)," February 28, 2008.
- 2-2 LTR-CDME-07-72, "Response to NRC Request for Additional Information Relating to LTR-CDME-05-209-P of the Wolf Creek Generating Station (WCGS) Permanent B* License Amendment Request," Westinghouse Electric Company LLC, Pittsburgh, PA, April 24, 2007 (Enclosure to WCNO Letter WO 07-0012, dated May 3, 2007).
- 2-3 LTR-CDME-07-198, "Response to NRC Request for Additional Information Relating to LTR-CDME-07-72 P-Attachment and LTR-CDME-05-209-P of the Wolf Creek Generating Station (WCGS) Permanent B* License Amendment Request," Westinghouse Electric Company LLC, Pittsburgh, PA, September 24, 2007 (Enclosure to WCNO Letter ET 07-0043, dated September 27, 2007).
- 2-4 WCNO Letter ET 06-0004, "Revision to Technical Specification 5.5.9, Steam Generator Tube Surveillance Program," February 21, 2006.
- 2-5 NRC Letter, "Wolf Creek Generating Station – Request for Additional Information (RAI) Related to License Amendment Request (LAR) to Revise the Steam Generator Program (TAC No. MD0197)," June 27, 2007.
- 2-6 NRC Letter, "Meeting with Representatives of Wolf Creek Nuclear Operating Corporation for Wolf Creek Generating Station (TAC No. MD0197)," August 7, 2007.

Table 2-1 NRC Technical Issue Response Road Map

Technical Issue No.	Issue Description	Report Section Addressing Technical Issue
1	Contact pressure between the tube and the tubesheet (Need to define method for computing residual contact pressure from pull out tests)	Section 7.1 ⁽¹⁾
2		
3	Allowed degree of slippage at tube pull out loads	Appendix A ⁽²⁾
4	Dimensions and yield strength of test specimens	Appendix A ⁽²⁾
5		
6		
7		
8	Pull out test database adequacy for uncertainties	Section 7.2 ⁽³⁾
9		
10		
11	Thermal expansion coefficient values and variability	Section 3.1 and Appendix B
12	Statistical performance standard for H* adequacy	Section 4.1
13	Propagate input uncertainties to H* uncertainties	Section 7.0 and Section 8.0
14	Accuracy of 2-D Finite Element tubesheet model	Sections 6.1.2
15	Error in the unit load FE analyses for SLB	Section 6.1.2.1.5
16	Input random versus systematic uncertainties	Section 8.1.3 and Section 8.2.2
17	Incremental slippage under normal operation and monitoring	Section 9.8
18	Need to assess accident leakage for feedwater line break	Section 9.2.3
19	Conservatism of "limiting median crevice pressure approach"	Section 6.4.8 and Section 8.1.1
20	Beta factor adjustment to crevice pressure (tubesheet stiffness)	Section 6.2.4
A**	Consider assumptions on divider plate condition	Section 6.2.6
B**	Effects of hole dilation on leakage and contact pressure	Section 6.2.5
C**	Thermal expansion coefficient in the radial direction	Section 3.4 and Appendix B
D**	3D-FEA discrepancies with ANL (gap under DBA)	Section 6.4.6
	Accident Leakage Integrity	Section 9.2
** Identified based on Industry activities after February 2008		

⁽¹⁾ Residual contact pressure conservatively assumed to be zero in this report.

⁽²⁾ Only previous pull out test program results are included in this report. New pull out test results were not available at the time of printing of this report.

⁽³⁾ Residual contact pressure uncertainties are addressed analytically on this report.

Table 2-2 List of NRC RAI on H* and Resolution Status

RAI No	Source Document for Initial Response: LTR-CDME-07-72 (Reference 2-2)
1	<p>Enclosure 1 of the application, Sections 6.1 and 6.2 - What were the actual yield strengths and wall thicknesses of the tube specimens used for pull out and leakage testing? How do these values compare to minimum values of these parameters at Wolf Creek? Discuss the effect of tube yield strength and wall thickness on contact pressure between the tube and tubesheet after the tube expansion process (i.e., ignoring pressure and temperature loads). Discuss why the test specimen strengths and wall thicknesses were conservative from the standpoint of minimizing the contact pressures between the tube and tubesheet, or discuss what adjustments need to be made to test results to allow for the variability of yield strength and tube wall thickness.</p> <p><u>Issue Resolution Summary:</u></p> <p>Additional tube pull and leakage data for the original test specimens as requested by the NRC Staff is provided in Appendix A of this report. Other than to provide specific information about the test specimens used in the pull out test, additional test data, together with a new structural analysis which involves a fully probabilistic, whole bundle H* depth calculation for each of the Model F H* plants obviate the need to compare the original test data yield strengths and tube wall thicknesses with the tubes at Wolf Creek as requested in this RAI. This RAI has been superseded by Item Numbers 4 and 5 of the list of issues that were outstanding when the Wolf Creek Generating Station amendment was withdrawn. The road map for the resolution of these issues is provided in Section 2.1 of this report.</p>
2	<p>Enclosure 1, Section 6.2.1 - The section states that the leak test program utilized tubesheet simulants (collars) with the nominal tubesheet hole diameter. Was this also the case for the pull out tests? What were the diameters of the tube specimens used in the pull out and leakage tests? Discuss the effect that the field tolerances on these parameters can have on contact pressure between the tube and tubesheet after the tube expansion process (i.e., ignoring pressure and temperature loads). Discuss why the parameter values used for the test specimens were conservative from the standpoint of minimizing the contact pressures between the tube and tubesheet, or discuss what adjustments need to be made to test results to allow for the variability of these parameters.</p> <p><u>Issue Resolution Summary:</u></p> <p>In response to the residual technical issues identified by the Staff, the capability to provide residual contact pressure variability as an input to the H* integration model was developed. The mean value of residual contact pressure is based on test data, and the variability around the mean value is determined for each relevant input variable based on analysis (see Section 7.0 of this report). The individual variability distribution for residual contact pressure are combined in the same manner as discussed above for the probabilistic H* determination (see Section 8.0 of this report). It is noted that the reference H* calculation provided in this report assumes residual contact pressure to be zero. Any positive value of residual contact pressure will decrease the final value of H*.</p>
3	<p>Enclosure 1, Section 6.1, page 27 of 127 - Why was the pull out data evaluated at the lower 95th percentile? Discuss how this supports the ability of tubes to sustain pull out loads, versus using an absolute lower bound value? Given the limited number of tests performed (and the many thousands of tubes in the SGs), should not the lower bound value be evaluated to a high confidence value?</p> <p><u>Issue Resolution Summary:</u></p> <p>See the response to NRC RAI 2 above.</p>

Table 2-2 (Continued) List of NRC RAI on H* and Resolution Status

RAI No	Source Document for Initial Response: LTR-CDME-07-72 (Reference 2-2)
4	<p>Enclosure 1, Section 6.2.1.2 - The section states that the hydraulic expansion pressure was approximately [proprietary information]. Was hydraulic expansion pressure a measured parameter during SG fabrication that was used for acceptance of each joint? Was the lower limit of the acceptance standard the same as the lower limit of the assumed [proprietary information]? If the answer to either of these questions is no, what is the basis for the assumed [proprietary information]?</p> <p><u>Issue Resolution Summary:</u></p> <p>See the response to NRC RAI 2 above.</p>
5	<p>How does pressure and temperature cycling affect the pull out and leakage resistance of the joints? Cite the available data on this topic, and why it is appropriate that the proposed inspection depths need not specifically account for such cycling.</p> <p><u>Issue Resolution Summary:</u></p> <p>This RAI has been superseded by Item Number 16 of the list of issues that were outstanding when the Wolf Creek Generating Station amendment was withdrawn. The road map for the resolution of these issues is provided in Section 2.1 of this report.</p>
6	<p>Pull out resistance per unit length associated with the tube expansion process (residual pull out resistance) was determined on the basis of pull out tests and on the assumption that pull out resistance is uniform along the length of the joint. The axial force in the tube is maximum at the top of the tubesheet and decreases as joint friction incrementally picks up some of the load with increasing distance into the tubesheet. As axial force in the tube declines, with increasing distance in the tubesheet, the Poisson's contraction of the tube diameter decreases causing contact pressure to increase until it reaches a constant value at the location where axial force in the tube has been reduced to zero. At the pull out load, the pull out resistance per unit length near the bottom of the joint will be higher than the average pull out resistance along the entire joint. The pull out resistance over the upper portion of the joint will be less than the average resistance. Referring to Tables 7-6 to 7-10 in Enclosure 1, would not consideration of the actual distribution of the residual pull out resistance as a function of distance below the top of the tubesheet lead to larger H* values than shown on these tables? If not, explain why not.</p> <p><u>Issue Resolution Summary:</u></p> <p>See the response to NRC RAI 2 above.</p>

Table 2-2 (Continued) List of NRC RAI on H* and Resolution Status

RAI No	Source Document for Initial Response: LTR-CDME-07-72 (Reference 2-2)
7	<p>The models used to develop the H* lengths are complex. Describe how these models have been verified to yield conservative H* values. Have these models been verified by test? For example, how well do these models predict the actual residual pull out loads for joint test samples with typical H* lengths (i.e., provide comparative data)?</p> <p><u>Issue Resolution Summary:</u></p> <p>This RAI has been superseded by Item Number 12 of the list of issues that were outstanding when the Wolf Creek Generating Station amendment was withdrawn. The road map for the resolution of this issue is provided in Section 2.1 of this report.</p>
8	<p>Enclosure 1, Section 6.2.2 - The section states that room temperature leakage tests were performed on all test specimens at test pressures of 1900, 2650, and 3100 pounds per square inch (psi) (presumably applied on the primary side with nothing more than atmospheric pressure at the top of the joint). However, Table 6-2 only presents room temperature data for a differential pressure of 1000 psi. Where is this latter data discussed? Why aren't the room temperature data for the tests described in Section 6.2.2 included in Table 6-2 and Figure 6-6?</p> <p><u>Issue Resolution Summary:</u></p> <p>The response to this NRC RAI is provided for historical purposes only. The original response to this RAI in LTR-CDME-07-72, "Response to NRC Request for Additional Information Relating to LTR-CDME-05-209-P of the Wolf Creek Generating Station (WCGS) Permanent B* License Amendment Request," still applies.</p>
9	<p>Enclosure 1, Section 6.2.2-1 - The section states that the elevated temperature tests were performed following the room temperature tests. Section 6.2.2.2 states that the room temperature tests were performed following the elevated temperature tests. Please clarify this discrepancy.</p> <p><u>Issue Resolution Summary:</u></p> <p>The response to this NRC RAI is provided for historical purposes only. The original response to this RAI in LTR-CDME-07-72, "Response to NRC Request for Additional Information Relating to LTR-CDME-05-209-P of the Wolf Creek Generating Station (WCGS) Permanent B* License Amendment Request," still applies.</p>

Table 2-2 (Continued) List of NRC RAI on H* and Resolution Status

RAI No	Source Document for Initial Response: LTR-CDME-07-72 (Reference 2-2)
10	<p>Enclosure 1, Section 6.2.2-2 - The section states that a 1900 psi test pressure was used (simulating normal operating pressure) to keep the pressurizing fluid above saturation pressure. As the Staff understands the report, the pressure at the upper end of the test joint is at atmospheric pressure which is not prototypic for normal operating conditions. As the test leakage goes from the bottom of the joint to the top, pressure at some point drops to less than saturation. Why would the test be expected to show as much leakage through the joint as would be the case under prototypic normal operating conditions?</p> <p><u>Issue Resolution Summary:</u></p> <p>The original response to this RAI in LTR-CDME-07-72, "Response to NRC Request for Additional Information Relating to LTR-CDME-05-209-P of the Wolf Creek Generating Station (WCGS) Permanent B* License Amendment Request," still applies. This RAI has been superseded by Item Number 18 of the list of issues that were outstanding when the Wolf Creek Generating Station amendment was withdrawn. The road map for the resolution of this issue is provided in Section 2.1 of this report.</p>
11	<p>The plot of Model F loss coefficient versus contact pressure in Figure 6-6 of Enclosure 1 exhibits a higher slope than is the case for Model D5. The difference appears attributable to lower loss coefficients at lower contact pressures for Model F than for Model D5. Discuss the differences between the Model F and D5 SG designs that explain their different behaviors. If no significant design differences can be identified, discuss the credibility of the loss coefficient data.</p> <p><u>Issue Resolution Summary:</u></p> <p>This RAI has been superseded by Item Number D** of the list of issues that remain outstanding when the Wolf Creek Generating Station amendment was withdrawn and as a result of industry activities after February 2008. The road map for the resolution of this issue is provided in Section 2.1 of this report.</p>
12	<p>Enclosure 1, Section 6.2.2.1 - The section states that the leak test results averaged 16 drops per minute (dpm) per joint at 1900 psi compared to 59 dpm at higher pressures. This is a factor of 3.7 difference. Discuss why this difference is so high compared to the factor of 2 which, under the bellwether principle, is assumed to bound the increase in leakage going from normal operating to accident conditions.</p> <p><u>Issue Resolution Summary:</u></p> <p>The response to this NRC RAI is provided for historical purposes only. The original response to this RAI in LTR-CDME-07-72, "Response to NRC Request for Additional Information Relating to LTR-CDME-05-209-P of the Wolf Creek Generating Station (WCGS) Permanent B* License Amendment Request," still applies.</p>

Table 2-2 (Continued) List of NRC RAI on H* and Resolution Status

RAI No	Source Document for Initial Response: LTR-CDME-07-72 (Reference 2-2)
13	<p>Enclosure 1, Section 7.1.2, page 45 of 127: Was the primary pressure unit load applied only to the primary face of the tubesheet, and not to the side of the tubesheet bore holes? Was the secondary pressure unit load applied only to the secondary face of the tubesheet, and not to the side of the tubesheet bore holes? Was the tube end cap pressure load (due to primary and secondary pressures) included in the finite element analyses?</p> <p><u>Issue Resolution Summary:</u></p> <p>The response to this NRC RAI is provided for historical purposes only. The original response to this RAI in LTR-CDME-07-72, "Response to NRC Request for Additional Information Relating to LTR-CDME-05-209-P of the Wolf Creek Generating Station (WCGS) Permanent B* License Amendment Request," still applies. This RAI has been superseded by Item Number 19 of the list of issues that were outstanding when the Wolf Creek Generating Station amendment was withdrawn. The road map for the resolution of this issue is provided in Section 2.1 of this report.</p>
14	<p>Enclosure 1, Section 7.1.2, page 45 of 127: The 500 of unit loads represent which of the following; heating up from 70 to 500 °F, or from 70 to 570 °F? If the former, why isn't 70 °F subtracted from 500 °F in the radial deflection scaling factors in Section 7.1.3 (page 46 of 127)?</p> <p><u>Issue Resolution Summary:</u></p> <p>The response to this NRC RAI is provided for historical purposes only. The original response to this RAI in LTR-CDME-07-72, "Response to NRC Request for Additional Information Relating to LTR-CDME-05-209-P of the Wolf Creek Generating Station (WCGS) Permanent B* License Amendment Request," still applies.</p>
15	<p>Enclosure 1: Regarding the equation for ΔR_{prTS} top of page 48 of 127, should not P_i be P_o consistent with the last equation appearing on page 48? If not, why not?</p> <p><u>Issue Resolution Summary:</u></p> <p>The response to this NRC RAI is provided for historical purposes only. The original response to this RAI in LTR-CDME-07-72, "Response to NRC Request for Additional Information Relating to LTR-CDME-05-209-P of the Wolf Creek Generating Station (WCGS) Permanent B* License Amendment Request," still applies.</p>

Table 2-2 (Continued) List of NRC RAI on H* and Resolution Status

RAI No	Source Document for Initial Response: LTR-CDME-07-72 (Reference 2-2)
16	<p>Enclosure 1, Section 7.1.3 - The tube inside and outside radii within the tubesheet after expansion shown on page 49 of 127 appear not to be entirely consistent with the numbers on page 44 of 127. Explain this inconsistency or, alternatively, show that this inconsistency does not significantly affect the outcome of the overall analysis.</p> <p><u>Issue Resolution Summary:</u></p> <p>The response to this NRC RAI is provided for historical purposes only. The original response to this RAI in LTR-CDME-07-72, "Response to NRC Request for Additional Information Relating to LTR-CDME-05-209-P of the Wolf Creek Generating Station (WCGS) Permanent B* License Amendment Request," still applies.</p>
17	<p>Enclosure 1, Section 7.1.4 - Near the top of page 50 of 127, it is stated that the secondary pressure is conservatively assumed to act on the outside of the tube and the inside of the tubesheet hole. The Staff agrees that this is conservative from the standpoint of maximizing leakage under normal operating conditions, but is concerned that it may be non-conservative from the standpoint of determining conservative ratios of accident leakage to normal operating leakage. Wouldn't the assumption of no secondary pressure yield a lesser value of normal operating leakage, leading to a higher ratio of accident to normal operating leakage? What is the basis for describing the assumption on secondary pressure as conservative?</p> <p><u>Issue Resolution Summary:</u></p> <p>This RAI has been superseded by Item Numbers 18, 19 and D** of the list of issues that remain outstanding when the Wolf Creek Generating Station amendment was withdrawn and as a result of industry activities after February 2008. The road map for the resolution of these issues is provided in Section 2.1 of this report.</p>
18	<p>Enclosure 1, Section 8.2 - The ligament tearing discussion in Section 8.2 (starting on page 75 of 127) only addresses circumferential cracks. Please provide corresponding discussion for axial cracks.</p> <p><u>Issue Resolution Summary:</u></p> <p>The original response to this RAI in LTR-CDME-07-72, "Response to NRC Request for Additional Information Relating to LTR-CDME-05-209-P of the Wolf Creek Generating Station (WCGS) Permanent B* License Amendment Request," still applies. The original response is also included as Section 9.7.2 of the Final H* Report.</p>

Table 2-2 (Continued) List of NRC RAI on H* and Resolution Status

RAI No	Source Document for Initial Response: LTR-CDME-07-72 (Reference 2-2)
19	<p>The structural and leakage assessments supporting the proposed technical specification amendment are for tubes with no degradation in the proposed inspection zone. The proposed inspection depths make no allowance for degradation which may occur within this zone prior to the next scheduled inspection. Assess the potential impact of degradation in the inspection zone on (1) contact pressures between the tube and tubesheet, (2) on tube pull out capacity, and (3) on leakage under normal and accident conditions. (Although flaws in this zone will be plugged on detection, this question is relevant to satisfying the tube integrity performance criteria with respect to condition monitoring and operational assessments.) This assessment should address potential axial and circumferential stress corrosion cracks (SCC) and volumetric intergranular attack (IGA) flaws.</p> <p><u>Issue Resolution Summary:</u></p> <p>The original response to this RAI in LTR-CDME-07-72, "Response to NRC Request for Additional Information Relating to LTR-CDME-05-209-P of the Wolf Creek Generating Station (WCGS) Permanent B* License Amendment Request," still applies.</p>
20	<p>Describe the methodology to be employed for performing condition monitoring and operational assessments for the tubesheet inspection zone (for pull out and accident leakage) assuming that SCC and or IGA mechanisms have started to be active.</p> <p><u>Issue Resolution Summary:</u></p> <p>The original response to this RAI in LTR-CDME-07-72, "Response to NRC Request for Additional Information Relating to LTR-CDME-05-209-P of the Wolf Creek Generating Station (WCGS) Permanent B* License Amendment Request," still applies.</p>
21	<p>Enclosure 1: The development of the B* distances assumes that crack leakage resistance is not significant relative to the tube-to-tubesheet joint resistance. Discuss the conservatism of the B* distances given the assumption that crack leakage resistance is the dominant resistance to leakage under normal operating conditions. To the extent this discussion relies on assumptions about contact pressure between the tube and tubesheet local to the crack, justify assumptions relative to the influence of the crack on local contact pressure.</p> <p><u>Issue Resolution Summary:</u></p> <p>The response to this NRC RAI is provided for historical purposes only. The original response to this RAI in LTR-CDME-07-72, "Response to NRC Request for Additional Information Relating to LTR-CDME-05-209-P of the Wolf Creek Generating Station (WCGS) Permanent B* License Amendment Request," still applies.</p>

Table 2-2 (Continued) List of NRC RAI on H* and Resolution Status

RAI No	Source Document for Initial Response: LTR-CDME-07-72 (Reference 2-2)
22	<p>Describe the methodology for performing condition monitoring and operational assessments for accident induced leakage stemming from locations below the specified tubesheet inspection depths.</p> <p><u>Issue Resolution Summary:</u></p> <p>This RAI has been superseded by Item Number D** of the list of issues that remain outstanding when the Wolf Creek Generating Station amendment was withdrawn and as a result of industry activities after February 2008. The road map for the resolution of this issue is provided in Section 2.1 of this report.</p>
23	<p>By letter dated March 28, 2006, you provided revisions to your proposed technical specifications (TS) in accordance with TSTF-449, Rev. 4, to include the following additional sentence into TS 5.5.9 c.1:</p> <p>"All tubes with degradation identified in the portion of the tube within the region from the top of the hot leg tubesheet to 17 inches below the top of the tubesheet shall be removed from service."</p> <p>Describe your plans for revising these words to reflect the February 21, 2006 license amendment and for submitting revisions to this amendment.</p> <p><u>Issue Resolution Summary:</u></p> <p>This RAI does not apply to the Model F H* plants going forward.</p>

Table 2-2 (Continued) List of NRC RAI on H* and Resolution Status

RAI No	Source Document for Initial Response: LTR-CDME-07-72 (Reference 2-2)
24	<p>Discuss your plans to revise TS 5.6.10 to include reporting requirements applicable to the implementation of the tubesheet inspection and alternate repair criteria. For example:</p> <p>*A breakout of indications detected within the tubesheet inspection depths with respect to their location, orientation, and measured size. (The only difference here relative to proposed changes associated with Technical Specification Task Force (TSTF) 449, Revision 4, is that the indications in the tubesheet region would be listed separately from those elsewhere.)</p> <p>*The operational primary to secondary leakage rate observed in each steam generator during the cycle preceding the inspection which is the subject of the report, and (2) the calculated accident leakage rate for each steam generator from the portion of tubing below the tubesheet inspection depths for the most limiting accident. If the calculated accident leakage rate for any steam generator is less than 2 times the total observed operational primary to secondary leakage rate, the 12-month report should describe how it was determined.</p> <p><u>Issue Resolution Summary:</u></p> <p>Proposed changes to the technical specification for the steam generator tube inspection report are provided by the utility as part of the license amendment request.</p>
25	<p>Enclosure 1, Section 7.1.3, page 46 of 127: The tubesheet bow analysis takes credit for resistance against bow provided by the divider plate. Cracks in the welds connecting the tubesheet and divider plate have been found by inspection at certain foreign steam generators. Describe what actions you are taking to ensure that the divider plates can perform their function, including providing the assumed resistance against tubesheet bow.</p> <p><u>Issue Resolution Summary:</u></p> <p>This RAI has been superseded by Item Number 20 of the list of issues that remain outstanding when the Wolf Creek Generating Station amendment was withdrawn and as a result of industry activities after February 2008. The road map for the resolution of this issue is provided in Section 2.1 of this report.</p>

Table 2-2 (Continued) List of NRC RAI on H* and Resolution Status

RAI No	Source Document for Initial Response: LTR-CDME-07-198 (Reference 2-3)
1	<p>Reference 1, Enclosure I, Table 6-4 - Are the listed F/L, force per length, values correct? If so, please describe in detail how they were calculated. If not correct, please provide all necessary revisions to the H* analysis results. [For Byron 2, Braidwood 2, and Seabrook, F/L is calculated as follows:</p> $F/L = (\text{Pull Force/specimen length}) \times (\text{net contact pressure/total contact pressure})$ <p>A consistent approach for Wolf Creek (based on allowing 0.25 inch slip) would yield F/L values on the order of 200 pounds per inch (lb/inch) rather than 563 lb/inch as shown in the Table.]</p> <p><u>Issue Resolution Summary:</u></p> <p>In response to the residual technical issues identified by the Staff, the capability to provide residual contact pressure variability as an input to the H* integration model was developed. The mean value of residual contact pressure is based on test data, and the variability around the mean value is determined for each relevant input variable based on analysis (see Section 7.0 of this report). The individual variability distribution for residual contact pressure are combined in the same manner as discussed above for the probabilistic H* determination (see Section 8.0 of this report). It is noted that the reference H* calculation provided in this report assumes residual contact pressure to be zero. Any positive value of residual contact pressure will decrease the final value of H*.</p> <p>This RAI has been superseded by Item Numbers 1 and 2 of the list of issues that remain outstanding when the Wolf Creek Generating Station amendment was withdrawn and as a result of industry activities after February 2008. The road map for the resolution of these issues is provided in Section 2.1 of this report.</p>

Table 2-2 (Continued) List of NRC RAI on H* and Resolution Status

RAI No	Source Document for Initial Response: LTR-CDME-07-198 (Reference 2-3)
2	<p>Reference 2, Enclosure I, Response to RAI questions 1 and 2 - provides the sensitivity of contact pressure to many of the material and geometric parameters used in the analyses. The response provides only a qualitative assessment of these sensitivities to support the conclusion that the values assumed in the H* analyses support a conservative calculation of H*. For example, the sensitivity study showed that contact pressure is sensitive to the yield strength of the tubing. The response states that the yield strength of the tubing used in the pull out test specimens was higher than the documented mean yield strength for prototypical tubing material, but did not indicate to what extent the yield strength of the test material bounds the range of prototypic yield strength variability. Thus, the Staff has no basis to agree or disagree with the conclusion that test specimen contact pressures are conservatively low. The steam generators contain up to 5620 tubes, and it needs to be demonstrated that the computed H* distances are conservative for all the tubes, not simply the average tubes or 95% of the tubes. Please provide a quantitative assessment demonstrating that the assumed values of the material and geometric parameters support a conservative H* analysis for all tubes. This assessment should consider thermal expansion coefficient (TEC) for the tube and tubesheet in addition to the parameters included in the Reference 2 response.</p> <p><u>Issue Resolution Summary:</u></p> <p>This RAI has been superseded by Item Number 9 of the list of issues that remain outstanding when the Wolf Creek Generating Station amendment was withdrawn and as a result of industry activities after February 2008. The road map for the resolution of this issue is provided in Section 2.1 of this report.</p>
3	<p>The H* analyses in References 1 and 2 are based, in part, on pull out resistance associated directly with hydraulic expansion process. This pull out resistance was determined by subtracting out the effects of differential thermal expansion between the tube and tubesheet test collar from the measured pull out load. The calculated differential thermal expansion effect was based, in part, on an assumed TEC value of 7.42E-06 in/in/°F for the 1018 steel tubesheet test collar. What is the impact of considering an alternative TEC value of 7E-06 in/in/°F (from Matweb.com for 1018 steel interpolated at 600 degrees Fahrenheit) on the computed pull out force determined from the pull out test and on the computed H* distances?</p> <p><u>Issue Resolution Summary:</u></p> <p>This RAI has been superseded by Item Number 12 of the list of issues that remain outstanding when the Wolf Creek Generating Station amendment was withdrawn and as a result of industry activities after February 2008. The road map for the resolution of this issue is provided in Section 2.1 of this report.</p>

Table 2-2 (Continued) List of NRC RAI on H* and Resolution Status

RAI No	Source Document for Initial Response: LTR-CDME-07-198 (Reference 2-3)
4	<p>Reference 2, Enclosure I, Response to RAI question 7 - The Model D5 steam generator (SG) pull out data in Table 2 indicate that pull out force increases with temperature for the 3-inch long specimens and decreases with temperature for the 6-inch long specimens. For the 4-inch specimens, pull out force increases with temperature to 400°F and decreases with temperature beyond that point. Discuss the reasons for this apparent discrepancy in trends among the data. Discuss whether the reduction in tube yield strength with temperature might be sufficient for some specimens to limit any increase in contact pressure associated with differential thermal expansion between the tube and tubesheet.</p> <p><u>Issue Resolution Summary:</u></p> <p>In response to the residual technical issues identified by the Staff, the capability to provide residual contact pressure variability as an input to the H* integration model was developed. The mean value of residual contact pressure is based on test data, and the variability around the mean value is determined for each relevant input variable based on analysis (see Section 7.0 of this report). The individual variability distribution for residual contact pressure are combined in the same manner as discussed above for the probabilistic H* determination (see Section 8.0 of this report). It is noted that the reference H* calculation provided in this report assumes residual contact pressure to be zero. Any positive value of residual contact pressure will decrease the final value of H*.</p>
5	<p>Following up on question 4 above, is there a possibility that any tubes could be stressed beyond the compressive yield strength (at temperature) of the tube material due to differential thermal expansion, internal pressure, and tubesheet hole dilation for the range of yield strengths in the field? Describe the basis for either yes or no to this question. If yes, how has this been factored into the contact pressures, accumulated pull out resistance load as a function of elevation, and H* in Tables 7-6 through 7-10 and 7-6a through 7-10a of Reference 2, Enclosure I?</p> <p><u>Issue Resolution Summary:</u></p> <p>The original response to this RAI in LTR-CDME-07-198, "Response to NRC Request for Additional Information Relating to LTR-CDME-07-72 P-Attachment and LTR-CDME-05-209-P of the Wolf Creek Generating Station (WCGS) Permanent B* License Amendment Request," still applies.</p>

Table 2-2 (Continued) List of NRC RAI on H* and Resolution Status

RAI No	Source Document for Initial Response: LTR-CDME-07-198 (Reference 2-3)
6	<p>Reference 2, Enclosure I, Response to RAI question 17 - The response states near the bottom of page 30 of 84 that Case 1 results shown in Table 3.0 are for the limiting cold leg analysis and reflect the following assumption: "Although the pull out test data indicated positive residual mechanical joint strength, the residual joint strength is ignored for SLB [steam line break] accident condition[s] to conservatively account for postulated variability of the coefficient of thermal expansion." The NRC Staff notes, however, that the limiting H* value shown in Table 3.0 for Case 1 is that necessary to resist three times the normal operating pressure end cap load, not that needed to resist 1.4 times SLB. It is the Staff's understanding based on review of Tables 7-6 through 7-10 and 7-6a through 7-10a that the residual mechanical joint strength (522 lb/inch) was reflected in the H* computations for normal operating and accident conditions, including SLB. Discuss and clarify these apparent discrepancies.</p> <p><u>Issue Resolution Summary:</u></p> <p>A new structural analysis which involves a fully probabilistic, whole bundle H* depth calculation for each of the Model F H* plants obviates the need to address the sub-parts of this RAI.</p>
7	<p>Reference 2, Enclosure I, Table 7-6 - This table states that the required pull out force is 1680 lb. Table 7-6 indicates that for a tubesheet radius of 12 inches the needed depth of engagement is less than 10.52 (about 10.2 using linear interpolation). However, the table states that an engagement depth slightly greater than 10.52 (i.e., 10.54) is needed. Discuss and explain this apparent (minor) discrepancy.</p> <p><u>Issue Resolution Summary:</u></p> <p>A new structural analysis which involves a fully probabilistic, whole bundle H* depth calculation for each of the Model F H* plants obviates the need to address this RAI.</p>

Table 2-2 (Continued) List of NRC RAI on H* and Resolution Status

RAI No	Source Document for Initial Response: LTR-CDME-07-198 (Reference 2-3)
8	<p>Reference 1, Enclosure I, Table 6-4 - The listed F/L values are based on allowing 0.25 inch slippage. Reference 1 does not address the potential for limited, but progressive incremental slippage under heatup/cooldown and other operational load cycles. Nor does Reference 1 address the effects of slippage on normal operating leakage and on accident-induced leakage or the ratio of normal operating and accident induced leakage. The response to RAI question 5 in Reference 2, Enclosure I, does not provide any further insight into this issue. That response specifically addressed test results for tubes with a hard roll expansion, and the Staff believes that the slippage versus axial load characteristics for such an expansion may be entirely different than for a hydraulic expansion. Discuss and address the potential for progressive incremental slippage under heatup/cooldown and other operational load cycles. In addition, address the potential for slippage under operational and accident conditions to affect the ratio of accident-induced leakage to operational leakage.</p> <p><u>Issue Resolution Summary:</u></p> <p>This RAI has been superseded by Item Number 16 of the list of issues that remain outstanding when the Wolf Creek Generating Station amendment was withdrawn and as a result of industry activities after February 2008. The road map for the resolution of this issue is provided in Section 2.1 of this report.</p>
9	<p>Discuss your plans for revising the proposed technical specification (TS) amendment to monitor the tube expansion transition locations relative to the top of the tubesheet to ensure that the tubes are not undergoing progressive, incremental slippage between inspections.</p> <p><u>Issue Resolution Summary:</u></p> <p>This RAI has been superseded by Item Number 16 of the list of issues that remain outstanding when the Wolf Creek Generating Station amendment was withdrawn and as a result of industry activities after February 2008. The road map for the resolution of this issue is provided in Section 2.1 of this report.</p>

Table 2-2 (Continued) List of NRC RAI on H* and Resolution Status

RAI No	Source Document for Initial Response: LTR-CDME-07-198 (Reference 2-3)
10	<p>Reference 1, Enclosure I, Section 7.1.4.2 - This section provides a brief discussion of SLB, feed line break (FLB), and loss-of-coolant accident (LOCA) in terms of which is the most limiting accident in terms of tube pull out potential. Expand this discussion to indicate whether SLB and FLB are the most limiting accidents among the universe of design basis accidents (DBA) (or other faulted conditions in the design basis) in terms of both tube pull out, and the margin between the calculated accident-induced tube leakage for each DBA and the assumed accident-induced tube leakage in the safety analysis for that DBA.</p> <p><u>Issue Resolution Summary:</u></p> <p>This RAI has been superseded by Item Numbers 17, A** and D** of the list of issues that remain outstanding when the Wolf Creek Generating Station amendment was withdrawn and as a result of industry activities after February 2008. The road map for the resolution of these issues is provided in Section 2.1 of this report.</p>
11	<p>Figure 11 of Reference 2, Enclosure I contains loss coefficient data for Model F SG tubing that was not included in Figure 6-6 of Reference 1, Enclosure 1. This data was for contact pressures ranging from about 1200 psi to about 2000 psi. Why was this data not included in Figure 6-6? Discuss if this is this because of low expansion pressures and if the data that is not included in Figure 6-6 is room temperature data. [If yes, then the NRC Staff observes that the room temperature loss coefficients for the Model F specimens are relatively invariant with contact pressure above a contact pressure threshold of around 700 psi. The 600 degree F data is also invariant with contact pressure. Thus, loss coefficient may not be a direct function of contact pressure once a threshold degree of contact pressure is established. The difference in loss coefficient data between the 600°F data and the room temperature may be due to parameter(s) other than contact pressure. This other parameter(s) may not be directly considered in the B* analysis.]</p> <p><u>Issue Resolution Summary:</u></p> <p>This RAI has been superseded by Item Numbers 17, A** and D** of the list of issues that remain outstanding when the Wolf Creek Generating Station amendment was withdrawn and as a result of industry activities after February 2008. The road map for the resolution of these issues is provided in Section 2.1 of this report.</p>

Table 2-2 (Continued) List of NRC RAI on H* and Resolution Status

RAI No	Source Document for Initial Response: LTR-CDME-07-198 (Reference 2-3)
12	<p>Figure 13 of Reference 2, Enclosure I contains additional loss coefficient data taken from the crevice pressure study in the white paper. Provide a figure showing all individual data points from which Figure 13 was developed. Describe the specific applied pressure differentials from the crevice pressure study used to calculate the contact pressure for each data point.</p> <p><u>Issue Resolution Summary:</u></p> <p>This RAI has been superseded by Item Numbers 17, A** and D** of the list of issues that remain outstanding when the Wolf Creek Generating Station amendment was withdrawn and as a result of industry activities after February 2008. The road map for the resolution of these issues is provided in Section 2.1 of this report.</p>
13	<p>Although the means of the regression fits of the loss coefficient data for the Model F and Model D SGs are shown in Figure 13 of Reference 2, Enclosure I, to be within a factor of three of each other, the slope and intercept properties remain highly divergent, seeming to cast further doubt that loss coefficient varies with contact pressure (above some threshold value of contact pressure). Discuss this and describe any statistical tests that have been performed to establish the significance of correlation between loss coefficient and contact pressure. In addition, describe any statistical tests that have been performed to confirm that it is appropriate to combine the data sets to establish the slope and intercept properties of loss coefficient versus contact pressure.</p> <p><u>Issue Resolution Summary:</u></p> <p>This RAI has been superseded by Item Numbers 17, A** and D** of the list of issues that remain outstanding when the Wolf Creek Generating Station amendment was withdrawn and as a result of industry activities after February 2008. The road map for the resolution of these issues is provided in Section 2.1 of this report.</p>

Table 2-2 (Continued) List of NRC RAI on H* and Resolution Status

RAI No	Source Document for Initial Response: LTR-CDME-07-198 (Reference 2-3)
14	<p>Reference 2, Enclosure I, page 25 of 84 - For the case of assumed zero slope of loss coefficient versus contact pressure, two constant loss coefficient values were compared. Does the first assumed value come from Figure 14? If not, provide additional information on where this assumption comes from. If yes, explain the relationship between the assumed value and Figure 14. Does the second assumed value come from Figure 12? If not, provide additional information on where this assumption comes from. If yes, explain the relationship between the assumed value and Figure 12.</p> <p><u>Issue Resolution Summary:</u></p> <p>The response to this NRC RAI is provided for historical purposes only. The original response to this RAI in LTR-CDME-07-198, "Response to NRC Request for Additional Information Relating to LTR-CDME-07-72 P-Attachment and LTR-CDME-05-209-P of the Wolf Creek Generating Station (WCGS) Permanent B* License Amendment Request," still applies.</p>
15	<p>Reference 2, Enclosure I, Figure 15 - clarify the title of Figure 15 in terms of whether it reflects consideration of residual mechanical strength in the joint during an SLB. Is Figure 15 for the hot or cold leg? Explain the following: (1) why the B* values at small tubesheet radii are less than those listed in Reference 1, Enclosure I, Table 11-1 and (2) why the contact pressures shown in Reference 1, Enclosure I, Figures 9-6 and 9-7 are different from those shown in Tables 7-6 and 7-8 of Reference 1, Enclosure I.</p> <p><u>Issue Resolution Summary:</u></p> <p>A new structural analysis which involves a fully probabilistic, whole bundle H* depth calculation for each of the Model F H* plants and a new leakage analysis obviate the need to provide a detailed response to this RAI.</p>
16	<p>Reference 2, Enclosure I - Provide a description of the revised finite element model used to support the revised H* calculations in Tables 6-7 through 6-10 and Tables 6-7a through 6-10a. Compare this revised model to the original model which supported the Reference 1 analysis. Explain why the revised model is more realistic than the original model.</p> <p><u>Issue Resolution Summary:</u></p> <p>A new structural analysis which involves a fully probabilistic, whole bundle H* depth calculation for each of the Model F H* plants obviates the need to provide a detailed response to this RAI.</p>

Table 2-2 (Continued) List of NRC RAI on H* and Resolution Status

RAI No	Source Document for Initial Response: LTR-CDME-07-198 (Reference 2-3)
17	<p>Reference 2, Enclosure 1, Attachment 1 (The Westinghouse Letter Summary of Changes to B* and H*), page 14 - address the status of the divider plate evaluation being performed under EPRI sponsorship, and the schedule for completion of the various topics being addressed in the evaluation. Describe any inspections that have been performed domestically that provide insight on whether the extent and severity of divider plate cracks is bounded by the foreign experience. Discuss the available options for inspecting the divider plates.</p> <p><u>Issue Resolution Summary:</u></p> <p>This RAI has been superseded by Item Number 20 of the list of issues that remain outstanding when the Wolf Creek Generating Station amendment was withdrawn and as a result of industry activities after February 2008. The road map for the resolution of this issue is provided in Section 2.1 of this report.</p>
18	<p>Discuss how the ability of the divider plates at Wolf Creek to resist tubesheet deflection (without failure) under operating and accident loads is assured in the short term, pending completion of the EPRI evaluation. Include in this discussion the actions that are planned in the near term to ensure that the divider plates are capable of resisting tubesheet deflection.</p> <p><u>Issue Resolution Summary:</u></p> <p>This RAI has been superseded by Item Number 20 of the list of issues that remain outstanding when the Wolf Creek Generating Station amendment was withdrawn and as a result of industry activities after February 2008. The road map for the resolution of this issue is provided in Section 2.1 of this report.</p>

Table 2-2 (Continued) List of NRC RAI on H* and Resolution Status

RAI No	Source Document for Initial Response: LTR-CDME-07-198 (Reference 2-3)
19	<p>Reference 2, Enclosure 1, Attachment 1 - Provide a description of the Crevice Pressure Test. This description should address, but not necessarily be limited to the following:</p> <ol style="list-style-type: none"> a. Description of test specimens, including sketches. b. Description of "pre-treatments" of test specimens (hydraulic expansion pressure, heat relief, etc.). c. Description of test setup, including sketches. d. Description of test procedure. e. What were the secondary side temperatures in Tables 1 and 2 corresponding to the listed secondary side pressures and how were the secondary side pressure and temperatures controlled and monitored? f. How long did each test run and how stable were the pressure readings at each of the pressure taps during the course of each test? g. What was the temperature of (1) the coolant in the crevice and (2) the tube and tubesheet collar as a function of elevation? h. How were the temperature distributions for item g determined? Were direct temperature measurements of the tubesheet collar performed as a function of elevation? <p><u>Issue Resolution Summary:</u></p> <p>The original response to this RAI in LTR-CDME-07-198, "Response to NRC Request for Additional Information Relating to LTR-CDME-07-72 P-Attachment and LTR-CDME-05-209-P of the Wolf Creek Generating Station (WCGS) Permanent B* License Amendment Request," still applies.</p>

Table 2-2 (Continued) List of NRC RAI on H* and Resolution Status

RAI No	Source Document for Initial Response: LTR-CDME-07-198 (Reference 2-3)
20	<p>Reference 2, Enclosure 1, Attachment 1 - The pressure tap locations in Figure 2 are different from those shown in Figure 3. Discuss and explain this difference or provide corrected figures.</p> <p><u>Issue Resolution Summary:</u></p> <p>The original response to this RAI in LTR-CDME-07-198, "Response to NRC Request for Additional Information Relating to LTR-CDME-07-72 P-Attachment and LTR-CDME-05-209-P of the Wolf Creek Generating Station (WCGS) Permanent B* License Amendment Request," still applies.</p>
21	<p>Reference 2, Enclosure 1, Attachment 1 - Figures 2 and 3 assume crevice pressure at the top of tubesheet is at the saturation pressure for the primary system. Discuss and explain the basis for this assumption. Why wouldn't the crevice pressure trend to the secondary side pressure near the top of the tubesheet?</p> <p><u>Issue Resolution Summary:</u></p> <p>The original response to this RAI in LTR-CDME-07-198, "Response to NRC Request for Additional Information Relating to LTR-CDME-07-72 P-Attachment and LTR-CDME-05-209-P of the Wolf Creek Generating Station (WCGS) Permanent B* License Amendment Request," still applies.</p>
22	<p>Reference 2, Enclosure 1, Attachment 1 - Figure 3 refers to tests labeled SLB 9 and SLB 10 which are not listed in Table 2. Discuss and explain this, or provide a revised Table 2 and Figure 3 showing all test results.</p> <p><u>Issue Resolution Summary:</u></p> <p>The original response to this RAI in LTR-CDME-07-198, "Response to NRC Request for Additional Information Relating to LTR-CDME-07-72 P-Attachment and LTR-CDME-05-209-P of the Wolf Creek Generating Station (WCGS) Permanent B* License Amendment Request," still applies.</p>

Table 2-2 (Continued) List of NRC RAI on H* and Resolution Status

RAI No	Source Document for Initial Response: LTR-CDME-07-198 (Reference 2-3)
23	<p>Reference 2, Enclosure 1, Attachment 1 - Page 6 states in part that the following change should be made to the H*/B* analyses: "The driving head of the leaked fluid has been reduced." Discuss and clarify this sentence. The Staff notes that resistance to leakage occurs from two sources: resistance from the flaw and resistance from the crevice. Because the crevice pressure was assumed to be equal to the secondary pressure, the original analysis assumed the entire pressure drop (the driving head) was across the flaw. The tests described in the white paper eliminate any pressure across the flaw (by using holes rather than cracks) and force the entire pressure drop to occur along the crevice. Thus, there is no net change in the total driving head between the primary and secondary sides. In fact, the driving head from the bottom to the top of the crevice would seem to have been increased.</p> <p><u>Issue Resolution Summary:</u></p> <p>A new structural analysis which involves a fully probabilistic, whole bundle H* depth calculation for each of the Model F H* plants which applies a depth-based crevice pressure obviates the need to provide a detailed response to this RAI.</p>
24	<p>Reference 2, Enclosure 1, Attachment 1 - The top paragraph on page 10 states, in part, "the median value of the crevice pressure ratios provides a conservative value that is an average representation of the behavior at the top of the tubesheet. The median is typically a better statistical representation of the data than the mean because the median is not influenced by a smaller data set but by the total range in values in the sample set." The Staff has the following questions regarding these sentences:</p> <ol style="list-style-type: none"> Discuss and clarify what data set "median value" applies to. For example, does the "median value" for the NOP data set in Table 1 mean the median value of the 15 pressure tap data points obtained during three tests, or does it mean a median value of a subset of these 15 data points? If a subset, what subset and why? Alternatively, does it mean the median value at each pressure tap location? Discuss why this median value is a conservative representation of the behavior at the top of the tubesheet. Discuss what is meant by "top of the tubesheet." For 17-inch inspection zone amendments, shouldn't this mean the upper 17-inches to ensure a conservative analysis? If not, why not? To ensure a conservative analysis for H* and B*, should not the objective be to establish crevice pressure as a function of elevation that can be directly applied into the H* and B* computations. Discuss why the median is not influenced by a smaller data set and how the median is influenced by the total range of values in the sample set. <p><u>Issue Resolution Summary</u></p> <p>A new structural analysis which involves a fully probabilistic, whole bundle H* depth calculation for each of the Model F H* plants which applies a depth-based crevice pressure obviates the need to provide a detailed response to this RAI (see Sections 6.0 and 8.0).</p>

Table 2-2 (Continued) List of NRC RAI on H* and Resolution Status

RAI No	Source Document for Initial Response: LTR-CDME-07-198 (Reference 2-3)
25	<p>Reference 2, Enclosure 1, Attachment 1 - Provide a copy of Reference 3. The cited web page appears to be no longer available. Also, provide copy of Reference 4.</p> <p>Issue Resolution Summary</p> <p>The response to this NRC RAI is provided for historical purposes only. The original response to this RAI in LTR-CDME-07-198, "Response to NRC Request for Additional Information Relating to LTR-CDME-07-72 P-Attachment and LTR-CDME-05-209-P of the Wolf Creek Generating Station (WCGS) Permanent B* License Amendment Request," still applies. A new structural analysis which involves a fully probabilistic, whole bundle H* depth calculation for each of the Model F H* plants which applies a depth-based crevice pressure obviates the need to provide a detailed response to this RAI.</p>
26	<p>Reference 2, Enclosure 1, Attachment 1 - What were the specific data sets used to compute the Dixon Ratio values at the top of page 11?</p> <p>Issue Resolution Summary</p> <p>The response to this NRC RAI is provided for historical purposes only. The original response to this RAI in LTR-CDME-07-198, "Response to NRC Request for Additional Information Relating to LTR-CDME-07-72 P-Attachment and LTR-CDME-05-209-P of the Wolf Creek Generating Station (WCGS) Permanent B* License Amendment Request," still applies. A new structural analysis which involves a fully probabilistic, whole bundle H* depth calculation for each of the Model F H* plants which applies a depth-based crevice pressure obviates the need to provide a detailed response to this RAI.</p>
27	<p>Reference 2, Enclosure 1, Attachment 1 - In Table 5 under the heading of outliers, rows 1 and 2 refer to "total set," whereas lines 3 and 4 refer to "included." Does "included" mean the same thing as "total set." If not, how does it differ from "total set," and how does it differ from "excluded?"</p> <p>Issue Resolution Summary</p> <p>The response to this NRC RAI is provided for historical purposes only. The original response to this RAI in LTR-CDME-07-198, "Response to NRC Request for Additional Information Relating to LTR-CDME-07-72 P-Attachment and LTR-CDME-05-209-P of the Wolf Creek Generating Station (WCGS) Permanent B* License Amendment Request," still applies. A new structural analysis which involves a fully probabilistic, whole bundle H* depth calculation for each of the Model F H* plants which applies a depth-based crevice pressure obviates the need to provide a detailed response to this RAI.</p>

Table 2-2 (Continued) List of NRC RAI on H* and Resolution Status

RAI No	Source Document for Initial Response: LTR-CDME-07-198 (Reference 2-3)
28	<p>Reference 2, Enclosure 1, Attachment 1 - Provide a step-by-step description (including an example) of how the values in Table 5 were obtained.</p> <p>Issue Resolution Summary</p> <p>The response to this NRC RAI is provided for historical purposes only. The original response to this RAI in LTR-CDME-07-198, "Response to NRC Request for Additional Information Relating to LTR-CDME-07-72 P-Attachment and LTR-CDME-05-209-P of the Wolf Creek Generating Station (WCGS) Permanent B* License Amendment Request," still applies. A new structural analysis which involves a fully probabilistic, whole bundle H* depth calculation for each of the Model F H* plants which applies a depth-based crevice pressure obviates the need to provide a detailed response to this RAI.</p>
29	<p>Reference 2, Enclosure 1, Attachment 1 - Confirm that the "unaltered" case in Table 5 reflects the use of the improved tubesheet/divider plate model with a "divider plate factor" of 0.399.</p> <p>Issue Resolution Summary</p> <p>The response to this NRC RAI is provided for historical purposes only. The original response to this RAI in LTR-CDME-07-198, "Response to NRC Request for Additional Information Relating to LTR-CDME-07-72 P-Attachment and LTR-CDME-05-209-P of the Wolf Creek Generating Station (WCGS) Permanent B* License Amendment Request," still applies. A new structural analysis which involves a fully probabilistic, whole bundle H* depth calculation for each of the Model F H* plants which applies a depth-based crevice pressure obviates the need to provide a detailed response to this RAI.</p>

3.0 TEST PROGRAM IN SUPPORT OF H*

Following the withdrawal by Wolf Creek Nuclear Operating Corporation of its License Amendment Request (Reference 3-1), the NRC Staff issued a summary (Reference 3-2) of its technical concerns regarding the technical justification of H* (References 3-3, 3-4 and 3-5). The issues noted in Reference 3-2 that dealt with coefficient of thermal expansion and residual contact pressure (the interaction between the tubesheet and tube resulting from only the hydraulic expansion) were addressed by test programs during 2008 and 2009. The following sections describe the tests that were performed in support of the H* technical justification.

3.1 COEFFICIENT OF THERMAL EXPANSION (CTE) OF ALLOY 600 AND SA508 STEEL

The strength of the hydraulically expanded tube-to-tubesheet joint in a steam generator (SG) is due, in large part, to the difference of thermal expansion between the tube and the tubesheet. The tube, which is made of A600, expands more at a given temperature than does the tubesheet, which is made of A508 material, resulting in mechanical interference between the two.

In 2007, the NRC Staff provided data that suggested that there may be cases where the thermal expansion mismatch between the tube and the tubesheet do not follow the expected behavior, i.e., the tubesheet may expand more at a given temperature than the tube, resulting in loss of contact pressure between the tube and the tubesheet at elevated temperature. Because the technical basis of H* (tube pull out) is significantly dependent on differential thermal expansion between the tube and the tubesheet, the Staff provided the following summary of the outstanding issue (Item No. 10 from Reference 3-2):

– The [H report of record] report considered two different nominal values of thermal expansion coefficient (TEC) for alloy 600 tubing and two different nominal values for the A508 tubesheets. The nominal TEC values are based on (1) nominal ASME Code values for both the tube and tubesheet and (2) data from ANTER Laboratories Inc. for both the tube and tubesheet. TEC variability relative to these nominal values was assumed to have a standard deviation of 1.5% based on reported measurement uncertainty associated with the ANTER data. However, the report provided no evidence that either TEC model (i.e., that based on Code values versus that based on the ANTER data) captures the range of TEC values that may be encountered in the field. In addition, recent TEC data from PMIC indicate smaller TEC differences between the tube and tubesheet materials than is indicated by either of the above TEC models, thus adding to the Staff's concern as whether either TEC model captures the range of TEC values which may exist in the field. A more complete technical justification for the TEC model is needed in terms of its ability to capture the range of TEC differences between the tube and tubesheet that may be encountered in the field. This technical justification should address, but not necessarily be limited to the following:*

- a. Literature search for relevant TEC data, and evaluation of that data. If the PMIC data is considered not relevant, what is the basis? Apart from the American Society of Mechanical Engineers (ASME) Code vetting process, is there any reason to believe that the pedigree of the PMIC data (or ANTER data) is not as good as the data upon which the Code values are based? What is the feasibility of subjecting the PMIC and ANTER data to a review similar to that performed as part of the Code vetting process?*

- b. *Expert opinion and experience on the variability of TEC that may be exhibited by materials such as alloy 600 and A508 steel that may have fabricated from different heats of material, at different times, and with different processing histories (e.g., mill annealed versus thermally-treated alloy 600, temperatures experienced during post weld heat relief).*
- c. *Expert opinion and experience on potential changes to alloy 600 TEC due to hydraulic expansion process. Data concerning sensitivity of TEC to cold working for metals in general needs to be provided.*

3.1.1 Review of Industry Data

In response to the issue summarized in Reference 3-2, industry experts were consulted and a literature search was performed to: (1) identify the sources of coefficient of thermal expansion (CTE) data, and in particular, the sources of the CTE contained in the ASME Code, (2) determine how the Code mean value for CTE was derived and (3) determine what the statistical interpretation of the 10% variability noted on the Code should be. Further, the data provided by the NRC Staff was reviewed to determine the material pedigree, the handling history of the material, the test process and the analysis of the test data. A summary report was prepared which is included in this report as Appendix B. Generally, one of the data points provided by the Staff (referred to as the ANTER data) was found to be reasonably consistent with the available industry data. However, the second data point for SA508 material (referred to as the PMIC data) was found to have deficiencies in the material temperature exposure history and in the test process and was, therefore, not included in the final evaluation for the mean value and variability of CTE. Appendix B of this report provides the details of the data literature search, the results of the analysis, and a rationale for not including the PMIC data. The discussion in Appendix B includes the additional data from a test program discussed in the following section.

3.2 CTE TESTS

Because the body of available industry data on CTE of SA508 and A600 was limited, a test program was completed to acquire CTE data for both A508 and A600 material for conditions specifically of interest to H*. This test program was intended to determine whether the ASME Code reasonably represents the mean CTE values of these materials, and to characterize the statistical variability of CTE for these materials. The ASME Code (Reference 3-6) provides mean values of the CTE and a general statement that the values could vary by +/-10%. Because a probability statement is required for H*, specification of a broad range of variability without a statistical interpretation was unacceptable.

3.2.1 Description of the CTE Tests

3.2.1.1 Materials

SA508

Two grades and four heats of A508 pressure vessel steel were tested under this program: SA-508 Grade 3 Class 1 (Heat 03D958-1-6), SA-508 Grade 3 Class 2 (Heats 97D28-1-1, 97B80-1-11, and 97D258-1-1). These materials were provided in block form by Babcock and Wilcox Canada. The chemical

certifications of these materials are contained in Table 3-1, and their mechanical property certifications are contained in Table 3-2.

Alloy 600

Nine tubes of A600 thermally-treated material, each approximately twelve inches long, were used to perform the CTE measurements on A600 material. Three different heats of material were tested for each of the three sizes of SG tube under consideration (Model F – 0.688 inch dia, Model D5 – 0.750 inch dia., and Model 44F and 51F – 0.875 inch dia.). The Model F SG tubes were represented by Heats NX0419, NX9749, and NX9821, the Model D5 SG tubes were represented by Heats NX1002, NX1019, and NX1145, and the Model 44F/51F SG tubes were represented by Heats NX9180, NX9292, and NX1518. All of these heats of material are from archive samples of tubing heats that were included in production SGs.

The matrix of the tubes with their corresponding heats and nominal outer diameter is contained in Table 3-3, while the chemical and mechanical property certifications are contained in Tables 3-4 and 3-5, respectively.

3.2.1.2 Sample Preparation

Each block of A508 material was cut into specimens that were 0.25 inch x 0.25 inch x 2 inches long rectangular prisms. The cutting process utilized was a water cooled cut-off wheel to avoid excessive local heating of the material and to provide lubrication.

The tubes of A600 material were first cut in half lengthwise; one half was used for the non-strain hardened CTE measurements, and the other half was saved for the strain hardened part of the test program. The first half of each of the tubes was subsequently cut into strips whose chord length was 0.25 inch and whose length was 2 inch. The length dimension was parallel to the axis of the original tube.

In order to strain harden the tube, the tubes were hydraulically expanded at a nominal pressure of 31,000 psi into split collars made of 1018 carbon steel, which were designed to simulate the stiffness of the tubesheet based on the results of Middlebrooks et al. (Reference 3-7). Specifically, the collars were manufactured so that a ratio between the outer diameter of the tubesheet and the outer diameter of the tube were kept to 2.42 as closely as possible. Drawings of the split collars for each of the SG models used in the current test program are shown in Figures 3-1 through 3-3. The dimensions are such that the ratio of 2.42 was maintained between the center hole and the upper/lower surface of the block, between the center hole and the bolt hole (horizontally), and between the center hole and the counter bore of the bolt hole. The resulting radial strain on the material was approximately 3%. These tubes were then cut in the same manner as the non-strain hardened tube with the exception that care was taken to make sure that all of the strips were removed from the expanded section only.

3.2.2 CTE Tests

Table 3-6 shows the complete test matrix for the CTE tests performed. A total of 132 individual CTE tests were performed. All CTE testing was performed in air in a Unitherm 1091™ unit according to

ASTM E228-06 (Reference 3-8). The tests ran from room temperature to 700°F and were heated at a rate of approximately 3.6°F/min. (2°C/min. specified). All tests were performed by ANTER Laboratories.

Four types of tests were performed:

The first test was a determination of the CTE under heat-up conditions, consistent with the accepted test practice. In addition, industry experts recommended that using heat-up only data would avoid hysteresis effects upon cooling. Ten specimens from each of the four heats of A508 material were tested. Similarly, all of the A600 heats were tested. The ten specimens were on a tube diameter basis instead of a heat basis. Thus, for the Model F steam generator tube (0.688 inch dia.), 4 specimens from Heat NX0419 were tested and 3 specimens from each of Heat NX9749 and Heat NX9821 were tested. For the Model D5 steam generator tube (0.750 inch dia.), 4 specimens from Heat NX1002 were tested and 3 specimens from each of Heat NX1019 and Heat NX 1145 were tested. Likewise, for the Model 44F/51F steam generator tube (0.875 inch dia.), 4 specimens from Heat NX9180 were tested and 3 specimens from each of Heat NX9292 and Heat NX1518 were tested.

The second test was the determination of repeatability of results. Ten heat-up tests of A508 material (Heat 97D258-1-1, Sample #8) and ten heat-up tests of A600 material (Heat NX1019, Sample #3) were performed. These two specific samples were chosen because they most closely exhibited the mean behavior of their respective materials from Test 1.

The third test was the heat-up of the strain hardened A600 material. Just like the non-strain hardened A600 CTE tests, the three heats of material for each SG model were tested in the ratio of 4:3:3. That is, for the Model F SG tube, 4 specimens were tested from Heat NX0419 and 3 specimens from each of Heat NX9749 and Heat NX9821 were tested. For the Model D5 SG tube, 4 specimens were tested from Heat NX1002 and 3 specimens from each of Heat NX1019 and Heat NX 1145 were tested. Likewise, for the Model 44F SG, 4 specimens were tested from Heat NX9180 and 3 specimens from each of Heat NX9292 and Heat NX1518 were tested:

Anomalous behavior in some of the individual specimens was observed in this test. Specifically, some specimens exhibited decreasing CTE with increasing temperature, reaching a minimum CTE value at approximately 200°F to 300°F, and then showing increasing CTE values with increasing temperature from approximately 300°F to 700°F. The anomalous behavior of some of the test specimens was addressed in the subsequent test.

The fourth test was a diagnostic test to explain some anomalous behavior observed in the prior (third) test. It was postulated by Begley (Reference 3-9) that if strain hardened A600 was subjected to temperatures above approximately 600°F, it should revert to its non-strain hardened behavior. Thus, three samples that exhibited anomalous behavior were retested 3 times each, and 1 sample that initially exhibited “normal” behavior was retested 3 times. The anomalous samples chosen for retest were from Model F, Heat NX0419, Sample 3; Model D5, Heat NX1019, Sample 2; and Model 44F, Heat NX9180, Sample 4. One sample that initially exhibited “normal” behavior was Model D5, Heat NX1145, Sample 3.

3.3 CTE TEST RESULTS

The complete data package for the CTE tests is documented in Reference 3-11. Due to the extensive list of figures to describe the results of the testing, a summary table, Table 3-7, lists the tests, materials, and figure numbers. Briefly, Figures 3-4 through 3-24 show the results of the heat-up testing on the A508 and non-strain hardened A600 material, Figures 3-25 and 3-26 show the results of the multiple tests on one sample each of A508 material and A600 material, Figures 3-27 through 3-35 show the results of the tests on strain hardened A600 material, and Figures 3-36 through 3-39 show the results of the 3 repeat tests on A600 strain hardened material that initially exhibited anomalous behavior and the 1 repeat test on A600 strain hardened material that initially exhibited "normal" behavior.

3.4 DISCUSSION

SA508 Material

The heat-up tests on A508 material all exhibit a trend of increasing CTE value with increasing temperature, and the shape is consistently non-linear. The scatter is divided into two regions; the scatter below approximately 350°F is more significant than the scatter in the region above approximately 350°F, but still well within 10% of the individual mean curves. The data in the higher temperature region are quite close to the individual mean curves. The scatter in the lower temperature region is believed to be due to (1) thermal inertia and (2) measurement inaccuracy due to very small thermal expansions in that temperature range (fractions of microns) (Reference 3-10). Expansions below 200°F were typically less than 0.1%. This translates into less than 2 mils of growth, which is approximately the same as the measurement tolerance of the dilatometer used to measure CTE.

A plot of the mean curves of the individual heats of A508 material versus the ASME Code data shows that the current test data diverge from the mean ASME Code curve below approximately 350°F and align very well with the ASME Code data above approximately 350°F (see Figure 3-8). A few CTE measurements lie slightly outside the uncertainty associated with the ASME Code curve ($\pm 10\%$) at 100°F, but this is not a concern because of the reasons outlined above. Thus, use of the ASME Code curve in steam generator tube-to-tubesheet joint thermal calculations is generally conservative as discussed in Appendix B.

Non-Strain Hardened A600 Material

The curves of CTE versus temperature for the non-strain hardened A600 material also exhibit increasing CTE values with increasing temperature, and most are non-linear. Unlike the A508 material, however, a few of the CTE versus temperature curves for non-strain hardened A600 material show an almost linear behavior. The data scatter is also more pronounced in the lower temperature region and small in the upper temperature region.

Comparing these data to the ASME Code curve (see Figures 3-13, 3-18, 3-23, and 3-24), the mean curves for the individual heats of material generally lie above the mean of the ASME Code curve. This would imply that, in a SG tube-to-tubesheet joint thermal calculation, use of the ASME Code curve would be conservative (the tube is predicted to expand less than the test data show). Taken together with the data for the A508 material, the ASME Code curves would predict that the tubesheet will expand more and the

tube will expand less than the current data show. Thus, use of the ASME Code curves will predict less contact pressure due to thermal growth and mismatch than the data indicate, and is therefore conservative.

Repeat Tests

One sample from the A508 material (Heat 97D258-1-1, Sample #8) and one sample from the A600 material (Heat NX1019, Sample #3) were tested multiple times in an effort to determine the repeatability of the data. In both cases, the means of the repeat test data are slightly higher than their respective original tests at 100°F, but otherwise, they are nearly identical to the original curves. The scatter on these curves is again similar to the other plots, i.e., there is more scatter in the lower temperature regime than in the upper temperature regime. Therefore, there is ample evidence that the tests are repeatable.

Strain Hardened A600 Material

The results of the CTE measurements made on strain hardened A600 material lend themselves to three noteworthy observations: (1) there is more scatter in the lower temperature regime than in the upper temperature regime, (2) some curves exhibit "normal" behavior defined as increasing CTE values with increasing temperature while other curves contain data that initially show a decrease of CTE value with increasing temperature followed by expected behavior, and (3) the mean curves of the strain hardened data are rotated clockwise from their non-strain hardened counterparts, i.e., the mean CTE values are higher in the low temperature regime and lower in the high temperature regime than CTE values of the non-strain hardened data. One may expect a differing behavior in CTE measurements between the strain hardened and non-strain hardened material due to the increase in the number of vacancies as well as the increasing number of, and entangling of, dislocations during plastic deformation. The tests performed immediately after cold working show this. However, this effect is not present after cold working and subsequent exposure of the specimens to temperatures above 600°F.

The hypothesis that this effect can be alleviated by thermal treatment above 600°F (Reference 3-9) led to the decision to perform repeat tests on a number of previously tested strain hardened specimens. Three samples were chosen because of the originally anomalous behavior of their data (Model F tube, Heat NX0419; Model D5 tube, Heat NX1019; and Model 44F tube, Heat NX9180), and one was chosen because it initially exhibited "normal" behavior (Model D5 tube, Heat NX1145). These are shown in Figures 3-36 through 3-39, respectively. In all cases initially exhibiting anomalous behavior, the effect did not recur, and the mean of the retest data CTE curves align much more closely with the non-strain hardened curves. Recall that the initial CTE tests on the strain hardened material were taken to 700°F. This is beyond the postulated 600°F and indicates that the strain hardened material has experienced some elastic recovery. Further, since the strain hardening only worked the material to approximately 3% strain, there is little plastic deformation incurred.

3.5 CONCLUSIONS

1. The data indicate that use of the ASME Code curves for A508 and A600 material would be conservative for a SG tube-to-tubesheet joint calculation. That is, the tubesheet is predicted by the ASME Code curve to expand more than the data show, and the tubes are predicted by the ASME Code curve to expand less than the data show. This would have the effect of lessening the

thermal mismatch between the tube and the tubesheet, and it would then decrease the thermal component of the contact pressure between them.

2. The mean curves of CTE versus temperature for the A508 material all lay within the uncertainty associated with the ASME Code curves. Some individual data lay outside the lower bound on the curve at 100°F, but this is of no concern since the expansion of the material at these temperatures is well within the measurement tolerance of the instrumentation. The mean curves of CTE versus temperature for the A600 material and all of the individual data lay within the uncertainty associated with the ASME Code curves.
3. All samples show a general curve of increasing CTE with increasing temperature. All of the A508 material show non-linear behavior, while some of the A600 material shows nearly linear behavior.
4. The data scatter is more pronounced in the temperature regime below approximately 350°F than in the regime above approximately 350°F. This is due to thermal inertia and measurement uncertainty due to very small thermal expansions in that temperature range (fractions of microns).
5. Performing multiple tests on a single specimen results in a similar data scatter pattern as that on data from individual heats of material. This suggests that the variability is inherent to the test apparatus and does not reflect actual variability of CTE. It is concluded that within the accuracy of the test method, the CTE values are repeatable and consistent.
6. Strain hardening does not affect the CTE of A600 material after exposure of the strain hardened material to temperatures of 600 degrees or greater. While initial tests of strain hardened samples of A600 material show a mean CTE versus temperature curve that has been rotated relative to the original, non-strain hardened mean CTE versus temperature curve, re-testing of these specimens returns the CTE behavior to its original, non-strain hardened behavior. Some individual curves exhibit anomalous behavior at low temperature increase, i.e., an initially decreasing CTE value with increasing temperature. The tests showed that this behavior is eliminated upon retesting, due to the fact that temperatures above approximately 600°F provide enough thermal energy to induce elastic recovery. In addition, the plastic strain introduced by the strain hardening was small.
7. A detailed analysis of the CTE data was performed to determine the mean value and variability of the CTE of SA508 and A600 material. This analysis is included in Appendix B of this report and shows that the use of the ASME Code CTE mean properties is conservative for H* calculations. Statistical variability parameters are also provided for both materials.

3.6 REFERENCES

- 3-1 WCNOC Letter ET 08-0010, "Withdrawal of License Amendment Request for a Permanent Alternate Repair Criteria in Technical Specification (TS) 5.5.9, Steam Generator (SG) Program," February 14, 2008.

- 3-2 NRC Letter, "Wolf Creek Generating Station – Withdrawal of License Amendment Request on Steam Generator Tube Inspections (TAC No. MD1097)," February 28, 2008."
- 3-3 Wolf Creek Letter ET 06-0004, "Revision to Technical Specification 5.5.9, Steam Generator Tube Surveillance Program," February 21, 2006.
- 3-4 Wolf Creek Letter WO 07-0012, "Response to Request for Additional Information Related to License Amendment Request to Revise the Steam Generator Program," May 3, 2007.
- 3-5 Wolf Creek Letter ET 07-0043, "Response to Request for Additional Information Related to License Amendment Request to Revise the Steam Generator Program," September 27, 2007.
- 3-6 ASME Boiler and Pressure Vessel Code, Section II, New York: ASME International, 2007.
- 3-7 W. B. Middlebrooks, D. L. Harrod, and R. E. Gold, *Nuclear Engineering and Design* 143, 1993, pp. 159-169.
- 3-8 ASTM E228-06, "Standard Test Method for Linear Thermal Expansion of Solid Materials with a Push-Pull Rod Dilatometer," West Conshohocken: ASTM International, 2006.
- 3-9 J. Begley, private communication.
- 3-10 D. Gaal, Laboratory Director, ANTER Corporation, private communication.
- 3-11 Westinghouse CN-SGMP-09-2, "Analysis of the Coefficients of Thermal Expansion of A600 and A508 Material."

Table 3-1¹ Chemical Certifications (in Weight Percent) for A508 Pressure Vessel Steel Used in the CTE Test Program

Heat	C	Si	Mn	P	S	Ni	Cr	Mo	V	Cu	Al
03D958-1-6	0.24 max.	0.15/ 0.40	1.14/ 1.56	0.010 max.	0.010 max.	0.37/ 1.03	0.15/ 0.25	0.42/ 0.53	0.010 max.	0.10 max.	0.040 max.
97D28-1-1	0.22	0.23	1.41	0.005	0.001	0.94	0.20	0.52	<0.003	0.03	0.018
97B80-1-11	0.21	0.23	1.49	0.007	0.001	0.93	0.19	0.51	<0.003	0.05	0.019
97D258-1-1	0.20	0.23	1.47	0.005	0.001	0.93	0.18	0.51	<0.003	0.03	0.022

Table 3-2² Mechanical Certifications for A508 Pressure Vessel Steel in the CTE Test Program

Heat	Yield Strength (ksi)	Tensile Strength (ksi)	Elongation (%)	Reduction of Area (%)
03D958-1-6	68.8	90.3	29.2	74.6
97D28-1-1 ³	73.9	96	28	73
	75.5	97.4	28.4	73.4
97B80-1-11	74	96.7	28	71.7
97D258-1-1	70.3	92.0	29.2	71.7
	71.4	93.8	28	70.4

¹ Chemical certifications provided courtesy of the Muroran Plant of The Japan Steel Works, Ltd.

² Mechanical certifications provided courtesy of B&W Canada.

Table 3-3³ Summary of the A600 Tubes Used in the CTE Test Program

Steam Generator Model	Heat	Condition	Nominal Outer Diameter (in.)
F	NX0419	Thermally-Treated	0.688
F	NX9749	Thermally-Treated	0.688
F	NX9821	Thermally-Treated	0.688
D5	NX1002	Thermally-Treated	0.750
D5	NX1019	Thermally-Treated	0.750
D5	NX1145	Thermally-Treated	0.750
44F	NX9180	Thermally-Treated	0.875
44F	NX9292	Thermally-Treated	0.875
44F	NX1518	Thermally-Treated	0.875

Table 3-4⁴ Chemical Certifications (in Weight Percent) of the A600 Tubes Used in the CTE Test Program

Heat	C	Mn	Fe	S	Si	Cu	Ni	Cr	Al	Ti	Co	P	B
NX0419	0.029	0.13	9.16	0.001	0.20	0.28	74.26	15.94	0.30	0.26	0.03	0.012	0.004
NX9749	0.040	0.23	8.14	0.001	0.29	0.22	74.99	16.09	0.21	0.24	0.04	0.010	0.005
NX9821	0.028	0.16	7.47	0.001	0.22	0.42	75.76	15.94	0.31	0.22	0.02	0.008	0.005
NX1002	0.027	0.29	9.67	0.003	0.12	0.28	73.83	15.78	0.13	0.13	0.04	0.010	0.004
NX1019	0.047	0.26	9.00	0.001	0.18	0.28	74.49	15.74	0.24	0.23	0.04	0.008	0.005
NX1145	0.037	0.29	9.39	0.001	0.15	0.30	73.64	16.19	0.30	0.23	0.05	0.009	0.004
NX9180	0.030	0.19	9.77	0.003	0.12	0.41	73.48	16.00	0.33	0.25	0.02	0.009	0.005
NX9292	0.020	0.23	8.99	0.002	0.10	0.38	75.15	15.13	0.25	0.22	0.04	0.010	0.004
NX1518	0.030	0.34	8.82	0.001	0.28	0.20	74.46	15.87	0.19	0.23	0.05	0.008	0.004

³ Two values were reported for this heat of material.⁴ All values provided courtesy of Westinghouse STD.

Table 3-5⁴ Mechanical Certifications of the A600 Tubes Used in the CTE Test Program

Heat	Yield Strength (ksi)	Tensile Strength (ksi)	Elongation (%)	Hardness (R _B)
NX0419	51	106	37.5	84
NX9749	49	106	38.5	85
NX9821	53	106	38.0	84
NX1002	44	100	40.5	79
NX1019	52	111	36.5	85
NX1145	55	111	35.5	86
NX9180	51	101	41.5	85
NX9292	47	98	45.5	83
NX1518	51.5	107.4	38.5	87

⁴ All values provided courtesy of Westinghouse STD.

Table 3-6 Matrix for Coefficient of Thermal Expansion Tests

Material	Heat No.	Tube Dia. (in.)	Heat-Up CTE	Repeatability	Strain Hardened	Retest of Strain Hardened
A508	03D958-1-6	na	10 ⁽¹⁾	na	na	na
	97D28-1-1	na	10 ⁽¹⁾	na	na	na
	97B80-1-11	na	10 ⁽¹⁾	na	na	na
	97D258-1-1	na	10 ⁽¹⁾	10 (sample 8) ⁽²⁾	na	na
A600	NX0419	0.688	3 ⁽¹⁾	na	3 ⁽¹⁾	3(sample 3) ⁽²⁾
	NX9749		4 ⁽¹⁾	na	4 ⁽¹⁾	na
	NX9821		3 ⁽¹⁾	na	3 ⁽¹⁾	na
	NX1002	0.750	4 ⁽¹⁾	na	4 ⁽¹⁾	na
	NX1019		3 ⁽¹⁾	10 (sample 3) ⁽²⁾	3 ⁽¹⁾	3 (sample 2) ⁽²⁾
	NX1145		3 ⁽¹⁾	na	3 ⁽¹⁾	3 (sample 3) ⁽²⁾
	NX9180	0.875	4 ⁽¹⁾	na	4 ⁽¹⁾	3 (sample 4) ⁽²⁾
	NX9292		3 ⁽¹⁾	na	3 ⁽¹⁾	na
	NX1518		3 ⁽¹⁾	na	3 ⁽¹⁾	na
Total Tests			70	20	30	12
Notes:						
1. Different specimens						
2. Same specimen; retested						

Table 3-7 Listing of the Test Results and Their Corresponding Figure Numbers

Material	Heat	Test Description	Figure No.
A508 Gr. 3 Cl. 1	03D958-1-6	Heat-up	4
A508 Gr. 3 Cl. 2	97D28-1-1	Heat-up	5
A508 Gr. 3 Cl. 2	97B80-1-11	Heat-up	6
A508 Gr. 3 Cl. 2	97D258-1-1	Heat-up	7
A508	All	Mean curves versus ASME Code	8
A600 (0.688 inch dia.)	NX9749	Heat-up	9
A600 (0.688 inch dia.)	NX0419	Heat-up	10
A600 (0.688 inch dia.)	NX9821	Heat-up	11
A600 (0.688 inch dia.)	All	Heat-up	12
A600 (0.688 inch dia.)	All	Mean curves versus ASME Code	13
A600 (0.750 inch dia.)	NX1002	Heat-up	14
A600 (0.750 inch dia.)	NX1019	Heat-up	15
A600 (0.750 inch dia.)	NX1145	Heat-up	16
A600 (0.750 inch dia.)	All	Heat-up	17
A600 (0.750 inch dia.)	All	Mean curves versus ASME Code	18
A600 (0.875 inch dia.)	NX9180	Heat-up	19
A600 (0.875 inch dia.)	NX9292	Heat-up	20
A600 (0.875 inch dia.)	NX1518	Heat-up	21
A600 (0.875 inch dia.)	All	Heat-up	22
A600 (0.875 inch dia.)	All	Mean curves versus ASME Code	23
A600	All	Mean curves versus ASME Code	24
A508 Gr. 3 Cl. 2	97D258-1-1	Multiple tests on Sample 8	25
A600 (0.750 inch dia.)	NX1019	Multiple tests on Sample 3	26
A600 (0.688 inch dia.)	NX9749	Strain hardened, heat-up	27
A600 (0.688 inch dia.)	NX0419	Strain hardened, heat-up	28
A600 (0.688 inch dia.)	NX9821	Strain hardened, heat-up	29
A600 (0.750 inch dia.)	NX1002	Strain hardened, heat-up	30
A600 (0.750 inch dia.)	NX1019	Strain hardened, heat-up	31
A600 (0.750 inch dia.)	NX1145	Strain hardened, heat-up	32
A600 (0.875 inch dia.)	NX9180	Strain hardened, heat-up	33
A600 (0.875 inch dia.)	NX9292	Strain hardened, heat-up	34
A600 (0.875 inch dia.)	NX1518	Strain hardened, heat-up	35
A600 (0.688 inch dia.)	NX0419	Strain hardened, repeat testing on Sample 3	36
A600 (0.750 inch dia.)	NX1019	Strain hardened, repeat testing on Sample 2	37
A600 (0.875 inch dia.)	NX9180	Strain hardened, repeat testing on Sample 4	38
A600 (0.750 inch dia.)	NX1145	Strain hardened, repeat testing on Sample 3	39



Figure 3-1 Model F Steam Generator Split Collar Used to Strain Harden A600 Tubing

a,c,e



Figure 3-2 Model D5 Steam Generator Split Collar Used to Strain Harden A600 Tubing



Figure 3-3 Model 44F Steam Generator Split Collar Used to Strain Harden A600 Tubing

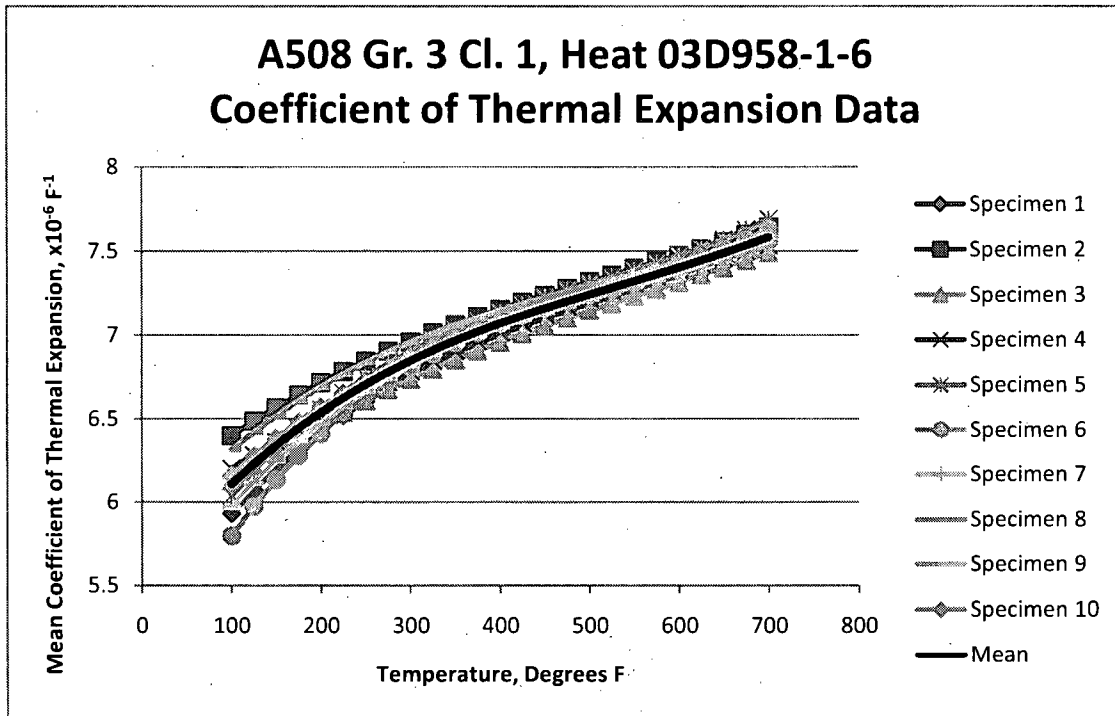


Figure 3-4 Heat-Up Test on A508 Gr. 3 Cl. 1 Material

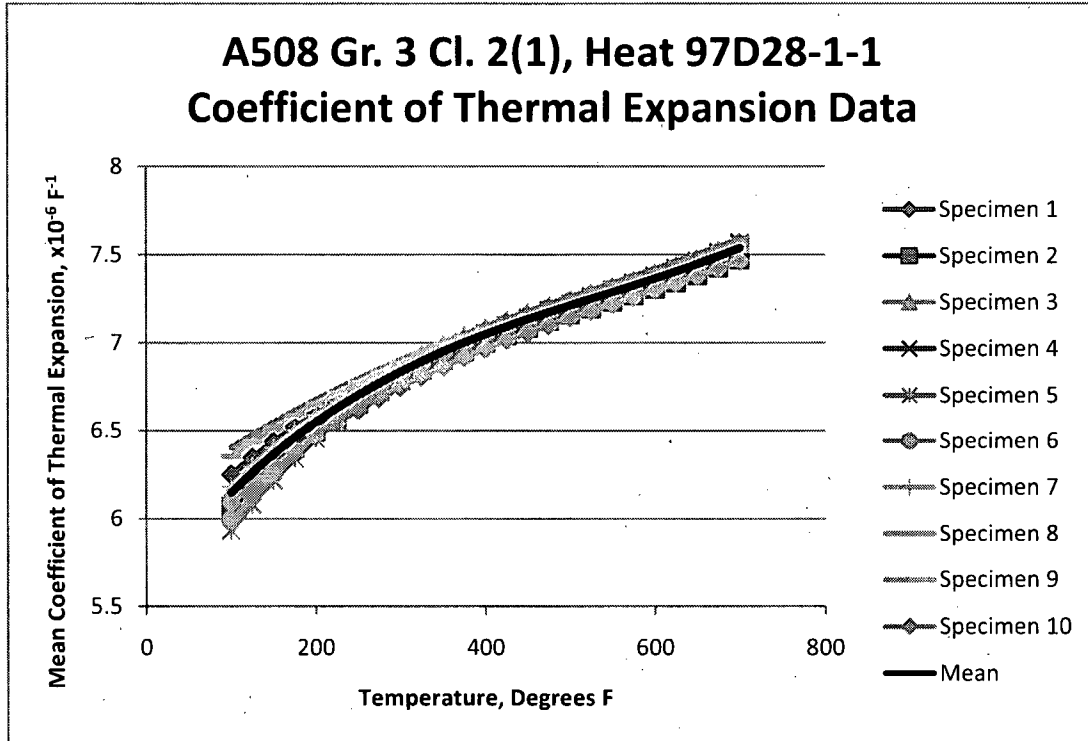


Figure 3-5 Heat-Up Test on A508 Gr. 3 Cl. 2 Material

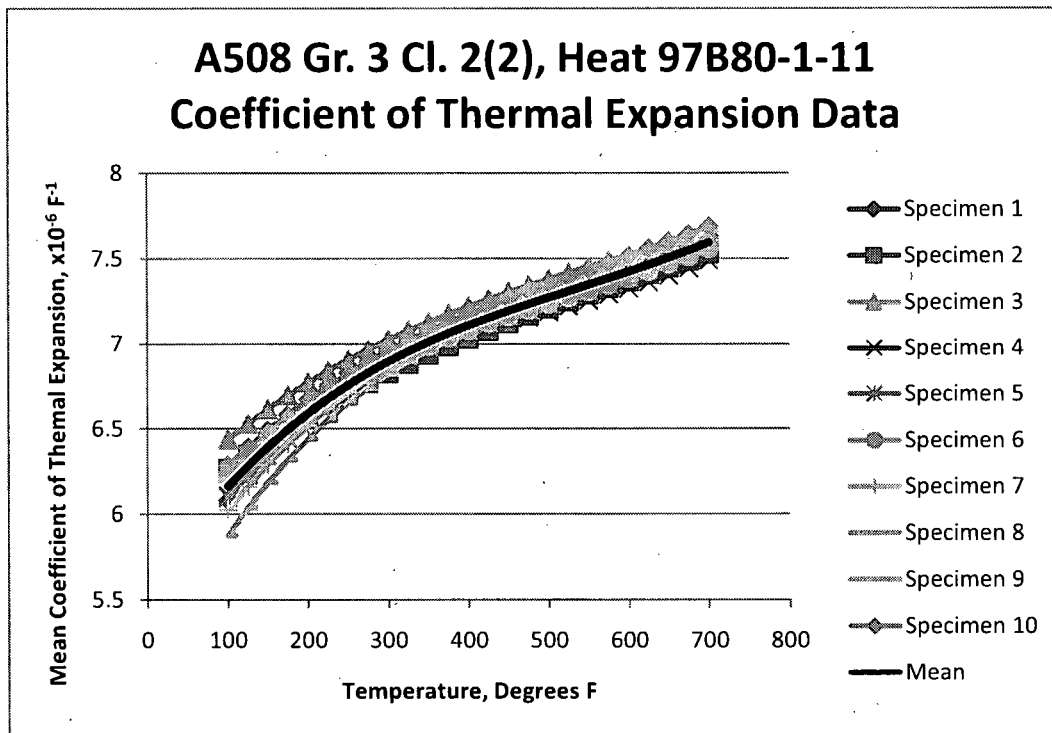


Figure 3-6 Heat-Up Test on A508 Gr. 3 Cl. 2 Material

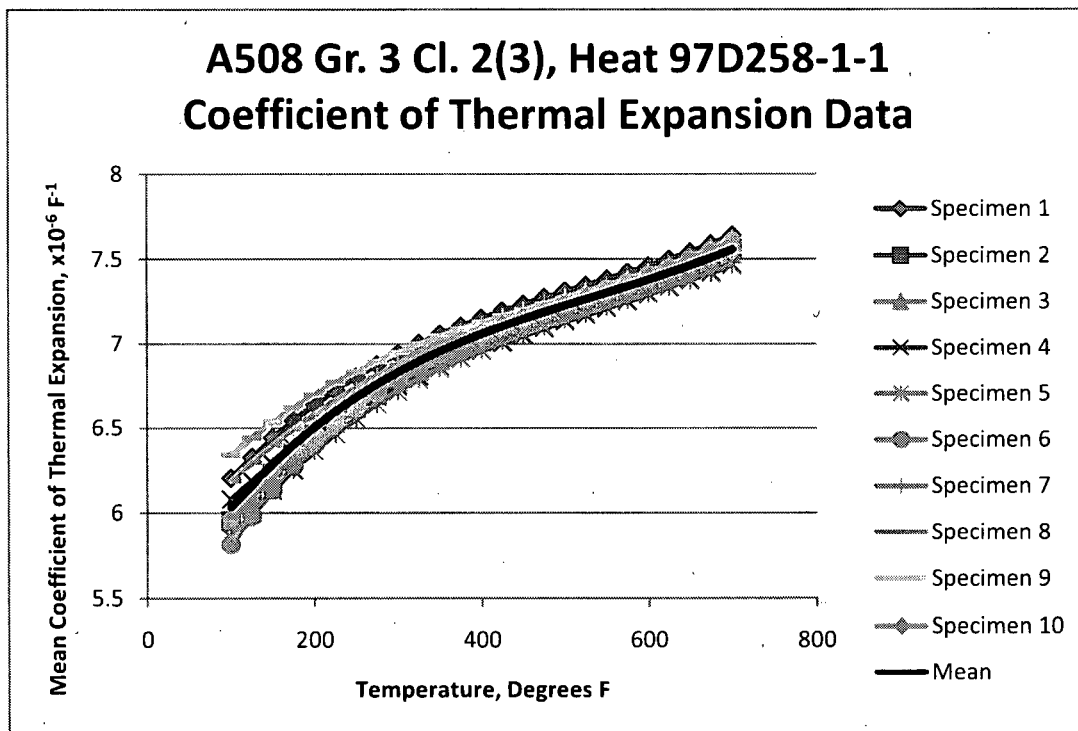


Figure 3-7 Heat-Up Test on A508 Gr. 3 Cl. 2 Material

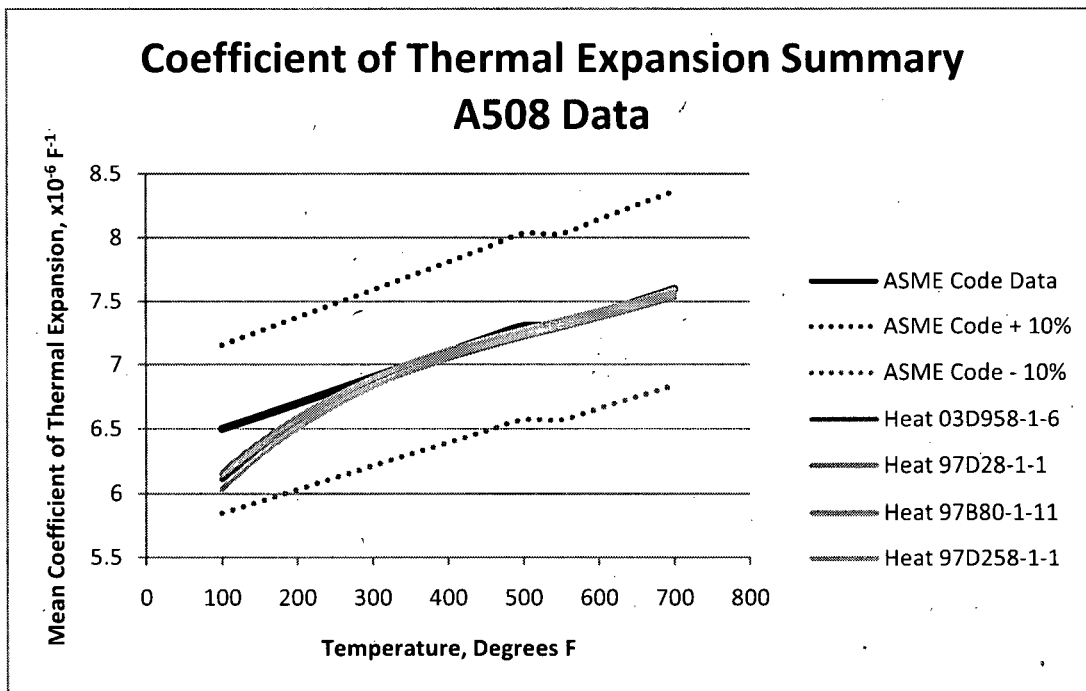


Figure 3-8 A508 Mean Curves Versus the ASME Code Curves

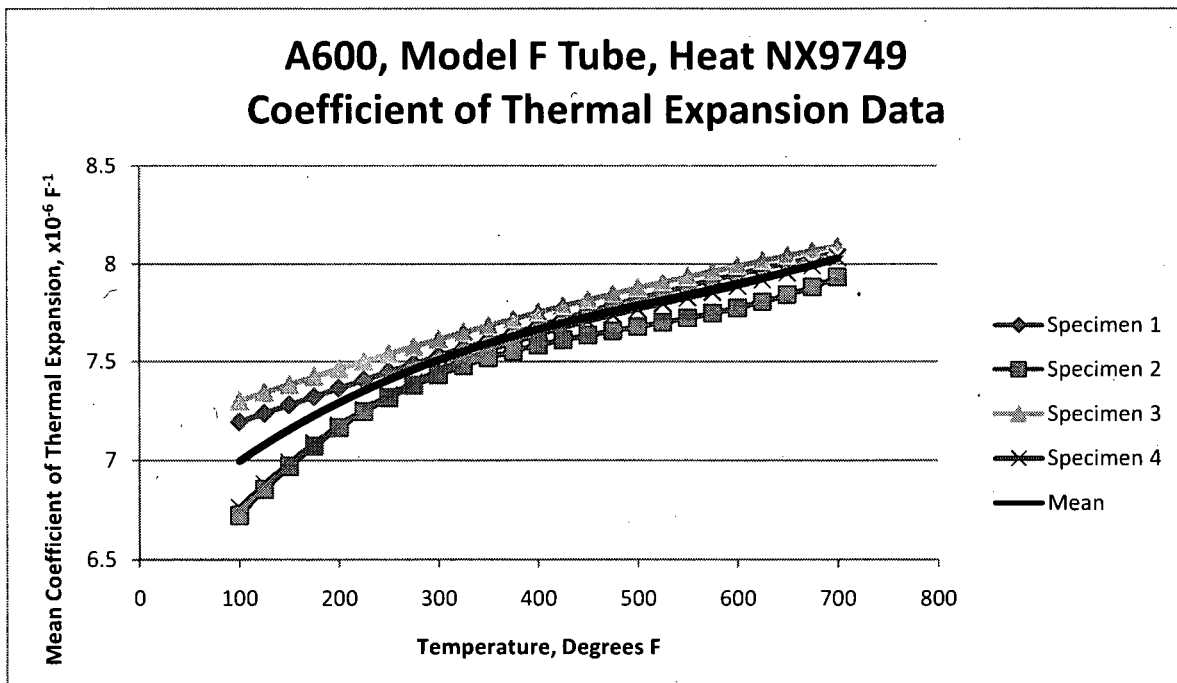


Figure 3-9 Heat-Up Test on A600, Model F Tube, Heat NX9749

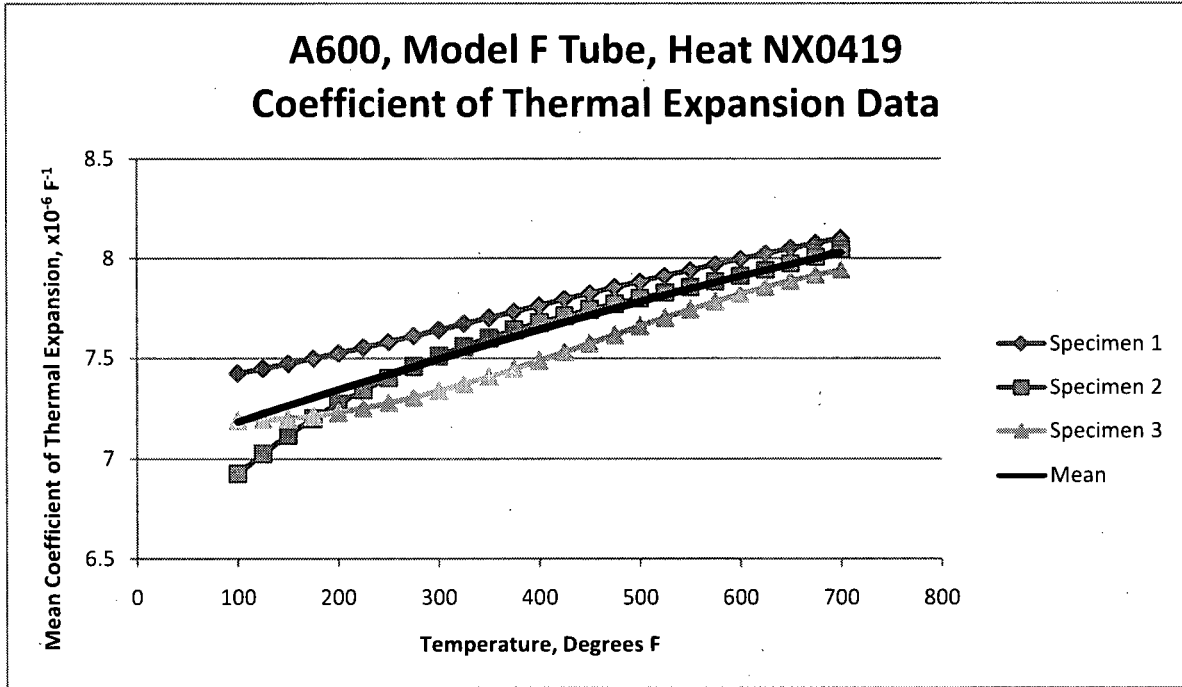


Figure 3-10 Heat-Up Test on A600, Model F Tube, Heat NX0419

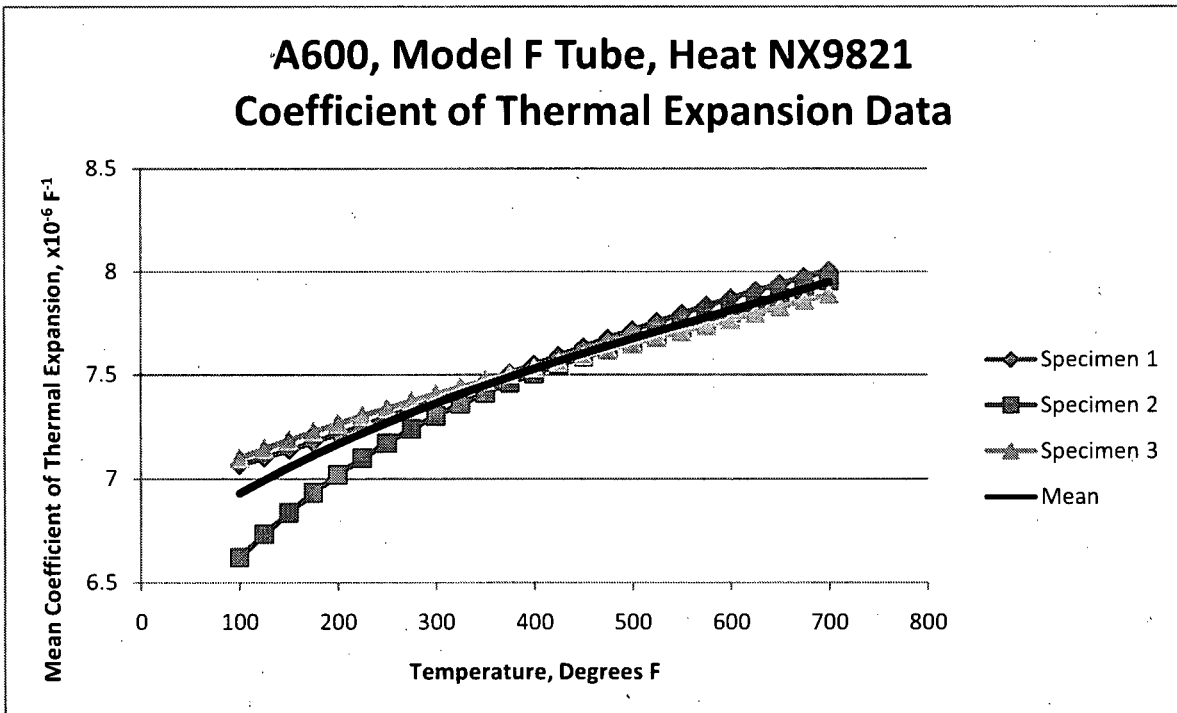


Figure 3-11 Heat-Up Test on A600, Model F Tube, Heat NX9821

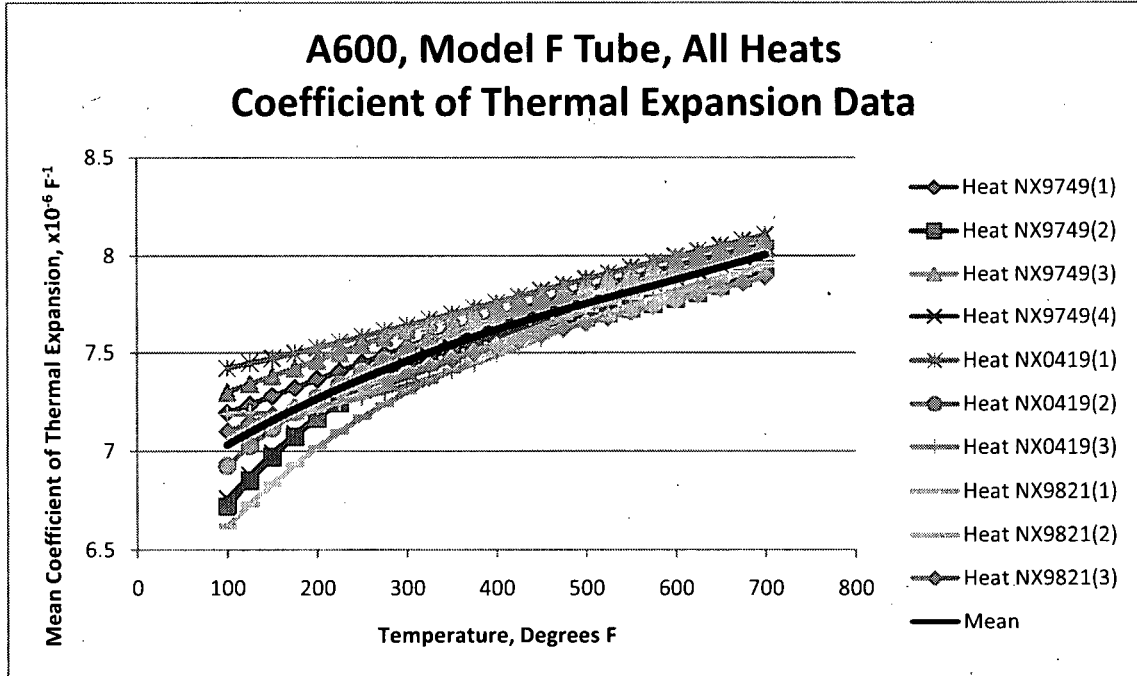


Figure 3-12 Summary of Heat-Up Testing of All Heats of A600 Model F Tube

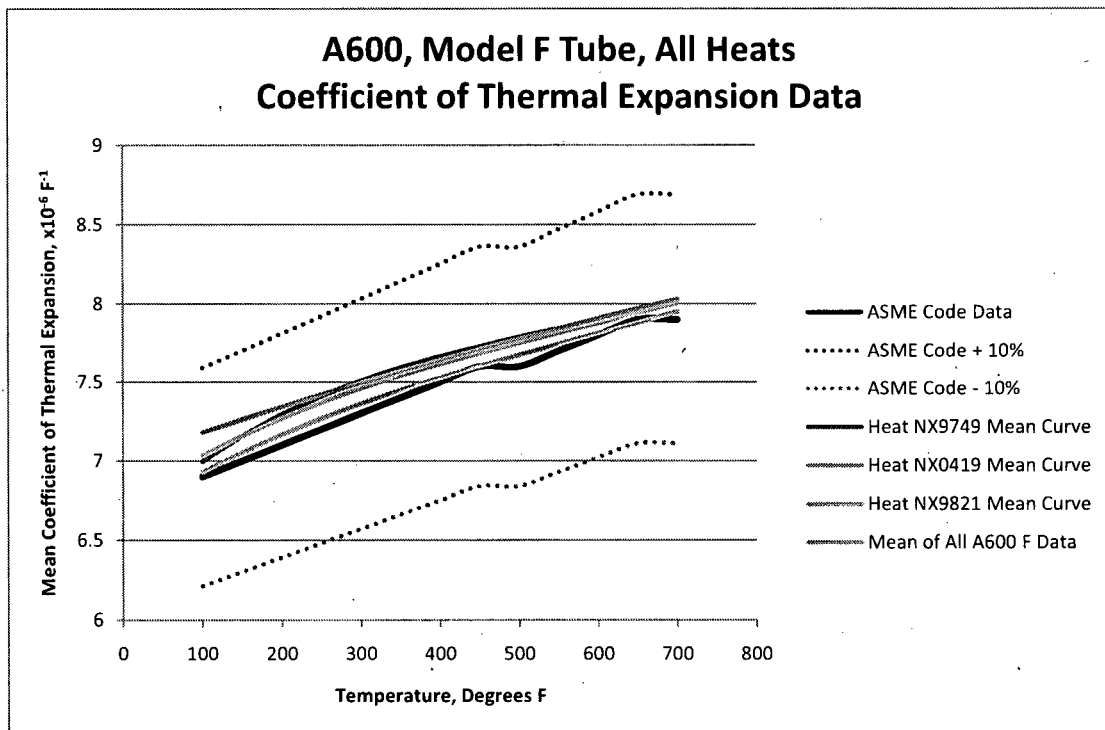


Figure 3-13 Mean Curves of Heats of A600 Model F Tube Versus the ASME Code Curve

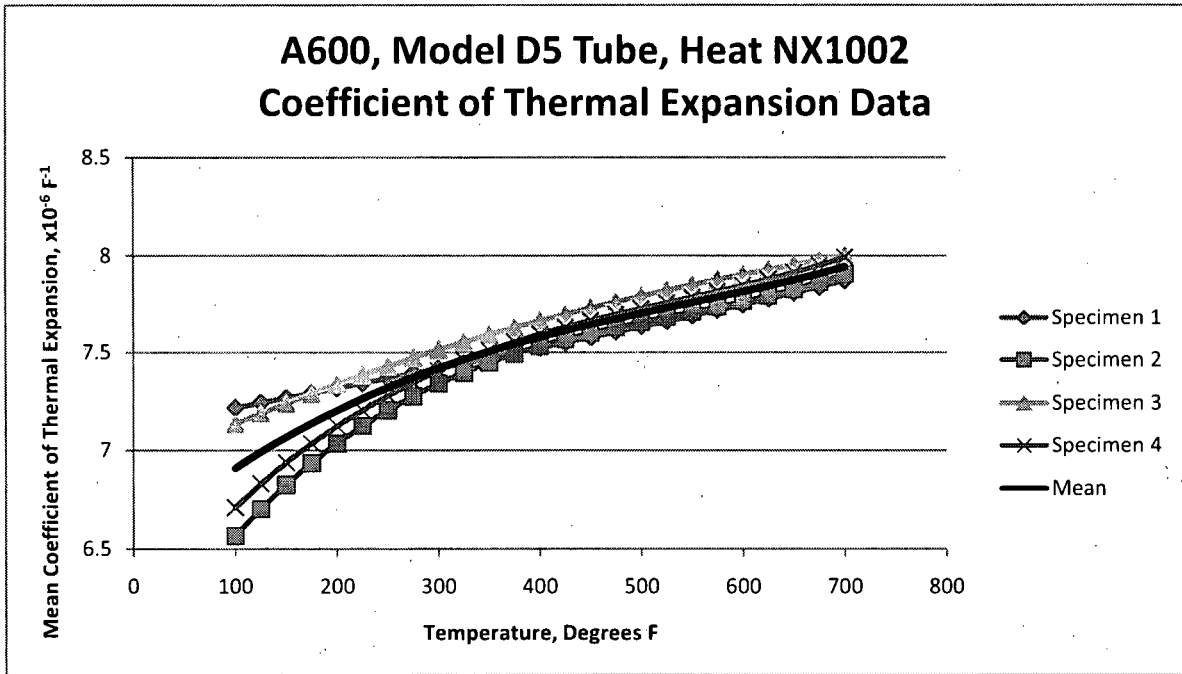


Figure 3-14 Heat-Up Test of A600, Model D5 Tube, Heat NX1002

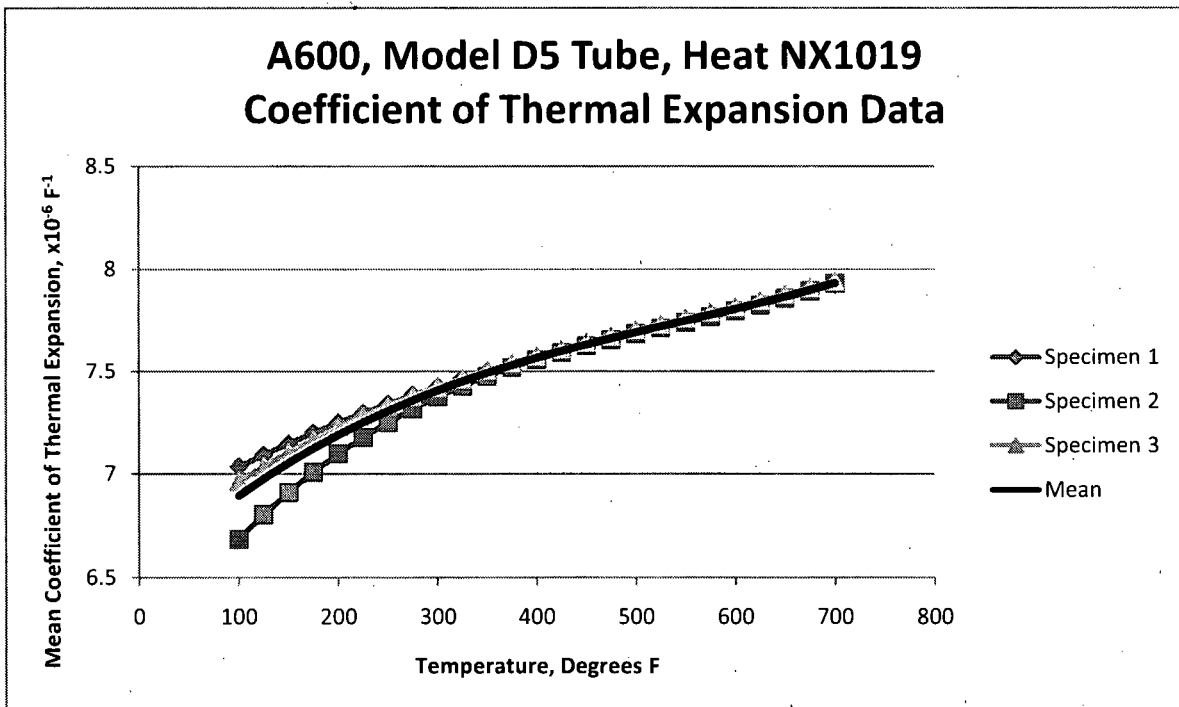


Figure 3-15 Heat-Up Test of A600, Model D5 Tube, Heat NX1019

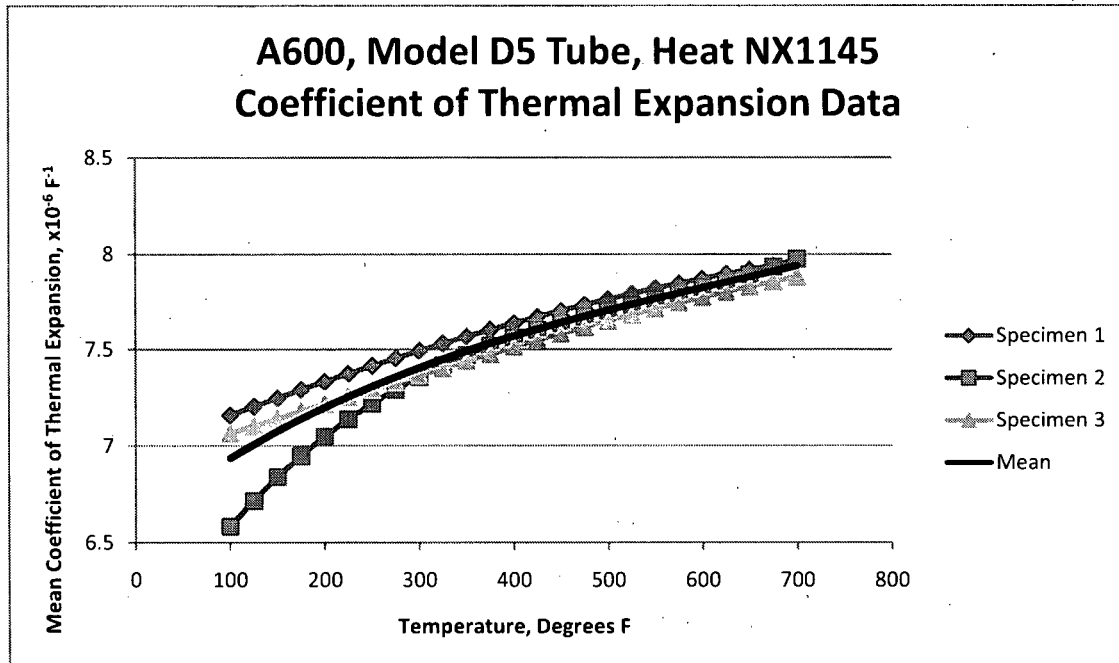


Figure 3-16 Heat-Up Test of A600, Model D5 Tube, Heat NX1145

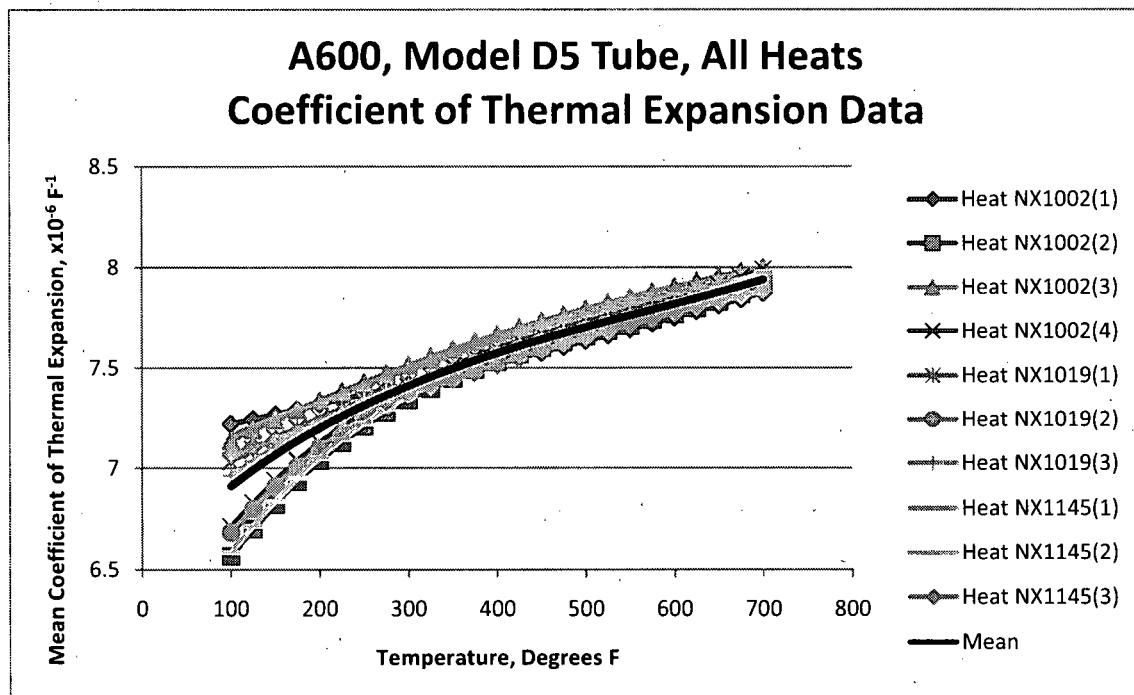


Figure 3-17 Summary of Heat-Up Testing of All Heats of A600 Model D5 Tube

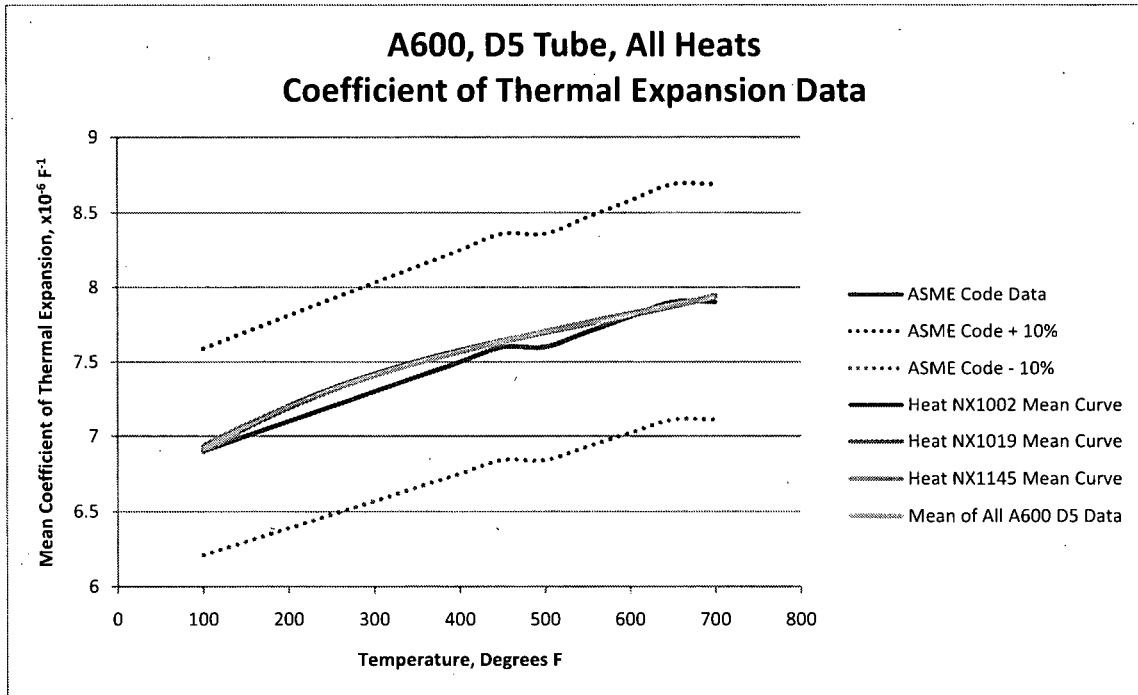


Figure 3-18 Mean Curves of Heats of A600 Model D5 Tube Versus the ASME Code Curve

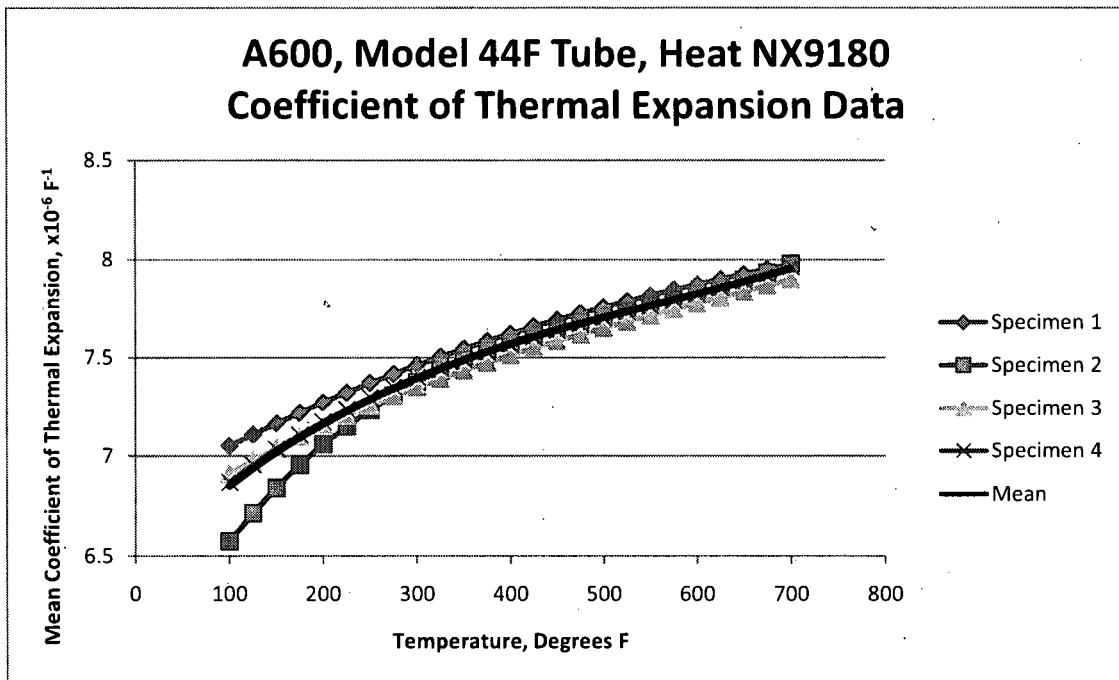


Figure 3-19 Heat-Up Tests of A600, Model 44F Tube, Heat NX9180

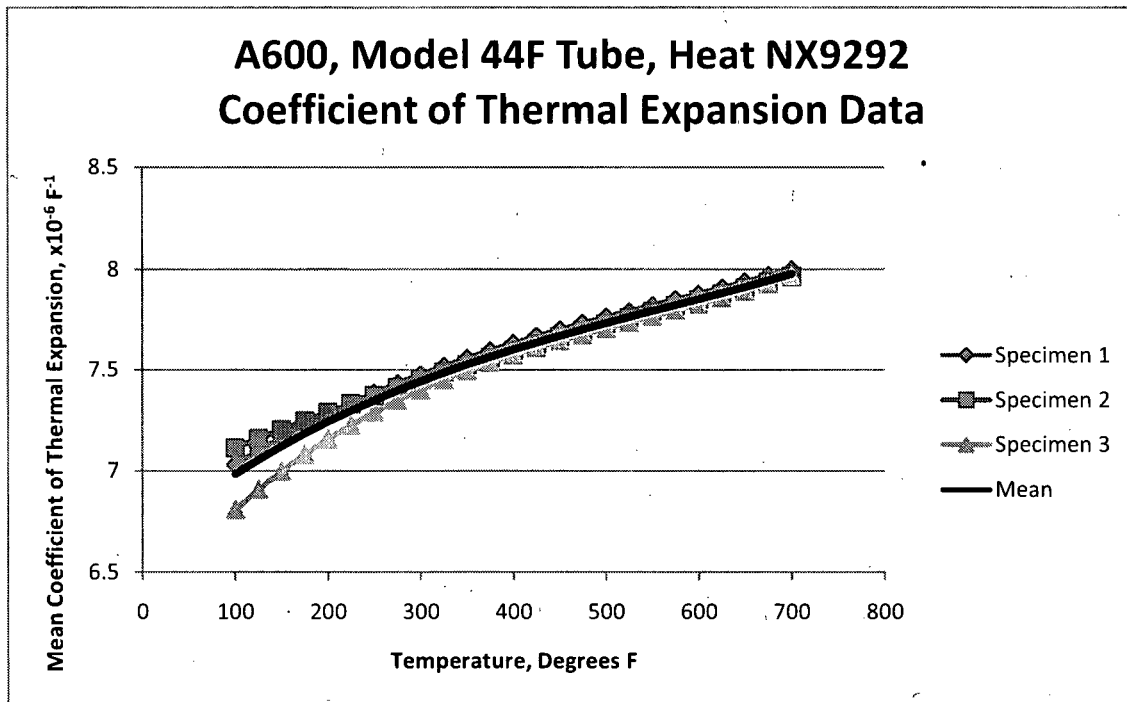


Figure 3-20 Heat-Up Tests of A600, Model 44F Tube, Heat NX9292

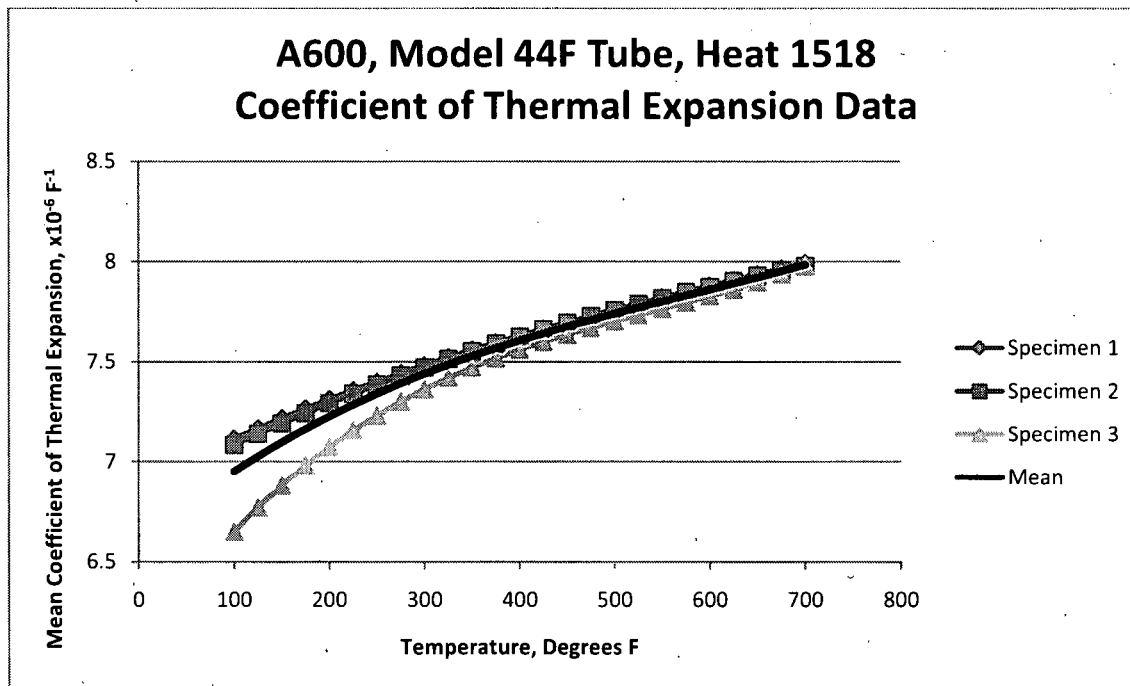


Figure 3-21 Heat-Up Tests of A600, Model 44F Tube, Heat NX1518

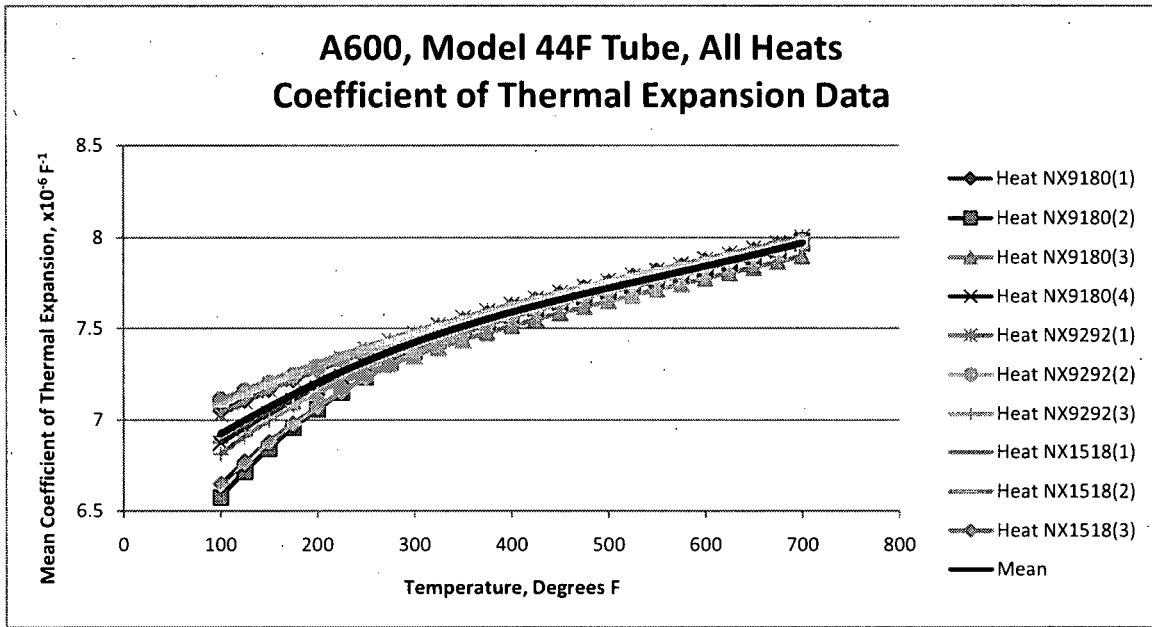


Figure 3-22 Summary of Heat-Up Testing of All Heats of A600 Model 44F Tube

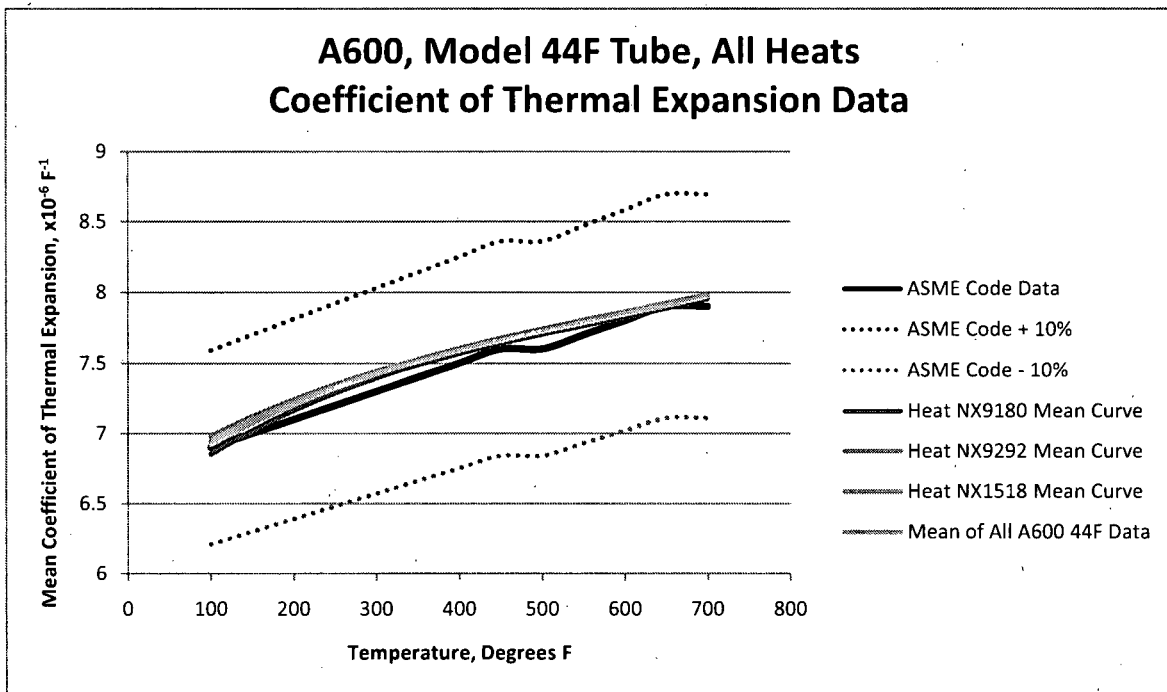


Figure 3-23 Mean Curves of Heats of A600 Model 44F Tube Versus the ASME Code Curve

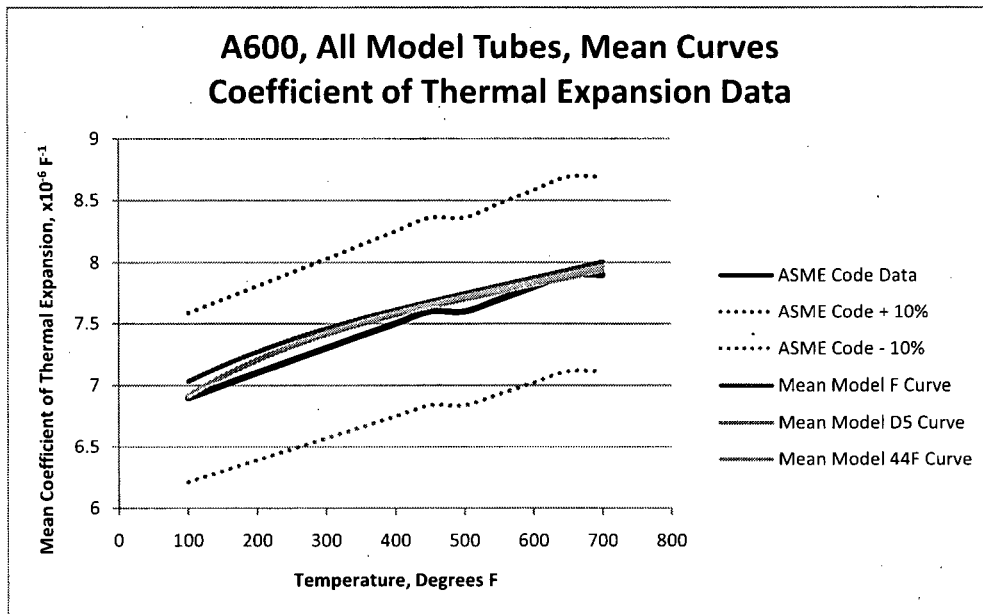


Figure 3-24 Mean Curves of All A600 Steam Generator Model Data Versus the ASME Code Curve

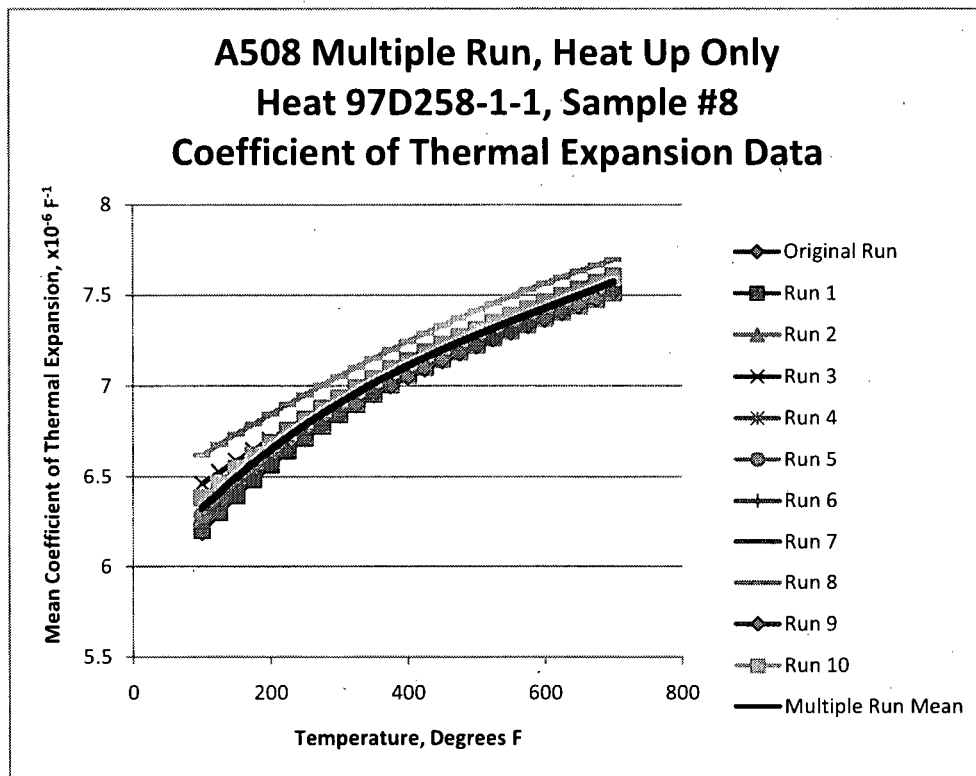


Figure 3-25 A508, Heat 97D258-1-1, Sample 8 Multiple Testing

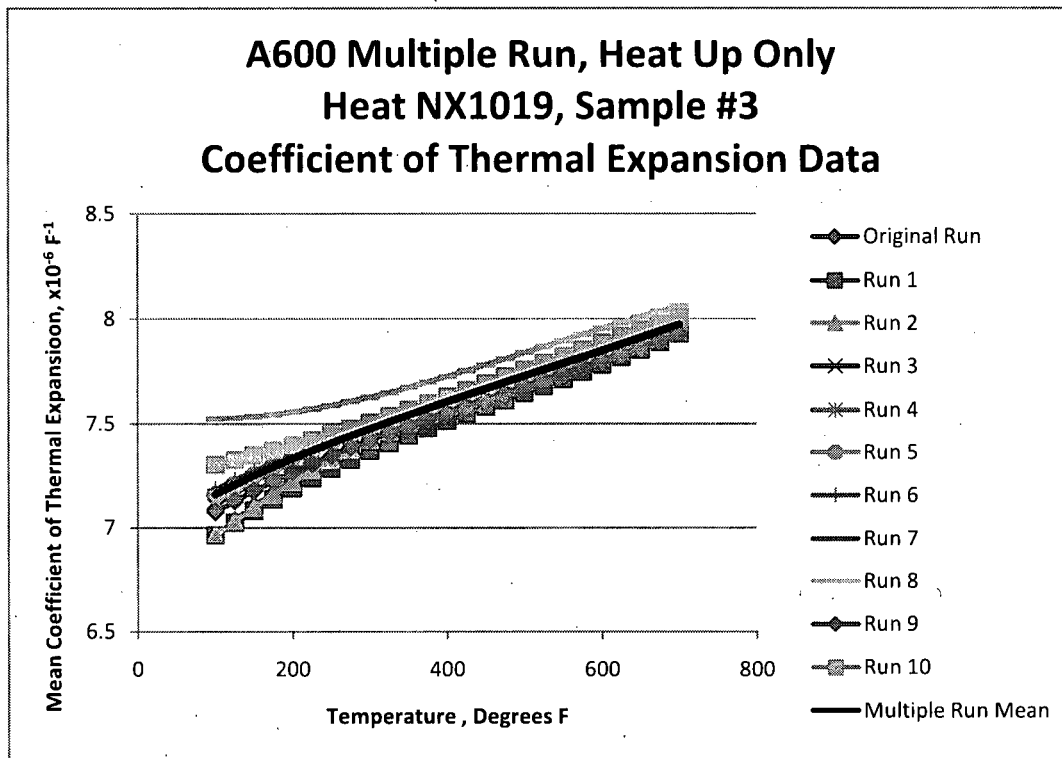


Figure 3-26 A600, Heat NX1019, Sample 3 Multiple Testing

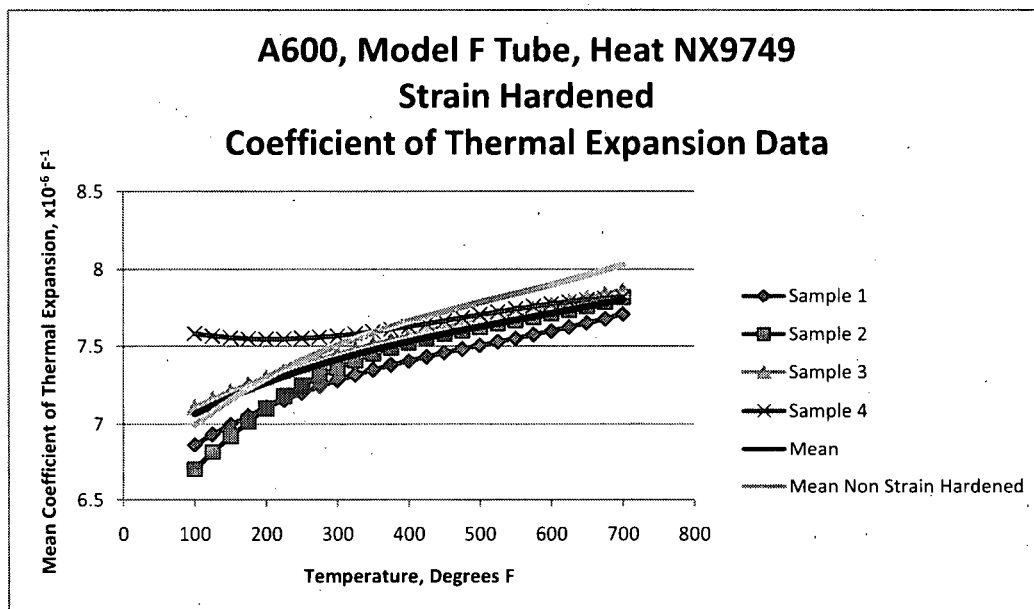


Figure 3-27 Heat-Up Tests of Strain Hardened A600 Model F Tubing, Heat NX9749

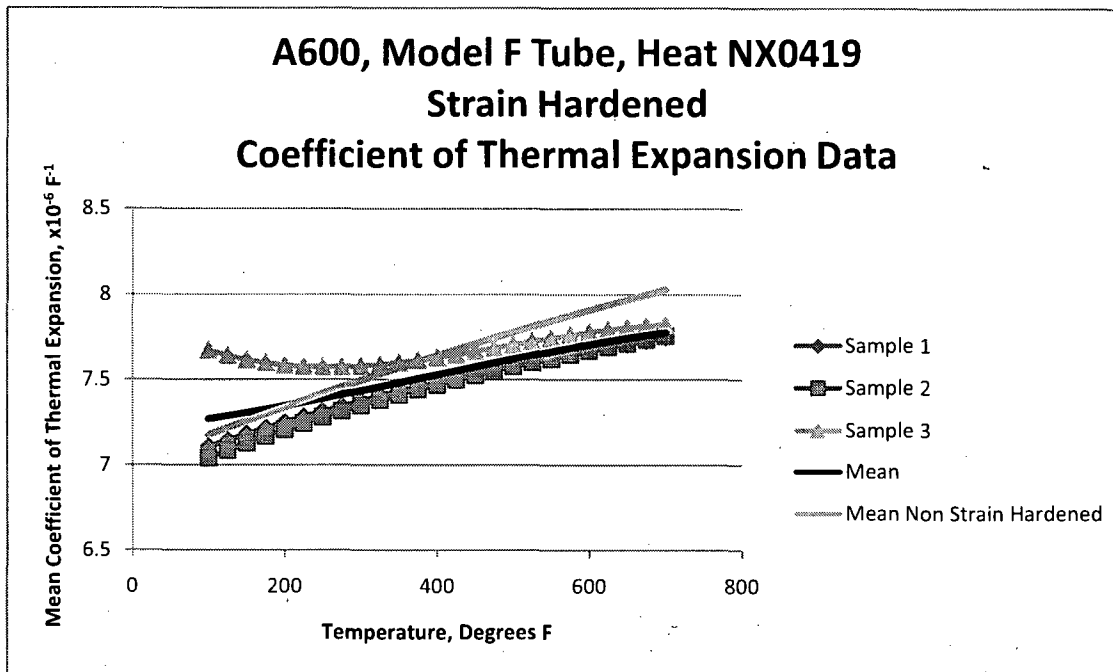


Figure 3-28 Heat-Up Tests of Strain Hardened A600 Model F Tubing, Heat NX0419

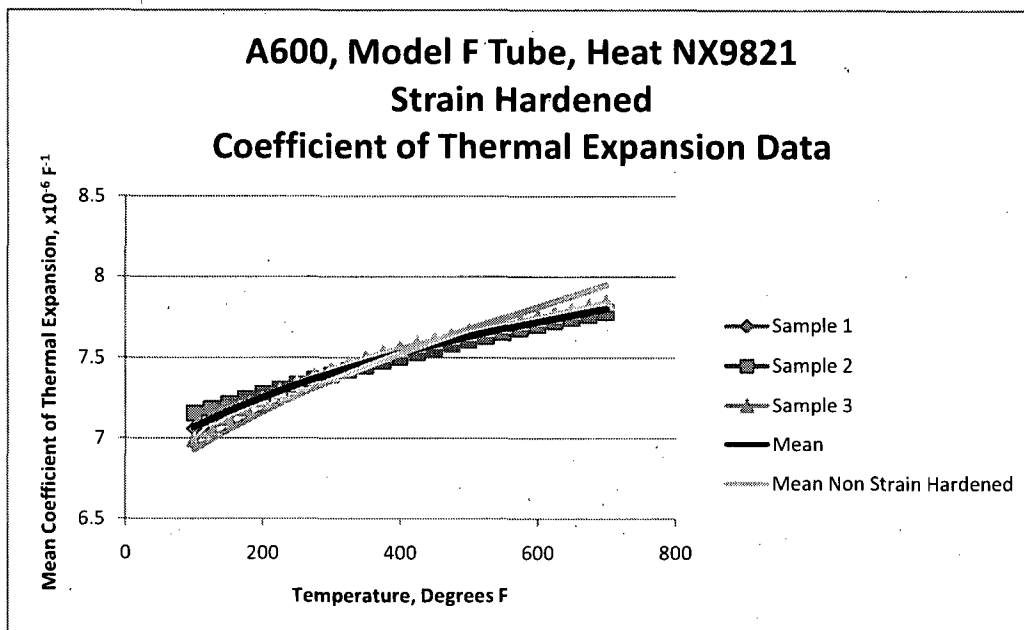


Figure 3-29 Heat-Up Tests of Strain Hardened A600 Model F Tubing, Heat NX9821

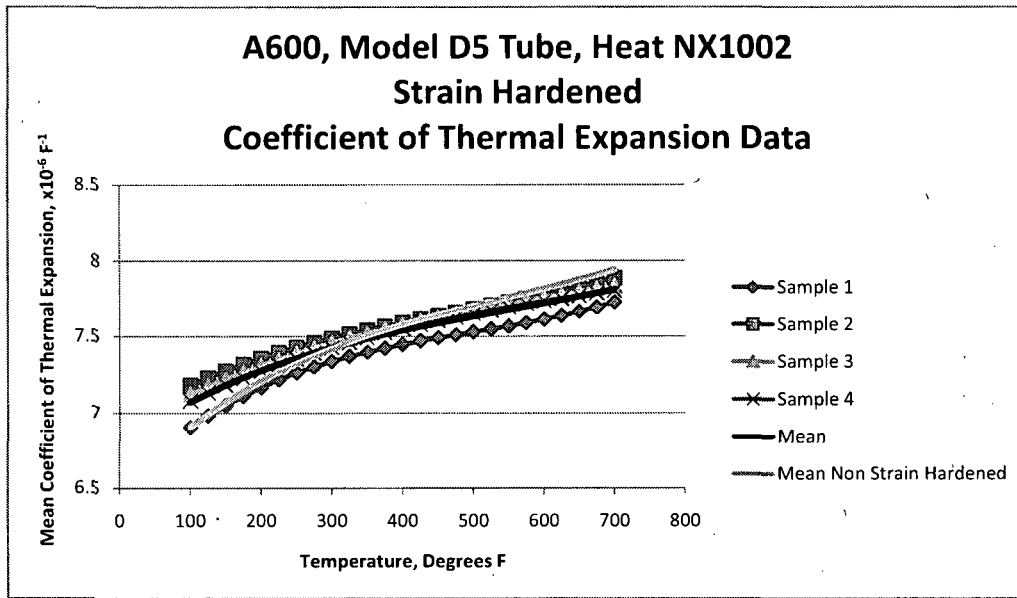


Figure 3-30 Heat-Up Tests of Strain Hardened A600 Model D5 Tubing, Heat NX1002

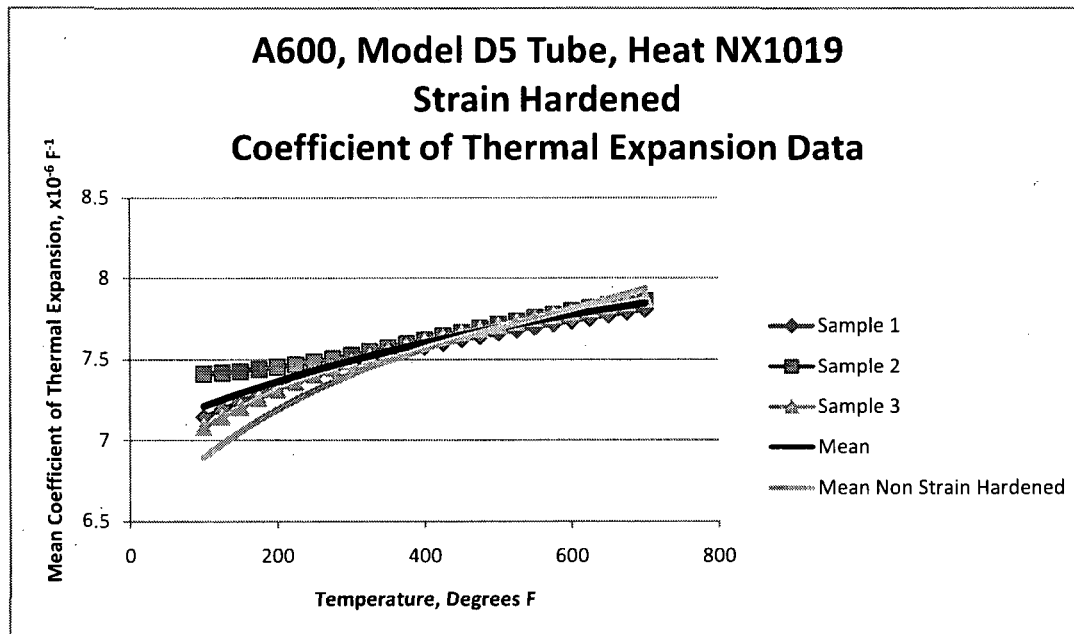


Figure 3-31 Heat-Up Tests of Strain Hardened A600 Model D5 Tubing, Heat NX1019

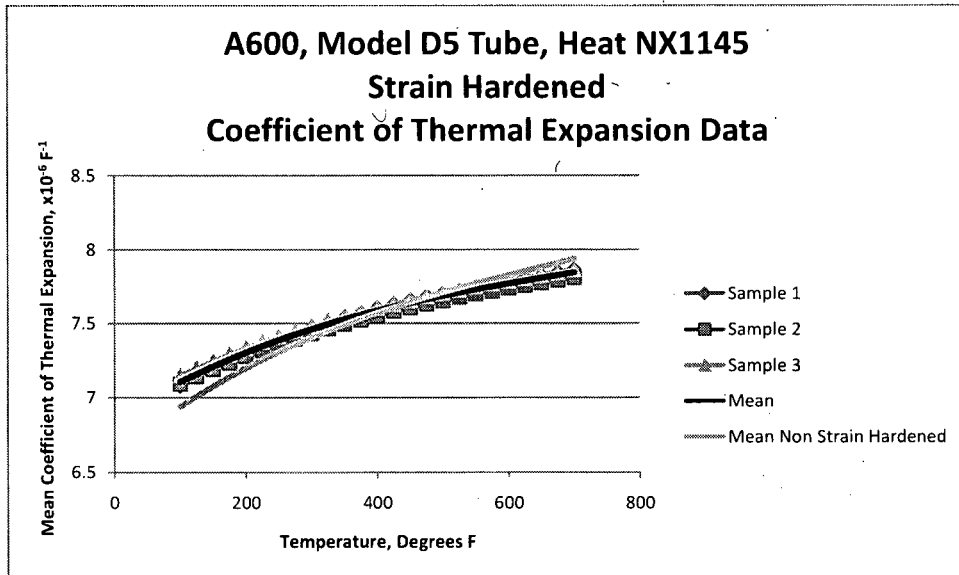


Figure 3-32 Heat-Up Tests of Strain Hardened A600 Model D5 Tubing, Heat NX1145

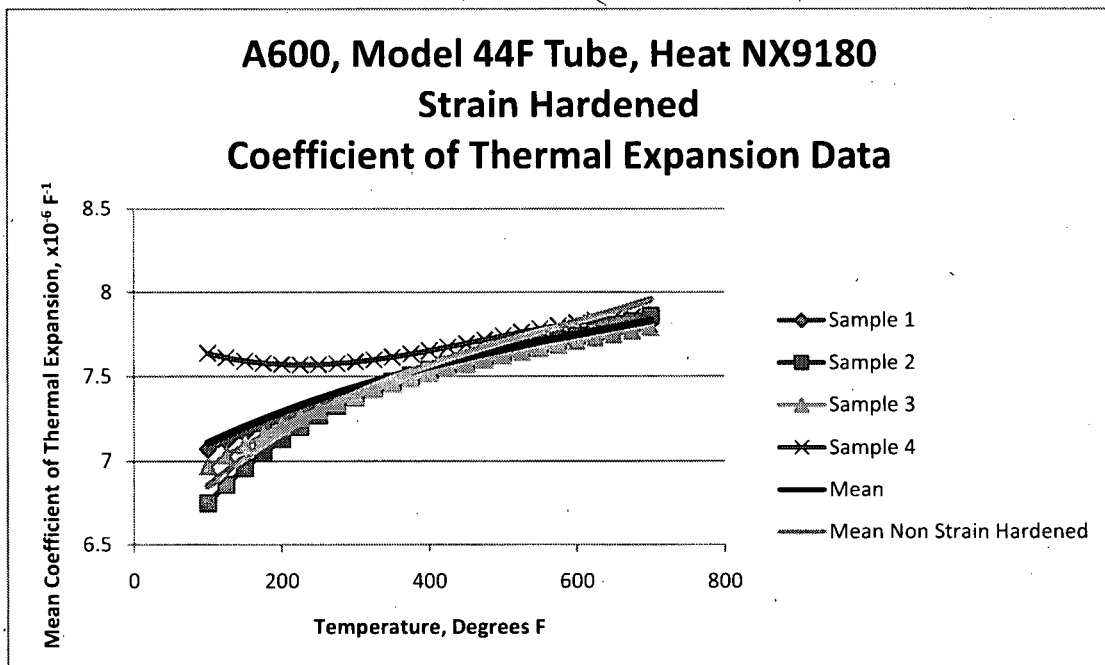


Figure 3-33 Heat-Up Tests of Strain Hardened A600 Model 44F Tubing, Heat NX9180

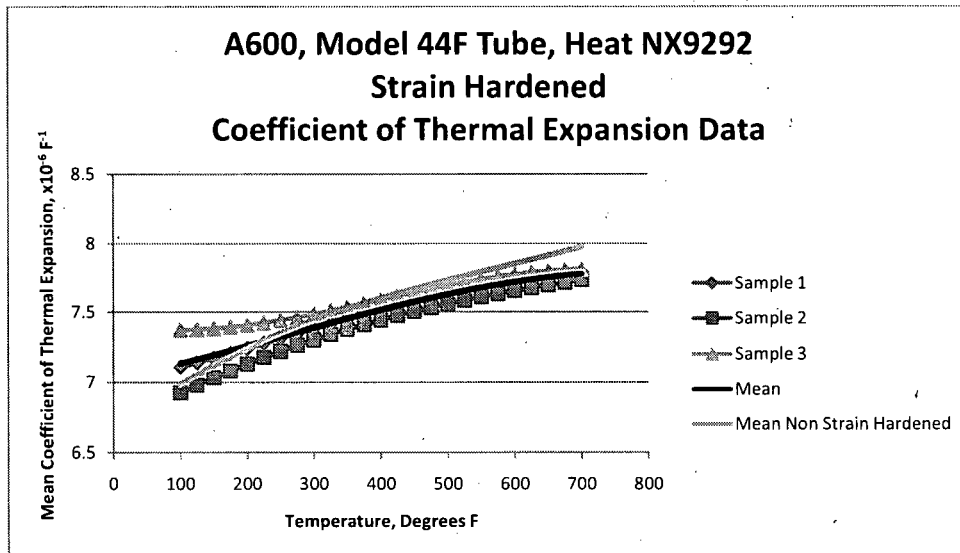


Figure 3-34 Heat-Up Tests of Strain Hardened A600 Model 44F Tubing, Heat NX9292

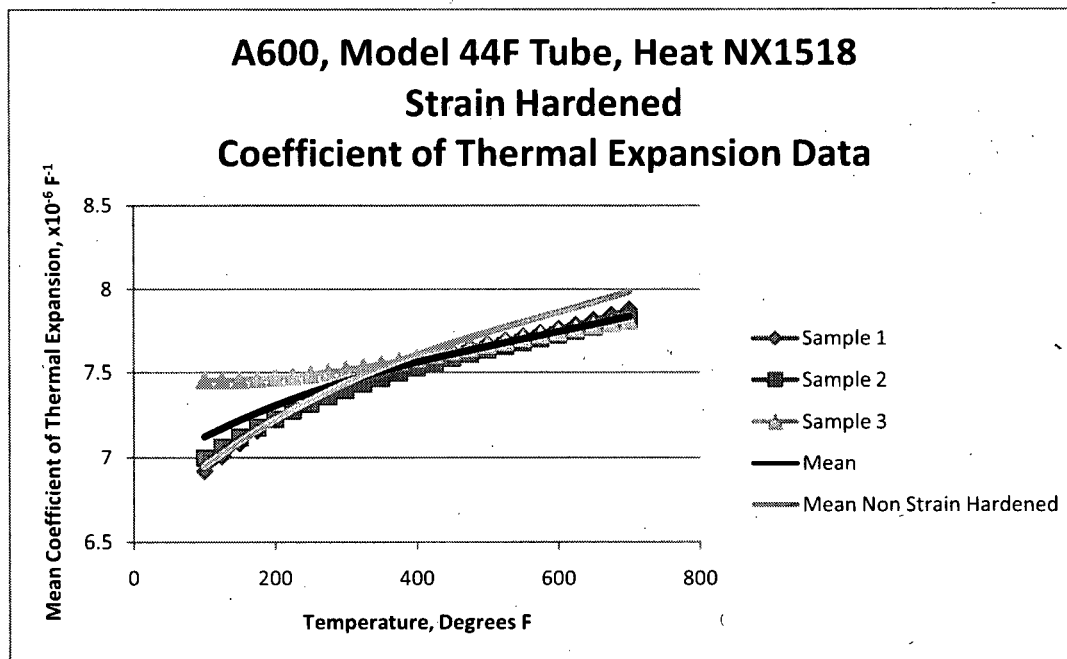


Figure 3-35 Heat-Up Tests of Strain Hardened A600 Model 44F Tubing, Heat NX1518

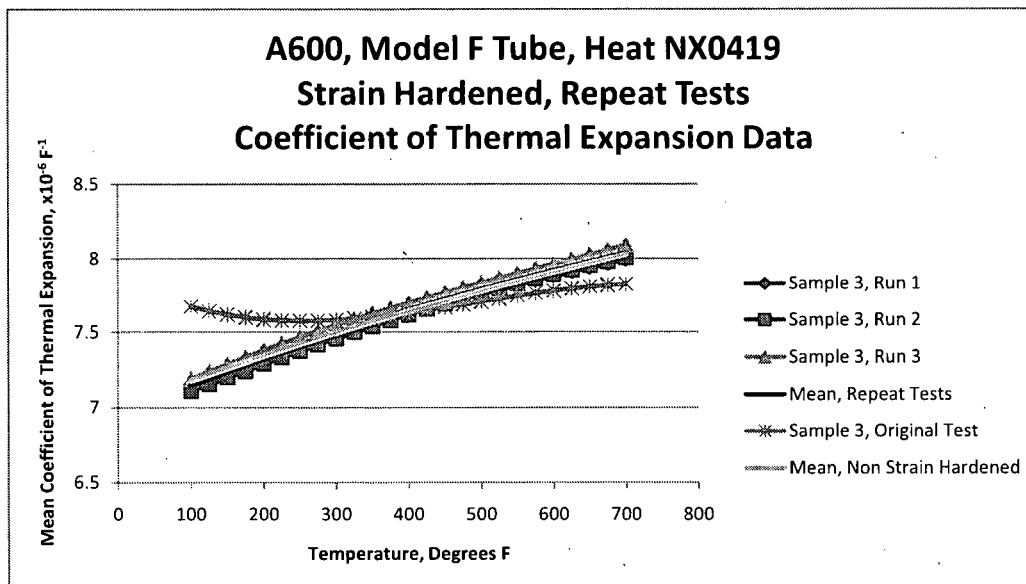


Figure 3-36 A600 Model F Tube, Heat NX0419, Repeat Test

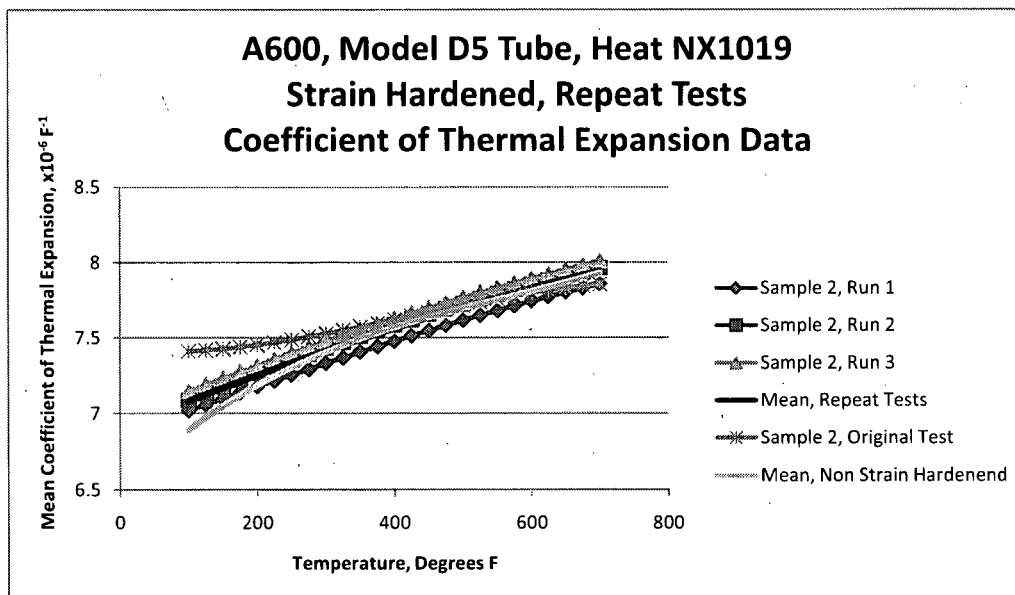


Figure 3-37 A600 Model D5 Tube, Heat NX1019, Repeat Test

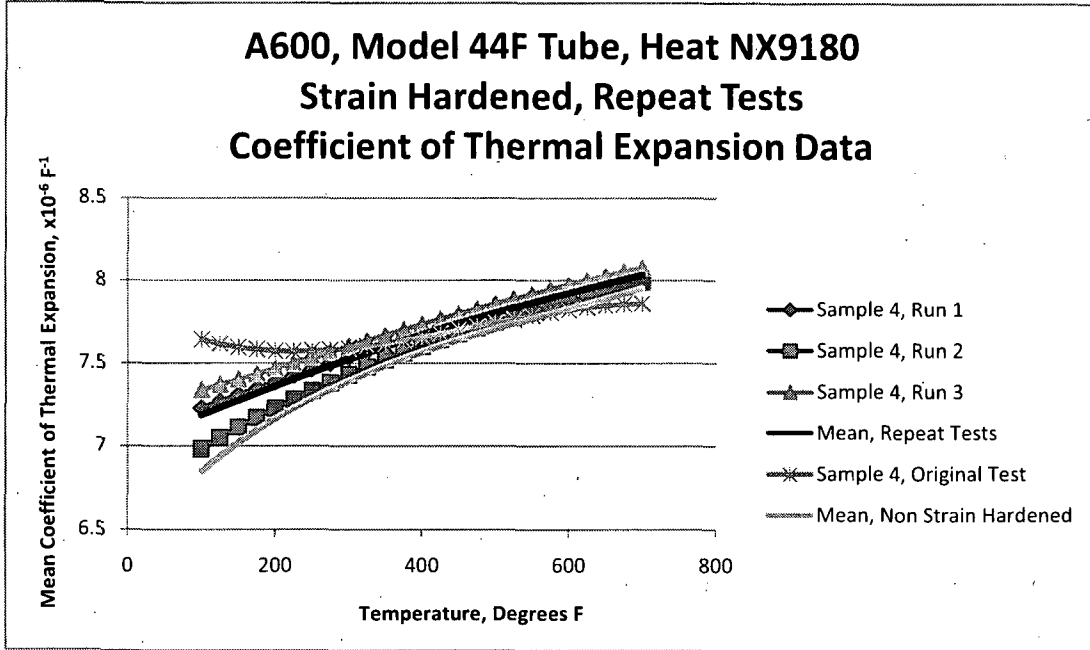


Figure 3-38 A600 Model 44F Tube, Heat NX9180, Repeat Test

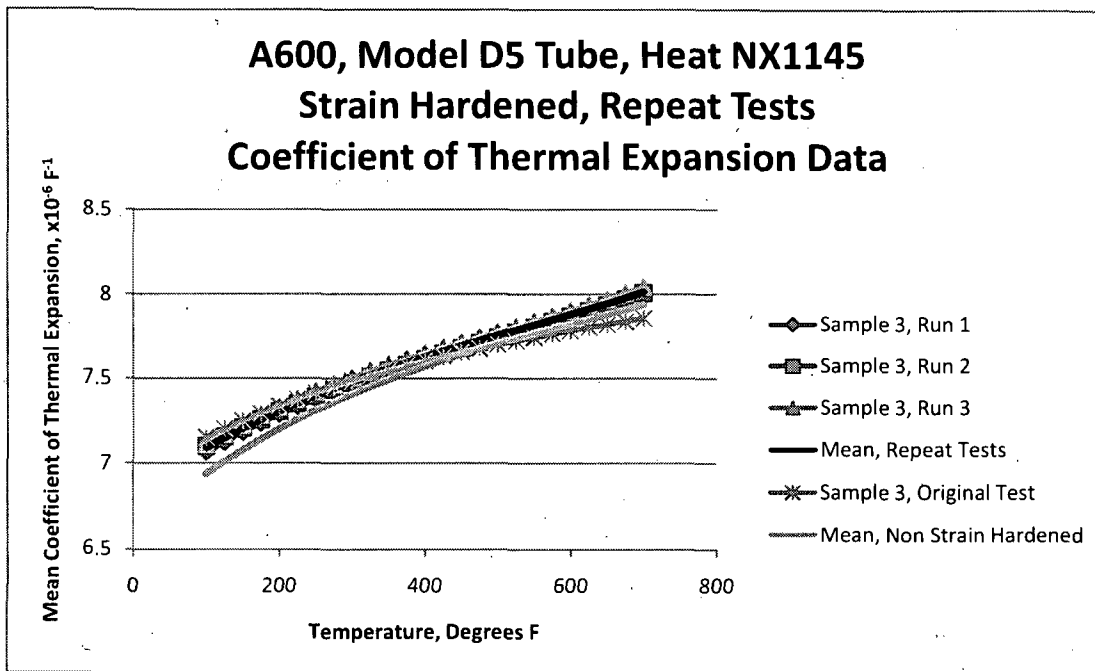


Figure 3-39 A600 Model D5 Tube, Heat NX1145, Repeat Test

4.0 STRUCTURAL AND LEAKAGE INTEGRITY ACCEPTANCE CRITERIA

As noted in NEI 97-06, Rev. 2 (Reference 4-1), the steam generator (SG) performance criteria identify the standards against which tube integrity is to be measured. Meeting the three performance criteria – structural integrity, accident-induced leakage and operational leakage – provides reasonable assurance that the SG tubing will remain capable of fulfilling the specific function of maintaining reactor coolant pressure boundary integrity throughout each operating cycle.

The structural integrity performance criterion from Reference 4-1 is:

“All in-service steam generator tubes shall retain structural integrity over the full range of normal operating conditions (including startup, operation in the power range, hot standby, and cooldown and all anticipated transients included in the design specification) and design basis accidents. This includes retaining a safety factor of 3.0 against burst under normal steady-state full power operation primary-to-secondary pressure differential and a safety factor of 1.4 against burst applied to the design basis accident primary-to-secondary pressure differentials. Apart from the above requirements, additional loading conditions associated with the design basis accidents, or combination of accidents in accordance with the design and licensing basis, shall be evaluated to determine if the associated loads contribute significantly to burst or collapse. In the assessment of tube integrity, those loads that do significantly affect burst or collapse shall be determined and assessed in combination with the loads due to pressure with a safety factor of 1.2 on combined primary loads and 1.0 on axial secondary loads.”

The accident-induced leakage performance criterion from Reference 4-1 is:

“The primary-to-secondary accident-induced leakage rate for all design basis accidents, other than the steam generator tube rupture, shall not exceed the leakage rate assumed in the accident analysis in terms of total leakage rate for all steam generators and leakage rate for the individual steam generator. Leakage is not to exceed 1.0 gpm per SG, except for specific types of degradation at specific locations as documented in the Steam Generator Program technical specifications.”

The operational leakage performance criterion from Reference 4-1 is:

“The reactor coolant system (RCS) operational primary-to-secondary leakage through any one steam generator shall be limited to 150 gallons per day.”

Reference 4-2 provides guidance for implementing NEI 97-06 and, thus, meeting the integrity assessment performance criteria described in NEI 97-06. This document reflects current industry practices and represents an acceptable method for integrity assessment.

Since 2003, an alternate repair criterion (ARC) titled H* has been under development and Nuclear Regulatory Commission (NRC) review. The key technical issues have been: 1) the acceptance criterion for H*, 2) the methodology for demonstrating an acceptable probability of meeting the acceptance criterion, and 3) the methodology for addressing primary-to-secondary leakage during postulated design

basis accident (DBA) conditions. The acceptance criteria for the alternate repair criteria for hydraulically expanded tube joints are based on current industry SG guidelines and are discussed in detail below.

The program elements described in Reference 4-1 provide guidance on structuring steam generator programs to meet the challenges posed by SG tube degradation. The EPRI Guidelines that form the basis of the SG program requirements are:

- PWR Steam Generator Examination Guidelines
- PWR Primary-to Secondary Leak Guidelines
- PWR Secondary Water Chemistry Guidelines
- PWR Primary Water Guidelines
- Steam Generator Integrity Assessment Guidelines
- Steam Generator In-situ Pressure Testing Guidelines

The Steam Generator Integrity Assessment Guideline document is used to develop the requirements and methodology used to meet the performance criteria defined in NEI 97-06, Rev. 2.

The availability of TSTF-449, Rev. 4, "Steam Generator Tube Integrity," was announced in the Federal Register on May 6, 2005 as part of the NRC Staff consolidated line item improvement process (CLIP). By letter dated September 3, 2005, the NRC Staff agreed with the observation that NEI 97-06, Rev. 2, "Steam Generator Program Guidelines," is consistent with Technical Specification Task Force Traveler (TSTF 449, Rev. 4) and that the adoption of TSTF-449 by all pressurized water reactors (PWRs) will result in an improved regulatory framework.

Based on the above, it is concluded that compliance with the requirements and methodologies described in NEI 97-06, Rev. 2 and the EPRI guideline documents represents the best path for regulatory approval of the proposed alternate repair criterion, H*.

4.1 STRUCTURAL INTEGRITY ACCEPTANCE CRITERIA

The primary justification of H* is the completion of a semiprobabilistic, whole bundle H* depth calculation using a three-dimensional finite element analysis (3D FEA) structural model for calculating tubesheet displacement. A mean H* value is calculated for selected radii throughout the tube bundle to represent the tube structural limit along with the consideration of appropriate uncertainties in the input parameters and material properties that affect tubesheet displacements and, therefore, the H* pull out length. The uncertainties considered in the analysis include residual contact pressure and material properties such as Young's Modulus and the coefficient of thermal expansion of the tube and the tubesheet. Residual contact pressure (the contact pressure resulting from only the hydraulic expansion process) is assumed to be zero for this analysis, although prior and in-progress tests show that there is a positive value of residual contact pressure. An uncertainty assessment for residual contact pressure is provided that includes the effects of variation in material yield strength, initial gap between the tube and the tubesheet before hydraulic expansion, hydraulic expansion pressure variation, and strain hardening (see Section 7.0 of this report for more detail). It is noted that assuming the residual contact pressure to

be zero is a significant conservatism in this analysis; any positive value of residual contact pressure will reduce the value of H^* .

All tubes in the SG tube bundle are shown to have an H^* value from the top of the tubesheet with a 0.95 probability with 50 percent confidence (see Section 8.0) of meeting the structural integrity performance criteria (SIPC) margin requirements as defined in NEI 97-06, Rev. 2. H^* values are calculated for normal operating, postulated steam line break and feedwater line break conditions. Section 5.0 of this report provides the rationale for not considering the locked rotor and control rod ejection events in the calculation of the H^* value.

Tube burst cannot occur within the thickness of the tubesheet. Therefore, tube pull out is the structural failure mode of interest in the development of the H^* criterion since the tubes are radially constrained against axial fish-mouth rupture by the presence of the tubesheet. Because burst cannot occur in the tubesheet region, the structural criteria from Reference 4-2 do not directly address tube degradation in the tubesheet expansion region. However, absent other directly applicable criteria, the NRC Staff has, in prior reviews of H^* justification submittals, treated failure to meet H^* equivalent to burst.

The axial force that could produce pull out derives from the tube end cap loads due to primary-to-secondary pressure differentials associated with normal operating and design basis accident conditions. The NRC Staff, in its approval of a 17 inch non-permanent H^* (Reference 4-4), has accepted that it is adequate to determine the required engagement distance on the basis of maintaining a factor of three (3) against tube pull out under normal operating conditions and a factor of 1.4 against pull out under accident conditions. Given that the H^* distance of each individual tube has a certain probability of not meeting the performance criteria, it must be verified that the probability of any tube in the bundle in the faulted loop failing to meet the performance criteria is less than 0.05 with 50 percent confidence.

Because failure to meet H^* is interpreted as being equivalent to burst, the criteria applied for H^* justification are extremely conservative. The probability of a single tube failing to meet the H^* distance is extremely small because, for a Model F SG, each bundle contains 5626 tubes and the entire bundle is shown to meet H^* at the 0.95 probability. Failure to meet H^* (pull out) is defined as small incremental motion, such that a postulated tube severance may be slightly above the defined H^* distance, and not complete separation of the tube from the tubesheet. Because there is no possibility of burst of the tube within the tubesheet, and because the factors of safety of three (3) on the normal operating loads and 1.4 on design basis accident loads are already included in the justification of H^* , failure to meet H^* has negligible impact on the primary pressure boundary. Indeed, the H^* justification is based on meeting the probabilistic criteria above without any slippage.

4.2 PRIMARY-TO-SECONDARY LEAKAGE ACCEPTANCE CRITERIA

Industry guidelines (Reference 4-2) permit application of either a deterministic approach or a probabilistic approach that satisfies the limit requirements for the accident-induced limiting performance criterion (AILPC) of at least 0.95 at 50 percent confidence.

Upon implementation of the H^* criterion, the existence of 100 percent through-wall cracks will be assumed below the H^* depth because no inspections of the tube below H^* will be required. Therefore, the potential for leakage of primary coolant through the crack and through the hydraulically expanded

joint between the tubes and tubesheet to the secondary system must be evaluated. A detailed leakage prediction model has been developed in support of the H* criterion that considers the resistance to leakage within the thickness of the tubesheet. The model is based on the Darcy flow equation, which is described in detail in Section 9.0 of this report. The NRC Staff has noted that the use of the Darcy equation, which states that leakage is proportional to the applied pressure differential, is conservative relative to other alternative models such as the Bernoulli or orifice models, which assume leak rate to be proportional to the square root of the differential pressure.

The original manifestation of the leakage analysis (Reference 4-3) was known as B*. In lieu of the original B* approach, which required the definition of a leak loss coefficient, the margin against leakage during an accident event is now defined by developing the ratio of accident-induced leakage to normal operating leakage by the following process (see Section 9.0 for a detailed discussion):

1. Based on test data, show that the loss coefficient is constant under normal operating and design basis accident conditions.
2. Determine the ratio of design basis accident pressure differential to normal operating pressure differential.
3. Multiply the pressure differential ratio by the ratio of the dynamic viscosity (μ_{NOP}) during normal operating conditions to dynamic viscosity during accident conditions (μ_{DBA}).
4. Multiply the result of Item 3 by the ratio of effective flow path length (l_{NOP}) under normal operating conditions to effective flow path length under steam line break conditions (l_{DBA}).

The effective flow path length is the crevice length, above the H* distance, over which there is contact between the tube and the tubesheet. It has been shown by the 3D FEA for the Model F SGs (Section 6.0) that contact between the tubes and the tubesheet is assured during all plant conditions for each tube through the entire length of the tubesheet thickness. Therefore, the effective flow path length ratio, $l_{\text{NOP}}/l_{\text{DBA}}$, above the H* length for each transient condition that models primary-to-secondary leakage is 1.0.

For a postulated design basis accident, the expected increase in leakage is a function of only the increase in pressure differential that occurs across the tubesheet during the plant transient and the change in dynamic viscosity. Plant-specific leak rate factors have been developed for each of the H* plants and are included within this report in Section 9.0.

For the condition monitoring assessment, the component of leakage from below the H* distance observed during the prior cycle will be added to that from all other sources and compared to the allowable leakage limit for each design basis accident that models primary-to-secondary leakage. For the operational assessment, the difference in leakage from each design basis accident analysis assumption used in the plant's Final Safety Analysis Report (FSAR) and the accident leakage from all other sources will be divided by the leakage factor for the appropriate design basis accident and compared to the observed operational leakage and, if the result is less than the observed leakage, an administrative limit (for operational leakage) will be established not to exceed the calculated value.

4.3 REFERENCES

- 4-1 NEI 97-06, Rev. 2, "Steam Generator Program Guidelines," Nuclear Energy Institute, Washington, DC, May 2005.
- 4-2 Steam Generator Integrity Assessment Guidelines: Revision 2, EPRI, Palo Alto, CA, 1012987, July 2006.
- 4-3 WCAP-15932-P (Proprietary), Revision 1, "Improved Justification of Partial-Length RPC Inspection of the Tube Joints of Model F Steam Generators of Ameren-UE Callaway Plant," Westinghouse Electric Company LLC, Pittsburgh, PA, May 2003.
- 4-4 USNRC; Safety Evaluation by the Office of Nuclear Regulation Related to Amendment No. 150 to Facility Operating License No. NPF-37, Amendment No. 150 to Facility Operating License No. NPF-66---IARC SER, Amendment No. 144 to Facility Operating License No. NPF-72, and Amendment No. 144 to Facility Operating License No. NPF-77; Exelon Generating Company, LLC, Byron Station, Unit Nos. 1 and 2, Braidwood Station Units 1 and 2; Docket Nos. STN 50-455, STN 50-456 and STN 50-457; April 2007.

5.0 PLANT OPERATING CONDITIONS AND LOADINGS (MODEL F)

5.1 NORMAL OPERATING CONDITIONS AND LOADINGS

Table 5-1 provides values for the current steam generator (SG) thermal-hydraulic parameters during normal operating conditions for each of the H* plants with Model F SGs. These conditions are used to establish the H* distances and to determine overall leakage factors identified in this report for each plant.

5.2 FAULTED CONDITIONS

Each of the faulted events are considered in this section and are described below. These include: steam line break (SLB), feedwater line break (FLB), locked rotor (LR) and control rod ejection (CRE). The transient response curves for these events are included in Section 9.0 of this report.

Previous analyses have shown that FLB and SLB are the limiting faulted conditions, with tube lengths required to resist push out during a postulated loss-of-coolant accident (LOCA) typically less than one-fourth of the tube lengths required to resist pull out during FLB and SLB (References 5-1 and 5-2). Therefore, LOCA was not considered in the H* analysis.

5.2.1 Feedwater Line Break and Steam Line Break

In accordance with plant emergency operating procedures, it is expected that the operator would take action following a high energy secondary line break to stabilize the reactor coolant system conditions. The expectation for a SLB or FLB with credited operator action is to stop the system cooldown through isolation of the faulted SG and control temperature by the auxiliary feedwater system. Steam pressure control would be established by either the SG safety valves or control systems via steam dump or the atmospheric relief valves. For any of the steam pressure control options, the maximum temperature would be approximately the no-load temperature and would be well below the normal operating temperature for the plant. Subsequently, the operator would initiate a cooldown and depressurization of the reactor coolant. The peak pressure differential and asymptotic temperatures from the design specification transients are used in the structural analysis. The pertinent parameters for these transients are described in Tables 5-2 and 5-3.

5.2.2 Locked Rotor

This accident is based on the instantaneous seizure of the reactor coolant pump with the plant operating at full power¹. The locked rotor can occur in any loop. Reactor trip occurs almost immediately, as a result of low coolant flow in the affected loop. Following the trip, heat stored in the fuel rods continues to pass into the core coolant causing the coolant to expand. The rapid expansion of the coolant in the reactor core, combined with the reduced heat transfer to the secondary system, causes an in-surge into the pressurizer and a pressure increase throughout the reactor coolant system. The in-surge into the pressurizer compresses the steam volume, actuates the automatic spray system, opens the power-operated relief valves (PORVs), and eventually opens the pressurizer safety valves in that sequence. The two PORVs are designed for reliable operation and would be expected to function properly during the accident. Because of the short duration of the transient, the temperatures in the hot and cold leg of the SG and secondary side that correspond to the maximum pressure differential during the locked rotor event design basis accident are used in the structural and leakage analysis. The pertinent parameters of this transient are listed in Table 5-4.

5.2.3 Control Rod Ejection

This accident is based on the single-most reactive control rod being instantaneously ejected from the core. This reactivity insertion in a particular region of the core causes a severe pressure increase in the reactor coolant system such that the pressurizer safety valves will lift and also causes a more severe temperature transient in the loop associated with the affected region than in the other loops. For conservatism, the analysis is based on the reactivity insertion and does not include the mitigating effects (on the pressure transient) of coolant lowdown through the hole in the vessel head vacated by the ejected rod. Like the locked rotor transient, because of the short duration of the transient, the temperatures in the hot and cold legs of the SG and secondary side that correspond to the maximum pressure differential during the design basis accident are used in the structural and leakage analysis. The pertinent parameters of this transient are listed in Table 5-5.

¹ Two of the plants with Model F SGs assume that a SG power operated relief valve (PORV) becomes stuck open following a locked rotor event. For one plant, all the initial secondary side fluid, plus the feedwater flow and the primary coolant leakage for the first 20 minutes, is assumed to be released to the atmosphere. The affected SG is isolated, by operator action, to close the isolation valve upstream of the relief valve within 20 minutes. For both plants, the flow area through the stuck-open PORV is less than the flow area from a doubled-ended steam line break. From a primary-to-secondary leakage perspective, it is judged that the SLB/FLB leakage factor would bound the leakage factor for a locked rotor with a stuck-open SG PORV because the pressure differential across the tubesheet during a postulated SLB/FLB is larger than a locked rotor event. An engineering judgment is made on the outcome of the locked rotor transient with a stuck open PORV because it is not modeled in the design specification of the affected plants.

5.3 CALCULATION OF APPLIED END CAP LOADS

The tube pull out loads² (also called end cap loads) to be resisted during normal operating (NOP) and faulted conditions for the bounding Model F plant (Millstone Unit 3) for the hot leg are shown below. End cap load is calculated by multiplying the required factor of safety times the cross-sectional area of the tubesheet bore hole times the primary side to secondary side pressure difference across the tube for each plant condition.

Operating Condition	ΔP (psi) ($P_{pri}-P_{sec}$)	Area (in ²) (Note 1)	End Cap Load (lbs.)	Factor of Safety	H* Design End ap Load (Lbs.)

The above calculation of end cap loads is consistent with the calculations of end cap loads in prior H* justifications and in accordance with the applicable industry guidelines (Reference 5-3). This approach results in conservatively high end cap loads to be resisted during NOP and faulted conditions because a cross-sectional area larger than that defined by the tubesheet bore mean diameter is assumed.

The faulted condition end cap loads will not vary from plant to plant among the Model F population for the postulated FLB for 3- and 4-loop plants because the specified transient for both is the same. The value for end cap load for a 3-loop plant is different than the value for a 4-loop plant for a postulated SLB event and is also provided above. The values vary only slightly for the locked rotor event and control rod ejection event from plant to plant (see Table 5-6).

The end cap loads noted above include a safety factor of 3 applied to the normal operating end cap load and a safety factor of 1.4 applied to the faulted condition end cap loads to meet the associated structural performance criteria consistent with NEI 97-06, Rev. 2 (Reference 5-3).

Seismic loads have also been considered, but they are not significant in the tube joint region of the tubes (Reference 5-1).

H* values are not calculated for the locked rotor and control rod ejection transients because the pressure differential across the tubesheet is bounded by the FLB/SLB transient. For plants that have a locked rotor

² The values for end cap loads in this subsection of the report are calculated using an outside diameter of the tube equal to the mean diameter of the tubesheet bore plus 2 standard deviations.

with stuck open PORV transient included as part of the licensing basis, this event is bounded by the FLB/SLB event because the peak pressure during this transient is significantly less than that of the SLB/FLB transient.

In support of the leakage analysis provided in Section 9.0, the parameters included in Tables 5-1 through 5-5 are used to compare contact pressures during normal operating plant conditions and all design basis accident conditions for all radial locations throughout the thickness of the tubesheet.

5.4 REFERENCES

- 5-1 CN-SGDA-02-152, Rev. 1 (Proprietary), "Evaluation of the Tube-to-Tubesheet Contact Pressures for Callaway Model F Steam Generators," Westinghouse Electric, Pittsburgh, PA, March 2003.
- 5-2 CN-SGDA-03-133 (Proprietary), Rev. 0, "Evaluation of the H* Zone Boundaries for Specific Model D5 and Model F Steam Generators," Westinghouse Electric, Pittsburgh, PA, October 2003.
- 5-3 NEI 97-06, Rev. 2, "Steam Generator Program Guidelines," Nuclear Energy Institute, Washington, DC, May 2005.

Table 5-1 Operating Conditions - Model F H* Plant

Parameter and Units	Plant					
	Salem Unit 1 ⁽¹⁾	Millstone Unit 3 ⁽²⁾	Seabrook Unit 1 ⁽³⁾	Vogtle Units 1 and 2 ⁽⁴⁾	Wolf Creek ⁽⁵⁾	Vandellos II ⁽⁶⁾

a,c,e

Table 5-2 Steam Line Break Conditions

Parameters and Units	Salem Unit 1	Millstone Unit 3	Seabrook Unit 1	Vogtle Units 1 and 2	Wolf Creek	Vandellos II ⁽¹⁾

a,c,e

Table 5-3 Feedwater Line Break Conditions³

a,c,e

Parameters and Units	Salem Unit 1	Millstone Unit 3	Seabrook Unit 1	Vogtle Units 1 and 2	Wolf Creek	Vandellos II

Table 5-4 Locked Rotor Event Conditions

Parameters and Units	Salem Unit 1	Millstone Unit 3	Seabrook Unit 1	Vogtle Units 1 and 2	Wolf Creek	Vandelllos II

a,c,e

Table 5-5 Control Rod Ejection

Parameters and Units	Salem Unit 1	Millstone Unit 3	Seabrook Unit 1	Vogtle Units 1 and 2	Wolf Creek	Vandellors II	a,c,e

Table 5-6 Design End Cap Loads for Normal Operating Plant Conditions, Locked Rotor and Control Rod Ejection for Model F Plants

Plant	Low T_{avg} End Cap Load w/Safety Factor (lbf)	High T_{avg} End Cap Load w/Safety Factor (lbf)	Locked Rotor End Cap Load (lbf)	Control Rod Ejection End Cap Load (lbf)

a,c,e

6.0 STRUCTURAL ANALYSIS OF THE TUBE-TO-TUBESHEET JOINT

The H* structural analysis consists of four separate models as shown in the process description in Section 1.0. Tubesheet deflections are calculated using a three-dimensional finite element analysis (3D FEA) model. The tubesheet displacements are input to an MS Excel® spreadsheet model (Figure 1-1, H* Analysis Process for H*). The spreadsheet model calculates the contact pressure between the tubes and the tubesheet as a function of radial and axial position in the tubesheet. The contact pressure is transformed into an axial pull out resistance through friction and shear between the tube outside diameter (OD) surface and the tubesheet tube bore inside diameter (ID) surface. The pull out resistance is integrated as a function of axial position and compared to the applied end cap loads and axial forces. The axial distance below the top of the tubesheet (TTS) where the axial pull out resistance is equal to or greater than applied pull out forces is the calculated H* depth. In the following discussions, the structural analysis will commonly be referred to as the contact pressure analysis.

The third model is an Microsoft Excel® spreadsheet model that calculates the residual contact pressures (RCP) from the available pull out test data and provides the RCP as input to the H* Integrator model. In the current application, RCP is assumed to be zero (0 psi) and the RCP model is not utilized. A fourth finite element model is utilized to calculate the variability influence factors for residual contact pressure. Additional finite element models and results are used to support the H* analysis. Supporting analyses were performed to address specific issues such as definition of the “worst tube” in the bundle, tubesheet bore dilation effects on contact pressure, etc., that validate the use of the 3D FEA model.

The structural analysis for H* has evolved since the Wolf Creek License Amendment request in 2006 (see References 6-16 and 6-20). This evolution resulted from a number of studies that utilized the state-of-the-art structural analysis methods to benchmark the methods utilized in the Wolf Creek request. This report section describes the technical basis of these models and the benchmarking analyses performed to test and validate the model results.

6.1 RESULTS SUMMARY

The H* structural analysis conservatively calculates the tubesheet deflections as input to the analysis of the contact pressure distribution between the tube and the tubesheet for an assumed length of tube in the limiting region of the steam generator (SG) bundle to resist the applied pull out forces. The limiting region of the tubesheet is defined as that region of the tubesheet in which the deflections are calculated to be maximized, resulting in the largest value of H*. The length of tubing considered is the predicted length required to equilibrate the design basis pull out forces. The results of the structural analysis, for the bounding Model F SG in the fleet, show that a length of []^{a,c} inches provides sufficient engagement length into the tubesheet to resist the applied pull out loads during normal operations and limiting faulted conditions, assuming that all input variables are at their mean value and the crevice pressure adjustment to the final tube length is excluded. Figure 6-1 shows the distribution of the mean H* values as a function of tubesheet radius in the limiting sector of the tubesheet. The applied pull out loads include the required safety margins prescribed in NEI-97-06, Rev. 2 (Reference 6-2) and the analysis of the operating conditions and design transients meets the requirements defined in the ASME Code (Reference 6-3). The mean analysis results for H* are referenced in Reference (6-39).



Figure 6-1 Mean H* Values for the Limiting Model F Plant

6.1.1 Introduction

The H* analysis determines the required engagement length of an SG tube into the tubesheet necessary to resist pull out forces. Pull out forces develop from the temperatures and pressures that occur during normal, upset and accident operating conditions in the SG (see Section 5.3 for the calculation of the applicable pull out forces). The pull out load on a tube is resisted by local tube thermal and pressure-induced deformations and contact that transfer the load on a tube to the surrounding tubesheet material in shear via friction forces. The ability of a tube to transfer the pull out loads to the tubesheet through friction is directly related to the magnitude of the contact pressure between the inner diameter of the tubesheet bore and the outer diameter surface of the tube.

The temperatures and pressures that develop the pull out forces on the tube also act to deform the SG tubesheet such that it will both expand in the radial direction and deflect in the transverse (thickness) direction. The deformations in the perforated region of the tubesheet affect the resistance of the SG tubes to the applied pull out loads because a deformation that acts to increase the tube-hole size relative to the initial undeformed tube-hole configuration will decrease the contact pressure between the tube and the tubesheet. The reverse is also true; a decrease in the tube hole size relative to the initial undeformed tube hole configuration will increase the contact pressure between the tube and the tubesheet. Other factors, such as Poisson contraction of the tube cross section and the potential for fluid to be present between the tube outer diameter and the tubesheet inner diameter, also affect the contact pressure. The distribution of the contact pressure between the tube and the tubesheet varies as a function of radial position in the tubesheet and elevation within the tubesheet.

The H* structural analysis that provides the tubesheet radial and axial deflections utilizes a 3D finite element model that is described in Section 6.2. Section 6.2.2 discusses the analysis input. Section 6.2.3

discusses the determination of the limiting region of the tubesheet with respect to the tube pull out resistance. Section 6.2.4 discusses the radius specific treatment of the local tubesheet stiffness in the H* structural model. Section 6.2.5 discusses the effects of tubesheet hole dilation on the leakage and structural aspects of the H* analysis. Section 6.2.6 discusses the modeling of the SG divider plate and how the potential for degradation of the divider welds is accounted for in the analysis. Section 6.3 discusses the effects of tubesheet rotation and deformation and Section 6.4 discusses how the previous results are used to calculate the tube-to-tubesheet contact pressure. Section 6.4 also discusses the benchmark models used to validate the 3D finite element model.

The contact pressure results presented in this section include detailed sensitivity studies on the effect of material variability, SG design variability, variability in SG tube installation, operating condition variability and the effect of SG structures, such as the divider plate, that can alter the deflection of the tubesheet and tube bore. The finite element models that support the contact pressure analysis were compared to an independent analysis created by Argonne National Laboratories (ANL) using a different FEA code (ABAQUS). The ANL ABAQUS models produced essentially the same results when similar input conditions were used. The results described in this report conservatively bound the requirements for both the hot leg and the cold leg in any Model F SG.

The contact pressure results in this report are based on a proven theory of elasticity model (Reference 6-18) that uses results from the supporting finite element analyses as input. The results of the theory of elasticity model were benchmarked using alternative finite element models and shown to be conservative (see Section 6.4.5).

6.1.2 Evolution and Development of the H* Structural Model

Prior analyses for H* (Reference 6-24) utilized a two-dimensional (2D) axisymmetric structural model to calculate tubesheet displacements. The 2D model results came from a linear superposition of unit loads. In the linear superposition method, unit loads, both thermal and pressure, were applied to obtain deflections that were then scaled with a ratio according to the applicable pressure and temperature conditions to obtain the results for specific conditions such as normal operating conditions (NOP) or accident loading conditions. Due to temperature differences between different structures in the lower SG complex on the order of []^{a,c,co}F or more, different deflection results are obtained when the reference case for the model is changed. For example, when the model is loaded with pressures and temperatures similar to NOP conditions and those results are then scaled to represent steam line break (SLB) conditions, the results are different than when the model is directly loaded with pressures and temperatures similar to SLB. The discovery of this difference between the scaled results and the results of directly applying condition specific loads meant that new models were necessary to benchmark the 2D structural modeling approach. Further, although the 2D model was an axisymmetric model, this use of axisymmetry was questioned because of the presence of the uni-directional divider plate and tube lane. Questions were also raised about the effectiveness of the divider plate as a structural member. A three-dimensional (3D), non-axisymmetric, finite element analysis (FEA) model was created to benchmark the 2D model results. The initial goal of the 3D finite element model was to provide a comparison to the previously established 2D axisymmetric finite element model of the tubesheet, channelhead and stub barrel. The development of 3D FEA models to benchmark the 2D axisymmetric model led to the decision to replace the 2D model with the 3D FEA model.

The 3D FEA model was not initially considered as the reference analysis basis for H* because of a difficulty in obtaining the nodal outputs at the exact locations required by the H* integration routine. Therefore, the initial function of the 3D FEA model was to perform benchmark analyses to verify the results of the 2D axisymmetric model. However, processes were developed to overcome the node-matching issue with the H* integration routine during the continued evolution of the 3D FEA model. Because of this, and because the 2D axisymmetric model utilized the code WECAN (a finite element program that is no longer supported by Westinghouse or any other organization) a decision was made to adopt the state-of-the-art 3D FEA analysis model as the reference model for H* calculations.

The 3D finite element model allows for more detailed modeling of the lower SG complex than an axisymmetric finite element model. Some of the details that cannot be included in an axisymmetric finite element model are:

1. Tubesheet Tube Lane
2. Bearing/Support Pads
3. Divider Plate
4. Simultaneously Applied Hot Leg and Cold Leg Conditions

These non-axisymmetric features in the SG have a significant effect on the radial displacement of the tubesheet during all modeled plant operating conditions.

The force integration spreadsheet that is used to determine the H* distance was developed by assuming a radially and axially fixed nodal map of the tubesheet to provide a structured force integration and H* tubesheet mapping capability. The mesh for the perforated tubesheet region (the region of interest in the model) is seeded in a very specific fashion with []^{a,c,c} divisions over the radius of the tubesheet and []^{a,c,c} nodes through the thickness of the tubesheet. For example, Figure 6-6 shows a plot of the elements (also known as a screen shot) of a typical 2D axisymmetric finite element mesh of the lower SG complex without a tubesheet (TS) support ring.

The 3D model also has []^{a,c,c} horizontal divisions over the radial dimension and it also has []^{a,c,c} nodes through the thickness of the tubesheet in the region of interest. The 3D mesh is seeded without a bias at the top of the tubesheet (TTS) and the bottom of the tubesheet (BTS) but additional nodes are included in the model. The choice of higher order tetrahedral elements in the 3D perforated tubesheet region allows for interpolation of the tubesheet displacements at any elevation or radial location required.

The mesh density in both the 3D and the axisymmetric model was selected to produce a spatially converged result that gives a smooth radial displacement output in the perforated region of the tubesheet. Further refinement in the 3D finite element mesh did not yield a significant difference []^{a,c,c} in tubesheet displacement for the perforated region. [

Figure 6-7 shows a picture of a typical 3D finite element mesh of the lower SG complex with a tubesheet support ring.

The 3D finite element mesh was also defined azimuthally, with the mesh seeding at the 45° and 90° planes being equal to the mesh seeding and divisions at the 0° plane. See Figure 6-8 for a top plane view of the tubesheet mesh that shows the divisions at the 0°, 45° and 90° planes. See Figure 6-8 and Figure 6-9 for pictures of the rear of the 3D mesh.

There are a total of []^{a,c,c} solid higher order (10-node) tetrahedral and higher order quadrilateral elements in a typical 3D finite element model of the Model F SG. There are []^{a,c,c} nodes in the 3D model for a total of []^{a,c,c} degrees of freedom. Plant-specific finite element models may have more or less nodes than a typical Model F, but, that does not affect the final results of the analysis.

6.1.2.1 Comparison of 2D and 3D Model Boundary Conditions

It is expected that the results from a 3D finite element analysis of the lower SG complex and those from a 2D axisymmetric analysis will yield different results. The 3D analysis is capable of responding more realistically to variations in the operating conditions and material properties. The tubesheet displacements calculated from the 3D analysis accurately reflect the applied loading conditions for the material properties used in the analysis.

The results in Sections 6.2.1 through 6.2.3 were not considered in the tube-to-tubesheet contact pressure analyses prior to 2008. This is because the effect of the non-axisymmetric structures and boundary conditions could not be included in the axisymmetric model used to analyze the tubesheet displacements due to thermal and pressure load effects. Similarly, the effect of the non-axisymmetric structures on the deformations of the tube bore could not be included in the analysis of the contact pressure. The prior axisymmetric finite element analysis used displacement, pressure and temperature boundary conditions that are different from the ones discussed in Sections 6.2.2.2.2 through 6.2.2.2.5. The following sections summarize the boundary condition differences between a 3D analysis and a 2D axisymmetric analysis of the lower SG complex.

6.1.2.1.1 Displacement Boundary Conditions

An axisymmetric model is “pinned” with respect to the radial direction along the central axis of the model. This means that all vertical and radial displacements are calculated with respect to a fixed central axis that cannot translate or deflect in any direction. In the case of a SG with a tubesheet support ring, this requirement will alter the displaced shape of the tubesheet due to thermal and pressure loads. This condition also increases the tubesheet bow in the case of a tubesheet without a tubesheet support ring. However, the contact pressure results generated from the 2D axisymmetric tubesheet model displacements have been shown to be conservative when compared to the results of a contact pressure analysis using 3D tubesheet model displacements.

6.1.2.1.2 Applied Pressure Loads

The axisymmetric model cannot calculate the azimuthal variation of the tubesheet displacement due to pressure loads. The axisymmetric model also cannot calculate the deflection of the tubesheet for different simultaneously applied hot leg and cold leg primary fluid pressures.

6.1.2.1.3 Applied Thermal Loads

The axisymmetric model cannot calculate the deflection of the tubesheet for different simultaneously applied hot leg and cold primary fluid temperatures. The axisymmetric model over-estimates the tubesheet deflections due to thermal loads because the non-axisymmetric structures in the model influence how the tubesheet can deflect and rotate. Eliminating the non-axisymmetric structures from the analysis means that the stiffness of the tubesheet in those regions will be significantly reduced at operating conditions and, therefore, the estimated thermal displacements will be greater.

6.1.2.1.4 Applied Boundary Conditions for the Linear Superposition Approach for Combining Tubesheet Axisymmetric Displacements

The tubesheet displacement calculations for the tube-to-tubesheet contact pressure prior to 2008 were based on unit load combinations, not the actual applied pressures and temperatures. The radial tubesheet displacement was recorded during each unit load case as a function of tubesheet radius and elevation. The unit load approach consisted of the following pressure cases:

- 1000 psia pressure on all primary faces at room temperature (ΔR_{PRI})
- 1000 psia pressure on all secondary faces at room temperature (ΔR_{SEC})

The unit load approach consisted of the following temperature cases:

- 500°F temperature difference on the stub barrel (ΔR_{SB})
- 500°F temperature difference on the channelhead (ΔR_{CH})
- 500°F temperature difference on the tubesheet (ΔR_{TS})

with all other structures held at room temperature during each applied unit temperature load case. The stress free reference, or ambient room temperature, is assumed to be 70°F for each material in the analysis. The tubesheet displacement for a specific operating condition was then calculated using the equation:

a,c,e

The values for ΔT_{CH} , ΔT_{SB} and ΔT_{TS} were taken from the change in the fluid temperatures during each operating condition (relative to room temperature). The maximum radial tubesheet deflection predicted using this method for a Model F SG was approximately []^{a,c,e} inch. The minimum radial tubesheet deflection predicted using this method for a Model F SG was approximately []^{a,c,e} inch. In comparison, the maximum tubesheet deflection for a Model F SG using the 3D finite element analysis is approximately []^{a,c,e} inch or less. The minimum tubesheet deflection for a Model F SG using the 3D finite element analysis is approximately []^{a,c,e} inch.

6.1.2.1.5 Limits of the Linear Superposition Approach for Calculating Tubesheet Displacement

The purpose of the linear superposition method was to reduce the number of FEA models necessary to calculate the contact pressure. In theory, it also allowed for the simple calculation of a number of different effects on the contact pressure by simply changing the operating temperatures and pressures when post-processing the displacement results. However, there are three fundamental rules of a linear superposition analysis that must be considered when using the method for an analysis of the lower SG complex. The three fundamental rules of the linear superposition analysis are:

1. All connected structures should be at similar temperatures.
2. All connected structures should respond to changes in the environment in a linear fashion.
3. All connected structures should respond to changes in the applied load in a linear fashion.

The secondary face of the tubesheet and the stub barrel are at significantly different temperatures during all operating conditions. The smallest temperature difference between the primary fluid and the secondary fluid is more than 100°F. The thermal expansion coefficient and modulus of elasticity for the tubesheet, stub barrel and channelhead change at different rates with respect to temperature. This means that the way that each structure responds to changes in temperature is not necessarily linear with respect to changes in another structure's material property. Also, the stiffness of the connection between the tubesheet and the channelhead, or the tubesheet and the stub barrel, is very different when the two structures are at operating temperatures versus one or the other being at a room temperature. The tubesheet displacements cannot be accurately predicted based on linear scaling of the unit load results for the stub barrel and channelhead. This is especially true for different operating conditions with a large difference in primary and secondary fluid temperatures. For example, calculating the tubesheet displacements from a 500°F applied temperature difference and then scaling those results to represent a SLB condition ($\Delta T = 350^\circ\text{F}$) will give dramatically larger displacement results compared to calculating the tubesheet displacements from a 350°F temperature difference. This difference is exacerbated when variations in material properties are considered because the material stiffness of the connections between the tubesheet and the attached structures change at different rates with respect to temperature. The end result is that the calculated tubesheet displacements from a linear superposition of axisymmetric finite element results will have a very different distribution and magnitude compared to the applied conditions on a 3D finite element model.

The 3D finite element analysis results are the preferred analysis basis for the tube-to-tubesheet contact pressure analyses. This is because the 3D finite element analysis more correctly captures the SG operating conditions and accurately includes the significant structures in an operating SG. The 3D finite element analysis also responds to variations in input parameters in a more realistic fashion.

6.2 3D FINITE ELEMENT TUBESHEET DISPLACEMENT ANALYSIS

6.2.1 Description of the Tubesheet Complex Model

The channelhead, tubesheet, divider plate and lower shell (i.e., stub barrel) are typically referred to as the lower steam generator (SG) complex. See Figure 6-10 for a picture of the important structures in the lower SG complex model. The modeling of the tubesheet itself is broken up into two different material models in a non-axisymmetric fashion. There are four linear elastic material models in the analysis and one orthotropic elastic material model in the finite element analysis.

The tubesheet in a typical Model F SG consists of a large perforated region where the tube bundle is expanded into the tubesheet, a solid (non-perforated) lane of tubesheet material between the cold leg and hot leg sides of the bundle, and a ring of solid material on the periphery of the interior of the SG that also extends to a support ring structure outside of the internal SG structure. In the Model F SG without support rings, the lower SG complex is supported by four bearing pad connections on the channel at roughly 45° to either side of the tube lane. See Figure 6-11 for details of the different regions of the tubesheet.

The displacement inputs to the H* integration model are generated by a 3D finite element model created in ANSYS WorkBench, Versions 10 and 11. ANSYS WorkBench is a computer aided engineering (CAE) and modeling tool designed as a front end and interactive graphic user interface for the finite element code ANSYS. Although created initially to benchmark the 2D axisymmetric model (Reference 6-20), the 3D FEA models were modified to represent plant-specific geometry and design conditions to determine the limiting plant among the Model F population.

Each plant or SG design-specific model includes the appropriate solid representations for the stub barrel (or lower shell), the perforated region of the tubesheet, the solid portion of the tubesheet and the support ring (if it is present in the specific plant of interest), the divider lane, the divider plate, and the channelhead. The combination of these structures is referred to as the lower SG complex. An undegraded divider plate is included in the model. Tubesheet displacements are scaled to account for potential divider plate degradation in post-processing. The perforated region of the tubesheet is modeled using effective orthotropic properties to account for the square pitch tube bore perforations. All other solid structures are modeled using linear, temperature dependent, material properties. The material input properties are taken from the 1989 edition of the ASME Boiler and Pressure Vessel Code.

The perforated region of the tubesheet is modeled using effective orthotropic elastic material properties according to Slot (Reference 6-5). The tube lane (also referred to as the divider lane) and the divider plate (also referred to as the partition plate) represent significant structures in the tubesheet complex and both affect the radial displacements of the tubesheet. The radial displacement of the tubesheet with a divider lane and an intact divider plate during NOP is typically on the order of []^{a,c,c} inch, or less. The vertical displacement of the tubesheet with a divider lane and an intact divider plate during NOP is typically on the order of []^{a,c,c} inch, or less. The original analysis for the Model F and Model 51-type SGs noted that including the tube lane reduces the vertical displacements at the centerline of the tubesheet by more than []^{a,c,c}% (Reference 6-6), relative to a tubesheet with no divider lane. The original analysis for the Model F and Model 51-type SGs noted that including a divider plate without fully considering the channelhead-to-divider plate welds reduces the vertical displacements at the centerline of the tubesheet by at least []^{a,c,c}% (Reference 6-28), relative to a tubesheet without a divider plate. The divider plate

reduces both the radial and vertical displacements of the tubesheet because it restricts the rotation of the tubesheet and vertical displacement of the tubesheet. In fact, if the vertical connection of the divider plate to the primary face of the tubesheet is assumed to be severed, the net reduction in displacement is still at least []^{a,c,c}% (Reference 6-7) due to the remaining welded connections between the divider plate and the channelhead reducing the rotation of the tubesheet. If all of the divider plate connections are considered intact, the tubesheet displacements are reduced by approximately []^{a,c,c}% (Reference 6-7). See Section 6.2.6 for a detailed discussion of divider plate modeling.

The tubesheet support ring is another significant structure to consider when estimating tubesheet displacements. The tubesheet support ring acts to “girdle” the perforated region of the tubesheet and is the structure where the Model F SG is typically supported and connected to the containment structure. All but one of the H* plants with a Model F SG have a support ring. If a SG does not have a support ring, the boundary conditions that apply to the SG change to reflect the required bearing support pad structures. The bearing support pad structures reduce the displacement of the channelhead structure and have less of an effect on the tubesheet displacements. See Table 6-7 for a list of the plants in the H* fleet with and without tubesheet support rings. The operating parameters and conditions for all of the Model F plants in the H* fleet are listed in Table 5-1. The applied operating pressures and temperatures for each analysis condition, and for each operating SG in the H* fleet, are listed in Section 5.0 of this report.

The tubesheet is a thick plate and the application of the pressure load results in a generalized plane strain condition. The pitch of the square, perforated hole pattern is []^{a,c,c} inch and the tubesheet hole diameter is conservatively assumed to be []^{a,c,c} inch, noting that the nominal bore diameter is []^{a,c,c} inch. The inside diameter (ID) of the tube after expansion into the tubesheet is taken to be about []^{a,c,c} inch based on an approximation of []^{a,c,c}% thinning during installation associated with constant material volume. Equivalent properties of the tubesheet are calculated without taking credit for the stiffening effect of the tubes, which results in a conservatively calculated tubesheet deflection.

The tubesheet ligament efficiency, η , is defined as:

$$\eta = \frac{h_{\text{nominal}}}{P_{\text{nominal}}}$$

$$\begin{aligned} h_{\text{nominal}} &= P_{\text{nominal}} - d_{\text{maximum}} \text{ (ligament thickness)} \\ P_{\text{nominal}} &= []^{\text{a,c,c}} \text{ inch, the pitch of the square hole pattern} \\ d_{\text{maximum}} &= []^{\text{a,c,c}} \text{ inch, the tube hole diameter} \end{aligned}$$

Therefore, $h_{\text{nominal}} = [\quad]^{a,c,e}$ inch (i.e., $[\quad]^{a,c,e}$ and $\eta = [\quad]^{a,c,e}$ when the tubes are not included. From Slot (Reference 6-5) the in-plane mechanical properties for Poisson's ratio of 0.3 are:

where the subscripts p and d refer to the pitch and diagonal directions, respectively. These values are substituted into the expressions for the anisotropic elasticity coefficients given previously. The coordinate system used in the analysis and derivation of the tubesheet equations is given in Reference 6-4. Using the equivalent property ratios calculated above in the equations presented at the beginning of this section yields the elasticity coefficients for the equivalent solid plate in the perforated region of the tubesheet for the finite element model.

The three-dimensional structural model is used in two different analyses: 1) a static structural analysis with applied pressure loads at a uniform temperature and 2) a steady-state thermal analysis with applied surface loads. The solid model and mesh is the same in the structural and thermal analyses but the element types are changed to accommodate the required degrees of freedom (e.g., displacement for structural, temperature for thermal) for each analysis. The tubesheet displacements for the perforated region of the tubesheet in each analysis are recorded for further use in post-processing. Figure 6-2 and Figure 6-3 are screen shots of the three-dimensional solid model of the Model F SG. Figure 6-4 shows the entire 3D model mesh.

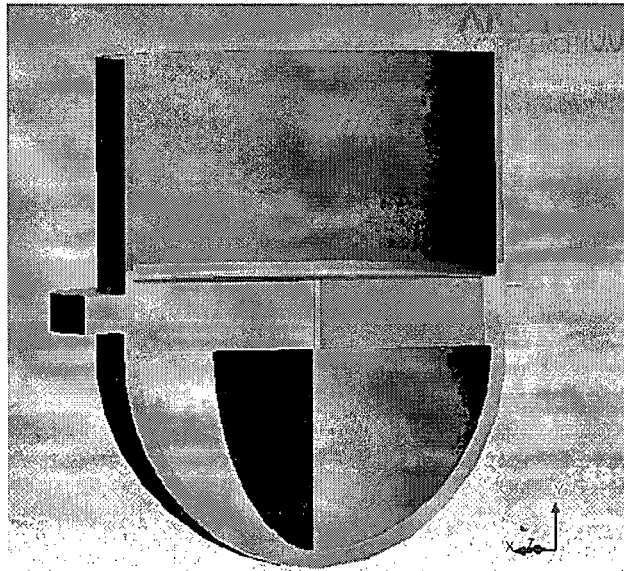


Figure 6-2 Solid 3D Model of a Typical SG With a Tubesheet Support Ring

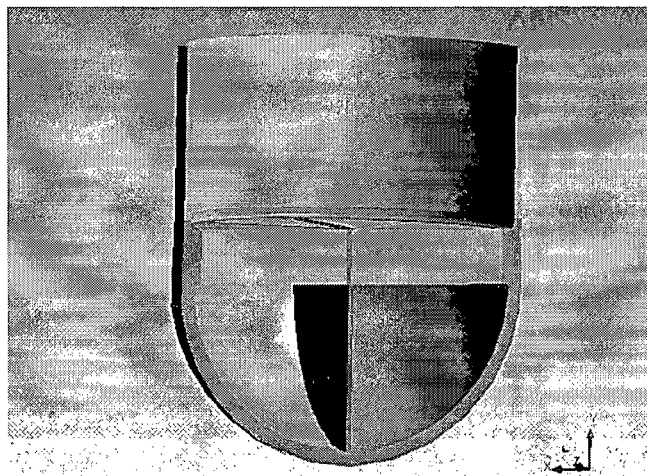


Figure 6-3 Solid 3D Model of a Typical SG Without a TS Support Ring



Figure 6-4 3D Model Mesh Screen Shot



Figure 6-5 Close-Up of Tubesheet Junction Mesh in a Model Without a TS Support Ring

a,c,e

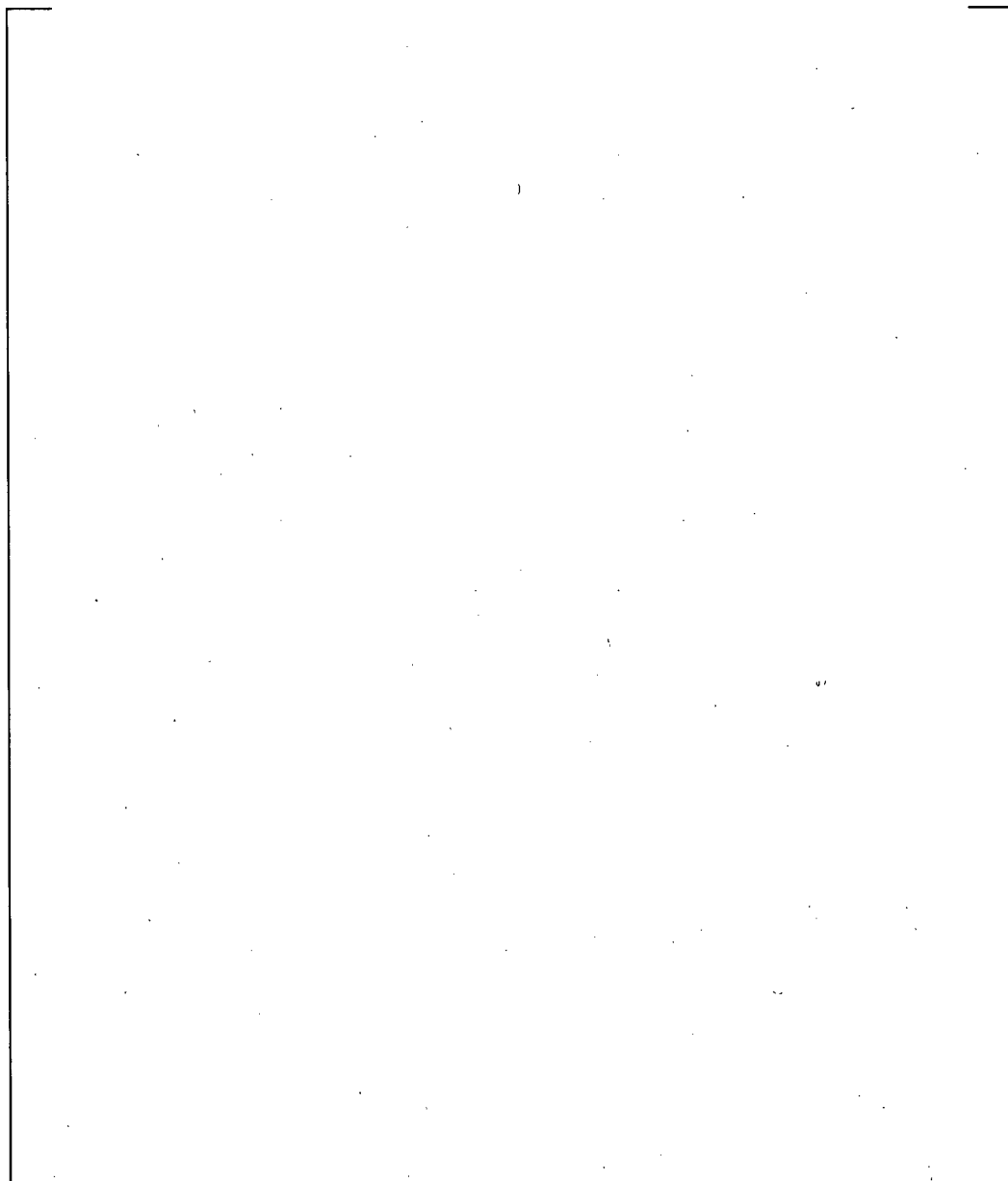


Figure 6-6 Typical Finite Element Mesh for a Prior Axisymmetric Tubesheet-Channelhead-Stub Barrel Model

(Note that this model does not have a tubesheet support ring.)

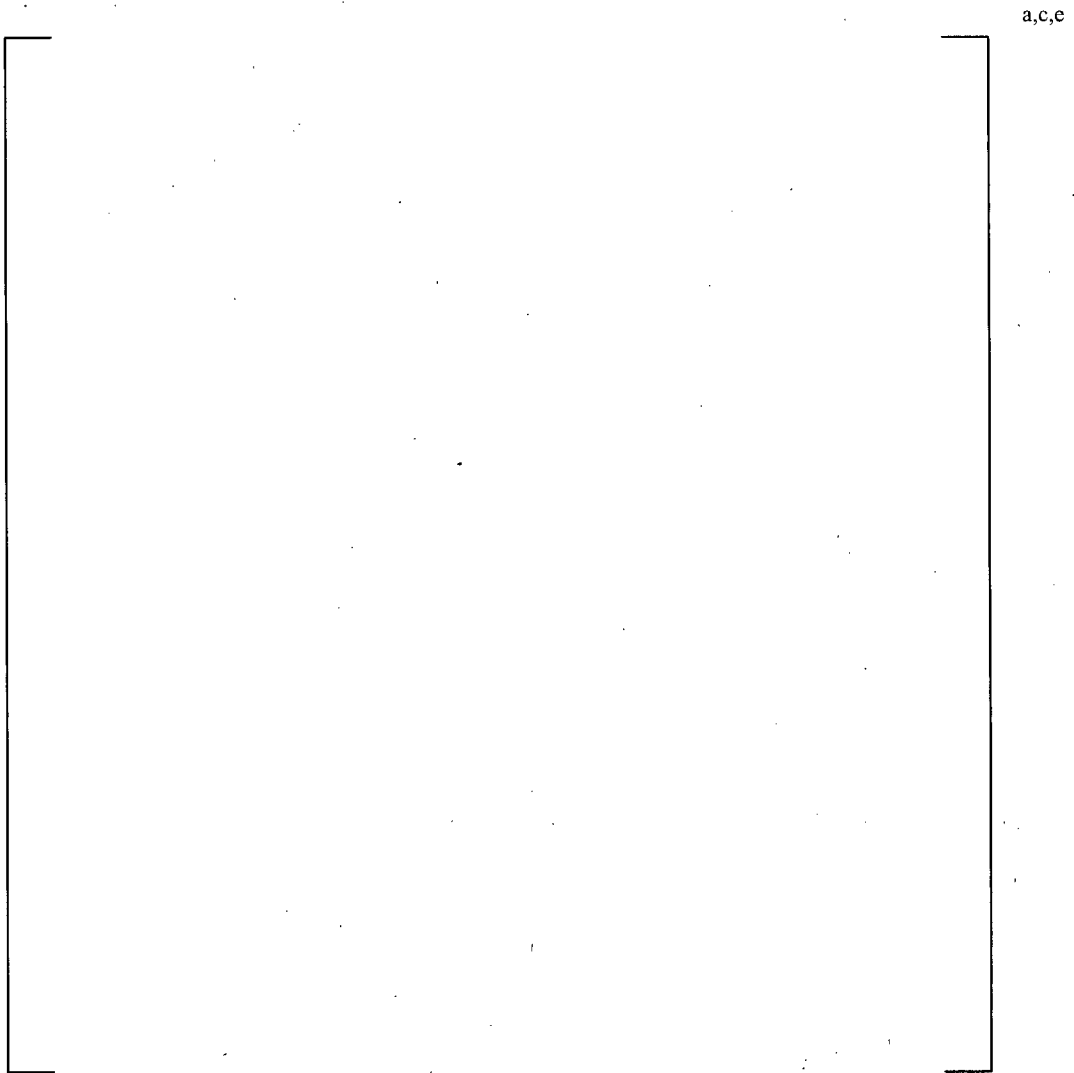


Figure 6-7 3D Tubesheet Mesh Close-Up Screen Shot

a,c,e



Figure 6-8 Top Plane View of Perforated Tubesheet Mesh

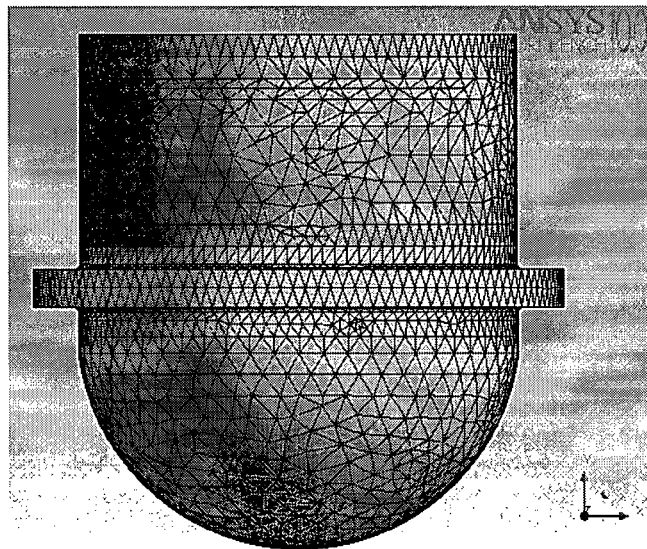


Figure 6-9 Rear View of 3D Model Mesh

6.2.2 Inputs to the Model and Their Variability

6.2.2.1 3D FEA Model Materials and Material Properties

The materials used in modeling the 3D Model F SG are the same as those noted in the engineering and design specification of the Model F SG. See Reference 6-16 for a description of the typical material properties used in a contact pressure analysis. See Reference 6-4 for a discussion of the reference design specification data and material properties in the 3D finite element model. The material properties for each material in the analysis are the mean material properties taken from the 1989 American Society of Mechanical Engineers Boiler and Pressure Vessel (ASME B&PV) Code unless otherwise noted.

Table 6-1 List of Lower SG Complex Materials

Component	ASME Code Specification
Tubesheet	SA-508 Class 2a
Lower Shell	SA-533 Grade A Class 2
Channelhead	SA-216 Grade WCC
Divider Plate	Alloy 600

The tubes in the Model F SGs are fabricated from Alloy 600 thermally-treated (A600TT) material. Summaries of the applicable mechanical and thermal properties for the tube material are provided in Table 6-2. Table 6-3 summarizes the material of fabrication for the tubesheet (SA-508, Class 2a). The shell material is SA-533, Grade A, Class 2, and its properties are in Table 6-4. Finally, the channelhead material is SA-216, Grade WCC, and its properties are in Table 6-5. The divider plates are fabricated from A600 material (see Reference 6-7). The material properties were all obtained from the ASME B&PV Code, Reference 6-3. See Table 6-6 for a list of representative mean operating input properties used in the Model F H* contact pressure analysis.

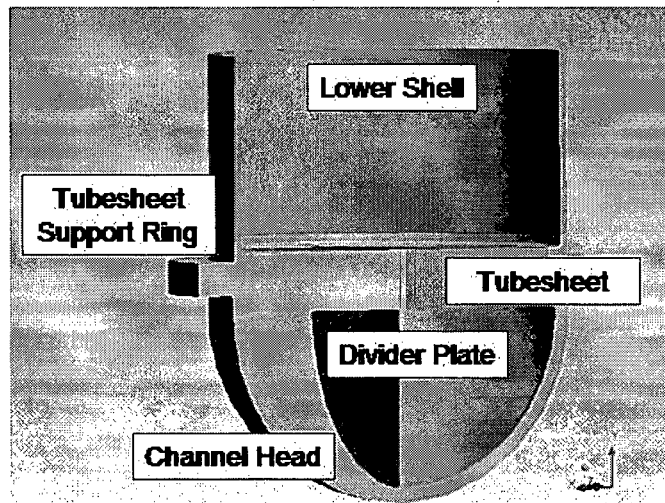


Figure 6-10 Important Structures in the Lower SG Complex

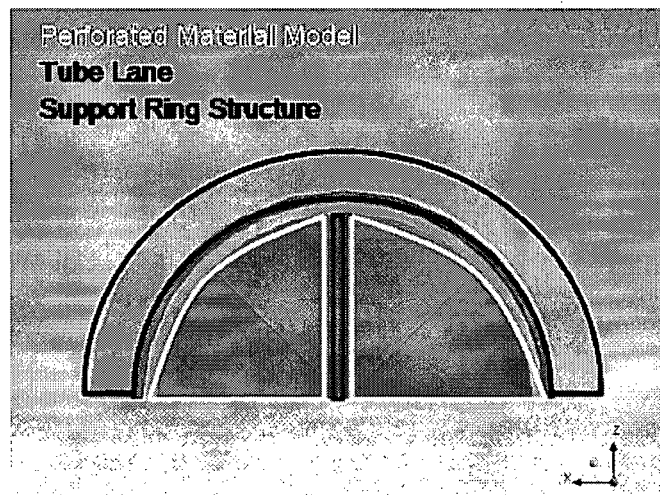


Figure 6-11 Top View of Tubesheet Showing Different Tubesheet Structures

The effective orthotropic material properties of the tubesheet were calculated using the method described by Slot (Reference 6-5).

The perforated tubesheet in the Model F channelhead assembly is treated as an equivalent solid plate in the finite element analysis. An accurate model of the overall plate behavior was achieved by using the concept of an equivalent elastic material with anisotropic properties. For square pitch tubesheet hole patterns, the equivalent material properties depend on the orientation of loading with respect to the symmetry axes of the pattern. The stress-strain relations for the axisymmetric perforated part of the tubesheet are given by:

$$\left[\begin{array}{c} \\ \\ \end{array} \right] \quad \text{a,c,e}$$

with the elasticity coefficients calculated as:

$$\left[\begin{array}{c} \\ \\ \end{array} \right] \quad \text{a,c,e}$$

$$\left[\begin{array}{c} \\ \\ \end{array} \right] \quad \text{a,c,e}$$

$$\left[\begin{array}{c} \\ \\ \end{array} \right] \quad \text{a,c,e}$$

$$\left[\begin{array}{c} \\ \\ \end{array} \right] \quad \text{a,c,e}$$

$$\left[\begin{array}{c} \\ \\ \end{array} \right] \quad \text{a,c,e}$$

$$\left[\begin{array}{c} \\ \\ \end{array} \right] \quad \text{a,c,e}$$

$$\left[\begin{array}{c} \\ \\ \end{array} \right] \quad \text{a,c,e}$$

$$\left[\begin{array}{c} \\ \\ \end{array} \right] \quad \text{a,c,e}$$

where

The variables in the equation are:

- \bar{E}_p^* = Effective elastic modulus for in-plane loading in the pitch direction,
- \bar{E}_z^* = Effective elastic modulus for loading in the thickness direction,
- $\bar{\nu}_p^*$ = Effective Poisson's ratio for in-plane loading in the thickness direction,
- \bar{G}_p^* = Effective shear modulus for in-plane loading in the pitch direction,
- \bar{G}_z^* = Effective shear modulus for transverse shear loading,
- \bar{E}_d^* = Effective shear modulus for in-plane loading in the diagonal direction,
- $\bar{\nu}_d^*$ = Effective Poisson's ratio for in-plane loading in the diagonal direction, and,
- ν = Poisson's ratio for the solid material,
- E = Elastic modulus of solid material,
- γ_{RZ} = Transverse shear strain
- τ_{RZ} = Transverse shear stress,
- $[D]$ = Elasticity coefficient matrix required to define the anisotropy of the material.

Table 6-2 Summary of Material Properties for Alloy 600 Tube and Divider Plate Material

Property	Temperature (°F)						
	70	200	300	400	500	600	700
Young's Modulus (psi·10 ⁶)	31.00	30.20	29.90	29.50	29.00	28.70	28.20
Thermal Expansion (in/in/°F·10 ⁻⁶)	6.90	7.20	7.40	7.57	7.70	7.82	7.94
Density (lb-sec ² /in ⁴ ·10 ⁻⁴)	7.94	7.92	7.90	7.89	7.87	7.85	7.83
Thermal Conductivity (Btu/sec-in-°F·10 ⁻⁴)	2.01	2.11	2.22	2.34	2.45	2.57	2.68
Specific Heat (Btu-in/lb-sec ² -°F)	41.2	42.6	43.9	44.9	45.6	47.0	47.9

Table 6-3 Summary of Material Properties for SA-508 Class 2a Tubesheet Material

Property	Temperature (°F)						
	70	200	300	400	500	600	700
Young's Modulus (psi·10 ⁶)	29.20	28.50	28.00	27.40	27.00	26.40	25.30
Thermal Expansion (in/in/°F·10 ⁻⁶)	6.50	6.67	6.87	7.07	7.25	7.42	7.59
Density (lb-sec ² /in ⁴ ·10 ⁻⁴)	7.32	7.30	7.29	7.27	7.26	7.24	7.22
Thermal Conductivity (Btu/sec-in-°F·10 ⁻⁴)	5.49	5.56	5.53	5.46	5.35	5.19	5.02
Specific Heat (Btu-in/lb-sec ² -°F)	41.9	44.5	46.8	48.8	50.8	52.8	55.1

Table 6-4 Summary of Material Properties for SA-533 Grade A Class 2 Shell Material

Property	Temperature (°F)						
	70	200	300	400	500	600	700
Young's Modulus (psi·10 ⁶)	29.20	28.50	28.00	27.40	27.00	26.40	25.30
Thermal Expansion (in/in/°F·10 ⁻⁶)	7.06	7.25	7.43	7.58	7.70	7.83	7.94
Density (lb-sec ² /in ⁴ ·10 ⁻⁴)	7.32	7.30	7.283	7.265	7.248	7.23	7.211

Table 6-5 Summary of Material Properties for SA-216 Grade WCC Channelhead Material

Property	Temperature (°F)						
	70	200	300	400	500	600	700
Young's Modulus (psi·10 ⁶)	29.50	28.80	28.30	27.70	27.30	26.70	25.50
Thermal Expansion (in/in/°F·10 ⁻⁶)	5.53	5.89	6.26	6.61	6.91	7.17	7.41
Density (lb-sec ² /in ⁴ ·10 ⁻⁴)	7.32	7.30	7.29	7.27	7.26	7.24	7.22

Table 6-7: List of SG Models and H* Plants With Tubesheet Support Ring Structures

a,c,e

** Model 44 F – These original SGs have been replaced.

*** Model 51F – These original SGs have been replaced.

6.2.2.2 Applied 3D Boundary Conditions

The calculated radial tubesheet deflection is the starting point for determining the effect of tubesheet bending and tube bore distortion on the contact pressure. The boundary conditions in the finite element model reflect the applied loading conditions in an operating SG as well as conservatively calculating the radial tubesheet deflection. The H* analysis is a static, steady-state, analysis by definition because the maximum pressures and temperatures are applied as if they were constant during SG operation. Applying the maximum temperatures and pressures in this fashion maximizes the radial deflection of the tubesheet due to thermal growth and pressure differential and also maximizes the applied end cap load on the tubes. Time varying, or transient, analyses of the operating pressures and temperatures reduce the thermal and pressure loads on the tube and tubesheet.

There are three categories of applied boundary conditions in the 3D finite element model:

1. Displacements
2. Pressures
3. Temperatures

The applied displacement boundary conditions in the model are required to prevent rigid body translation of the model. The displacement boundary conditions were also selected to conservatively account for deflection modes of the tubesheet. The applied pressures represent the primary and secondary conditions in the SG and are based on the most recent bounding plant operating conditions and parameters available. The applied temperatures are selected based on the secondary and primary fluid operating temperatures. Each of the boundary conditions used in the finite element analysis and a comparison to the previous axisymmetric model boundary conditions are provided in the following sections.

6.2.2.2.1 Applying Boundary Conditions in the 3D Finite Element Model

There are five possible surface groups to apply pressure and temperature loads in the 3D finite element model of the lower SG complex. These surface groups are:

1. Hot Leg/Cold Leg Primary Surfaces
2. Secondary Surfaces
3. Lower Shell Cut Face
4. Exterior Surfaces
5. Lower SG Complex Symmetry Plane

See Figure 6-12 for an illustration of the surface groups in the model.

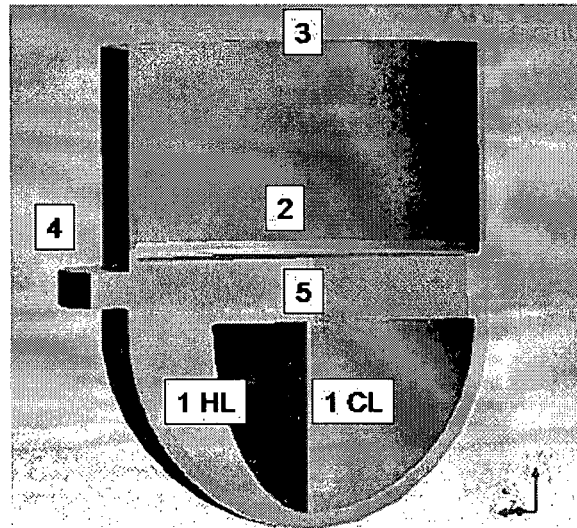


Figure 6-12 Surface Groups for a Typical SG FEM

There are also three edges in the model that are used to apply displacement boundary conditions. These edges are:

1. Lower edge of the tubesheet solid/tubesheet support ring
2. Centerline of the divider lane
3. Lower edge of the divider plate solid

Figure 6-13 and Figure 6-14 illustrate the edges in the model.

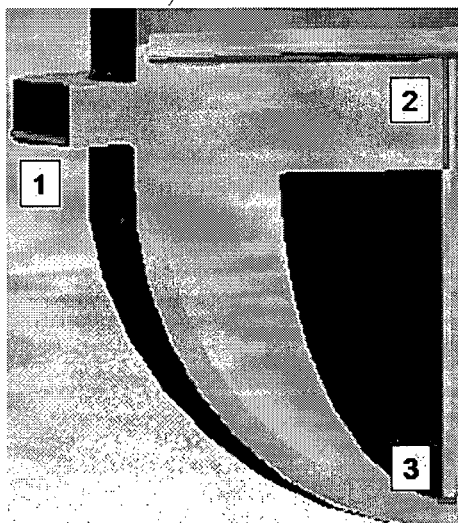


Figure 6-13 Important Edges in a Typical SG FEM With a Tubesheet Support Ring

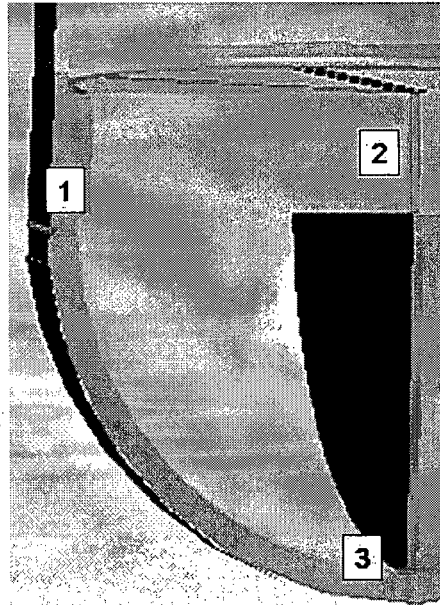


Figure 6-14 Important Edges in a Typical SG FEM Without a Tubesheet Support Ring

6.2.2.2.2 Discussion of Displacement and Pressure Boundary Conditions

The choice of boundary conditions is the most important factor in determining the tubesheet displacement output. The support structures and bearing pads for an SG typically restrain the structure in the vertical and horizontal directions and connect it to the floor of the containment building. In the case of the Model F SG, this connection is achieved through the tubesheet support ring. The tubesheet support ring acts to restrain the motion of the SG in the vertical and horizontal directions. See Figure 6-14 for an illustration of how the boundary conditions for a non-support ring model are applied. The boundary conditions in the structural model reflect these constraints. However, the SG is freely allowed to expand in a stress free fashion during heat-up. The boundary conditions in the thermal model reflect the ability of the SG to expand radially without restraint. Figure 6-15 and Figure 6-16 are illustrations of the typical applied load conditions in the structural model and the thermal model. Figure 6-17 and Figure 6-18 are illustrations of the boundary conditions typically applied to the tubesheet to prevent rigid body translation.

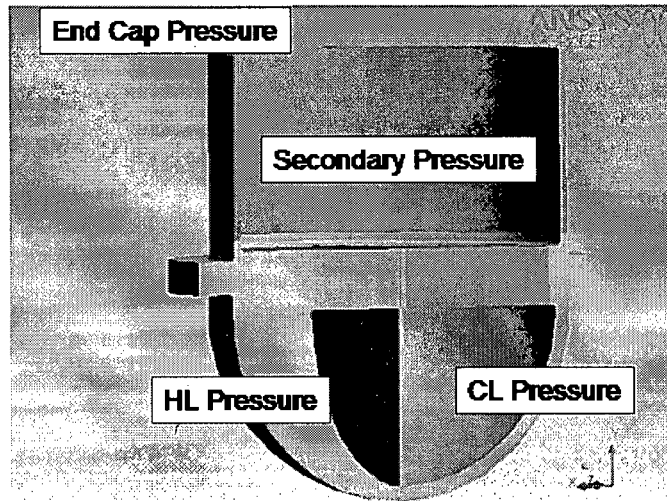


Figure 6-15 Typical Structural Model Applied Loads

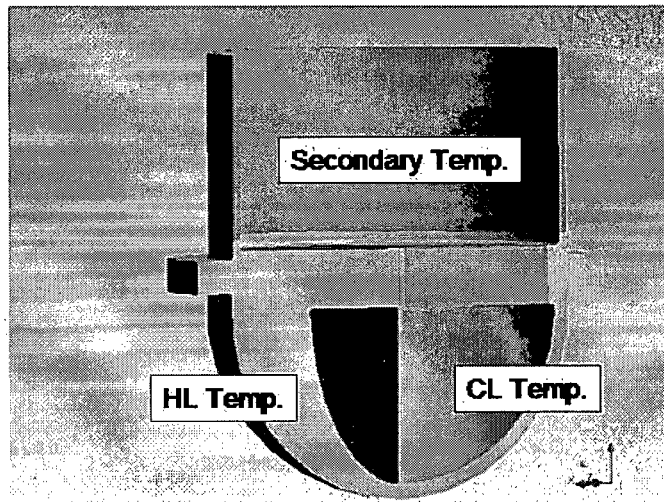


Figure 6-16 Typical Thermal Model Applied Loads

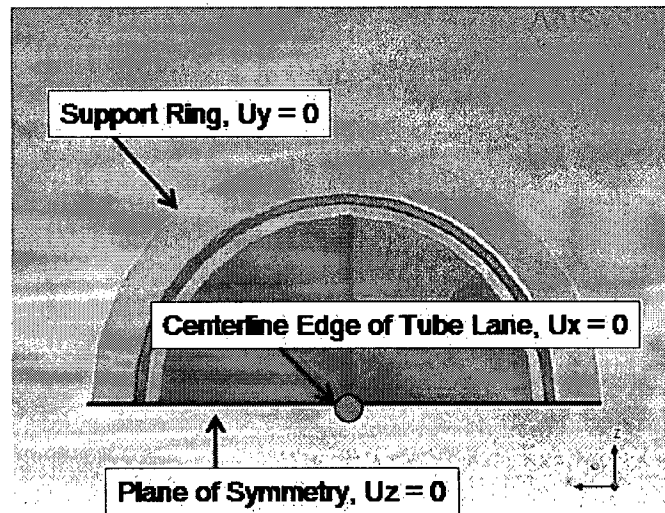


Figure 6-17 Typical Thermal Model Tubesheet Boundary Conditions Shown on Top View SG

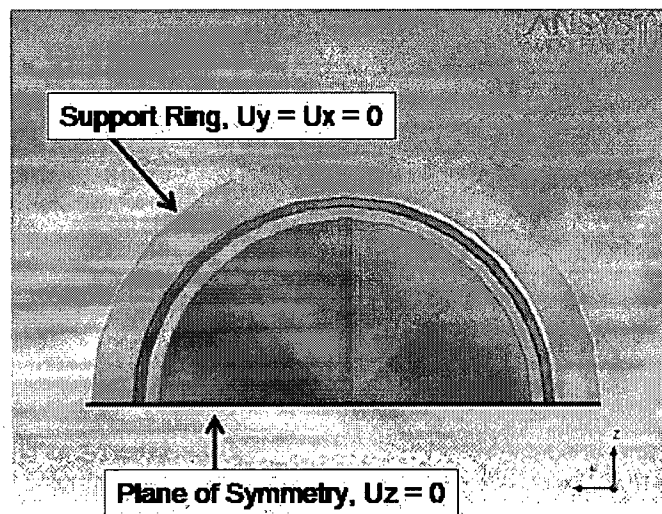


Figure 6-18 Typical Structural Model Tubesheet Boundary Conditions Shown on Top View of Model F

In Figure 6-15 and Figure 6-16, displacement in the Z-direction (perpendicular to the page) is fixed at the half-symmetry plane that bisects the lower shell, tubesheet, channelhead and divider plate. The displacements in the vertical (Y-axis) and horizontal (X-axis) directions are fixed at zero on the outer-most, lower edge, of the support ring. The primary and secondary pressure loads are applied to the primary and secondary surfaces. The vessel end cap pressure load is calculated using the thin shell relationship ($\sigma = p_{sec}r_m/2t$) and applied along the top surface of the lower shell. The lower shell dimensions typically place it in the thin shell regime. The ratio of the lower shell radius to its wall thickness does not exceed the criteria for a thin shell analysis. The primary pressure in the hot and cold leg chambers in the channelhead are modeled separately based on the system curves and the appropriate

transient analysis details. The height of the lower shell included in the model is equal to at least $4.6\sqrt{R_m t}$, per ASME Code requirements, unless a drawing reference dimension specifies a lower height, to attenuate any effects from the cut edge of the vessel and the applied end cap load so that loads are transmitted to the tubesheet region in a correct fashion. A portion of the transition shell is included in the model if the height of the lower shell is less than the ASME Code limit. No plants with Model F SGs have a lower shell less than the ASME Code limit.

[

]^{a,c}. The reference temperature for the structural model is also set to the hot leg primary fluid temperature so that no temperature differential is considered in the structural pressure load model. This is conservative because it uniformly reduces the stiffness of the solid and perforated regions of the tubesheet to the lowest level for each operating condition. The reference temperature in the thermal load model is set to 70 °F so that all displacements and strains are measured with respect to ambient room temperature. The typical thermal analysis boundary conditions are shown in Figure 6-17. The typical structural analysis boundary conditions are shown in Figure 6-18. Notice that the horizontal displacements are fixed at the centerline of the tubesheet instead of at the support ring in the thermal analysis. The temperature conditions are applied as surface loads and then the analysis determines what the final steady-state temperature distribution is due to conduction. The surfaces of the model are considered to be perfectly insulated and neither radiation nor convection losses are permitted. This is a conservative assumption that is consistent with the steady-state, static, nature of the analysis that considers only the maximum or minimum applied temperatures and pressures rather than the more realistic conditions taken from the system operating curves or the transient definitions in the SG design specification.

The current operating parameters in the Model F H* fleet are listed in Table 5-1. The generic parameters for a Model F 4-loop H* plant are listed in Table 6-8 through Table 6-13. The parameters in Table 6-8 and Table 6-13 are based on conservative assumptions drawn from Table 5-1. Please refer to Table 6-8 through Table 6-13 for the pressures and temperatures in each operating condition. The details in the operating condition tables come from the System Curve reference for a Model F operating plant (SSDC-1.3F) and the latest, approved and published PCWG conditions for Millstone Unit 3 (PCWG-06-9). The Millstone Unit 3 conditions were used as a comparison because they represent the highest operating temperatures in the Model F fleet. These selected conditions cannot actually occur in an operating SG but are used in a comparative analysis described in Section 6.4.7 to determine the effect on H* for postulated normal operating conditions. For example, it is not possible to have both a low secondary side pressure and a high secondary side fluid temperature, but using the maximum and minimum conditions from Table 5-1 assumes those conditions can exist simultaneously. The determination of the limiting plant in the Model F fleet is made using the actual specified plant operating conditions and not the generic conditions from Table 6-8 through Table 6-13.

Table 6-8 Conservative Generic NOP Pressures and Temperatures for 4-Loop Model F
 (These values do not exist in operating SG and are produced by examining worst-case comparisons.)

		a,c,e

Table 6-9 Generic NOP Low T_{avg} Pressures and Temperatures for 4-Loop Model F

		a,c,e

Table 6-10 Generic NOP High T_{avg} Pressures and Temperatures for 4-Loop Model F

		a,c,e

Table 6-11 Generic SLB Pressures and Temperatures for 4-Loop Model F

		a,c,e

Table 6-12 Generic FLB Pressures and Temperatures for 4-Loop Model F

		a,c,e

Table 6-13 Conservative Generic SLB Pressures and Temperatures for 4-Loop Model F
 (These values do not exist in operating SG and are produced by examining worst-case comparisons.)

		a,c,e

6.2.2.2.3 Effect of Tubesheet Support Ring on Displacement Boundary Conditions

The tubesheet support ring is used to attach the lower SG complex to the containment building floor through a system of structural supports. Not all SG models have a tubesheet support ring. If a SG does not have a tubesheet support ring then bearing pads mounted on the exterior surface of the channelhead are used to connect the SG to the containment building floor (see Figure 6-14). These two different possibilities represent two different ways to apply displacement boundary conditions in the structural analysis of the finite element model. One option is to fix the centerline of the tubesheet, through the thickness of the divider lane, in the global X-direction so that the centerline of the tubesheet does not change position during the analysis. Another option is to radially constrain the edge of the tubesheet support ring ($U_R = 0$) so that the tubesheet centerline does not change position during the analysis. A study was performed to see if there was a significant difference between the displacement results due to pressure loading for the centerline fixed and tubesheet ring fixed boundary condition options. The study showed that there was a small difference between the two boundary conditions but that it had an insignificant effect on the resulting contact pressure distribution.

The study used the boundary NOP temperatures, primary, and secondary pressure loads from Table 6-8. Using the values from Table 6-8 means that the highest operating temperatures in the H* fleet are used which will result in the least stiff tubesheet material. Using the upper bound temperatures to obtain the least stiff tubesheet structure is conservative because it highlights the contribution of the tubesheet support ring to the analysis. See Figure 6-19 for a graph comparing the tubesheet deflection for the centerline fixed and tubesheet support ring fixed boundary conditions for the bottom of the tubesheet (BTS) surface and the top of the tubesheet (TTS) surface for both the hot leg (HL) and the cold leg (CL) of the SG.



Figure 6-19 Comparison of the Tubesheet Deflection for the Centerline Fixed and Tubesheet Support Ring Fixed Boundary Conditions for the Bottom of the Tubesheet (BTS) Surface and the Top of the Tubesheet (TTS) Surface for Both the HL and the CL of the SG

The results in Figure 6-19 cannot be examined as if one condition is more conservative than the other or that one condition predicts more displacement than the other. The question is whether the act of constraining the nodes along the centerline of the tubesheet to remain in the same location (which cannot occur in a real SG) gives a markedly different result from constraining the tubesheet support ring in the radial direction (which is most similar to what occurs in a real SG). The results in Figure 6-19 show that the difference between a realistic boundary condition and an unrealistic boundary condition is small. The ring fixed boundary condition predicts larger displacements at the near radii while the centerline fixed model predicts larger displacements at radii greater than 10 inches. The maximum difference between the pressure deflection of the tubesheet for the model with the tubesheet support ring fixed condition and the tubesheet centerline fixed condition was []^{a,c,c} inch. This difference in deflection had only a small effect on contact pressure. The decrease in contact pressure is less than []^{a,c,c}% when utilizing the fixed center boundary condition; however, the centerline fixed conditions does not realistically represent the actual physical condition. Therefore, it is appropriate to use the tubesheet support ring fixed boundary condition in the finite element analysis of the tubesheet deflections due to the pressure load.¹

6.2.2.2.4 Applied Pressures

The primary fluid pressure is applied to the interior primary surface of the channelhead, the primary face of the tubesheet, and the surface of the divider plate. The hot leg pressure is applied to the inlet chamber of the channelhead plenum, the hot leg primary face of the tubesheet, and the hot leg surface of the divider plate. The cold leg pressure is applied to the outlet chamber of the channelhead plenum, the cold leg primary face of the tubesheet, and the cold leg surface of the divider plate. The secondary fluid pressure is applied to the interior secondary face of the tubesheet and the lower shell. The lower shell cut face is the surface where the vessel end cap load is applied to the model. The vessel end cap load is calculated using the thin shell pressure vessel calculations unless the ratio of the lower shell wall thickness to the inner radius of the lower shell dictates that the thick shell end cap load equations should be used instead (Reference 6-8). The exterior surface of the SG includes the exterior surface of the channelhead, the exterior surface of the tubesheet, and the exterior surface of the lower shell. The pressures applied to each of the surfaces is the absolute pressure, not the gauge pressure; therefore the exterior surface of the SG can be pressurized to 15 psi (atmospheric pressure). [

]^{a,c,c}. The effect of atmospheric pressure on the exterior surfaces is conservatively ignored in the H* analysis and the finite element analysis.

6.2.2.2.5 Applied Temperatures

Each of the transient analysis conditions applied to the finite element model are considered to be static and steady-state. In the context of the thermal analysis, the static assumption means that there is zero heat transfer from radiation and convection mechanisms in the SG. The static condition assumption also means that there is no primary fluid flow through the SG tubes. The static assumption in the SG means that the temperature profile through the tubesheet will develop based on the conduction properties of the tubesheet material. Pure conduction through the tubesheet will result in a linear distribution of

¹ The results in Section 6.2.2.2.3 do not apply in the case of an SG model without a tubesheet support ring. Currently, there are no existing domestic Model F SG's without a tubesheet support ring. In the event that a SG model does not have a tubesheet support ring the boundary conditions are moved lower on the SG complex structure and the discussion in Section 6.2.2.2.3 becomes irrelevant.

temperature ranging from the primary fluid temperature at the primary face of the tubesheet to the secondary fluid temperature at the secondary face of the tubesheet. The linear temperature distribution is reasonable during the feedwater line break (FLB) and the steam line break (SLB) conditions due to the assumed static analysis conditions. The linear temperature distribution is also reasonable during the faulted conditions because the tubesheet rapidly approaches equilibrium with the primary and secondary fluids during the SLB and FLB transients due to the low thermal mass of the perforated tubesheet and the large difference in primary and secondary fluid temperatures.

The normal operating conditions (NOP) are analyzed using different assumptions. During NOP, it is reasonable to assume that primary fluid is flowing in the tubes. Therefore, heat transfer across the tube wall from the primary fluid is the main heat source within the tubesheet during NOP. Previous analysis (Reference 6-9) suggests that the temperature throughout the thickness of the tubesheet during NOP is nearly uniform at the primary side temperature until the upper 2 inches of the tubesheet. The tubesheet displacements due to pressure already assume that the tubesheet is uniformly at the highest primary fluid temperature, so this assumption does not affect the pressure related displacement results. The effect of the different temperature distribution during NOP was studied using two different sets of boundary conditions and meshing schemes in the finite element analysis. All methods assumed a primary fluid temperature equal to the highest normal operating temperature (NOP Hi- T_{avg}) in the Model F fleet (622.6 °F). The secondary fluid temperature in both methods assumed that the secondary fluid was at a constant value equal to the average of the feedwater temperature and the steam outlet temperature for Millstone Unit 3 (490°F). A higher secondary fluid temperature in this context is conservative because it means that both surfaces of the tubesheet are at high temperatures and will radially expand more. The difference between the two methods lies in how the heat is distributed through the thickness of the tubesheet. The linear temperature distribution assumes that the tubes contribute no heat to the tubesheet and that the final thermal distribution is determined by pure conduction. [

]^{a,c} See Figure 6-20 for a graph comparing the linear temperature distribution to the modified temperature distribution used in the study.



Figure 6-20 Comparison of Different Temperature Distributions Through the Tubesheet due to Varying Boundary Conditions

The tubesheet displacements for the modified and linear temperature distributions were then compared to determine what the difference in H^* was between the two assumptions using the two finite element models with different meshes to accommodate the modified temperature distribution. The comparison showed that the modified distribution predicted similar displacements to the linear distribution at TS radii less than []^{a,c,e} inches but that the modified temperature distribution predicted larger displacements at TS radii greater than []^{a,c,e} inches. The tubesheet displacement results from the linear temperature distribution were then scaled to match the results from the modified temperature distribution and used as input to an H^* analysis. See Figure 6-21 for a graph of the non-scaled linear and modified thermal distribution radial tubesheet expansion and Figure 6-22 for a graph of the scaled linear and modified thermal distribution tubesheet expansion.



Figure 6-21 Radial Tubesheet Expansion due to Temperature

(The solid and dashed lines on the graph are from the linear temperature distribution. The points on the graph are from the modified temperature distribution.)



Figure 6-22 Graph Comparing the Radial Tubesheet Expansion of the Modified Thermal Distribution and the Scaled Linear Thermal Distribution Results

The results from the H^* study showed that the maximum difference of the H^* value between the linear temperature distribution and the modified temperature distribution is []^{a,c,e} inches, assuming zero residual contact pressure and a coefficient of friction of []^{a,c,e}. The maximum value of H^* at the limiting tubesheet radius was []^{a,c,e} inches. See Figure 6-23 for a graph of the difference in H^* between the two different thermal distributions.



Figure 6-23 Graph of Difference in H^* Values at the Limiting TS Radius (Max H^*) for the NOP Hi- T_{avg} Condition Using the Linear and Modified Thermal Distributions

The difference between H^* for the linear thermal distribution and the modified thermal distribution decreases rapidly with increasing residual contact pressure. For instance, assuming that the residual contact pressure contributes at least []^{a,c,e} lbf/in, approximately []^{a,c,e}% of the residual contact pressure value from prior test data, decreases the difference in H^* at the limiting TS radius by []^{a,c,e} inch. If the average value of residual contact pressure, from prior test data is used, approximately []^{a,c,e} lbf/in, the difference in H^* at the limiting TS radius is decreased by roughly []^{a,c,e} inches. Similarly, decreasing the primary fluid temperature decreases the difference between the linear and modified thermal distribution H^* results at the limiting TS radius. The difference in the H^* results for the NOP Hi- T_{avg} case bound (i.e., predict larger H^* due to the difference in thermal distribution) the results for the NOP Low- T_{avg} case. Therefore, it is conservative to apply the modified thermal distribution NOP Hi- T_{avg} results to both NOP conditions. The results for the hottest primary and secondary fluid temperatures in the H^* fleet are applied across the fleet to all plant-specific H^* analyses. The final analysis for H^* adds a value of []^{a,c,e} inches to the H^* value at a tubesheet radius if NOP is determined to be the limiting H^* condition at that radius.

6.2.2.3 Variability in Material Properties and Input Conditions

6.2.2.3.1 Material Property Variability

The materials properties of the tube and the tubesheet affect the distribution of contact pressure between the tube and the tubesheet. The material inputs and related inputs in the contact pressure analysis are:

1. Young's Modulus (E)
2. Coefficient of Thermal Expansion (α)
3. Poisson's Ratio (ν)

The effect of varying the material properties in either the tube or the tubesheet develops from the related stiffness coefficients in finite element analysis of the tubesheet deflections and the theory of elasticity analysis which determines how the tube and the representative tubesheet structure respond to the applied loads and deformations.

The linear material and orthotropic material models used in the analysis follow from a direct application of Hooke's Law; therefore, E and ν are inter-related. Either E or ν can vary with respect to temperature or material effects, but not both. The values for E vary according to temperature and material structure and the values for ν are held constant at 0.3 in the analysis. The mean values for E for each material, with respect to temperature, in the contact pressure analysis are taken from the ASME Code. The one sigma (1σ) variability of E at any given temperature is defined as []^{a,c,e}% (Reference 6-13). The mean values of coefficient of thermal expansion (α) are taken from the ASME Code for each material in the analysis. The one sigma (1σ) variability of α is defined for both the tube and the tubesheet material as []^{a,c,e}% and []^{a,c,e}%, respectively (Reference 6-14).

The yield strength of the tube material (Y) and the tangent modulus (E_T) of the tube material are not required in the contact pressure analysis. Instead, the effect of varying both parameters separately is included in the residual contact pressure analysis described in Section 7.0 of this report.

6.2.2.3.2 Design and Process Related Input Variability

The geometric and design/process tolerances for the SG tubes and tubesheet tube bore can influence the contact pressure distribution. These variables include:

1. Tube Outer Diameter (OD)
2. Tube Wall Thickness
3. Tubesheet Tube Bore Inner Diameter (ID)
4. Tubesheet Collar OD
5. Hydraulic Expansion Pressure

The tube ID and tube OD, as well as the tubesheet ID, are varied according the reported tolerances described in Section 7.0. Most of these sources of variability affect the calculation of residual contact pressure (RCP) variability only. The variability in these parameters has negligible effect on H^* if the RCP is assumed to be zero. The variables that affect RCP variability are:

- Initial gap between the tube OD and the tubesheet tube bore ID
- Variability in the hydraulic expansion pressure

The RCP variability with respect to each parameter is discussed in Section 7.0. The current H^* analysis assumes zero (0 psi) residual contact pressure in the contact pressure analysis. The tube OD and tube ID are explicitly used in the contact pressure analysis to determine the stiffness coefficients. The tubesheet collar OD and tube bore ID are also explicitly used in the contact pressure analysis to determine the stiffness coefficients of the representative tubesheet collar in the theory of elasticity analysis. A value of

the mean tubesheet bore ID plus two standard deviations ($+2\sigma$) is conservatively used to maximize the tube end cap load.

6.2.2.3.3 Coefficient of Friction Variability

The coefficient of friction between two materials is a property of the surface characteristics and loading method leading to different cases of friction (e.g., static, sliding, stiction, etc.). A value of []^{a,c,c} is the lowest estimate from prior test data (Reference 6-12) and is more conservative than the published coefficient for greased nickel sliding over a steel surface of 0.3 (Reference 6-11). Other test and analysis data suggest that the coefficient of friction between the tube and the tubesheet could be as high as []^{a,c,c} (Reference 6-12). A coefficient of friction of []^{a,c,c} is recommended for the H* contact pressure analysis. For simplicity and conservatism, the coefficient of friction is conservatively assumed to be []^{a,c,c} in the integration of contact pressure to determine the pull out resistance.

6.2.3 Bounding Sector Analysis

A 3D FEA model was developed to determine the limiting region of the tubesheet to be considered for the H* calculations. This model was originally intended to benchmark the earlier 2D axisymmetric model. The perforated tubesheet region of the three-dimensional finite element model was partitioned into sectors to study the asymmetric tubesheet displacements. Figure 6-24 is an illustration of the tubesheet sectors used in the finite element study.

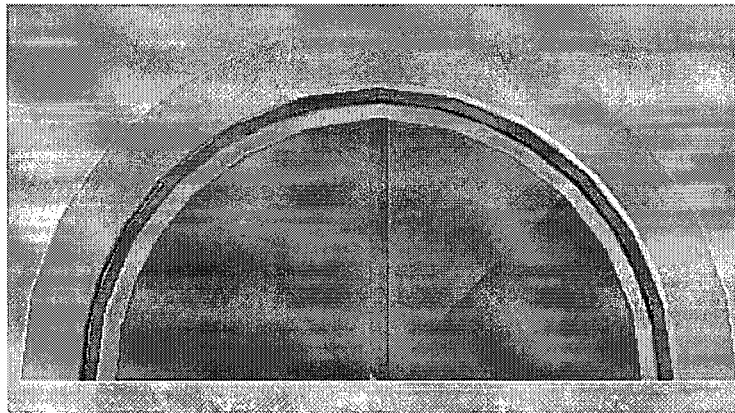
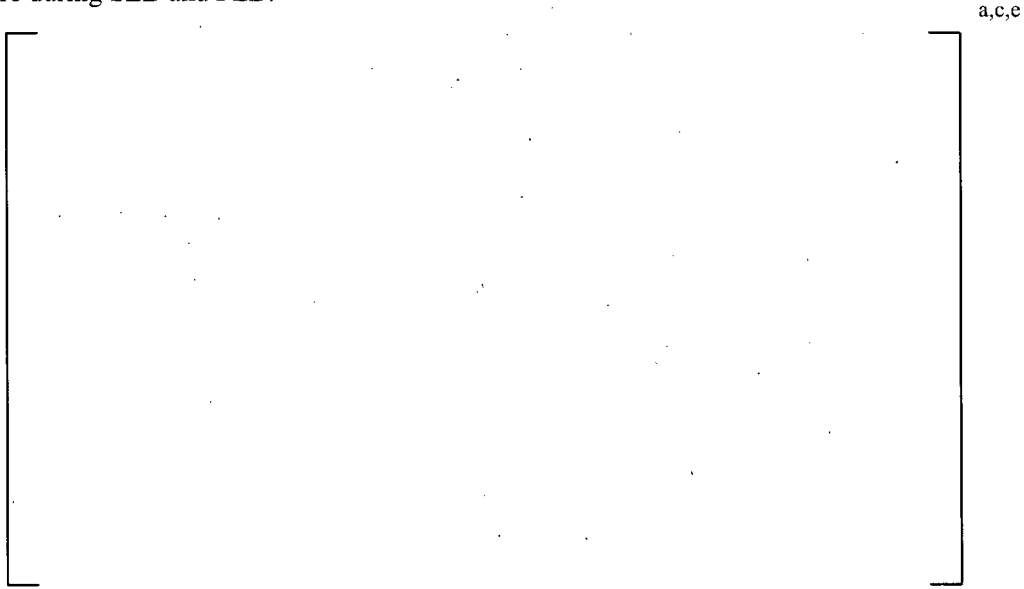


Figure 6-24 Top View of Model F Tubesheet Showing Sector Regions for Displacement Analysis

The finite element analysis used the Model F FLB, SLB and NOP conditions in Table 6-8, Table 6-12 and Table 6-13. A summary of the condition-specific temperatures and pressures for those conditions is provided in Section 5.0. The displacement results for the 0°, 45° and 90° sector boundaries were obtained using a macro code written in the native ANSYS Program Development Language (APDL). The 0° sector boundary is the edge of the tubesheet perpendicular to the face of the divider plate (i.e., along the symmetry plane of the tubesheet). The 45° sector boundary is the edge 45° clockwise from the symmetry plane of the SG tubesheet. The 90° sector boundary is the edge of the tubesheet perpendicular to the tubesheet symmetry plane, parallel to the divider plate face, along the edge of the tube lane. The results at each sector boundary face were obtained as a function of both elevation and radius for comparison and use in contact pressure calculations.

The results of the study showed that the maximum radial tubesheet displacement for the applied pressure loading occurred perpendicular to the face of the divider plate. The radial displacement for the applied thermal loading does not vary azimuthally during NOP or SLB because the thermal properties of the tubesheet and the resulting thermal gradients do not vary as a function of sector angle. See Figure 6-25 for representative curves of the radial tubesheet displacements during NOP. It should be noted that the azimuthal radial displacements due to pressure during NOP bound the azimuthal radial displacement due to pressure during SLB and FLB.



**Figure 6-25 Radial TS Displacement due to Pressure at TTS and BTS for
TS Radius = 60 in. During NOP**

It is logical for the 0° sector boundary face to be the limiting face for radial displacement because it is furthest away from the constraints of the divider plate and tube lane. The results of the azimuthally varying radial tubesheet displacements in the analysis of the tube-to-tubesheet contact pressures show that the lowest contact pressure occurs on the 0° face. [

] ^{a,c,e}. The radial displacements due to the pressure differential were linearly scaled by the difference in the azimuthal radial displacement to study the effect of the change in contact pressure as a function of TS angle. [

] ^{a,c,e}. See Figure 6-26 for a typical graph showing the effect of decreasing radial tubesheet displacement as a function of sector angle and the related increase in tube pull out resistance during NOP conditions.



**Figure 6-26 Relative Change in Tubesheet Displacement as a Function of Sector Angle During
NOP**

**(The effect of the decreasing radial tubesheet displacements on tube pull out resistance is noted in
5% increments.)**

Figure 6-26 shows that the pull out resistance of a tube increases the closer that tube is to the tube lane. The pull out resistance of a tube increases by roughly []^{a,c,e}% for every []^{a,c,e}% decrease in the radial tubesheet displacement. Therefore, the 0° sector face, normal to the tube lane, is the limiting sector in the tube bundle and all of the tubes outside of the []^{a,c,e} degree sector can be shown to have greater pull out resistance to applied end cap loads. The azimuthal variation of the radial tubesheet displacement is conservatively ignored during both NOP and SLB conditions in the contact pressure analysis in favor of using the results for the limiting sector. Only the most limiting tubes in the bundle at the 0° face of the tubesheet, for both the hot leg and cold leg sides of the tubesheet, are considered in the H* contact pressure analysis.

6.2.4 Radius Dependent Tubesheet Stiffness Analysis

6.2.4.1 Summary

The Goodier model (Reference 6-18) for calculating the tube-to-tubesheet contact pressure assumes that a representative collar of tubesheet (TS) material can be removed from the tubesheet and still provide the same constraint as if the tube and tubesheet structure were still in the tubesheet. The expansion of the pressurized tube bore, local to a tube of interest, can change the predicted values of the tube bore dilation due to internal pressure. In other words, the deflections of a single tubesheet cell are not independent from the deflections of other tubesheet cells. A combined planar, tube and tubesheet model is studied so that this effect can be included in the effective tubesheet collar approach used in the Goodier model. Two finite element models were used to examine the character of the local deformations of a tubesheet hole ID surface for the case where the tube location in the bundle varies and the tubes in the vicinity of the tube of interest may or may not be pressurized. Different values of primary pressure are used to envelope both the high and low values of applied pressure in the problem and possible combinations of pressurized and un-pressurized tubes surrounding a tube of interest. The end result of this study is a ratio that can be used to modify the tubesheet collar thickness, as a function of position, to approximate the constraint that a pressurized tubesheet would provide on a single tube.

6.2.4.2 Introduction

The radial expansion of the inner surface of an open thick shell, or collar, due to internal pressure, is given by the equation:

$$\left[\frac{P_{crev}}{E_{TS}} \left(\frac{D^2 + C^2}{D^2 - C^2} - N \right) \right]_{a,c,e} \quad (6-1)$$

Where

- P_{crev} = the crevice pressure acting on the ID surface of the tubesheet collar and the OD surface of the tube
- E_{TS} = the elastic modulus of the tubesheet material
- C = the inner radius (IR) of the tubesheet collar
- D = the outer radius (OR) of the tubesheet collar and
- N = the Poisson's ratio of the collar material

The thickness of the representative tubesheet collar wall was determined by 2D finite element analysis in 1993 (Reference 6-23). The collar thickness was calculated so that the tubesheet cylinder wall thickness would provide the same radial stiffness as the surrounding tubesheet material for the case of a single pressurized tube in a bundle of non-pressurized tubes. The original analysis (Reference 6-23) considered only the effective stiffness of a collar necessary to account for the material around a single pressurized tube within a tubesheet. This was a conservative approach to approximate the behavior of a single TS collar for most thermal and pressure related deformations because it maximized the tubesheet deflection.

However, there is pressure acting on all of the non-plugged TS cells simultaneously during operating conditions. The effect of all of the tubes in a bundle acting to simultaneously pressurize the perforated region of the tubesheet is not captured when a single removed TS collar is analyzed. The compatibility condition for the analysis of the tubesheet to tube friction interface does account for the tubesheet collar expanding due to an applied pressure on the ID surface of the tubesheet, but the amount of expansion is calculated assuming that the collar acts as a single thick walled cylinder, not a cellular unit within a tubesheet that has a number of ID surfaces that are also pressurized.

The approximate perforated plate material model accurately captures the total radial and axial deformations of the perforated tubesheet but the deformations and stresses at the local tube-to-tubesheet surface level are not calculated in the analysis. Analysis of the deformations and stresses in the vicinity of a single tube hole due to pressure and temperature requires a model detailed of a perforated tubesheet with the correct operating conditions applied to each tube bore. The deformation of a single tubesheet perforation will be affected by the primary side pressure transmitted through the tube wall, the temperature of the tubesheet, the distribution of any crevice pressure due to a tube with a 100% through-wall flaw, the presence of other structures that can limit local deformations in the tube hole and the deformation of the tube holes nearest the tubesheet cell of interest. The possibility exists that tubes in the vicinity may be plugged which would negate any effect due to the pressure deformation of that specific hole. However, in the limit, for a tube in the middle of the bundle with no other pressurized tubes around it, the original analysis accurately describes the behavior of a tubesheet cell. For tubes in the near radius (close to the divider lane) or the periphery, the presence of other structures such as the tube lane and the tubesheet annulus act to reduce tubesheet deflections and radial expansions. A change in the predicted amount of tube bore dilation due to internal pressure directly affects the tube-to-tubesheet contact pressure calculated by the Goodier model (Reference 6-18). The deformations of a tube surrounded by pressurized tubes will be different from that of a lone pressurized tube in the center of a bundle. This study quantifies the difference in stiffness between the case of a single pressurized tube in a tubesheet and the case of a pressurized tube in a tubesheet surrounded by other pressurized tubes.

6.2.4.3 Background

An important concern relating to the structural model was raised at the December 13th, 2007 meeting with the NRC Staff at Waltz Mill (Reference 6-25). The concern was that current thick shell equations that model the contact pressure between the tube and the tubesheet do not include any restoring forces for the tubesheet. These restoring forces are generated by the elastic resistance to deformation of the tubesheet material surrounding a tube and also by the simultaneous inflation of adjacent tubes in contact with the tubesheet. The current tube-to-tubesheet contact model is based on the theory of elasticity and the work of Goodier and Schoessow (Reference 6-18). The model considers the relative elastic flexibility between a single tube that has been expanded to contact with an equivalent collar that simulates the constraint of the surrounding tubesheet material. The results are combined using the principle of linear superposition to describe the resulting net effect on radial displacement in order to calculate the net contact pressure between the tube and the tubesheet. No additional forces or stiffness are added to the tubesheet model; therefore it is theoretically possible for the tubesheet material to expand proportionally to the increase in crevice pressure without limit.

In prior submittals of H^* (Reference 6-20), the pressure in the crevice between the tube and the tubesheet was assumed to be at the secondary side saturation pressure. The crevice pressure acted on the ID of the

tubesheet material and the OD of the tube material. The results of the crevice pressure testing that disproved that fundamental model assumption were summarized in a White Paper provided to the NRC Staff (Reference 6-28). The result of test data was to increase the crevice pressure for the purposes of calculating the contact pressure between the tube and the tubesheet because the data showed that leakage from the primary side remains in the liquid phase for most of the length of the crevice. The crevice prevents the fluid from rapidly expanding or moving through the crevice medium (thereby keeping the static portion of the fluid energy large). Therefore, the component of radial displacement that is caused by the tubesheet collar ID deflecting away from the OD of the tube increased. The amount that the tube OD expanded into contact with the ID of the tubesheet was reduced due to a reduction of the pressure differential across the tube wall. The net effect of both of these changes on the tube-to-tubesheet contact pressure model is to reduce the contact pressure and increase the required H* inspection distance.

The impact of the crevice pressure test data led to two additional important realizations regarding the analysis model for contact pressure:

1. The contact pressure analysis model did not properly apply the increased crevice pressure to the ID of the tubesheet collar. Instead, the secondary side pressure was still being applied to the tubesheet ID.
2. A built-in factor in the H* analysis model, known as the beta, or β , factor, intended to correct for the crevice pressure issue, was not being properly applied by the model.

The required changes to the spreadsheet model for the increased crevice pressure condition and the prior reduced secondary side pressure in the crevice pressure model were compared. The details of the comparison revealed that the tube-to-tubesheet contact pressure reduction increased when the tubesheet bore ID expansion was increased by the increased crevice pressure. When Items 1 and 2 above were addressed, the applied crevice pressure was reduced on the tubesheet bore ID and the tube-to-tubesheet contact pressure increased. Using the secondary side pressure as the crevice pressure reduced the crevice pressure applied to the tubesheet tube bore ID by roughly []^{a,c,c}% compared to the crevice pressure model based on the test data.

The current H* modeling approach does not use a β factor, nor does it reduce the applied crevice pressure when calculating the tube bore expansion due to internal pressure. The test data is applied to the OD of the tube wall and the ID of the tubesheet tube bore as a function of elevation for each operating condition.

During the continuing development of the H* methodology, the model was modified to exclude application of the β factor, but to represent the same effect through a modification of the collar thickness of the surrounding effective tubesheet material in the Goodier analysis to account for the difference in stiffness due to a pressurized tubesheet. This approach was reviewed by a panel of industry experts in structural analysis and is included in the current analysis for H*.

6.2.4.4 Finite Element Model Details and Results

The TS ID study used two different 2D plane stress models. The first model (Model 1) represents the tubes along the plane of half symmetry in the SG. The second model (Model 2) represents the tubes perpendicular to the plane of symmetry and parallel to the tube lane. The calculated tubesheet

deformation changes as a function of tubesheet radius, elevation and azimuthal angle with respect to the divider lane. See Section 6.2.3 for a discussion of the azimuthal change in the tubesheet displacements, and the related azimuthal dependence of the tube pull out resistance. Both models neglect the tube lane and solid rim material (tubesheet annulus) which includes the lower shell, divider plate and channelhead connections. The presence of the tube lane is represented by the applied boundary conditions. Additional material is modeled in each finite element analysis to prevent artificially induced deflections due to the boundary conditions and reduce the effect of a stiff boundary by representing the additional tubesheet material that would be present in a real SG. In prior analyses (Reference 6-23) a radius equal to []^{a,c,e} tube pitches were determined to be adequate. A []^{a,c,e} pitch boundary of additional tubesheet material was added in Model 1 and Model 2 based on the prior analysis results. It is important to note that these models do not represent symmetry planes or symmetric sections of the tubesheet but are instead isolated sections of the perforated tubesheet region that are defined by the similarity in radial displacement among the tubes represented in the model. Figure 6-27 shows the arrangement of the finite element models used to study the problem. See Figure 6-28 for an illustration of the Model 1 geometry and Figure 6-29 for an illustration of the Model 2 geometry.

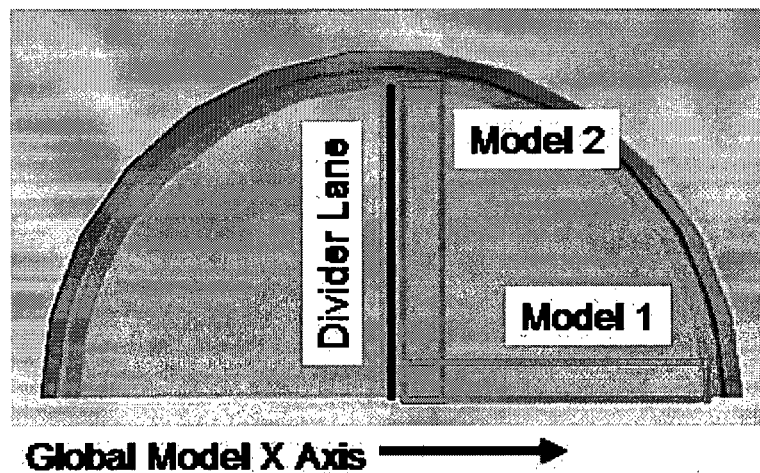


Figure 6-27 FEA Model Orientations as Shown From a Top View of a Typical Tubesheet

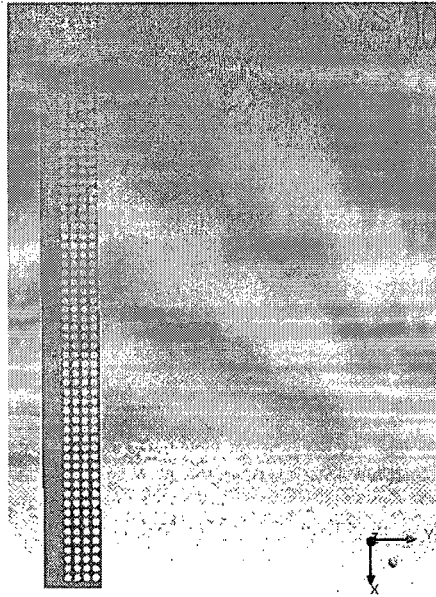


Figure 6-28 Model 1 Geometry, Region of Tubesheet Perpendicular to Tube Lane
(The material to the left of the perforations is added to soften the applied displacement boundary conditions.)

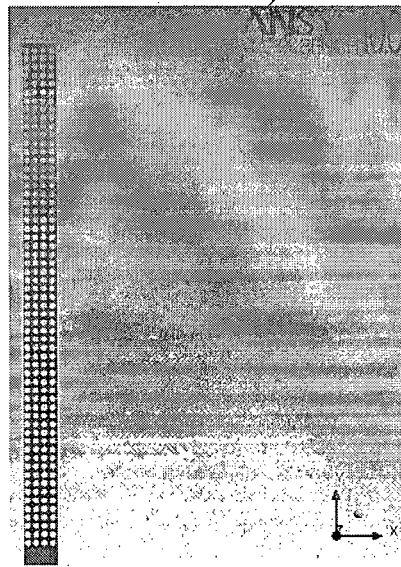


Figure 6-29 Model 2 Geometry, Region of Tubesheet Parallel to Tube Lane
(The material on the bottom of the model is added to soften the applied displacement boundary conditions.)

The focus of the study was purely on the effect that the perforated portion of the tubesheet structure has on the local displacement of the tubesheet hole ID surface. The lower shell, associated component welds and junctions and the tubelane act as girdles which reduce the TS displacement and therefore also limit the local deformation of the tubesheet hole ID. Including the structures attached to the tubesheet further decreases the pressure expansion of the perforated region of the tubesheet, which would act to increase

the restoring forces on the tube bore resisting the pressure expansion. Therefore, it is conservative to ignore these structures in the model and they are not required in the planar analysis. See Figure 6-30 and Figure 6-31 for pictures of the applied boundary conditions in each model.

Each individual TS hole was pressurized with either the NOP primary side pressure (2250 psig) or the SLB primary side pressure (2560 psig) as the bounding upper limit for the internal pressure acting on the face of the tubesheet tube bore. The TS holes were also pressurized with the primary side condition saturation pressures. The NOP saturation pressure was []^{a,c,e} psia and the SLB saturation pressure was []^{a,c,e} psia. The saturation pressures represent the lower bounding limits for the tubesheet tube bore. The upper bounding limit on tube bore pressure occurs near the bottom of the tubesheet for the case when the tubesheet surface is directly exposed to the primary fluid, such as in the case of a through-wall crack. The lower bounding limit on the tube bore pressure occurs when the tubesheet surface is in contact with pressurized crevice fluid that is near to, or has already, flashed to steam at the top of the tubesheet crevice (Reference 6-24). Three holes were chosen in each model to illustrate the different effects that TS constraint and tube pressurization have on the local deformation of a tube hole surface. In addition to the other pressurized conditions, several cases were run so that the three tubes of interest were the only tubes in the bundle that were pressurized. The hole locations in Model 1 are shown in Figure 6-32 through Figure 6-35. The tubes of interest correspond to a radius of roughly 2 inches (“inside” tube bore), 30 inches (“middle” tube bore) and 59 inches (“outside” tube bore).

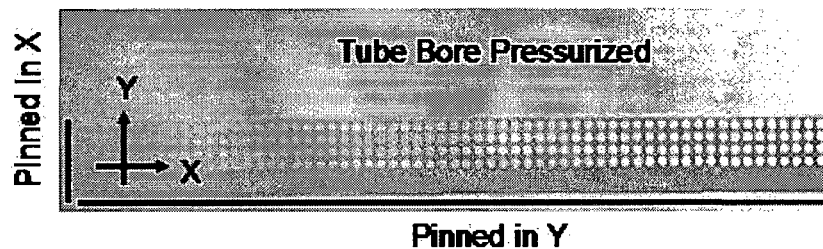


Figure 6-30 Model 1 Applied Boundary Conditions - Perpendicular to Divider Lane.

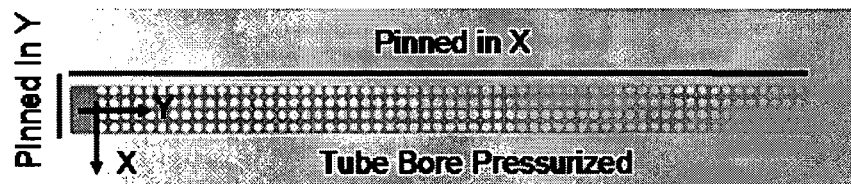


Figure 6-31 Model 2 Applied Boundary Conditions - Parallel to Divider Lane

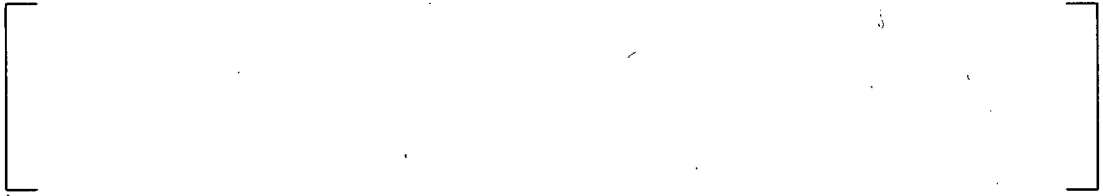


Figure 6-32 Relative Location of the Three Tube Holes of Interest in Model 1 and Model 2
(The tubes of interest correspond to a radius of roughly 2 inches (“inside” tube bore), 30 inches (“middle” tube bore) and 59 inches (“outside” tube bore).)

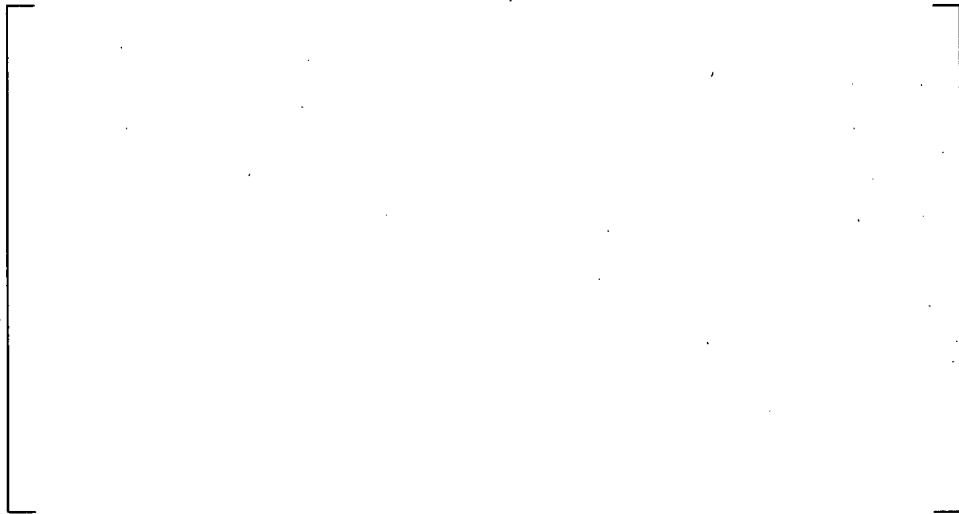


Figure 6-33 Close-Up of Inside Hole Location
(Red circles added for clarity)



Figure 6-34 Close-Up of Middle Hole Location
(Red circles added for clarity)



Figure 6-35 Close-Up of Outside Hole Location
(Red circles added for clarity)

The hole locations in Model 2 are achieved by rotating the holes in Model 1 through 90° counter clockwise. The boundary conditions for each 2D model were compared to the displacements of the perforated region of the tubesheet from the 3D finite element model in order to benchmark the 2D results. The same temperature difference and primary side pressure load was applied from the 3D model. In both Model 1 and Model 2, the difference in the radial displacement at the mid-plane of the tubesheet between the 2D perforated region and the 3D perforated region with the approximate material properties was on the order of []^{a,c,e} or less. The results of the 2D planar analysis are not dependent on tubesheet thickness and can be assumed to be constant throughout the thickness of the tubesheet. The final analysis of the tube hole deformation at each location used only an [

[]^{a,c,e}. The body temperature for NOP and FLB was 620°F (~622.6°F at Millstone Unit 3) and the body temperature for SLB was 450°F. Both temperatures are representative of the highest operating primary fluid temperatures in the H* fleet and result in the TS being evaluated when the ligaments have the least resistance (i.e., lowest Young’s Modulus) to expansion. This is a conservative assumption because [

[]^{a,c,e}.

6.2.4.5 Calculation Method and Results

The displacements in the X and Y directions around each of the three tube bores of interest were calculated as a function of angular position relative to the center of each hole. The coordinates of each hole in the deformed configuration were shifted so that only tube hole deformation was considered and no tube hole translation was retained. The deformation of the tube hole for NOP and SLB conditions is then calculated as a function of circumferential angle for each tube location. The net deflection of a tube hole, at a given point around the circumference, is defined as:

$$[] \quad \text{a,c,e} \quad (6-2)$$

where the values of U_x and U_y represent the translation of the hole center, relative to the global finite element model reference coordinate system from the initial undeformed configuration to the final deformed state. In this analysis, only the deformation of the circumference of the tube hole (or the deflection of the tube hole OD) is examined.² The results for the Net FEA deflection are plotted as a function of circumferential angle to compare against the unit deflection predicted by the thick shell equations (see Figure 6-37 through Figure 6-42). The result from the TS hole ID expansion calculated using thick shell equations is subtracted from the net total displacement so that equivalent measures are compared to calculate the total difference between the thick shell equation result and the finite element results (see Equation 3). A value greater than zero for the total difference indicates that the effective stiffness of the tubesheet collar can be reduced, by changing the thickness of the collar, when calculating the expansion of the tubesheet ID due to internal pressure. A value less than zero indicates that the tubesheet collar thickness should be increased when calculating the expansion of the tubesheet ID due to internal pressure.

$$\left[\begin{array}{c} \text{Net FEA Deflection} \\ \text{minus} \\ \text{Thick Shell Equation Result} \end{array} \right]_{a,c,e} \quad (6-3)$$

The average value of the FEA result is obtained by calculating the area under the curve for the Net FEA Deflection as a function of tube hole angle and dividing that result by 360°. The end result of this comparison is a relationship that estimates the limiting tubesheet collar thickness as a function of TS radius.

The total radial deformation for each tube of interest in Model 1 is shown in Figure 6-37 through Figure 6-42. The results plotted include only the direct dilation or deformation of the tube hole and not the translation of the tube hole due to expansion of the entire tubesheet. The tube hole deformation plotted in Figure 6-37 through Figure 6-42 directly compares to the predicted displacement from the thick shell calculation (see Equation 6-1). In several cases during SLB conditions, the net displacement of the TS hole ID surface around the circumference of the hole is negative, which means that the deflection of the other pressurized holes in the tubesheet acts to compressively deform the tube hole into greater contact with the tube. This result means that regardless of the location of the tube in the bundle, in the presence of other pressurized tubes the effective thickness of the TS collar is greater than the TS collar thickness for a pressurized tube that is not surrounded by pressurized tubes. The results in Figure 6-37 through Figure 6-42 show that the calculated tube bore dilation using the thick shell equations included in the H* integration model is greater than the predicted tube bore dilation using the finite element analysis for most, or all, of the tube bore circumference. The tube hole deformation results are referenced to the convention shown in Figure 6-36.

² The terms dilation, deformation and deflection are used throughout Section 6.0. In general, deformation is the change in a material relative to an unloaded initial configuration. Dilation is the growth or expansion of a surface due to some pressure. Deflection is the change in a surface relative to an unloaded initial configuration.

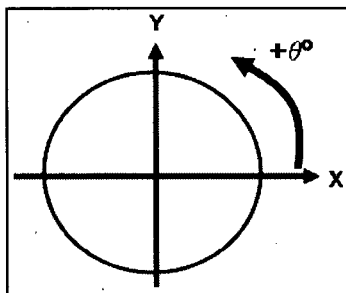


Figure 6-36 Reference Configuration for Tube Bore Deflection Plots

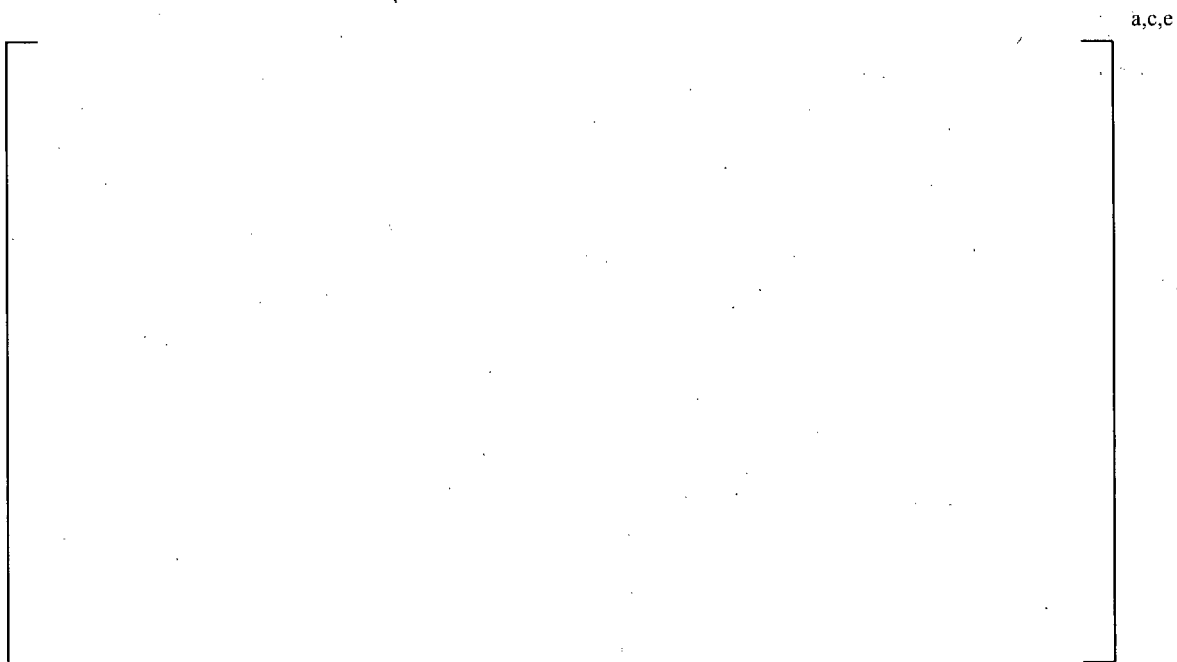


Figure 6-37 Inside Hole Results for NOP Conditions, $P_{pri} = 2250$ psi, for Model 1



Figure 6-38 Middle Hole Results for NOP Conditions, $P_{pri} = 2250$ psi, for Model 1



Figure 6-39 Outside Hole Results for NOP Conditions, $P_{pri} = 2250$ psi, for Model 1



Figure 6-40 Inside Hole Results for SLB Conditions, $P_{pri} = 2560$ psi, for Model 1



Figure 6-41 Middle Hole Results for SLB Conditions, $P_{pri} = 2560$ psi, for Model 1

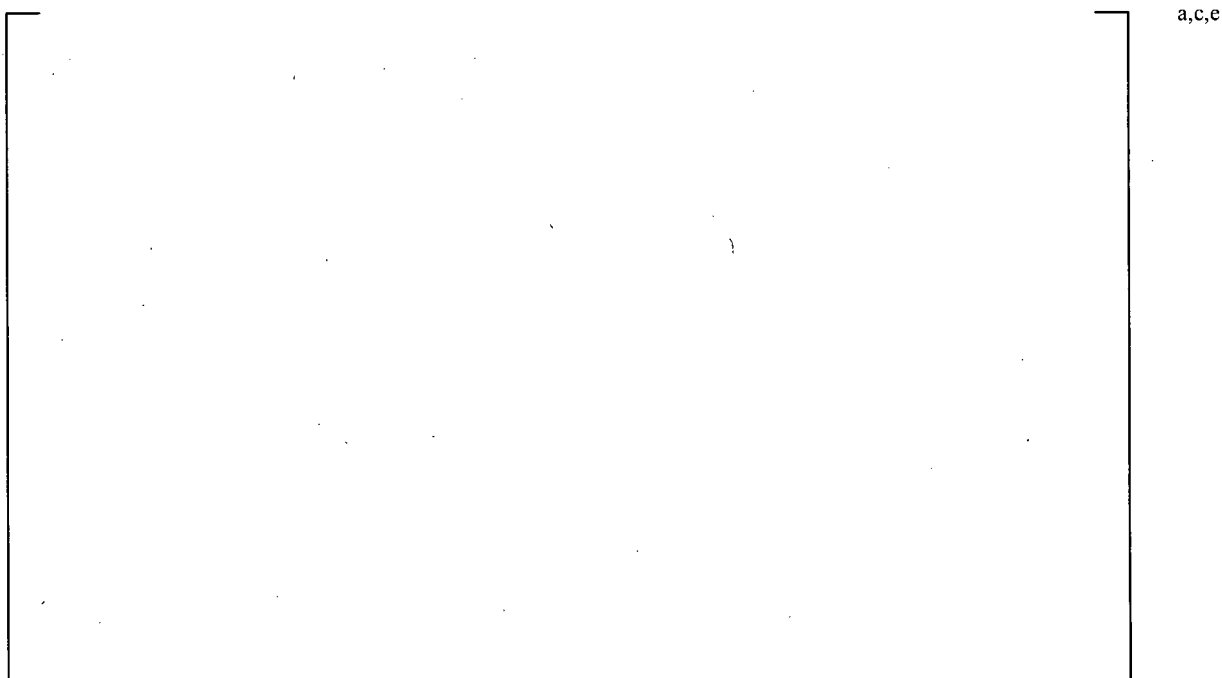


Figure 6-42 Outside Hole Results for SLB Conditions, $P_{pri} = 2560$ psi, for Model 1

The results in Figure 6-37 through Figure 6-42 for Model 1 bound the results for tube hole deformation in Model 2, with the exception of the inside hole, which is the same in both models and has the same deformation in both orientations. The results of Equations (6-1) and (6-2) are shown in Figure 6-43. These results do not significantly change when the tube material is introduced to the tubesheet. The tube material conforms to the deformation of the tubesheet material with no gaps forming between the OD of the tube and the ID of the tubesheet tube bore in all cases. It is important to note that the results discussed in Section 6.2.4 pertain to applied pressure loads acting on a material at operating temperature, but without any applied temperature differentials. Therefore, these results ignore [

] ^{a,c,e}. Refer to Section 6.2.5 for a discussion of tube dilation within a tubesheet cell due to both temperature and pressure effects and Section 6.4.5 for a discussion of the combined effect of pressure and temperature differentials on tube-to-tubesheet contact pressure.

a,c,e



Figure 6-43 Comparison of FEA Results and Thick Shell Equations for NOP and SLB Using Equations (6-1) and (6-2)

a,c,e



**Figure 6-44 Typical Result for Including the Tube Cross Section Within the Tube Bore, for the Outside Hole, When All of the Tube Bores are Pressurized
(The displacement results in the figure are magnified 500x)**

The effect of nearby plugged tubes, leaking tubes, and the practical bounds of variability on the radial dilation of the tube bore due to changing crevice pressure was also examined. The study of the different pressure combinations focused on the inside tube bore because the results in Figure 6-37 through Figure 6-43 show that the inside tube bore had the greatest magnitude of radial deflection. The result of the different pressurized tube bore study showed that varying combinations of pressure in the tube bore at different locations in the bundle do not result in a tube deformation that exceeds the case when all of the tube bores are pressurized to the full primary side pressure. This result is true for the SLB case and the NOP case. This result is also true for the case when the primary side saturation pressure is applied to the inside tube bore at varying locations. The calculated thick shell tube bore dilation due to internal pressure exceeded the average total deflection for all cases and combinations of pressure loading.

The internal pressure in the combination study was applied separately to four different regions: the internal pressure in the tube bore of interest, the tube bore local to the inside tube bore (local), the tube bore radii that bound the effective collar thickness determined by Reference 6-23 (mid-range), and the tube bore more than three times the effective collar thickness determined in Reference 6-23 (far field) (see Figure 6-45). The results of comparing different combinations of pressure in the four different tube bore regions are given in Table 6-14. The SLB tube deflections are bounded by the NOP tube bore deflections because the tubesheet Young's modulus during NOP (620°F) is less than the tubesheet Young's modulus at SLB (450°F). The results in Table 6-14 show that the thick shell calculation for the dilation of the inner surface of the tubesheet collar bound the deflection of all possible combinations of pressure, in and around, the tube of interest. The average total deformation results (without subtracting the translation of the tube hole)³ of the FEA solution when all of the tube bores are pressurized to the full NOP primary side pressure for the interior dilation of the inside inner tube bore surface []^{a,c,c} is []^{a,c,c}% less than the predicted thick shell results []^{a,c,c}. If only the tube bore deflection is considered, by subtracting the effect of tube bore translation, the FEA solution for the inside tube bore dilation []^{a,c,c} is []^{a,c,c}% less than the predicted thick shell results []^{a,c,c}. Therefore, the thick shell calculations on an effective tubesheet collar for the assumed case of a tube bundle pressurized to the full primary side pressure conservatively bound the results of any FEA result for tube bore dilation due to any applied internal pressure or combination of pressurized tubes. It is important to note that the results for the planar model assume that both the pressure and temperature remain at the worst-case conditions throughout the tubesheet crevice without changing. Any reduction in temperature or pressure, relative to the primary fluid pressure and temperature used in the model, would act to reduce the predicted tube bore dilation.

³ The translation of the center of the tube hole of interest changes with each combination of applied pressure in Table 6-14. Because the tube of interest in the cases shown in Table 6-14 is the inside hole, and the magnitude of the tube bore translation is small for the inside hole, it is acceptable to consider all of the results in Table 6-14 as comparable.



Figure 6-45 Graphic of Applied Pressure Regions in Separate Pressure Combination Study

The results in the Table 6-14 Cases 5 through 12 are provided to illustrate possible combinations of pressures in the vicinity of the tube of interest. These cases are not intended to reflect actual plant operating conditions. They are provided as evidence that regardless what combination of plugged, leaking, or fully pressurized tube bore surround a given tube, the greatest deflection of the tube bore is obtained when the entire perforated region is fully pressurized to the primary fluid pressure. This result makes intuitive sense because reducing the number of pressurized tube bores in the tubesheet directly reduces the strain in the tubesheet, which will directly decrease the deflections of the tube bore.

Table 6-14 Analysis Results of Model 1 Inside Hole Deflection for Multiple Pressure Load Combinations

a,c,e

	Pressure Load		Deflection			
	1	2	1	2	3	4

The FEA results pose a difficulty in modeling the predicted dilation of the tube bore ID. All of the FEA results predict non-uniform dilation which at some points in a tube bore becomes negative. It is not logical, or feasible, to use Equation (6-1) to predict a negative dilation from a positive pressure applied to the tube bore ID. Further, the range of deformations predicted by the FEA results cannot be calculated using Equation (6-1). The tubesheet expansion equation is asymptotic with respect to d for values much greater than the initial d . See Figure 6-46 for a graph of the calculated TS deflection during NOP as a function of d .

a,c,e



Figure 6-46 Tube Bore ID Deflection due to a Constant Applied Internal Pressure as a Function of Outer Collar Radius

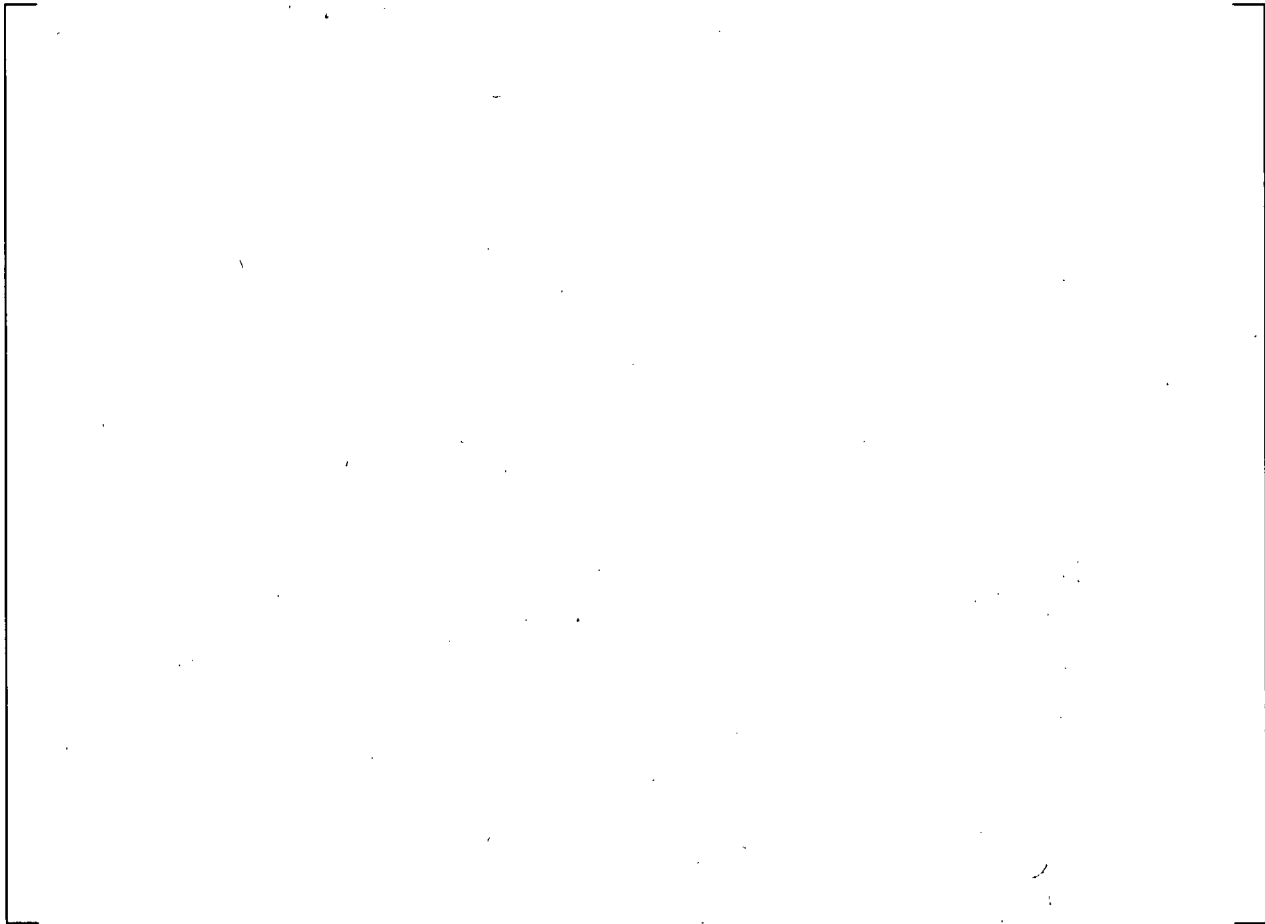
The relationship between d and the tubesheet collar inside radius (IR) deflection in Figure 6-46 shows that the effect of d on the stiffness of a []^{a,c,e} inch (or greater) collar wall is the same as that of a []^{a,c,e} inch thick collar wall. This is because the tubesheet material, from the perspective of Poisson effects due to axial loads on the tube and the corresponding deformations of the tubesheet collar, only “sees” a limited radius of the effective tubesheet collar. Beyond a certain radius, the interaction of the additional tubesheet material collar stiffness to the tube deflections, or the tube bore dilation, is irrelevant.

The relationship between d and the TS ID surface expansion means that calculating the equivalent tubesheet expansion based upon the exact FEA results could yield a tubesheet collar thickness much larger than the original d . Very large values of d , more than []^{a,c,e} times the original thickness, begin to call into question the basis for the Goodier model and the compatibility relationship used to solve for the tube bore dilation. Very large values of d are also not conservative because the parameter d appears in both the numerator and denominator of the equation used to evaluate the contact pressure between the tube and the tubesheet in the Goodier model (Reference 6-18). Therefore, it is appropriate to consider the

results from the FEA as a general trend that describes the effective behavior of the tubesheet collar at different locations in a tubesheet.

The following approach accommodates the Goodier model framework in a conservative and appropriate manner while also taking into consideration the FEA results:

a,c,e



The FEA results are compared to results of the thick shell equations in Table 6-15. The calculation of the adjusted d values is shown in Table 6-16. The comparison of the tube bore ID dilation for the initial d value and the adjusted d value is given in Table 6-17. The calculated tube bore ID dilation results using this procedure are slightly reduced from the initial results and also accommodate the trend from the finite element analysis (see Figure 6-37 through Figure 6-42). The original goal of this process was to approximate the trend from the FEA because the actual values from the FEA cannot be obtained using the thick shell relationships. The trend from the FEA results is that there is a marked difference between the FEA and the thick cylinder results as the position in the TS changes. In order to capture that trend, it is necessary to define the difference between the two analyses. The inner diameter (c) cannot change in either analysis. Further, it is required that the internal pressure, Young's modulus (E) and Poisson's ratio (ν) are the same in both analyses. Therefore, the only parameter that can reasonably be changed to accommodate this trend, is the d value.

The limiting case for both the NOP and SLB operating conditions occurs when all tubes are pressurized at the full primary side pressure. The limiting case is defined as the greatest positive net deflection of the tube bore ID in the finite element analysis for the three tubes of interest. This result bounds the case when no tubes are pressurized in the vicinity of the tube of interest and when select tube bores are either pressurized or unpressurized based on the assumption of locally plugged tube holes adjacent to the tube bore of interest. The calculated deflection using the thick shell results is always greater than the average predicted deflection of the tubesheet hole ID surface using FEA.

Using the inside collar deflection as the reference case means that the middle and outside collar locations should have a thickness between []^{a,c,e} times the initial *d* value that would be calculated assuming no other tubes in the bundle are pressurized (see Table 6-16). The ratio approach is used in order to maintain compatibility in the H* calculation method. The use of the limiting pressure and temperature results for the Model F SG means that these results may be considered generally applicable regardless of the plant-specific operating conditions. This approach also considers the results in Reference 6-12 and Reference 6-24 which show that the lower tubesheet radius tubes (i.e., TS radius less than 30 inches) have the limiting (i.e., lowest value) tube-to-tubesheet contact pressures. Therefore, maximizing the tube bore dilation due to internal pressure and minimizing the tubesheet collar stiffness in the lower tubesheet radius tubes when calculating contact pressures is conservative. The relationship between TS radius and the *d* parameter for SLB and NOP conditions is shown in Figure 6-47.

Table 6-15 Comparison of FEA Results and Thick Shell Results

Location	Condition	(1)	(2)	(3)	Thick Shell Results	(3) - (4)
		FEA Deflection Results				
		Max	Min	Avg		Total Difference
-	-	in	in	in	in	in

a,c,e

Table 6-16 Calculation of Adjusted *d*

Location	Condition	(1)	(2)	(3)	(2) x (3)
		Total Difference	Deflection Difference Ratio	Initial <i>d</i>	Adjusted <i>d</i>
-	-	in	in/in	in	in

a,c,e

Table 6-17 Comparison of Thick Shell Results for Initial d and Adjusted d Values

Location	Condition	Thick Shell Results		
		Avg. FEA in	Initial in/in	Adjusted in

a,c,e

a,c,e

Figure 6-47 Linear Relationships Between Applied Effective Outer Radius (d) and TS Radius for the NOP and SLB Conditions

The results in Figure 6-47 are conservative because they are based on the calculated deflections from the case of the entire tubesheet being fully pressurized to the primary side pressure throughout the entire tubesheet depth. The amount of the dilation in the contact pressure analysis will use the depth based crevice pressure distribution based on Specimen 8 data (Reference 6-28) to determine the applied crevice pressure in the probabilistic analysis of the contact pressure distribution. The relationship for the d parameter as a function of tubesheet radius is based on the adjusted d values in Table 6-16 using the Case 1 and Case 3 results in Table 6-14.

The final effect on the tube-to-tubesheet contact pressure, and therefore, the value of H^* , calculated by using the Goodier analysis approach with the tubesheet radius dependent collar stiffness applied to the result of a three-dimensional finite element analysis of tubesheet displacements is small,

increasing by []^{a,c,e}%. The final effect on the tube-to-tubesheet contact pressure calculated by reducing the interior dilation of the tube bore to the values predicted by the finite element study is an increase of approximately []^{a,c,e}%. Therefore, using the calculated thick shell results for the tube bore dilation of an effective tubesheet collar due to internal pressure is conservative.

A significant result is that the varying collar stiffness reduces the sensitivity of the H* model to material data input variations. Constant tubesheet collar stiffness for each operating condition produces an unrealistic profile in the contact pressure distribution as a function of tubesheet radius that exaggerates the effect of tubesheet deflection when the coefficient of thermal expansion or the Young's modulus of the tubesheet are varied in the worst-case direction. Adjusting the tubesheet collar stiffness as a function of the tubesheet radius for each operating condition produces a smooth contact pressure relationship. The FEA results reinforce the conservatism used in the representative TS collar thickness analysis approach and in the pull out study tests.

6.2.4.6 Conclusions and Discussion

A series of finite element models explored the interaction between tubes and tubesheet bore in a fully pressurized bundle. Several combinations of internal pressure were applied so that the possibility of a tube surrounded by cracked tubes, or a cracked tube surrounded by uncracked tubes, or a cracked/un-cracked tube surrounded by plugged tubes, are all accounted for in the analysis. The results of the analyses are two equations that can be used to modify the tubesheet collar thickness as a function of tubesheet radius. The most limiting relationship comes from a linear fit of the model results during NOP and SLB, for the case of all tubes in the bundle being cracked and fully pressurized. See Figure 6-47 for a graph of the two linear relationships.

The relationship for the NOP case is:

$$\left[\begin{array}{l} \text{ } \\ \text{ } \\ \text{ } \end{array} \right] \quad \text{a,c,e}$$

The relationship for the SLB case is:

$$\left[\begin{array}{l} \text{ } \\ \text{ } \\ \text{ } \end{array} \right] \quad \text{a,c,e}$$

The NOP relationship is applied to the FLB operating condition, but the FLB pressures are used to calculate the tube bore dilation. This is conservative because a hotter tubesheet, with reduced elastic modulus, is used to calculate the adjusted d values, and because the NOP relationship predicts a smaller value of d as a function of tubesheet radius than the SLB relationship.

6.2.5 Tubesheet Tube Bore Dilation

6.2.5.1 Background

Section 6.2.4 discussed the results of the radius dependent tubesheet stiffness analysis. The results of that analysis showed that tubesheet bore ovalization caused a variable deflection profile around the tubes (see Figure 6-37 through Figure 6-42). The variable profiles led to questions regarding the tube conformity to

the tubesheet bore holes. The analysis discussed in this section addresses this issue to show that the tubes conform to the shape of the tubesheet bore in all cases.

The purpose of this analysis is to determine the effect of local tubesheet distortion on the contact pressure distribution between the surface of the outer tube diameter and the inner surface of the tubesheet tube bore. This analysis also provides an alternative way to verify the range of contact pressure calculated by the H^* analysis due to pressure effects.

6.2.5.2 Analysis

The source of local tubesheet bore distortion is the deflection of the tubesheet due to pressure and thermal loads. The pressure loads acting on the tubesheet and the tubesheet bore distorts the tube bore material in two different ways. The pressure difference between the primary and secondary faces of the tubesheet acts to deflect, or “bow”, the tubesheet in the direction of the greatest pressure differential. The primary fluid pressure acting on the internal surface of the tubes in the bundle also acts on the pressurized tube bore. The internal pressure distorts the tube bore differently depending on the location of the tube bore relative to other pressurized tubes and the non-perforated regions of the tubesheet structure such as the divider lane and the solid peripheral rim (Reference 6-29).

The contact pressure studied in this analysis is generated, in general, by the residual installation effects from hydraulic tube expansion and the applied pressure differential acting on the inner surface of the tube. The contact pressure generated by the installation and expansion process is referred to as the residual contact pressure. The starting point for this analysis is the mean residual contact pressure calculated in Reference 6-30. Although Reference 6-30 includes calculations of residual contact pressure for Model F, Model D5 and Model 44F SGs under various conditions of dimensional tolerances and material properties, this analysis will only use the nominal dimensions and material properties for the Model F. The Model F has the lowest residual contact stress for nominal conditions in Reference 6-30; therefore, this analysis conservatively bounds the conditions for the Model D5 and Model 44F. The analysis described in this section is contained in Reference 6-40.

A 2D plane strain ANSYS finite element model (FEA) is used to explore the effects of tube bore distortion. The model is shown in Figure 6-48. This model is similar to the models in Reference 6-30 except that the model in this analysis is square and represents a single tube/tubesheet unit cell of the Model F SG. The X-Y coordinate system for this model is shown on Figure 6-36. The dimensions of the model are:

- Outside dimension of tubesheet square = []^{a,c,e} inch (equal to the tube center to center distance of the Model F SG)
- Inside diameter of tubesheet hole = []^{a,c,e} inch
- Unexpanded tube outside diameter = []^{a,c,e} inch
- Tube wall thickness = []^{a,c,e} inch

This model simulates the tube expansion during the manufacturing process, distortion of the tubesheet during operation, and tube pressurization during operation. The model is run in seven loading steps. These are, in order of application in the model:

1. Initialize the Model: No loads, zero stress.
2. Initial Expansion Pressure Step (Pressurize the tube to []^{a,c,e} psi). The tube expansion pressure is broken into two steps so that the FEA does not overcompensate for the stiffening effect of the tube and predict a greater residual contact pressure than would actually develop during tube installation.
3. Increase pressure on the tube to []^{a,c,e} psi. This is a conservatively low estimate of the actual manufacturing expansion pressure range of []^{a,c,e} ksi to []^{a,c,e} ksi.
4. Release pressure on tube. This step locks in the tube with strain hardening effects and initializes the model for the application of operating pressure loads.
5. Displace the tubesheet cell. The applied range of displacement includes both the thermal loads and the pressure loads acting to deflect the tubesheet, but both the tube and the tubesheet are considered to be at ambient conditions (70°F).
6. Pressurize tube to []^{a,c,e} psi (equal to primary side pressure minus secondary side pressure at no load; []^{a,c,e} psi). The presence of secondary fluid (at the top of the tubesheet) or primary fluid (from a leak within the tubesheet portion of the tube) in the crevice between the tube and the tubesheet would reduce the pressure differential across the tube wall. Reducing the pressure differential across the tube wall means that less contact pressure will develop between the tube and the tubesheet.
7. Increase internal pressure on the tube to 2250 (equal to primary side pressure under no load and operating conditions). Note that this pressure is conservatively lower than the operating primary pressure during feedwater line break (FLB) and steam line break (SLB) conditions.

Thermal expansions under operating conditions were not included in this model.

Steps 1 through 4 simulate the tube expansion process during manufacturing. During this process, the tube will exceed the yield stress and will act in a plastic manner. When the expansion pressure is released in Step 4, there will be a residual stress between the tube and tubesheet and the tube will be strain hardened. The maximum expansion pressure in this analysis was selected to give the same residual contact pressure at the end of Step 4 as the Model F nominal condition in Reference 6-30 []^{a,c,e} psi). (Although the H* analysis assumes zero residual contact pressure for conservatism of the pull out calculations, the value of residual contact pressure used for this study is a reasonable estimate of the actual expected residual contact pressure.) The application of the full expansion pressure would result in a greater magnitude of residual contact pressure and strain hardening. Therefore, the results presented in this analysis should be considered conservative lower estimates of the contact pressure between the tube and the tubesheet. Step 5 applies tubesheet distortion under operating conditions to determine the effects on contact stresses between the tube and tubesheet. The source of the distortion is a combination of the tubesheet bow due to pressure loads, thermal expansion distortions and the potential for distortion of the tube bore and ligaments due to local effects from neighboring tubes. There are several different postulated types and amounts of tubesheet distortion. Steps 6 and 7 add in the pressure that the tube would see under operating conditions.

During Steps 1 through 4, the boundary conditions are the same for all of the computer runs. The outside edges of the tubesheet are constrained from moving. The tube is constrained to stay centered in the hole in the tubesheet to prevent free body movement of the tube. This is shown in Figure 6-49. The outside of the tube and the inside of the hole in the tubesheet have contact elements to allow separation between the tube and tubesheet but allow transfer of load when contact is made.

Several different configurations of tubesheet distortion were analyzed. Each represents the bounding assumptions on the potential cause of the tubesheet bore distortion and the possible location of the unit tube/tubesheet bore cell in the tube bundle.

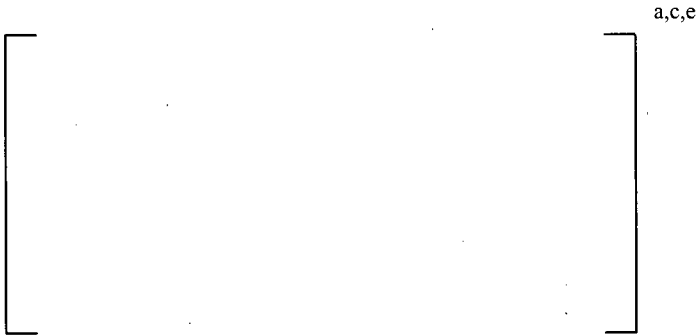
The first type of tubesheet distortion simulated is stretching of the tubesheet in the direction parallel to the Y axis (called square displacement) of the model with the model fixed to allow no movement at the edges in the X direction. This type of idealized distortion is similar to the deflection in the tube bore directly perpendicular to the face of the divider plate in the middle of the bundle. The distortion generated by these boundary conditions represents a worst-case condition with respect to contact pressure because the tube bore material can only distend and is not allowed to redistribute the strain around the tube bore. Redistributing the strain around the tube bore due to Poisson effects would act to pinch the tube and increase contact pressure. These boundary conditions are applied by displacing the “top” edge of the model by half the stretching amount in the +Y direction, displacing the “bottom” edge of the model by half the stretching amount in the -Y direction and fixing the “sides” of the model in the X direction. Note that the use of the terms “top”, “bottom” and “sides” refer only to the orientation as shown in Figure 6-49 and other figures in this analysis and not to the orientation of the actual SG tubesheet. Figure 6-50 shows the displaced shape in solid lines and shaded elements (with displacements exaggerated) and the undisplaced shape in dashed lines without shaded elements. Note the top and bottom edges of the model are displaced but the sides are not displaced. Six different displacements are investigated and these computer runs are labeled as follows.



The maximum value of the predicted tubesheet tube bore distortion from the H^* calculation is typically on the order of []^{a,c,e} inch or less (see Section 6.3 for a discussion of the equations used to calculate those distortions and dilations due to pressure and thermal effects). The maximum value of the tubesheet tube bore distortion predicted by FEA is []^{a,c,e} inch or less. Therefore, these applied displacements are conservative and bound the predicted range of distortion from both FEA and classical thick shell equations.

The second type of tubesheet distortion simulated allows the tubesheet cell material to redistribute the strain according to Poisson effects. The distortion is same as the first type in the Y direction but with the sides of the tubesheet portion of the model free to move in the X direction but constrained to stay in a

straight line. This is achieved by node coupling in the X direction on the side edges of the model. The displaced and undisplaced shapes for this condition are shown in Figure 6-51. Note here that the top and bottom edges of the model are displaced similar to Figure 6-50, but the sides of the model have displaced inward from the undisplaced sides. The computer run labels are as follows.



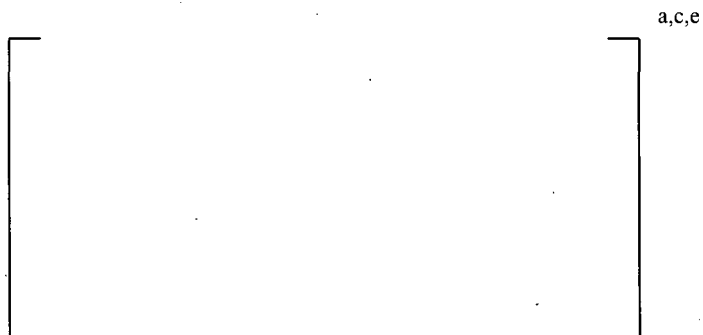
The next type of tubesheet distortion simulated is displacement in a tube pattern diagonal direction. This type of distortion is similar to the tube bore deflections experienced by the tube bore at some angle to the face of the divider plate in the bundle. The upper right corner of the model is displaced in the upper right diagonal direction by half the total displacement and the lower left corner is displaced in the lower left diagonal direction by half the total displacement. The other two corners are fixed and the edges of the tubesheet portion of the model are constrained to be straight lines between the corners using linear constraint equations. The node constraints for this model are shown in Figure 6-52. The expansion pressure in Step 3 was changed to []^{a,c,e} psi in order to achieve a residual contact pressure of []^{a,c,e} psi at the end of Step 5 due to the diagonal model orientation to make the initial conditions from the RCP variability study as similar as possible to the initial conditions in the tubesheet dilation study. The displaced and undisplaced shapes for this model are shown in Figure 6-53. Note that the upper right and lower left corners of the model are displaced, but the other two corners are not displaced. Again, six different displacements were investigated and the computer run labels are as follows:



The total displacement is the vector sum of the X and Y displacement. Note that these displacements are the S.1.X model displacements from above times the square root of two. Since the square model displacements are measured from one side to the opposite side of the model, and the diagonal model displacements are measured for one corner to the opposite corner, the diagonal model displacements have the same displacement per inch as the square model displacements.

The last type of tubesheet distortion simulated is same as the previous type in displacement in the diagonal direction of the upper right and lower left corners but the other two corners are free to move. The displaced and undisplaced shapes for this condition are shown in Figure 6-54. Note that the upper

right and lower left corners are displaced similar to Figure 6-53, but the other two corners are allowed to displace inward from the undisplaced corners. The computer run labels are as follows.



Tables 1 and 2 show the contact pressure results between the tube and the tubesheet for all the steps for all the computer runs.

Figure 6-55 through Figure 6-67 show the stress intensity and contact pressure for each step in a typical computer run – in this case Run S.1.5. The S.x.5 cases are the most representative of the tube bore dilations that result from the applied pressures and temperatures acting on the tubesheet. The figures are shown to assist in visualizing what is happening during a run. On all of these figures the stress intensity and contact pressures are in psi. Displacements shown are in true scale, with no magnification of the results (i.e., 1 to 1).

Figure 6-55 shows the stress intensity for Step 1. Since there is no displacement or pressure in Step 1, the stress intensity is zero everywhere. Figure 6-55 shows that there is an initial gap between the tube and the tubesheet. Since there is no contact between the tube and the tubesheet there is no contact pressure between the tube and the tubesheet.

In Step 2 of the computer run, the inside of the tube is pressurized to []^{a,c,e} psi. The resulting stress intensity is shown in Figure 6-56. Note that the stress intensity in the tube is in the range of []^{a,c,e} to []^{a,c,e} psi which is above the yield stress of []^{a,c,e} psi. The tube has plastically deformed and the gap between the tube and tubesheet has closed. The maximum stress in the tubesheet is less than []^{a,c,e} psi. Figure 6-57 shows the contact pressure at the end of Step 2. The contact pressure is very close to uniform at about []^{a,c,e} psi. Note that the tube expansion during manufacturing is done in a single step to maximum pressure. Step 2 is in the analysis to make it easier to see the stresses, displacement and contact stresses about half way through the expansion process.

In Step 3 of the computer run, the inside of the tube is pressurized to about []^{a,c,e} psi. The resulting stress intensity is shown in Figure 6-58. Note that the maximum stress in the tube has only increased from about []^{a,c,e} psi in Step 2 to []^{a,c,e} in Step 3 even though the tube internal pressure has almost doubled. This is because the tube is in the plastic region of the stress strain curve where the tangent modulus is much less than the elastic modulus of the tubesheet. The stress in the tubesheet has increased significantly, but is still below about []^{a,c,e} psi. The contact pressure at the end of Step 3 is shown in Figure 6-59. This contact pressure is close to []^{a,c,e} psi and is very uniform around the circumference of the tube.

In Step 4 of the computer run, the pressure inside the tube is reduced to zero. This corresponds to the end of the tube expansion manufacturing process. Figure 6-60 shows the stress intensity at the end of Step 4. The residual stress in the tube is less than []^{a,c,e} psi and the residual stress in the tubesheet is less than []^{a,c,e} psi. The loading at the end of Step 4 is the same as in Step 1, that is, no displacement or pressure load applied to the model. The reason that the tube does not return to the condition of Step 1 (Figure 6-55) is that the tube has been plastically deformed during Steps 2 and 3. Figure 6-61 shows the residual contact pressure between the tube and tubesheet. The residual contact pressure varies between 316 and 421 psi with an average of 372 psi.

In Step 5 the tubesheet is stretched, the upper edge by []^{a,c,e} inch in the upper direction and the lower edge by []^{a,c,e} in the lower direction. The side edges of the tubesheet are fixed in the X direction. Figure 3 shows the displacement greatly magnified. Figure 6-62 shows the stress intensity in the tube and tubesheet at the end of Step 5. The maximum stress in the tube has decreased slightly, and the maximum stress in the tubesheet is less than []^{a,c,e} psi. The maximum stress in the tubesheet occurs at the side edges of the tube hole which is to be expected given the tubesheet stretching in the vertical direction. Figure 6-63 shows the contact pressure between the tube and tubesheet at the end of Step 5. This contact stress is less than in Step 4 but it is always positive and no gaps have opened between the tube and tubesheet.

Steps 6 and 7 pressurize the inside of the tube with pressure seen at the hot standby condition in operation. At hot standby, the primary pressure is 2250 psi and the secondary pressure is 1020 psi. Step 6 uses a tube pressure of 1230 psi which is equal to the difference between the primary side pressure and the secondary side pressure. This would be the net pressure on the tube if there was a gap between the tube and tubesheet. Step 7 uses a tube pressure of 2250 psi. This is the pressure on the tube if there is no gap between the tube and the tubesheet. Figure 6-64 shows the stress intensity and Figure 18 shows the contact pressure at the end of Step 6. Figure 6-66 shows the stress intensity and Figure 6-67 shows the contact pressure at the end of Step 7. Since there are no gaps at the end of Step 6 (the contact pressure is positive all the way around in Figure 6-65), then Step 7 is valid for this tubesheet displacement condition. The final contact pressure varies from []^{a,c,e} to []^{a,c,e} psi. The magnitude of the final contact pressure would be different if a smaller or zero value of residual contact pressure were assumed. The value of contact pressure assumed in this analysis is solely for the purposes of matching the initial conditions from the RCP variability study and it is impossible to obtain the same level of strain hardening in a tube approximately []^{a,c,e} % and not have some calculated value of residual contact pressure. However, the trend in the results would be the same and the final effect (i.e., the variation of the contact pressure around the circumference of the tube is small) is also expected to be the same.

The idealized distortion cases from the S.1.x runs had the limiting contact pressure distributions and values for all conditions. The contact pressure was always greater than zero for the entire circumference of the tube at the expected level of distortion during operating conditions. The variation in the contact pressure distributions for the expected maximum distortion was on the order of []^{a,c,e} psi for Step 6 and Step 7. A variation of 50 psi in the contact pressure represents a []^{a,c,e}% difference, or less, compared to the average contact pressure value around the circumference of the tube. Refer to Section 7.0 for a discussion on the average contact pressure for the mean Model F material and geometric properties. Therefore, it can be concluded that the contact pressure does not significantly vary around the circumference of the tube during operating conditions and that no gaps between the outer tube surface and the inner tubesheet tube bore surface develop due to pressure effects or tubesheet distortion.

6.2.5.3 Summary of Results

The tubesheet tube bore dilation study results show that tubesheet deformations in the range predicted for the plants in the H* fleet does not create a gap between the tube OD and the tubesheet tube bore ID. Two models were used to study this effect: a square unit cell model and a diagonal, or “diamond”, unit cell model. Each model represented the potential direction of the applied loads on a tube within a tubesheet tube bore. The square unit cell model predicted more uniform contact pressure results due to the applied dilation and the diamond model tended to predict contact pressures that were skewed to the maximum value in the distribution. The absolute maximum tube bore dilation predicted in Reference 6-29 is less than []^{a,c,c} inch. The average predicted tube bore dilation in the H* contact pressure analysis is approximately []^{a,c,c} inch. The average predicted tube bore dilation from the tubesheet stiffness study is on the order of []^{a,c,c} inch (see Section 6.2.4). The variation in the residual contact pressure around the circumference of the tube, due to a tube bore dilation of []^{a,c,c} inch an unpressurized tube at room temperature, for the square tubesheet cell boundary conditions in Table 6-18 is less than []^{a,c,c} psi. The variation in the residual contact pressure around the circumference of the tube, due to a tube bore dilation of []^{a,c,c} inch in an unpressurized tube at room temperature, for the diagonal tubesheet cell boundary conditions in Table 6-19 is less than []^{a,c,c} psi. There was residual contact pressure present for all applied boundary conditions, regardless of the tubesheet cell model used in the analysis, for the bounding tube bore dilation of []^{a,c,c} inch. In the case of a pressurized tube in the square tubesheet cell, the variation around the circumference of the tube was also less than []^{a,c,c} psi. In the case of a pressurized tube in the diagonal tubesheet cell, the variation around the circumference of the tube was less than []^{a,c,c} psi. A variation of less than []^{a,c,c} psi for a tube at room temperature with an internal primary fluid pressure of 2250 psi and an applied tube bore dilation of []^{a,c,c} inch is equal to a []^{a,c,c}% variation, or less, in the contact pressure around the circumference of the tube. The variation in the contact pressure around the circumference of the tube decreases to []^{a,c,c}%, or less, for the maximum calculated tube bore dilation from Reference 6-29. Therefore, it is not necessary to consider the circumferential variation in the contact pressure distribution between a tube and the tubesheet. It is also concluded that the tube OD and tubesheet tube bore ID always maintain contact in the predicted range of tubesheet displacements.

Table 6-18 Contact Pressure for Square Displacement Model ⁽¹⁾

a,c,e

- (1) All contact pressures in psi.
- (2) Each displaced side of square displaced to half this distance.
- (3) For run names S.1.X, the non-displaced sides of the square are fixed in the X direction. For run names S.2.X, the non-displaced sides of the square are free to move in the X direction but constrained to be a straight line.

Table 6-19 Contact Pressure for Diagonal Displacement Model ⁽¹⁾

a,c,e

- (1) All contact pressures in psi.
- (2) Each displaced corner of square displaced to half this distance.
- (3) For Run Names D.1.X, non-displaced corners are fixed. For Run Names D.2.X, non-displaced corners are free



Figure 6-48 Finite Element Model



Figure 6-49 Boundary Conditions for Square Displacement Model



Figure 6-50 Displaced Shape for S.1.1 Through S.1.6 Computer Runs



Figure 6-51 Displaced Shape for S.2.1 Through S.2.6 Computer Runs



Figure 6-52 Boundary Conditions for Diagonal Displacement Model

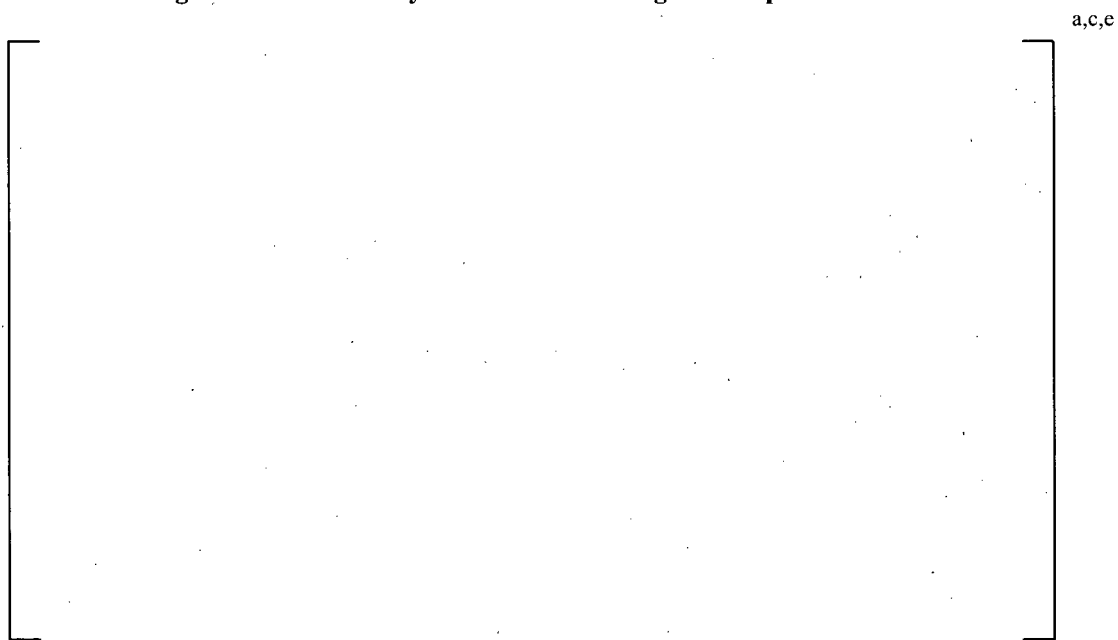


Figure 6-53 Displaced Shape for D.1.1 Through D.1.6 Computer Runs



Figure 6-54 Displaced Shape for D.2.1 Through D.2.6 Computer Runs



Figure 6-55 Computer Run S.1.5, Step 1, Stress Intensity



Figure 6-56 Computer Run S.1.5, Step 2, Stress Intensity



Figure 6-57 Computer Run S.1.5, Step 2, Contact Pressure

a,c,e



Figure 6-58 Computer Run S.1.5, Step 3, Stress Intensity

a,c,e



Figure 6-59 Computer Run S.1.5, Step 3, Contact Pressure



a,c,e

Figure 6-60 Computer Run S.1.5, Step 4, Stress Intensity



a,c,e

Figure 6-61 Computer Run S.1.5, Step 4, Contact Pressure



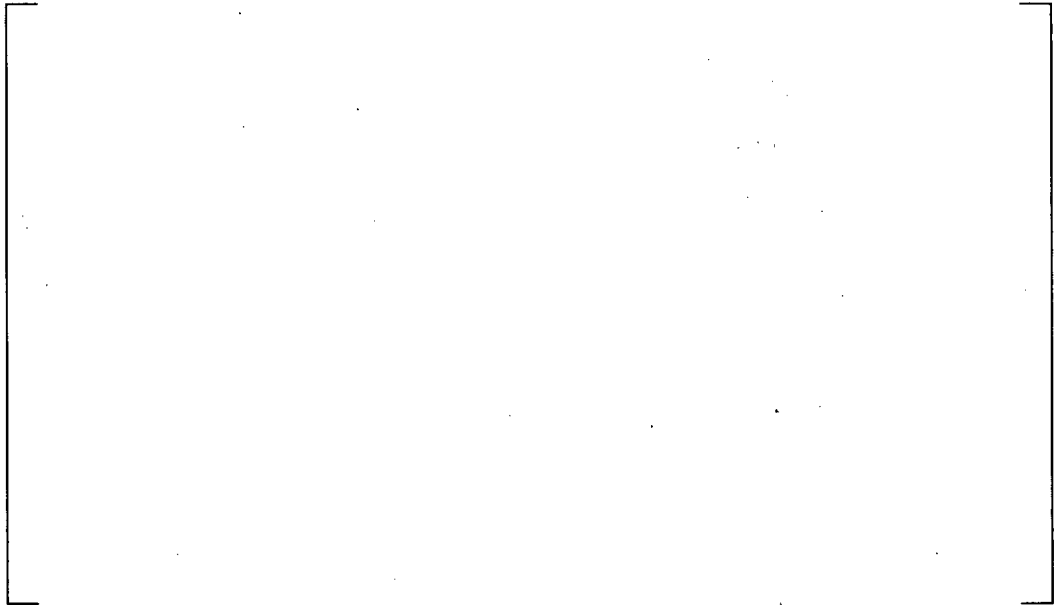
a,c,e

Figure 6-62 Computer Run S.1.5, Step 5, Stress Intensity



a,c,e

Figure 6-63 Computer Run S.1.5, Step 5, Contact Pressure



a,c,e

Figure 6-64 Computer Run S.1.5, Step 6, Stress Intensity



a,c,e

Figure 6-65 Computer Run S.1.5, Step 6, Contact Pressure



Figure 6-66 Computer Run S.1.5, Step 7, Stress Intensity



Figure 6-67 Computer Run S.1.5, Step 7, Contact Pressure

6.2.6 Divider Plate Modeling

The effect of the divider plate is modeled in the H* Integration model (Excel® spreadsheet model) through an adjustment factor to account for the presence or absence of the divider plate. The divider plate factor is normalized to the condition represented in the ASME Code Stress Report that assumes a non-functional, (or missing) divider plate to maximize the design stresses on the tubesheet. The tubesheet deflection corresponding to the ASME Code stress analysis of the tubesheet without the divider plate, therefore, results in a divider plate factor of []^{a,c,c}. Based on the use of the original structural model for the divider plate, the divider plate factor for the case of a fully functional divider plate is []^{a,c,c} because the tubesheet deflection would be decreased relative to the reference case.

During the development, the structural model of the tubesheet complex was significantly improved by including structural features such as the solid tubesheet rim and solid, non-perforated section in the tubelane, divider plate structural support of the channelhead, as well as other features that more correctly represented the tubesheet complex structure. Analysis of the tubesheet deflection using the improved model results in reduced predicted tubesheet deflection. For the case of a fully functional divider plate, the predicted deflection normalized to the original tubesheet deflection yields a divider plate factor of []^{a,c,c}. For the case of a non-functional divider plate, represented by eliminating the upper []^{a,c,c} inches of the divider plate where it attached to the tubesheet, but retaining the divider plate in the channelhead, results in a divider plate factor of []^{a,c,c}.

Cracking has been observed in the heat affected zone of the stub runner to divider plate welds in foreign SGs (Reference 6-7). The cracks appear to be the result of combined primary water stress corrosion cracking (PWSCC) and mechanical fatigue. Degradation of the divider plate to stub runner connections can affect the deflection of the tubesheet due to pressure loads. This degradation could affect an analysis that depends upon the divider plate to limit the vertical displacement of the tubesheet as well as analyses that take credit for a divider plate factor (DPF).

As noted above, the H* analysis bounds the effect of a severely degraded divider plate by increasing the tubesheet deflections by the ratio of the DPF for a degraded divider plate []^{a,c,c} to the DPF for an intact divider plate []^{a,c,c}, or []^{a,c,c}. In the context of the lower SG complex model and the H* contact pressure analysis, a degraded divider plate is considered a divider plate with the upper []^{a,c,c} inches of the weld, stub runner, and heat affected zone of the divider plate removed. This level of degradation has never been observed in any foreign SG and is extremely conservative compared to the reported levels of degradation over the prior 15 years of inspections in the foreign fleet (References 6-33, 6-34, and 6-35). See Reference 6-7 for a description of the divider plate factor for different levels of weld degradation and how the divider plate factor is calculated. Refer to Section 6.2.1 for a description of how the divider plate is included in the lower SG complex model.

Degradation of the divider plate does not significantly affect the pressures or temperatures of the primary fluid during any operating condition (Reference 6-36). The limiting sector of the tubesheet is perpendicular to the face of the divider plate. Refer to Section 6.2.3 for a discussion of the tubesheet displacements as a function of azimuthal position. The combined radial tubesheet displacements at the 90° plane of the perforated tubesheet region (parallel to the face of the divider plate along the edge of the divider lane) are typically []^{a,c,c}% less than the tubesheet displacements perpendicular to the face of the divider plate. Reducing the tubesheet displacements increases the contact pressure between the tube and

the tubesheet. See Figure 6-26 for a graph showing the increase in pull out resistance as a function of azimuthal angle in the tubesheet. Increasing the contact pressure between the tube and the tubesheet reduces the calculated H^* value. See Figure 6-68 for a comparison of the mean H^* values for a degraded divider plate and an intact divider plate. Note that the tubesheet displacements with a degraded divider plate predict a larger value of H^* than the tubesheet displacements with an intact divider plate.



Figure 6-68 Comparison Between H^* Values for a Degraded Divider Plate (DPF = []^{a,c,e}) and an Intact Divider Plate (DPF = []^{a,c,e}).

6.3 TUBESHEET ROTATION EFFECTS

The H^* integrator model includes a calculation for tubesheet hole dilation due to tubesheet rotations. A study was performed to evaluate if the tube bore dilation model from the reference case (Reference 6-15) in the H^* integration is appropriate when the 3D FEA displacements are used. The study compared the results for tubesheet bore dilation from the original 2D axisymmetric model and those from the 3D FEA model. This section summarizes the results of this study.

Loads are imposed on the tube OD as a result of tubesheet deflections. The interaction between the tubesheet and the other structures in the lower SG complex results in the tubesheet rotating due to the deflections under the applied pressure and temperature conditions. The radial displacements produced by the thermal loads are unaffected by the divider plate. The analysis results in this report conservatively assume (see Section 6.2.6) that the stub-runner-to divider plate weld is non-functional (i.e., there is no restraint provided to the vertical displacement of the tubesheet by the divider plate). The radial deflection, U_R , at any point within the tubesheet is found by combining the radial tubesheet deflections at that location according to:

$$\left[\quad \quad \quad \right] \text{ a,c,e}$$

where

DPF = the divider plate factor,

$U_{\Delta P}$ = the radial tubesheet deflections at the 0° face of the tubesheet (see Section 6.2.3) due to the applied pressure loads on the lower SG complex for the specific operating condition and

$U_{\Delta T}$ = the radial tubesheet deflections due to the applied temperature loads on the lower SG complex for the specific operating condition.

This expression is used to determine the radial deflections along a line of nodes at a constant axial elevation (e.g., top of the tubesheet, mid-plane, etc.) within the perforated area of the tubesheet. The expansion of a hole of diameter D in the tubesheet at a radius R is given by:

$$\begin{aligned} \text{Radial:} & \quad \Delta D = D \{dU_R(R)/dR\} \\ \text{Circumferential:} & \quad \Delta D = D \{U_R(R)/R\} \end{aligned}$$

U_R is available directly from the finite element results. The value for dU_R/dR is obtained by numerical differentiation of the combined displacement field. The maximum expansion of a hole in the tubesheet is in either the radial or circumferential direction. Typically, these two values are within []^{a,c,e}% of each other. Since the analysis for calculating contact pressures is based on the assumption of axisymmetric deformations with respect to the centerline of the hole, a representative value for the hole expansion must be used that is consistent with the assumption of axisymmetric behavior. A two-dimensional finite element study (Reference 6-15) was performed to determine the effect of hole "out-of-roundness" on the contact pressures between a sleeve and a tube, and between the tube and tubesheet. The equation used for the hole ΔD , $D_{\max} - D_{\min}$, is:

$$\left[\quad \quad \quad \right] \text{ a,c,e}$$

where SF is a scale factor between []^{a,c,c} and []^{a,c,c}. For the eccentricities typically encountered during tubesheet rotations, SF varies between approximately []^{a,c,c} and []^{a,c,c}. The eccentricities on the tube bore are due to combined pressure and temperature effects (e.g., tubesheet bow, thermal expansion, etc.). Eccentricity in this context is taken to mean the difference between the maximum hole diameter and the minimum hole diameter (ΔD). These values are listed in the following table:

Table 6-20 Scale Factor as a Function of Initial Eccentricity

a,c,e

The data for initial eccentricities were fit to the following polynomial equation (Reference 6-15):

$$[\hspace{15em}] \quad \text{a,c,e}$$

The hole expansion calculation as determined from the 3D finite element results includes the effects of tubesheet rotations and deformations caused by the system pressures and temperatures. It does not include the local effects produced by the interactions between the tube and tubesheet hole. The hole expansion equation was compared against the range of calculated displacements from the 3D finite element analysis. Both the previously calculated scale factors and ΔD factors were applicable when the displacements from the 3D finite element analysis were used. The results of the 2D hole expansion calculation were shown to be conservative and both increased hole growth and reduced contact pressure compared to the 3D results. Refer to Section 6.2.5 for a discussion of contact pressure variation due to tubesheet tube bore dilation. Therefore, the 2D hole expansion calculation is reasonable when the 3D FEA displacement results are used and the ΔD and SF equations can be used in the H* contact pressure analysis.

6.4 CALCULATION OF TUBE-TO-TUBESHEET CONTACT PRESSURE

6.4.1 Calculation of Local Effects Due to Interaction of the Tube and Tubesheet Hole

Standard thick shell equations, including accountability for the end cap axial loads in the tube (Reference 6-17), in combination with the hole expansions results from Section 6.3, are used to calculate the contact pressures between the tube and the tubesheet. The thick shell equations are assembled using the model provided by Goodier (Reference 6-18). The unrestrained radial expansion of the tube OD due to thermal expansion is calculated as:

$$[\hspace{15em}] \quad \text{a,c,e}$$

and, from pressure acting on the inside and outside of the tube as,

$$\left[\begin{array}{c} \text{---} \\ \text{---} \\ \text{---} \end{array} \right]^{a,c,e}$$

where:

- P_i = Internal primary side pressure, P_{pri} psi
- P_o = Crevice pressure, P_{cp} psi
- b = Inside radius of tube = []^{a,c,e} inch
- c = Outside radius of tube = []^{a,c,e} inch
- α_t = Coefficient of thermal expansion of tube, in/in/°F
- E_t = Modulus of Elasticity of tube, psi
- T_t = Temperature of tube, °F, and,
- ν = Poisson's Ratio of the material

The thermal expansion of the hole ID is included in the finite element results and does not have to be expressly considered in the algebra; however, the expansion of the hole ID produced by pressure is given by:

$$\left[\begin{array}{c} \text{---} \\ \text{---} \\ \text{---} \end{array} \right]^{a,c,e}$$

where:

- E_{TS} = Modulus of Elasticity of tubesheet, psi
- d = Outside radius of cylinder which provides the same radial stiffness as the tubesheet

Note that the outside radius of the representative tubesheet cylinder, d , is modified using the results described in Section 6.2.4. If the unrestrained expansion of the tube OD is greater than the expansion of the tubesheet hole, then the tube and the tubesheet are in contact. The inward radial displacement of the outside surface of the tube produced by the contact pressure is given by (Note: the use of the term δ in this section is unrelated to its potential use elsewhere in this report):

$$\left[\begin{array}{c} \text{---} \\ \text{---} \\ \text{---} \end{array} \right]^{a,c,e}$$

The radial displacement of the inside surface of the tubesheet hole produced by the contact pressure between the tube and hole is given by:

$$\left[\dots \right]^{a,c,e}$$

The equation for the contact pressure (P_2) is obtained from:

$$\left[\dots \right]^{a,c,e}$$

where ΔR_{ROT} is the hole expansion produced by tubesheet rotations obtained from finite element results. The ΔR 's are:

$$\left[\dots \right]^{a,c,e}$$

$$\left[\dots \right]^{a,c,e}$$

The resulting equation is:

$$\left[\dots \right]^{a,c,e}$$

where:

- P_i = Internal primary side pressure, P_{pri} psi
- P_{cp} = Crevice pressure, psi
- b = Inside radius of tube, in
- c = Outside radius of tube, in
- α_t = Coefficient of thermal expansion of tube, in/in/°F
- E_t = Modulus of Elasticity of tube, psi
- T_t = Temperature of tube, °F, and,
- ν = Poisson's Ratio of the material.
- P_2 = Contact Pressure

For a given set of primary and secondary side pressures and temperatures, the above equation is solved for selected elevations in the tubesheet to obtain the contact pressures between the tube and tubesheet as a

function of radius. The elevations selected ranged from the top to the bottom of the tubesheet. The contact pressure calculation results are limited to a minimum value of zero (0 psi) because it is not possible to have less than zero contact pressure between two objects. The OD of the tubesheet cylinder in the analysis is initially equal to that of the cylindrical (simulate) collars ([]^{a,c,e} inches) designed to provide the same radial stiffness as the tubesheet, which was determined from a finite element analysis of a section of the tubesheet (References 6-19 and 6-20). See Section 6.2.4 for a discussion of how the tubesheet cylinder OD is modified in the contact pressure analysis as a function of tubesheet radius. The tube inside and outside radii within the tubesheet are obtained by assuming a nominal plus 2 sigma diameter for the hole in the tubesheet ([]^{a,c,e} inch) and wall thinning in the tube equal to the average of that measured during hydraulic expansion tests. That thickness is []^{a,c,e} inch for the tube (Model F tube wall thickness after hydraulic expansion).

6.4.1.1 Changes in the Contact Pressure Calculation and H* Calculation Methodology

The contact pressure analysis methodology has not changed since 2007 (Reference 6-21). However, the inputs to the contact pressure analysis and how H* is calculated have changed in that period of time. For example, the effective stiffness of the simulated tubesheet collar can now vary as a function of tubesheet radius in the contact pressure analysis (see Section 6.2.4). The details describing the inputs to the contact pressure analysis are discussed in Section 6.0.

The calculation for H* includes the summation of axial pull out resistance due to local interactions between the tube bore and the tube. The calculation for H* conservatively ignores any additional pull out resistance due to tube bending within the tubesheet or Poisson expansion effects acting on the severed tube end. In previous submittals, the force resisting pull out acting on a length of a tube between any two elevations h_1 and h_2 was defined in Equation (6-4):

$$\left[\int_{h_1}^{h_2} \left(F_{HE} + \mu P \frac{d}{4} \right) dh \right]^{a,c,e} \quad (6-4)$$

where:

- F_{HE} = Resistance per length to pull out due to the installation hydraulic expansion,
- d = Expanded tube outer diameter (not related to the tubesheet collar outer diameter),
- P = Contact pressure acting over the incremental length segment dh , and,
- μ = Coefficient of friction between the tube and tubesheet, conservatively assumed to be []^{a,c,e} for the pull out analysis to determine H*.

The current H* analysis generally uses the following equation to determine the axial pull out resistance of a tube between any two elevations h_1 and h_2 :

$$\left[\dots \right]^{a,c,e} \quad (6-5)$$

Where the other parameters in Equation (6-5) are the same as in Equation (6-4) and μ_E and F_{HE}^{APP} are new parameters that account for the differences in modeling the effect of the installation hydraulic expansion. The μ_E parameter is the effective coefficient of friction evaluated for the final length of the tube portion within the tubesheet. The effective coefficient of friction can be calculated using Soler's method (Reference 6-37) or it can be an assumed value. The F_{HE}^{APP} is the applied effective resistance per length to pull out due to the installation hydraulic expansion, based on the work of Goodier (Reference 6-18). The combination of Soler's method with Goodier's analysis provides two equations to solve for the two unknowns in the residual contact pressure analysis: the distribution of the residual contact pressure for a given tube length, and the coefficient of friction between the tube and the tubesheet (Reference 6-38). The H* analysis has the option of calculating the residual resistance to pull out for any given tube length based on test data alone, calculations involving the test data, or some other user-defined distribution of residual effects. This means that if an H* analysis uses any value of residual contact pressure, the distribution of residual contact pressure is also adjusted in the final calculation of the H* value during the adjustment for the crevice pressure distribution. Refer to the H* analysis process diagram, Figure 2-1, for an illustration of the analysis sequence. However, the reference basis for the H* analysis is the assumption that residual installation pressure contributes zero (0) additional resistance to tube pull out. Therefore, the equation to calculate the pull out resistance in the H* analysis is:

$$\left[\dots \right]^{a,c,e} \quad (6-6)$$

The contact pressure is assumed to vary linearly between adjacent elevations in the top part of Table 6-25, Table 6-26 and Table 6-27. Substitution of a linear distribution of contact pressure into Equation (6-6) gives the following result between any two elevations in the tubesheet (L_1 and L_2)

$$\left[\dots \right]^{a,c,e}$$

or,

$$\left[\dots \right]^{a,c,e}$$

so that,

$$\left[\frac{F_{i+1} - F_i}{z_{i+1} - z_i} \right]_{a,c,e} = \frac{F_{i+1} - F_i}{z_{i+1} - z_i} \quad (6-7)$$

Equation (6-7) is used to calculate the accumulated force resisting pull out from the top of the tubesheet to each of the elevations listed in the lower parts of Table 6-25 through Table 6-27. The initial estimate for H^* is the point at which the result of Equation (6-7) is equal to, or greater than, the applied pull out loads given in Section 5.0. The available pull out resistance in the tube, (F_i), is linearly interpolated between the top of the tubesheet and any given elevation below the top of the tubesheet so that the equality in Equation (6-8) is true at the H^* depth.

$$\left[\frac{F_{i+1} - F_i}{z_{i+1} - z_i} \right]_{a,c,e} = F_i \quad (6-8)$$

Where the F in Equation (6-8) is equal to the applied end cap load for a specific operating condition as calculated in Section 5.0. The H^* spreadsheet model does not allow any pull out resistance to accumulate below []^{a,c,e} inch from the top of the tubesheet. The practical significance of that limit is that H^* cannot be less than []^{a,c,e} inch, because the rate of pull out resistance accumulation cannot exceed the applied pull out load until []^{a,c,e} inch. However, if an H^* depth of less than []^{a,c,e} inch is calculated using this process, for any operating condition at any tubesheet radius, the resulting H^* value is increased to a value of at least []^{a,c,e} inch. Any further modifications to H^* , such as increases for uncertainty in the location of the bottom of the expansion transition, are added to the minimum value of []^{a,c,e} inch.

6.4.2 General Description of 3D FEA Model Results

The three-dimensional finite element model calculates all normal and shear displacements for the tubesheet with respect to the undeformed condition in the global coordinate system. Results are available for all regions of the model, but, only the results for the perforated region of the tubesheet at the 0° hot leg face (symmetry plane) are required for the contact pressure analysis. This is because the displacements on the 0° face of the tubesheet generate the least contact pressure and produce the largest H^* values. Each SG in the Model F fleet has a slightly different set of displacements because of the small variations in the as-built design and plant-specific operating condition. However, the results from a plant-specific contact pressure analysis of the Model F fleet show that the radial displacements for the region of interest in the tubesheet are very similar. The NOP conditions generate the largest combined thermal and pressure displacements. The resulting contact pressure distributions throughout the Model F fleet are also very similar in the region of interest at the limiting tubesheet radius. The major component of tubesheet displacement in the finite element model is the deflection due to thermal growth. See Figure 6-69 and Figure 6-70 for graphs of the combined tubesheet deformations in the 3D finite element model for Millstone Unit 3. The results for Millstone Unit 3 are bounding for a 4-loop Model F SG plant. In general, the displacement and contact pressure results for a 3-loop Model F plant are bounded by the results for a 4-loop Model F plant. See Figure 6-71 through Figure 6-73 for graphs of the combined radial tubesheet displacement for Millstone Unit 3. The results shown in Figure 6-71, Figure 6-72 and Figure 6-73 are the sum of the scaled pressure displacements (i.e., multiplied by the divider plate factor

ratio of 1.60) and the thermal displacements for different tubesheet elevations. As expected, the bottom of the tubesheet is “tighter” than the top of the tubesheet and there is no bending at the neutral axis of the tubesheet. The resulting contact pressure distribution for Millstone Unit 3, at the limiting tubesheet radius of 20.5 in, is shown in Figure 6-74. The mean H^* distribution for Millstone Unit 3, as a function of tubesheet radius is shown in Figure 6-1.

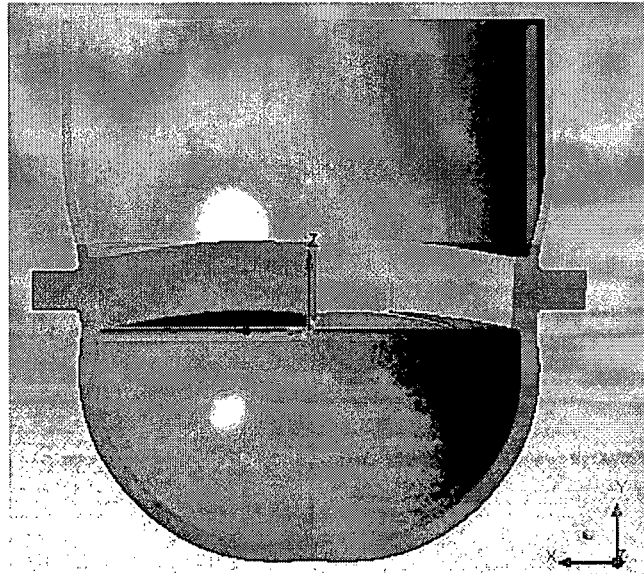


**Figure 6-69 Typical Combined Displacement for 3D Model During NOP
(Plotted on deflected mode shape, with a displacement magnification of 100x)**

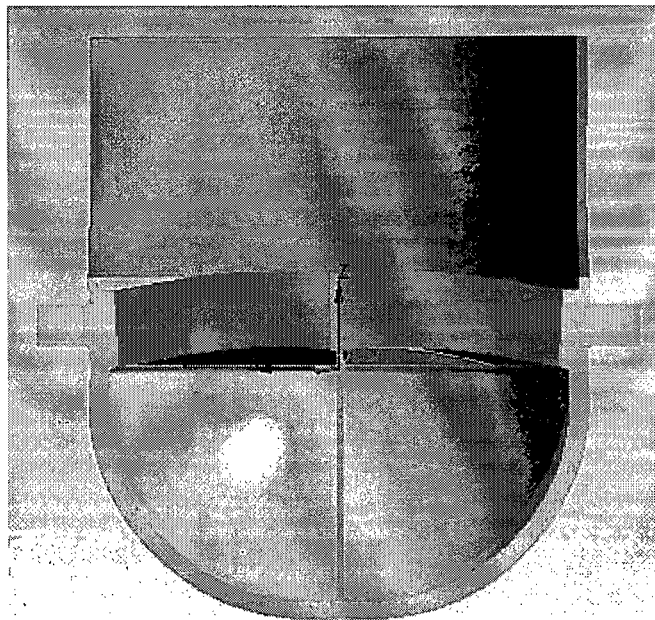


**Figure 6-70 Typical Combined Displacement for 3D Model During SLB
(Plotted on deflected mode shape, with a displacement magnification of 100x)**

a,c,e

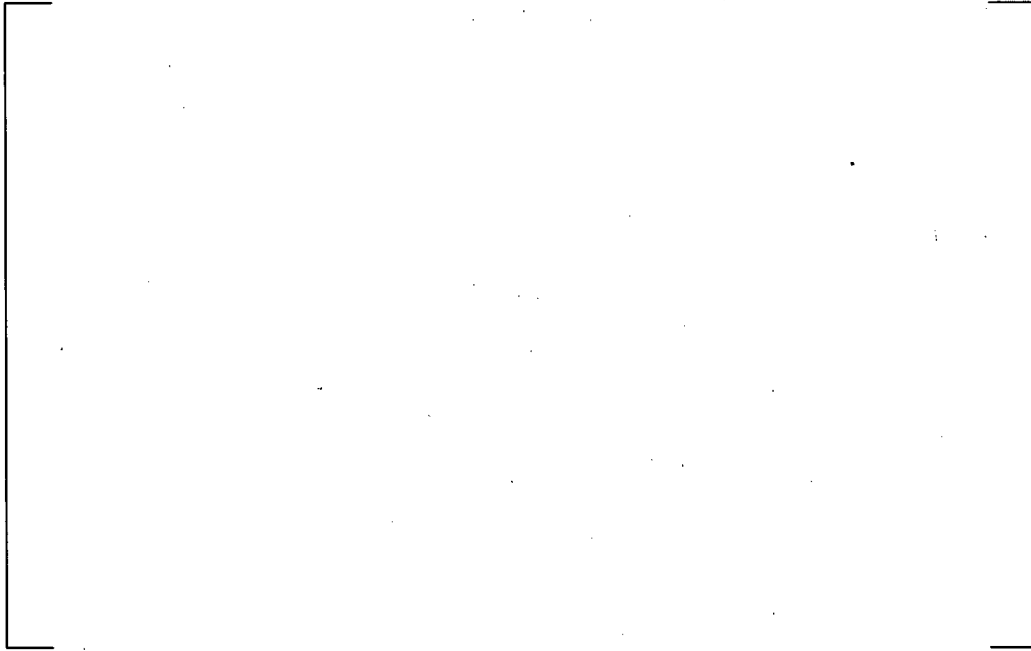


Figure 6-71 Combined Thermal and Pressure Tubesheet Radial Displacement for Millstone Unit 3 at the Bottom of the Tubesheet, DPF = []^{a,c,e}

a,c,e



Figure 6-72 Combined Thermal and Pressure Tubesheet Radial Displacement for Millstone Unit 3 at the Neutral Axis of the Tubesheet, DPF = []^{a,c,e}



Figure 6-73 Combined Thermal and Pressure Tubesheet Radial Displacement for Millstone Unit 3 at the Top of the Tubesheet, DPF = []^{a,c,e}

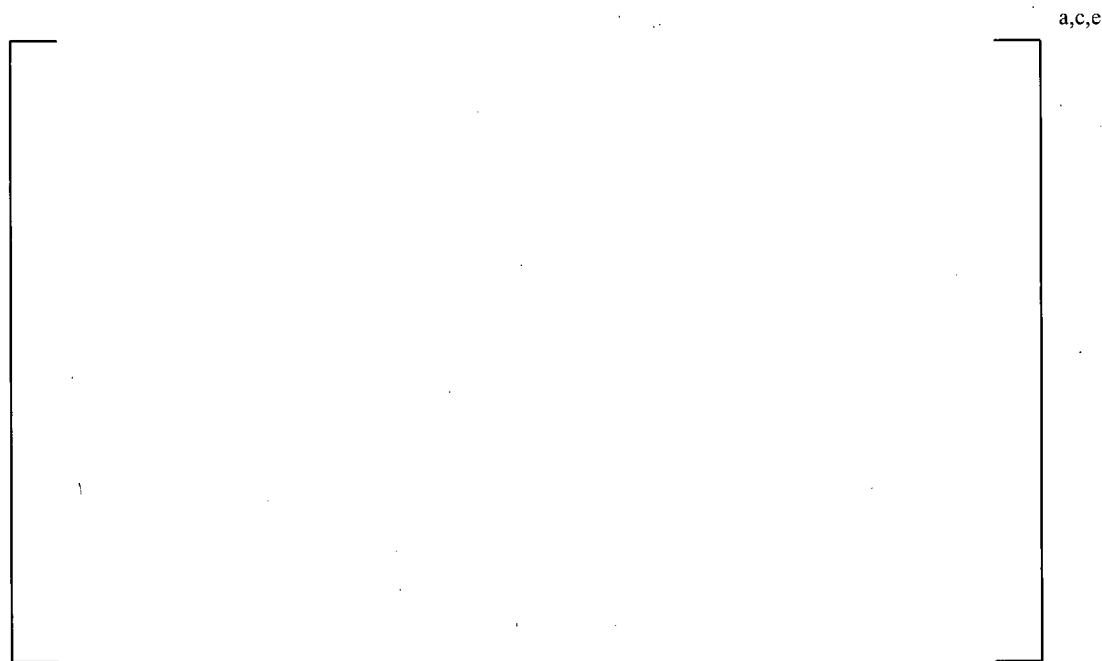


Figure 6-74 Comparison of Tube-to-Tubesheet Contact Pressure for Millstone Unit 3 at the Limiting Tubesheet Radius of []^{a,c,e} inches

(Results include all crevice pressure specimen data.)

6.4.3 General Description of 3D FEA Post-Processing

The structural analysis of the tubesheet complex provides the input displacement to the H* Integrator Excel® model (see Figure 2-1). In prior analyses for H*, the nodal arrangement in the 2D axisymmetric model was matched to the axial and radial nodes in the Excel® model so that the output matrix of tubesheet deflections could be used directly in the H* integration model. The 3D FEA model has a slightly different arrangement of nodes in the perforated tubesheet region due to the different plant-specific geometries and the higher order nodes. Therefore, it was necessary to “post-process” the deflection outputs from the 3D FEA model for use in the H* Integrator.

The result of the finite element analysis in ANSYS WorkBench is a binary data file that contains information about all of the requested displacements in the model at every node in the model. An ANSYS APDL macro routine is used to post-process the binary data file to obtain the necessary tubesheet displacement data. The output of the APDL macro is a 4 column by 1171 row vector that contains the ANSYS node number, radial coordinate, vertical elevation coordinate and the radial tubesheet displacement for each node on the 0° face of the tubesheet. The output from the APDL macro is the input for a spreadsheet that interpolates the tubesheet displacement data. The output from the spreadsheet is the input for the H* contact pressure analysis. This process is repeated for the thermal and pressure related displacements for each of the limiting operating conditions. The APDL macro and interpolation spreadsheet are capable of obtaining data from any azimuthal slice in the tubesheet. Only the results on the 0° tubesheet face are specified in this analysis because it has been shown to be the limiting region in the tubesheet (see Section 6.2.3).

6.4.4 Determination of Limiting Model F SG Plant in the H* Fleet

The limiting Model F H* plant was determined by a contact pressure analysis of each specific plant in the Model F fleet. The choice of the limiting Model F plant was based on three criteria:

1. The lowest calculated contact pressure at the bottom of the tubesheet.
2. The smallest rate of increase of the contact pressure from the top of the tubesheet to the mid-plane.
3. The greatest degree of sensitivity to variations in material properties due to plant operating conditions.

The comparison of the tube-to-tubesheet contact pressures was done on the zero degree (0°) face of the tubesheet at all tubesheet radii. See Figure 6-75 for a comparison of the mean tube-to-tubesheet contact pressure results at the limiting TS radius []^{a,c,e} inch) for all plants in the Model F fleet.

Criterion 1 is important because it describes how much potential margin is available for the contact pressure results. For example, if an analysis predicts lower contact pressures at the top of the tubesheet but greater contact pressures in the identified region of interest in a SG tube (due to potential flaws) that tube is at a lower risk of pull out.

Criterion 2 is also important because a greater rate of contact pressure increase indicates that less axial tube length is required to meet the pull out load.

Criterion 3 is the most significant because the final H^* and contact pressure analysis is a full bundle analysis that primarily depends upon a statistical variation in the (E) Young's Modulus and Coefficient of Thermal Expansion (α) of the tube and tubesheet.



Figure 6-75 Comparison of Contact Pressures for Model F Fleet Including All Crevice Pressure Data At Limiting TS Radius []^{a,c,e}

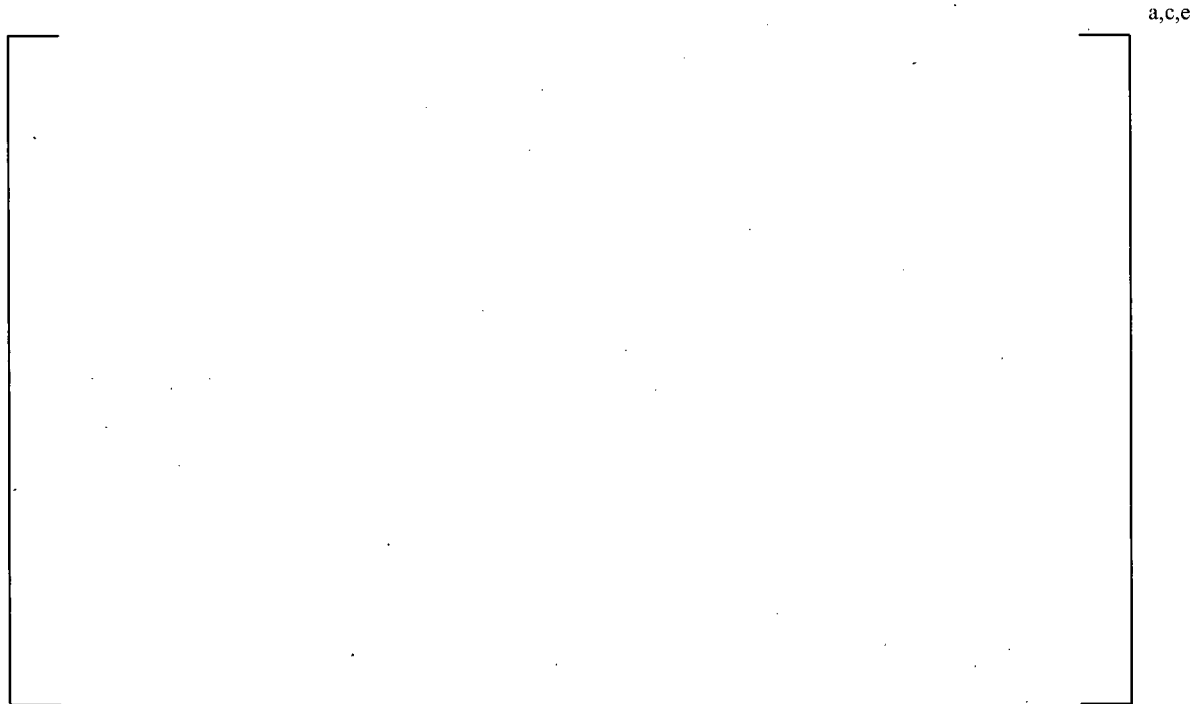


Figure 6-76 Tube-to-Tubesheet Contact Pressure for the Limiting Model F Plant (Millstone Unit 3) at the Limiting TS Radius Using Only the Specimen 8 Crevice Pressure Data

The Model F plant that satisfies all three criteria is Millstone Unit 3, for the post-uprating condition. All of the Model F plants are similar with respect to Criteria 1 and 2, although the Millstone results indicate lower contact pressures at the bottom of the tubesheet and a smaller contact pressure gradient at the limiting radius. However, Millstone has the highest specified operating temperature (see Table 5-1). This is important because the difference in the coefficient of thermal expansion for the tube and the tubesheet decreases with increasing temperature. The hotter that a plant operates, the more sensitive it is to variations in the thermal expansion coefficient. The difference in the coefficient of thermal expansion for the tube and the tubesheet between 600°F and 700°F is 4.00E-7 or less. Because Millstone Unit 3 operates at the highest fluid temperatures, it is more likely that the differential thermal component of the contact pressure calculation will be minimized and, at the other extreme, that the thermal growth of the tubesheet will be maximized. Therefore, the results from a Model F contact pressure analysis using the geometry and operating conditions from Millstone Unit 3 are the conservative bounding results for the Model F fleet.

6.4.5 Sample Mean H* and Contact Pressure Calculation

The calculation of H* relies upon the input for the finite element models discussed in Section 6.2, the operating parameters for a specific plant, and material properties. The initial value of H*, and the contact pressure, are modified by allowances for inspection uncertainty, temperature distribution and crevice pressure. The initial H* results come from a comparison of the pull out resistance at a given radius to the uniformly applied pull out loads. The calculated tube engagement length required to equilibrate the loads on the tube for each operating condition in the analysis is calculated and the maximum engagement length at any given radius is used as the initial H* value for that radius. It is typical for one operating condition to produce the lowest tube-to-tubesheet contact pressures at all radii which generates the largest (bounding) H* values for the plant. If a value of less than one inch is predicted at any given radius the final H* value at that radius is adjusted to a minimum value of one inch. See Table 6-21 for a summary of the initial mean H* values using the mean material inputs and operating parameters for Millstone Unit 3 based on the tubesheet displacements at the zero (0°) degree face of the tubesheet.

Table 6-21 Initial Mean H* Values

a,c,e

The maximum H* values occur during the NOP Low-T_{avg} condition and those values bound the H* results at all other tube radii. The limiting H* result, or the worst-case tube, is at the []^{a,c,e} inch radius. The maximum H* values occur during the NOP condition. Therefore, the H* results must be adjusted to account for the difference in the thermal distributions at NOP and accident conditions ([]^{a,c,e} inch). See Section 6.2.2.2.5 for the effect of assuming different tubesheet displacements due to

different thermal distributions. See Table 6-22 for a summary of the mean H* values with the thermal distribution adjustment.

Table 6-22 Mean H* Values Adjusted for Thermal Distribution Effect

a,c,e

The mean H* values are further adjusted to include the offset for the uncertainty in the location of the bottom of the expansion transition (BET). The BET offset for a Model F SG is 0.3 inch. This offset was developed from an uncertainty analysis of the location of the BET documented in Reference 6-22. Table 6-23 provides a summary of the adjusted mean H* values including the BET offset. The results in Table 6-23 are shown in Figure 6-1.

Table 6-23 Mean H* Values Including BET Offset

a,c,e

The adjusted H* values with the BET offset represent the first estimate of the final tube engagement length based on the assumption that the tube is severed at the bottom of the tubesheet. The definition of H* is that the tube below the specified H* depth is assumed to be nonexistent. Therefore, the initial estimate for H* must be adjusted so that the final tube length accommodates the crevice pressure distribution referenced to the calculated H* value. Changing the length in the analysis of the tube portion within the tubesheet redistributes the crevice pressure and changes the resulting contact pressure distribution. The result of shortening the tube length within the tubesheet (i.e., the difference between the initial assumption of the location of the severance and the initial prediction of H*) is to increase the calculated H* distance, typically increasing H* between []^{a,c,e} inch and []^{a,c,e} inches depending on the initial predicted value of H*. The adjustment required is proportional to the predicted initial H*. The result of including the thermal distribution adjustment, the BET offset and the crevice pressure adjustment is the final H* value. Table 6-24 summarizes the final mean H* values. The contact pressures related to the results in Table 6-21 are given in Table 6-25, Table 6-26 and Table 6-27.

Table 6-24 Final Mean H* Values

a,c,e

The variations in H* for a probabilistic study do not include the BET offset or the crevice pressure adjustment. The recommended input deck from a Monte Carlo analysis is used to determine the final H* values at a probabilistic confidence level and the resulting tube length that gives the crevice pressure adjustment. A final H* value calculated using the square root sum of the squares (SRSS) approach includes the thermal distribution effect and the BET and a conservative estimate of the crevice pressure adjustment. See Figure 1-1 for a graphical representation of the multiple passes required to generate the Final H* value with the crevice pressure adjustment.

6.4.6 Validation of Calculated Contact Pressures and Supporting Models

The results of the contact pressure and lower SG complex models were verified using two different means:

- Independent peer review using alternate models
- Alternate calculation method using Finite Element Analysis

Comparing the H* analysis results to these alternate analyses showed that the H* contact pressure analysis, and the related analysis models, are reasonable.

A comparison of the tubesheet complex structural model with a similar structural model prepared by Argonne National Laboratory (ANL) was performed during the development of the H* analysis, thus providing an independent assessment of the model. ANL created a similar finite element model, with some geometry differences, of the lower SG complex using ABAQUS. The tubesheet model included a single tube bore with a contact law to approximate the contact pressure distribution between a tube and the tubesheet at the limiting radius.

The comparison with the ANL model included a comparison of the maximum vertical (transverse) displacement of the tubesheet during NOP and SLB conditions for essentially the same input conditions. The ANL review also included a comparison of the calculated contact pressure at the limiting tubesheet radius as a function of the elevation within the tubesheet. The maximum vertical tubesheet deflections calculated in the H* lower SG complex model and the ANL finite element model were within []^{a,c,e}% of each other when the same material properties, pressure loads and temperatures were used. Therefore, the deflections in the H* lower SG model are reasonable and agree with the results from a different and independent finite element analysis.

The contact pressure results of the ANL model closely agreed with the contact pressure results from the H* analysis. The characteristic of the contact pressure distributions in the H* analysis and the ANL analysis were within []^{a,c,e}% of each other when the same material properties and boundary conditions were used. The same trend in the contact pressure distributions (minimum tube-to-tubesheet contact pressure at the top of the tubesheet, maximum tubesheet contact pressure at the bottom) was also observed. Both the ANL model and the H* model showed that the SLB contact pressure increased relative to the NOP contact pressure when the model boundary conditions changed from NOP to SLB. It is significant to note that the ANL model relied on a contact law with a different meshing scheme to achieve these results. Based on this comparison, it is concluded that the H* contact pressure analysis is reasonable and validated by a completely different model and analysis approach.

Because the H* contact pressure analysis is a complex process, a separate analysis was performed to verify the contact pressure analysis. The tubesheet deformations, tube bore deformations due to pressure and temperature, tube deformations due to pressure and temperature, strain hardening effects from installation, effects due to thermal lock-up between the tube and the tubesheet, etc., are all combined to calculate the contact pressure distribution between the tube OD and the tube bore ID. To verify the accuracy of the H* contact pressure analysis, a separate 2D planar finite element model of a tube within a single tubesheet cell was created. The tube and tubesheet cell model boundary conditions allowed the model to simulate separately each effect that the H* contact pressure model used in the calculation. The boundary conditions on the 2D planar tubesheet/tube cell model included:

1. Tube Expansion
2. Permanent Strain Hardening of the Tube
3. Installation Pressure Release
4. Tube Bore Dilation due to Pressure and Temperature loads on the Tubesheet
5. Heat-Up of the Tube and Tubesheet
6. Pressurization of the Tube to an Internal Pressure of 1220 psi
7. Pressurization of the Tube to an Internal Pressure of 2250 psi

Items 6 and 7 in the applied boundary conditions allow the 2D planar model to compare contact pressure results at different tubesheet elevations. The case of the reduced pressure (1220 psi) in Item 6 represents the upper 6 inches of the tube bore (close to the top of the tubesheet) when the crevice pressure acting on the tube is reduced but still affecting the total pressure differential across the tube wall. The case of the increased internal pressure (2250 psi) in Item 7 models the condition of no crevice pressure acting on the tube. The mean material properties were used for both the tube and the tubesheet in the 2D planar model and the H* contact pressure analysis. The maximum tube bore dilation for the NOP case, as calculated using the results from Section 6.2.4, were used for the 2D planar model, were applied so that the tubesheet bore could only extend along a major axis without acting to "pinch" the tube in the orthogonal axis (i.e., zero Poisson contraction). The tube bore dilations in the H* contact pressure analysis were calculated using the tubesheet deflections and the eccentricity relationship described in Section 6.3. The contact pressure result at an elevation that had approximately the same tube bore dilation as the input to the 2D planar model was used to compare the two different methods. Both the tube and the tubesheet were heated to 600°F in the 2D planar model. The H* contact pressure analysis used the boundary

conditions for a typical Model F SG in the domestic fleet. The 2D finite element analysis showed that the tube and the tubesheet always maintain contact throughout Steps 1 through 7. Further, the 2D planar analysis showed that the variation in contact pressure around the circumference of a tube and tubesheet cell with applied deformations, pressures and temperatures was minimal and remained close to the average value around the entire tube OD. The H* contact pressure analysis predicted less contact pressure between the tube OD and the tube bore ID than the 2D FEA model predicted for every case. For example, in the case of feedwater line break, ΔP across the tubesheet equal to 2650 psi, both the tube and the tubesheet at the temperature of 622.6° F, at a tubesheet radius of []^{a,c,c} inches, at an elevation of approximately 2 inches above the tube end weld, with a tube bore eccentricity of []^{a,c,c} inch, and zero residual contact pressure (0 psi) the 2D finite element model predicts an average tube-to-tubesheet (T-TS) contact pressure around the circumference of the tube of []^{a,c,c} psi. The H* contact pressure analysis predicts a tube-to-tubesheet (T-TS) contact pressure of []^{a,c,c} psi for the same conditions, tube bore eccentricity, radius and elevation. Similarly for the case of NOP, with a ΔP across the tubesheet equal to 1453 psi ($P_{pri} = 2250$ psia, $P_{sec} = 797$ psia), with both the tube and the tubesheet at 622.6° F, at a tubesheet radius of []^{a,c,c} inches, at a elevation approximately []^{a,c,c} inches above the tube end weld, with a tube bore eccentricity of []^{a,c,c} inch, and zero residual contact pressure (0 psi) the 2D finite element model predicts a maximum T-TS contact pressure of []^{a,c,c} psi. The H* contact pressure analysis predicts a maximum T-TS contact pressure of []^{a,c,c} psi for the same conditions, tube bore eccentricity, radius and elevation. Therefore, the results of the H* contact pressure analysis included in the H* Integrator model are a reasonable estimate of calculated contact pressure available between the tube and the tubesheet during operating conditions based on conservative FEA results.

6.4.7 Distribution of Tube-to-Tubesheet Contact Pressure as a Function of Tubesheet Elevation

Previous H* submittals include data that showed a contact pressure profile that is similar to a typical bending stress profile through the thickness of the tubesheet. In that case, for a positive pressure difference between the primary and secondary faces of the tubesheet, the tubesheet will “bow” upward away from the channelhead. This deflection “pinches” the tubesheet bores at the primary surface of the tubesheet and acts to “open” the crevice at the top of the tubesheet. The change from the ALSP model to the 3D model also demonstrates this kind of behavior in the tubesheet deflection. See Figure 6-77 and Figure 6-78 for graphs of the deflection through the tubesheet at three tubesheet radii using the operating conditions in Table 6-8 for NOP and Table 6-8 for SLB.

The FEA results from the 3D models were obtained using the boundary conditions described in Section 6.2.2.2 and the procedure described in Section 6.4.3 to post-process the 3D FEA results into the required H* analysis input format.



**Figure 6-77 TS Radial Displacement Under Combined Thermal and Pressure Loads During SLB
TTS = TS Elevation 21.0 in, BTS = TS Elevation 0.0 in.**



**Figure 6-78 TS Radial Displacement Under Combined Thermal and Pressure Loads for NOP
TTS = TS Elevation 21.0 in, BTS = TS Elevation 0.0 in.**

The tubesheet displacements in Figure 6-77 and Figure 6-78 show that the combined displacements for the NOP cases are larger than the combined displacement for the SLB case at each of the radii. The rates of increase of the combined tubesheet displacements for the SLB case are also greater than the rate of slope increase of the combined tubesheet displacements during NOP. The FEA results in Figure 6-77 and Figure 6-78 show that the tubesheet is "tighter" at the bottom of the tubesheet than at the top of the tubesheet and that the tubesheet is tighter at the SLB conditions than at NOP conditions. If actual SLB and NOP conditions are used to model the radial displacements in the tubesheet, the trend of the results in Figure 6-77 and Figure 6-78 remain but the magnitude of the displacements are different. Figure 6-79 and Figure 6-80 use the input data from Table 6-9 and Table 6-10 for NOP conditions and the input data from Table 6-11 for SLB. This data represents the bounding operating conditions from a single plant instead of the generic operating conditions from a postulated Model F plant.



Figure 6-79 Combined Thermal And Pressure Load Tubesheet Radial Displacements for NOP
TTS = TS Elevation 21.0 in, BTS = TS Elevation 0.0 in.

The tubesheet displacements shown in Figure 6-79 and Figure 6-80 show that both the gradient of the tubesheet displacements as a function of tubesheet elevation and the magnitude of the radial tubesheet displacements in Figure 6-77 and Figure 6-78 are conservative relative to actual plant operating conditions.



**Figure 6-80 Combined Thermal and Pressure Load Tubesheet Radial Displacements for SLB
TTS = TS Elevation 21.0 in, BTS = TS Elevation 0.0 in.**

The deflection profiles shown in Figure 6-77 through Figure 6-80 show that the contact pressure distribution between the tube and the tubesheet approximately follows the assumed bending stress profile (tight at the bottom of the tubesheet, looser at the top of the tubesheet). They also indicate that the contact pressure distribution for SLB conditions exceeds the contact pressure distribution for NOP conditions at some depth within the tubesheet for expected input operating conditions. See Figure 6-81 for a graph of the tube-to-tubesheet contact pressures during SLB and NOP conditions when the generic input for NOP conditions (Table 6-9 and Table 6-10) are used and the generic input conditions for SLB (Table 6-11) are used. It is concluded from Figure 6-79 that the contact pressure at SLB conditions exceeds that for NOP conditions. Although Figure 6-79 shows the axially distributed contact pressure at the limiting radial location, the same conclusions also apply for all other radial location in the tubesheet.



Figure 6-81 Mean Contact Pressure Distribution Case for Millstone Unit 3 Conditions at a TS
 Radius of []^{a,c,e} inches TTS = TS Elevation 0.0 in, BTS = TS Elevation 21.03 in.

6.4.8 Effect of Excluding Specimen 7 Crevice Pressure Data on Contact Pressure Results

The crevice between the tube and the tubesheet is an important component of the H* contact pressure analysis. Reference 6-28 documents data from a test whose purpose it was to determine the crevice pressure distribution assuming a primary-to-secondary leak in the expanded region of the tubesheet. The data from Reference 6-28 was included with a prior analysis of H* (Reference 6-24) together with a basis for applying the test data. Subsequently, a recommendation was received from the NRC to apply the test data in a different fashion termed a “distributed,” or, “depth-based” pressure distribution. The depth-based crevice pressure distribution has been adopted as the reference analysis case for H*. See Reference 28 for a description of how the crevice pressure data is applied in the H* analysis.

Crevice pressure and leakage tests are extremely difficult to perform, especially at elevated temperature, because the leakage is very small and difficult to measure even over an extended period of time. Some of the data, identified as Specimen 7, in Reference 6-28 appears counter-intuitive, suggesting a reversal of flow near the exit from the crevice. During a review of this data with the NRC Staff and ANL, it was concluded that the counter-intuitive data (from Specimen 7) in the crevice pressure experiment should be excluded from the final H* contact pressure distribution analysis. In general, exclusion of the data from Specimen 7 results in less conservative results for H*. The final analysis for H* excludes the data from Specimen 7; however, the analysis to determine the limiting plant was based on the use of the entire data set, including Specimen 7. This was done to make sure that all of the collected test data was used in a conservative fashion when determining the limiting plant in the Model F fleet and any contact pressure related sensitivities (e.g., see Sections 6.2.4, 6.2.3, 6.2.5, 6.3, 6.4, 6.4.1 and 6.4.4). It was determined that the reduction in the mean H* value as a function of tubesheet radius when the Specimen 7 data is

excluded is small. The effect of excluding the Specimen 7 data on the associated contact pressure and sensitivity studies can also be assumed to be small. Therefore, the conclusion from this analysis is that Model F H^* population is not affected by excluding the Specimen 7 crevice pressure data from the contact pressure analysis. Figure 6-82 compares the crevice pressure as a function of tubesheet elevation with the test data from Specimen 7 and Specimen 8 included and the crevice pressure distribution using only the Specimen 8 data. The resulting H^* distributions for the different crevice pressure distributions are shown in Figure 6-83.



Figure 6-82 Comparison of the Average Crevice Pressure Data as a Function of Depth Ratio for the Entire Crevice Pressure Data Set and the Data Set When Only Specimen 8 is Considered



Figure 6-83 Comparison of H^* for Different Crevice Pressure Data Input

6.5 CONCLUSIONS

The results of the H* contact pressure analysis demonstrates that there is sufficient contact pressure between the tube and the tubesheet due to thermal effects, pressure effects, tubesheet deflections and tube deflections to justify moving the primary pressure boundary and load path from the tube end weld to the tube-to-tubesheet expansion joint. The NOP contact pressure distribution is bounded by the SLB and FLB contact pressures throughout the tubesheet for the mean input case. The H* contact pressure analysis results also show that the contact pressure increases from the top of the tubesheet to the bottom of the tubesheet. See Figure 6-81 for a graph of the contact pressure at the limiting tubesheet radius in the limiting Model F plant. See Table 6-25, Table 6-26 and Table 6-27 for summaries of the mean contact pressure distributions in the limiting plant with Specimen 8 crevice pressure data input only. The limiting case, in the limiting sector, and throughout the tubesheet, is NOP Low-T_{avg}. This case bounds all other load combinations and tubesheet displacement to produce the limiting H* in the tube bundle. See Figure 6-1 for a graph of the mean value of H* as a function of tubesheet radius. The significant conclusions in Section 6.0 are summarized in the list below:

1. The calculated mean value of H*, []^{a,c,c} inches, is based on the limiting tube location at a radius of []^{a,c,c} inches in the limiting sector of the tubesheet. All other tubes will have a lower (i.e., better) value of H*.
2. The reference structural model for the H* analysis is a 3D FEA model that replaces the 2D ALSP model utilized in prior H* evaluations. The 3D model shows that the results from the 2D model were conservative.
3. The 3D FEA model has been validated by comparing it to another model of the same structure, as well as a model by an independent organization, and achieving the same results.
4. The limiting tubesheet displacements in the bundle occur on the line that is perpendicular to the divider plate (referenced to the 0° face of the half symmetry tubesheet in the 3D FEA model). Tubesheet displacements at all other azimuthal positions in the bundle are less than the displacements on the zero (0) degree face.
5. A greater value of H* results when the divider plate is assumed to provide no support to the tubesheet. This conclusion applies for all radii on the tubesheet.
6. The effect of excluding Specimen 7 from the crevice pressure data is to slightly decrease the value of H*.
7. Leakage channels in the crevice do not develop as a result of tubesheet bore dilation. The tube has been shown to remain in contact with the tubesheet bore for all predicted deformations of the tubesheet bore. The variation in contact pressure around the circumference of the tube is very small for the expected range of deformations.
8. The contact pressure between the tube and the tubesheet is greater during SLB/FLB conditions than at NOP conditions at all locations in the tubesheet, for all plants in the Model F fleet.
9. The bounding plant among the Model F population is Millstone Unit 3. Millstone Unit 3 meets all of the criteria established to define the bounding plant. In particular, Millstone Unit 3 has the highest specified operating temperature among the candidate Model F plants.

6.6 REFERENCES

- 6-1 NEI 97-06, Rev. 2, "Steam Generator Program Guidelines," Nuclear Energy Institute, Washington, DC, May 2005 (issued for use by NEI on September 2, 2005 and confirmed by the NRC Staff as complying with TSTF-449 on October 3, 2005). Implementation is mandatory by March 2, 2006.
- 6-2 RIS 2007-20, NRC Regulatory Issue Summary 2007-20, "Implementation of Primary-to-Secondary Leakage Performance Criteria," August 23, 2007.
- 6-3 ASME Boiler and Pressure Vessel Code, Section 111, "Rules for Construction of Nuclear Power Plant Components," The American Society of Mechanical Engineers, New York, NY, 1989, No Addenda.
- 6-4 LTR-NCE-08-184, "Documentation of the Drawings and Input Data used in the creation of the FE Models of the Model 44F, D5 and F Steam Generators," October 31, 2008.
- 6-5 T. Slot, Stress Analysis of Thick Perforated Plates, 1972.
- 6-6 WTD-ED(SA)-70-037, "Influence of the Divider Lane on Tubesheet Stresses," September 1970.
- 6-7 *Divider Plate Cracking in Steam Generators: Results of Phase I: Analysis of Primary Water Stress Corrosion Cracking and Mechanical Fatigue in the Alloy 600 Stub Runner to Divider Plate Weld Material*. EPRI, Palo Alto, CA: 2007. 1014982.
- 6-8 A.P. Boresi, R.J. Schmidt, Advanced Mechanics of Materials, 6th Edition.
- 6-9 WTD-SM-75-072, "Temperature Distributions for Calculation of Secondary Skin Stress in D2-D3 Tubesheet Analysis," August 1975.
- 6-10 NCE-88-271 (Proprietary), "Assessment of Tube-to-Tubesheet Joint Manufacturing Processes for Sizewell B Steam Generators Using Alloy 690 Tubing," Westinghouse Electric, Pittsburgh, PA, November 1988.
- 6-11 Mark's Standard Handbook for Mechanical Engineers, 10th Ed., Editors: E.A. Avallone, T. Baumeister III, 2007.
- 6-12 WCAP-15932-P (Proprietary), Revision 1, "Improved Justification of Partial-Length RPC Inspection of the Tube Joints of Model F Steam Generators of Ameren-UE Callaway Plant," Westinghouse Electric Company LLC, Pittsburgh, PA, May 2003.
- 6-13 TID-26666, Vol 1, Design Data, Nuclear Systems Materials Handbook, ORNL, 1988.

-
- 6-14 WEST-13-402, Rev. 1, "An Evaluation of the Statistical Variability in Coefficient of Thermal Expansion Properties of SA-508 and Alloy-600," December 2008.
- 6-15 SM-94-58, Rev. 1, "Doel 4 Elevated Tubesheet Sleeve – ASME Code Evaluation and Effect of Tubesheet Rotations on Contact Pressure."
- 6-16 CN-SGDA-03-99 (Proprietary), "Evaluation of the Tube/Tubesheet Contact Pressures for Wolf Creek, Seabrook, and Vogtle Unit 1&2 Model F Steam Generators," Westinghouse Electric Company LLC, Pittsburgh, PA, September 2003.
- 6-17 SM-98-102 (Proprietary), Rev. 2, "Tube/Tubesheet Contact Pressures for Yonggwang 2," Westinghouse Electric, Pittsburgh, PA, November 1998.
- 6-18 Goodier, J., Schoessow, G., "The Holding Power and Hydraulic Tightness of Expanded Tube Joints: Analysis of Stress and Deformation," Transactions of the ASME, Vol. 65, July 1943.
- 6-19 STD-TP-1997-7951, Rev. 1, "Vogtle-1 SG 4 Tube-to-Tubesheet Joint Evaluation (Hydraulic Expansion Only to Determine Leakage and Loading Resistance)," Westinghouse Electric, Pittsburgh, PA, May 19, 1997.
- 6-20 CN-SGDA-03-99 (Proprietary), "Evaluation of the Tube/Tubesheet Contact Pressures for Wolf Creek, Seabrook, and Vogtle Unit 1&2 Model F Steam Generators," Westinghouse Electric Company LLC, Pittsburgh, PA, September 2003.
- 6-21 Wolf Creek Generating Station – Withdrawal of License Amendment Request on Steam Generator Tube Inspections (TAC No. MD0197)," United States Nuclear Regulatory Commission, Washington, D.C., February 28, 2008.
- 6-22 LTR-SGDA-03-129, "Responses to NRC RAIs on Partial-Length RPC Inspection of the Tubesheet Region of the Callaway Plant Steam Generators to AmerenUE Callaway (Class 2 Document)," June 2, 2003.
- 6-23 W. B. Middlebrooks, D. L. Harrod, and R. E. Gold, *Nuclear Engineering and Design* 143, 1993, pp. 159-169.
- 6-24 WCAP-16794-P, "Steam Generator Tube Alternate Repair Criteria for the Portion of the Tube Within the Tubesheet at the Vogtle Unit 1 & 2 Electric Generating Plants," October 2007.
- 6-25 Remaining Technical Issues Related to Technical Specification Amendment Request Regarding Steam Generator Tube Inspections Based on H*/B* Methodology, TAC No. MD0197, Wolf Creek Generating Station, Docket No. 50-482, January, 2008.
- 6-26 Reference Number Intentionally Not Used.

- 6-27 WCAP-16145-P, "Justification for the Partial-Length Rotating Pancake Coil (RPC) Inspection of the Tube Joints of the Vogtle Units 1 & 2 Model F Steam Generators," October 2003.
- 6-28 LTR-SGDA-07-4 (Proprietary), "Letter Summary of Changes to B* and H* Analysis due to New Crevice Pressure and Divider Plate Data," Westinghouse Electric Company LLC, Pittsburgh, PA, January 17, 2007.
- 6-29 C.D. Cassino, LTR-SGMP-09-17, "Pressurized Tubesheet Stiffness Analysis."
- 6-30 CN-SGMP-08-3, "Residual Contact Pressure Between Steam Generator Tube and Tubesheet After Tube Expansion – Parametric Study."
- 6-31 Reference Number Intentionally Not Used.
- 6-32 WCAP-16228-P, "PWSCC Susceptibility Assessment of the Alloy 600 and Alloy 82/182 Components in Wolf Creek," March 2004.
- 6-33 D'Annucci, F., "Inspection of the Steam Generator Partition Plate," Proceedings of ICAPP '05, Seoul, Korea, May 15-19, 2005, Paper 5711.
- 6-34 MRP-EDF-SGPP02, "DAMPIERRE 1/2 NPP – Unit 1 – Chemical, Metallurgical and Mechanical Characterizations of the Weld Joining the Partition Stub, the Divider Plate and the Channelhead Bowl."
- 6-35 MRP-EDF-SGPP04, "CHINON B NPP – Unit 4 – Characterization of Indications Discovered on the SG #2 Stud / Partition Plate Weld Surface."
- 6-36 *Divider Plate Cracking in Steam Generators: Results of Phase II: Evaluation of the Impact of a Cracked Divider Plate on LOCA and Non-LOCA Analyses.* EPRI, Palo Alto, CA: 2008. 1016552.
- 6-37 Soler, A. et al., 1984, Mechanical Design of Heat Exchanger and Pressure Vessel Components, Arcturus Publishers, Cherry Hill, NJ.
- 6-38 Allam, M., Bazergui, A., Axial Strength of Tube to Tubesheet Joints, Journal of Pressure Vessel Technology, Volume 124, February 2002.
- 6-39 CN-SGMP-09-14, "Plant – Specific Finite Element Analyses of Model F Plants for H*," April 2009.
- 6-40 LTR-SGMP-09-22, "H* Analysis Section 6 Summary Letter," April 2009.

7.0 RESIDUAL CONTACT PRESSURE

Residual Contact Pressure (RCP) is defined as the pressure between the tube and the tubesheet at room temperature resulting from the hydraulic expansion of the tubes into the tubesheet. Pull out tests have been performed to support prior submittals of the H^* justifications (Reference 7-1) and in conjunction with leakage tests to support return to power reports for plants that have experienced tube end damage due to failure of a split pin (Reference 7-3 and 7-4). These tests have been performed at both room temperature and at elevated temperatures. The tests utilized steel collars that simulated the stiffness and strength of unit cells of tubesheets with different dimensions of the square pitch and tube bore diameter.

Residual contact pressure derived from the measured pull out forces from tests that simulate the as-manufactured condition of the steam generators (SGs). All of the tests that have been performed to date have demonstrated that a positive value of RCP exists after the hydraulic expansions. However, the results from pull out test depend on a number of factors, including dimensional variations of the tubes and the tubesheet collars, surface finish variations, potential manufacturing artifacts in the tubesheet (collar) bore, process variables such as expansion pressures, etc. For elevated temperature pull out testing, the derivation of the RCP from the test data depends on the specific values of the coefficient of thermal expansion for the materials used for the test specimens that are generally not specifically known but fall within a small range (see Appendix B). As a result, elevated temperature pull out test data are not used for this evaluation. Nevertheless, data scatter is anticipated in the pull out tests and reduction of the test data to determine RCP due to the factors noted above. Uncertainty in the RCP value used was the source of staff concerns in prior submittal of H^* (Reference 7-1).

Another area of concern identified by the NRC staff was that only limited pull out data exists from which the residual contact pressures are estimated. The NRC staff stated in Reference 7-2 that insufficient information had been provided to establish whether the pull out test specimens used to determine residual contact pressure adequately envelop the range of values of these parameters which might be encountered for the expected range of the H^* value. Note that the prior analysis for H^* was very conservative and that larger values of H^* than provided in Section 6.0 were conservatively predicted. In prior submittals of H^* , the predicted H^* value was conservatively estimated using a 2-dimensional axisymmetric structural model, and temporary applications of H^* at 17 inches were approved (Reference 7-5). However, the pull out test specimen lengths were significantly shorter than the approved value of H^* , leading to questions if the force per unit length (F/L) calculations were reliable for the longer specified value of H^* .

To address these issues, a new pull out test program was initiated to support the development of H^* as described in this report. In addition, an analysis was performed to evaluate the uncertainties applicable to RCP (see Table 7-1). The purpose of the test program was to provide additional pull out data for longer test specimens than tested previously, which would be used to establish a conservative value of the expected mean RCP. The parallel analysis program provided the uncertainties that should be applied to the mean RCP determined from the pull out test program and prior pull out test data.

This section provides the results of the pull out test program and the results of the analytical uncertainty study the parameters that affect the RCP.

7.1 PULL OUT TEST PROGRAM

The objective of the pull out test program was to define a conservative mean value of residual contact pressure for use in the H^* analysis. Pull out tests provide load vs. displacement data for specimens of different lengths that represent both the range of potential values of H^* and the different tube diameters among the population of H^* candidates (11/16 inch, 3/4 inch and 7/8 inch). The RCP is calculated from the recorded pull out forces from these tests assuming the same coefficient of friction (0.2) that was assumed in Section 6.0 for the H^* structural analysis. This section, which summarizes the pull out test results and analysis for mean residual contact pressure, is currently in preparation. When completed, this section will provide the mean value of RCP that can be applied in the H^* justification, together with the uncertainty analysis provided in Section 7.2.

The reference value for RCP assumed in this report for H^* is assumed to be zero. The mean value of H^* provided in Section 6.0 and the probabilistic assessment in Section 8.0 are based on the assumption of zero residual contact pressure. Any positive value of RCP will reduce the mean value of H^* provided in section 6.0 and the probabilistic value of H^* discussed in Section 8.0.

7.2 ANALYSIS FOR UNCERTAINTIES IN RCP

7.2.1 Variables that Affect the Value of RCP

Table 7.1 summarizes the variables that impact the uncertainty of the RCP and that were considered in the calculations for RCP uncertainty.

For the component dimension variables, the mean values were determined from the applicable manufacturing drawings. The limits of the drawing tolerance were interpreted as $[]^{a,c,e}$ values and the $[]^{a,c,c}$ values were determined from this definition. This is conservative because component dimensions exceeding the drawing tolerances would be rejected. Since all components will meet the drawing dimensions unless documented by a manufacturing deviation notice as isolated cases, the limits of the drawing tolerances represent the total distribution of the variables.

For material properties, S_y , E_T and E_{TS} , the limits of the material specification were conservatively interpreted as $[]^{a,c,c}$ values and the $[]^{a,c,c}$ values were determined from this definition. This is conservative because materials exhibiting property values outside the specification would be rejected for use.

The Young's moduli, E_T and E_{TS} , are also parameters that directly affect the structural calculation for H^* in Section 6.0 and, consequently, the probabilistic evaluation for H^* in Section 8.0. The influence of the Young's moduli on both the structural analysis and on the RCP analysis is very small. Therefore, the Young's moduli of the tube and tubesheet materials are considered independently in the structural analysis and RCP analysis. No effort was made to coordinate the specific values of Young's modulus between the structural analysis and the analysis for RCP.

For the uncertainty analysis, the mean tube expansion pressure was conservatively assumed to be the minimum acceptable expansion pressure from the manufacturing specification for the Model F SGs. A $[]^{a,c,c}$ standard deviation of the minimum acceptable expansion pressure was assumed to account for

expansion equipment instrumentation error. The manufacturing procedures prevent the as-built expansion pressure to be less than the lower tolerance of the specification. Tubes that initially did not meet the minimum expansion pressure were re-expanded at a higher pressure to assure compliance with the process specification. Therefore, the expansion pressure assumed for this study is a conservative, lower bound value when considering the absolute values of calculated residual contact pressures. Any expansion pressure greater than the assumed minimum value will result in an increase in the predicted residual contact pressure.

7.2.2 Structural Analysis Model

The analysis model to evaluate the contact stresses was a 2 dimensional plane strain finite element model using the ANSYS computer code (Reference 7-9). Both the tube and tubesheet are represented using the ANSYS []^{a,c,e} finite element, which is a 2-dimensional plane structural element. The model is a full 360° representation of the tube and tubesheet. The finite element mesh consists of []^{a,c,e} nodes about the circumference of both the tube and tubesheet. []^{a,c,e} elements are used radially through the tube wall and []^{a,c,e} elements are used radially through the tubesheet collar.

The contact interaction between the tube and tubesheet during hydraulic expansion is represented analytically as a []^{a,c,e}.

Figure 7-1 shows an overall view of the finite element model. This view shows the Model F model. The finite element models for Model D5 and 44F are similar; only the dimensions differ slightly. Figure 7-2 shows a close up of the tube region of the model.

7.2.2.1 Dimensions, Boundary Conditions and Loads

The model simulates the unit cell representation of the tubesheet, using the same approach used in Section 6.0 to calculate contact pressure. The external dimensions of the collar that simulates the stiffness of the tubesheet unit cell is the same as that utilized in the pull out tests (Reference 7-9) for the different models of SG represented. The collar bore and tube dimensions are initially the mean values specified on Table 7-1.

Because there are no physical boundary conditions for the tube-to-tubesheet interaction, the boundary conditions in the finite element model are used to prevent singularity errors due to unimpeded rigid body motion during the analysis. As such, the boundary conditions were chosen to minimize the impact on the analysis results. On the outer circumference of the tubesheet collar, the four principal directions are set on []^{a,c,e}.

[]^{a,c,e}. This is shown in Figure 7-2. The pressure load is applied to the inside surface of the tube in []^{a,c,e}. The pressure load is []^{a,c,e}.

7.2.2.2 Solution Process

The hydraulic expansion process was simulated in ANSYS via a [

]a,c,c.

Residual contact pressure is the desired output for this parametric sensitivity study. Because of the symmetry of the geometry, boundary conditions and loading, the residual contact pressure is expected to be uniform around the circumference of the tube/tubesheet. However, the results show a slight variation in residual contact pressure distribution, which is a result of mathematical computations within ANSYS.

The average residual contact pressure reported was determined by averaging the minimum and maximum value calculated. Because the variation of the distribution around the circumference is small and is due to mathematical computations rather than a physical phenomenon, this averaging technique is judged to be a valid representation of the residual contact pressure.

7.2.3 Structural Analysis Results

The results of the contact stress parametric study are contained in Tables 7-2, 7-3, and 7-4 for the Model F, Model D5 and Model 44F, respectively. The parameter that most affects the residual contact pressure is the [

]a,c,c.

7.2.4 RCP Uncertainty Evaluation

The combined uncertainty of residual contact pressure, when all input variables are considered, is developed using an influence factor approach. In Tables 7-2, 7-3 and 7-4, the mean and two standard deviation values of contact stress (pressure) are provided for each input variable. Therefore, the necessary parameters are available to define a distribution of residual contact stress (residual contact pressure) for each variable. Tables 7-2, 7-3 and 7-4 show that the effect on RCP is different for positive or negative variations of individual parameters. Because it is of primary interest to determine the

minimum RCP, the individual distributions of RCP in each variable were based on only the parameter that would reduce the RCP. For example, on Table 7-2, the variation of RCP for a $+2\sigma$ variation in tube OD is []^{a,c,c} psi, whereas the variation of RCP for a -2σ variation of tube OD is []^{a,c,c} psi. To establish the distribution of RCP for variation of tube OD, only the []^{a,c,c} psi variation is considered. The result of this approach is that the reduction of RCP is properly modeled, but that the potential increase in RCP may be over-estimated. Overestimating the RCP does not affect the conclusions for H^* because, while higher RCP reduces the value of H^* , only the lower tail of the H^* distribution is of interest in the probabilistic analysis of H^* .

Residual contact pressure cannot be less than zero. For this reason, the individual distributions of RCP for the eight significant variables were modeled as Weibull distributions. The Weibull distribution parameters, α and β , were iterated until the distribution yielded the correct mean value of RCP and the correct value of standard deviation. Table 7-5 summarizes the Weibull distribution parameters along with the resulting mean and variance for each input variable. These values define the distribution of each influence function, which, if expressed as a cumulative distribution function (CDF) as shown in Figure 7-3, can be directly sampled using a Monte Carlo technique. The CDF for each variable is normalized by the predicted mean residual contact stress. The distribution of the final RCP variability is determined by the following equation:

$$[]^{a,c,c}$$

Where $FRCP_i$ is the multiplier for the applicable mean RCP determined in Section 7.1, and v_{1i} , v_{2i} , v_{8i} are the influence factor values for the i^{th} pick.

One hundred thousand simulations for the RCP variability multiplier were performed. The resulting distribution of the variability multiplier is shown in Figure 7-4.

7.2.5 Application to H^* Calculation

To apply the RCP distribution in Figure 7-4 to the H^* calculation, it is necessary to represent the RCP factor distribution in terms of H^* . This is readily accomplished by calculating H^* as a function of the RCP multiplier assuming that the mean value of RCP is known. As noted in Section 7.1, the mean value of RCP has not been finally determined from the test data. However, to illustrate the application to the H^* analysis, the estimate of mean RCP derived analytically in the RCP variability study is used. Based on this calculated value of mean RCP, []^{a,c,c} psi, an influence factor for H^* was calculated that can be sampled along with the influence factors for the variables that directly affect the calculation of H^* (see Section 8.0).

Figure 7-5 shows the influence of a mean value of RCP = []^{a,c,c} psi on the value of H^* . The cumulative distribution function from Figure 7-4 expressed in terms of the value of H^* is shown on Figure 7-5. If the multiplier on RCP from Figure 7-4 is zero, the value of H^* is the value calculated for zero RCP. A value of CDF equal to []^{a,c,c} (see Figure 7-4) represents the effect of the mean value of RCP on the value of H^* . As is seen from figure 7-5, the effective multiplier on H^* is approximately []^{a,c,c} for a mean value of RCP of []^{a,c,c} psi. This represents a reduction in the H^* value for zero RCP of approximately []^{a,c,c} inches. Smaller values of mean RCP will result in smaller reduction in the value of H^* and larger values of mean RCP will result in larger reduction.

It is concluded from this evaluation that the assumption of zero RCP for the reference value of H* is extremely conservative. Depending on the value of mean RCP finally determined for the test data, the zero RCP value of H* is estimated to include at least 1-2 inches of margin compared to a more realistic value of H* that includes a real value of RCP.

7.3 REFERENCES

- 7-1 LTR-CDME-07-198, "Response to NRC Request for Additional Information Relating to LTR-CDME-07-02 P-Attachment and LTR-CDME-05-209-P of the Wolf Creek Generating Station (WCGS) Permanent B* License Amendment Request," September 24, 2007.
- 7-2 NRC Letter, "Wolf Creek Generating Station-Withdrawal of License Amendment Request on Steam Generator Tube Inspections (TAC No. MD1097)," United States Nuclear Regulatory Commission, Washington, D.C., February 28, 2008.
- 7-3 CN-SGDA-03-99 (Proprietary), "Evaluation of the Tube/Tubesheet Contact Pressure for Wolf Creek, Seabrook, and Vogtle Unit 1&2 Model F Steam Generators," Westinghouse Electric Company, LLC, Pittsburgh, PA, September 2003.
- 7-4 DP-SGDA-03-1 (Proprietary), "Model D Tube-to-Tubesheet Joint Determination of Pull Out Resistance for H-Star (Program for Comanche Peak 2, Catawba Unit 2, Byron 2 and Braidwood 2)," Westinghouse Electric Company, LLC, Pittsburgh, PA, 2003.
- 7-5 NRC Letter, "Braidwood Station, Units 1 and 2 – Issuance of Exigent Amendment Re: Steam Generator Tube Surveillance Program (TAC No. MC6757)," United States Nuclear Regulatory Commission, Washington, D.C., April 28, 2005.
- 7-6 1001191, "Steam Generator Degradation Specific Management Flaw Handbook," EPRI, Palo Alto, CA, January 2001.
- 7-7 ASME Boiler and Pressure Vessel Code, "Rules for Construction of Nuclear Power Plant Components," The American Society of Mechanical Engineers, New York, NY, 1989.
- 7-8 Begley, J.A., "Mechanical and Corrosion Properties of Ni-Cr-Fe Alloy 600 Related to Primary Side IGSCC," Final Report, EPRI Research Project S303-8, October, 1986.
- 7-9 CN-SGMP-08-3 (Proprietary), "H* FEA Parametric Modeling," April 2009.
- 7-10 TP-CDME-08-1 (Proprietary), "Pull Out Test Program for H*," Westinghouse Electric Company, LLC, Pittsburgh, PA, 2008.

Table 7-1 Variables That Affect Residual Contact Pressure

a,c,e

Table 7-2 Residual Contact Stress Model F Steam Generator

a,c,e

Table 7-3 Residual Contact Stress Model D5 Steam Generator

a,c,e

Table 7-4 Residual Contact Mode 44F Steam Generator

a,c,e

Table 7-5 Weibull Parameters for Residual Contact Pressure Variation

a,c,e



Figure 7-1 Finite Element Model – Overall View



Figure 7-2 Finite Element Model – Node Constraints

a,c,e

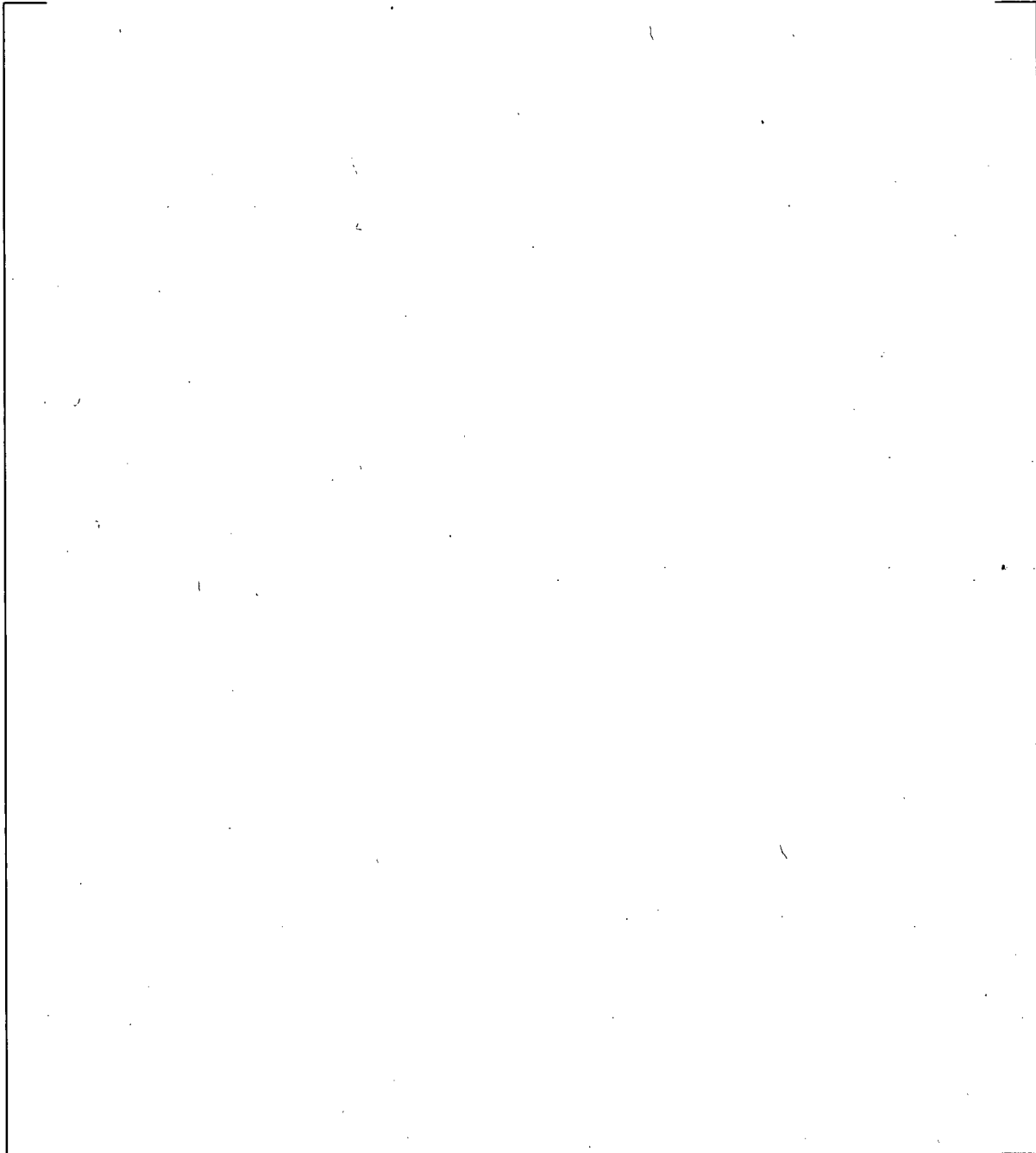
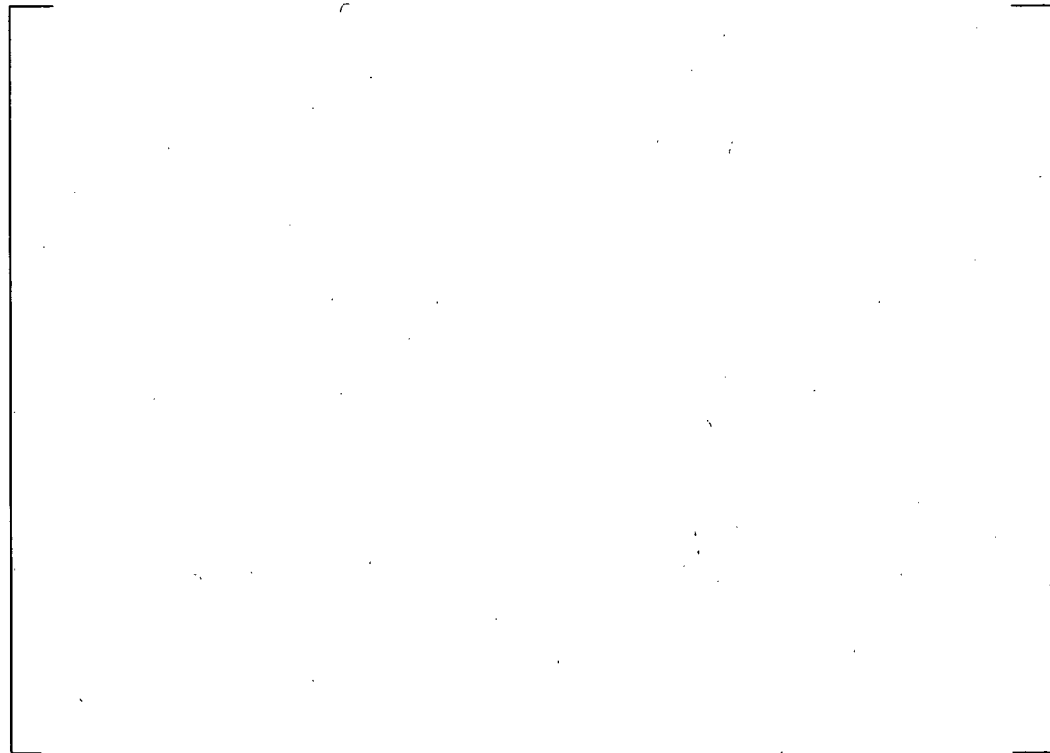


Figure 7-3 Cumulative Distribution Functions of RCP Variables Factors



a,c,e

Figure 7-4 Composite Variability of Residual Contact Pressure



a,c,e

Figure 7-5 Illustration of Adjustment to H^* for Positive RCP

8.0 DETERMINATION OF H* AT THE REQUIRED PROBABILITY AND CONFIDENCE

The applicable probabilistic criteria for H* were provided in Section 4.0 of this report. Each tube in the tube bundle must meet the H* value with a probability of 95% at a confidence level of 50%. This definition is also known as a whole bundle analysis at 95/50.

Several approaches to meeting the probabilistic requirement are available. The EPRI Tube Integrity Guidelines (Reference 8-1) provide a simplified statistical approach under which the uncertainties on the mean prediction of H* are combined as the square root of the sum of the squares (SRSS). The guidelines also provide for a fully probabilistic analysis utilizing a Monte Carlo sampling technique. While both methods are used in this report for developing the whole bundle H* value at 95/50, the more simple and conservative method, SRSS, is the reference basis for determining the probabilistic value of H*.

Section 6.0 of this report provides the structural basis for the limiting mean value of H*, []^{a,c,c} inches, which includes the adjustment for the location of the bottom of the expansion transition (BET) and the adjustment for tubesheet NOP thermal distribution. Figure 6-1 provides the mean H* value as a function of tubesheet radius within the limiting tubesheet sector for the bounding Model F steam generator (SG) plant. It was noted in Section 6.0 that the limiting mean value of H* applies for the tube located at the limiting radius in the limiting sector of the tube bundle. Every other tube in the bundle would be expected to have a lower value of H*. The H* value for this limiting tube is utilized as the basis for the probabilistic evaluation included in this section.

8.1 PROCESS

8.1.1 Effect of Crevice Pressure on H*

Section 6.4.5 discusses the analysis iteration performed during the H* calculation process to define the final H* distance for a distributed crevice pressure (P_{crev}) model referenced to the location of the predicted H*. Referring to Figure 1-1, the H* process diagram, the first prediction of H* assumes that the postulated flaw exists at the bottom of the tubesheet. Thus, the crevice pressure distribution is initially applied assuming that it is distributed over the entire thickness of the tubesheet. The resulting prediction of H* implies that the postulated flaw exists just below the predicted H* distance. The final calculation of H* assumes that the flaw is located at the initial predicted value of H* and applies the crevice pressure distribution accordingly. This process adds a nominal length to the first H* prediction because changing the crevice pressure axial location reference changes the contact pressure distribution above H*.

The incremental value of H* due to the application of the crevice pressure profile (see Figure 6-82) varies with the initial prediction of H* but has a unique value for each H* value. Multiple cases were evaluated in which the applicable input parameters identified in Section 8.1.2 were varied singly or in combination, an initial value of H* was calculated and the necessary adjustment due to the re-application of the crevice pressure distribution was determined. Figure 8-1 shows the resulting adjustment for crevice pressure for the range of initially predicted values of H* for the Model F SG. The characteristic of the P_{crev} adjustment curve is as expected. An initially predicted small value of H* depends principally on contact pressure derived from thermally and pressure-induced contact forces between the tube and the tubesheet

with very little influence from the crevice pressure. Thus, the crevice pressure has little impact on the result and a small crevice pressure adjustment would be expected. As the initially predicted H^* length increases, the effect of the crevice pressure adjustment also increases because the thermal and pressure-induced contact pressures are proportionately less compared to the crevice pressure. Therefore, a larger impact of crevice pressure on the predicted value of H^* would be expected. At some value of initially predicted H^* , the slope of the crevice pressure adjustment begins to approach the initial crevice pressure distribution slope, based on the entire thickness of the tubesheet, and the relative adjustment due to the crevice pressure decreases to zero at the originally assumed distribution as the initial prediction of H^* approaches the full thickness of the tubesheet.

Because the P_{crev} adjustment is shown to be a unique function of the value of the first prediction of H^* , independent of parameter variations that result in the first predicted value of H^* , the adjustment for P_{crev} can be applied after the determination of the probabilistic value of H^* and is not a parameter in the probabilistic analysis.

8.1.2 Definition of Variables and Their Variability

The complete calculation for H^* , shown in the process diagram on Figure 1-1, depends on a number of input parameters whose value can vary. Not all of the variables affect every part of the calculation. Table 8-1 summarizes the input variables and their applicability to the separate models that are utilized in the H^* calculation process. Four input parameters directly affect the results of the contact pressure calculations: Young's modulus of the tubesheet and tube material (E_T , E_{TS}) and coefficient of thermal expansion (CTE) of the tube and tubesheet materials (α_T , α_{TS}). Variations in the tubesheet bore and the tube outer diameter and tube wall thickness do not directly affect the contact pressure calculations because the initial condition for the contact pressure calculations assume line-on-line contact between the tube and the tubesheet. However, geometric variability of the components is introduced into the calculations through the residual contact pressure (RCP) variability discussed in Section 7.0. The reference basis for the H^* calculations in this report is the assumption of zero residual contact pressure. All prior tube pull out testing has shown that there is a positive value for RCP. If a positive value of RCP is included in the H^* calculation, the value of H^* will decrease; thus, the assumption of zero residual contact pressure is conservative.

Table 8-2 summarizes the variables that affect the H^* calculations. The table includes the mean value of the variables, the predicted mean value of H^* and the resulting variability of H^* for perturbations of individual variables around their means. All of the material properties that are used as input variables in the H^* analysis are natural variables. An analysis parameter is considered to be a natural variable if the range of values that it is assumed to have is not affected by a process related to the analysis or is an intrinsic characteristic. For example, the CTE of Alloy 600 is not affected by the application of end cap loads on the tube and remains the same regardless of the volume of Alloy 600 that is present. Therefore, the CTE of Alloy 600 is considered an intrinsic material property and can be assumed to vary within a natural distribution of values. It is reasonable to assume that natural variables have normal (Gaussian) distributions because variations in material structures and properties (e.g., crystal structures, grain boundaries, etc.) are likely to be concentrated around some average value with an equal chance of being either below the average or above it. For example, the distributions of the two most significant variables, α_T and α_{TS} were shown to be reasonably approximated by a normal distribution in the analysis of the coefficient of thermal expansion tests, Appendix B of this report.

The variation of H^* with respect to a known change of a single parameter over a defined range is called an influence factor. The concept of influence factors is well known in structural analysis and the application of the concept for the H^* analysis is the same. An influence factor was calculated for each of the relevant input parameters (i.e., α_T , α_{TS} , E_T , E_{TS}) about a mean value determined from the ASME Code and a 1, or more, standard deviation variance based on established test data or reference literature [e.g., Appendix B, Reference 8-4]. The influence factors were calculated by repeating the entire calculation process shown in Figure 1-1, except the RCP calculations, by varying only one input variable at a time while holding all other inputs at their mean value. These calculations were repeated at different input parameter variances to account for possible non-normality of the resulting H^* influence factor distributions for each variable. It is seen from Table 8-2 that among the four variables affecting the value of H^* , the variation due to Young's Modulus, E , for both the tubesheet and tubing materials is very small compared to the variability of the coefficient of thermal expansion for both materials. Nevertheless, the variability in H^* due to all four properties was included in the probabilistic assessment.

8.1.3 Interaction Among the Applicable Variables

Application of the SRSS method of combining uncertainties assumes that each input parameter and the effect on H^* of varying that parameter, is independent of the other input parameters. The Monte Carlo influence factor approach also assumes that variables are independent. A variable is considered to be independent with respect to another variable if a change in that variable does not affect the variability of the other. With respect to H^* , a variable is independent if the characteristic of the change in H^* due to a variation of that parameter is not affected by a simultaneous change in another parameter. The characteristic variation of H^* in the four individual random variables affecting its value is shown in Figure 8-2. Each variable was changed from its mean value by a number of standard deviations while all other variables were held at their mean and the value of H^* was determined. Figure 8-3 shows the percent change in the "raw" mean H^* prediction plotted on the same scale to provide perspective on the significance of each variable. The raw mean H^* prediction is the predicted value of H^* before any adjustments are made for location of the BET, normal operating NOP thermal distribution (see Section 6.4.5) and crevice pressure adjustment.

Figure 8-3 shows that the most significant variables for H^* are the CTE of the tubesheet (α_{TS}) and of the tube materials (α_T). The tube CTE clearly dominates, resulting in approximately a []^{a,c,c}% increase in H^* from the mean if its value is approximately at the mean minus 3σ . While the tubesheet material CTE is also significant, a mean plus 3σ value for it results in approximately a []^{a,c,c}% increase in the value of H^* over its mean value. The remaining variables, the Young's Moduli of the tubesheet and tubing material are very weak variables, resulting in less than 2% increase in the H^* value at their means minus 3σ values. []

]^{a,c,c}

If the input variables are independent, their combined effect on H^* is expected to be a cumulative effect rather than a multiplicative effect. Figure 8-4 illustrates the expected effect of simultaneous variation of the CTE of the tube and the CTE of the TS, assuming true independence. From Figure 8-3, a -1σ variation of the CTE of the tubesheet results in a []^{a,c,c}% decrease in the value of H^* . Similarly, a $+2\sigma$ variation of the CTE of the tubesheet results in approximately a []^{a,c,c}% increase in the value of H^* . Based on this logic, assuming the CTE of the tube and tubesheet to be independent, a family of curves was constructed to show the expected change in H^* when both the CTE of the tubes and the tubesheet are

varied simultaneously, Figure 8-4. The difference between the individual curves is the constant offset from the mean H^* value for each different variation of both the tube and tubesheet CTE.

To determine if each of the variables affecting H^* are independent, a large number of influence factor calculations was performed in which two or more input parameters were varied over a wide range of their uncertainties. The result of these calculations is reflected in the variation of H^* . A matrix of interactions was considered for the four applicable variables for the determination of H^* as shown on Table 8-3.

Figure 8-5 shows the results of the interaction study for the coefficient of thermal expansion of the tubesheet and the coefficient of thermal expansion of the tube. The figure shows the percent variation from the calculated mean value of H^* when the coefficient of thermal expansion for the tube varies from $+5\sigma$ to -5σ and when the coefficient of thermal expansion for the tubesheet is also varied from -1σ to $+5\sigma$. The shape of the curves is similar, suggesting that there are no discontinuities at which a value of H^* cannot be defined; however, the curves are rotated about the mean value of the tube CTE resulting in a convergence of the net effect on H^* when the CTE of the tubesheet is positively varied, and a divergence when the CTE of the tubesheet is negatively varied. If the variables were independent, a point-by-point difference of approximately []^{a,c}% change in H^* would be expected (see Figure 8-3) when the tubesheet CTE is at a value of mean $+2\sigma$. Over a 3σ variation of the tube CTE, the point-by-point change in H^* is shown to vary (see Figure 8-4) from []^{a,c}% at mean tube CTE to []^{a,c}% at the mean minus 3σ value of tube CTE. Therefore it is concluded that the tube CTE and tubesheet CTE have some interaction effect over a wide range of tube CTE variation.

Figures 8-2 and 8-3 show that the influence of Young's Modulus for both the tube (E_T) and tubesheet (E_{TS}) materials is essentially negligible. For a 4σ variation of E_{TS} , the effect on H^* is less than []^{a,c}%. Similarly, for a 4σ variation of E_T , the effect on H^* is less than []^{a,c}%. The effect of E_{TS} is greater than that of E_T because the structural response of the tubesheet and the tube to tubesheet contact pressure both involve this variable, whereas E_T is reflected in only the contact pressure calculation.

Figures 8-6 through 8-10 show the degree of interaction among the applicable variables:

- Figure 8-6: Interaction between α_{TS} and E_{TS} . The slope of the curve for variation of E_{TS} alone (Figure 8-2c) is unchanged by a simultaneous 1σ positive variation of α_{TS} . The absolute difference between the two curves reflects only the effect of α_{TS} on H^* . A negative variation of α_{TS} would decrease the value of H^* and is of no consequence here.
- Figure 8-7: Interaction between α_{TS} and E_T . The figure shows that there is no interaction between these variables. The curves are parallel and reflect only the impact of varying α_{TS} on the value of H^* .
- Figure 8-8: Interaction between α_T and E_T . The figure shows that there is no interaction between these variables. The curves are parallel and reflect only the impact of varying α_T on the value of H^* .
- Figure 8-9. Interaction between α_T and E_{TS} . The figure shows that there is no interaction between these variables.

- Figure 8-10: Interaction between E_T and E_{TS} . The figure shows that there is no interaction between these variables. The figure also shows that Young's Modulus is an extremely weak variable in regard to their effect on H^* .

It is concluded that α_T and α_{TS} are somewhat interdependent, but insufficiently so to suggest that a discontinuity exists where the value of H^* is not defined within the degree of variability of interest for the probabilistic H^* value. Each of the other variables is independent and is not significantly affected by variation of any other variable as reflected by the predicted value of H^* .

The interdependence of α_T and α_{TS} requires special consideration to assure that a value of H^* exists, and is not excessively large, when an extremely unlikely combination of values of α_T and α_{TS} is considered. To address this issue, all of the input variables were set at their []^{a,c,c} value in the direction of increasing H^* , and a new H^* was calculated. The mean value of H^* for this very unlikely case increased by approximately []^{a,c,c} inch, indicating that H^* is not significantly sensitive to the input parameters.

8.1.4 Influence Factor Distributions

As noted in Figure 1-1 of this report, the calculation process for H^* is complex, involving 4 different models (only 3 if RCP is assumed to be zero). For this reason, it is not practicable to perform a classical Monte Carlo simulation in which multiple simulations are performed by randomly choosing values from the distributions of the input variables, performing a calculation for the dependent variable (in this case, H^*) and rank ordering the solutions to determine the value at the desired probability and confidence level. To implement a classical Monte Carlo approach for H^* would require completing the entire structural calculation for the number of simulations desired (10K – 1M), including the 3D FEA analysis for tubesheet deflections and the H^* integration process, which is an extremely time and cost-intensive effort. However, the process can be made more practicable by developing distributions of H^* in each variable and then sampling these distributions using a Monte Carlo technique to determine the combined probability of H^* in all variables. This is termed the “Influence Factor Approach”.

To implement the influence factor approach, a best estimate (mean) value of H^* is calculated, assuming that all input variables are at their mean values (see Section 6.4.5). Subsequently, one variable at a time is perturbed by $\pm 1\sigma$ (standard deviation) or greater and the corresponding values of H^* are determined. In this manner, individual distributions of H^* as a function of each variable are developed. It is assumed that the influence factor distributions are reasonably normally distributed; therefore, each H^* influence distribution is defined by the known mean value of H^* and the calculated variance of H^* from the perturbation of the input parameter. Thus, if an input parameter is varied by one standard deviation, the resulting H^* influence factor value would also be considered a 1σ deviation. In this manner, because there are four parameters that affect the H^* calculation, four influence factor distributions are developed from which to sample to determine the final combined distribution of H^* .

The influence factor approach assumes that the individual influence distributions are essentially normally distributed. This appeared to be a reasonable assumption because the variables that affect the H^* calculation are all “natural” variables, which tend to be normally distributed (see Table 8-1). Examination of Table 8-2 shows that the H^* influence factors are not truly normally distributed, particularly for the variables that have the most significant influence on H^* because the variations at multiple standard deviations are greater than the 1σ variation multiplied by the number of standard

deviations considered. For example, the variation of H^* for a 5σ variation of αTS is greater than five times the H^* variation for a 1σ variation of αTS . To address this, the distributions from which to sample were conservatively biased by basing them on only the influence function distribution that increased the value of H^* (see Figure 8-11). For example, for the variation of H^* for tubesheet coefficient of thermal expansion in Table 8-2, the H^* influence function was constructed using the positive variation result for H^* , 0.25 inch, to most accurately represent the influence function. This process biases the determination of the final H^* distribution to the conservative side (increased H^* length) since the lower tail of the distribution is not relevant. Influence factors were calculated in this manner for [

] ^{a,c,c} parameter variations as shown in Table 8-2.

Table 8-1 H* Input Variables and Their Applications

Variable	Application			
	Tubesheet Displacement	Contact Pressure Calculation	Mean Residual Contact Pressure	Residual Contact Pressure Variability

a,c,e

Note: "X" indicates that the variable is used.

Table 8-2 H* Variables and Influence Factors

a,c,e

Table 8-3 Matrix of Variable Interaction Study for H*

a,c,e

a,c,e



Figure 8-1 Adjustment to H* for Distributed Crevice Pressure Referenced to Initial Prediction of H*



Figure 8-2 H* Variation of H* with Individual Input Variables

a,c,e



Figure 8-3 Variability of H*with All Relevant Parameters



Figure 8-4 Expected Variation of H^* When Both α_T and α_{TS} are Varied and are Independent

a,c,e



Figure 8-5 Interaction Between α_{TS} and α_T

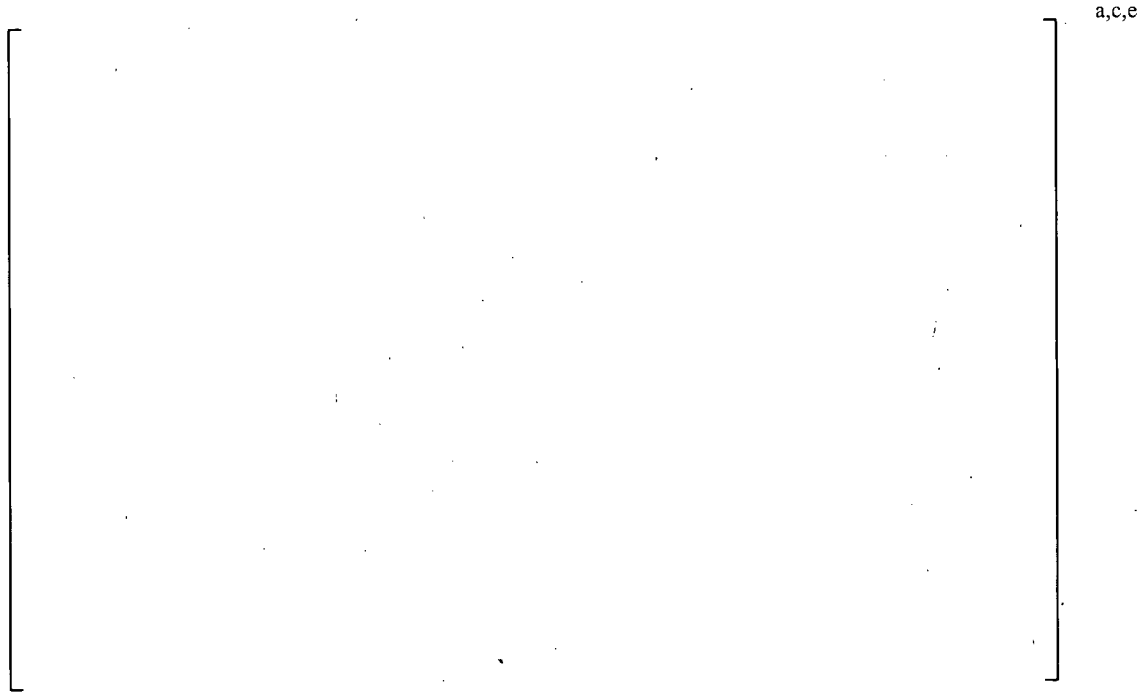


Figure 8-6 Interaction Between α_{TS} and E_{TS}



Figure 8-7 Interaction Between α_{TS} and E_T



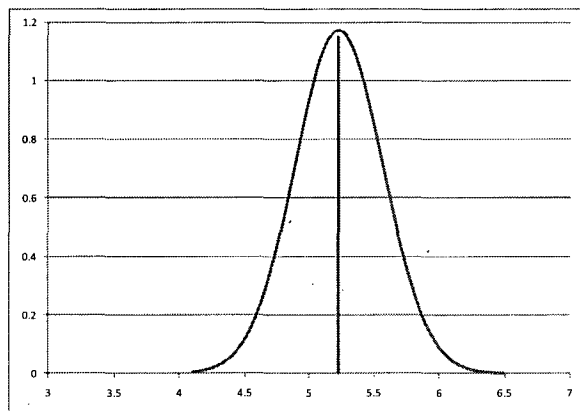
Figure 8-8 Interaction Between α_T and E_T



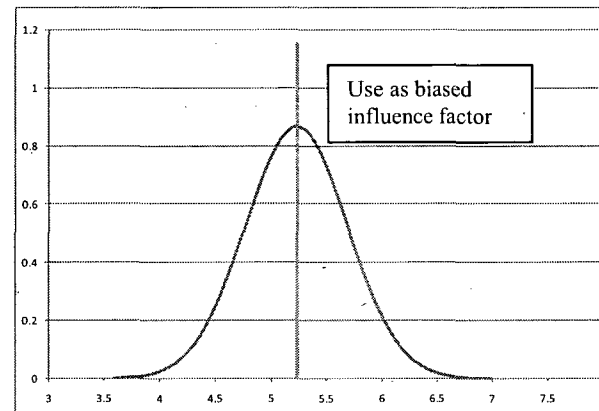
Figure 8-9 Interaction Between α_T and ETS



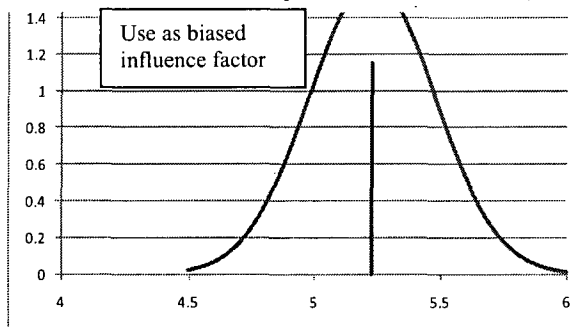
Figure 8-10 Interaction Between E_{TS} and E_T



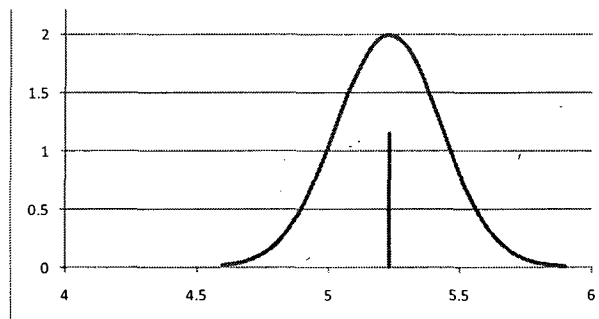
Variation of H* for +1σ variation of αT ($\mu = 5.23$; $\sigma = -0.34$)
 (H* decreases for positive variation of αT)



Variation of H* for -1σ variation of αTS ($\mu = 5.23$, $\sigma = +0.46$)
 (H* increases for negative variation of αT)



Variation of H* for +1σ variation of αTS ($\mu = 5.23$; $\sigma = 0.25$)
 (H* increases for positive variation of αTS)



Variation of H* for +1σ variation of αTS ($\mu = 5.23$; $\sigma = -0.20$) (H* decreases for positive variation of αTS)

Figure 8-11 Illustration of Biased Influence Factors

8.2 CALCULATION OF PROBABILISTIC H*

8.2.1 Square Root of the Sum of the Squares (SRSS) Approach

The Square Root of the Sum of the Squares (SRSS) approach is the reference approach for calculating the whole bundle value of H* at 95% probability and 50% confidence.

The simplified statistical approach provided in Reference 8-1 permits combining the variability of multiple parameters by the square root of the sum of the squares (SRSS). This approach assumes that the variability of each parameter is reasonably approximated by a normal distribution. For the H* calculation, this approach requires calculating the variation of the H* influence factors for each input variable. An influence factor is defined as the variation in H* from its mean value when each separate variable is perturbed while holding all other variables at their mean values. In other words, it is necessary to develop influence factors for each variable on H* for the $\pm n\sigma$ values of the variables where σ is the standard deviation and n is a multiplier chosen to represent the desired probability of occurrence of the variation. The choice of the value of n provides a basis for examining the assumption of normality of the distribution and investigating highly improbable occurrences of specific parameter variation, such as the assumption of specific tubesheet properties in recognition that the population of tubesheets is relatively small compared to the population of tubes. The results of varying one input at a time to determine the effect of such a variation on H* are included in Table 8-2 and Figure 8-2.

As shown on Table 8-2, the H* influence factors are reasonably represented by a normal distribution, except for α_T which exhibits significant non-linearity with increased variation from the mean. For example, the H* value for a 5σ variation divided by 5 is []^{a,c}% greater than the 1σ variation in the direction of increasing H*. For this analysis, the H* influence factor distributions were based on only the parameter variations that increased the value of H*. These are called “biased influence factors” as discussed in Section 8.1.3 and illustrated on Figure 8-11. For example, on table 8.2, a negative 1σ variation of the coefficient of thermal expansion of the tube (α_T) results in a positive variation of H* of 0.46 inch, whereas a positive 1σ variation of α_T results in a reduction of the value of H* of -0.34 inch. To address the apparent non-normal distributions of the significant H* influence factor, influence factors were calculated for a range of parameter variation up to 5σ as shown on table 8-2. No discontinuities of H* in any of the input parameters were identified. For the H* evaluation, only the variation in the direction of increasing H* was considered for the influence factors for both the 1σ and 4.285σ parameter variation. The use of the 4.285σ influence factors reasonably addresses the concern regarding the non-normality of the H* influence factor distributions by examining the far tail of the distribution. Recall that only the biased influence factors were used.

Calculations for determining the required single tube reliability were performed using standard functions in Excel® (Reference 8-3). Since the requirement for H* is to achieve a whole bundle reliability of 95%, it is first necessary to calculate the required single tube reliability based on a bundle population of tubes equal to 5626. For this, the Excel® function BINOMDIST(s, T, Pb, L) is used, where

s is the number of allowed failures = 0

T is the number of trials = 5626

P_b is the desired probability = 95%

L is a logical argument that directs the function to return the value of the cumulative distribution function, which is the probability that there are no more than s failures.

For the required whole bundle reliability (probability of success) of 95%, the function returns a value for the required single tube probability of failure (known as the individual term binomial distribution probability). For the required whole bundle reliability of 95%, the permitted single tube probability of failure (P_f) is 9.15E-06 for a bundle of 5626 tubes assuming no tubes are plugged.

The required single tube reliability (P_s) is the complement of the permitted single tube probability of failure:

$$P_s = 1 - P_f = (1 - 9.15E-06) = 0.99999085$$

The Excel® function NORMSINV® returns the number of standard deviations required to achieve a desired reliability, R , of a single tube. When considering a single tube, the necessary multiplier on the combined variance is 1.645 to achieve a 95% probability at 50% confidence (Reference 8-2). For the single tube reliability required to achieve a whole bundle reliability of 95% probability at 50% confidence, the function returns a value of 4.285 as the multiplier on the standard deviation.

Figure 8-12 shows the variation of the required single tube reliability, expressed in numbers of standard deviations from the mean as a function of number of tubes in the bundle to meet the 95% whole bundle reliability criterion. Hypothetically, if the bundle consisted of only a single tube, the multiplier required to meet 95% reliability is 1.645. For a full complement of 5626 tubes, the multiplier is 4.285.

Two different evaluations were made to develop the 95/50 value for the full bundle using the SRSS approach and to develop the sensitivity of H^* to the input variables.

1. The SRSS combined result based on the 1σ variation of H^* in all four input variables was multiplied by 4.285 to determine the full bundle 95/50 H^* value.
2. The SRSS combined result based on the 4.285σ variation of H^* in all four input variables was calculated directly. This approach takes into account that the H^* influence factors are not true normal distributions as noted above.

Table 8-4 summarizes the H^* probabilistic predictions including the adjustment for applying the crevice pressure to the depth of the initially predicted H^* value. Cases S-1, S-2 and S-3 are the results for the different evaluations.

Case S-0: For this evaluation, the influence factors for H^* were determined for 1σ variation of each variable affecting the H^* calculation as summarized in Table 8-2. Because it was noted that the variations of H^* were not true normal distributions in each variable, the deviation of each variable was chosen in the direction that maximized the value of H^* , i.e., using the biased influence factors. For example, considering the two most influential variables, the coefficients of thermal expansion (α) of the tubesheet and tubing material, the positive variation of the tubesheet α and the negative variation of the tube α were

chosen. Although much less significant, the same process was applied for the variation of Young's Modulus for both materials. The resulting combined H^* variance, []^{a,c,c} inch by the SRSS method, was determined. When multiplied by the factor 1.645, the resulting increase from the mean of the predicted H^* value is []^{a,c,c} inch. When the adjustment is made for the crevice pressure referenced to the initially predicted value of H^* (see Figure 8-1), the final value of H^* is []^{a,c,c} inches. This value is the 95% probability, 50% confidence value of H^* for a single tube.

Case S-1: For this evaluation, the biased influence factors from Case S-0 were utilized. To extend the evaluation to include the full tube bundle complement of 5626 tubes, the applicable multiplier for the single tube analysis is 4.285. The resulting increase from the predicted mean H^* value is []^{a,c,c} inches. When the adjustment is made for the crevice pressure distribution referenced to the predicted H^* , the final value of H^* for the entire bundle at 95% probability and 50% confidence is []^{a,c,c} inches.

Case S-2: As noted above, influence factors for H^* were calculated based on parameter variances of 4.285σ . Only the variations that would increase the value of H^* were considered. It is seen from Figure 8-2 and Table 8-3 that the most significant influencing variable is the tube α . The predicted result for H^* for a variation of α_T of 4.285σ is greater than 4.285 multiplied by the 1σ variability of H^* . However, the variation of H^* at a 4.285σ variation of the tubesheet α_{TS} is only slightly greater than 4.285 times the 1σ variation of H^* in the tubesheet α . When the adjustment is made for the crevice pressure distribution referenced to the predicted H^* , the final value of H^* for the entire bundle at 95% probability and 50% confidence is 11.2 inches. This case is the recommended value of H^* at 95% probability and 50% confidence for the entire bundle of 5626 tubes.

Case S-3: This case replicates Case S-2 except that the biased influence factors are based on 5σ variations of each of the input parameters. The predicted value of H^* for this case is []^{a,c,c} inches. The H^* probability for this case is far in excess of 95/50 for a tube population of 5626 tubes. Application of 5σ parameter variations is well in excess of the required parameter variation, 4.285σ , to satisfy the 95% whole bundle probability requirement. This case shows that H^* is not highly sensitive to extreme parameter variations and validates the recommended H^* value of 11.2 inches from Case S-2 above.

Case S-4: Because there is interaction between α_{TS} and α_T , this case assumes that both α_{TS} and α_T are at their 2σ values in the direction of increasing H^* to define a very conservative biased mean value of H^* . The influence factors at 4.285σ were combined by SRSS. The resulting value of H^* , []^{a,c,c} inches, significantly exceeds the whole bundle probability requirements of 95% at 50% confidence. This case further demonstrates that highly improbable input parameter combinations do not significantly increase the value of H^* .

8.2.2 Monte Carlo Sampling Approach to Calculating the Probabilistic Value of H^*

The process described in this section, based on a Monte Carlo sampling technique, was utilized to provide a check of the method described in Section 8.2.1.

A Monte Carlo sampling process was utilized, using the commercially available program "@RISK," to develop the final H^* distribution for all parameters combined (Reference 8-5). The biased influence factors developed for each variable are randomly sampled to develop the final H^* distribution. The combined distribution is defined by the following equation:

$$[\quad]^{a,c,e} \quad (8-1)$$

where v_i is the randomly sampled value of H^* from each individual influence factor distribution.

Table 8-4 summarizes the results of various Monte Carlo cases considered.

Case M-0: Because the -1σ variation of each variable results in a different variation in H^* than the $+1\sigma$ variation (see Table 8-2), effectively there are 2 possible influence distributions for each variable. Hence, a total of 8 influence distributions can be constructed. For this case, the distributions that were constructed from the $+1\sigma$ variable variation were sampled; 10,000 simulations were performed and the final H^* distribution was constructed. The results of this simulation are presented in Table 8-4. The final H^* value, less than [\quad]^{a,c,e} inches, represents the 95% probability at 50% confidence value of H^* for this particular set of inputs after the adjustments for BET and crevice pressure have been made. Because the input variations chosen are arbitrary, there is no physical significance to this result, except to provide information on the sensitivity of H^* to variations of the input parameters.

Case M-1: This case is the same approach as Case M-0 except that the influence distributions from all of the -1σ variations of the input variables were utilized. The results of this simulation are presented in Table 8-4. The final H^* value, less than [\quad]^{a,c,e} inches, represents the 95% probability value of H^* for this particular set of inputs. Because the inputs chosen are arbitrary, there is no physical significance to this result, except to provide information on the sensitivity of H^* to variations of the input parameters. The case demonstrates the greater influence of the negative variation of αT on H^* .

Cases M-0 and M-1 were initial analyses to scope the sensitivity of H^* to variations in the input parameters. Comparing the H^* results for these influence factor variations leads to two observations:

1. The change in the predicted H^* value is not significantly sensitive to the variations of the input parameters in either the positive or negative direction, and,
2. The variation of H^* is principally driven by the value of αT . The results of these initial analyses suggested the conservative path for evaluating the probabilistic value of H^* , which was to bias all of the influence function in the direction of increasing H^* .

Case M-2: The 8 possible influence distributions from Cases 1 and 2 were reduced to 4 by selecting only those that resulted in an increased value of H^* as suggested by Cases M-0 and M-1. For example from Table 8-2 for the $\pm 1\sigma$ variations of the variables, the influence distributions were based on the following parameter variations:

E_{TS} : -1σ variation	Results in 0.02 inch increase in H^*
α_{TS} : $+1\sigma$ variation	Results in 0.25 inch increase in H^*
E_T : -1σ variation	Results in 0.01 inch increase in H^*
α_T : -1σ variation	Results in 0.46 inch increase in H^*

This set of influence parameters are referred to as the “biased influence factors” because all of the variable variations were chosen to maximize the H* value.

Using the influence distributions determined from the mean H* []^{a,c,c} inches, including the BET and NOP temperature distribution adjustments and the standard deviations noted above, 100K simulations were performed to determine the combined H* distribution. The 95% probability value was chosen from the resulting combined distribution. This case represents a conservatively biased estimate of a single tube H* value at 95% probability and 50% confidence. The final calculated value of H* for this case is no greater than []^{a,c,c} inches.

Case M-3: As an extension of Case M-2, the final H* distribution from case M-2 was sampled 5626 times, and the resulting H* values were rank ordered from high to low. The maximum value of H* from this sampling was determined to be less than []^{a,c,c} inches as shown on Table 8-4. This case is not a complete extreme value evaluation but it provides insight into the combined distribution of H*, particularly when compared to Cases M-2 and M-4.

Case M-4: This case is a further extension of Case M-2 and Case M-3. The distribution from Case M-2 is sampled similarly to Case M-3, except that the sampling of the Case M-2 results is repeated 1000 times. The maximum values from each of the 1000 repeats of the 5626 sample from the distributions are recorded and rank ordered. From this ranking, the 950th value is chosen, which is the 95% probability at 50% confidence of the distribution of extreme values. This case represents a true extreme value evaluation for the case when all the influence factors are conservatively biased in the direction of a greater H*. The resulting extreme value of H* is []^{a,c,c} inches. Comparing this value with that from Case M-3 shows that there is very little change in the value of H* when 1000 samples of the maximum values are taken compared to only a single sample.

Case M-5: This case considers the biased influence factors for the 4.285σ variation from Table 8-2 divided by 4.285 to give equivalent 1σ factors that take into account the non-normality of the influence factor distributions. Monte Carlo sampling from each influence distribution was performed 100,000 times to determine the resulting distribution of H*, and the 95% probability, 50% confidence value is reported from this distribution. It is noted that each of the 100K simulations assumes a new value for the tubesheet properties. Interaction effects are included because the 4.285σ variations were used that already include the effective interactions among the variables. The predicted whole bundle H* value at 95/50 is []^{a,c,c} inches. When compared to Case M-2, this case illustrates the effect of the non-normality of the influence factors.

This case is the Monte Carlo analogy to Case S-2, representing a whole bundle analysis at the desired probabilistic criteria. It is expected that Monte Carlo sampling of the variances would result in a smaller value of H* than that obtained from the SRSS combination of uncertainties.

Case M-6: This case is highly conservative for three reasons noted below and is provided only as a benchmark analysis:

- The H* influence factors are based on parameter variations at 4.285σ from Table 8-2.
- The influence factors are biased toward maximizing the value of H*

- It is an extreme value evaluation.

Recognizing that there is a limited population of tubesheets among the H* candidate plants, this case provides an extreme value H* assuming a limited population of tubesheets. An iterative sampling scheme was applied in which the tubesheet properties were sampled once and, while holding the tubesheet properties at that chosen value, the tube properties were sampled 5626 times and the maximum value of the resulting H* was recorded. This process was repeated for 1000 random picks of tubesheet properties. The recorded 1000 maximum H* values were rank ordered and the 950th value was selected. This value, []^{a,c,c} inches, represents the extreme value of H* at a probability exceeding 95% at 50% confidence for the entire bundle of 5626 tubes.

This case demonstrates that H* is not significantly sensitive to extremely conservative assumptions and it validates the SSRS-based recommended value of H* of 11.2 inches.

Case M-7: The extreme conservatism of this case defines it as a bounding case which cannot reasonably occur. The influence factors for this case are based on 2σ variation of all variables, biased in the direction of a greater value of H*. The influence factor distributions are sampled 100K times to develop the H* distribution. The H* distribution was sampled 5626 times, and that sampling was repeated 1000 times. The maximum values from each of the 1000 replicates of 5626 samples were retained and rank ordered. The 950th rank value, []^{a,c,c} inches (before the P_{crev} correction), represents the 95% probability at 50% confidence of the extreme value of this biased case. It is noted that the 2σ influence factors are not simply double the 1σ influence factors, but are the true H* calculation process response to the inputs. Therefore, this case includes an interaction effect between the two principal variables, αT and αTS .

After the correction for the effect of crevice pressure referenced to the location of the predicted H* is added, the final value of H* for this extremely conservative case is []^{a,c,c} inches. This case exceeds the requirement of 95% probability at 50% confidence for the whole bundle by a significant margin.

8.3 SUMMARY AND CONCLUSIONS

The input variables that affect the calculations for tubesheet displacement, tube-to-tubesheet contact pressures and residual contact pressure were defined. The variation of these parameters was previously defined in Section 6.0. Only four parameters, the coefficient of thermal expansion for the tubesheet and the tube material and the Young's Modulus of the tubesheet and the tube material, affect the calculation of H* if it is assumed that the residual contact pressure is zero. The impact of variability of each of these parameters on H* was determined. Two approaches were utilized to determine the probabilistic value of H* that meets the requirement of 95% probability at 50% confidence for all of the 5626 tubes in the Model F tube bundle, combination of uncertainties by the square root of the sum of the squares (SRSS), and a Monte Carlo sampling method.

The following conclusions were reached:

1. The recommended 95/50 whole bundle value of H* is 11.2 inches (Case S-2). This value meets the requirements of whole-bundle based 95% probability at 50% confidence, and is the most conservative of all of the results obtained from various different assessments of H* that did not intentionally bias the results. It is based on the use of the SRSS method of combining

uncertainties. The uncertainties are based on variation of the individual parameters of 4.285 standard deviations from their respective mean values.

2. An assessment of the extreme value of H* for all of the tubes (5626 for a Model F SG) in a SG tube bundle shows that the extreme value of H* based on the use of variances biased to maximizing the value of H* (Case M-4) is enveloped by the recommended value of H*.
3. Four input parameters affect the value of H*: The coefficients of thermal expansion of the tubesheet and tubing materials and the Young's moduli for the tube and tubesheet materials. The parameter that most influences the H* value is the coefficient of thermal expansion of the tubing material (A600) and the second most important variable is the coefficient of thermal expansion of the tubesheet material (SA508). Variations of Young's Modulus of both materials have only minor influence on the value of H*.
4. The input variables are generally not interdependent. Some interdependence between the coefficients of thermal expansion of the tube material and of the tubesheet material exists, but without any discontinuities at which the value of H* becomes undefined. An analysis showed that the other input parameters independently affect the value of H* without regard to the variation of any other parameter.
5. The 95/50 value of H* is not significantly sensitive to extreme variations of the input parameters as shown by the relatively narrow distribution of results for all of the cases considered.
6. If the number of tubesheet samples is reduced to account for the limited population of tubesheets among the H* candidate plants, the extreme value of H* of []^{a,c,c} inches (Case M-6) validates the recommended value of 11.2 inches.
7. The recommended value of H* is based on the mean value of H* for the single worst tube in the bundle at []^{a,c,c} inches radius in the sector of tubes shown to have the limiting H* values. All other tubes will have a lesser value of H*.

8.4 REFERENCES

- 8-1 EPRI 1012987, Revision 2, Steam Generator Integrity Assessment Guidelines; July 2006.
- 8-2 LTR-SST-05-19, Rev. 1, "System State Equivalency Testing Not Required for Windows XP SP-2," June 20, 2005.
- 8-3 MS Excel Function Reference; Document Number AB26298-0392; Microsoft Corporation; Redmond, WA.
- 8-4 ID-26666, Vol. 1, Design Data, Nuclear Systems Materials Handbook, ORNL, 1988.
- 8-5 LTR-SGMP-09-55, "Monte Carlo Analyses in Support of the H-Star Program," Westinghouse Electric Company LLC, Pittsburgh, PA, April 20, 2009.

Table 8-4 Summary of Probabilistic Analysis

Case	Description (see Sections 8.2.1 and 8.2.2 for complete descriptions)	Condition (1)	Mean H* (in.)	ΔH* (in.)	Probabilistic H* at 95/50 (in.)	Pcr Adjust- ment ⁽⁴⁾	Final H* (in.)

a,c,e

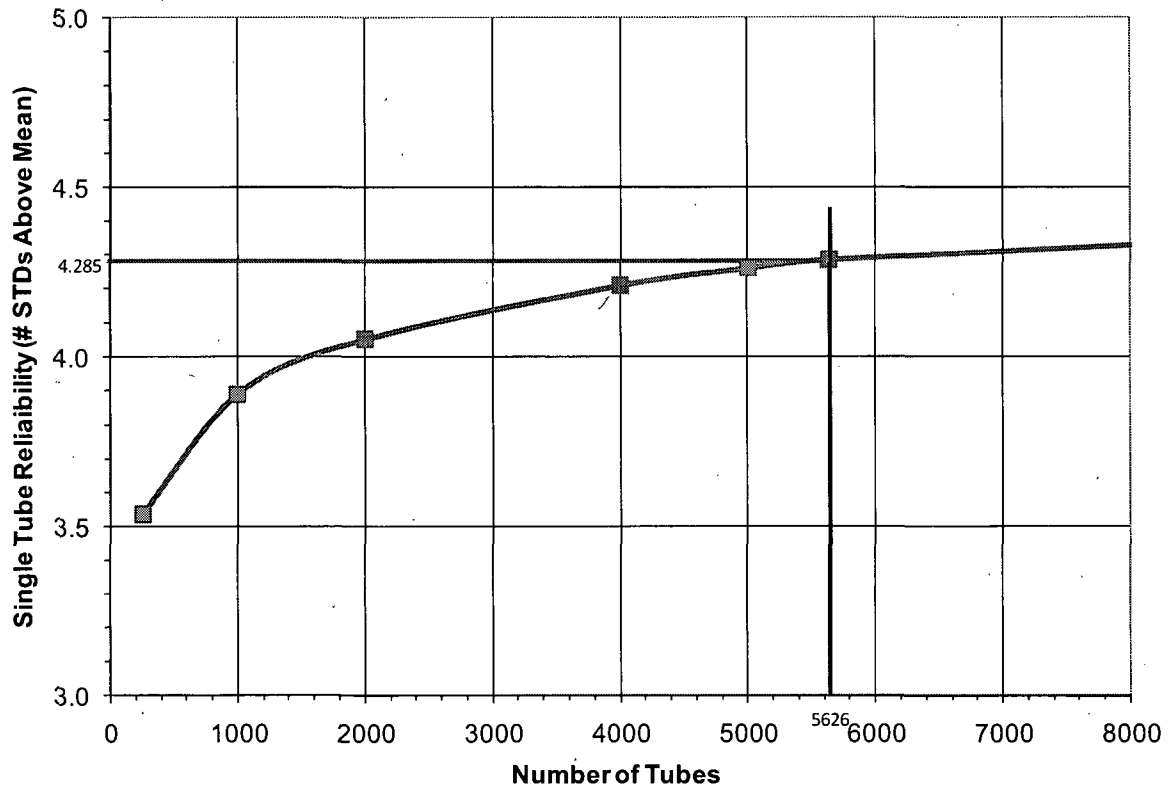


Figure 8-12 Single Tube Required Reliability, Expressed as Number of Standard Deviations from the Mean to Meet a Whole-Bundle (5626 Tubes) Reliability of 95%

Serial No: 09-525
Docket No. 50-423

ENCLOSURE 11

Westinghouse Electric Company LLC, LTR-SGMP-09-100 NP-Attachment, Response to NRC Request for Additional Information on H*; Model F and Model D5 Steam Generators, dated August 12, 2009.

NON-PROPRIETARY

**DOMINION NUCLEAR CONNECTICUT, INC.
MILLSTONE POWER STATION UNIT 3**

WESTINGHOUSE NON-PROPRIETARY CLASS 3

LTR-SGMP-09-100 NP-Attachment

Westinghouse Electric Company

**Response to
NRC Request for Additional Information on H*;
Model F and Model D5 Steam Generators**

August 12, 2009

Westinghouse Electric Company LLC
P.O. Box 158
Madison, PA 15663

© 2009 Westinghouse Electric Company LLC
All Rights Reserved

**Response to
NRC Request for Additional Information on H*;
Model F and Model D5 Steam Generators**

References:

1. NL-09-0547, Vogtle Electric Generating Plant License Amendment Request to Revise Technical Specification(TS) Sections 5.5.9, "Steam Generator (SG) Program" and TS 5.6.10, "Steam Generator Tube Inspection Report for Permanent Alternate Repair Criteria," Southern Company, May 19, 2009.
2. RS-09-071, " License Amendment Request to Revise Technical Specifications (TS) for Permanent Alternate Repair Criteria," Exelon Nuclear, June 24, 2009.
3. CP-200900748, Log # TXX-09075, "Comanche Peak Steam Electric Station (CPSES) Docket Nos. 50-445 and 50-446, License Amendment Request 09-007, Model D5 Steam Generator Alternate Repair Criteria," Luminant, June 8, 2009.
4. SBK-L-09118, "Seabrook Station: License Amendment Request 09-03; Revision to Technical Specification 6.7.6.k, "Steam Generator (SG) Program," for Permanent Alternate Repair Criteria (H*)," May 28, 2009.
5. Vogtle Electric Generating Plant, Units 1 and 2, Request for Additional Information Regarding Steam Generator Program (TAC Nos. ME1339 and ME1340)," United States Nuclear Regulatory Commission, July 10, 2009.
6. Braidwood Station, Units 1 and 2, and Byron Station, Unit Nos. 1 and 2 – Request for Additional Information Related to Steam Generator Permanent Alternate Repair Criteria (TAC Nos. ME1613, ME1614, ME1615, and ME1616)," United States Nuclear Regulatory Commission, July 20, 2009.
7. Comanche Peak Steam Electric Station, Units 1 and 2 – Request for Additional Information Regarding the Permanent Alternate Repair Criteria License Amendment Request (TAC Nos. ME1446 and ME1447)," United States Nuclear Regulatory Commission, July 23, 2009.
8. WCAP-17071-P, "H*: Alternate Repair Criteria for the Tubesheet Expansion Region in Steam Generators with Hydraulically Expanded Tubes (Model F)," Westinghouse Electric LLC, April 2009.
9. WCAP-17072-P, "H*: Alternate Repair Criteria for the Tubesheet Expansion Region in Steam Generators with Hydraulically Expanded Tubes (Model D5)," Westinghouse Electric LLC, May 2009.
10. "Vogtle Electric Generating Plant, Units 1 and 2, Request for Additional Information Regarding Steam Generator Program (TAC Nos. ME1339 and ME1340)," United States Nuclear Regulatory Commission, August 5, 2009

Introduction

In response to formal requests for technical specification amendments, References 1, 2, 3 and 4, the USNRC formally requested additional information in References 5, 6 and 7. A preliminary request was received in response to Reference 4. This document provides responses to NRC RAI on the Vogtle, Byron/Braidwood and Comanche Peak requests for a permanent license amendment to implement H*. These plants represent the Model F and Model D5 steam generators for which the H* technical justification is provided in Reference 8 and 9. It is anticipated that similar RAIs may be issued as other LARs are submitted that include other models of SG, specifically Models 44F and 51F. The intent of these responses is to provide a generic response for all applicable models of SGs to the extent possible, recognizing that there may be specific numerical differences for the models of SG not yet addressed (Model 44F and Model 51F). If necessary, a second issue of these responses will be provided to specifically address the Model 44F and Model 51 RAI when they are received.

The NRC questions are repeated verbatim for each of the plants who received formal or draft RAI in the tables preceding the response to each question. The current NRC RAIs are specifically in regard to WCAP-17071-P (Model F H*) and WCAP-17072-P (Model D5 H*); responses are provided primarily for these reports, but additional information is provided as appropriate for the H* reports for the other models of SGs, WCAP-17091-P for the Model 44F and WCAP-17092-P for the Model 51 F. Because the reports all utilize the same methodology, model-specific information provided will generally be different in only the numerical information.

Subsequent to the initial issue of the RAI (References 5, 6 and 7), the NRC issued follow-up questions (Reference 10) to question numbers 4, 20 and 24 and an additional question regarding a TS commitment for applying the leakage factors. The responses to the follow-up questions to original question numbers 20 and 24 are included directly in the response to these questions below. The response to RAI#4 and the follow-up question to RAI#4 will be provided under separate cover.

Where references are made in a response to other responses included in this document, the basis for the reference is the RAI received by Vogtle. For example, the Vogtle RAI#20 response applies to the Byron/Braidwood RAI#21 as noted in the tabularization of the questions preceding each response.

RAI	Vogtle	1. Reference 1, page 6-21, Table 6-6: This table contains a number of undefined parameters and some apparent inconsistencies with Table 5-2 on page 5-6. Please define the input parameters in Table 6-6.
	WCGS	1. Reference 1, page 6-21, Table 6-6: This table contains a number of undefined parameters and some apparent inconsistencies with Table 5-2 on page 5-6. Please define the input parameters in Table 6-6.
	B/B	1. Reference 1, Page 6-21, Table 6-6: This table contains a number of undefined parameters and some apparent inconsistencies with Table 5-2 on page 5-6. Please define the input parameters in Table 6-6.
	CPSES	1. Reference 1, page 6-21, Table 6-6: This table contains a number of undefined parameters and some apparent inconsistencies with Table 5-2 on page 5-6. Please define the input parameters in Table 6-6.
	Seabrook	1. Reference 1, Page 6-21, Table 6-6: This table contains a number of undefined parameters and some apparent inconsistencies with Table 5-2 on page 5-6. Please define the input parameters in Table 6-6.

Response:

Table 6-6 in WCAP-17071-P and WCAP-17072-P is provided principally as a reference to provide a bridge to the source of basic design data maintained by Westinghouse and as a historical reference from prior H* reports. Although many of the entries in Table 6-6 are not used in the H* analysis, the table was provided to show traceability to the principal sources of the design data, the Westinghouse Power Capability Working Group (PCWG) sheets and the Systems Standards 1.3F and 1.3, which provide transient response data for component design. The references to Millstone Unit 3 in WCAP-17071-P and to Byron Unit 2 in WCAP-17072-P reflect that these plants are the limiting plants for the Model F and Model D5 SGs that are candidates for application of H*.

Updated Tables 6-6 for the Model F and Model D5 are provided as Tables RAI1-2 and RAI1-3. The references in the tables have been updated from those contained in Revision 0 of WCAP-17071-P and WCAP-17072-P.

Table RAI1-1
Updated Table 6-6 of WCAP-17071-P: Summary of H* Millstone Unit 3 Analysis
Mean Input Properties

Plant Name	Millstone Unit 3		
Plant Alpha	NEU		
Plant Analysis Type	Hot Leg		
SG Type	F		
Input	Value	Unit	Reference
Accident and Normal Temperature Inputs			
a,c,e			
NOP T _{hot}		°F	PCWG-06-9
NOP T _{low}		°F	PCWG-06-9
SLB TS ΔT		°F	1.3F
SLB CH ΔT		°F	1.3F
Shell ΔT		°F	1.3F
FLB Primary ΔT Hi		°F	1.3F
FLB Primary ΔT Low		°F	1.3F
SLB Primary ΔT		°F	1.3F
SLB Secondary ΔT		°F	1.3F
Secondary Shell ΔT Hi		°F	PCWG-06-9
Secondary Shell ΔT Low		°F	PCWG-06-9
Cold Leg ΔT		°F	PCWG-06-9
Hot Standby Temperature		°F	PCWG-06-9
Operating Pressure Input			
Faulted SLB Primary Pressure	2560.0	psig	1.3F
Faulted FLB Primary Pressure	2642.0 ⁽¹⁾	psig	1.3F
Normal Primary Pressure	2235.0	psig	PCWG-06-9
Cold Leg ΔP		a,c,e psig	NSD-RMW-90-070
NOP Secondary Pressure – Low		psig	PCWG-06-9
NOP Secondary Pressure – Hi		psig	PCWG-06-9
Faulted FLB Secondary Pressure	0.0	psig	1.3F
Faulted SLB Secondary Pressure	0.0	psig	1.3F

Notes. 1. The value for Faulted FLB Primary Pressure used in the H* analysis is 2650 psi which conservatively bounds the limiting value of 2642 psi as identified in SSDC 1.3F for the Model F SGs. The value of 2642 psig for peak primary-secondary pressure differential differs from the value provided in Table 5-3 (2657 psig) reported in WCAP-17071-P.

Table RAI1-2
Updated Table 6-6 of WCAP-17072-P: Summary of H* Byron Unit 2 Analysis
Mean Input Properties

Plant Name	Byron 2		
Plant Alpha	CBE		
Plant Analysis Type	Hot Leg		
SG Type	D5		
Input	Value	Unit	Reference
Accident and Normal Temperature Inputs			
		a,c,e	
NOP T _{hot}		°F	PCWG-2741
NOP T _{low}		°F	PCWG-2741
SLB TS ΔT		°F	1.3, Rev. 2
SLB CH ΔT		°F	1.3, Rev. 2
Shell ΔT		°F	1.3, Rev. 2
FLB Primary ΔT		°F	1.3, Rev. 2
SLB Primary ΔT		°F	1.3, Rev. 2
SLB Secondary ΔT		°F	1.3, Rev. 2
Secondary Shell ΔT Hi		°F	PCWG-2741
Secondary Shell ΔT Low		°F	PCWG-2741
Cold Leg ΔT		°F	PCWG-2741
Hot Standby Temperature*		°F	PCWG-2741
Operating Pressure Input			
Faulted SLB Primary Pressure	2560.0	psig	1.3, Rev. 2
Faulted FLB Primary Pressure	2560.0	psig	1.3, Rev. 2
Normal Primary Pressure	2235.0	psig	PCWG-2741
Cold Leg ΔP		a,c,e psig	NSD-RMW-90-070
NOP Secondary Pressure – Low		psig	PCWG-2741
NOP Secondary Pressure – Hi		psig	PCWG-2741
Faulted FLB Secondary Pressure	0.0	psig	1.3, Rev. 2
Faulted SLB Secondary Pressure	0.0	psig	1.3, Rev. 2

Much of the data provided in Table 6-6 is not utilized in the final H* analysis. Table RAI1-3 provides a summary of whether the data is utilized in the reference analysis of H* and in which analysis model it is used (See Figure 1-1 in the respective reports). It is emphasized that changes made in Tables RAI1-1 and RAI1-2 do not affect the H* results provided in References 7 and 8 of this document.

**Table RAI1-3
Utilization of Data from Table 6-6**

Input	Where Used
Accident and Normal Temperature Inputs	
NOP T _{hot}	H* Integrator Spreadsheet
NOP T _{low}	H* Integrator Spreadsheet
SLB TS ΔT	Not Used
SLB CH ΔT	Not Used
Shell ΔT	Not Used
FLB Primary ΔT Hi	Not Used
FLB Primary ΔT Low	Not Used
SLB Primary ΔT	Not Used
SLB Secondary ΔT	Not Used
Secondary Shell ΔT Hi	H* Integrator Spreadsheet; same as Secondary Fluid Temperature at NOP High T _{avg} Conditions
Secondary Shell ΔT Low	H* Integrator Spreadsheet; same as Secondary Fluid Temperature at NOP Low T _{avg} Conditions
Cold Leg ΔT	Not Used
Hot Standby Temperature	H* Integrator Spreadsheet
Operating Pressure Input	
Faulted SLB Primary Pressure	H* Integrator Spreadsheet
Faulted FLB Primary Pressure	H* Integrator Spreadsheet
Normal Primary Pressure	H* Integrator Spreadsheet
Cold Leg ΔP	Not Used
NOP Secondary Pressure – Low	H* Integrator Spreadsheet
NOP Secondary Pressure – Hi	H* Integrator Spreadsheet
Faulted FLB Secondary Pressure	Not Used
Faulted SLB Secondary Pressure	Not Used

The definitions of the entries in the Table 6-6 of WCAP-17071-P and WCAP17072-P are presented below. Also, discussion is provided regarding the consistency of the values in Table 6-6 of the respective reports with Tables 5-1 through 5-6 of the reports.

NOP T_{hot}

The steam generator hot leg temperature at high T_{avg} normal operating conditions at 100% power (considered to be the same as the reactor vessel outlet temperature).

Model F: []^{a,c,e} °F at the inlet of the tubes at high T_{avg} normal operating conditions at 100% power for Millstone Unit 3 is consistent with the value provided in Table 5-1 (WCAP-17071-P).

Model D5: []^{a,c,e} °F at the inlet of the tubes at high T_{avg} normal operating conditions at 100% power Byron Unit 2 is consistent with the value provided in Table 5-1 (WCAP-17072-P).

NOP T_{low}

The steam generator hot leg temperature at the inlet of the tubes at low T_{avg} normal operating conditions at 100% power (considered to be the same as the reactor vessel outlet temperature).

Model F: []^{a,c,e} °F is consistent with the value provided in Table 5-1.

Model D5: []^{a,c,e} °F is consistent with the value provided in Table 5-1.

SLB TS ΔT

Model F: []^{a,c,e} °F, ([]^{a,c,e} °F - 70°F) = []^{a,c,e} °F: The steam generator hot and cold leg temperature difference that occurs during a postulated steam line break event during the maximum pressure difference across the tubesheet of 2560 psi between the steady-state tubesheet metal temperature and the ambient temperature surrounding the steam generator (assumed to be 70°F). The value of []^{a,c,e} °F is not used in the analysis.

Model D5: []^{a,c,e} °F, ([]^{a,c,e} °F - 70°F) = []^{a,c,e} °F: The steam generator hot and cold leg temperature difference that occurs during a postulated steam line break event during the maximum pressure difference across the tubesheet of 2560 psi between the steady-state tubesheet metal temperature and the ambient temperature surrounding the steam generator (assumed to be 70°F). The value of []^{a,c,e} °F is not used in the H* analysis.

SLB CH ΔT

Model F: 348°F, []^{a,c,e} °F: The steam generator hot and cold leg temperature difference that occurs during a postulated steam line break event during the maximum pressure difference across the tubesheet of 2560 psi between the steady-state channelhead metal temperature and the ambient temperature surrounding the steam generator (assumed to be 70°F). The value of []^{a,c,e} °F is not used in the H* analysis.

Model D5: 227°F , ($[\]^{a,c,e} \text{ }^{\circ}\text{F}$): The steam generator hot and cold leg temperature difference that occurs during a postulated steam line break event during the maximum pressure difference across the tubesheet of 2560 psi between the steady-state channelhead metal temperature and the ambient temperature surrounding the steam generator (assumed to be 70°F). The value of $[\]^{a,c,e} \text{ }^{\circ}\text{F}$ is not used in the H^* analysis.

Shell ΔT

Model F: ($[\]^{a,c,e} \text{ }^{\circ}\text{F} - 70^{\circ}\text{F}$) = $[\]^{a,c,e} \text{ }^{\circ}\text{F}$: The steam generator secondary side temperature difference that occurs during a postulated steam line break event during the maximum pressure difference across the tubesheet of 2560 psi between the steady-state secondary side shell metal temperature and the ambient temperature surrounding the steam generator (assumed to be 70°F). The $[\]^{a,c,e} \text{ }^{\circ}\text{F}$ value is not used in the H^* analysis.

Model D5: $[\]^{a,c,e} \text{ }^{\circ}\text{F}$. The steam generator secondary side temperature difference that occurs during a postulated steam line break event during the maximum pressure difference across the tubesheet of 2560 psi between the steady-state secondary side shell metal temperature and the ambient temperature surrounding the steam generator (assumed to be 70°F). The $[\]^{a,c,e} \text{ }^{\circ}\text{F}$ value is not used in the H^* analysis.

The secondary side temperature during a postulated SLB is used in the H^* analysis for both the Model F ($[\]^{a,c,e} \text{ }^{\circ}\text{F}$) and Model D5 ($[\]^{a,c,e} \text{ }^{\circ}\text{F}$) SGs.

FLB Primary ΔT_{Hi}

The reduction in NOP T_{hot} temperature that occurs during a postulated feedwater line break during the maximum pressure difference across the tubesheet of 2642 psi (Model F), 2560 psi (Model D5) corresponding to the high T_{avg} plant condition.

Model F: $[\]^{a,c,e} \text{ }^{\circ}\text{F}$ is consistent with the value provided in Table 5-3 ($[\]^{a,c,e} \text{ }^{\circ}\text{F} - 54^{\circ}\text{F} = [\]^{a,c,e} \text{ }^{\circ}\text{F}$). The -54°F value is not used in the H^* analysis.

Model D5: $[\]^{a,c,e} \text{ }^{\circ}\text{F}$ is consistent with the value provided in Table 5-3 ($[\]^{a,c,e} \text{ }^{\circ}\text{F} - [\]^{a,c,e} \text{ }^{\circ}\text{F} = [\]^{a,c,e} \text{ }^{\circ}\text{F}$). The $[\]^{a,c,e} \text{ }^{\circ}\text{F}$ value is not used in the H^* analysis.

The primary side temperature that occurs during a postulated FLB initiating from the high T_{avg} plant condition, $[\]^{a,c,e} \text{ }^{\circ}\text{F}$ is used in the H^* analysis for the Model F SG. The no load temperature of $[\]^{a,c,e} \text{ }^{\circ}\text{F}$ is used for the Model D5 SGs.

FLB Primary ΔT_{Low}

The reduction in NOP T_{low} temperature that occurs during a postulated feedwater line break during the maximum pressure difference across the tubesheet of 2642 psi.

Model F: []^{a,c,e} °F is consistent with the value provided in Table 5-3 ([]^{a,c,e} °F []^{a,c,e} °F = []^{a,c,e} °F). The -54°F value is not used in the H* analysis.

Model D5: []^{a,c,e} °F is not included in WCAP-17072-P. The []^{a,c,e} °F value is not used in the H* analysis.

The primary side temperature that occurs during a postulated FLB initiating from the low T_{avg} plant condition, []^{a,c,e} °F, is used in the H* analysis for the Model F. The no load temperature of []^{a,c,e} °F is used for the Model D5 SGs.

SLB Primary ΔT

Model F: The reduction in no load temperature of []^{a,c,e} °F ([]^{a,c,e} °F) to []^{a,c,e} °F that occurs in the reactor coolant system during a postulated SLB during the maximum pressure difference across the tubesheet of 2560 psi. The value in Table 6-6 should be []^{a,c,e} °F to be consistent with SSDC 1.3F and Table 5-2. The []^{a,c,e} °F value is not used in the H* analysis.

Model D5: The reduction in no load temperature of []^{a,c,e} °F ([]^{a,c,e} °F) to []^{a,c,e} °F that occurs in the reactor coolant system during a postulated SLB during the maximum pressure difference across the tubesheet of 2560 psi. The value in Table 6-6 is consistent with SSDC 1.3, Rev 2 and Table 5-2. The []^{a,c,e} °F value is not used in the H* analysis.

The primary side temperature that occurs during a postulated SLB, []^{a,c,e} °F, is used in the H* analysis for the Model F. The primary side temperature, []^{a,c,e} °F, is used for the Model D5 SGs.

SLB Secondary ΔT

Model F: The reduction in no load temperature of []^{a,c,e} °F ([]^{a,c,e} °F) to []^{a,c,e} °F that occurs on the secondary side of the steam generator during a postulated SLB during the maximum pressure difference across the tubesheet of 2560 psi. The value in Table 6-6 should be []^{a,c,e} °F to be consistent with Table 5-2.

Model D5: The reduction in no load temperature of []^{a,c,e} °F ([]^{a,c,e} °F) to []^{a,c,e} °F that occurs on the secondary side of the steam generator during a postulated SLB during the maximum pressure difference across the tubesheet of 2560 psi. The value in Table 6-6 should be []^{a,c,e} °F to be consistent with SSDC 1.3, Rev. 2 and Table 5-2.

As noted above, the secondary side temperature during a postulated SLB is used in the H* analysis for both the Model F ([]^{a,c,e} °F) and Model D5 ([]^{a,c,e} °F) SGs.

Secondary Shell ΔT_{Hi}

For the Model F SG, []^{a,c,e} °F (should be []^{a,c,e} °F) is the average temperature between the secondary side steam temperature and the feedwater temperature during NOP Hi T_{avg} operation ([]^{a,c,e} °F + []^{a,c,e} °F). This value is the same as the secondary fluid temperature during high T_{avg} normal operating conditions. The same value calculated for the Model D5 SGs is []^{a,c,e} °F.

Secondary Shell ΔT_{Low}

For the Model F SGs, []^{a,c,e} °F is the average temperature between the secondary side steam temperature and the feedwater temperature during NOP Low T_{avg} operation ([]^{a,c,e} °F + []^{a,c,e} °F)/2 = []^{a,c,e} °F). This value is the same as the secondary fluid temperature during low T_{avg} normal operating conditions. The same value calculated for the Model D5 SGs is []^{a,c,e} °F.

Cold Leg ΔT

Model F: The temperature difference between the hot and cold leg of the Millstone 3 SGs during NOP Low T_{avg} is 66.6°F. This value is not used in the H* analysis.

Model D5: The temperature difference between the hot and cold leg of the Byron 2/Braidwood 2 SGs during NOP Low T_{avg} is 63°F. This value is not used in the H* analysis.

Hot Standby Temperature

The zero load temperature, []^{a,c,e} °F.

This value is used in the H* analysis for both the Model F and Model D5 SGs.

Faulted SLB Primary Pressure

The maximum pressure difference that occurs across the tubesheet during a postulated SLB.

Model F: 2560 psig is consistent with the value reported in Table 5-2.

Model D5: 2560 psig is consistent with the value reported in Table 5-2.

Faulted FLB Primary Pressure

The maximum pressure difference that occurs across the tubesheet during a postulated FLB.

Model F: The value (2650 psig) used for the Model F SG in the H* analysis bounds the actual FLB pressure differential, 2642 psi identified in SSDC 1.3F. As noted above, Table 5-3 of

WCAP-17071-P should be corrected to 2642 psig for the entries for peak primary-to-secondary pressure.

Model D5: The maximum FLB pressure differential for the Model D5 SGs is 2560 psi.

Normal Primary Pressure

The primary side pressure during normal operation.

Model F: 2235 psig is consistent with the absolute primary pressure reported in Table 5-1 of 2250 psia.

Model D5: 2235 psig is consistent with the absolute primary pressure reported in Table 5-1 of 2250 psia.

Cold Leg ΔP

The overall pressure drop that occurs in a steam generator tube as fluid flows through the tube from hot leg to cold leg.

Model F: []^{a,c,e} psig (Millstone 3). This value is not used in the H* analysis.

Model D5: []^{a,c,e} psig (Byron 2/Braidwood 2). This value is not used in the H* analysis.

NOP Secondary Pressure Low

The steam pressure on the secondary side of the steam generators for NOP Low T_{avg} .

Model F: []^{a,c,e} psig is consistent with the value reported in Table 5-1 as []^{a,c,e} psia.

Model D5: []^{a,c,e} psig is consistent with the value reported in Table 5-1 as []^{a,c,e} psia.

NOP Secondary Pressure Hi

The steam pressure on the secondary side of the steam generators for NOP Hi T_{avg} .

Model F: []^{a,c,e} psig is consistent with the value reported in Table 5-1 as []^{a,c,e} psia.

Model D5: []^{a,c,e} psig is consistent with the value reported in Table 5-1 as []^{a,c,e} psia.

Faulted FLB Secondary Pressure

0 psig, for the Model F and Model D5 SGs, the steam pressure on the secondary side of a steam generator during a postulated FLB. This value is not used in the H* analysis.

RAI	<i>Vogtle</i>	2. <i>Reference 1, page 6-23, Section 6.2.2.2: Why was the finite element analysis not run directly with the modified temperature distribution rather than running with the linear distribution and scaling the results?</i>
	<i>WCGS</i>	2. <i>Reference 1, Section 6.2.2.2: Please explain why the finite element analysis not run directly with the modified temperature distribution rather than running with the linear distribution and scaling the results?</i>
	<i>B/B</i>	2. <i>Reference 1, Section 6.2.2.2: Why was the finite element analysis not run directly with the modified temperature distribution rather than running with the linear distribution and scaling the results?</i>
	<i>CPSES</i>	2. <i>Reference 1, Section 6.2.2.2: Please explain why the finite element analysis was not run directly with the modified temperature distribution rather than running with the linear distribution and scaling the results?</i>
	<i>Seabrook</i>	2. <i>Reference 1, Section 6.2.2.2: Why was the FEA analysis not run directly with the modified temperature distribution rather than running with the linear distribution and scaling the results?</i>

Response:

The finite element analysis was run with the modified temperature distribution as described in section 6.2.2.2.5 of WCAP 17071-P (Model F) and WCAP-17072-P (Model D5). However, since the modified temperature distribution required a different meshing scheme, the displacement results could not initially be used as inputs to the H* contact pressure analysis. The difficulty in applying the results for the modified temperature distribution is what led to the development of Figures 6-21 through Figure 6-23. Additional tools were developed to accommodate the displacement results from the modified temperature distribution during the course of refining the analysis procedures to accommodate other steam generator designs. When the actual tubesheet displacements from the modified thermal distribution are used, instead of the results from the linear temperature distribution being scaled, the actual change in H* distance is much less than the []^{a,c,e} inches reported in Section 6.2.2.2.5. The value of the adjustment for the thermal distribution effect in H* for the different models of SG in the H* fleet is given in Table RAI2-1. All of the values in Table RAI2-1 assume zero residual contact pressure from tube installation effects. The results in column (3) come from using the scaled linear tubesheet displacements in the H* contact pressure analysis. The results in column (4) come from using the tubesheet displacements from the modified thermal distribution.

**Table RAI2-1
Updated NOP Thermal Offset Factors**

SG Model	Report	Thermal Offset (Scaled Result)	Thermal Offset (Applied)
(1)	(2)	(3)	(4)
Model F	WCAP 17071-P	[] ^{a,c,e} in.	[] ^{a,c,e} in.
Model D5	WCAP 17072-P	[] ^{a,c,e} in.	[] ^{a,c,e} in.
Model 44F	WCAP 17091-P	0.00 in.	0.00 in.
Model 51F	WCAP 17092-P	0.00 in.	0.00 in.

RAI	Vogtle	3. Reference 1, page 6-38, Section 6.2.3: Why is radial displacement the "figure of merit" for determining the bounding segment? Does circumferential displacement not enter into this? Why is the change in the tube hole diameter not the "figure of merit?"
	WCGS	3. Reference 1, Section 6.2.3: Please explain why radial displacement is the "figure of merit" for determining the bounding segment? Does circumferential displacement not enter into this? Why is the change in tube hole diameter not the "figure of merit?"
	B/B	3. Reference 1, Section 6.2.3: Why is radial displacement the "figure of merit" for determining the bounding segment? Does circumferential displacement not enter into this? Why is the change in tube hole diameter not the "figure of merit?"
	CPSSES	3. Reference 1, Section 6.2.3: Please explain why radial displacement is the "figure of merit" for determining the bounding segment. Does circumferential displacement not enter into this? Why is the change in tube hole diameter not the "figure of merit?"
	Seabrook	3. Reference 1, Section 6.2.3: Why is radial displacement the "figure of merit" for determining the bounding segment? Does circumferential displacement not enter into this? Why is the change in tube hole diameter not the "figure of merit?"

Response:

Radial displacement is calculated in two different ways in the H* analysis: the global scale and the local scale.

On the scale of the steam generator itself, otherwise referred to as the global scale, the radial displacement of the entire tubesheet is calculated. At this level, the tubes are not included in the structural model and there is no direct way to calculate the change in the tube hole diameter. It is not possible to calculate the change in the tube hole diameter at the global scale because the tube holes physically do not exist but are represented by

the effective anisotropic material properties of the tubesheet. Therefore, from the global perspective, it is not possible to use the change in hole diameter as a "figure of merit."

On the local scale, the displacements of the tube and tubesheet collar are calculated in the radial and circumferential directions. As described in Section 6.3 of WCAP-17071-P (Model F) and WCAP -17072-P (Model D5), the expansion of a hole of diameter D in the tubesheet at a radius R is given by:

$$\text{Radial:} \quad \Delta D = D \{dU_R(R)/dR\}$$

$$\text{Circumferential:} \quad \Delta D = D \{U_R(R)/R\}$$

U_R is available directly from the finite element results as the global radial displacement for a given point in the tubesheet. The value for $dU_R(R)/dR$ is obtained by numerical differentiation of the combined displacement field. The maximum expansion of a hole in the tubesheet is in either the radial or circumferential direction. Typically, these two values are within []^{a,c,e}% of each other. However, it is clear from the relationship described in Section 6.3 that maximizing the radial displacement at the global scale (i.e., increasing U_R) results in maximizing the circumferential and radial displacement of the tubesheet material at the local scale.

The connection between the local and global scales is the global radial displacement of the tubesheet. This is because the applied boundary conditions and the structures attached to the tubesheet have the greatest effect on the displacement in the radial direction. The tubesheet displacement in the circumferential direction due to the applied pressure loading is typically constant at a small negative value on the order of []^{a,c,e} inch or less. Therefore, the radial displacement is the best indicator, or "figure of merit," of the effect of different operating conditions on tubesheet displacement due to pressure loading. Radial displacement is also a good "figure of merit" for the change in tube hole diameter because maximizing the global radial displacement leads to the maximum calculated circumferential and radial tubesheet displacements at the local level. Therefore, the global radial displacement of the tubesheet as described in Section 6.2.3 is the appropriate choice for determining the bounding segment of the tubesheet with respect to the contact pressure analysis.

RAI	Vogtle	4. Reference 1, page 6-69: In Section 6.2.5.3, it is concluded that the tube outside diameter and the tubesheet tube bore inside diameter always maintain contact in the predicted range of tubesheet displacements. However, for tubes with through-wall cracks at the H^* distance, there may be little or no net pressure acting on the tube for some distance above H^* . In Tables 6-18 and 6-19, the fourth increment in the step that occurs two steps prior to the last step suggests that there may be no contact between the tube and tubesheet, over a portion of the circumference, for a distance above H^* . Is the conclusion in Section 6.2.5.3 valid for the entire H^* distance, given the possibility that the tubes may contain through-wall cracks at that location?
	WCGS	4. Reference 1, page 6-69: In Section 6.2.5.3, it is concluded that the tube outside diameter and the tubesheet tube bore inside diameter always maintain contact in the predicted range of tubesheet displacements. However, for tubes with through-wall cracks at the H^* distance, there may be little or no net pressure acting on the tube for some distance above H^* . In Tables 6-18 and 6-19, the fourth increment in the step that occurs two steps prior to the last step suggests that there may be no contact between the tube and tubesheet, over a portion of the circumference, for a distance above H^* . Is the conclusion in 6.2.5.3 valid for the entire H^* distance, given the possibility that the tubes may contain through-wall cracks at that location?
	B/B	4. Reference 1, Page 6-7: In Section 6.2.5.3, it is concluded that the tube outside diameter and the tubesheet tube bore inside diameter always maintain contact in the predicted range of tubesheet displacements. However, for tubes with through-wall cracks at the H^* distance, there may be little or no net pressure acting on the tube for some distance above H^* . In Tables 6-18 and 6-19, the fourth increment in the step that occurs two steps prior to the last step suggests that there may be no contact between the tube and tubesheet, over a portion of the circumference, for a distance above H^* . Is the conclusion in 6.2.5.3 valid for the entire H^* distance, given the possibility that the tubes may contain through-wall cracks at that location.

CPSES	4. Reference 1, page 6-70: In Section 6.2.5.3, it is concluded that the tube outside diameter and the tubesheet tube bore inside diameter always maintain contact in the predicted range of tubesheet displacements. However, for tubes with through-wall cracks at the H^* distance, there may be little or no net pressure acting on the tube for some distance above H^* . In Tables 6-18 and 6-19, the fourth increment in the step that occurs two steps prior to the last step suggests that there may be no contact between the tube and tubesheet, over a portion of the circumference, for a distance above H^* . Is the conclusion in Section 6.2.5.3 valid for the entire H^* distance, given the possibility that the tubes may contain through-wall cracks at that location?
Seabrook	4. Reference 1, Page 6-69: In Section 6.2.5.3, it is concluded that the tube outside diameter and the tubesheet tube bore inside diameter always maintain contact in the predicted range of tubesheet displacements. However, for tubes with through-wall cracks at the H^* distance, there may be little or no net pressure acting on the tube for some distance above H^* . In Tables 6-18 and 6-19, the fourth increment in the step that occurs two steps prior to the last step suggests that there may be no contact between the tube and tubesheet, over a portion of the circumference, for a distance above H^* . Is the conclusion in 6.2.5.3 valid for the entire H^* distance, given the possibility that the tubes may contain through-wall cracks at that location?

Reference 10 provided follow-up questions to RAI#4. In Reference 10, the follow questions to RAI#4 were titled RAI#1. The follow-up questions from Reference 10 are reproduced below:

RAI#1 (Reference 10)

1. Address following questions as part of response to RAI 4 (Vogtle):

- a. Clarify the nature of the finite element model ("slice" model versus axisymmetric SG assembly model) used to generate the specific information in Tables 6-1, 2, and 3 (and accompanying graph entitled "Elliptical Hole Factors") of Reference 6-15. What loads were applied? How was the eccentricity produced in the model? (By modeling the eccentricity as part of the geometry? By applying an axisymmetric pressure the inside of the bore?) Explain why this model is not scalable to lower temperatures.
- b. Provide table showing maximum delta diameters (total diameter distortion) and maximum eccentricities (maximum diameter minus minimum diameter) from the 3 dimensional (3-D) finite element analysis for normal operating and steam line break (SLB), for model F and D5.
- c. In Figure 2 of the White Paper, add plot for original relationship between reductions in contact pressure and eccentricity as given in Reference 6-15 in the graph

accompanying Table 6-3. Explain why this original relationship remains conservative in light of the new relationship. Explain the reasons for the differences between the curves.

- d. When establishing whether contact pressure increases when going from normal operating to steam line break conditions, how can a valid and conservative comparison be made if the normal operating case is based on the original delta contact pressure versus eccentricity curve and the SLB case is based on the new curve?*

Response:

The responses to RAI#4 of References 5, 6 and 7 and to the follow-up question, RAI#1 of Reference 10, will be provided under separate cover.

RAI	Vogtle	5. Reference 1, Page 6-87: -Are the previously calculated scale factors and delta D factors in Section 6.3 conservative for steam line break and feedwater line break? Are they conservative for an intact divider plate assumption? Are they conservative for all values of primary pressure minus crevice pressure that may exist along the H* distance for intact tubes and tubes with through-wall cracks at the H* distance? How is tube temperature (TT) on page 6-87 determined? For normal operating conditions, how is the TT assumed to vary as function of elevation?
	WCGS	5. Reference 1, Section 6.3: Please verify if the previously calculated scale factors and delta D factors in Section 6.3 conservative for (1) steam line break (SLB) and a feedwater line break (FLB); (2) an intact divider plate assumption; and (3) all values of primary pressure minus crevice pressure that may exist along the H* distance for intact tubes and tubes with through-wall cracks at the H* distance.
	B/B	5. Reference 1, Page 6-86, Section 6: Are the previously calculated scale factors and delta D factors in Section 6.3 conservative for steam line break and feedwater line break (FLB)? Are they conservative for an intact divider plate assumption? Are they conservative for all values of primary pressure minus crevice pressure that may exist along the H* distance for intact tubes and tubes with through-wall cracks at the H* distance?
	CPSES	5. Reference 1, Section 6.3, Page 6-86: Please verify if the previously calculated scale factors and delta D factors in Section 6.3 are conservative for (1) a steam line break (SLB) and a feedwater line break (FLB); (2) an intact divider plate assumption; and (3) all values of primary pressure minus crevice pressure that may exist along the H* distance for intact tubes and tubes with through-wall cracks at the H* distance.
	Seabrook	5. Reference 1, Section 6.3: Are the previously calculated scale factors and delta D factors in Section 6.3 conservative for steam line break (SLB) and feed line break (FLB)? Are they conservative for an intact divider plate assumption? Are they conservative for all values of primary pressure minus crevice pressure that may exist along the H* distance for intact tubes and tubes with through-wall cracks at the H* distance?

Response:

Note: The page reference, 6-87 (Model F) appear to be incorrect in the question. Section 6.3 begins on page 6-83 (Model F). The page reference for the Model D5 is correct as stated in the Byron/Braidwood RAI.

- 1) The previously calculated scale factors and delta D factors in Section 6.3 are conservative for all of the analyzed Model F and Model D5 conditions, including normal operating, steam line break and feedwater line break, as appropriate. Use of the contact pressure data described in Reference RAI5-1 would increase the tube-to-tubesheet contact pressure in the Model F H* analysis.
- 2) The previously calculated scale factors and delta D factors in Section 6.3 are conservative for an intact divider plate assumption. The results on page 6-87 assume that a greater level of weld and divider plate degradation exists in the SG (DPF = []^{a,c,e}) than in the rest of the H* structural analysis (DPF = []^{a,c,e}). (DPF = Divider Plate Factor).
- 3) The previously calculated scale factors and delta D factors in Section 6.3 are conservative for all values of primary pressure minus crevice pressure regardless of their location within the tubesheet. This is because the calculated scale factors and delta D factors applied unit pressure loads to either side of the tube and weld structure in the model such that either the primary side of the tube and tubesheet were pressurized or the secondary side of the tube and tubesheet (including the crevice) were pressurized. In the reference elliptical hole study, the gap elements that were selected for use in the two dimensional study also penalized the tube-tubesheet contact pressure by preventing line on line contact between the tube outside diameter (OD) and the tubesheet/sleeve inside diameter (ID) which results in a lower estimate of the tube-to-tubesheet contact pressure.
- 4) The tube temperature (T_T) is assumed to be equal to the primary fluid temperature for the operating condition of interest. The tube temperature is assumed to not vary as a function of elevation within the tubesheet.

RAI5 References:

RAI5-1. LTR-NRC-09-26, "LTR-SGMP-09-66 P-Attachment, "White Paper: Low Temperature Steam Line Break Contact Pressure and Local Tube Bore Deformation Analysis for H*" (Proprietary)," May 13, 2009

RAI	WCGS	6. <i>Reference 1, page 6-87: Please provide information on how the tube temperature (T_T) on page 6-87 was determined? For normal operating conditions, how is the T_T assumed to vary as function of elevation?</i>
	B/B	6. <i>Reference 1, Page 6-9: How is tube temperature (T_T) on page 6-96 determined? For normal operating conditions, how is the T_T assumed to vary as a function of elevation?</i>
	CPSES	6. <i>Reference 1, page 6-96: Please provide information on how the tube temperature (T_T) on page 6-96 was determined. For normal operating conditions, please explain how the T_T is assumed to vary as function of elevation.</i>
	Seabrook	6. <i>Reference 1, Page 6-8: How is tube temperature (T_T) on page 6-87 determined? For normal operating conditions, how is the T_T assumed to vary as function of elevation?</i>

Response:

The tube temperature (T_T) is assumed to be equal to the primary fluid temperature for the operating condition of interest. The tube temperature is assumed to not vary as a function of elevation within the tubesheet.

RAI	Vogtle	6. Reference 1, page 6-97, Figure 6-75:-Contact pressures for nuclear plants with Model F SGs are plotted in Figure 6-75, but it is not clear what operating conditions are represented in the plotted data, please clarify.
	WCGS	7. Reference 1, page 6-97, Figure 6-75: Contact pressures for nuclear plants with Model F SGs are plotted in Figure 6-75, but it is not clear what operating conditions are represented in the plotted data. Please clarify.
	B/B	7. Reference 1, Page 6-104, Figure 6-77: Contact pressures for nuclear plants with Model D5 steam generators are plotted in Figure 6-77, but it is not clear what operating conditions are represented for the plants shown in the plotted data; please clarify.
	CPSSES	7. Reference 1, page 6-104, Figure 6-77: Contact pressures for nuclear plants with Model D5 SGs are plotted in Figure 6-77, but it is not clear what operating conditions are represented for the plants shown in the plotted data. Please clarify.
	Seabrook	7. Reference 1, Page 6-97, Figure 6-75: Contact pressures for nuclear plants with Model F steam generators are plotted in Figure 6-75, but it is not clear what operating conditions are represented in the plotted data, please clarify.

Response:

Figure 6-75 (WCAP-17071-P) shows the contact pressure results for the fleet of Model F steam generators for the main feedwater line break (FLB), main steam line break (SLB) and normal operating low average temperature (NOP Low T_{avg}) conditions. Figure RAI6-1 provides an update of Figure 6-75 in WCAP-17071-P with an expanded legend that describes each curve in the figure.

Figure 6-77 (WCAP-17072-P) shows the contact pressure results for the fleet of Model D5 steam generators for the main feed line break (FLB), main steam line break (SLB) and normal operating low average temperature (NOP Low T_{avg}) conditions. Figure RAI6-2 provides an update of Figure 6-77 in WCAP-17072-P with an expanded legend that describes each curve in the figure.

Figure RAI-6-1
Revised Figure 6-75 (WCAP-17071-P)

a,c,e

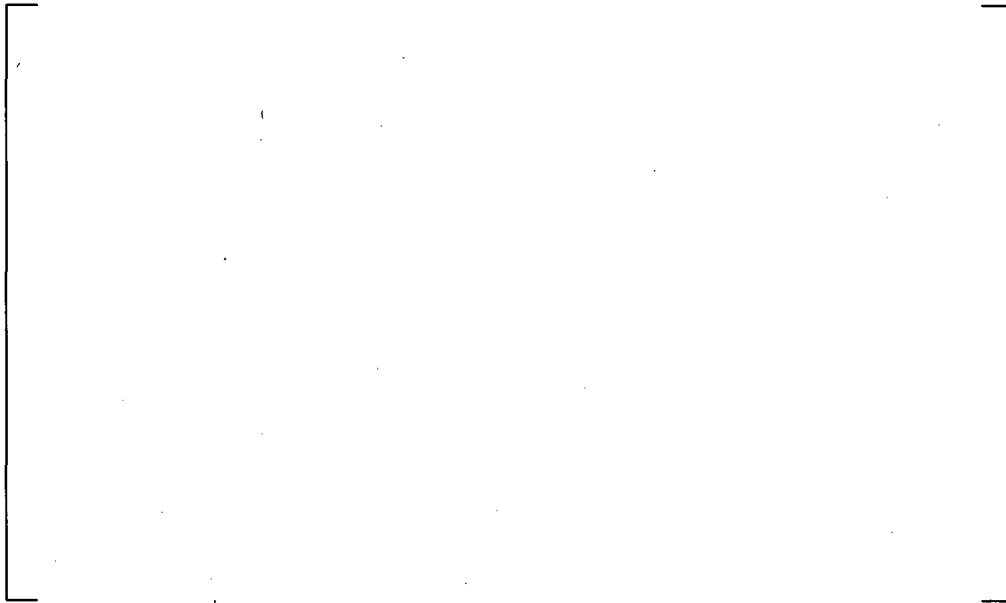


Figure RAI6-2
Revised Figure 6-77 (WCAP-17072-P)

a,c,e



RAI	Vogtle	7. Reference 1, page 6-113, Reference 6-5: This reference seems to be incomplete; please provide a complete reference.
	WCGS	8. Reference 1, page 6-112, Reference 6-5: This reference seems to be incomplete. Please provide a complete reference.
	B/B	8. Reference 1, Page 6-120, Reference 6-5: This reference seems to be incomplete; please provide a complete reference.
	CPSES	8. Reference 1, page 6-120, Reference 6-5: This reference appears to be incomplete. Please provide a complete reference.
	Seabrook	8. Reference 1, Page 6-112, Reference 6-5: This reference seems to be incomplete; please provide a complete reference.

Response:

The complete reference is:

Slot, Thomas, "Stress Analysis of Thick Perforated Plates," TECHNOMIC Publishing Company, Inc., Westport, Connecticut, 1972.

RAI	Vogtle	8. Reference 1, page 6-113, Reference 6-15: Table 6-3 in Reference 6-15 (SM-94-58, Rev 1) appears inconsistent with Table 6-2 in the same reference. Explain how the analysis progresses from Table 6-2 to Table 6-3.
	WCGS	9. Reference 1, page 6-113, Reference 6-15: Table 6-3 in Reference 6-15 (SM-94-58, Revision 1) appears inconsistent with Table 6-2 in the same reference. Please explain how the analysis progresses from Table 6-2 to Table 6-3.
	B/B	9. Reference 1, Page 6-121, Reference 6-15: Table 6-3 in Reference 6-15 (SM-94-58, Rev. 1) appears inconsistent with Table 6-2 in the same reference. Explain how the analysis progresses from Table 6-2 to Table 6-3.
	CPSES	9. Reference 1, Page 6-121, Reference 6-15: Table 6-3 in Reference 6-15 (SM-94-58, Revision 1) appears to be inconsistent with Table 6-2 in the same reference. Please explain how the analysis progresses from Table 6-2 to Table 6-3.
	Seabrook	9. Reference 1, Page 6-113, Reference 6-15: Table 6-3 in Reference 6-15 (SM-94-58, Rev 1) appears inconsistent with Table 6-2 in the same reference. Explain how the analysis progresses from Table 6-2 to Table 6-3

Response:

The values for initial and final eccentricity for the contact pressure ratio of 0.91 listed in Table 6-3 of Reference 6-15 (SM-94-58, Rev. 1) are calculated as follows using the values from Table 6-2:

$$\text{Initial Eccentricity} = (D_{\text{max}} - D_{\text{min}}) / [\quad]^{a,c,e} \text{ inch Tube Hole ID} = [\quad]^{a,c,e}$$

$$\text{Final Eccentricity} = ((\text{Hole Delta D (90}^\circ) - \text{Hole Delta D (0}^\circ)) / [\quad]^{a,c,e} \text{ inch Tube Hole ID}) = [\quad]^{a,c,e}$$

The values for eccentricity in Table 6-2 of the reference should have been divided by the nominal diameter of the tubesheet hole [$\quad]^{a,c,e}$ inch) to be consistent with Table 6-3.

RAI	Vogtle	9. Reference 1, page 8-9, Figure 8: -There is an apparent discontinuity in the plotted data of the adjustment to H* for distributed crevice pressure, please provide any insight you may have as to why this apparent discontinuity exists.
	WCGS	10. Reference 1, page 8-9, Figure 8-1: There is an apparent discontinuity in the plotted data of the adjustment to H* for distributed crevice pressure. Please provide any insight you may have as to why this apparent discontinuity exists.
	B/B	10. Reference 1, page 8-9, Figure 8-1: There is an apparent discontinuity in the plotted data of the adjustment to H* for distributed crevice pressure. Please provide any insight you may have as to why this apparent discontinuity exists.
	CPSES	10. Reference 1, page 8-9, Figure 8-1: There is an apparent discontinuity in the plotted data of the adjustment to H* for distributed crevice pressure. Please provide any insight you may have as to why this apparent discontinuity exists.
	Seabrook	10. Reference 1, Page 8-9, Figure 8-1: There is an apparent discontinuity in the plotted data of the adjustment to H* for distributed crevice pressure, please provide any insight you may have as to why this apparent discontinuity exists.

Response:

Figure 8-1 (WCAP-17071-P, WCAP-17072-P) summarizes the variability cases run to determine the H* value response to variation of the input parameters (α_T , α_{TS} , E_T , E_{TS}) individually or in combination. The values of the variables were chosen to provide sufficient data to define the potential surface of interactions between the variables. No attempt was made to bias the variables in a manner that would yield H* values in the range between 3.8 inches and 4.2 inches; therefore this gap is coincidental.

Figure RAI9-1 shows a composite of the P_{crev} corrections for all of the models of SGs considered, Models F, D5, 44F and 51F SGs under H^* (Ref: WCAP-17071-P, WCAP-17072-P, WCAP-17091-P and WCAP-17092-P). Figure RAI9-1 shows the same characteristic shape of the P_{crev} correction but also shows that the H^* responses are different for the different structures. The "apparent discontinuity" in the curve for the Model F is much less pronounced for the Model D5 and other models of SG and, in the case of the Model 44F, is populated by calculated data points. Because the same analysis methods are employed for all of the Model-specific structures, it is concluded that the apparent discontinuity in Figure 8-1 of WCAP-17071-P and WCAP-17072-P is related principally to the structural response of the specific SG model being addressed, and does not imply a potential calculation error.

Figure RAI9-1 also shows that in each of the structures considered, there are steps in the P_{crev} correction curves (e.g., between 3.8 and 4.2 inches in the Model F, at about 6.6 inches in the Model D5, at about 3.5 inches and 4.5 inches for the Model 44F and 51F). To investigate the step in the curve between initial predictions of H^* and the P_{crev} correction, several cases were considered for the Model F SGs for H^* values between 3.8 inches and 4.2 inches as a typical case to evaluate the issue generically. These cases were synthesized by adjusting the values of the four influencing parameters (α_T , α_{TS} , E_T and E_{TS}), based on interpolation among existing variabilities, in an attempt to yield H^* values in this range. Each of the four parameters was adjusted in at least one case to meet this objective.

The following are the additional cases that were examined:

Input Parameters				$H^*(raw)$	P_{crev}	Comment
a_{TS}	E_{TS}	a_T	E_T			
1	-1	-2	-2			Original Case
5	4	0	0			
-1	0	-3.25	0			
-1	0	-3	-5			
4.5	0	0	0			
5	4	0	-1			
4.5	0	0	-1			
5	0	0	0			Original Case

Figure RAI9-2 shows the results of this study. The P_{crev} correction values are essentially constant within the narrow range of initial H^* predictions that define the step in the overall curve, Figure RAI9-1, except for a single point at approximately []^{a,c,e} inches. As discussed below, the interpolation between the limited number of points representing the crevice pressure distribution and the fixed number of points representing the thickness of the tubesheet leads to isolated conditions at which the integration scheme cannot converge to a single value. A minor departure (less than about 0.005 inch) in either direction results in convergence of the integration. The point at []^{a,c,e} inches is at such a condition. It does not suggest that the crevice pressure correction is undefined at that location.

As described in each of the H* WCAP reports, the correction for P_{crev} is an iterative process. Following the initial prediction of H*, which assumes that a tube separation is located at the primary face of the tubesheet and, therefore, assumes the crevice pressure is distributed over the entire thickness of the tubesheet, the calculation process depicted in Figure 1-1 of the report is repeated but with the crevice pressure distributed over the length of the initial prediction of H*. The resulting prediction of H* will exceed the initial prediction. This process is iterated until the input values and output values of H* converge to the same number. The convergence criteria are set to 2 decimals because the H* distance cannot practically be measured to the second decimal. In some instances, depending on the specific combination of input parameters that lead to the initial prediction of H*, the variation of H* is less than the convergence criteria. In that case, the default is at the larger value of the P_{crev} .

The H* integrator model utilizes discrete, dimensionally fixed points through the thickness of the tubesheet to represent the tube to tubesheet contact pressure. The representation of the distributed crevice pressure as discussed in Section 6 of the report utilizes a discrete number of points whose axial dimensions vary according to the assumed position of the flaw. Thus, the same number of points describes the crevice pressure profile regardless if the flaw is assumed at the bottom of the tubesheet or at some other location within the tubesheet. Only the slope of the distribution between the points changes. Because of a mismatch between the crevice pressure axial definition and the tubesheet contact pressure axial definition, the integration model cannot converge to a single value at certain discrete points, depending on the model of SG under consideration. For the Model F SG, this point occurs at approximately 4 inches from the top of the tubesheet. The axial range within which this occurs is extremely narrow, less than []^{a,c,e} inch (see Figure RAI9-2), and the non-convergence results in a very limited range of the axial crevice pressure correction factor, less than []^{a,c,e} inch. For the Model F SG, a variation of initial H* prediction of approximately 0.005 inch from the critical axial length results in the model converging again at the lower value of P_{crev} correction as also shown on Figure RAI9-2. This result applies generically to the Model D5, 44F and 51F SGs as well.

For practical application in determining the final value of H*, it is noted that when the adjustments for BET and NOP thermal distribution are included, the predicted values of H* are far removed from the points in the P_{crev} correction curves where the model does not converge for all models of SGs. The recommended values of H*, prior to the correction for P_{crev} , for the different models of SG are:

Model F:	9.81 inches (Ref: WCAP-17071-P)
Model D5	12.11 inches (Ref: WCAP-17072-P)
Model 44F	11.06 inches (Ref: WCAP-17091-P)
Model 51F	11.14 inches (Ref: WCAP-17092-P)

In all cases, the point of non-convergence of the model does not affect the final recommended value of H*.

Figure RAI9-1
 P_{crev} Correction Profiles for Models F, D5, 44F and 51F SGs



Figure RAI9-2



RAI	Vogtle	10. Reference 1, Page 8-6, Section 8.1.4: Clarify whether the "biased" H* distributions for each of the four input variables are sampled from both sides of the mean H* value during the Monte Carlo process, or only on the side of the mean H* value yielding an increased value of H*.
	WCGS	11. Reference 1, Page 8-6, Section 8.1.4: Please clarify whether the "biased" H* distributions for each of the four input variables are sampled from both sides of the mean H* value during the Monte Carlo process, or only on the side of the mean H* value yielding an increased value of H*.
	B/B	11. Reference 1, Page 8-6, Section 8.1.4: Clarify whether the "biased" H* distributions for each of the four input variables are sampled from both sides of the mean H* value during the Monte Carlo process, or only on the side of the mean H* value yielding an increased value of H*.
	CPSSES	11. Reference 1, Page 8-6, Section 8.1.4: Please clarify whether the "biased" H* distributions for each of the four input variables are sampled from both sides of the mean H* value during the Monte Carlo process, or only on the side of the mean H* value yielding an increased value of H*.
	Seabrook	11. Reference 1, Page 8-6, Section 8.1.4: Clarify whether the "biased" H* distributions for each of the four input variables are sampled from both sides of the mean H* value during the Monte Carlo process, or only on the side of the mean H* value yielding an increased value of H*.

Response:

As shown in Figure 8-11 of the report (WCAP-17071-P, WCAP-17072-P, WCAP-17091-P and WCAP-17092-P), the variation of the parameters that resulted in the greatest increase in the value of H* were chosen as the "biased" influence factors from which to sample in the Monte Carlo (MC) process. These distributions were normal distributions determined from the mean H* and greatest H* variation resulting from equal valued positive and negative variations of the respective parameters. Note that for the case of coefficient of thermal expansion of the tube, a decrease in the coefficient results in an increase in the H* value and also reflects the broadest distribution. For the coefficient of thermal expansion of the tubesheet, an increase in the coefficient results in increasing H* and also results in the broadest distribution.

Both sides of the biased influence factors were sampled during the Monte Carlo analysis. Sampling from the broadest distributions results in the broadest H* distribution and the largest values of H* corresponding to the desired probabilistic goal, in this case, 95/50.

Figure RAI10-1 shows the results of the Monte Carlo sampling from the interaction surface (see RAI#20) for the resulting values of H* between the upper 93% and 98% of the simulations. (The 98% upper limit was chosen for convenience). The highest values

of H^* are concentrated in a well defined region bounded approximately by the tube coefficient of thermal expansion (α_T) between []^{a,c,e} and tubesheet coefficient of thermal expansion (α_{TS}) between []^{a,c,e}. The conclusion that the maximum values of H^* are produced from samples in approximately the center of the interaction surface defined by Figure 8-5 in the report applies to both the Model F and Model D5 SGs. Consequently, the use of the broadest distributions that increase the value of H^* will tend to focus on the region in question because the broadest H^* distributions are defined by negative variations of α_T and by positive variations of α_{TS} . Selections from the negative sides of the broadest distributions will not result in maximum values of H^* . If picks are made from both distributions on the negative side of the biased influence distributions, the result will be an over-prediction of the lower tail of the H^* distribution. This is noted in WCAP-17071-P, WCAP-17072-P, WCAP-17091-P and WCAP17092-P and is of no consequence because only the maximum value of H^* is of concern.

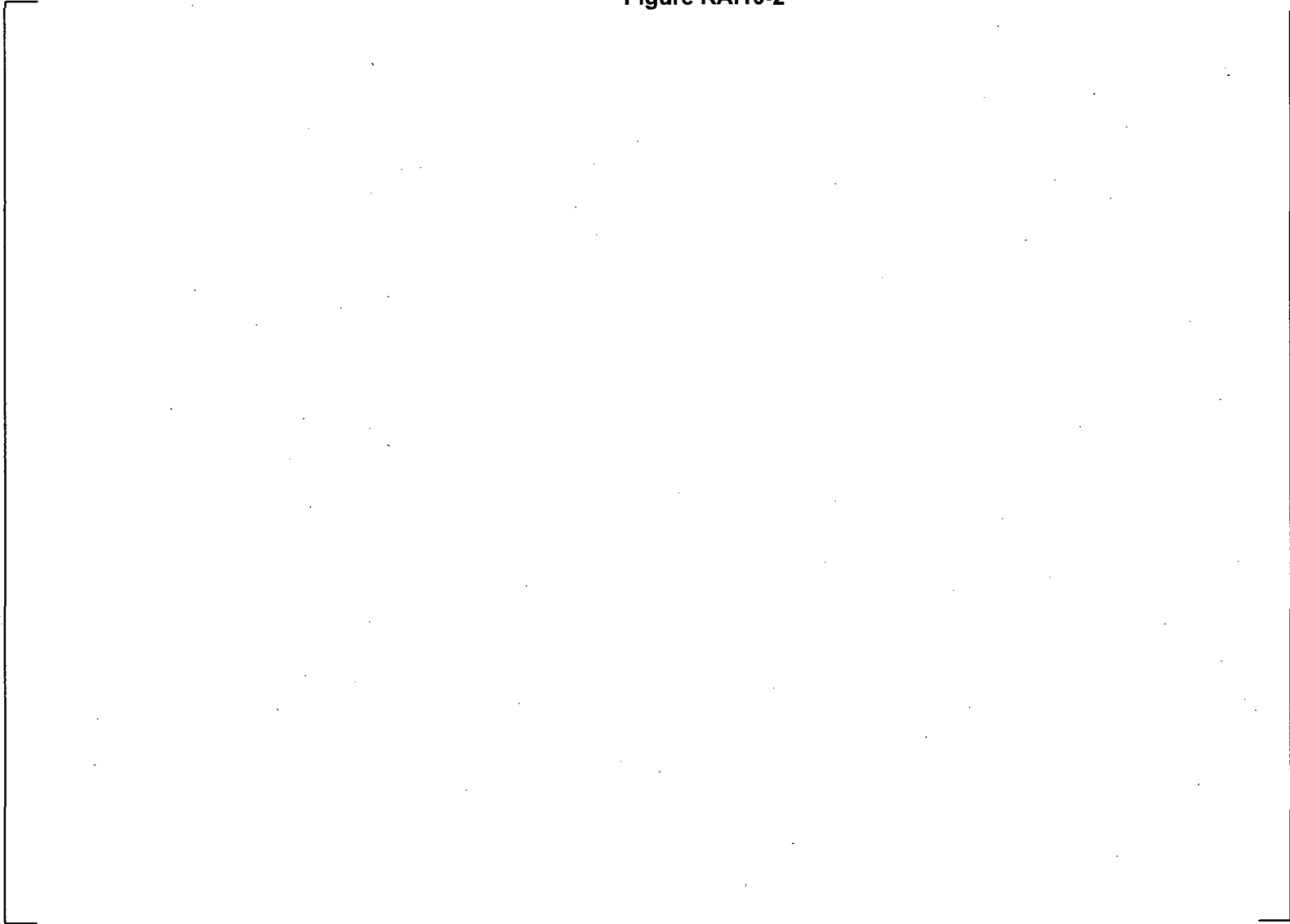
Figure RAI10-1

a,c,e



Figure RA110-2

a,c,e



RAI	Vogtle	11. Reference 1, page 8-14, Figure 8-6: The legend for one of the interactions shown between α_{TS} and E_{TS} appears to have a typo in it, please review and verify that all values shown in the legend are correct.
	WCGS	12. Reference 1, page 8-14, Figure 8-6: The legend for one of the interactions shown between the coefficient of thermal expansion of the tube (α_{TS}) and tubesheet (E_{TS}) appears to contain typographical error. Please review and verify that all values shown in the legend are correct.
	B/B	12. Reference 1, Page 8-14, Figure 8-6: The legend for one of the interactions shown between α_{TS} and E_{TS} appears to have a typo in it. Please review and verify that all values shown in the legend are correct.
	CPSES	12. Reference 1, page 8-14, Figure 8-6: The legend for one of the interactions shown between the coefficient of thermal expansion of the tubesheet (α_{TS}) and Young's modulus of the tubesheet (E_{TS}) appears to contain a typographical error. Please review and verify that all values shown in the legend are correct.
	Seabrook	12. Reference 1, Page 8-14, Figure 8-6: The legend for one of the interactions shown between α_{TS} and E_{TS} appears to have a typo in it, please review and verify that all values shown in the legend are correct.

Response:

The uppermost curve, defined by the star point, which is currently labeled as $a_{TS}=-3$ should be labeled as $a_{TS}=+3$. All other values in the legend are correct.

RAI	Vogtle	12. Reference 1, page 8-20, Case S-4: Why does the assumption of a 2-sigma value for the coefficient of thermal expansion of the tube (αT) and the tubesheet (αTS) to determine a "very conservative biased mean value of H^* " conservatively bound the interaction effects between αT and αTS ? Describe the specifics of how the "very conservative biased mean value of H^* ," as shown in Table 8-4, was determined.
	WCGS	13. Reference 1, page 8-20, Case S-4: Why does the assumption of a 2-sigma value for the coefficient of thermal expansion of the tube (αT) and the tubesheet (αTS) to determine a "very conservative biased mean value of H^* " conservatively bound the interaction effects between αT and αTS ? Please describe the specifics of how the "very conservative biased mean value of H^* ," as shown in Table 8-4, was determined.
	B/B	13. Reference 1, Page 8-20, Case S-4: Why does the assumption of a 2-sigma value for the coefficient of thermal expansion of the tube (α_T) and the tubesheet (α_{TS}) to determine a "very conservative biased mean value of H^* " conservatively bound the interaction effects between α_T and α_{TS} ? Describe the specifics of how the "very conservative biased mean value of H^* ," as shown in Table 8-4, was determined.
	CPSES	13. Reference 1, page 8-20, Case S-4: Why does the assumption of a 2-sigma value for the coefficient of thermal expansion of the tube (αT) and tubesheet (αTS) to determine a "very conservative biased mean value of H^* " conservatively bound the interaction effects between αT and αTS ? Please describe how the "very conservative biased mean value of H^* ," as shown in Table 8-4, was determined.
	Seabrook	13. Reference 1, Page 8-20, Case S-4: Why does the assumption of a 2-sigma value for the coefficient of thermal expansion of the tube (αT) and the tubesheet (αTS) to determine a "very conservative biased mean value of H^* " conservatively bound the interaction effects between αT and αTS ? Describe the specifics of how the "very conservative biased mean value of H^* ," as shown in Table 8-4, was determined.

Response:

The very conservative mean value of H^* , []^{a,c,e} inches (Model F), []^{a,c,e} inches, (Model D5), is determined by arbitrarily assuming that the 2-sigma values of all variables defines the mean value of H^* . To determine these values, it was assumed that the input variables to the structural evaluation (i.e, the entire H^* calculation process as shown in

Figure 1-1 of the report) were set at their 2-sigma values, and the resulting H^* was termed the “conservative mean.” Table RAI12-1 illustrates the input values that define the mean value of H^* and the “very conservative mean” value of H^* . The SRSS approach was then applied using the influence factors from Table 8-2 in the report for the 95/50 whole-bundle value appropriate to the model SG being considered. The result is essentially equivalent to the 5-sigma variation case, Case S4 on Table 8-3 of the report. Note that because the 2-sigma input parameter value of H^* was determined by the entire calculation process shown in Figure 1-1 of WCAP, the interaction effects of the variables at the 2-sigma level are included in this calculation.

Table RAI12-1
Definition of “Conservative Mean” H^*

Definition	Analysis Input Parameters and their Values			
	α_T	α_{TS}	E_T	E_{TS}
Mean H^*	mean	mean	mean	mean
Conservative Mean H^*	Mean- $2\sigma^{(1)}$	Mean+ $2\sigma^{(1)}$	Mean- $2\sigma^{(1)}$	Mean- $2\sigma^{(1)}$
(1) Values chosen in direction of increasing H^*				

RAI	Vogtle	13. Reference 1, page 8-22, Case M-5: The description for this case seems to correspond to a single tube H* estimate rather than a whole bundle H* estimate. How is the analysis performed for a whole bundle H* estimate?
	WCGS	14. Reference 1, page 8-22, Case M-5: The description for this case seems to correspond to a single tube H* estimate rather than a whole bundle H* estimate. Please explain how is the analysis performed for a whole bundle H* estimate?
	B/B	14. Reference 1, Page 8-22, Case M-5: The description for this case seems to correspond to a single tube H* estimate rather than a whole bundle H* estimate. How is the analysis performed for a whole bundle H* estimate?
	CPSES	14. Reference 1, page 8-22, Case M-5: The description for this case seems to correspond to a single tube H* estimate rather than a whole bundle H* estimate. Please explain how the analysis is performed for a whole bundle H* estimate?
	Seabrook	14. Reference 1, Page 8-22, Case M-5: The description for this case seems to correspond to a single tube H* estimate rather than a whole bundle H* estimate. How is the analysis performed a whole bundle H* estimate?

Response:

Case M-5 is the Monte Carlo (MC) sampling analogy to Case S-2. A single tube analysis would sample from the 1σ influence distributions to determine the overall distribution of H*, and from the resulting H* distribution, choose the 95% probability value of the upper tail. Case M-5 pre-biases the influence factor distributions by choosing the influence factor distributions at the 4.285σ (Model F) (4.237σ Model D5) values divided by 4.285 (Model F) (4.237 , Model D5). Thus, the input distributions are pseudo- 1σ distributions that are already biased by the number of standard deviations required to represent a whole bundle analysis as was done in Case S-2. The use of the greater value influence functions results in a broader final H* distribution from which the 95/50 value represents the whole bundle. The basis for the 4.285σ (Model F) (4.237σ , Model D5) value to represent the whole bundle case is discussed in the report.

It was recognized that the assumption of normality of the influence factor distribution could influence the results from the MC approach included in the report. Nevertheless, the MC cases were included in the report to provide a basis for evaluating multiple variability cases that could not be considered using the SRSS approach. The response to RAI#20 provides a comprehensive analysis based on the interaction surface of Figure 8-5 and utilization of the Monte Carlo technique.

RAI	Vogtle	14. Reference 1, page 8-2: Case M-5 states, "Interaction effects are included because the 4.285 sigma variations were used that already include the effective interactions among the variables." Case M-5 also states that the 4.285 sigma variations come from Table 8-2. However, Table 8-2 does not appear to include interactions among the variables. Explain how the 4.285 sigma variations include the effect of interactions among the variables.
	WCGS	15. Reference 1, page 8-22: Case M-5 states, "Interaction effects are included because the 4.285 sigma variations were used that already include the effective interactions among the variables." Case M-5 also states that the 4.285 sigma variations come from Table 8-2; however, Table 8-2 does not appear to include interactions among the variables. Please explain how the 4.285 sigma variations include the effect of interactions among the variables.
	B/B	15. Reference 1, Page 8-22: Case M-5 states, "Interaction effects are included because the 4.237 sigma variations were used that already include the effective interactions among the variables." Case M-5 also states that the 4.237 sigma variations come from Table 8-2. However, Table 8-2 does not appear to include interactions among the variables. Explain how the 4.237 sigma variations include the effect of interactions among the variables.
	CPSES	15. Reference 1, page 8-22: Case M-5 states, "Interaction effects are included because the 4.237 sigma variations were used that already include the effective interactions among the variables." Case M-5 also states that the 4.237 sigma variations come from Table 8-2; however, Table 8-2 does not appear to include interactions among the variables. Please explain how the 4.237 sigma variations include the effect of interactions among the variables.
	Seabrook	15. Reference 1, Page 8-22: Case M-5 state,: "Interaction effects are included because the 4.285 sigma variations were used that already include the effective interactions among the variables." Case M-5 also states that the 4.285 sigma variations come from Table 8-2. However, Table 8-2 does not appear to include interactions among the variables. Explain how the 4.285 sigma variations include the effect of interactions among the variables.

Response:

Because the 4.285 σ (Model F), 4.237 σ (Model D5) variations were calculated using the complete calculation process depicted in Figure 1-1 of the report (WCAP-17071-P, WCAP-17072-P), the variations include the structural interaction effects for each variable assuming that all other variables are at their mean value. If multiple variables were

perturbed simultaneously, a greater effect on H* would be expected. The Monte Carlo sampling scheme used did not support the use of compound parameter variations.

The response to RAI#20 provides an in-depth analysis of the interaction effects among the significant variables using the Monte Carlo method and sampling from the interaction surface of Figure 8-5.

RAI	Vogtle	15. Reference 1, page 8-22, Case M-6, first bullet: Should the words "divided by 4.285" appear at the end of the sentence?
	WCGS	16. Reference 1, page 8-22, Case M-6, first bullet: Please verify if the words "divided by 4.285" appear at the end of the sentence.
	B/B	16. Reference 1, Page 8-22, Case M-6, first bullet: Should the words "divided by 4.237" appear at the end of the sentence?
	CPSES	16. Reference 1, page 8-22, Case M-6, first bullet: Please verify if the words "divided by 4.237" should appear at the end of the sentence?
	Seabrook	16. Reference 1, Page 8-22, Case M-6, first bullet: Should the words "divided by 4.285" appear at the end of the sentence?

Response:

The first bullet under Case M-6 on page 8-22 is clarified by adding the phrase "divided by 4.285" (Model F) ("4.237"-Model D5) between "4.285 σ " (Model F) ("4.237 σ "-Model D5) and "from."

RAI	Vogtle	16. Reference 1, page 8-23, Case M-7: Was the "2 sigma variation of all variables" divided by a factor of 2?
	WCGS	17. Reference 1, page 8-23, Case M-7: Please verify if the "2 sigma variation of all variables" divided by a factor of 2.
	B/B	17. Reference 1, Page 8-23, Case M-7: Was the "2 sigma variation of all variables" divided by a factor of 2?
	CPSES	17. Reference 1, page 8-23, Case M-7: Please verify if the "2 sigma variation of all variables" was divided by a factor of 2.
	Seabrook	17. Reference 1, Page 8-23, Case M-7: Was the "2 sigma variation of all variables" divided by a factor of 2?

Response:

For case M-7, the 2-sigma variation was treated as if it were 1-sigma variation. This assumption is somewhat arbitrary and intended only as a hypothetical case to show the effect on H* if it were assumed that the calculated standard deviation are much larger. Therefore, the 2-sigma variation was NOT divided by 2.

This case is an arbitrary sensitivity study that addresses the H* result if the 1σ influence factors were more than doubled. Starting from the basic mean structural prediction of H*, []^{a,c,e} for the Model F ([]^{a,c,e}, for the Model D5) inches, it was assumed that the 2σ influence distributions applied instead of the 1σ influence distributions, and the MC sampling was from the 2σ distributions. The principal objective of this case was to show that very conservative assumptions do not lead to a major impact on the value of H*.

RAI	Vogtle	17. Reference 1, page 8-23, Case M-7: Explain how this case includes the interaction effects between the two principle variables, α_T and α_{TS} .
	WCGS	18. Reference 1, page 8-23, Case M-7: Please explain how this case includes the interaction effects between the two principle variables, α_T and α_{TS} .
	B/B	18. Reference 1, Page 8-23, Case M-7: Explain how this case includes the interaction effects between the two principle variables, α_T and α_{TS} .
	CPSSES	18. Reference 1, page 8-23, Case M-7: Please explain how this case includes the interaction effects between the two principal variables, α_T and α_{TS} .
	Seabrook	18. Reference 1, Page 8-23, Case M-7: Explain how this case includes the interaction effects between the two principle variables, α_T and α_{TS} .

Response:

Case M-7 assumes that the 1σ variability of H^* in the parameters is based on the 2σ influence factors calculated for each parameters. Because the influence factors are calculated using the entire calculation flow depicted in Figure 1-1 of the report, the interactive effect of the key parameters at the 2σ is reflected. The calculations were performed by perturbing one parameter at a time; therefore, the combined interaction of perturbing multiple parameters is not reflected. However, the assumption that the 2σ variation in the direction of increasing H^* represent one standard deviation of the H^* influence factors and the extreme value calculation process provide a very conservative estimate of H^* .

The response to RAI#20 provides an in-depth analysis of the interaction effects among the significant variables.

RAI	Vogle	18. Reference 1, page 8-25, Table 8-4: Explain why the mean H* calculated in the fifth case does not require the same adjustments, as noted by the footnotes, that all other cases in the table require.
	WCGS	19. Reference 1, page 8-25, Table 8-4: Please explain why the mean H* calculated in the fifth case does not require the same adjustments, as noted by the footnotes, that all other cases in the table require.
	B/B	19. Reference 1, Page 8-25, Table 8-4: Explain why the mean H* calculated in the fifth case does not require the same adjustments, as noted by the footnotes, that all other cases in the table require.
	CPSES	19. Reference 1, page 8-25. Table 8-4: Please explain why the mean H* calculated in the fifth case does not require the same adjustments, as noted by the footnotes, that all other cases in the table require.
	Seabrook	19. Reference 1, Page 8-25, Table 8-4: Explain why the mean H* calculated in the fifth case does not require the same adjustments, as noted by the footnotes, that all other cases in the table require.

Response:

The superscripts referring to the notes were inadvertently omitted from the mean H* value for Case S-4 in Table 8-4. The mean value of H* shown, []^{a,c,e} inches (Model F) ([]^{a,c,e} inches, Model D5), includes the adjustment for BET and for the NOP thermal distribution.

This omission exists also in WCAP-17072-P for the Model D5 SGs, but has been corrected on subsequent H* reports for the Model 44F and 51F SGs (WCAP-17091-P and WCAP17092-P).

RAI	Vogtle	19. Reference 1, page 8-25, Table 8-4: Verify the mean H^* shown in the last case in the table.
	WCGS	20. Reference 1, page 8-25, Table 8-4: Please verify the mean H^* shown in the last case in the table.
	B/B	20. Reference 1, Page 8-25, Table 8-4: Verify the mean H^* shown in the last case in the table.
	CPSES	20. Reference 1, page 8-25, Table 8-4: Please verify the mean H^* shown in the last case in the table.
	Seabrook	20. Reference 1, Page 8-25, Table 8-4: Verify the mean H^* shown in the last case in the table

Response:

(Please also see the response to Question 16.)

The mean value of H^* for Case M7 is correct as shown on Table 8-4.

The purpose of this case was to determine the whole bundle, extreme value of H^* and to show the effect on H^* if the uncertainties were doubled at the same time as discussed in the response to Question 16. The process to achieve this was to calculate the mean H^* as for all other cases, except case S4, on Table 8-4, but then to arbitrarily assume that the 2σ variations as the values for the 1σ influence distributions of H^* . The intent of this case was to show that extreme assumptions of variability do not invalidate the H^* concept.

RAI	Vogtle	20. Section 8 of Reference 1: The variability of H^* with all relevant parameters is shown in Figure 8-3. The interaction between α_T and α_{TS} are shown in Figure 8-5. Please explain why the direct relationships shown in these two figures were not sampled directly in the Monte Carlo analysis, instead of the sampling method that was chosen. Also, please explain why the sampling method chosen led to a more conservative analysis than directly sampling the relationships in Figures 8-3 and 8-5.
	WCGS	21. Section 8 of Reference 1: The variability of H^* with all relevant parameters is shown in Figure 8-3. The interaction between α_T and α_{TS} are shown in Figure 8-5. Please explain why the direct relationships shown in these two figures were not sampled directly in the Monte Carlo analysis, instead of the sampling method that was chosen. Also, please explain why the sampling method chosen led to a more conservative analysis than directly sampling the relationships in Figures 8-3 and 8-5.
	B/B	21. Section 8 of Reference 1: The variability of H^* with all relevant parameters is shown in Figure 8-3. The interaction between α_T and α_{TS} are shown in Figure 8-5. Please explain why the direct relationships shown in these two figures were not sampled directly in the Monte Carlo analysis, instead of the sampling method that was chosen. Also, please explain why the sampling method chosen led to a more conservative analysis than directly sampling the relationships in Figures 8-3 and 8-5.
	CPSES	21. Section 8 of Reference 1: The variability of H^* with all relevant parameters is shown in Figure 8-3. The interaction between α_T and α_{TS} are shown in Figure 8-5. Please explain why the direct relationships shown in these two figures were not sampled directly in the Monte Carlo analysis, instead of the sampling method that was chosen. Also, please explain why the sampling method chosen led to a more conservative analysis than directly sampling the relationships in Figures 8-3 and 8-5.
	Seabrook	21. Section 8 of Reference 1: The variability of H^* with all relevant parameters is shown in Figure 8-3. The interaction between α_T and α_{TS} are shown in Figure 8-5. Please explain why the direct relationships shown in these two figures were not sampled directly in the Monte Carlo analysis, instead of the sampling method that was chosen. Also, please explain why the sampling method chosen led to a more conservative analysis than directly sampling the relationships in Figures 8-3 and 8-5.

Response:

General

The recommended value of H^* is based on the square root of the sum of the squares (SRSS) approach to combining the uncertainties for H^* . The Monte Carlo cases included in the report were included as a vehicle to study different sensitivities to H^* parameters variations and were provided as support for the SRSS recommendation. The peer review (Expert Panel's) conclusions were that the SRSS approach was a suitably conservative approach given the many conservatisms built into the H^* analysis. The significant conservatisms included in the H^* analysis are summarized in Section 1 of the report(s) and again identified in Section 10 of the report(s).

Figures 8-3 and 8-5 were developed during, and immediately after, the peer review of the H^* project, which was followed in close order by publishing the report. The staff's observation that Figures 8-3 and 8-5 reasonably define an interaction surface, which could be utilized directly for a Monte Carlo sampling assessment, is correct. Therefore, a Monte Carlo analysis based on the interaction surface defined by Figure 8-4 in the respective WCAP reports for the different models of SGs was completed. This analysis provided the opportunity to quantify some of the conservatisms that are included in the technical justification of H^* . The approach to this issue was to consider the most significant conservatisms in the overall H^* analysis and quantify their effects on the recommended value of H^* to show that the recommended value of H^* is conservative. The sequence of the analysis was as follows:

1. Application of the Monte Carlo methodology discussed in the H^* reports, except for case M-6, assumes that each simulation of H^* includes a different value of the properties of the tubesheet. Thus, if 100,000 simulations are performed, each simulation includes a different random pick of tubesheet properties. Among the population of H^* candidate plants, there are 60 steam generators; therefore, the actual population of tubesheets is limited to 60. To better address the limited population of tubesheets, the reference MC sampling is a staged process corresponding to the simulation of one steam generator tubesheet/tube bundle combination. A set of tubesheet properties is selected, and for that set, the corresponding tube properties are sampled 5626 times for the Model F SG tube population (4570 times for the model D5 SG tube population), and as appropriate for the other models of SGs. The above process is repeated 10,000 times. This provides a more accurate simulation reflecting the limited number of tubesheets in the population.
2. The probabilistic analysis in Section 8 of the report(s) assumes that the entire tube bundle consists of tubes located at the worst case location in the tube bundle (e.g., the most limiting radius in the most limiting sector of the tube bundle as shown in Section 6.2.3). As shown in Figure 6-1 of the report, the worst tube is defined by a very narrow segment of tubes, while all other tubes are shown to have a lower value

of H^* . Therefore, the bundle was divided into a number of sectors as discussed below, and the 0.95 probability at 50% confidence value of H^* was defined on the combined probability of the sector probability for all tubes. This analysis is still quite conservative because all tubes are still assumed to be in the limiting azimuthal sector of the tube bundle (the sector perpendicular to the divider plate including about 5° from the centerline of the tubesheet. See Section 6.2.3 of the report). Tubes more than about 5 pitches removed from the centerline perpendicular to the divider plate have been shown to have lower values of H^* .

3. The current analysis for the Model F and Model D5 SGs includes a correction factor for the NOP thermal distribution through the tubesheet. The factor was developed very conservatively using a ratio technique (see report Section 6.2.2.2.5). This correction factor was re-evaluated (see the response to RAI#2) and a more realistic value of it is applied in this analysis. The correction factor does not apply equally to all models of SG; therefore, the effect of the correction factor is SG model-specific and has already been included in the reports for the Model 44F and Model 51F SGs (WCAP-17091-P and WCAP-17092-P). The analysis results below identify the SG models where this improved analysis applies.
4. The H^* analysis assumes no contribution from residual contact pressure (RCP). All test data to date, including data from tests performed prior to 2008, has shown that a positive value of RCP exists after hydraulic expansion of the tubes. Tests were performed during the current H^* program that confirmed a significant level of RCP, and also showed that within a short distance of motion, the forces required to continue to move the tube by far exceeded the maximum pull out forces that could be generated under very conservative assumptions. The analysis quantifies the effect of RCP on the calculated value of H^* and benchmarks the RCP to the tests that were performed during the H^* development.

A. Sector Analysis

Based on the profile of the predicted mean H^* , the tube bundle is divided into 9 annular sectors as shown in Figures RAI20-1, -2, -3 and -4 for the models of SG included in the H^* population (Reference RAI20-1). (In Figure RAI20-4, for the Model 51F SGs, the appropriate sector division results in only 7 sectors; however, additional sectors with 1 tube, each, were added at both ends for convenience of the calculations.) The normalized H^* is determined from the raw H^* calculation results, prior to adjustment of the H^* value by the addition of correction factors for the BET and NOP tubesheet thermal profile. This is done to obtain a true normalization, unaffected by any constants. However, the final value of H^* , after the MC sampling for ΔH , is based on the adjusted maximum mean value of H^* as shown in the appropriate sector in Tables 1, 2, 3 and 4. The adjustment for crevice pressure referenced to the predicted H^* is made after the all other factors have been accounted for. Thus, for each sector:

[a,c,e]

Where,

F is the sector normalization factor from Figures RAI20-1, -2, -3 and -4,

$H^*_{(BET+Tnop)}$ is the raw H^* value adjusted for BET and NOP thermal distribution

ΔH^*_{uncert} is the adjustment for interaction effects from the MC analysis

ΔH^*_{pcrev} is the adjustment for crevice pressure

The normalized value of H^* in each sector is based on the maximum value of H^* in that sector; thus, the sector evaluation is inherently conservative.

The number of tubes in each sector is determined from the row and column numbers and the model-specific pitch of the tubes. Tables RAI20-1, -2, -3, and -4 summarize the sector populations for each of the models of SGs.

B. Interaction Surface and Monte Carlo Sampling

A simulation model was developed to evaluate limiting values of H^* for specific classes of steam generators. The Monte-Carlo based model evaluates extreme values of H^* on a single steam generator basis, repeating the process to construct a distribution of maximum H^* values. The final output of the model is the 95/50 estimate of extreme H^* within any one steam generator.

The components of variance included in the model are the coefficients of thermal expansion (CTE's) for the tubesheet and the individual tubes. These have been shown in the H^* reports to be, by far, the most significant contributors to variations in H^* for the tubesheet/tube bundle combinations. The essential function describing H^* variation for specific value pairs of the thermal expansion coefficients has been developed and is shown in Figure 8.5 of the H^* reports. It should be noted that full interaction effects are included.

The basic structure of the simulation is shown in Figure RAI20-5 and represents one Monte Carlo trial. The process shown produces one realization of the extreme H^* for a given steam generator. Repetition, involving 10,000 trials produces a distribution from which a 95/50 estimate of H^* can be obtained by robust nonparametric means. As shown in Figure RAI20-5, the core process involves a random selection of one value of tubesheet CTE and N values of tube CTE, where N is the number of tubes in the steam generator or specific region of interest. The resulting N pairs are propagated through the

fitted surface to produce N values of H* which are then sorted to identify the maximum (extreme) value of H* which is stored for further use.

The above process can be easily applied on a regional (SG sector) basis by running the simulation for each region separately based on region-specific values on tube population size and average H*. The composite H* for the entire steam generator can be obtained by the following equation:

$$H^*_c = [\dots]^{a,c,e} \text{ for M Region model}$$

It is most important that the H* values for the individual regions are not sorted prior to application of the above post-processing because of the need to maintain tubesheet identity between regions.

C. Sector Application of Interaction Effects

The interaction data shown in Figure 8-5 of the H* WCAPs were developed for the limiting tube radius (i.e., the tubesheet radius in Figures 1, 2, 3 and 4) where the normalized value of H* is 1. Because of the complex nature of the H* analysis, it was necessary to determine if the interaction effects at the limiting H* radius adequately represented the interactions at other tubesheet radii. Two radii were selected to represent the most probable locations where significant effects, if they exist, might materialize: 1) A tubesheet sector near the limiting radius, and 2) A tubesheet sector far removed from the limiting radius.

It was shown in the reports that the influence of Young's modulus on the final values of H* is negligible and that there was no significant interaction between the Young's moduli of the materials and the coefficient of thermal expansion of the materials. The existing interactions are limited to the coefficients of thermal expansion of the tube and tubesheet materials. Therefore, the same matrix of sensitivity cases that defined Figure 8-5 in the reports was run for each of the two tubesheet sector chosen as noted above.

In all cases it was determined that the interaction effects defined in Figure 8-5 of the report(s) for the location of the maximum mean H* value bounded the interaction effects of the other sectors considered. Therefore, for conservatism and simplicity, the range of interaction effects (i.e., $\Delta H^* = f(\alpha_T, \alpha_{TS})$) for the maximum mean value of H* shown on Figure 8-5 was applied for all sectors of the tubesheet.

Figures RAI20-6 and RAI20-7 show the results of this evaluation for the tubesheet sectors selected for the Model F and Model D5 SGs. The interaction profile for the mean, 3σ and 5σ variation of tubesheet coefficient of thermal expansion are shown to cover the significant range of variability. In all cases, the variability of the location of the maximum value of H* is greater than, or equal to, the variability at other radial locations on the tubesheet. Therefore, the application of the variability for the radial location of the maximum value of H* for all other radial locations is justified and conservative.

D. Results from Sector Based Sampling from the Interaction Surfaces

Table RAI20-5 (a) summarizes the recommended values of H^* from the H^* reports for all of the affected Model SGs together with the results of the Monte Carlo (MC) sampling from the interaction surface defined in Figure 8-5 of each report. The MC sampling was based on the sector approach described above and also the approach shown in Figure RAI20-5 to limit the number of tubesheet simulation. The result from this sampling must be adjusted for the crevice pressure distribution referenced to the location of the initially predicted value of H^* . The correction for crevice pressure is taken from Figure 8-1 of the respective reports. After the adjustments are made for the crevice pressure reference location, the values of H^* are slightly greater than the recommended values of H^* from the respective reports.

Table RAI20-5(b) extends the evaluation of the conservatism of the recommended SRSS-based values of H^* by adjusting the Monte Carlo sampling results for the updated values of the adder for the NOP thermal distribution in the tubesheet for the Model F and Model D5 SGs. The updated NOP thermal distribution factor for the Model 44F and Model 51F SGs are already included in the respective reports (WCAP-17091-P and WCAP-17092-P); consequently there is no adjustment made for these models of SG.

The original NOP thermal distribution adjustment factor was developed on a very conservative basis, using the scaling method described in Section 6.2.2.2.5 of WCAP-17071-P and WCAP-17072-P. As the analysis for H^* evolved, a direct method of applying the tubesheet NOP thermal distribution in the structural analysis was developed; this method is describe in Section 6.2.2.2.5 of WCAP-17072-P (Model D5 report). For the Model D5 SG, the necessary correction based on the updated method was []^{a,c,e} inch compared to []^{a,c,e} inch based on the scaling technique. A similar analysis was subsequently performed for the Model F SG and it was determined that the appropriate correction for the NOP thermal distribution is []^{a,c,e} inch instead of the []^{a,c,e} inches included in the recommended value of H^* in WCAP-17071-P.

When the updated correction for the NOP thermal distributions are applied, and the necessary correction for crevice pressure reference location is applied, the final value of H^* for the Model F SG is []^{a,c,e} inches and, for the Model D5, is []^{a,c,e} inches (see Table RAI20-5(b)). Both of these values are less than the recommended values of H^* , respectively, for the Model F and Model D5 SGs. Thus, it is concluded that the recommended values of H^* , based on the SRSS approach as shown in the respective reports for the Model F and Model D5 SGs, are conservative.

It should be noted that the adjustment of the NOP thermal distribution correction factor does not impact which operating condition, NOP or SLB, is the limiting condition. The limiting value of H^* is determined by three times normal operating pressure before and after the adjustment for the NOP thermal distribution. Section 6.4.5 of the Model F report, WCAP-17071-P, and the Model D5 report, WCAP-17072-P, discusses the determination of the H^* values. When the NOP thermal distribution is directly included in

the structural analysis to determine tubesheet displacements, the NOP condition remains the limiting condition for H^* .

E. Determination of Residual Contact Loads from Pull Out Tests

In prior analyses for H^* , pull out test data has been used to calculate a residual contact pressure, which is distributed over the length of the tubesheet and included in the integration of pull out force over length to determine the length at which the pull out and resisting forces are equal. However, the pull out resistance can also be used to offset the pull out forces. Both methods were studied and it was determined that the same result was achieved, regardless of which method was applied. Because offsetting the applied loads requires fewer assumption (i.e., coefficient of friction) and results in more conservative values of H^* , this approach was selected to determine the effect of the hydraulic expansion only on the calculated value of H^* .

Reference RAI20-2, provided as Appendix A to this document, summarizes the pull out test program performed in support of the H^* development. The data from the pull out tests and Monte Carlo simulation were used to determine a conservative value of end cap load reduction. As in prior pull out tests, there was considerable scatter in the pull test data. The highest pull force recorded at 0.25 inch cross head displacement was []^{a,c,e} lbf, and the lowest pull force recorded at 0.25 inch cross head displacement was []^{a,c,e} lbf. Monte Carlo simulation was then used to determine a 5/50 value (i.e., the lower 95% bound) of the pull test data.

The Monte Carlo simulations used the pull test data to establish means and standard deviations for the pull forces that were observed. Two sets of data for each of three tube diameters (0.688 inch, 0.750 inch, and 0.875 inch) were provided: One considered the 13 in. expansion lengths only and the other considered all expansion lengths (13, 15 and 17 inches) combined. Seven distributions were used: 1) A truncated (at 0) normal distribution, 2) a lognormal distribution, 3) an Erlang distribution, 4) a Gamma distribution, 5) an inverse Gaussian distribution, 6) a Pearson Type V distribution, and 7) a Weibull distribution. All except the truncated normal were chosen because their domains range from 0 to + infinity, their domains are continuous, and their fitting parameters for the means and standard deviations used were within their allowable values. One hundred thousand iterations were run for each simulation, and the 5/50 values of pull force recorded for each distribution. The most conservative result, []^{a,c,e} lbf, came from the simulation that used the Weibull distribution, and this number is very consistent with the lowest observed pull test datum. Note that the Weibull distribution is widely recommended to model distributions in lieu of a truncated normal distribution. The figure below illustrates the results of the Monte Carlo sampling based on the Weibull distribution of the test data. Complete details of the above analysis can be found in Reference RAI20-2.

The recommended end cap load reduction is []^{a,c,e} lbf.



(Figure corresponding to the Monte Carlo simulation using a Weibull distribution for the Model F SG data, using the 13 inch expansion length only. The 5/50 value of pull force is []^{a,c,e} lbf.)

F. Application of Residual Contact Load

The H* results in Figure 8-5 of WCAP-17071-P, WCAP-17072-P, WCAP-17091-P and WCAP-17092-P show that H* is sensitive to the variations in the coefficient of thermal expansion (CTE) of the tube (α_T) and the tubesheet (α_{TS}). The reports also show that H* is not significantly sensitive to variations in the Young's modulus (E) of the tube or the tubesheet. The results in Figure 8-5 in WCAP-17071-P, WCAP-17072-P, WCAP-17091-P and WCAP-17092-P also demonstrate that the worst case trend in the variation of the thermal expansion coefficients is when the α_T is decreasing and α_{TS} is increasing. In other words, H* increases the most when the coefficients of thermal expansion are varied to reduce the contact pressure between the tube and the tubesheet due to thermal growth.

It is possible to reduce the order of the problem (i.e., reduce the number of dimensions involved in the sensitivity study) given the knowledge of which values and directions of variation in CTE are most important to the problem. Figures RAI10-1 and RAI10-2 show the combinations of α_T and α_{TS} that are most likely to produce a worst case H* value. The values of CTE standard deviations for both the tube and tubesheet are combined into an effective variable using the following relationship:

$$\alpha_{srss} = \sqrt{(-\sigma_{\alpha T})^2 + (\sigma_{\alpha TS})^2}$$

The possible variation in sign of either CTE standard deviations is not included in this equation because the only values of interest occur when the tube CTE variation is negative relative to the mean and the tubesheet CTE variation is positive relative to the mean. This reduced form of variation in CTE is then used to compare the change in H^* due to the application of residual pre-load between the tube and the tubesheet due to the installation and hydraulic expansion of the tube.

There are multiple ways to achieve the same value of α_{srss} . For example, a TS CTE variation of $+5\sigma$ about the mean and a tube CTE variation of -5σ about the mean are each equal to a combined α of 5 (assuming only one is non-zero). Likewise, a combination of tube and TS CTE variations of $-3/+4$ and $-4/+3$ will also yield an α of 5. However, the net change in H^* with respect to the material properties are very similar for a single value of α_{srss} regardless of values of its component parts. In cases where there are multiple possibilities for a unique value of α_{srss} , the combination of TS and tube CTE that produced the smallest reduction in H^* was used. Figure RAI20-8 shows the multiple curves that were used to create the surface seen in RAI20-9.

Hydraulic expansion of the tube into contact with the tubesheet tube bore introduces a pre-load that must be overcome before the tube can translate within the tubesheet tube bore. This means that in addition to the pull out resistance that a tube develops due to internal pressure, thermal growth, etc., the pull out resistance of the tube due to the hydraulic expansion must also be overcome in order for the tube to freely translate within the tube bore. However, the hydraulic expansion process has only a small effect on the development of contact pressure between the tube and the tubesheet compared to that developed due to operating pressure and temperature. Therefore, the installation effect, termed residual contact load (RCL), is included as a reduction of the applied end cap load. Recall that the end cap loads are based on the mean $+2\sigma$ tubesheet bore diameter and are thus very conservative.

The reduction in end cap load, for the i^{th} value of pull out resistance due to installation effects is:

$$P_i = \text{End Cap Load} = n\Delta p \pi r_o^2 - DL - RCL_i$$

Where,

n is the applicable safety factor for the SG operating condition based on the SIPC,

Δp is the primary to secondary pressure differential,

r_o is the outside tube radius,

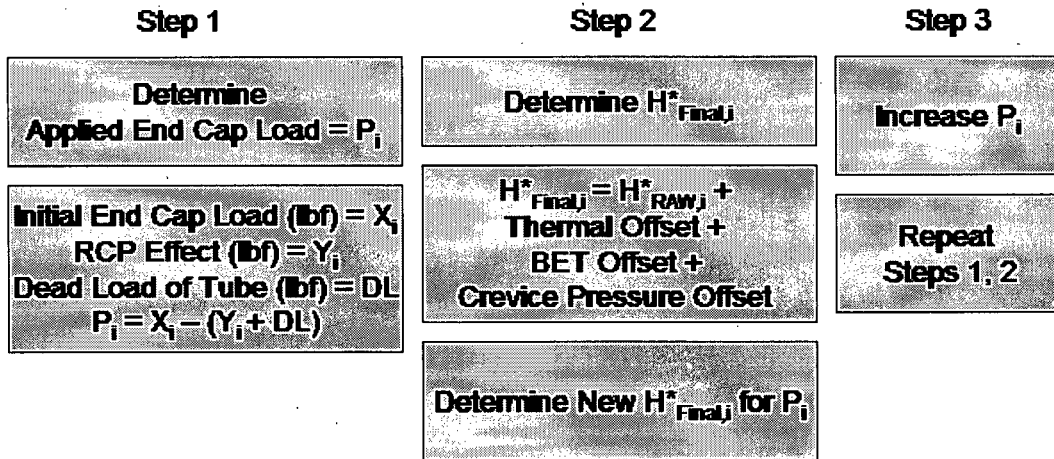
DL is the dead load of the tube straight leg above the top of the tubesheet and RCL is the value of installation pre-load determined from test results.

The minimum pull out force from section F above, []^{a,c,e} lbf, was used. The dead weight of the straight leg portion of the tube above the tubesheet was also included because it also provides a resistance to tube pull out. The dead weight of the straight legs of the tubes varies between []^{a,c,e} and []^{a,c,e} lbs depending on the length of the tube straight leg; an average value of []^{a,c,e} lbs was used.

As an example, for the NOP Low T_{avg} condition at Millstone Unit 3, the end cap load due to the pressure acting on the tube is []^{a,c,e} lbf. Assuming the minimum value of pull out force from the test data and an average dead weight of the tube straight leg, the applied end cap load that must be balanced by the distribution of contact pressure between the tube and the tubesheet is equal to []^{a,c,e} lbf – []^{a,c,e} lbf – []^{a,c,e} lbf, or []^{a,c,e} lbf.

Using the RCL to reduce the end cap load on the tube has been shown to be conservative in a direct comparison with the alternative method, that is, converting the pull out force to a residual contact pressure and including it in the integration for H^* . Further, reduction of the applied load does not affect the contact pressure distribution between the tube and the tubesheet. For instance, if there was a combination of material properties and operating conditions that resulted in a very small or zero value of contact pressure for some portion of the tube below the top of the tubesheet, the application of RCL as a reduction of applied load does not change the predicted contact pressure. The first point of positive contact between the tube and the tubesheet is still determined based on the structural analysis of the tubesheet. An additional benefit from applying the RCL as a reduction to the applied end cap load is that there is no need to develop a distribution of the residual effect of the tube installation as a function of elevation in the tubesheet. The test results can be directly used to determine the pre-load on the tube.

A value of H^* is determined for any value of RCL for the limiting SG operating condition at the limiting TS radius and sector in the bundle. The process for determining the H^* value is shown in the following flow chart.



The result of this process is a surface of the response in H^* to changes in RCL and α_{srss} (the square root of the sum of squares of the specific variations in CTE from one MC simulation). If the values for RCL are normalized to an assumed value, say []^{a,c,e} lbf, and the values of H^* are taken as the change in H^* relative to the value of H^* with an RCL of zero, the result is a non-dimensional surface that can be used in conjunction with a Monte Carlo analysis to determine the reduction in H^* due to the inclusion of RCL. Figure RAI20-9 is a surface plot of the change in the Model F H^* values as a function of RCL and α_{srss} . Figure RAI20-10 is a surface plot of the change in the Model D5 H^* values as a function of RCL and α_{srss} .

Figure RAI20-9 and RAI20-10 illustrate that the effect of including the RCL as a reduction in the applied tube end cap load is dependent on both the H^* value and the material parameters. This is a logical result because if H^* is small (correlated to a small value of α_{srss}) then the effect of RCL should also be small because there is enough contact pressure to maintain equilibrium with the load on the tube regardless of the value of RCL. However, if H^* is large, because of some combination of material parameters or operating conditions that produce less contact pressure between the tube and the tubesheet, then the presence of any value of RCL has a much larger effect on H^* . For example, in Figure RAI20-8, assuming an RCL ratio of 1 (RCL ~ []^{a,c,e} lbf) with an α_{srss} of 0 results in a very small correction to the final H^* distance on the order of []^{a,c,e} inch. However, if the RCL ratio is equal to 1 and α_{srss} is equal to 5, the change in H^* is 2 or more inches, or a factor of 4 greater.

The effects of residual contact pressure (RCP) are implemented in the extreme-value simulation model using a functional representation of the developed steam generator-specific data described above. The function describes the correction term (ΔH^*) in terms of two variables:

$$\Delta H^* = G(\text{RCL}, \text{Alpha})$$

Where:

RCL = Residual contact load

Alpha = Effective thermal expansion coefficient

A typical description of this surface is shown in Figure RAI20-8. As can be seen from the figure, the behavior of the function is somewhat complex. The value of the function generally increases with both independent variables which makes some simplification possible based on a conservatively low estimate of one of the variables.

A lower limit constant value of RCL was chosen, in part to assure a more robust computational behavior in the implementation of the RCL effects modeling. The value cited in the response to part F of this RAI corresponds to a RCL ratio of approximately 1.0. Figure RAI20-11 shows the resulting ΔH^* as a function only of Alpha. This and corresponding functions for each steam generator class, were implemented in the full simulation model.

The actual implementation into the simulation model was straightforward. Since the RCL correction is subtractive, the computation of Alpha and ΔH^* is performed directly after the computation of H^* within the simulation. The computation is performed for all tube/tubesheet combinations in the entire simulation process. The reduction in the computed extreme values of H^* is typically on the order of 1-2 inches, and is steam generator-specific.

It is important to note that the change in H^* due to the crevice pressure adjustment, thermal offset and BET is already included in the analysis. The distribution of the crevice pressure adjustment shown in Figure 8-1 of the H^* reports is not required in this instance. That is because the reduction of the end cap load changes how the H^* value will react to a change in contact pressure distribution. So it is necessary to incorporate the change in H^* due to the RCL reduction of the end cap load with the crevice pressure adjustment to produce a net change in H^* using consistent methods. Therefore, the result of using the RCL surface to determine the change in H^* is the net effect of all adjustments to H^* and no further corrections are required.

Table RAI2-05(c) summarizes the effects of the application of residual pull out load (RCL) on the value of H^* . When the 5/50 pull out force from the test data is applied using the Monte Carlo approach that samples from Figure 8-5 in the reports and also from the RCL correction surface discussed above, the values of H^* are reduced approximately 1 to 2 inches for all affected models of SGs. The resulting values of H^* for the Model F and Model D5 SGs are further reduced by application of the updated NOP temperature distribution correction factor. As can be seen from Table RAI20-5, the recommended values of H^* for the respective SGs in the applicable reports exceeds the values determined when the conservative factors inherent in the recommended values are considered in the analysis.

G. Summary and Conclusions

The recommended values of H^* for the different models of SGs as provided in the respective reports (WCAP-17071-P [Model F], WCAP-17072-P [Model D5], WCAP-17091-P [Model 44F] and WCAP-17092-P [Model 51F]) were based on very conservative assumptions. Additional analysis, using Monte Carlo techniques and the variables interaction surfaces defined in Figure 8.5 of the reports, was performed to quantify the conservatism of these assumption with regard to the recommended values of H^* for the different models of SGs. Four principal conservatisms were evaluated:

1. The number of tubesheets was limited to a number less than the number of tubes in the bundles of the respective SG models. The total population of SGs among the H^* candidate plants is 60 including 4 different models of SGs. The number of tubesheets simulated for each SG was limited to 10,000.
2. Instead of assuming that all tubes in the bundle are located at the single worst case position that defines the recommended value of H^* , the bundles were divided into sectors. This approach retains significant conservatism because the maximum value of H^* in each sector was used for the analysis and the limiting interaction variances were applied to all sectors. It is noted that all sectors considered are located in the limiting azimuthal sector of the tubesheet as discussed in Section 6.2.3 of the reports.
3. The conservative adder for NOP tubesheet thermal distribution was re-evaluated by including the thermal distribution directly in the structural analysis. The resulting adders to H^* are realistic values that reflect the actual response of the tubesheet structure to the applied thermal distribution. This applies only for the Model F and Model D5 SGs because the updated thermal correction factor is already included in the recommended H^* values for the Model 44F and 51F SG. Modification of the thermal distribution factors does not change that the NOP conditions are the limiting conditions that determine the value of H^* .
4. Based on pull out tests performed during the H^* development, the effect of the minimum measured pull out forces at 0.25 inch of tube travel on the values of H^* were evaluated. The pull out force data was applied directly as a reduction of the applied loading instead of utilizing an intermediate conversion of pull out force to contact pressure. This approach is more direct, and its specific application is conservative because the 5/50 value of pull out force was used. In reality, much greater values of pull out force were demonstrated in the tests at 0.25 inch travel. Still greater pull out forces were observed during the tests for greater values of tube travel, even exceeding the limiting applied design loads for H^* . Therefore, the application of the 5/50 value of pull out force from the tests is conservative.

After addressing the above factors, the final values of H^* are significantly less than the values recommended for all affected models of SGs. Therefore, the recommended values of H^* for each of the models of SG are shown to be conservative.

RAI#20 References:

RAI20-1 LTR-SGMP-09-92;"Tubesheet Sector Definition for H* Revised Probabilistic Analysis," July 10, 2009.

RAI20-2 LTR-SGMP-09-98, "H* Pull Test Program Summary," July 27, 2009.

**Figure RAI20-1
Model F**



a,c,e

**Figure RAI20-2
Model D5**



a,c,e

**Figure RAI20-3
Model 44F**

a,c,e



**Figure RAI20-4
Model 51F**

a,c,e

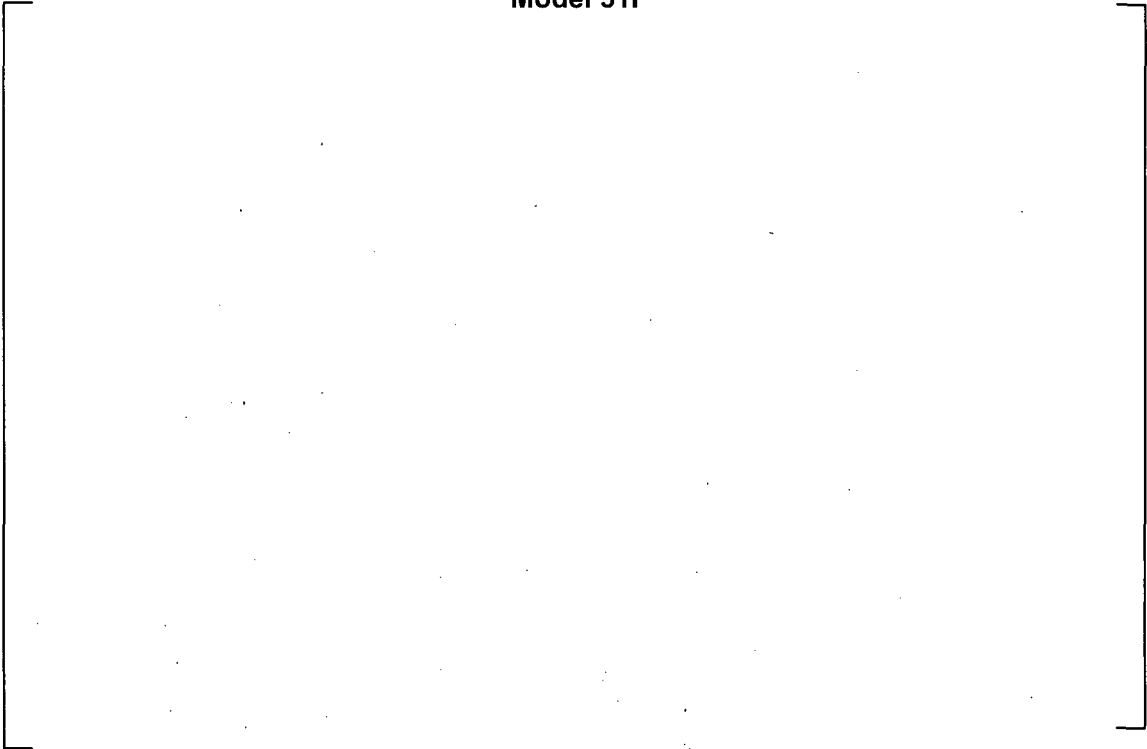


**Figure RAI20-5
Monte Carlo Simulation Process**

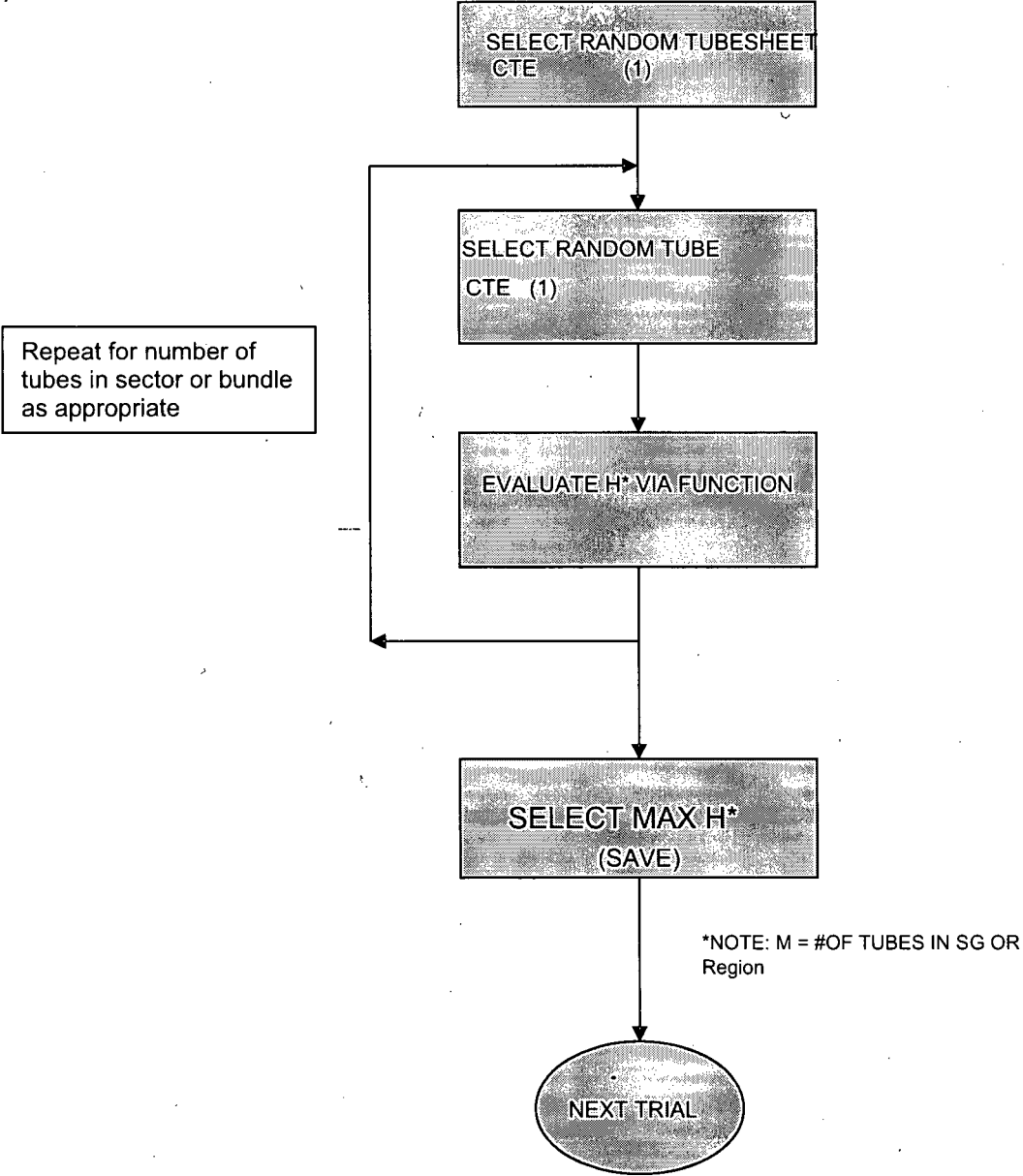


Figure RA120-6
Model F: Interaction Profiles for Sector-Base Sampling

a,c,e



Figure RAI20-7
Model D: Interaction Profiles for Sector-Base Sampling

a,c,e



Figure RA120-8
 ΔH^* for Various Values of α_{srss} and RCL Ratio
($a = \alpha_{srss}$, $RCL_{ref} = 800\text{lb}$)

a,c,e

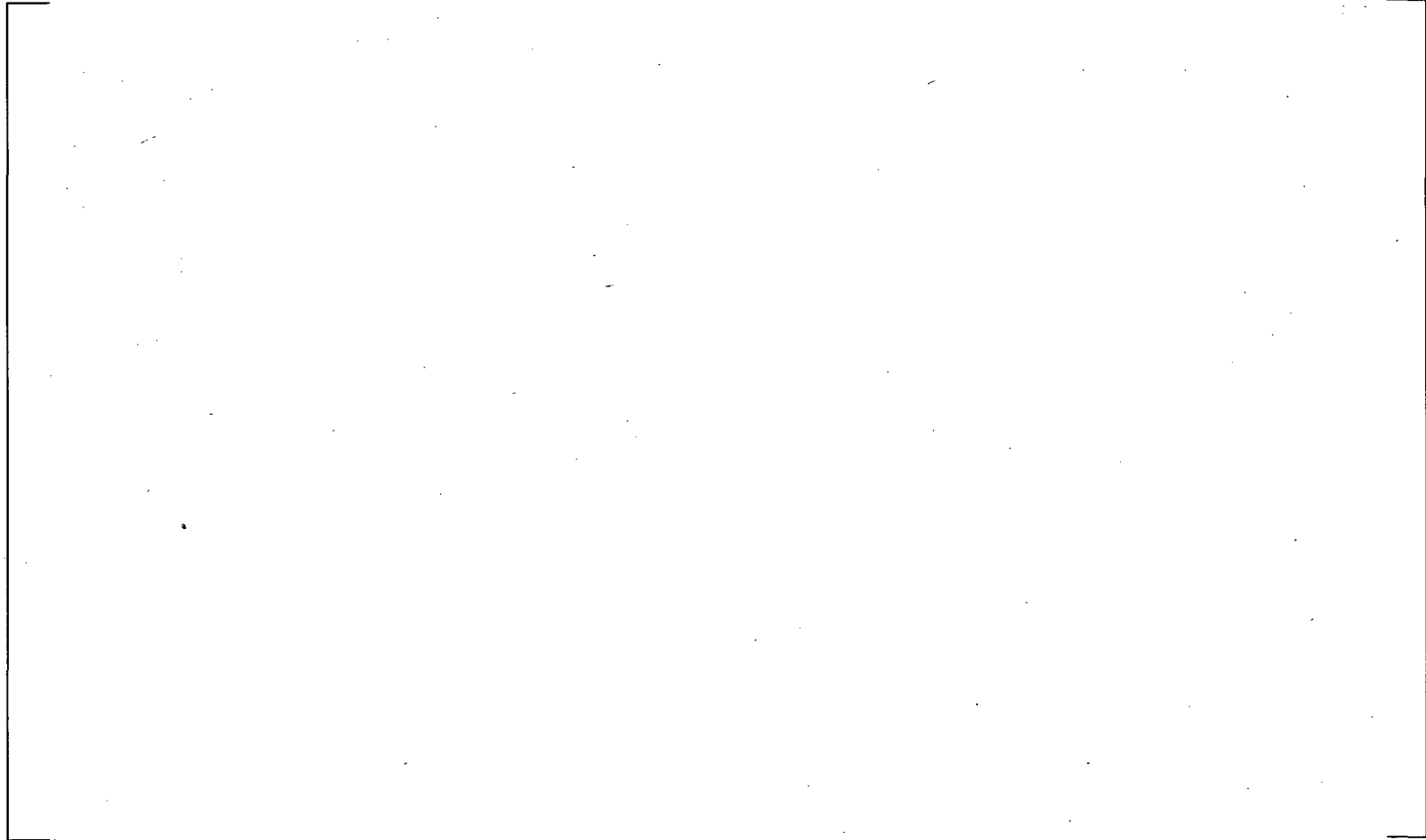


Figure RAI20-9
Model F Response Surface for the Change in H* as a Function of RCL and α_{srss}



a,c,e

Figure RAI20-10
Model D5 Response Surface for the Change in H^* as a Function of RCL and α_{srss}



a,c,e

Figure RAI20-11
Change in H^* as a Function of α_{srss}



a,c,e

**Table RAI20-1
Model F SG Sector Populations**

Model F									
TS Radius	0-11	11-17	17-23	23-29	29-35	35-41	41-47	47-53	53-60
Max Mean H*			[] ^{a,c,e}						
Max Mean H*Factor	[]
Number of Tubes	[]

a,c,e

**Table RAI20-2
Model D5 SG Sector Populations**

Model D5									
TS Radius	0-6	6-12	12-18	18-24	24-30	30-36	36-42	42-48	>48
Max Mean H*					[] ^{a,c,e}				
Max Mean H*Factor	[]
Number of Tubes	[]

a,c,e

**Table RAI20-3
Model 44F SG Sector Populations**

Model 44F									
TS Radius	<9	9-15	15-21	21-27	27-33	33-39	39-45	45-51	>51
Max Mean H*			[] ^{a,c,e}						
Max Mean H*Factor	[]
Number of Tubes	[]

a,c,e

**Table RAI20-4
Model 51F SG Sector Populations**

Model 51F								
TS Radius		<9	9-17	17-24	24-32	32-41.85	41.85-52.52	>52.52
Max Mean H*				[] ^{a,c,e}				
Max Mean H*Factor		[]
Number of Tubes		[]

a,c,e

**Table RAI20-5
Results of Monte Carlo Sampling and Valuation of Conservatism**

SG Model	Report Case S-2			Surface Sampling from Figure 8-5 of the Report(s) with Limited Number of Tubesheets and Sector Based Approach		
	95/50 (inch)	P _{crev} (inch)	Final H*(inch)	95/50 (inch)	P _{crev}	Final H*
F			11.2			
D5			13.8			
44F			13.31			
51F			13.14			

(a) Sampling from Interaction Surface Figure 8-5

SG Model	H* After Surface Sampling	Correction for NOP Thermal Distribution		a,c,e	Surface Sampling, Limited Tubesheets Corrected for NOP Thermal Offset		
	95/50 H*(inch)	Original (inch)	Revised (inch)		95/50 H*(inch)	P _{crev} (inch)	Final H*(inch)
F				=			
D5				=			
44F				=			
51F				=			

SG Model	Surface Sampling from Figure 8-5 of the Report(s) with Limited Number of Tubesheets	□H* for Minimum Pull Out Force (inch)	Final H* After Including Minimum Pull Out Force	Correction for NOP Thermal Distribution	Final H* (inch)
	95/50 (inch)	NA	(95/50) (inch)	(inch)	(95/50) (inch)
F					
D5					
44F					
51F					

(c) Adjustment for Residual Contact Pressure

Notes:

1. The value of H* before correction for P_{crev} is used because the interaction surface is based on the H* value without the P_{crev} adjustment.

There are a number of utility specific RAIs with numbers in the range of RAI 21 through 23, depending on the specific utility. The responses to utility-specific RAIs are provided under separate cover by the utilities.

RAI	Vogtle	24. Reference 1, Page 9-6, Section 9.2.3.1: The feedwater line break heat-up transient is part of the plant design and licensing basis. Thus, it is the NRC staffs position that H* and the "leakage factors," as discussed in Section 9.4, should include consideration of this transient. Explain why the proposed H* and leakage factor values are conservative, even with consideration of the feedwater line break heat-up transient.
	WCGS	24. Reference 1, page 9-6, Section 9.2.3.1: The FLB heat-up transient is part of the plant design and licensing basis. Thus, it is the staff's position that H* and the "leakage factors," as discussed in Section 9.4, should include consideration of this transient. Explain why the proposed H* and leakage factor values are conservative, even with consideration of the FLB heat-up transient.
	B/B	23. Reference 1, Page 9-6, Section 9.2.3.1: The FLB heat-up transient is part of the plant design and licensing basis. Thus, it is the NRC staffs position that H* and the "leakage factors," as discussed in Section 9.4, should include consideration of this transient. Explain why the proposed H* and leakage factor values are conservative, even with consideration of the FLB heat-up transient.
	CPSES	24. Reference 1, page 9-6, Section 9.2.3.1: The FLB heat-up transient is part of the plant design and licensing basis. Thus, it is the NRC staff's position that H* and the "leakage factors," as discussed in Section 9.4, should include consideration of this transient. Please explain why the proposed H* and leakage factor values are conservative, even with consideration of the FLB heat-up transient.
	Seabrook	24. Reference 1, Page 9-6, Section 9.2.3.1: The feedwater line break heat-up transient is part of the plant design and licensing basis. Thus, it is the staff's position that H* and the "leakage factors," as discussed in Section 9.4, should include consideration of this transient. Explain why the proposed H* and leakage factor values are conservative, even with consideration of the feedwater line break heat-up transient.

Response:

Radiological consequences are a function of the source term and activity transport.

- Source term refers to the activity available for release. This is controlled by the Tech Specs on primary and secondary activity and the iodine spike

considerations required by the NRC. Fuel damage is not expected for either the SLB or the FLB. As a result, the source term would be the same. This is the case for the H* plants under consideration.

- Activity transport is dependent upon initial locations of the activity and the mechanism for transport that are applicable. For both the SLB and the FLB events, the dose calculation would use the Tech Spec leakage rate for tube leakage. For both the SLB and FLB events, the secondary break would be assumed to occur outside containment such that the faulted SG releases would occur directly to the atmosphere. As a result, the activity transport would be the same.

Therefore, calculation of the dose consequences for the SLB event would be identical to the calculations that would be made for a FLB event. In this subject, the item that is addressed by the H* program is to define a criterion such that the Tech Spec tube leakage is adequately bounding for both the FLB and SLB. The approach that is used is to define single values for a conservative temperature and conservative pressure differential for the determination of the leakage rate. For the purposes of the dose calculation, these single values are effectively assumed both to be simultaneously occurring and to be continuous for the duration of the calculation. In the dose calculations, these leakage conditions are assumed to last anywhere from multiple hours to multiple days. In some cases, the timeframe is based on allowing for plant cooldown to 212°F which would also require depressurization of the RCS and, therefore reducing the severity of conditions contributing to the tube leakage. However, as noted above, the dose calculations do not consider a more realistic set of conditions for tube leakage.

With respect to temperature transients, a review of the steam generator design transients and the FSAR safety analyses determined that they are not appropriate for defining a temperature basis for the leakage calculations. Those calculations are focused on different criteria and include assumptions which would be overly conservative and operationally limiting for the H* program. For secondary side breaks occurring outside containment, reasonable assumptions would result in a much greater cooling capability of the steam generator secondary side inventory in comparison to FSAR safety analyses. Moreover, based on engineering judgment, a more realistic time-dependent leakage for these events, would result in dose consequences that are less than those reported in the UFSAR under the current licensing basis for both a postulated SLB and FLB event (including a FLB heatup event) due to the reduction in pressure across the tubes and tubesheet that occurs over the long term duration of the accident that is not currently accounted for in the dose analysis. This effect has not been quantified nor does it need to be. It is simpler to define a reasonable peak temperature to use as a basis for the duration of the dose calculation. As identified in WCAP-17071-P and WCAP-17072-P, Westinghouse believes that, with assumptions consistent with an outside containment break, and considering operator actions that are consistent with current Emergency Operating Procedures (EOPs), the no-load condition for a plant is a reasonable condition to use as the basis of the primary to secondary

leakage. The EOPs, for an event which results in a Safety Injection, provide for reduction/termination of safety injection flow and for initiation of cooldown and depressurization of the reactor coolant system to the point that the RHR system can be placed in operation for continued cooling of the RCS. These actions will significantly reduce the pressure and temperature of the RCS to conditions less than the limiting conditions proposed for use in the H* calculations. The cooldown is initiated by releasing steam from the steam generators by using the systems that are available at the time. The steaming of the steam generators provides the additional benefit of increasing the available AFW flow injection due to a reduced pressure that the AFW pumps have to overcome. Either by considering a reduction in dose consequences due to a more realistic time dependent leakage for these events or by considering that the FLB event is best represented as a cooldown event, it is concluded that no change is required to the leakage factors for the Model F and D5 SGs as reported in WCAP-17071-P and WCAP-17072-P.

However, the NRC staff has pointed out that the "figure of merit" in the technical specification performance criterion is "the leakage rate assumed in the accident analysis" and that a FLB heatup event is part of the current licensing basis for certain plants in the H* fleet. Therefore, to ensure that there is sufficient margin between the accident leakage and operational leakage during a postulated FLB as required by the plant Technical Specifications and to ensure that the implementation of the H* criterion remains within the current licensing basis, an adjustment to the leakage factors provided in Table 9-7 of WCAP-17071-P and WCAP-17072-P has been made that accommodates the design specification FLB heatup event. As noted above, the use of temperatures from this transient is judged to be non-realistic and overly conservative. As described in WCAP-17071-P and WCAP-17072-P, for the Model F SGs, the FLB design transient represents a double-ended rupture of the main feedwater line concurrent with both a Station Blackout (loss of main feedwater and reactor coolant pump coastdown) and Turbine Trip. For the Model D5 SGs, the maximum RCS temperature of 670°F exceeds the saturation temperature which is not predicted to occur by the worst case Chapter 15 Safety Analysis Transient response.

Because a FLB heat-up event would result in an increase in primary-to-secondary leakage due to the reduction in viscosity of the reactor coolant, the extent of temperature increase must be quantified to address the impact on radiological consequences for the H* plants with Model F and Model D5 steam generators. Referring to references 9-12 and 9-13 of WCAP-17071-P and WCAP-17072-P, the maximum temperature rise for a Model F SG is less than 6.5°F above the normal operating hot leg temperature (approximately 630°F). For the Model D5 steam generator, the maximum increase in temperature is 50°F above the normal operating hot leg temperature (approximately 670°F). This would require a negligible increase in leakage factor for the Model F SGs reported in Table 9-7 (to a maximum of 2.05 from 2.03) and a slight increase in leakage factors reported for the Model D5 steam generators (to a maximum of 2.31 from 2.03).

The maximum temperature rise for a Model F SG is 66°F above the normal operating cold leg temperature (to approximately 620°F). For the Model D5 steam generator, the maximum increase in cold leg temperature is 120°F above the normal operating cold leg temperature (to approximately 670°F). This would require a maximum increase in leakage factor of 1.23 times the factors provided for the individual Model F SGs in Table 9-7 (to a maximum value of 2.50) and a maximum increase in leakage factor of 1.63 times the factors provided for the individual Model D5 steam generators to a maximum value of 3.16. The leakage factor for the cold leg is limiting for a FLB heat-up event and should be incorporated into the reporting requirements for the plant technical specifications.

Revised versions of Tables 9-1 and 9-7 from WCAP-17071-P and WCAP-17072 -P are provided in this RAI response to reflect the potential increase in temperature that may occur during a postulated FLB event.

Finally, the feedwater line break heat-up transient definition is not a concern for the H* structural analysis. The SIPC requirement for calculating the end cap load during the faulted condition (1.4DP) during the feedwater line break condition does not exceed the end cap load applied to the tubes during NOP (3.0DP). In fact, the applied end cap load during feedwater line break, regardless of whether it is a heat-up or cool down feedwater line break, is several hundred pounds less than the end cap load applied during normal operating conditions. Therefore, normal operating conditions are bounding for the structural determination of H* in all cases. Please refer to Section 5 and Section 6 in the WCAP 17071-P and WCAP-17072-P for a discussion of the calculated end cap loads and the contact pressure results for the feedwater line break condition.

Table RAI24-1
Revised Table 9-1 Reactor Coolant System Temperature Increase Above Normal
Operating Temperature Associated With Design Basis Accidents

(References 9-12 and 9-13)

SG Type	Steam Line/Feedwater Line Break ⁽¹⁾		Locked Rotor (Dead Loop)		Locked Rotor (Active Loop)		Control Rod Ejection	
	SG Hot Leg (°F)	SG Cold Leg (°F)	SG Hot Leg (°F)	SG Cold Leg (°F)	SG Hot Leg (°F)	SG Cold Leg (°F)	SG Hot Leg (°F)	SG Cold Leg (°F)

a,c,e

(1) The postulated SLB does not result in a temperature increase above normal operating conditions as the SLB is a cooldown transient, only the postulated FLB can result in a heatup event dependent upon accident analysis assumptions. The postulated FLB is not part of the licensing basis for plants with Model 44F and Model 51F SGs.

**Table RA124-2
Revised Table 9-7 Final H* Leakage Analysis Leak Rate Factors (Revised)**

Transient Plant Name	SLB/FLB			Locked Rotor				Control Rod Ejection			
	FLB- SLB/NOP ΔP Ratio (High T_{avg}) ⁽²⁾	VR ^(3,4) @ 2642 psig	SLB/FLB Leak Rate Factor(LRF)	LR/NOP ΔP Ratio	VR ³ @ 2711 psia	Leak Rate Factor (LRF)	Adjusted LR LRF ⁽¹⁾	CRE/NOP ΔP Ratio	VR ³ @ 3030 psia	Leak Rate Factor (LRF)	Adjusted CRE LRF ¹
Byron Unit 2 and Braidwood Unit 2	1.93	1.61	3.11								
Salem Unit 1	1.79	1.21	2.16								
Robinson Unit 2	1.82	1	1.82								
Vogtle Unit 1 and 2	2.02	1.23	2.48								
Millstone Unit 3	2.02	1.23	2.49								
Catawba Unit 2	1.75	1.52	2.65								
Comanche Peak Unit 2	1.94	1.63	3.16								
Vandellos Unit 2	1.97	1.22	2.41								
Seabrook Unit 1	2.02	1.23	2.49								
Turkey Point Units 3 and 4	1.82	1	1.82								
Wolf Creek	2.03	1.23	2.50								
Surry Units 1 and 2	1.80	1	1.80								
Indian Point Unit 2	1.75	1	1.75								
Point Beach Unit 1	1.73	1	1.73								

a,c,e

1. Includes time integration leak rate adjustment discussed in Section 9.5.
2. The larger of the ΔP 's for SLB or FLB is used.
3. VR – Viscosity Ratio
4. VR – Viscosity Ratio in SG cold leg during a postulated FLB heatup event

APPENDIX A
SUMMARY OF 2008-2009 PULL OUT TEST PROGRAM IN SUPPORT OF H*

Abstract

Steam generator tubes made of Alloy 600 (A600) were hydraulically expanded in AISI 1018 cold rolled, carbon steel, cylindrical collars, which simulate the steam generator tubesheet, and then pulled by an MTS machine out of the collars in order that tube-to-tubesheet joint (hereafter referred to as "joint" or "the joint") strength might be measured. Nine tubes from each of Model F, Model D5, and Model 44F tubes were tested for pull out resistance, three at each expansion length (13 inches, 15 inches, and 17 inches). The pull out test parameters were established so that the results can be considered to be prototypic of the as-built condition of the steam generators within the H* fleet (i.e., the test specimens were designed and manufactured to be within the manufacturing tolerances for dimensional variations, material properties, and process control parameters for the H* fleet steam generator tube joints).

The pull force capacity associated with 0.25 inch tube displacement relative to the tubesheet ranged from approximately []^{a,b,c} lbf to approximately []^{a,b,c} lbf. The values for the maximum pull force ranged from approximately []^{a,b,c} lbf to approximately []^{a,b,c} lbf within a maximum relative displacement of 2.02 inches, regardless of the tube outside diameter or hydraulic expansion length[10].

Monte Carlo simulations were performed in order to better define a 5/50 value of pull force, which is based on the presence of residual contact pressure, for use in the H* analysis. The minimum 5/50 value of the pull force has been observed to be []^{a,b,c} lbf, and this corresponds very well to the lowest recorded pull force from the testing.

Introduction

H* (pronounced "H star") is the length of hydraulically expanded steam generator tube that must remain intact within the tubesheet in order for the joint to resist pull out and leakage due to normal operating or accident conditions. The basis of the H* program is such that residual contact pressure between the tube and the tubesheet is not considered in the structural or leakage calculations. Hence, any indication of joint strength from test program data is a measure of conservatism contained in the H* analysis.

Westinghouse commenced a test program in which steam generator tubes were hydraulically expanded in cylindrical collars representing the tubesheet and pulled to measure joint strength. There were no tack expansions, hard rolled expansions, or welds to consider. Initially, the H* program applied to Model F steam generators, but it has been expanded to include Model D5, Model 44F, and Model 51F steam generators. The following sections of this document summarize the results of this test program.

Experimental

Materials

Alloy 600 tubes representing those from Model F, Model D5, and Model 44F steam generators were cut to seventeen, nineteen, and twenty-one inch lengths. The Model F steam generator tube was taken from Heat NX7368 and is believed to be mill annealed. The Model D5 and Model 44F steam generator tubes were taken from Heats 2645 and 752570, respectively, and both are in the thermally treated condition. The chemical analyses for these materials are contained in Table 1 and the mechanical properties are contained in Table 2. Note that the mechanical properties listed in Table 2 are from the providers' certifications and from testing done at Industrial Testing Laboratory Services (ITLS). The latter tests were done according to ASTM E8-08 [1].

The cylindrical collars representing the tubesheet were cut to fifteen, seventeen, and nineteen inch lengths from AISI 1018 cold-rolled, carbon steel. The chemical analysis and mechanical properties of Heat 777553 are contained in Tables 3 and 4, respectively. It should be noted that the outer diameters of the collars were chosen to be []^{a,c,e} times the outer diameter of the tubes so that the stiffness of the actual tubesheet plate is correctly represented. This ratio is based on the work of Middlebrooks et al. [2].

The list of tube and collar pairings is presented in Table 5. The indices are to be read as follows: the first two indices refer to the overall length of the tube or collar, the second three indices refer to the nominal OD of the tube or the nominal ID of the collar, and the last two indices refer to the sample number. The "A" suffix refers to a second manufacture of the same sample. It should be noted that two of the tests done were originally planned to be diagnostic in nature. The collars were rebores so that they would contain an inner diameter surface finish of 250 micro-inch rms max. vice an engineered finish of 250 micro-inch rms. These collars were from Heat 730492, and its properties are also contained in Tables 3 and 4.

Pre-Expansion Measurements

The inner diameters of the collars were measured by the vendor (Tooling Specialists, Inc., Latrobe, PA) at distances corresponding to 25%, 50%, and 75% of the length of the collar, relative to the serialized end. Two measurements, ninety degrees apart, were made with an intramic at each location, and the two values at each location were then averaged. Surface roughness measurements were also made by the vendor at the 25% and 75% distances using a profilometer. Lack of an extension device for the profilometer did not permit roughness measurements at the 50% distance.

After being cut, the inner and outer diameters of the A600 tubes were measured by an intramic and the surface roughness of the outer diameters were measured with a profilometer at Westinghouse RRAS (R. Fetter). The diameter measurements were made, relative to the non serialized end, at distances that overlap those made in the collars. Thus, the 25%, 50%, and 75% distances correspond to those percents of the collar's length, not the tube's length. The

inner and outer diameters were also measured at two points for each distance, ninety degrees apart, and the two values were averaged.

Hydraulic Expansion

The tubes were inserted in the collars such that the non serialized end of the tube was flush with the serialized end of the collar. Thus, the serialized end of the tubes protruded from the collars by two inches. The tube/collar assemblies were then inserted on an O-ring mandrel, which was connected to a screw drive pressurizing system. The tube/collar assemblies were pressurized to a nominal pressure of []^{a,c,e} psi per Process Specification 81013RM, Revs. 4 through 10 applicable []. The nominal expansion pressure was typically exceeded, but the excess was less than []^{a,c,e} psi, which is within the tolerance of the equipment ([]^{a,c,e} psi). This work was performed at Westinghouse's Waltz Mill facility by M. Gallik and A. Stett. The details of the tube expansion test plan are contained in [4].

Post-Expansion Measurements

After the hydraulic expansions were completed, measurements of the tubes' inner diameters were again made with an intramic by Westinghouse RRAS (R. Fetter), and eddy current measurements of individual tube/collar assemblies were performed by Westinghouse with the 3-coil +point and standard bobbin coil probes (R. Pocratsky). Once the measurements were complete, the end caps were welded to the tubes at their serialized ends. The tube/collar assemblies with the end caps welded on are shown in Figures 1 through 9.

Heat Treatment

Real tubesheet Z-channels are given a post-weld heat treatment (PWHT) with an electric "belt" wrapped around the channel. In order to simulate that PWHT, the tube/collar assemblies were heat treated in air at nominally []^{a,c,e} °F for nominally 3 hours in a Blue M furnace, Model B-2730-Q. This was accomplished at Westinghouse's Churchill site (A. Neville). The actual PWHT temperature applied to the Z-channel is 1150°F. However, it was determined [5] that []^{a,c,e} °F is higher than the vast majority of the tubes will experience by the PWHT.

Instrumentation

Prior to testing, the exposed ends of the tubes were fitted with two 350 ohm, quarter bridge strain gauges. Additionally, two linear variable differential transformers (LVDTs) were used in order to model the displacement of each end of the tube relative to the collar. All electronic readouts (load cell, cross-head displacement, displacements of the LVDTs, and strains) were recorded on a Strainbook data acquisition system.

Pull Tests

The pull tests were performed according to the test program described in [6] in air and at room temperature. The mechanical operation of the MTS system was performed by M. Gallik and

A. Stett, while the electronic recording of the data was done by A. Roslund, all of whom work at Westinghouse's Waltz Mill facility. The sequence of the testing was activation of the Strainbook and confirmation of its recording, initiation of the pull test, continuation of the pull test until approximately two inches of cross-head displacement were achieved, and finally, the cessation of pull testing and electronic recording of data.

Post-Test Evaluations

After the pull testing was complete, another set of eddy current measurements were made at Westinghouse's Waltz Mill facility by R. Pocratsky. Again, both the 3-coil +point and standard bobbin coil probes were used.

Monte Carlo Analysis

In support of the test program, Monte Carlo simulations were run, based on means and standard deviations from the test data, in order to determine a 5/50 bound on pull force. The simulations were performed in two ways and on a tube OD basis: one simulation considered the thirteen inch expansions only, and the other simulation considered all nine tests together, ignoring expansion length difference. Seven distributions were chosen and the fitting parameters set so that the resulting distribution has the mean and standard deviation of the test data. The first was a truncated normal distribution. The other six were chosen so that their domains span zero to positive infinity, their domains are continuous, and fitting parameters are within their allowable ranges. They were lognormal, Erlang, Gamma, inverse Gaussian, Pearson Type V, and Weibull. In each simulation, 100,000 iterations were run.

Discussion of Key Parameters

Tube pull out force capacity (based on residual contact pressure) can be derived from the measured pull out forces from the test that simulate the as-manufactured condition of the steam generators. All of the tests performed to date have demonstrated that a positive value of residual contact pressure exists after the hydraulic expansion process. However, the results from these tests depend on a number of factors including dimensional variations of the tubes and tube collars, surface finish variations, potential manufacturing artifacts on the tubesheet (collar) bore, tube joint process variables, and material properties of the test specimens. The key items identified are addressed below.

The NRC staff has raised the concern that sufficient information must be provided to adequately characterize the potential range in values of residual contact pressure between the tube and the tubesheet (due to the hydraulic expansion process) which may be encountered within the whole plant [7]. At that time, only limited pull out data existed upon which the residual contact pressure was estimated. The staff pointed out [7] that the residual contact pressure, and thus the residual load capacity, is highly sensitive to several parameters including hydraulic expansion pressure, tube yield strength, tube material strain hardening properties, and initial (pre-expansion) gap between the tube and the tubesheet. The NRC staff further pointed out in [7] that additional information was necessary to establish whether the pull out test specimens

adequately envelop the range of values of those parameters that may be encountered in the as-built steam generators.

Consequently, two actions have been taken to address the NRC staff concerns. First, an analysis was performed to identify the key parameters that affect the residual contact pressure and to quantify the effects of uncertainties. Secondly, a new pull out test program was initiated to provide test results that can be directly compared to the key parameters as identified by analysis in support of the development of the H* criterion.

The analysis model used to evaluate the residual contact pressure was a two-dimensional, plane strain, finite element model using the ANSYS computer code as described in Section 7 of [8]. Based on a review of Table 7-3 of [8], the key parameters impacting pull out force capacity are:

- Initial tube gap
- Tube yield strength
- Tube joint expansion pressure
- Strain hardening.

Other parameters important to pull out force capacity not considered in the analytical model are surface roughness and variations in the diameter of the tubesheet bore (waviness).

Table 6 provides a comparison of the as-built to as-tested parameters in the new test program. Based on a review of Table 6, several points can be made regarding the key parameters of the pull out testing.

- It is expected that standard gun drilling practices used in the manufacture of steam generators would typically result in nominal gaps between the tube and tubesheet. No special controls were placed on the initial gap size as the test program was meant to be as prototypic as possible.
- The yield strength of the tubes used for the test specimens simulating the as-built configuration of the Model F and Model D5 steam generators was conservatively high compared to the as-built mean values ([]^{a,b,c} ksi vs. []^{a,b,c} ksi), because higher yield strengths result in less tube deformation for a given expansion pressure. The yield strength for the tubes used for the Model 44F steam generators was slightly less than the as-built mean yield strength ([]^{a,b,c} ksi vs. []^{a,b,c} ksi).
- The expansion pressure used in the manufacture of the test specimen was consistent with what is specified in [3] and is directly applicable to the as-built conditions of the steam generators in the H* fleet.
- The surface roughness of the tubes outer diameters and the collars inner diameters was well within the tolerances of the as-built conditions of the steam generators in the H* fleet.
- The mechanical properties of the materials used for the test specimens are within ASME Code specifications for the respective materials. Thus, use of the ASME Code values for the key parameters of the H* study is valid.

Other differences between the materials used for the test specimens for the pull out tests are addressed below.

The use of mill annealed tube vice thermally treated tubing for the Model F specimens has been evaluated and found to be acceptable. For room temperature testing, the key material property affecting the residual contact pressure is yield strength. The difference between yield strength of mill annealed material and thermally treated material is presented in Table 7 and further discussed below. Based on the similarity of mechanical properties between the two materials, it is concluded that there is no adverse effect on the test results. The yield strength value used for the Model F test specimens was []^{a,b,c} ksi, which would result in a reduction of residual contact pressure [9].

The test specimen collar is manufactured from AISI 1018 cold rolled, carbon steel. The material used in the H* fleet is actually A508 Class 2a carbon steel. The use of the different material does not adversely affect the pull test results since the primary property of the material in this case is elastic flexural rigidity of the tubesheet (i.e., elastic modulus), and since the tube expansion operation does not produce significant yielding of the tubesheet (the yield strength of the AISI 1018 cold rolled, carbon steel at room temperature is ~83 ksi), the use of higher strength material for the collar is acceptable (see pp. 8-9 of [8]). Thus, it is concluded that the pull out testing is representative of the as-built condition of the steam generators in the H* fleet.

Results

Table 8 shows the results of the pull tests, while Table 9 through Table 15 shows the results of the Monte Carlo simulations. The latter results are calculated for the pull out force at 0.25 inch displacement.

Discussion

Discussion between Westinghouse and the NRC staff has led to the decision that the pull out force of record should be the pull out force at 0.25 inch cross head displacement. The following discussion and analysis will, therefore, be based on that quantity.

Figure 10 plots the pull out force as a function of the collar ID surface roughness. The graph also provides information on the tube expansion lengths and the tube diameters that were tested. Intuitively, it would be expected that tube pull out force would increase with increasing tube diameter (which provides greater surface area in contact), increasing tube expansion length (which does the same thing), and increasing surface roughness. However, the results in Figure 10 do not necessarily support these assumptions. The highest pull out force for 0.25 inch cross head displacement (approximately []^{a,b,c} kips) occurred for both a test specimen with the largest tube OD, the largest collar ID surface roughness, and the smallest expansion length, as well as for a test specimen having the largest tube OD, one of the lowest collar ID surface roughness values, and the smallest expansion length. The next highest pull out force ([]^{a,b,c} kips) occurred for tubes with varying degrees of collar ID surface roughness, for all tube ODs, and for all expansion lengths. The lowest pull out force ([]^{a,b,c} lbf) occurred for a test

specimen with a 0.75 inch tube OD, a collar ID surface roughness of ~ 50 micro-inch (rms), and an expansion length of 15 inches. The lowest pull out force for a Model F test specimen was less than []^{a,b,c} kips. This specimen had a collar ID surface roughness less than 40 micro-inch (rms) and an expansion length of 13 inches. The lowest pull out force for a Model 44F specimen was less than []^{a,b,c} kips. This specimen had a collar ID surface roughness of less than 40 micro-inch (rms) and a tube expansion length of 15 inches.

Similarly, the pull test results are shown as a function of tube expansion length in Figure 11. These results also show the lack of correlation between pull out force and tube OD and expansion length.

The pull force necessary to move a tube in the collar is a consequence of three main factors: the residual contact pressure due to the hydraulic expansion, the surface roughness of the tube and the collar, and any geometric irregularities due to machining of the tube and collar, which are then subject to hydraulic expansion. As shown by analysis, the initial gap between the outer diameter of the unexpanded tube and the tubesheet bore hole can adversely affect the resulting residual contact pressure. Small variations along the length of the collar ID (waviness) due to the gun drilling process are significant contributors to the pull out resistance. Geometric irregularities are present as initial gaps between the tube and the collar and as bulges in the tubes. One possible explanation for the significant variation in the test results may be that the waviness was not well profiled due to the difficulty of quantifying this variable. Nonetheless, the pull out test results do appear to be consistent with the expected as-built condition.

Recall that nine pull out tests were performed for each tube OD. Analysis of variance (ANOVA in statistics) is a collection of statistical models and their associated procedures in which the observed variance is partitioned into components due to different explanatory variables. In its simplest form, ANOVA provides a statistical test of whether the means of several groups of data are all equal. One such method is called the F-test. Therefore, the F-test was conducted on the pull out test capabilities comparing the variance of each set of 9 samples for each tube diameter using Microsoft EXCEL. The F-test was used to determine whether or not there was any statistical difference between tube OD and pull test results. The answer was that it cannot be concluded that there is any difference in the variance between each sample set and that the means for tube pull out force for each of the outer diameters may be equal. Therefore, it is judged that all of the data can be considered to be one data set.

However, the NRC staff stated in [7] that there is a need to adjust the pull out data so as to produce an estimate of the residual contact pressure that is conservative for the range of H* values that are being proposed. In order to address this concern for the new pull out test data (i.e., the expansion length of some of the pull out test data exceed the calculated H* values), the sample sets for the different tube ODs were not combined. They were separated by expansion length, even though the F-test results suggest that the mean values of the tube pull out capacity are the same for different tube ODs and considering variations in expansion length and surface roughness.

To investigate this further, the Monte Carlo simulations were performed. Each tube OD was broken up into two sets (13 inch expansion length only and all expansion lengths) and

distributions were chosen based on the criteria previously defined. Using the calculated means and standard deviations from each data set, the fitting parameters for the seven distributions chosen were calculated. Note that the fitting parameters for the normal and lognormal distributions are simply the mean and standard deviation. In each case the 5/50 value was recorded, and the lowest of these corresponded to a pull force of []^{a,c,e} lbf. This was calculated for the Model F tube, 13 inch expansion length only, and using the Weibull distribution (see Table 15). This value is very consistent with the lowest actual pull force from the test data ([]^{a,b,c} lbf).

Conclusion

Based on the results of the pull tests and Monte Carlo analyses, it is concluded that the end cap load used in the H* analysis can be conservatively reduced by []^{a,c,e} lbf. H* can then be recalculated accordingly.

References

- (1) ASTM E8/E8M-08, "Standard Test Method for Tension Testing of Metallic Materials," West Conshohocken: ASTM International, 2008.
- (2) W. B. Middlebrooks, D. L. Harrod, and R. E. Gold, *Nuclear Engineering and Design* 143, 1993, pp. 159-169.
- (3) Process Specification 81013RM, "Hydraulic Tube Expansion," Rev.4 through Rev. 10, February 1, 1979 through July 24, 1981.
- (4) J. T. Kandra, TP-CDME-08-3, "Test Procedure for Tube Expansion for H*," August 25, 2008.
- (5) D. L. Harrod, WNEP-9725, "The Westinghouse Tube-to-Tubesheet Joint Hydraulic Expansion Process," July 1997.
- (6) J. T. Kandra, TP-CDME-08-1, "Pull-Out Test Program for H*," August 25, 2008.
- (7) NRC Letter, "Wolf Creek Generating Station – Withdrawal of License Amendment on Steam Generator Tube Inspections (TAC No. MD0197)," United States Nuclear Regulatory Commission, Washington, D.C., February 28, 2008.
- (8) WCAP-17071-P, "H*: Alternate Repair Criteria for the Tubesheet Expansion Region in Steam Generators with Hydraulically Expanded Tubes (Model F)," April 2009.
- (9) DP-SGDA-05-2, "Data Package for H-Star Pull Test of 7/8 Inch Tubing form Simulated Tubesheet, PA-MS-0199 WOG Program for Steam Generator Models 44F and 51F," November 2005.
- (10) LTR-SGMP-09-98, "H* Pull Test Program Summary," Westinghouse Electric Company LLC, July 27, 2009.

Table 1
Chemical Analyses of the A600 Materials Used in This Test Program

Steam Generator Model	F	D5	44F
Chemical Analysis Source	Plymouth Tube Co. Salisbury, MD	Huntington Alloys, Inc. Huntington, WV	AB Sandvik Steel
Heat	NX7368	2645	752570
Element (w/o)			
C	0.04	0.033	0.025
Mn	0.41	0.34	0.79
P	N/A	0.007	0.009
S	0.001	0.001	0.002
Si	0.30	0.09	0.33
Cr	14.87	15.44	16.60
Ni	76.21	75.45	72.45
Cu	0.15	0.23	0.010
Co	0.04	0.04	0.011
Fe	7.98	8.42	9.29
B	N/A	0.003	N/A

Table 2
Mechanical Properties of the A600 Materials Used in This Test Program

Steam Generator Model	Heat	Mechanical Property Source	σ_Y (psi)	σ_{UT} (psi)	Elongation (%)
F	NX7368	Vendor	59,700	106,600	39
		ITLS	58,000	108,000	32
D5	2645	Vendor	43,000	97,000	41.5
		ITLS	54,000	110,000	35
44F	752570	Vendor	47,500	101,700	45.5
		ITLS	46,000	101,000	40

Table 3
Chemical Analyses of the 1018 Cold-Rolled, Carbon Steel Used in This Test Program

Steel	Chemical Analysis Source	Heat	Element (w/o)				
			C	Mn	Si	S	P
AISI 1018	Steel Bar Corp. Greensboro, NC	777553	0.17	0.84	0.27	0.030	0.005
AISI 1018	Steel Bar Corp. Greensboro, NC	730492	0.18	0.79	0.22	0.030	0.010

Table 4
Mechanical Properties of the 1018 Cold-Rolled, Carbon Steel Used in This Test Program

Steel	Heat	Mechanical Property Source	σ_y (ksi)	σ_{UT} (ksi)	Elongation (%)
AISI 1018	777553	DuBose National Energy Services, Inc. Clinton, NC	83.0	90.0	18
AISI 1018	730492	DuBose National Energy Services, Inc. Clinton, NC	67.5	79.3	25

Table 5
Steam Generator Tube and Collar Pairings Used in This Test Program

Tube	Heat	Collar	Heat
17-688-01A	NX7368	15-699-01A	777553
17-688-02A	NX7368	15-699-02A	777553
17-688-03	NX7368	15-699-03A	777553
19-688-01	NX7368	17-699-01A	777553
19-688-02	NX7368	17-699-02A	777553
19-688-03	NX7368	17-699-03A	777553
21-688-01	NX7368	19-699-01A	777553
21-688-02	NX7368	19-699-02A	777553
21-688-03	NX7368	19-699-03A	777553
17-750-01A	2645	15-762-01A	777553
17-750-02A	2645	15-762-02A	777553
17-750-03	2645	15-699-03	730492
19-750-01	2645	17-762-01A	777553
19-750-02	2645	17-762-02A	777553
19-750-03	2645	17-762-03A	777553
21-750-01	2645	19-762-01A	777553
21-750-02	2645	19-762-02A	777553
21-750-03	2645	19-762-03A	777553
17-875-01A	752570	15-888-01A	777553
17-875-02A	752570	15-888-02A	777553
17-875-03	752570	15-762-03	730492
19-875-01	752570	17-888-01A	777553
19-875-02	752570	17-888-02A	777553
19-875-03	752570	17-888-03A	777553
21-875-01	752570	19-888-01A	777553
21-875-02	752570	19-888-02A	777553
21-875-03	752570	19-888-03A	777553

Table 6
Residual Contact Pressure Critical Parameter Comparison

Key Parameters	Model F		Model D5		Models 44F -51F		
	As-Built	As-Tested	As-Built	As-Tested	As-Built	As-Tested	
Average Initial Gap (inches)							a,c,e
Tube Yield Strength (ksi)							
Expansion Pressure (ksi)							
Tube Outer Diameter Surface Roughness μ in. rms							
Collar Inner Diameter Surface Roughness μ in. rms							
Tube OD (in)							
Collar ID (in)							

Table 7
Comparison of Yield Strength Between Mill Annealed and Thermally Treated Alloy 600

	Alloy 600 Mill Annealed As-Tested	Alloy 600 Thermally Treated As-Built	
Minimum]]	a,c,e
Mean			
Maximum			
Standard Deviation			
Number of Tests	361	307	
Tube Size (OD)	7/8 inch	7/8 inch	
Data	Reference [1]	Reference [1]	
Yield Strength values are in units of ksi.			

**Table 8
Results of the Pull Testing**

Tube ID	Heat	Collar ID	Heat	Load at 0.25" Displacement (kip)	Max. Load (kip)	Displacement at Max. Load (in)
17-688-01A	NX7368	15-699-01A	777553			
17-688-02A	NX7368	15-699-02A	777553			
17-688-03	NX7368	15-699-03A	777553			
19-688-01	NX7368	17-699-01A	777553			
19-688-02	NX7368	17-699-02A	777553			
19-688-03	NX7368	17-699-03A	777553			
21-688-01	NX7368	19-699-01A	777553			
21-688-02	NX7368	19-699-02A	777553			
21-688-03	NX7368	19-699-03A	777553			
17-750-01A	2645	15-762-01A	777553			
17-750-02A	2645	15-762-02A	777553			
17-750-03	2645	15-699-03	730492			
19-750-01	2645	17-762-01A	777553			
19-750-02	2645	17-762-02A	777553			
19-750-03	2645	17-762-03A	777553			
21-750-01	2645	19-762-01A	777553			
21-750-02	2645	19-762-02A	777553			
21-750-03	2645	19-762-03A	777553			
17-875-01A	752570	15-888-01A	777553			
17-875-02A	752570	15-888-02A	777553			
17-875-03	752570	15-762-03	730492			
19-875-01	752570	17-888-01A	777553			
19-875-02	752570	17-888-02A	777553			
19-875-03	752570	17-888-03A	777553			
21-875-01	752570	19-888-01A	777553			
21-875-02	752570	19-888-02A	777553			
21-875-03	752570	19-888-03A	777553			

a,b,c

Table 9
Monte Carlo Results for the Truncated Normal Distribution

Distribution	Normal Distribution (truncated at 0)			
Case 1	Parameters to Define the Distribution			5/50 Pull Out Force (kip)
Model F 13" Expansion	Name	Mean	Stand. Dev.	[] ^{a,c,e}
	Symbol	μ	σ	
	Value	[] ^{a,c,e}	[] ^{a,c,e}	
Case 2	Parameters to Define the Distribution			5/50 Pull Out Force (kip)
Model F All Expansions	Name	Mean	Stand. Dev.	[] ^{a,c,e}
	Symbol	μ	σ	
	Value	[] ^{a,c,e}	[] ^{a,c,e}	
Case 3	Parameters to Define the Distribution			5/50 Pull Out Force (kip)
Model D5 13" Expansion	Name	Mean	Stand. Dev.	[] ^{a,c,e}
	Symbol	μ	σ	
	Value	[] ^{a,c,e}	[] ^{a,c,e}	
Case 4	Parameters to Define the Distribution			5/50 Pull Out Force (kip)
Model D5 All Expansions	Name	Mean	Stand. Dev.	[] ^{a,c,e}
	Symbol	μ	σ	
	Value	[] ^{a,c,e}	[] ^{a,c,e}	
Case 5	Parameters to Define the Distribution			5/50 Pull Out Force (kip)
Model 44F 13" Expansion	Name	Mean	Stand. Dev.	[] ^{a,c,e}
	Symbol	μ	σ	
	Value	[] ^{a,c,e}	[] ^{a,c,e}	
Case 6	Parameters to Define the Distribution			5/50 Pull Out Force (kip)
Model 44F All Expansions	Name	Mean	Stand. Dev.	[] ^{a,c,e}
	Symbol	μ	σ	
	Value	[] ^{a,c,e}	[] ^{a,c,e}	

Table 10
Monte Carlo Results for the LogNormal Distribution

Distribution	Lognormal Distribution			
Case 1	Parameters to Define the Distribution			5/50 Pull Out Force (kip)
Model F 13" Expansion	Name	Mean	Stand. Dev.	[] ^{a,c,e}
	Symbol	μ	σ	
	Value	[] ^{a,c,e}	[] ^{a,c,e}	
Case 2	Parameters to Define the Distribution			5/50 Pull Out Force (kip)
Model F All Expansions	Name	Mean	Stand. Dev.	[] ^{a,c,e}
	Symbol	μ	σ	
	Value	[] ^{a,c,e}	[] ^{a,c,e}	
Case 3	Parameters to Define the Distribution			5/50 Pull Out Force (kip)
Model D5 13" Expansion	Name	Mean	Stand. Dev.	[] ^{a,c,e}
	Symbol	μ	σ	
	Value	[] ^{a,c,e}	[] ^{a,c,e}	
Case 4	Parameters to Define the Distribution			5/50 Pull Out Force (kip)
Model D5 All Expansions	Name	Mean	Stand. Dev.	[] ^{a,c,e}
	Symbol	μ	σ	
	Value	[] ^{a,c,e}	[] ^{a,c,e}	
Case 5	Parameters to Define the Distribution			5/50 Pull Out Force (kip)
Model 44F 13" Expansion	Name	Mean	Stand. Dev.	[] ^{a,c,e}
	Symbol	μ	σ	
	Value	[] ^{a,c,e}	[] ^{a,c,e}	
Case 6	Parameters to Define the Distribution			5/50 Pull Out Force (kip)
Model 44F All Expansions	Name	Mean	Stand. Dev.	[] ^{a,c,e}
	Symbol	μ	σ	
	Value	[] ^{a,c,e}	[] ^{a,c,e}	

**Table 11
Monte Carlo Results for the Erlang Distribution**

Distribution	Erlang Distribution			
Case 1	Parameters to Define the Distribution			5/50 Pull Out Force (kip)
Model F 13" Expansion	Name	Cont. Shape Par.	Cont. Scale Par.	[] ^{a,c,e}
	Symbol	m	β	
	Value	[] ^{a,c,e}	[] ^{a,c,e}	
Case 2	Parameters to Define the Distribution			5/50 Pull Out Force (kip)
Model F All Expansions	Name	Cont. Shape Par.	Cont. Scale Par.	[] ^{a,c,e}
	Symbol	m	β	
	Value	[] ^{a,c,e}	[] ^{a,c,e}	
Case 3	Parameters to Define the Distribution			5/50 Pull Out Force (kip)
Model D5 13" Expansion	Name	Cont. Shape Par.	Cont. Scale Par.	[] ^{a,c,e}
	Symbol	m	β	
	Value	[] ^{a,c,e}	[] ^{a,c,e}	
Case 4	Parameters to Define the Distribution			5/50 Pull Out Force (kip)
Model D5 All Expansions	Name	Cont. Shape Par.	Cont. Scale Par.	[] ^{a,c,e}
	Symbol	m	β	
	Value	[] ^{a,c,e}	[] ^{a,c,e}	
Case 5	Parameters to Define the Distribution			5/50 Pull Out Force (kip)
Model 44F 13" Expansion	Name	Cont. Shape Par.	Cont. Scale Par.	[] ^{a,c,e}
	Symbol	m	β	
	Value	[] ^{a,c,e}	[] ^{a,c,e}	
Case 6	Parameters to Define the Distribution			5/50 Pull Out Force (kip)
Model 44F All Expansions	Name	Cont. Shape Par.	Cont. Scale Par.	[] ^{a,c,e}
	Symbol	m	β	
	Value	[] ^{a,c,e}	[] ^{a,c,e}	

Table 12
Monte Carlo Results for the Gamma Distribution

Distribution	Gamma Distribution			
Case 1	Parameters to Define the Distribution			5/50 Pull Out Force (kip)
Model F 13" Expansion	Name	Cont. Shape Par.	Cont. Scale Par.	[] ^{a,c,e}
	Symbol	α	β	
	Value	[] ^{a,c,e}	[] ^{a,c,e}	
Case 2	Parameters to Define the Distribution			5/50 Pull Out Force (kip)
Model F All Expansions	Name	Cont. Shape Par.	Cont. Scale Par.	[] ^{a,c,e}
	Symbol	α	β	
	Value	[] ^{a,c,e}	[] ^{a,c,e}	
Case 3	Parameters to Define the Distribution			5/50 Pull Out Force (kip)
Model D5 13" Expansion	Name	Cont. Shape Par.	Cont. Scale Par.	[] ^{a,c,e}
	Symbol	α	β	
	Value	[] ^{a,c,e}	[] ^{a,c,e}	
Case 4	Parameters to Define the Distribution			5/50 Pull Out Force (kip)
Model D5 All Expansions	Name	Cont. Shape Par.	Cont. Scale Par.	[] ^{a,c,e}
	Symbol	α	β	
	Value	[] ^{a,c,e}	[] ^{a,c,e}	
Case 5	Parameters to Define the Distribution			5/50 Pull Out Force (kip)
Model 44F 13" Expansion	Name	Cont. Shape Par.	Cont. Scale Par.	[] ^{a,c,e}
	Symbol	α	β	
	Value	[] ^{a,c,e}	[] ^{a,c,e}	
Case 6	Parameters to Define the Distribution			5/50 Pull Out Force (kip)
Model 44F All Expansions	Name	Cont. Shape Par.	Cont. Scale Par.	[] ^{a,c,e}
	Symbol	α	β	
	Value	[] ^{a,c,e}	[] ^{a,c,e}	

Table 13
Monte Carlo Results for the Inverse Gaussian Distribution

Distribution	Inverse Gaussian Distribution			
Case 1	Parameters to Define the Distribution			5/50 Pull Out Force (kip)
Model F 13" Expansion	Name	Cont. Par.	Cont. Par.	[] ^{a,c,e}
	Symbol	μ	λ	
	Value	[] ^{a,c,e}	[] ^{a,c,e}	
Case 2	Parameters to Define the Distribution			5/50 Pull Out Force (kip)
Model F All Expansions	Name	Cont. Par.	Cont. Par.	[] ^{a,c,e}
	Symbol	μ	λ	
	Value	[] ^{a,c,e}	[] ^{a,c,e}	
Case 3	Parameters to Define the Distribution			5/50 Pull Out Force (kip)
Model D5 13" Expansion	Name	Cont. Par.	Cont. Par.	[] ^{a,c,e}
	Symbol	μ	λ	
	Value	[] ^{a,c,e}	[] ^{a,c,e}	
Case 4	Parameters to Define the Distribution			5/50 Pull Out Force (kip)
Model D5 All Expansions	Name	Cont. Par.	Cont. Par.	[] ^{a,c,e}
	Symbol	μ	λ	
	Value	[] ^{a,c,e}	[] ^{a,c,e}	
Case 5	Parameters to Define the Distribution			5/50 Pull Out Force (kip)
Model 44F 13" Expansion	Name	Cont. Par.	Cont. Par.	[] ^{a,c,e}
	Symbol	μ	λ	
	Value	[] ^{a,c,e}	[] ^{a,c,e}	
Case 6	Parameters to Define the Distribution			5/50 Pull Out Force (kip)
Model 44F All Expansions	Name	Cont. Par.	Cont. Par.	[] ^{a,c,e}
	Symbol	μ	λ	
	Value	[] ^{a,c,e}	[] ^{a,c,e}	

Table 14
Monte Carlo Results for the Pearson Type V Distribution

Distribution	Pearson Type V Distribution			
Case 1	Parameters to Define the Distribution			5/50 Pull Out Force (kip)
Model F 13" Expansion	Name	Cont. Shape Par.	Cont. Scale Par.	[] ^{a,c,e}
	Symbol	α	β	
	Value	[] ^{a,c,e}	[] ^{a,c,e}	
Case 2	Parameters to Define the Distribution			5/50 Pull Out Force (kip)
Model F All Expansions	Name	Cont. Shape Par.	Cont. Scale Par.	[] ^{a,c,e}
	Symbol	α	β	
	Value	[] ^{a,c,e}	[] ^{a,c,e}	
Case 3	Parameters to Define the Distribution			5/50 Pull Out Force (kip)
Model D5 13" Expansion	Name	Cont. Shape Par.	Cont. Scale Par.	[] ^{a,c,e}
	Symbol	α	β	
	Value	[] ^{a,c,e}	[] ^{a,c,e}	
Case 4	Parameters to Define the Distribution			5/50 Pull Out Force (kip)
Model D5 All Expansions	Name	Cont. Shape Par.	Cont. Scale Par.	[] ^{a,c,e}
	Symbol	α	β	
	Value	[] ^{a,c,e}	[] ^{a,c,e}	
Case 5	Parameters to Define the Distribution			5/50 Pull Out Force (kip)
Model 44F 13" Expansion	Name	Cont. Shape Par.	Cont. Scale Par.	[] ^{a,c,e}
	Symbol	α	β	
	Value	[] ^{a,c,e}	[] ^{a,c,e}	
Case 6	Parameters to Define the Distribution			5/50 Pull Out Force (kip)
Model 44F All Expansions	Name	Cont. Shape Par.	Cont. Scale Par.	[] ^{a,c,e}
	Symbol	α	β	
	Value	[] ^{a,c,e}	[] ^{a,c,e}	

Table 15
Monte Carlo Results for the Weibull Distribution

Distribution	Weibull Distribution			
Case 1	Parameters to Define the Distribution			5/50 Pull Out Force (kip)
Model F 13" Expansion	Name	Cont. Shape Par.	Cont. Scale Par.	[] ^{a,c,e}
	Symbol	α	β	
	Value	[] ^{a,c,e}	[] ^{a,c,e}	
Case 2	Parameters to Define the Distribution			5/50 Pull Out Force (kip)
Model F All Expansions	Name	Cont. Shape Par.	Cont. Scale Par.	[] ^{a,c,e}
	Symbol	α	β	
	Value	[] ^{a,c,e}	[] ^{a,c,e}	
Case 3	Parameters to Define the Distribution			5/50 Pull Out Force (kip)
Model D5 13" Expansion	Name	Cont. Shape Par.	Cont. Scale Par.	[] ^{a,c,e}
	Symbol	α	β	
	Value	[] ^{a,c,e}	[] ^{a,c,e}	
Case 4	Parameters to Define the Distribution			5/50 Pull Out Force (kip)
Model D5 All Expansions	Name	Cont. Shape Par.	Cont. Scale Par.	[] ^{a,c,e}
	Symbol	α	β	
	Value	[] ^{a,c,e}	[] ^{a,c,e}	
Case 5	Parameters to Define the Distribution			5/50 Pull Out Force (kip)
Model 44F 13" Expansion	Name	Cont. Shape Par.	Cont. Scale Par.	[] ^{a,c,e}
	Symbol	α	β	
	Value	[] ^{a,c,e}	[] ^{a,c,e}	
Case 6	Parameters to Define the Distribution			5/50 Pull Out Force (kip)
Model 44F All Expansions	Name	Cont. Shape Par.	Cont. Scale Par.	[] ^{a,c,e}
	Symbol	α	β	
	Value	[] ^{a,c,e}	[] ^{a,c,e}	

Figure 1
The Model F 13 Inch Expansion Tube/Collar Assembly

a,c,e

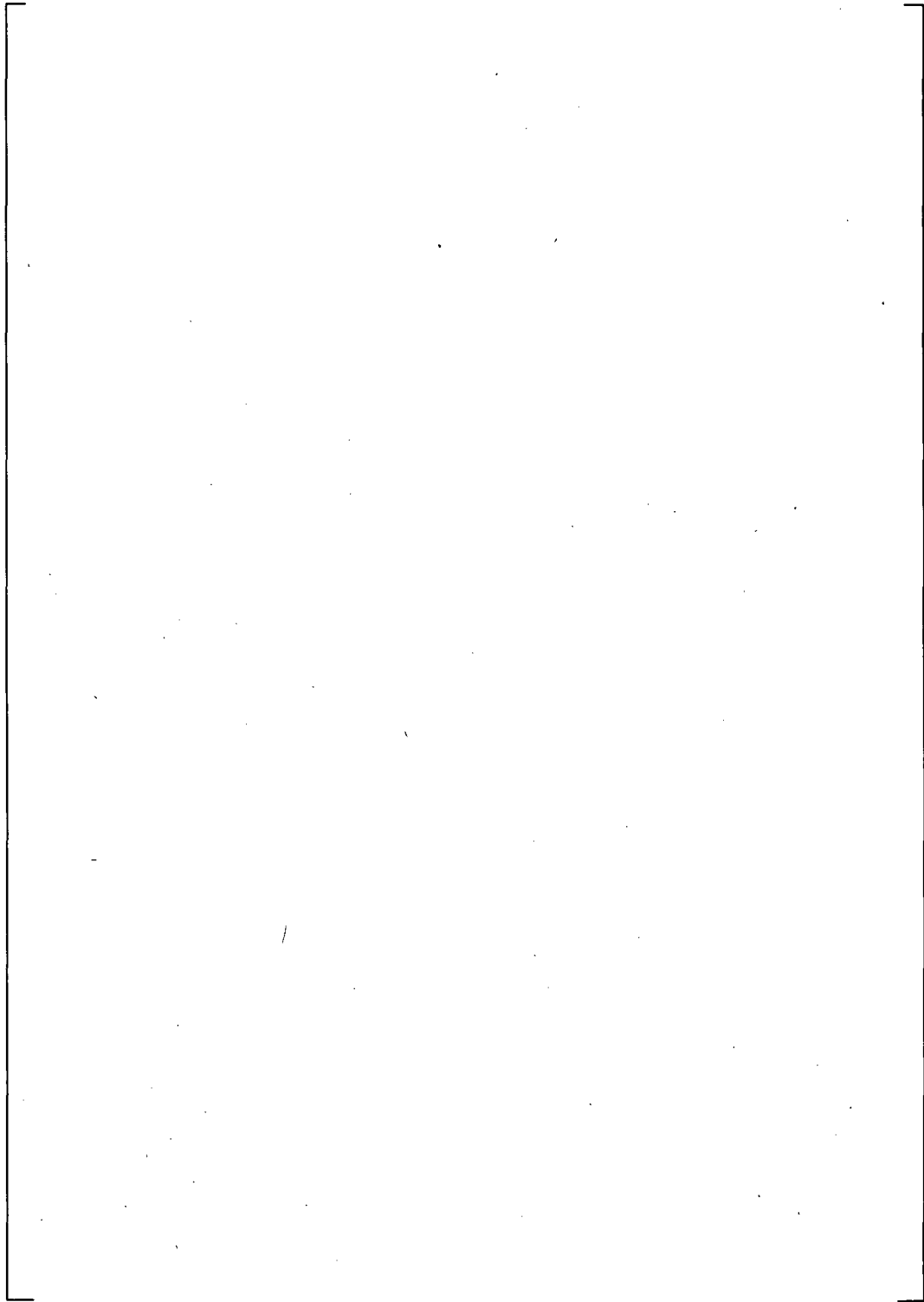


Figure 2
The Model F 15 Inch Expansion Tube/Collar Assembly

a,c,e

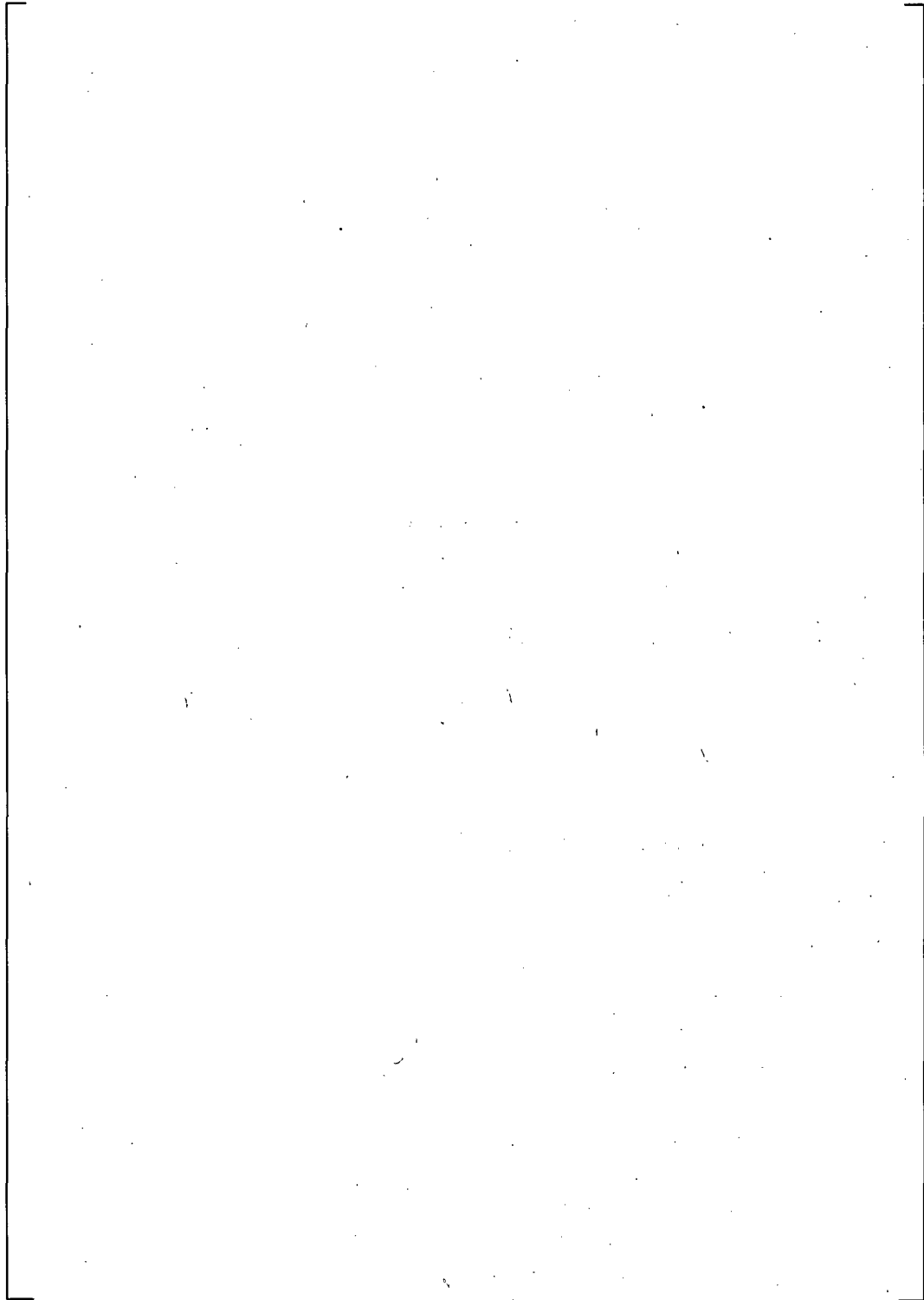


Figure 3
The Model F 17 Inch Expansion Tube/Collar Assembly

a,c,e

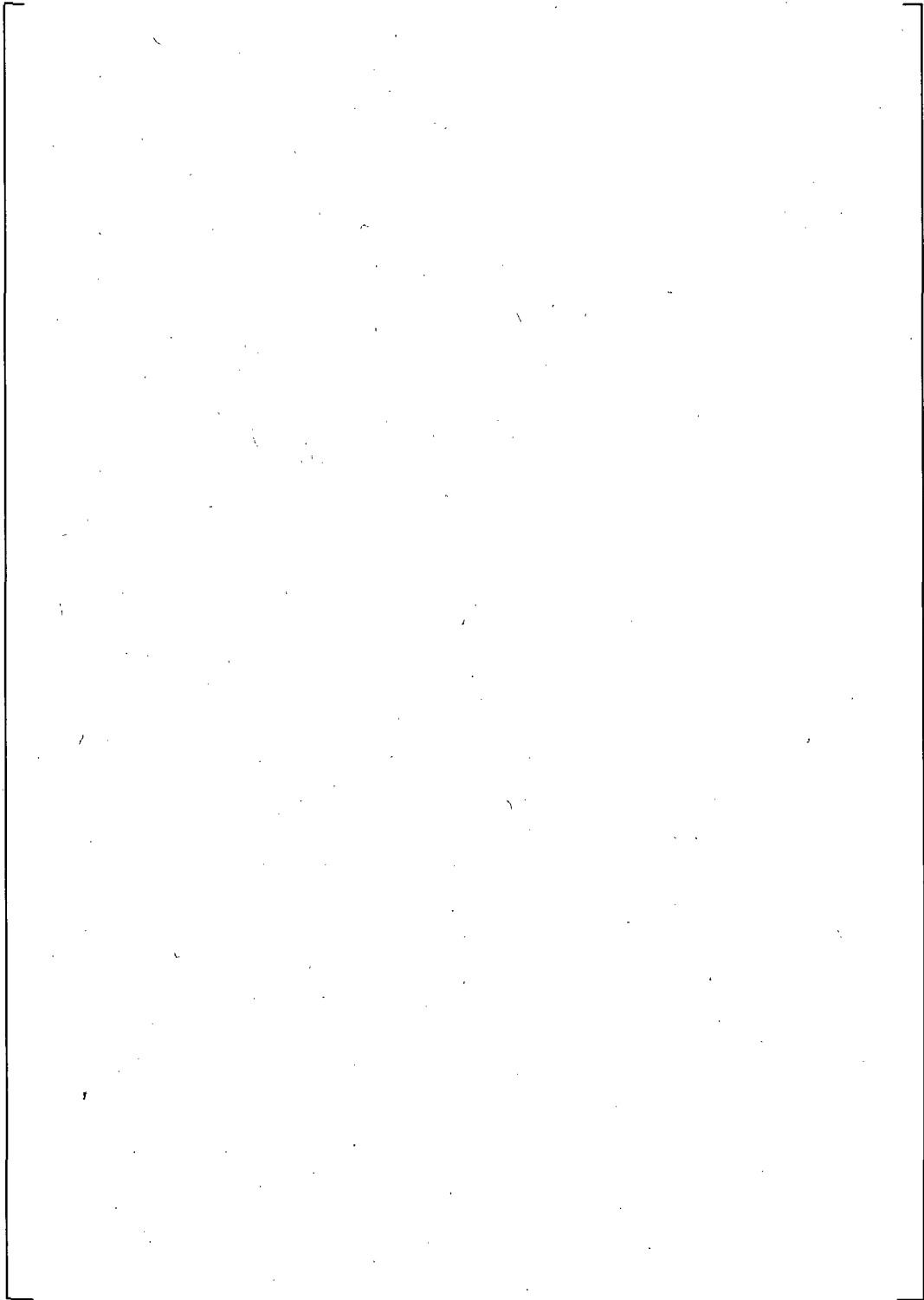


Figure 4
The Model D5 13 Inch Expansion Tube/Collar Assembly

a,c,e

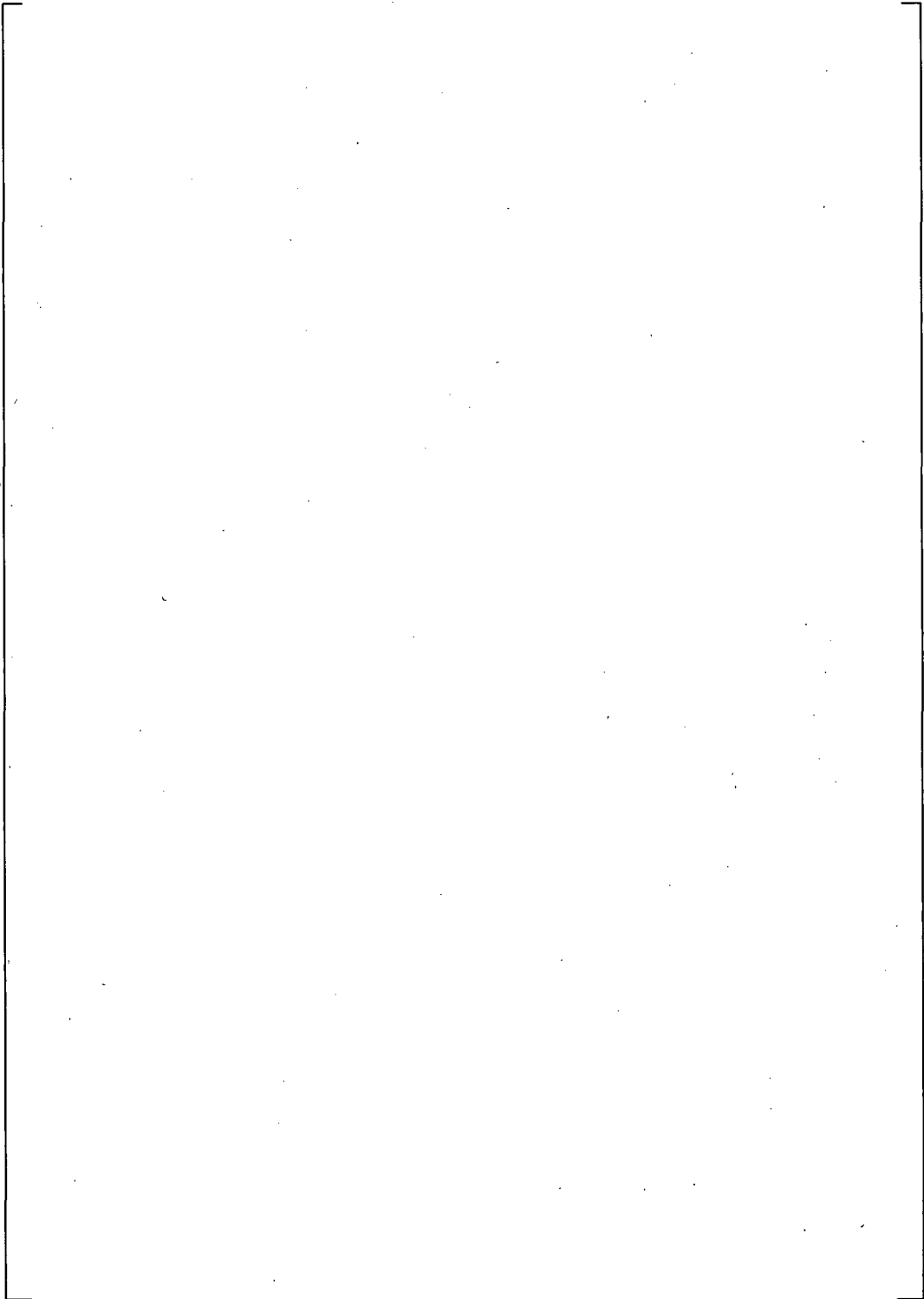


Figure 5
The Model D5 15 Inch Expansion Tube/Collar Assembly

a,c,e

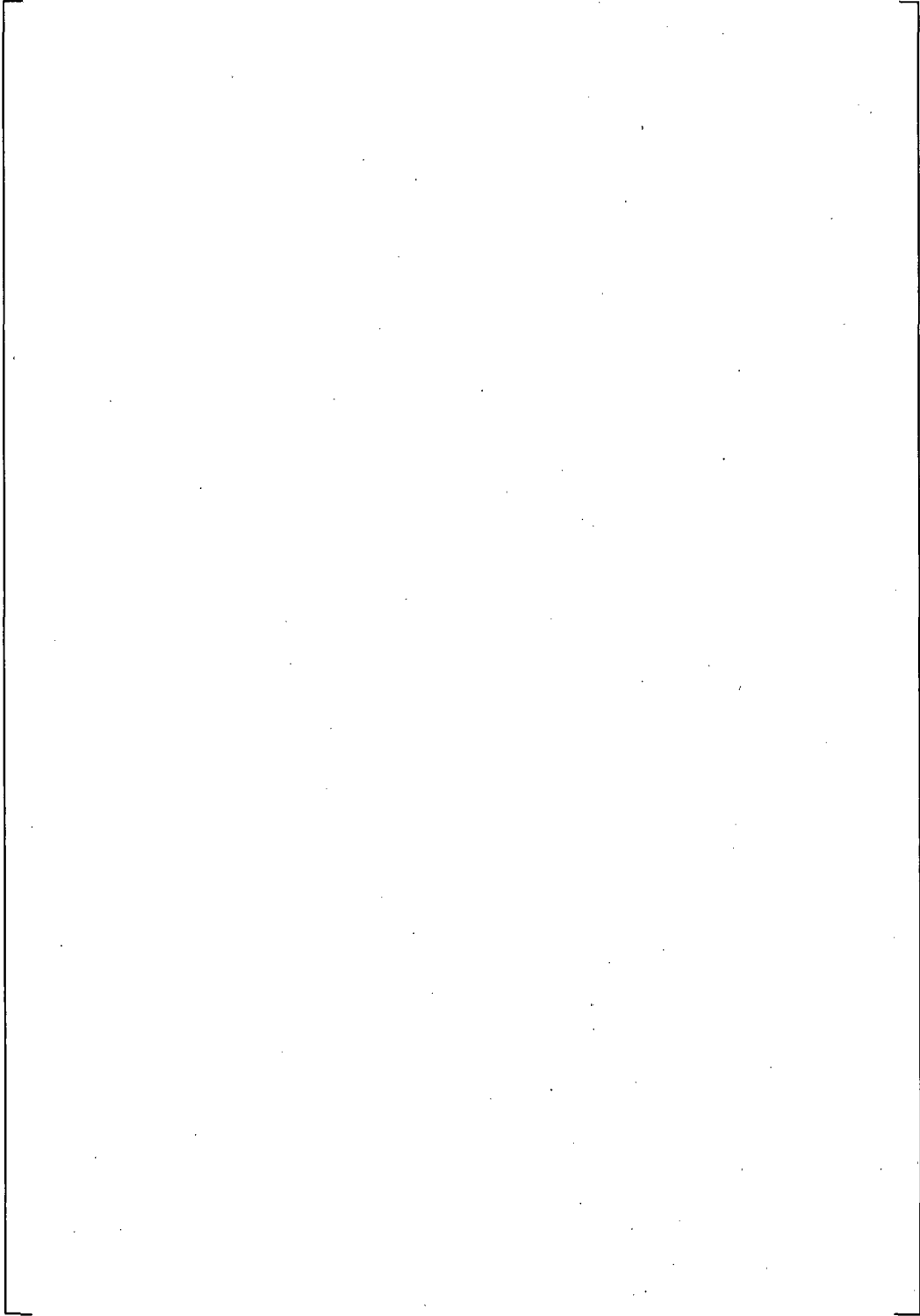


Figure 6
The Model D5 17 Inch Expansion Tube/Collar Assembly

a,c,e

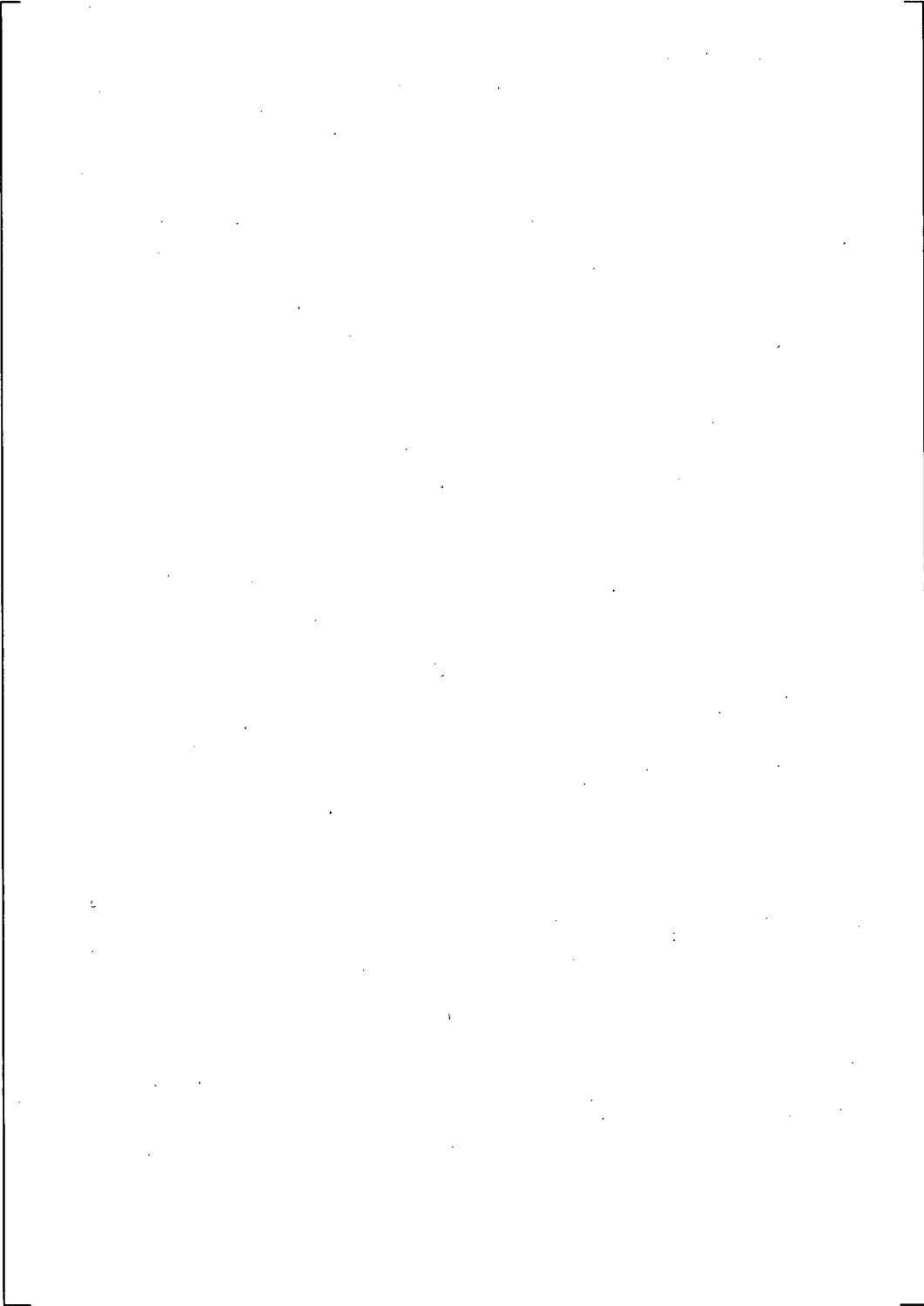


Figure 7
The Model 44F 13 Inch Expansion Tube/Collar Assembly

a,c,e

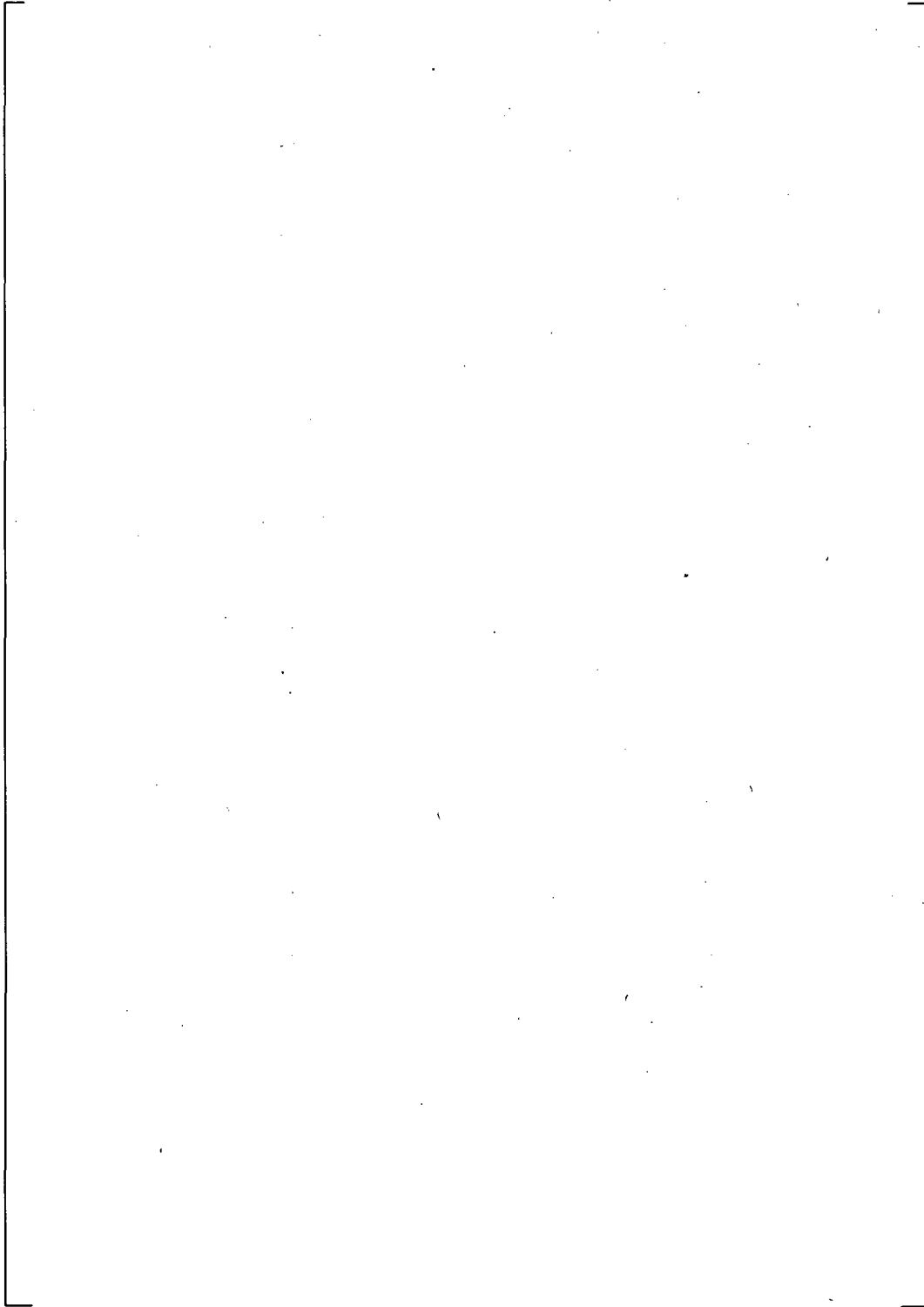


Figure 8
The Model 44F 15 Inch Expansion Tube/Collar Assembly

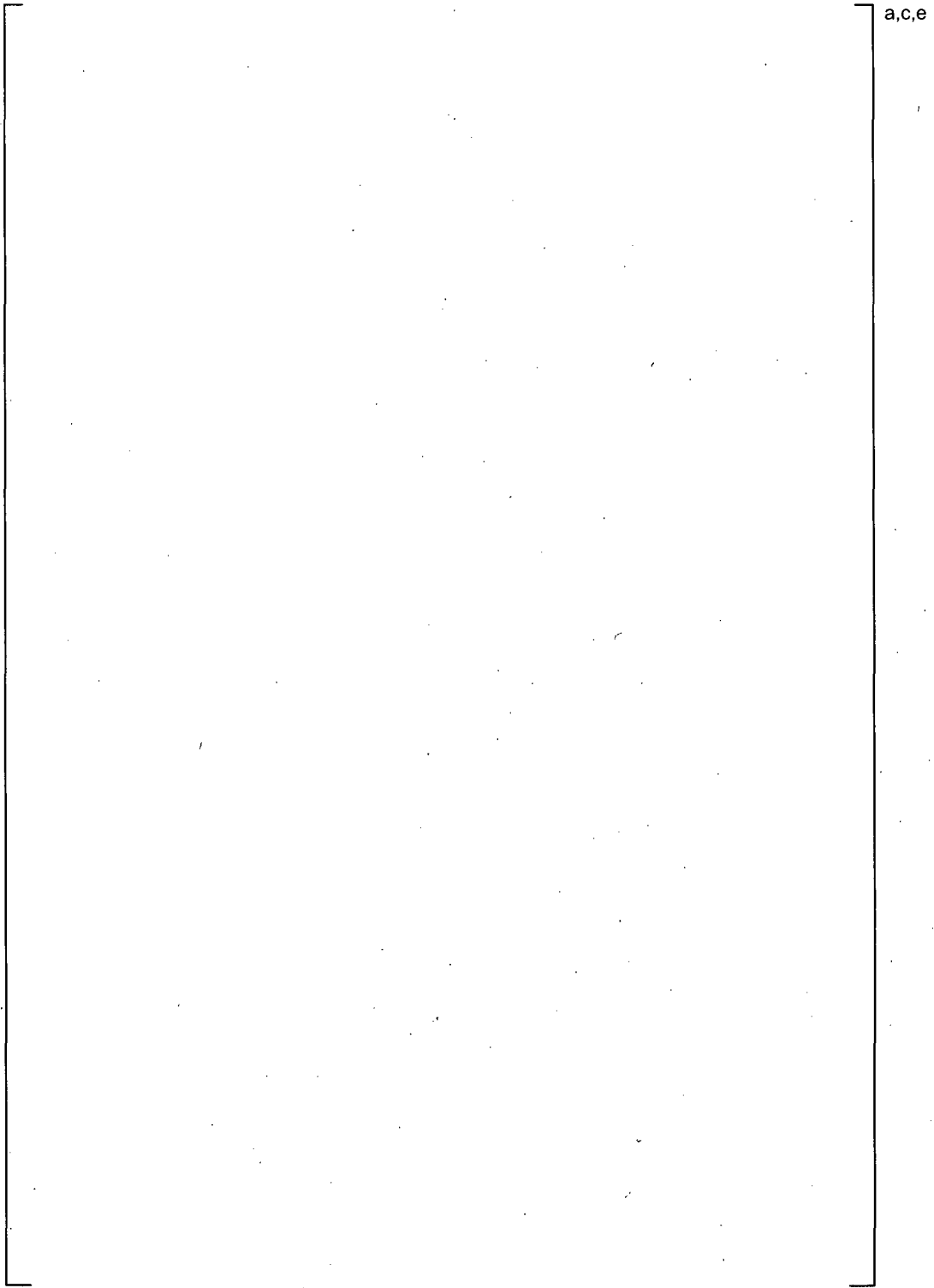


Figure 9
The Model 44F 17 Inch Expansion Tube/Collar Assembly

a,c,e

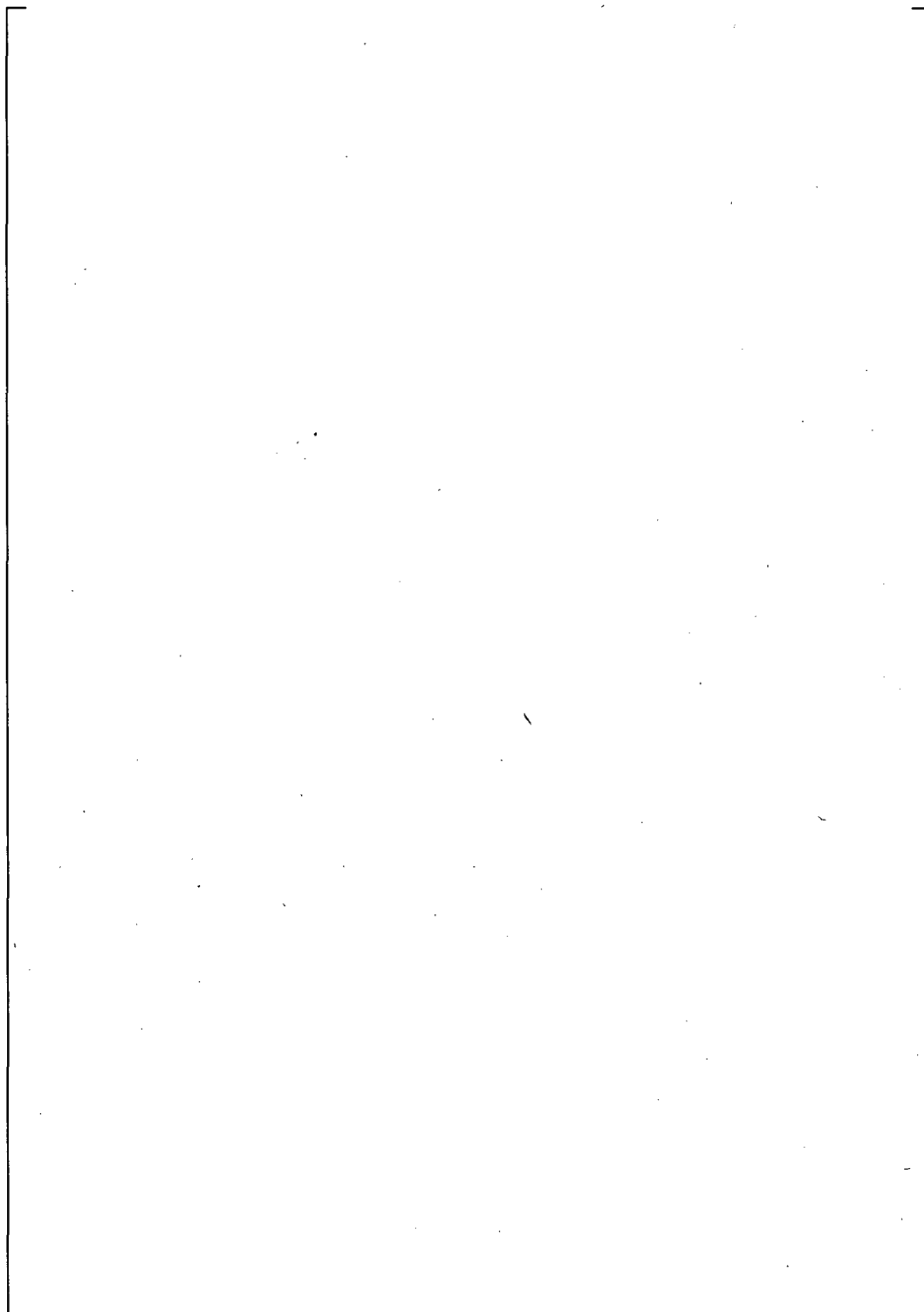
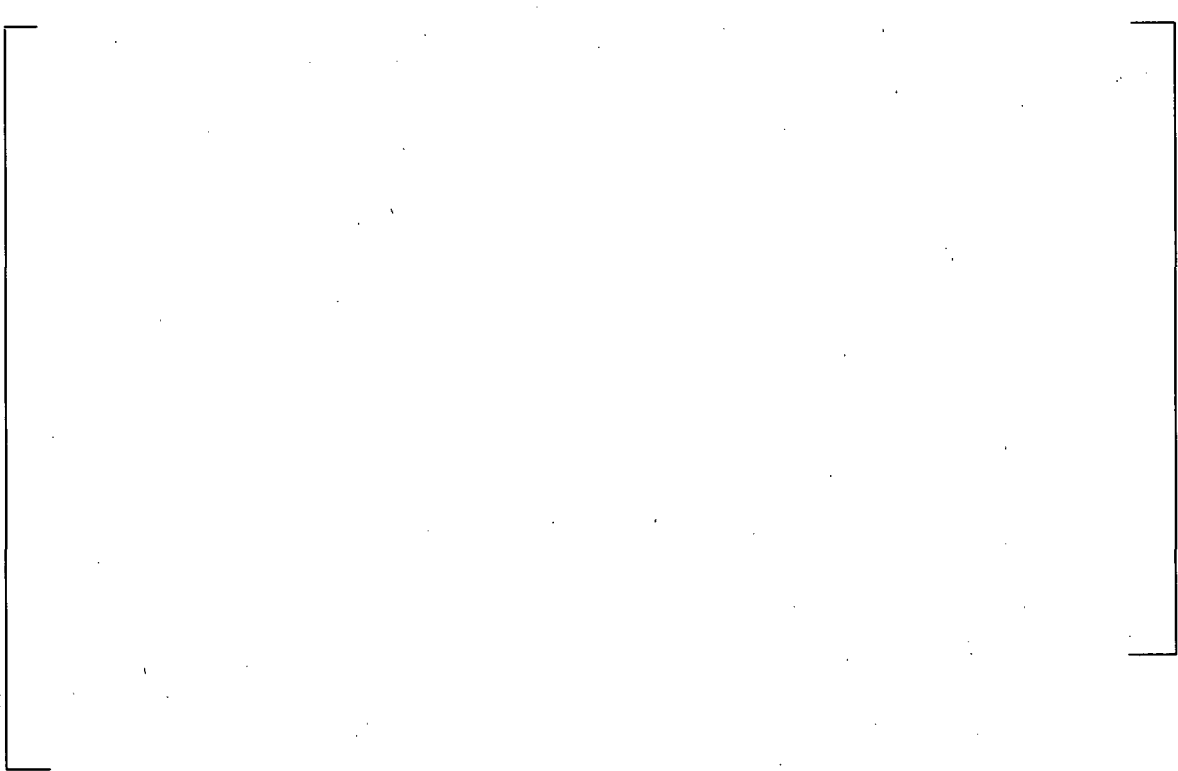


Figure 10
A Plot of Pull Out Force vs. Surface Roughness

a,c,e



Figure 11
The Pull Out Force vs. Expansion Length for a Given Tube OD



a,c,e

Serial No: 09-525
Docket No. 50-423

ENCLOSURE 12

**Westinghouse Electric Company LLC, LTR-SGMP-09-109 NP-Attachment, Response to
NRC Request for Additional Information on H*; RAI #4; Model F and Model D5 Steam
Generators, dated August 25, 2009.**

NON-PROPRIETARY

**DOMINION NUCLEAR CONNECTICUT, INC.
MILLSTONE POWER STATION UNIT 3**

Westinghouse Electric Company

**Response to
NRC Request for Additional Information on H*; RAI #4;
Model F and Model D5 Steam Generators**

August 25, 2009

Westinghouse Electric Company LLC
P.O. Box 158
Madison, PA 15663

© 2009 Westinghouse Electric Company LLC
All Rights Reserved

**Response to
NRC Request for Additional Information on H*; RAI #4;
Model F and Model D5 Steam Generators**

References:

1. NL-09-0547, Vogtle Electric Generating Plant License Amendment Request to Revise Technical Specification(TS) Sections 5.5.9, "Steam Generator (SG) Program" and TS 5.6.10, "Steam Generator Tube Inspection Report for Permanent Alternate Repair Criteria," Southern Company, May 19, 2009.
2. RS-09-071, "License Amendment Request to Revise Technical Specifications (TS) for Permanent Alternate Repair Criteria," Exelon Nuclear, June 24, 2009.
3. CP-200900748, Log # TXX-09075, "Comanche Peak Steam Electric Station (CPSES) Docket Nos. 50-445 and 50-446, License Amendment Request 09-007, Model D5 Steam Generator Alternate Repair Criteria," Luminant, June 8, 2009.
4. SBK-L-09118, "Seabrook Station: License Amendment Request 09-03; Revision to Technical Specification 6.7.6.k, "Steam Generator (SG) Program," for Permanent Alternate Repair Criteria (H*)," May 28, 2009.
5. Vogtle Electric Generating Plant, Units 1 and 2, Request for Additional Information Regarding Steam Generator Program (TAC Nos. ME1339 and ME1340)," United States Nuclear Regulatory Commission, July 10, 2009.
6. Braidwood Station, Units 1 and 2, and Byron Station, Unit Nos. 1 and 2 – Request for Additional Information Related to Steam Generator Permanent Alternate Repair Criteria (TAC Nos. ME1613, ME1614, ME1615, and ME1616)," United States Nuclear Regulatory Commission, July 20, 2009.
7. Comanche Peak Steam Electric Station, Units 1 and 2 – Request for Additional Information Regarding the Permanent Alternate Repair Criteria License Amendment Request (TAC Nos. ME1446 and ME1447)," United States Nuclear Regulatory Commission, July 23, 2009.
8. WCAP-17071-P, "H*: Alternate Repair Criteria for the Tubesheet Expansion Region in Steam Generators with Hydraulically Expanded Tubes (Model F)," Westinghouse Electric LLC, April 2009.
9. WCAP-17072-P, "H*: Alternate Repair Criteria for the Tubesheet Expansion Region in Steam Generators with Hydraulically Expanded Tubes (Model D5)," Westinghouse Electric LLC, May 2009.
10. "Vogtle Electric Generating Plant, Units 1 and 2, Request for Additional Information Regarding Steam Generator Program (TAC Nos. ME1339 and ME1340)," United States Nuclear Regulatory Commission, August 5, 2009

11. LTR-SGMP-09-100, "Response to NRC Request for Additional Information on H*; Model F and Model D5 Steam Generators," August 2009
12. LTR-NRC-09-26, "LTR-SGMP-09-66 P-Attachment, "White Paper: Low Temperature Steam Line Break Contact Pressure and Local Tube Bore Deformation Analysis for H* (Proprietary)," Westinghouse Electric Company LLC, May 13, 2009.
13. Seabrook Station, Unit No. 1- Request for Additional Information Regarding Steam Generator Program (TAC Nos. ME1386)," United States Nuclear Regulatory Commission, August 13, 2009

Introduction

In response to formal requests for technical specification amendments, References 1, 2, 3 and 4, the USNRC formally requested additional information in References 5, 6, 7 and 13. The Vogtle, Seabrook, Byron/Braidwood and Comanche Peak requests for a permanent license amendment to implement H* represent the Model F and Model D5 steam generators for which the H* technical justification is provided in References 8 and 9.

Subsequent to the initial issue of the RAI (References 5, 6, 7 and 13), the NRC issued follow-up questions (Reference 10) to questions numbers 4, 20 and 24 and an additional request regarding a technical specification (TS) commitment for applying the leakage factors. Except for RAI#4, responses to all of the RAIs, including the follow-up questions in Reference 10, were provided in Reference 11. The affected licensees provided separate responses in regard to the commitment for applying leakage factors.

The response to RAI#4 required additional explanation as discussed with the NRC staff on August 11, 2009 and was, therefore, not included in Reference 11. The additional questions related to RAI#4 that were identified during the August 11, 2009 telephone conference were summarized by Westinghouse and were the basis of the discussion at a meeting among the NRC, several licensees and Westinghouse on August 17 and 18, 2009. These additional questions are reproduced in the response to RAI#4, below. Specific discussion is included in the response to address the additional questions.

To summarize, this document provides the response to the initial RAI#4 as included in References 5, 6, 7 and 13, response to the follow-up question relating to RAI#4 in Reference 10 and response to the additional questions raised during the conference call on August 11, 2009.

Utilities, other than referenced in this document, have requested amendments to their licensees in parallel with the response to these RAIs. The technical RAIs are generic in nature because the analysis methods are the same for all affected plants. Therefore, this response to RAI#4 is generic for all Models of SGs that are candidates for application of H*. However, this letter

specifically augments Reference 11 to complete the responses to NRC RAIs for WCAP-17071-P (Model F H*) and WCAP-17072-P (Model D5 H*).

<p>RAI Part A</p>	<p>Vogtle</p>	<p>4. Reference 1, page 6-69: In Section 6.2.5.3; it is concluded that the tube outside diameter and the tubesheet tube bore inside diameter always maintain contact in the predicted range of tubesheet displacements. However, for tubes with through-wall cracks at the H* distance, there may be little or no net pressure acting on the tube for some distance above H*. In Tables 6-18 and 6-19, the fourth increment in the step that occurs two steps prior to the last step suggests that there may be no contact between the tube and tubesheet, over a portion of the circumference, for a distance above H*. Is the conclusion in Section 6.2.5.3 valid for the entire H* distance, given the possibility that the tubes may contain through-wall cracks at that location?</p>
	<p>WCGS</p>	<p>4. Reference 1, page 6-69: In Section 6.2.5.3, it is concluded that the tube outside diameter and the tubesheet tube bore inside diameter always maintain contact in the predicted range of tubesheet displacements. However, for tubes with through-wall cracks at the H* distance, there may be little or no net pressure acting on the tube for some distance above H*. In Tables 6-18 and 6-19, the fourth increment in the step that occurs two steps prior to the last step suggests that there may be no contact between the tube and tubesheet, over a portion of the circumference, for a distance above H*. Is the conclusion in 6.2.5.3 valid for the entire H* distance, given the possibility that the tubes may contain through-wall cracks at that location?</p>
	<p>B/B</p>	<p>4. Reference 1, Page 6-7: In Section 6.2.5.3, it is concluded that the tube outside diameter and the tubesheet tube bore inside diameter always maintain contact in the predicted range of tubesheet displacements. However, for tubes with through-wall cracks at the H* distance, there may be little or no net pressure acting on the tube for some distance above H*. In Tables 6-18 and 6-19, the fourth increment in the step that occurs two steps prior to the last step suggests that there may be no contact between the tube and tubesheet, over a portion of the circumference, for a distance above H*. Is the conclusion in 6.2.5.3 valid for the entire H* distance, given the possibility that the tubes may contain through-wall cracks at that location.</p>

CPSES	<p>4. Reference 1, page 6-70: In Section 6.2.5.3, it is concluded that the tube outside diameter and the tubesheet tube bore inside diameter always maintain contact in the predicted range of tubesheet displacements. However, for tubes with through-wall cracks at the H^* distance, there may be little or no net pressure acting on the tube for some distance above H^*. In Tables 6-18 and 6-19, the fourth increment in the step that occurs two steps prior to the last step suggests that there may be no contact between the tube and tubesheet, over a portion of the circumference, for a distance above H^*. Is the conclusion in Section 6.2.5.3 valid for the entire H^* distance, given the possibility that the tubes may contain through-wall cracks at that location?</p>
Seabrook	<p>4. Reference 1, page 6-69: In Section 6.2.5.3, it is concluded that the tube outside diameter and the tubesheet tube bore inside diameter always maintain contact in the predicted range of tubesheet displacements. However, for tubes with through-wall cracks at the H^* distance, there may be little or no net pressure acting on the tube for some distance above H^*. In Tables 6-18 and 6-19, the fourth increment in the step that occurs two steps prior to the last step suggests that there may be no contact between the tube and tubesheet, over a portion of the circumference, for a distance above H^*. Is the conclusion in 6.2.5.3 valid for the entire H^* distance, given the possibility that the tubes may contain through-wall cracks at that location?</p>

Part B: The additional questions relating to RAI#4 as provided in Reference 10 are:

Address following questions as part of response to RAI#4 (Vogtle):

- a. Clarify the nature of the finite element model ("slice" model versus axisymmetric SG assembly model) used to generate the specific information in Tables 6-1, 2, and 3 (and accompanying graph entitled "Elliptical Hole Factors") of Reference 6-15. What loads were applied? How was the eccentricity produced in the model? (By modeling the eccentricity as part of the geometry? By applying an axisymmetric pressure the inside of the bore?) Explain why this model is not scalable to lower temperatures.
- b. Provide table showing maximum delta diameters (total diameter distortion) and maximum eccentricities (maximum diameter minus minimum diameter) from the 3 dimensional (3-D) finite element analysis for normal operating and steam line break (SLB), for model F and D5.
- c. In Figure 2 of the White Paper, add plot for original relationship between reductions in contact pressure and eccentricity as given in Reference 6-15 in the graph accompanying Table 6-3. Explain why this original relationship remains conservative

in light of the new relationship. Explain the reasons for the differences between the curves.

- d. When establishing whether contact pressure increases when going from normal operating to steam line break conditions, how can a valid and conservative comparison be made if the normal operating case is based on the original delta contact pressure versus eccentricity curve and the SLB case is based on the new curve?

Part C: Additional Questions Provided in the August 11, 2009 telephone conference:

a. Overall High Level Question

1. Discuss if the eccentricity effect on contact pressure is occurring as described. It is the opinion of the NRC staff that the eccentricity effect may not be as significant as being reported by Westinghouse.

b. Other Key Questions

1. The eccentricities included in Table RAI 4-4 appear larger than anticipated. Need to confirm that positive contact pressure exists around the entire circumference of the tube and state this clearly in the response.
2. The difference between initial and final eccentricity included in Table RAI4-2 needs to be explained. In particular, the exclusive use of the relationship between initial eccentricity and scale factor in calculating contact pressure needs to be justified.
3. The basis for applying the correlation for scale factor outside an "eccentricity" range of between 1E-3 to 1E-4 inch in the calculation of contact pressure needs to be further explained. Values for displacements included in Table 6-18 (of WCAP-17071) suggest that contact pressure may be lost at displacement ranging between 1E-3 in to 1E-4 inch.
4. Provide the calculation basis for the upper and lower curves provided in Figure RAI 4-2
5. Resolve the apparent inconsistency between Item 4 on page 25 and the statement below Figure RAI4-1 regarding how the model in Figure RAI4-1 is loaded.

c. Key Remaining Issues

1. Provide the basis for why the ΔD_{hole} adjustment for contact pressure made using the old model remains conservative.
2. Provide an appropriate basis for demonstrating that joints tighten during a postulated SLB event. Why is it acceptable to compare the contact pressures calculated using the original model for NOP to the contact pressures calculated using the new model for SLB for the Model D5 SGs?
3. If both old and new models are conservative, is there an appropriate basis to show the relative conservatism of the methods?

To facilitate a continuous response to the total RAI#4 questions, the questions received originally (Part A), those received as follow-up questions (Part B) and those identified during the 8/11/09 telephone conference (Part C) are re-arranged as noted below. The location of responses to specific questions is shown in bold type after the question. Also, in the responses, the specific questions addressed by the responses are repeated in bold type in the box at the start of the response.

Part C: Sub a.

Discuss if the eccentricity effect on contact pressure is occurring as described. It is the opinion of the NRC staff that the eccentricity effect may not be as significant as being reported by Westinghouse. (See Section 1.0)

Part B

Address following questions as part of response to RAI#4 (Vogtle):

- a. *Clarify the nature of the finite element model ("slice" model versus axisymmetric SG assembly model) used to generate the specific information in Tables 6-1, 2, and 3 (and accompanying graph entitled "Elliptical Hole Factors") of Reference 6-15. What loads were applied? How was the eccentricity produced in the model? (By modeling the eccentricity as part of the geometry? By applying an axisymmetric pressure the inside of the bore?) Explain why this model is not scalable to lower temperatures. (See Section 1.2)*
- b. *Provide table showing maximum delta diameters (total diameter distortion) and maximum eccentricities (maximum diameter minus minimum diameter) from the 3 dimensional (3-D) finite element analysis for normal operating and steam line break (SLB), for model F and D5. (See Section 1.1)*
- c. *In Figure 2 of the White Paper, add plot for original relationship between reductions in contact pressure and eccentricity as given in Reference 6-15 in the graph accompanying Table 6-3. Explain why this original relationship remains conservative in light of the new relationship. Explain the reasons for the differences between the curves. (See Section 4.1)*
- d. *When establishing whether contact pressure increases when going from normal operating to steam line break conditions, how can a valid and conservative comparison be made if the normal operating case is based on the original delta contact pressure versus eccentricity curve and the SLB case is based on the new curve? (See Section 4.2)*

Part C: Sub b. Other Key Questions

1. The eccentricities included in Table RAI 4-4 appear larger than anticipated. Need to confirm that positive contact pressure exists around the entire circumference of the tube and state this clearly in the response. **(See Section 3)**
2. The difference between initial and final eccentricity included in Table RAI4-2 needs to be explained. In particular, the exclusive use of the relationship between initial eccentricity and scale factor in calculating contact pressure needs to be justified. **(See Section 1.2)**
3. The basis for applying the correlation for scale factor outside an "eccentricity" range of between 1E-3 to 1E-4 inch in the calculation of contact pressure needs to be further explained. Values for displacements included in Table 6-18 (of WCAP-17071) suggest that contact pressure may be lost at displacement ranging between 1E-3 in to 1E-4 inch. **(See Section 2.0)**
4. Provide the calculation basis for the upper and lower curves provided in Figure RAI 4-2. **(See Section 2.1)**
5. Resolve the apparent inconsistency between Item 4 on page 25 and the statement below Figure RAI4-1 regarding how the model in Figure RAI4-1 is loaded. **(See Section 1.2)**

Part C: Sub c. Key Remaining Issues

1. Provide the basis for why the ΔD_{hole} adjustment for contact pressure made using the old model remains conservative. **(See Section 2.2)**
2. Provide an appropriate basis for demonstrating that joints tighten during a postulated SLB event. Why is it acceptable to compare the contact pressures calculated using the original model for NOP to the contact pressures calculated using the new model for SLB for the Model D5 SGs? **(See Section 2.3)**
3. If both old and new models are conservative, is there an appropriate basis to show the relative conservatism of the methods? **(See Section 2.4)**

Part A: (Original RAI#4 from Reference 5)

Reference 1, Page 6-69: In Section 6.2.5.3, it is concluded that the tube outside diameter and the tubesheet tube bore inside diameter always maintain contact in the predicted range of tubesheet displacements. However, for tubes with through-wall cracks at the H^* distance, there may be little or no net pressure acting on the tube for some distance above H^* . In Tables 6-18 and 6-19, the fourth increment in the step that occurs two steps prior to the last step suggests that there may be no contact between the tube and tubesheet, over a portion of the circumference, for a distance above H^* . Is the conclusion in 6.2.5.3 valid for the entire H^* distance, given the possibility that the tubes may contain through-wall cracks at that location? **(See Section 5.0)**

1.0 General Background on Approach and Models

Discuss if the eccentricity effect on contact pressure is occurring as described. It is the opinion of the NRC staff that the eccentricity effect may not be as significant as being reported by Westinghouse.

Response:

The reference structural model for the H^* calculation as described in References 8 and 9 is a 3D FEA model that utilizes the equivalent properties approach for perforated plates in accordance with Reference 6-15 of the H^* WCAP reports. This model provides the tubesheet displacements that are utilized in the calculation of H^* . Included in the displacement output from the 3D FEA model are the radius and depth dependent x- and y- axis displacements for the tubesheet. These displacements are the input to the H^* integrator model that uses the inputs to calculate contact pressures based on thick-shell equations. The tubesheet displacements from the FEA model indicate that the tubesheet bores become eccentric after application of all thermal and pressure loads. The displacement results from the 3D FEA model are the difference between the completely unloaded case and the fully loaded case for the conditions of interest (i.e., NOP, SLB).

The information from the 3D FEA model, that the tubesheet bores become eccentric, led to a question regarding continued tube-to-tubesheet contact in the eccentric tubesheet bore. The impact of tubesheet bore hole out-of-roundness (eccentricity) on the calculation of tube to-tubesheet contact pressures was originally addressed using a scale factor approach as described below and in Reference 6-15 of the H^* WCAP reports. The fit developed in Reference 6-15, a third order polynomial, was appropriate for the conditions for which it was developed but it provided physically impossible results when extrapolated significantly outside its data basis such as was the case for the SLB conditions for the Model D5 SGs.

To resolve this issue, a separate model, was developed as described in Section 6.2.5 and shown in Figure 6-48 of Reference 8 and 9, to assess tube-to-tubesheet contact under the fully loaded condition (e.g., ΔP and thermal loading) for the small eccentricities that were calculated during the much "colder" temperature postulated SLB conditions for the Model D5 SGs than for the Model F SGs. To properly represent the tube in tubesheet condition, this model considered a tubesheet equivalent cell (the local TS material around a tubesheet bore) and a tube. To address the question if continued contact would exist between the tube and tubesheet after the tubesheet bore becomes eccentric, the tube expansion was analytically simulated to provide a condition of tube to tubesheet contact in a non-eccentric tubesheet bore. This condition was the reference condition for the subsequent loading of the model by pressure loads (thermal loads were not included) and by applying displacement boundary conditions (e -bar) to simulate the expected range of tubesheet bore eccentricity. The unloaded, post-tube expansion simulation conditions of the model was the reference condition for the displacements provided in Tables 6-18 and 6-19 of the H^* reports, References 8 and 9.

While eccentricity was the specific focus of this study because of the question raised about continued tube to tubesheet contact in an eccentric condition, the analytical model naturally also provided information on tubesheet bore dilation, the diametral growth of the tubesheet bore represented by the average of the maximum and minimum diameters of the eccentric tubesheet bore. Examination of the results from this model, as is discussed further below, resulted in two significant conclusions:

1. For the tubesheet bore eccentricities and dilation due to the applied loading in the limiting plants in the models of SG considered, the tube remains in contact with the tubesheet bore.
2. While tubesheet bore eccentricity contributes to the reduction in contact pressure between the tube and the tubesheet, tubesheet bore dilation appears to be the principal cause of reduction of contact pressure between the tube and the tubesheet.

1.1 Discussion of 3D FEA Model for H* Analysis

Provide table showing maximum delta diameters (total diameter distortion) and maximum eccentricities (maximum diameter minus minimum diameter) from the 3 dimensional (3-D) finite element analysis for normal operating and steam line break (SLB), for model F and D5.

Response:

The 3D FEA Model and its application for determining the tubesheet displacements are extensively described in Section 6 of the H* WCAP reports (References 8 and 9). It is important to note that the 3D FEA model includes the entire tubesheet complex (i.e., tubesheet, stub barrel, channelhead and divider plate) but excludes the tubes. The model utilizes an equivalent material approach from Reference 6-5 in the WCAP reports to represent the deformation of the tubesheet under the applied loading conditions (NOP, SLB/FLB). Displacements in Cartesian coordinates are calculated for these conditions at any location on the tubesheet. The displacements calculated are the changes from an unstressed, room temperature condition after all thermal and pressure loads appropriate to the operating conditions are applied. Application of a uniform temperature increase causes uniform dilation at each tubesheet bore. Application of pressure loads causes distortions in the structure due to bending. The 3D FEA model provides integrated total displacements of each tubesheet bore location.

Table RAI4-1 is a summary of the maximum eccentricities and ΔD s for the Model F and Model D5 limiting plants as calculated based on the U_R (tubesheet radial displacement) results from the 3-D lower SG complex model.

Table RAI4-1: Summary of Model D5 and Model F NOP and SLB Eccentricity Results

SG Model	Elev.	Avg. Eccentricity Data		Max. Eccentricity Data		Avg. Δ D		Max. Δ D	
		NOP	SLB	NOP	SLB	NOP	SLB	NOP	SLB
-	Above BTS ⁽¹⁾								
-	in	in/in	in/in	in/in	in/in	in	in	in	in
F									
F									
F									
D5									
D5									
D5									
F									
D5									

a,c,e

Notes:
1. BTS is Bottom of the Tubesheet

The original Table RAI4-4 is provided here for convenience

Plant	Condition	Value	Eccentricity, e	Δ D, 0°	Δ D, 90°
			inch/inch	inch	inch
Byron	SLB	MAX			
Byron	SLB	MIN			
Byron	SLB	AVG			
Millstone	SLB	MAX			
Millstone	SLB	MIN			
Millstone	SLB	AVG			
Byron	NOP	MAX			
Byron	NOP	MIN			
Byron	NOP	AVG			
Millstone	NOP	MAX			
Millstone	NOP	MIN			
Millstone	NOP	AVG			

a,c,e

1.2 Discussion of the "Slice" Model

Clarify the nature of the finite element model ("slice" model versus axisymmetric SG assembly model) used to generate the specific information in Tables 6-1, 2, and 3 (and accompanying graph entitled "Elliptical Hole Factors") of Reference 6-15. What loads were applied? How was the eccentricity produced in the model? (By modeling the eccentricity as part of the geometry? By applying an axisymmetric pressure the inside of the bore?) Explain why this model is not scalable to lower temperatures.

The difference between initial and final eccentricity included in Table RAI4-2 needs to be explained. In particular, the exclusive use of the relationship between initial eccentricity and scale factor in calculating contact pressure needs to be justified.

Resolve the apparent inconsistency between Item 4 on page 25 and the statement below Figure RAI4-1 regarding how the model in Figure RAI4-1 is loaded.

Response:

The "slice model" is shown in Figure 6-9 of Reference 6-15 in WCAP-17071-P, WCAP-17072-P, WCAP-17091-P, and WCAP-17092-P.

The data in Tables 6-1, 6-2, and 6-3 of Reference 6-15 of the H* WCAP reports, are derived from this plane stress model ("slice model") developed in WECAN/PLUS and the contact pressure equation identified on page 6-87 of WCAP-17071-P, page 6-95 of WCAP-17072-P, page 6-91 of WCAP-17091-P and page 6-84 of WCAP-17092-P as described below.

For convenience Tables 6-1, 6-2, and 6-3 of Reference 6-15 are replicated below and re-named as follows: Table 6-1 is renamed as Table RAI4-2, Table 6-2 is renamed as Table RAI 4-3, and Table 6-3 is renamed as Table RAI4-4.

The "initial" eccentricities (defined as $D_{MAX} - D_{MIN}$) applied in the "slice" model in Table RAI4-3 and Table RAI4-4 are directly incorporated into the model geometry. That is, the initial eccentricity is built into the model geometry. The eccentricity values in the model were assumed values for tubesheet tube bore deformation based on engineering judgment and prior experience.

In the "slice" model analysis, the tubesheet is assumed to have a thermal expansion coefficient of zero (0) in/in/°F and the tube material is assumed to have the appropriate ASME Code thermal expansion coefficient values. (The TS coefficient of thermal expansion is set to zero to provide a loading mechanism for the model. When a temperature is applied, the tube "grows" into the tubesheet collar. The temperature difference applied to the tube in the "slice" model was 500°F, for a total tube temperature of 570°F. [Applied 500°F + 70°F assumed room temperature]). The sole purpose of the development of the "slice" model was to provide a sensitivity study to relate the effects of assumed eccentricity ($D_{MAX} - D_{MIN}$) conditions to contact pressures from which the contact pressure ratios were developed. No attempt was made to

reproduce the contact pressures that would be calculated by the 2-D axisymmetric model that was previously used to develop the tubesheet displacements.

The "final" eccentricity ($D_{MAX} - D_{MIN}$) values in Table RAI4-3 and Table RAI4-4 were also determined using the "slice model": The final eccentricity values are the ($D_{MAX} - D_{MIN}$) results of applying the loading conditions on the slice model: The loads applied to the "slice" model were thermal loads only as follows:

- 0 psig - Primary Side Pressure
- 0 psig - Secondary Side Pressure
- 500 °F- Tubesheet ΔT
- 500 °F- Channel Head ΔT
- 500 °F- Shell ΔT

As discussed in Reference 6-15, Table RAI4-3 was constructed using the displacement results from the plane stress model analysis for the elliptical holes along with the contact pressure equations. The effective change in hole diameter was calculated as follows using a series of assumed scale factors:

$$\left[\begin{array}{c} \text{a,c,e} \\ \text{---} \\ \text{---} \\ \text{---} \end{array} \right] \quad \text{(RAI4-1)}$$

The ΔD_{MAX} and ΔD_{MIN} were taken from the radial and circumferential change in tube bore diameter in the "slice" model.

The corresponding contact pressure for each scale factor was then determined as follows:

$$\left[\begin{array}{c} \text{a,c,e} \\ \text{---} \\ \text{---} \\ \text{---} \end{array} \right] \quad \text{(RAI4-2)}$$

Equation RAI4-2 is a generic representation of how tube to tubesheet contact pressure is calculated in the H* integrator spreadsheet analysis. The equation is equivalent to the equation for P2 shown on page 6-87 in WCAP-17071-P, page 6-95 in WCAP-17072-P, page 6-91 in WCAP-10791-P and page 6-84 in WCAP-17092-P.

The scale factors for a given input eccentricity in Table RAI 4-3 result in contact pressure ratios using the thick shell equations that are equal to the contact pressure ratios calculated using the "slice" model for initial eccentricities (defined as $D_{MAX} - D_{MIN}$) equivalent to 0.0002, 0.0004, 0.0006 and 0.0008 inches, respectively, compared to the contact pressures for a circular hole ($D_{MAX} - D_{MIN} = 0$). These scale factors are identified in bold print in Table RAI4-3. The data for the scale factors as a function of "initial" eccentricity was fit by a third order polynomial equation provided on page 6-85 of WCAP-17071-P and page 6-86 of WCAP-17072-P.

Based on a review of Table RAI4-3 and Table RAI4-4, the scale factor []^{a,c,e} is the appropriate scale factor for calculating a reduction factor for contact pressure of []^{a,c,e} associated with an initial eccentricity of []^{a,c,e} ((D_{MAX} - D_{MIN})/ []^{a,c,e} inch) from the "slice" model. The scale factor of []^{a,c,e} relates to a contact pressure reduction factor of []^{a,c,e} and corresponds to an initial eccentricity of []^{a,c,e} inch, and so forth.

The "final eccentricity" values corresponding to the same scale factors highlighted in bold in Table RAI 4-3 (and Table RAI4-4) are not used in determining the reduction in contact pressure because the resulting third order polynomial relationship between scale factor and eccentricity is bounded by the relationship for "initial eccentricity", i.e., the resultant scale factors, and hence the reduction in contact pressure due to eccentricity, would be less using the third order fit resulting from the "final" eccentricity values from Table RAI 4-3. For example, for an eccentricity of 1E-3 in/in, the scale factor is []^{a,c,e} as compared to []^{a,c,e} for the trend line associated with the "initial" eccentricity results. Figure RAI 4-1 illustrates this. This figure shows a comparison of the trend line analysis for "initial" eccentricity and "final" eccentricity. Referring to Equation RAI 4-1, larger scale factors result in a greater reduction in contact pressure due to eccentricity.

Table RAI4-2
Reproduced Table 6-1 of Reference 6-15

Eccentricity (inch)	Sleeve O.D.			Tube O.D.		
	Average ⁽¹⁾	Ratio ⁽³⁾	Delta ⁽¹⁾⁽²⁾	Average ⁽¹⁾	Ratio ⁽³⁾	Delta ⁽¹⁾⁽²⁾
0.0000						
0.0002						
0.0004						
0.0006						
0.0008						

a,c,e

Notes: This table is developed from the model shown in Figure RAI4-1, below.

1. The units of these columns are stress in psi.
2. The "delta" in this table refers to the maximum deviation from a constant value of the mean linearized radial stress around the tube bore.
3. The ratio is calculated by dividing the contact pressure between the tube and the tubesheet at a given eccentricity by the contact pressure between the tube and the tubesheet in a round tube bore (e=0.0). For example, the ratio of []^{a,c,e} calculated in Table 6-1 is a ratio of the average contact pressure at an eccentricity of 0.0002 in of []^{a,c,e} psi divided by the average contact pressure at an eccentricity of []^{a,c,e} psi.

Table RAI4-3

Reproduction of Table 6-2 of Reference 6-15

Primary Pressure	0	psig
Secondary Pressure	0	psig
Tubesheet Delta T	500	°F
Shell Delta T	500	°F
Channel Head Delta T	500	°F
Sleeve OD Delta D	[] ^{a,c,e} in
Tube ID Delta D	[] ^{a,c,e} in
Tube OD Delta D (Thermal)	[] ^{a,c,e} in
Sleeve/Tube Interaction Coefficients	[] ^{a,c,e}
Tube/Tubesheet Interaction Coefficients	[] ^{a,c,e}

Eccentricity		(1)	(2)	(3)	(4)	(5)	(6)
Initial (inch)	Final (inch)	Max/Min Combination _{a,c,e}	Hole Delta D (0 Deg)	Hole Delta D (90 Deg)	S/T Contract Pressure	T/TS Contact Pressure	Ratio
0.0000		Minimum Average Maximum					
0.0002		Minimum Average _{a,c,e} <div style="border: 1px solid black; width: 50px; height: 50px; margin: 0 auto;"></div> Maximum					
0.0004		Minimum Average _{a,c,e} <div style="border: 1px solid black; width: 50px; height: 50px; margin: 0 auto;"></div> Maximum					

Table RAI4-3 (Cont'd.)

Eccentricity ^{a,c,e}	(1)	(2)	(3)	(4)	(5)	(6)	^{a,c,e}
0.0006	Minimum						
	Average ^{a,c,e}						
	Maximum						
0.0008	Minimum						
	Average ^{a,c,e}						
	Maximum						

Note: The values in **Bold** identify the source data for Table RAI4-3

Table RAI4-4

Reproduction of Table 6-3 of Reference 6-15

Initial Delta Dia (in)	Eccentricity ⁽¹⁾		Max/Min Factor	Pressure Ratio
	Initial (in/in)	Final (in/in)		
0.0000				
0.0002				
0.0004				
0.0006				
0.0008				

(1) These values are the values for initial and final eccentricity from Table RAI4-2 are divided by the nominal tubesheet hole diameter []^{a,c,e}

[]^{a,c,e}

a,c,e



Figure RAI4-2: Scale Factor Comparison (Initial versus Final Eccentricity)

The method for calculating the contact pressure for using the “old” method for the Model F SGs (all plant conditions) and the Model D5 SGs (NOP and FLB conditions) and the “new” method for calculating the contact pressure the Model D5 SGs only (SLB conditions) are described below:

Old Method (Reference 6-15):

1. The U_R used in the calculation of the circumferential and radial ΔD is based on the linearly scaled 2D axisymmetric FEA model (3-D model for the current H^* analysis) of the lower SG complex
2. The circumferential and radial ΔD 's are used in the scale factor (SF) equation to determine the ΔD_{hole} (see equation RAI4-1) that is used to determine the reduction in contact pressure as a function of eccentricity (e), equation RAI4-2.
3. The relationship between $11D$ and e is based on the 2-D plane model shown in Figure 6-9 of SM-94-58, Rev.1.

4. The model in Figure 6-9 of SM-94-58, Rev.1 includes the initial applied eccentricities ($D_{MAX} - D_{MIN}$) geometry definition of the model.
5. The "slice" model provides the input for using the SF relationship (Eqn. RAI4-1). The SF is determined by comparing the "slice" model results to the axisymmetric model results for a TS collar and tube model at a given radius in the TS over the full thickness of the TS.
6. The result is then used to calculate the reduction in contact pressure as a function of TS elevation and radius due to TS displacement and tube bore eccentricity. This is appropriate because the conditions for the Model F SG and Model D5 SG (NOP and FLB conditions) are within the range of data for which the scale factor relationship is applicable.

New Method (WCAP-17071-P, WCAP-17072-P):

1. The U_R used in the calculation of the circumferential and radial ΔD comes from a 3-D FEA model of the lower SG complex with condition-specific inputs applied.
2. The circumferential and radial ΔD 's are compared to determine the maximum ΔD that will give the maximum reduction in contact pressure as a function of eccentricity (e).
3. The relationship between ΔD and e is based on the 2-D []^{a,c,e} model shown in WCAP-17071-P and WCAP-17072-P, section 6.2.5. The model is shown in Figure 6-49 of the WCAP reports. The range of eccentricity used in this study conservatively exceeds the values of tube bore eccentricity calculated from the perforated TS model in Section 6.2.4.
4. The model in Figure 6-49 of the H* WCAP reports applies boundary conditions to the outer edge of the tube pitch material and does not directly affect the material that is deforming in the tube and tubesheet cell.
5. The TS deformations and tube to tubesheet contact pressure results that produce the maximum reduction in contact pressure at the minimum value of TS tube bore eccentricity are then fit with a linear relationship.
6. The result of the linear relationship is used to determine the reduction in contact pressure between the tube and the tubesheet directly. There are no intermediate equations or results.

A correct prediction of contact pressure loss requires the knowledge of both the proper values of D_{MAX} and D_{MIN} associated with the different pressure and temperature conditions at a given tubesheet radius and elevation as well as the value of eccentricity. The values of D_{MAX} and D_{MIN} are a function of the radial deflection of the tubesheet, U_R , as determined by the finite element analysis model (which previously was a 2-D axisymmetric model of the SG lower

assembly and at present, is a 3-D model of the SG lower assembly). The results from the "slice" model cannot be linearly scaled to lower temperatures because the method of superposition has been shown during the development of the current H* analysis to not apply to the non-linear combination of materials and loading in the lower SG complex. This conclusion led to the development of the 3D FEA model that is the reference model for the H* analysis. A discussion of this is provided in Section 6.1.2 of WCAP-17071-P and WCAP-17072-P.

1.3 Discussion of the Unit Cell Model to Calculate Contact Pressures

The "Unit Cell" model is extensively discussed in Section 6.2.5 of the H* WCAPs (References 8 and 9). The specific goal of this model was to determine if tube to tube contact would remain when the tubesheet is deformed due to operating loads. An equivalent tubesheet cell is modeled, that is, a tubesheet bore with surrounding tubesheet material, and a tube in the tubesheet bore (see Figure 6-48 of the H* WCAPs). For the primary purpose of this model – to study if tube-to-tubesheet contact is present during the limiting tubesheet deformations – the model was initialized by simulating the tube expansion process. The expansion process was conservatively simulated by applying a low value of expansion pressure []^{a,c,e} inside the tube, resulting in initial tube to tubesheet contact, and then removing the tube expansion internal pressure. The calculated dilation of the tubesheet bore due to the simulation of the tube expansion is []^{a,c,e} inch for all models of SG considered.

As discussed in Section 6.2.5 of the H* WCAP reports, the operating pressure loads, were applied to the initialized model in a sequential manner, and the resulting contact pressures were calculated when a range of displacements (termed "E-bar") were applied as boundary conditions to the model. Figure RAI4-2 shows the updated sequential loading (includes application of thermal loads) of the model and relates it to the steps discussed in Section 6.2.5 and Tables 6-18 and 6-19 of the H* WCAPs. The "E-bar" values shown as the displacement inputs on Tables 6-18 and 6-19 in the H* WCAP reports are uni-directional displacements (in inches) that are NOT the same as eccentricity and also not the same as ΔD . (Eccentricity is defined as the difference between the maximum and minimum diameters of a bore divided by the nominal diameter of the bore. The units of eccentricity are inch/inch.) The displacement inputs applied to the unit cell model are assumed values that based on prior analyses that envelope the expected tubesheet displacement for all of the applicable operating conditions. It is important to note that the unit cell model as described in Section 6.2.5 of the H* WCAP reports utilizes boundary conditions chosen to minimize the tube-to-tubesheet contact pressures for the applied relative displacements.

To interpret the results from the unit cell model properly, the following must be observed:

- To address if tube to tubesheet contact continues for all the assumed tubesheet displacements, the appropriate reference condition is the initialized condition (after Step 4) of the model that simulates a tube expanded in the tubesheet bore.

- To compare the results of the unit cell model with the 3D FEA model, the appropriate reference condition of the unit cell model is the initial model (Step 0) without the tube expansion simulated and thermal loads must be included.

Figures RAI4-3 and RAI4-4 show the average tubesheet bore dilation (ΔD) as a function of tubesheet relative displacement (E-bar) for the Model F and Model D5. The average tube bore dilation at zero E-bar input is the result of the temperature and pressure loading of the unit cell model. Initially, application of the displacement input "E-bar" results in more significant hole dilation, but rapidly takes on a shallower slope as the applied displacement increases. The curves are characteristically the same for the Model F and Model D5 steam generators and also for the different operating conditions, NOP and SLB, for the different models of SGs.

Similarly, Figures RAI4-5 and RAI4-6 show the tubesheet bore eccentricity "e" as a function of tubesheet relative displacement (E-bar) for the Model F and Model D5. Eccentricity initially increases with application of the displacement boundary condition (E-bar) simulating the load due to pressure differential across the tubesheet, but the rate of increase decays with increasing E-bar. A significant difference is noted between NOP and SLB conditions at large values of E-bar. This difference reflects the fact that the uniform growth of the tube bore hole due to increased temperature overwhelms the effect of application of the displacement boundary condition (E-bar) on tubesheet bore eccentricity. During the SLB event, the temperature is decreased and the differences in D_{MAX} and D_{MIN} remain more significant as the displacement boundary condition is increased, although the rate of increase in the difference between D_{MAX} and D_{MIN} is reduced at some point. Eventually, at NOP conditions, the difference between D_{MAX} and D_{MIN} tends to become decrease even though a greater displacement (E-bar) is applied, leading to a reduction of eccentricity "e."

Figures RAI4-7 and RAI4-8 show the contact pressure as a function of tubesheet relative displacement (E-bar) for the Model F and Model D5 for both NOP and SLB conditions based on the unit cell model. As expected, both NOP and SLB contact pressure decrease with increasing displacement inputs, ultimately going to zero at a very large value of applied displacements. It is to be noted that the maximum displacement assumed is significantly greater than would be predicted by the 3D FEA model. Over the entire range of assumed displacement conditions, the SLB contact pressure exceeds that for NOP conditions.

Table RAI4-5 summarizes the eccentricity, ΔD and predicted contact pressure using the unit cell model for various values of applied displacement (E-bar) for both the model F and Model D5 SGs. The true eccentricity $([D_{max}-D_{min}]/D_{nom})$ is shown for the applied displacement, E-bar. Table RAI4-5 also provides a comparison of the ΔD predicted by the unit cell model for the two reference conditions noted above, that is, for the total ΔD from the model without the simulated tube expansion (reference step 0 in Table 6-18) and for the initialized case with the tube expansion simulated (reference step 4 in Table 6-18).

Further, Table RAI4-5 provides a summary of contact pressures between the tube and the tubesheet for various applied values of $E\text{-}\bar{\Delta}$ for the Model F and Model D5 SGs. The "Modified Contact Pressure" is the "Raw Contact Pressure" from the unit cell model adjusted for the actual tube expansion process ([]^{a,c,e} psi compared to the simulation at []^{a,c,e} psi) real Model F and Model D5 geometry and more realistic operating conditions of pressures and temperatures. For all cases of applied displacement, positive contact pressure remains between the tube and tubesheet. It should be noted that the largest value of applied displacement ($E\text{-}\bar{\Delta}$) is well in excess of the displacement predicted by the 3D FEA model.

Table RAI4-6 provides similar data to that in Table RAI4-5, except that the data is based on the 3D FEA model.

Comparison of Tables RAI4-5 and RAI4-6 leads to the following observations:

1. The ΔD s from the 3D FEA model are significantly less than the corresponding ΔD s from the unit cell model from the unloaded to the fully loaded condition (i.e., from step 0 to step 9) for both NOP and SLB conditions. This leads to the conclusion that the unit cell model displacement results and contact pressure predictions conservatively represent the reference 3D FEA model results.
2. The eccentricities from the unit cell model are generally comparable to those from the 3D FEA model. A more exact comparison is difficult based on the available data; however, it is clear that the actual range of eccentricities from the 3D FEA model was adequately addressed by the unit cell model.
3. The method of Reference 6-15 of the H* WCAP report for adjusting contact pressure provides acceptable results for all conditions except the SLB condition for the Model D5 SGs. The method of Reference 6-15 significantly under-predicts contact pressure for the Model D5 SLB conditions. Referring to Figure RAI4-6, the method for calculating the reduction in contact pressure defined by the White Paper, when adjusted for temperature effects, shows that SLB contact pressure is increased relative to normal operating conditions.

**Table RAI4-5
Eccentricity, Contact Pressure and ΔD Results from Unit Cell Model**

SG Model	"E bar"	Square Cell Results		Square Cell Results		Square Cell Results		Square Cell - Average Delta D			
		Eccentricity		Raw Contact Pressure ⁽¹⁾		Modified Contact Pressure ⁽¹⁾		Step 0 ⁽²⁾ - Step 9 ⁽³⁾		Step 4 ⁽⁴⁾ - Step 9 ⁽³⁾	
		NOP	SLB	NOP	SLB	NOP	SLB	NOP	SLB	NOP	SLB
-	in	in/in	in/in	psi	psi	psi	psi	in	in	in	in
F											
F											
F											
F											
D5											
D5											
D5											
D5											

a,c,e

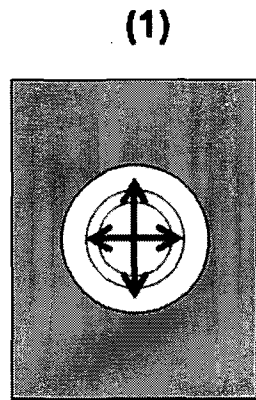
Notes:
 1. Accounts for expansion pressure and geometry.
 2. See Section 6.2.5 H* WCAP. Step 0 is the condition of the unit-cell model prior to any modifications for tube expansion, loading, etc.
 3. See Section 6.2.5 H* WCAP. Step 9 is the condition of the unit cell model after all loading conditions have been applied.
 4. See Section 6.2.5 H* WCAP. Step 4 is the initialized condition of the Unit Cell model after tube expansion has been simulated.

**Table RAI4-6
Eccentricity, Bore Dilation and Contact Pressure from 3D FEA Model**

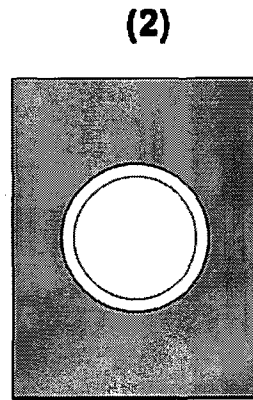
SG Model and Contact Pressure Reduction Model	Hstar Analysis		Hstar Analysis		Hstar Analysis - Avg. Δ D		a,c,e
	Eccentricity		Avg. Contact Pressure		No Load to Operating		
	NOP	SLB	NOP	SLB	NOP	SLB	
	in/in	in/in	psi	psi	in	in	
F - Ref. 6-15							
Limiting Radius - F - Ref. 6-15							
D5 - Ref. 6-15							
D5 - White Paper							
Limiting Radius - D5 - Ref. 6-15							
Limiting Radius - D5 - White Paper							
F - Updated Model ⁽¹⁾							
D5 - Updated Model ⁽¹⁾							

(1): Updated Model Results based on estimates from approximate values in finite element analysis and do not reflect the result of a regression analysis.

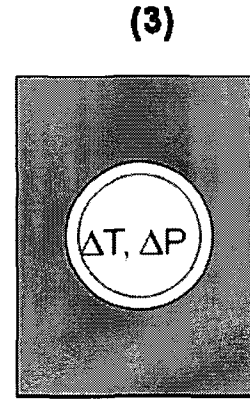
**Figure RA14-2
Unit Cell Model and Loading Sequence**



Step 0
 $\Delta P = 0$
 $\Delta T = 0$
 Unexpanded Tube
 $e = 0$
 $e \text{ bar} = 0$



Step 5
 $\Delta P = 0$
 $\Delta T = 0$
 Expanded Tube
 $e = 0$
 $e \text{ bar} = 0$



Step 6-9
 $\Delta P > 0$
 $\Delta T > 0$
 Expanded Tube
 $e > 0$
 $e \text{ bar} > 0$

Loading Steps:

0. Initial Model
1. Initial Tube to TS gap
2. Pressurize tube to 16ksi
3. Pressurize tube to 28ksi
4. Release Pressure on Tube
5. Apply $\Delta T^{(1)}$
6. Apply "E-bar"
7. Apply $\Delta P = [\quad]^{a,c,e}$ psi
8. Apply $\Delta P = [\quad]^{a,c,e}$ psi
9. Apply $\Delta P = [\quad]^{a,c,e}$ psi

Notes: (1) The application of the unit cell model in support of Tables 6-18 and 6-19 does not include application of ΔT .



a,c,e

Figure RAI4-3
Relationship between "E-bar" and ΔD ; Model F



a,c,e

Figure RAI4-4
Relationship between "E-bar" and ΔD ; Model D5



Figure RAI4-5
Relationship between "E-bar" and Eccentricity "e"; Model F



Figure RAI4-6
Relationship between "E-bar" and Eccentricity "e"; Model D5

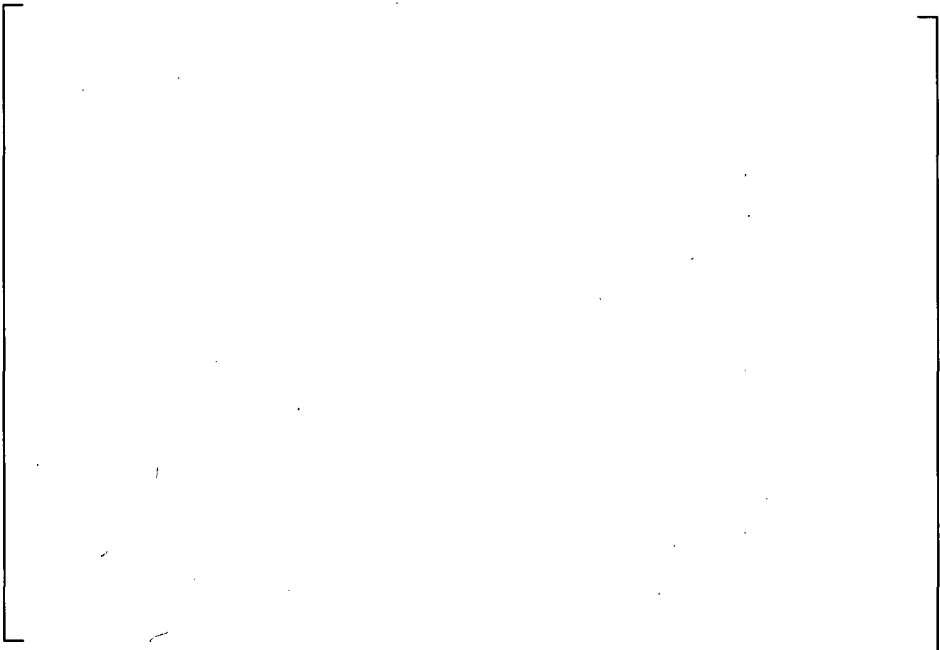


Figure RAI4-7
Relationship between "E-bar" and Contact Pressure; Model F



Figure RAI4-8
Relationship between "E-bar" and Contact Pressure; Model D5

2.0 Comparison of Slice Model and Unit Cell Model Results

The basis for applying the correlation for scale factor outside an “eccentricity” range of between 1E-3 to 1E-4 inch in the calculation of contact pressure needs to be further explained. Values for displacements included in Table 6-18 (of WCAP-17071) suggest that contact pressure may be lost at displacement ranging between 1E-3 in to 1E-4 in.

Response:

Interpretation of the displacements noted in Table 6-18 of the WCAP reports was clarified in the prior response, Section 1.3. The values noted in the column titled “Displacement Total” refer to the condition of the unit cell model after Step 4 of the loading sequence (See Figure RA14-2). When the true reference condition (Step 0) for total displacement is considered, the values of total displacement are significantly larger as noted previously.

Westinghouse agrees that the derivation of the fit in Reference 6-15 is non-intuitive and limited in its application. However, the results of applying the fit described in reference 6-15 are acceptable relative to a best case finite element model (unit cell with thermal and ΔP loading) for the reasons described below.

Westinghouse also agrees that the fit that describes the reduction in contact pressure for the steam line break condition in the Model D5 White Paper does not account for the reduction in contact pressure due to tube bore dilation in the same manner as the fit described in Reference 6-15. The results of using the fit described in Reference 6-15 also match the expected trend from a best case finite element model. See the response to b.4 below for more details.

A series of tubesheet tube bore eccentricities were applied to the tubesheet cell model and combined with different pressure and temperature loads. The average, maximum and minimum values of the tube-to-tubesheet (T/TS) contact pressures around the circumference of the tube were reported. The values of tubesheet relative displacement, pressure and temperature that were used in the analysis are summarized in the table below.

Input Conditions for Unit Cell Model (no correlation implied)		
\bar{e}	Internal Pressure	Temperature Difference
in	ΔP , psi	ΔT , °F _{a,c,e}
0.00	[]
2.0E-04	[]
4.0E-04	[]

Normal operating (NOP) conditions in the Model D5 and Model F steam generators are represented by a ΔP of []^{a,c,e} psi and a ΔT of []^{a,c,e} °F. Main steam line break (SLB) conditions in the Model D5 are represented by a ΔP of []^{a,c,e} psi and a ΔT of []^{a,c,e} °F. The value of ΔP in the tubesheet cell can change as a function of elevation in the tubesheet due to the distribution of crevice pressure. The results of the study include the data for a depth ratio of 0.9 which is an elevation roughly 2 inches below the top of the tubesheet. The values of ΔP represented in this study account for the region of interest near the top of the tubesheet where the maximum eccentricity in the tubesheet is expected and where the crevice fluid is transitioning from the crevice conditions to the secondary side fluid conditions. The region roughly 2 inches below the top of the tubesheet is also where a significant portion of the T/TS contact pressure develops so it is a good indicator of trends in the effect that different operating conditions have on the contact pressure.

The original results in section 6.2.5 of WCAP-17071-P were used to verify that the reduction in T/TS contact pressure as a function of tubesheet tube bore eccentricity was appropriate for the Model F SG. The original relationship that is used to define the reduction in T/TS contact pressure as a function of eccentricity is described in section 6.3 of WCAP 17071-P and WCAP 17072-P. However, the result of applying the fit described in section 6.3 to the Model D5 SG during SLB was shown to be inconsistent with the expected trend from the more detailed analysis described in section 6.2.5. The results of section 6.2.5 were then used to define a new relationship between the reduction in T/TS contact pressure and tube bore eccentricity. This new relationship is described in the Model D5 White Paper (Reference 12). Figure RAI4-8 shows the result of applying the new relationship to the Model D5 SLB conditions (i.e., White Paper results, Reference 12) in comparison with the results from the old 3rd order polynomial relationship. Because the tubesheet temperature induced hole dilation, potentially the most significant factor in contact pressure reduction, was not considered in the Model D5 condition results, a third curve was added to the figure titled "Model D5 FEA trend." This curve represents the most accurate calculation of the contact pressure ratio.

Figure RAI4-9 shows the contact pressure ratio (PC_{SLB}/PC_{NOP}) as a function of tubesheet relative displacement, $E\text{-bar}$. It is clear from Figure RAI4-9 that the results of using the old fit for the Model D5 SLB are inconsistent with the more detailed analysis. At SLB conditions, the tubesheet bore dilation is relatively larger than at NOP conditions due to the increased bending of the TS and decreased thermal expansion. Therefore, it is expected that the T/TS contact pressure ratio should increase by a factor of at least []^{a,c,e} (see Figure RAI4-9) when going from NOP to SLB. It is also expected that the tube to tubesheet contact pressure should decrease with increasing tube bore eccentricity. The H^* results using the old fit for the Model D5 clearly do not follow either expectation from the detailed analysis. However, when the new fit results are applied to the H^* calculation process the relationship between T/TS contact pressure in the Model D5 is much more reasonable and follows the expected trend from the more detailed analysis.

The Model F H^* contact pressure results, using the old fit, are well within the range predicted by the more detailed analysis in section 6.2.5 and the additional work described in this RAI response. See Figure RAI 4-10 below. This means that the old fit is appropriate to use for the

Model F NOP and SLB conditions and the NOP condition in the Model D5 SG. The results of using the fit described in Reference 6-15 match the expected trend from a best case finite element model for the NOP and SLB conditions for the Model F SGs and NOP conditions for the Model D5 SG.

To further address the concern that contact pressure may be lost at displacements ranging between 1E-3 in and 1E-4 in, the "Unit Cell" model is extensively discussed in Section 1.3 of this response above.

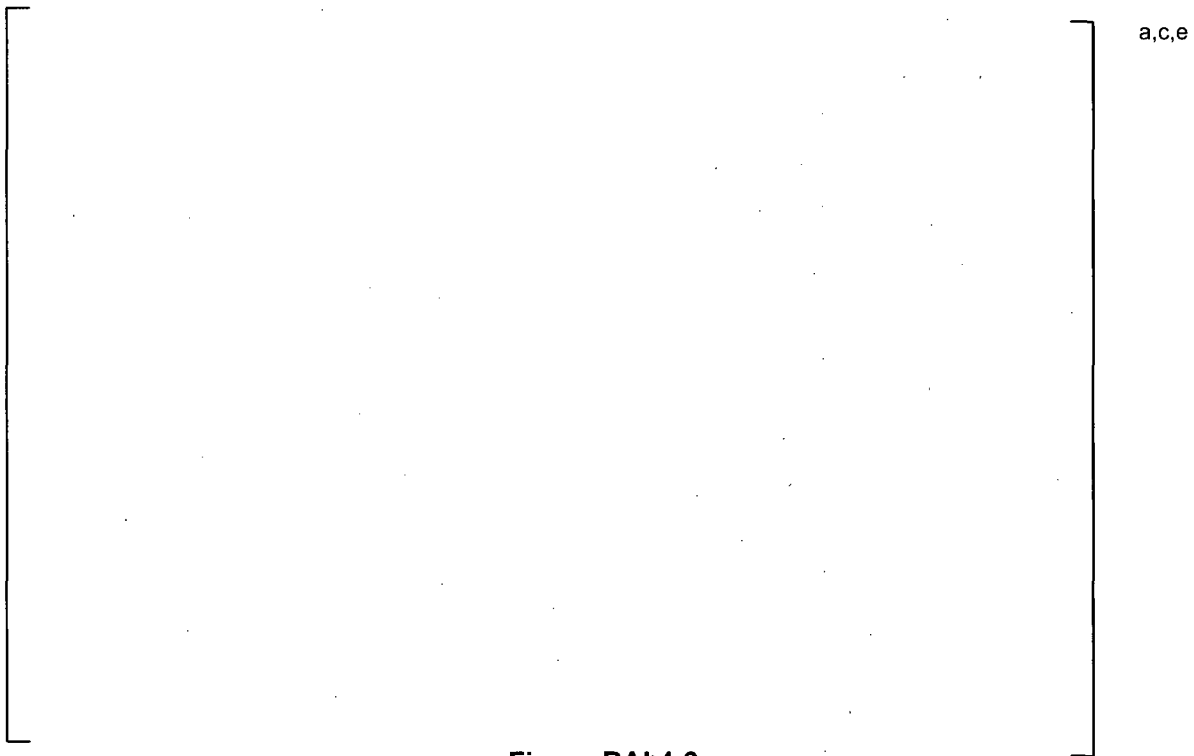


Figure RAI 4-9



Figure RAI 4-10

2.1 Calculation Basis for Contact Pressure Reduction Factors

Provide the calculation basis for the upper and lower curves provided in Figure RAI 4-2

Response:

The original figure RAI4-2, referred to in the question, is reproduced here as RAI4-10 to provide the foundation for the question and the response. Note that the scale of the y-axis has been corrected as discussed in the meeting on August 17, 2009.

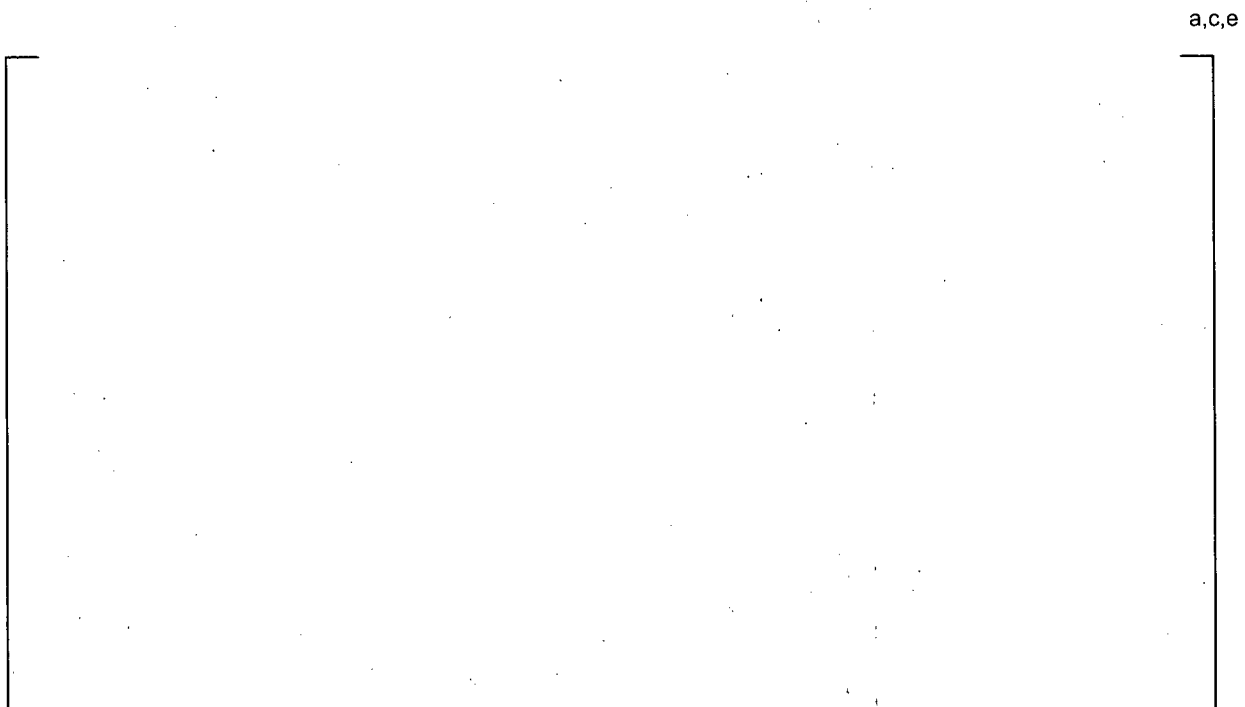


Figure RAI4-10 (original Figure RAI4-2)

The upper curve in the figure above is based on the data from the following table:

Eccentricity ($\Delta D_{max} - \Delta D_{min}$) (in)	Reduction in Contact Pressure (psi)(1)	Normalization Basis (psi)	Contact Pressure Reduction Factor(psi/psi)
0	0	1200	0
2E-4	[] ^{a,c,e} psi		[] ^{a,c,e}
4E-4	[] ^{a,c,e} psi		[] ^{a,c,e}
5E-4	[] ^{a,c,e} psi		[] ^{a,c,e}
6E-4	[] ^{a,c,e}		[] ^{a,c,e}
Notes: (1) Contact stress reductions are based on the values on Table RAI4-3			

Referring to Table RAI 4-3, the contact pressure for a round tube bore hole is calculated to be []^{a,c,e} psi (Ratio = 1.0). The contact pressure for a tube bore hole that results in a contact pressure ratio reduction of []^{a,c,e} (Ratio = []^{a,c,e}), which corresponds to an eccentricity of 2E-4 inch, is []^{a,c,e} psi. The absolute reduction in contact pressure is []^{a,c,e} psi.

The total reduction in contact pressure using the new model is approximately []^{a,c,e} psi (see Figure 6-69 of WCAP-17072-P). To plot the absolute reduction in contact pressure of []^{a,c,e} psi for an eccentricity of 2E-4 on Figure RAI4-10, the value is normalized by the total reduction in contact pressure of []^{a,c,e} psi from the new method. This value represents a reduction in contact pressure of []^{a,c,e}.

Again, referring to Table RAI 4-3, the contact pressure for a round tube hole is calculated to be []^{a,c,e} psi. The contact pressure for a tube bore hole that results in a contact pressure ratio reduction of []^{a,c,e} (Ratio = []^{a,c,e}), which corresponds to be eccentricity of 4E-4 inch, is []^{a,c,e} psi. The absolute reduction in contact pressure is []^{a,c,e} psi.

Again, the total reduction in contact pressure using the new model is approximately []^{a,c,e} psi (see Figure 6-69 of WCAP-17072-P). To plot the absolute reduction in contact pressure of []^{a,c,e} psi for an eccentricity of 4E-4 on Figure RAI4-10, the value is normalized by the total reduction in contact pressure of []^{a,c,e} psi from the new method. This value represents a reduction in contact pressure of []^{a,c,e}.

The same calculation was completed for an eccentricity of 6E-4 in. The value for 5E-4 in is an interpolated value between 4 E-4 in and 6E-4 in.

The bottom curve in the figure above is generated using the 3rd order polynomial fit. The results are summarized in the following table:

E, eccentricity (in)	T/TS Contact Pressure Reduction (psi)	Normalized Contact Pressure Reduction
6.36E-07	[] ^{a,c,e}	[] ^{a,c,e}
5.53E-05	[] ^{a,c,e}	[] ^{a,c,e}
3.16E-04	[] ^{a,c,e}	[] ^{a,c,e}
5.69E-04	[] ^{a,c,e}	[] ^{a,c,e}
9.07E-04	[] ^{a,c,e}	[] ^{a,c,e}

2.2 Conservatism of 3rd Order Polynomial Fit from WCAP Reference 6-15

Provide the basis for why the ΔD_{hole} adjustment for contact pressure made using the old model remains conservative.

Response:

The key conclusions from the comparison of the Reference 6-15 analysis, the WCAP results and the results of the square cell tubesheet model are:

- 1.) The fit described in Reference 6-15 of the H* WCAP reports is conservative when applied to the NOP condition in both the Model D5 and Model F SG. The fit tends to underestimate the contact pressure during NOP by as much as []^{a,c,e} psi to []^{a,c,e} psi for the Model F SG and as much as []^{a,c,e} % for the Model D5 SG ([]^{a,c,e} psi to []^{a,c,e} psi) (see Table RAI4-6).
- 2.) The fit described in Reference 6-15 of the H* WCAP reports is comparable when applied to the SLB condition in the Model F SG. The fit described in the Model D5 White Paper tends to over-estimate the contact pressure, by as much as []^{a,c,e} %, during SLB ([]^{a,c,e} psi to []^{a,c,e} psi) because the White Paper does not fully account for the change in tube bore diameter during the transient.
- 3.) The fit described in Reference 6-15 of the H* WCAP reports significantly under-estimates the contact pressure, by as much as []^{a,c,e} %, during the D5 SLB condition (from []^{a,c,e} psi to []^{a,c,e} psi).
- 4.) The square cell tubesheet finite element model shows an increase in contact pressure when going from NOP to SLB conditions in both the D5 and F SGs.

- 5.) Using the results from the square cell model to estimate the magnitude of the contact pressure reduction from the change in tube bore diameter calculated using the 3D finite element results from the lower SG tubesheet complex model show that the contact pressure still increases when going from NOP to SLB conditions in both the Model F and Model D5 SG.

The results of this analysis show that NOP contact pressures that define H^* in the Model F and Model D5 SG are conservative and that a more realistic model of contact pressure reduction as a function of tube bore deformation (including both dilation and eccentricity) would predict an increase in tube to tubesheet contact pressure at SLB conditions compared to NOP conditions.

(See also Section 2.3)

2.3 SLB vs. NOP Contact Pressures

Provide an appropriate basis for demonstrating that joints tighten during a postulated SLB event. Why is it acceptable to compare the contact pressures calculated using the original model for NOP to the contact pressures calculated using the new model for SLB for the Model D5 SGs?

Response:

Table RAI4-5 provides a summary of contact pressures between the tube and the tubesheet for various applied values of $E\text{-bar}$ for the Model F and Model D5 SGs. Comparison of the eccentricity values calculated using the unit cell model (see Table RAI4-5) with the eccentricity values calculated from the 3D FEA model (see Table RAI4-1) shows that the eccentricities from both models are comparable. It is not reasonable to expect exact matches of numbers between the two models, however, the order of magnitude of the calculated eccentricities is the same. Given that the two structural models provide similar eccentricities, the unit cell model shows that for these eccentricities, positive contact pressure exists between the tubes and the tubesheet for the entire range of displacements considered. Further, the results show that the contact pressures at SLB conditions exceed those at NOP conditions (See Table RAI4-6). See also the discussion in Section 2.4 below.

2.4 Relative Conservatism of “Old” and “New” Fit

If both old and new models are conservative, is there an appropriate basis to show the relative conservatism of the methods?

Response:

As noted above in Section 1.3 of this response, tube bore dilation is a more significant factor in determining tube-to-tubesheet contact pressure at higher temperatures and the effect of eccentricity on contact pressure is reduced at higher temperatures. The methodology for addressing the effect of eccentricity on contact pressure discussed in Reference 6-15 and utilized in WCAP-17071-P, WCAP-17072-P, WCAP-17091-P and WCAP-17092-P reflects this fact and it, therefore, provides acceptably accurate contact pressure results at higher temperatures (i.e., for all conditions except the “colder” SLB condition). This includes NOP, SLB (higher temperature, > 400°F, and FLB, where appropriate).

Also, as noted in Section 1.3 of this report, the effect of eccentricity on contact pressure loss is a more significant factor at the lower SLB temperatures for the Model D5 SG, but tube bore dilation due to temperature and pressure needs to be considered (which was not addressed in the “new” method, a.k.a the White Paper method discussed in WCAP-17072-P or 17091-P). Moreover, the original 3rd order polynomial fit significantly over-predicts contact pressure loss during the “colder” Model D5 SLB transient (and Model 44F two loop plant SLB).

Therefore, a more detailed model for contact pressure during a postulated SLB was developed. Referring to Table RAI4-6, it shows that contact pressure increases during a SLB event ([]^{a,c,e} psi) relative to NOP ([]^{a,c,e} psi) with primary and secondary side temperatures as low as 212°F when comparing contact pressures for NOP conditions for the unit cell to contact pressures for SLB for the unit cell.

Again, referring to Table RAI4-6, it has been shown when comparing contact pressures for NOP conditions for the unit cell to contact pressures for SLB for the unit cell for the Model F SG (higher temperature SLB conditions), that contact pressure increases during a postulated SLB (from []^{a,c,e} psi at NOP to []^{a,c,e} psi at SLB).

3.0 Comparison of 3D FEA and Unit Cell Model Results

The eccentricities included in Table RAI 4-4 appear larger than anticipated. Need to confirm that positive contact pressure exists around the entire circumference of the tube and state this clearly in the response.

Response:

Comparison of the eccentricity values calculated using the unit cell model (see Table RAI4-5) with the eccentricity values calculated from the 3D FEA model (see Table RAI4-1) shows that the eccentricities from both models are comparable. It is not reasonable to expect exact matches of numbers between the two models, however, the order of magnitude of the eccentricities calculated is the same. Given that the two structural models provide similar eccentricities, the unit cell model shows that for these eccentricities, positive contact pressure exists between the tubes and the tubesheet for the entire range of displacements considered. Further, the results show that the contact pressures at SLB conditions exceed those at NOP conditions.

4.0 Additional Background Information For Key Questions and Issues

RAI#4 evolved in several stages, each stage building on the prior stage. Reference 10 provided additional questions to augment those that were provided by Reference 5. Responses were prepared and were discussed in a telephone conference on August 11, 2009. During this telephone conference, additional questions were raised as identified in the introduction of this document. The following are responses that were provided in response to Reference 10 that were discussed in the August 11, 2009 telephone conference. They are historical in nature and are provided to complete the record of information provided in response to the NRC request for additional information.

4.1 Comparison of "Old and New" Relationship for Reduction in Contact Pressure and Eccentricity

In Figure 2 of the White Paper, add a plot for original relationship between reductions in contact pressure and eccentricity as given in Reference 6-15 in the graph accompanying Table 6-3. Explain why this original relationship remains conservative in light of the new relationship. Explain the reasons for the differences between the curves.

In order to superimpose the results of the "old" and "new" analyses for reduction in contact pressure related to eccentricity, the data for the "old" method must be normalized in the same fashion that Figure 2 has been normalized. The plot of contact pressure reduction included in

Figure 2 of the White Paper represents the total reduction in contact pressure associated with a given eccentricity. The information from Table 6-3 represents the ratio of the contact pressure calculated at a given eccentricity divided by the contact pressure calculated for a tubesheet bore with no eccentricity. For the new analysis, the total reduction in contact pressure for the eccentricities ($D_{MAX} - D_{MIN}$) for a range of up to []^{a,c,e} inch is determined to be []^{a,c,e} psi. For the old analysis, the total reduction in contact pressure for eccentricities in the same range is calculated to be []^{a,c,e} psi. The normalization basis is the same for both curves on the figure.

Figure RAI4-11, showing the normalized results as discussed during the August 17, 2009 meeting, is provided below. (Figure RAI4-11 is the same as Figure RAI4-10 in Section 2.1 of this document, except that the values of the "Old Polynomial Results" have been corrected on Figure RAI4-10 by a factor of 2 as discussed in the August 17, 2009 meeting.) The curve labeled "Old" Model Results is based on the data from Table RAI4-3 (Table 6-2 of Reference 15 of the WCAP report). The curve labeled "New" Model reproduces Figure 2 in the White Paper (Reference 12). The curve labeled "D5 SLB Polynomial Fit" are the results when the eccentricity data and ΔD_{hole} for the Model D5 SLB condition are applied directly to the polynomial fit, equation 6-8 in WCAP-17072-P and similar equation on page 6-85 in WCAP-17071-P. The latter curve is based on the maximum displacement conditions at the top of the tubesheet for the Model D5.

The curve labeled "Old Model Results" (top curve on Figure RAI4-11) is misleading relative to making an assessment of the conservatism of the new analysis method compared to the old analysis method. Unlike the new analysis method, which is only applied to the SLB case for the Model D5 SGs, the old analysis method has not been applied as a linear function as represented in the figure as the uppermost curve (solid squares). In reality, the old data fit (top curve on Figure RAI4-11), which is a 3rd order polynomial fit, when extrapolated significantly outside its supported data range (i.e., at temperatures either significantly above or below 500°F), provides physically unrealistic results as shown on Figure RAI4-11 (bottom curve, Δ -symbols). The Model D5 SLB condition puts the tubesheet at a nearly uniform temperature of less than 300°F, which is far outside of the range for which the eccentricity relationship was developed in Reference 6-15 in the WCAP reports.

The original relationship remains conservative because it predicts greater reduction of tube to tubesheet contact pressure than the new method for all operating conditions. However, the original relationship is only valid when ΔD_{min} and ΔD_{max} are within []^{a,c,e} % and eccentricity is within []^{a,c,e} inch to []^{a,c,e} inch range, (i.e., the basis of the original fit).

The maximum tube bore distortions occur at the top of the tubesheet. The results from applying the old fit for the relationship versus the new fit for the relationship for the Model D5 SLB tubesheet displacements and contact pressures are shown in Table RAI4-7. The tube-to-tubesheet (T/TS) contact pressure result due to thermal expansion of the tube and the pressure expansion of the tube including the effect of the crevice pressure distribution, is the same in the both the "old" and "new" cases in the Table RAI4-7.

**Table RAI4-7
Summary of Model D5 SLB Contact Pressure Results for
Different Eccentricity Fit Relationships**

Model D5			T/Ts P _{CON} Reduction		T/Ts P _{CON}	
Condition	Value	Eccentricity	Old	New	Old	New
SLB	Avg					
SLB	Max					
SLB	Min					

The results in Section 6.2.4 of WCAP-17071-P and WCAP-17072-P show that the average expected tubesheet-tube-bore eccentricity is on the order of []^{a,c,e} inch. The results in Table RAI4-7 show that the old method of calculating the reduction in contact pressure due to tubesheet-tube-bore eccentricity and change in diameter is conservative for larger values of eccentricity and ΔD (predicts greater decrease in contact pressure) than the new fit. However, it is inappropriate to use the old method at smaller values of eccentricity and ΔD because it provides physically impossible results (see Table RAI4-7). For example, the “old” method predicts a larger decrease in contact pressure for a smaller eccentricity on the order of 10⁻⁷ inch than for a larger eccentricity on the order of 10⁻³ inch. The “new” method, by comparison, predicts a slightly positive increase in contact pressure for an eccentricity of 10⁻⁷ inch and a large reduction in contact pressure for an eccentricity of 10⁻⁴ inch or greater, a physically realistic result. The reason that the “old” method predicts such a different reduction in contact pressure for small values of eccentricity is that these small eccentricity values are well outside the range of the data upon which the “old” relationship was developed. However, when used within its intended range of eccentricities and tubesheet bore displacement, the “old” method provides valid and conservative results. The “new” method of calculating the reduction in T/Ts contact pressure is linear and directly accommodates small calculated values of eccentricity. It is also clear from the results in Table RAI4-7 that the results from the old method when used in its supported eccentricity range are highly conservative compared to the “new” method.



Figure RAI4-11
Original Figure RAI4-2 Discussed at the August 17, 2009 Meeting

4.2 Use of Both “Old” and “New” Fit

When establishing whether contact pressure increases when going from normal operating to steam line break conditions, how can a valid and conservative comparison be made if the normal operating case is based on the original delta contact pressure versus eccentricity curve and the SLB case is based on the new curve?

Response:

It is important to note that the new analysis method is only used for the SLB condition for the Model D5 steam generators. Comparison of contact pressures between the normal operating condition and the SLB condition is made for the Model F steam generators in the H* fleet in WCAP-17071-P on a consistent basis.

It is Westinghouse's engineering judgment that the old methodology provides an accurate determination of contact pressures during normal operating conditions and postulated accident conditions (FLB and SLB) when peak temperatures range between []^{a,c,e} °F and eccentricities are between []^{a,c,e} inch and []^{a,c,e} inch and D_{max} and D_{min} are within []^{a,c,e} % of each other.

Application of the new method to calculate eccentricities and values of D_{max} and D_{min} that fall outside the above noted range provides conservative results because the plane strain model upon which it is based over-estimates the stiffness of the tube and tubesheet structure leading to lower contact pressure results as a function of eccentricity. The new method also excluded the effect of temperature and therefore, conservatively bounds the lower temperatures of the Model D5 SLB transient. The T/TS contact pressure results during SLB are still expected to bound the T/TS contact pressure results during NOP because, even though the tube bore eccentricity during SLB is generally greater than that during NOP, the overall growth of the tube bore during NOP is greater than that during SLB. Larger magnitudes of tube bore growth are directly related to decreasing tube-tubesheet contact pressure regardless of the value of calculated tube bore eccentricity.

It is appropriate to compare the Model D5 SLB contact pressure results from the “new” method to the Model D5 NOP results from the “old” method because each condition uses the appropriate fit to conservatively determine the reduction in T/TS contact pressure due to tube bore eccentricity and tube bore growth.

The sole purpose of the new methodology was to develop a more accurate way of calculating contact pressures during a postulated SLB for the Model D5 steam generators. The comparison provided in Figure 6-83 of WCAP-17072-P remains a valid comparison.

5.0 Part A (Original RAI#4)

Reference 1, Page 6-69: In Section 6.2.5.3, it is concluded that the tube outside diameter and the tubesheet tube bore inside diameter always maintain contact in the predicted range of tubesheet displacements. However, for tubes with through-wall cracks at the H^* distance, there may be little or no net pressure acting on the tube for some distance above H^* . In Tables 6-18 and 6-19, the fourth increment in the step that occurs two steps prior to the last step suggests that there may be no contact between the tube and tubesheet, over a portion of the circumference, for a distance above H^* . Is the conclusion in 6.2.5.3 valid for the entire H^* distance, given the possibility that the tubes may contain through-wall cracks at that location?

The following response to RAI#4 was included in Reference 11. The same response is included here to complete the record of information provided in regard to RAI#4 of References 5, 6 and 7.

Response:

The conclusions reached in Section 6.2.5.3 of WCAP-17071-P are valid for the entire H^* distance because of the following considerations:

1. The primary source of contact pressure between the tube and the tubesheet is differential thermal expansion between the tubes and the tubesheet. The analysis in Section 6.2.5.3 specifically excludes the effect of thermal expansion of the tube from the analysis. The tubesheet is assumed to deform due to the combination of pressure and thermal loads which produces the tube bore ovalization and leads to the displacements applied in this model. Only the residual effects from installation are considered for the tube in steps 1 through 5. The tube internal pressure applied in these steps only simulates the hydraulic expansion pressure to establish the initial conditions for the following step. The conditions assumed for this study are not possible during any operating condition in the steam generator but are conservative relative to actual SG conditions. (Note: Residual contact pressure is not used in the calculation of H^* values in Section 6. The residual effects of installation are included in the results of Section 6.2.5.3 so that the sensitivity of a strain hardened tube to tubesheet tube bore deformation can be studied.)
2. Step 5 on Tables 6-18 and 6-19 is not representative of any condition in the steam generator because it assumes that the tubesheet is at operating temperature with an applied primary-to-secondary pressure differential while the tubes remain at room temperature and are not pressurized. That is why Steps 1 through 5 are described as "initializing" steps in the process. It is physically impossible for these conditions to occur simultaneously in the same steam generator.

3. Because no pressure loading is applied to the tube in Step 5 of the analysis discussed in section 6.2.5, the results presented in Tables 6-18 and 6-19 are applicable regardless of whether, or not, a through-wall crack exists at the H^* location. The more representative case is Step 6 shown on Tables 6-18 and 6-19 in which tube internal pressure is included. For that case, the potential point of zero contact pressure is at an applied displacement a factor of 5 greater than for Step 5, and far in excess of what is reasonably predicted for the actual tubesheet deformation. The factor of 5 difference in required displacement to cause the contact pressure to reduce to zero more than adequately covers the postulated potential local reduction in crevice pressure due to a circumferential separation at the location of H^* . Recall also, that no thermal expansion of the tube is considered in this analysis.

It is also noted that tables 6-18 and 6-19 are the results of a sensitivity study that is not intended to represent the integrated calculation for H^* . The integrated H^* analysis is a complex process that combines the effects of several types of loading and deformation into an integrated estimate of the tube-to-tubesheet contact pressure. Therefore, it is not appropriate to consider a sensitivity study out of the context of the greater analysis. The integrated analysis presented in the complete Section 6 shows that for the combined case of the thermal effects, pressure effects, and tubesheet displacement there is tube-to-tubesheet contact pressure throughout the tubesheet.

It is acknowledged that the cut end of a tube is radially less stiff than a tube that is radially loaded at a point away from the tube end, and that the presumption of a tube sever at the H^* distance may represent the case of a tube end. The decreased tube-end stiffness is referred to as "compliance." In other words, a tube that is loaded at the cut end provides less resistance to the load than a tube with equal load applied a distance removed from the tube-end. Thus, conceptually, a local "end effect" could be expected to occur due to the increased compliance of the tube-end.

The calculation process for H^* shown in Figure 1-1 of the H^* WCAP reports and discussed in several places in the report notes that an adjustment is made to the initial prediction of H^* to account for the distributed crevice pressure referenced to the predicted H^* position. Thus, the greatest crevice pressure is always located at the final value of H^* . Increased tube compliance cannot result in a higher local crevice pressure than is already included in the analysis because, at the point of sever, the primary side pressure is the crevice pressure.

It may be postulated that the increased tube compliance results in reduced contact pressure because the net differential pressure across the tube wall is zero. At the tube-end, the current analysis already includes a zero differential pressure due to the adjustment process for distributed crevice pressure. Therefore, the net reduction in contact pressure would be limited to the axial length of the local effect and would further depend on the slope of the decrease in crevice pressure.

For the Model F and Model D5 SGs, the bounding value of isolation distance above the tube end is 0.6 inch based on classical solutions for the design of pressure vessels (Timoshenko).

The isolation distance is the generically applicable minimum separation distance from an applied load to a point of interest in order to safely assume that the load is in the far field relative to the point of interest. Specific structures and load cases may have different isolation distances but the classical result by Timoshenko for a pressure vessel will conservatively bound any specific cases. For this length, the slope of the contact pressure curve would have to decrease by a factor of at least $[]^{a,c,e}$ before the value of H^* is affected by more than $[]^{a,c,e}$ inch. If the tube is conservatively modeled as a center-loaded beam on an elastic foundation compared to an end-loaded beam on an elastic foundation, the resulting worst case change in structural compliance and the resulting contact pressure slope could be a factor of up to 2. Alternatively, similar analyses for the cross sections of curved beams suggest that the change in compliance of the structure could be as high as a factor of 6. Neither case approaches the factor of $[]^{a,c,e}$ required based on classical pressure vessel analysis to impact the value of H^* ; therefore, no additional adjustments to H^* are necessary to address the potential end effects.

6.0 Summary of the Response to RAI #4

A summary of the response to the original RAI# 4 and additional questions related to RAI 4 are provided below:

1. No additional adjustment to the value for H^* is necessary to address the potential for end effects. This is because the greatest crevice pressure is always located at the final value of H^* . At the H^* distance, the current analysis already includes a zero pressure differential due to the adjustment process for the distributed crevice pressure. Therefore, the net reduction in contact pressure would be limited to the axial length of the local effect and would further depend on the slope of the decrease in crevice pressure. It is judged that the slope of the contact pressure curve would not decrease at a rate such that the value of H^* would be affected.
2. Tube bore dilation is a more significant factor in determining tube-to-tubesheet contact pressure at higher temperatures and the effect of eccentricity on contact pressure is reduced at higher temperatures. The methodology for addressing the effect of eccentricity on contact pressure discussed in Reference 6-15 and utilized in WCAP-17071-P, WCAP-17072-P, WCAP-17091-P and WCAP-17092-P reflects this fact and, therefore, it provides acceptably accurate contact pressure results at higher temperatures (i.e., for all conditions except the "colder" SLB condition). This includes NOP, SLB (higher temperature, $> 400^\circ\text{F}$, and FLB, where appropriate).
3. The results of using the fit described in Reference 6-15 match the expected trend from a best case finite element model for the NOP and SLB conditions for the Model F SGs and NOP conditions for the Model D5 SG.
4. The ΔD s from the 3D FEA model are significantly less than the corresponding ΔD s from the unit cell model from the unloaded to the fully loaded condition (i.e.,

from step 0 to step 9) for both NOP and SLB conditions. This leads to the conclusion that the unit cell model displacement results and contact pressure predictions conservatively represent the reference 3D FEA model results.

5. The eccentricities from the unit cell model are generally comparable to those from the 3D FEA model. A more exact comparison is difficult based on the available data; however, it is clear that the actual range of eccentricities from the 3D FEA model was adequately addressed by the unit cell model.
6. Based on items 4) and 5) which demonstrate the acceptability of the use of the unit cell model for benchmarking the 3-D FEA model, the method for calculating the reduction in contact pressure defined by the unit cell model, when adjusted for temperature effects, shows that SLB contact pressure is increased relative to normal operating conditions for the Model D5 steam generators.
7. It has also been shown when comparing contact pressures for NOP conditions for the unit cell to contact pressures for SLB for the unit cell for the Model F SG (higher temperature SLB conditions), that contact pressure increases during a postulated SLB.
8. Given that the two structural models provide similar eccentricities, the unit cell model shows that for these eccentricities, positive contact pressure exists between the tubes and the tubesheet for the entire range of displacements considered.

Based on the above, it is concluded that the NOP contact pressures that define H^* in the Model F and Model D5 SG are conservative and that a more realistic model of contact pressure reduction as a function of tube bore deformation (including both dilation and eccentricity) would predict positive contact pressure around the entire circumference of the tube and an increase in tube to tubesheet contact pressure at SLB conditions compared to NOP conditions.

The conclusions reached in the response to RAI#4 apply equally for the Model 44F and Model 51F SGs.

Serial No: 09-525
Docket No. 50-423

ENCLOSURE 13

**Westinghouse Electric Company LLC, CAW-09-2569, "Application for Withholding
Proprietary Information from Public Disclosure," dated May 4, 2009.**

**DOMINION NUCLEAR CONNECTICUT, INC.
MILLSTONE POWER STATION UNIT 3**

Serial No: 09-525
Docket No. 50-423

ENCLOSURE 14

**Westinghouse Electric Company LLC, CAW-09-2632, "Application for Withholding
Proprietary Information from Public Disclosure," dated August 13, 2009.**

**DOMINION NUCLEAR CONNECTICUT, INC.
MILLSTONE POWER STATION UNIT 3**



Westinghouse Electric Company
Nuclear Services
P.O. Box 355
Pittsburgh, Pennsylvania 15230-0355
USA

U.S. Nuclear Regulatory Commission
Document Control Desk
Washington, DC 20555-0001

Direct tel: (412) 374-4643
Direct fax: (412) 374-3846
e-mail: greshaja@westinghouse.com

Our ref: CAW-09-2632

August 13, 2009

APPLICATION FOR WITHHOLDING PROPRIETARY
INFORMATION FROM PUBLIC DISCLOSURE

Subject: LTR-SGMP-09-100 P-Attachment, "Response to NRC Request for Additional Information on H*; Model F and Model D5 Steam Generators," dated August 2009 (Proprietary)

The proprietary information for which withholding is being requested in the above-referenced report is further identified in Affidavit CAW-09-2632 signed by the owner of the proprietary information, Westinghouse Electric Company LLC. The affidavit, which accompanies this letter, sets forth the basis on which the information may be withheld from public disclosure by the Commission and addresses with specificity the considerations listed in paragraph (b)(4) of 10 CFR Section 2.390 of the Commission's regulations.

Accordingly, this letter authorizes the utilization of the accompanying affidavit by Dominion Connecticut.

Correspondence with respect to the proprietary aspects of the application for withholding or the Westinghouse affidavit should reference this letter, CAW-09-2632, and should be addressed to J. A. Gresham, Manager, Regulatory Compliance and Plant Licensing, Westinghouse Electric Company LLC, P.O. Box 355, Pittsburgh, Pennsylvania 15230-0355.

Very truly yours,

A handwritten signature in black ink, appearing to read 'J.A. Gresham', written over a horizontal line.

J.A. Gresham, Manager
Regulatory Compliance and Plant Licensing

Enclosures

cc: G. Bacuta, (NRC OWFN 12E-1)

bcc: J. A. Gresham (ECE 4-7A) 1L
R. Bastien, 1L (Nivelles, Belgium)
C. Brinkman, 1L (Westinghouse Electric Co., 12300 Twinbrook Parkway, Suite 330, Rockville, MD 20852)
RCPL Administrative Aide (ECE 4-7A) 1L (letter and affidavit only)
G. W. Whiteman, Waltz Mill
H. O. Lagally, Waltz Mill
C. D. Cassino, Waltz Mill
J. T. Kandra, Waltz Mill
D. L. Rogosky, ECE 564A

AFFIDAVIT

COMMONWEALTH OF PENNSYLVANIA:

SS

COUNTY OF ALLEGHENY:

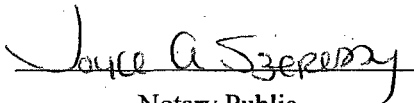
Before me, the undersigned authority, personally appeared J. A. Gresham, who, being by me duly sworn according to law, deposes and says that he is authorized to execute this Affidavit on behalf of Westinghouse Electric Company LLC (Westinghouse), and that the averments of fact set forth in this Affidavit are true and correct to the best of his knowledge, information, and belief:



J.A. Gresham, Manager

Regulatory Compliance and Plant Licensing

Sworn to and subscribed before me
this 13th day of August 2009



Notary Public

COMMONWEALTH OF PENNSYLVANIA
Notarial Seal
Joyce A. Szepessy, Notary Public
Monroeville Boro, Allegheny County
My Commission Expires April 16, 2013
Member, Pennsylvania Association of Notaries

- (1) I am Manager, Regulatory Compliance and Plant Licensing, in Nuclear Services, Westinghouse Electric Company LLC (Westinghouse), and as such, I have been specifically delegated the function of reviewing the proprietary information sought to be withheld from public disclosure in connection with nuclear power plant licensing and rule making proceedings, and am authorized to apply for its withholding on behalf of Westinghouse.
- (2) I am making this Affidavit in conformance with the provisions of 10 CFR Section 2.390 of the Commission's regulations and in conjunction with the Westinghouse "Application for Withholding" accompanying this Affidavit.
- (3) I have personal knowledge of the criteria and procedures utilized by Westinghouse in designating information as a trade secret, privileged or as confidential commercial or financial information.
- (4) Pursuant to the provisions of paragraph (b)(4) of Section 2.390 of the Commission's regulations, the following is furnished for consideration by the Commission in determining whether the information sought to be withheld from public disclosure should be withheld.

- (i) The information sought to be withheld from public disclosure is owned and has been held in confidence by Westinghouse.
- (ii) The information is of a type customarily held in confidence by Westinghouse and not customarily disclosed to the public. Westinghouse has a rational basis for determining the types of information customarily held in confidence by it and, in that connection, utilizes a system to determine when and whether to hold certain types of information in confidence. The application of that system and the substance of that system constitute Westinghouse policy and provide the rational basis required.

Under that system, information is held in confidence if it falls in one or more of several types, the release of which might result in the loss of an existing or potential competitive advantage, as follows:

- (a) The information reveals the distinguishing aspects of a process (or component, structure, tool, method, etc.) where prevention of its use by any of

Westinghouse's competitors without license from Westinghouse constitutes a competitive economic advantage over other companies.

- (b) It consists of supporting data, including test data, relative to a process (or component, structure, tool, method, etc.), the application of which data secures a competitive economic advantage, e.g., by optimization or improved marketability.
- (c) Its use by a competitor would reduce his expenditure of resources or improve his competitive position in the design, manufacture, shipment, installation, assurance of quality, or licensing a similar product.
- (d) It reveals cost or price information, production capacities, budget levels, or commercial strategies of Westinghouse, its customers or suppliers.
- (e) It reveals aspects of past, present, or future Westinghouse or customer funded development plans and programs of potential commercial value to Westinghouse.
- (f) It contains patentable ideas, for which patent protection may be desirable.

There are sound policy reasons behind the Westinghouse system which include the following:

- (a) The use of such information by Westinghouse gives Westinghouse a competitive advantage over its competitors. It is, therefore, withheld from disclosure to protect the Westinghouse competitive position.
- (b) It is information that is marketable in many ways. The extent to which such information is available to competitors diminishes the Westinghouse ability to sell products and services involving the use of the information.
- (c) Use by our competitor would put Westinghouse at a competitive disadvantage by reducing his expenditure of resources at our expense.

- (d) Each component of proprietary information pertinent to a particular competitive advantage is potentially as valuable as the total competitive advantage. If competitors acquire components of proprietary information, any one component may be the key to the entire puzzle, thereby depriving Westinghouse of a competitive advantage.
 - (e) Unrestricted disclosure would jeopardize the position of prominence of Westinghouse in the world market, and thereby give a market advantage to the competition of those countries.
 - (f) The Westinghouse capacity to invest corporate assets in research and development depends upon the success in obtaining and maintaining a competitive advantage.
- (iii) The information is being transmitted to the Commission in confidence and, under the provisions of 10 CFR Section 2.390, it is to be received in confidence by the Commission.
- (iv) The information sought to be protected is not available in public sources or available information has not been previously employed in the same original manner or method to the best of our knowledge and belief.
- (v) The proprietary information sought to be withheld in this submittal is that which is appropriately marked in LTR-SGMP-09-100 P-Attachment, "Response to NRC Request for Additional Information on H*; Model F and Model D5 Steam Generators," dated August 2009 (Proprietary), for submittal to the Commission, being transmitted by Dominion Connecticut letter and Application for Withholding Proprietary Information from Public Disclosure to the Document Control Desk. The proprietary information as submitted for use by Westinghouse for Millstone Unit 3 is expected to be applicable to other licensee submittals in support of implementing an alternate repair criterion, called H*, that does not require an eddy current inspection and plugging of steam generator tubes below a certain distance from the top of the tubesheet.

This information is part of that which will enable Westinghouse to:

- (a) Provide documentation of the analyses, methods, and testing which support the implementation of an alternate repair criterion, designated as H*, for a portion of the tubes within the tubesheet of the Millstone Unit 3 steam generators.
- (b) Assist the customer in obtaining NRC approval of the Technical Specification changes associated with the alternate repair criterion.

Further this information has substantial commercial value as follows:

- (a) Westinghouse plans to sell the use of similar information to its customers for the purposes of meeting NRC requirements for licensing documentation.
- (b) Westinghouse can sell support and defense of the technology to its customers in the licensing process.

Public disclosure of this proprietary information is likely to cause substantial harm to the competitive position of Westinghouse because it would enhance the ability of competitors to provide similar calculation, evaluation and licensing defense services for commercial power reactors without commensurate expenses. Also, public disclosure of the information would enable others to use the information to meet NRC requirements for licensing documentation without purchasing the right to use the information.

The development of the technology described in part by the information is the result of applying the results of many years of experience in an intensive Westinghouse effort and the expenditure of a considerable sum of money.

In order for competitors of Westinghouse to duplicate this information, similar technical programs would have to be performed and a significant manpower effort, having the requisite talent and experience, would have to be expended.

Further the deponent sayeth not.

PROPRIETARY INFORMATION NOTICE

Transmitted herewith are proprietary and/or non-proprietary versions of documents furnished to the NRC in connection with requests for generic and/or plant-specific review and approval.

In order to conform to the requirements of 10 CFR 2.390 of the Commission's regulations concerning the protection of proprietary information so submitted to the NRC, the information which is proprietary in the proprietary versions is contained within brackets, and where the proprietary information has been deleted in the non-proprietary versions, only the brackets remain (the information that was contained within the brackets in the proprietary versions having been deleted). The justification for claiming the information so designated as proprietary is indicated in both versions by means of lower case letters (a) through (f) located as a superscript immediately following the brackets enclosing each item of information being identified as proprietary or in the margin opposite such information. These lower case letters refer to the types of information Westinghouse customarily holds in confidence identified in Sections (4)(ii)(a) through (4)(ii)(f) of the affidavit accompanying this transmittal pursuant to 10 CFR 2.390(b)(1).

COPYRIGHT NOTICE

The reports transmitted herewith each bear a Westinghouse copyright notice. The NRC is permitted to make the number of copies of the information contained in these reports which are necessary for its internal use in connection with generic and plant-specific reviews and approvals as well as the issuance, denial, amendment, transfer, renewal, modification, suspension, revocation, or violation of a license, permit, order, or regulation subject to the requirements of 10 CFR 2.390 regarding restrictions on public disclosure to the extent such information has been identified as proprietary by Westinghouse, copyright protection notwithstanding. With respect to the non-proprietary versions of these reports, the NRC is permitted to make the number of copies beyond those necessary for its internal use which are necessary in order to have one copy available for public viewing in the appropriate docket files in the public document room in Washington, DC and in local public document rooms as may be required by NRC regulations if the number of copies submitted is insufficient for this purpose. Copies made by the NRC must include the copyright notice in all instances and the proprietary notice if the original was identified as proprietary.

Dominion Connecticut
Letter for Transmittal to the NRC

The following paragraphs should be included in your letter to the NRC:

Enclosed are:

1. 1 copy of LTR-SGMP-09-100 P-Attachment, "Response to NRC Request for Additional Information on H*; Model F and Model D5 Steam Generators," dated August 2009 (Proprietary):
2. 1 copy of LTR-SGMP-09-100 NP-Attachment, "Response to NRC Request for Additional Information on H*; Model F and Model D5 Steam Generators," dated August 2009 (Non-Proprietary).

Also enclosed is Westinghouse authorization letter CAW-09-2632 with accompanying Affidavit, Proprietary Information Notice, and Copyright Notice.

As Item 1 contains information proprietary to Westinghouse Electric Company LLC, it is supported by an affidavit signed by Westinghouse, the owner of the information. The affidavit sets forth the basis on which the information may be withheld from public disclosure by the Commission and addresses with specificity the considerations listed in paragraph (b) (4) of Section 2.390 of the Commission's regulations.

Accordingly, it is respectfully requested that the information which is proprietary to Westinghouse be withheld from public disclosure in accordance with 10 CFR Section 2.390 of the Commission's regulations.

Correspondence with respect to the copyright or proprietary aspects of the items listed above or the supporting Westinghouse affidavit should reference CAW-09-2632 and should be addressed to J. A. Gresham, Manager, Regulatory Compliance and Plant Licensing, Westinghouse Electric Company LLC, P.O. Box 355, Pittsburgh, Pennsylvania 15230-0355.

Serial No: 09-525
Docket No. 50-423

ENCLOSURE 15

**Westinghouse Electric Company LLC, CAW-09-2659, "Application for Withholding
Proprietary Information from Public Disclosure," dated August 27, 2009.**

**DOMINION NUCLEAR CONNECTICUT, INC.
MILLSTONE POWER STATION UNIT 3**



Westinghouse Electric Company
Nuclear Services
P.O. Box 355
Pittsburgh, Pennsylvania 15230-0355
USA

U.S. Nuclear Regulatory Commission
Document Control Desk
Washington, DC 20555-0001

Direct tel: (412) 374-4643
Direct fax: (412) 374-3846
e-mail: greshaja@westinghouse.com

Our ref: CAW-09-2569

May 4, 2009

APPLICATION FOR WITHHOLDING PROPRIETARY
INFORMATION FROM PUBLIC DISCLOSURE

Subject: WCAP-17071-P, "H*: Alternate Repair Criteria for the Tubesheet Expansion Region in Steam Generators with Hydraulically Expanded Tubes (Model F)," dated April 2009 (Proprietary)

The proprietary information for which withholding is being requested in the above-referenced report is further identified in Affidavit CAW-09-2569 signed by the owner of the proprietary information, Westinghouse Electric Company LLC. The affidavit, which accompanies this letter, sets forth the basis on which the information may be withheld from public disclosure by the Commission and addresses with specificity the considerations listed in paragraph (b)(4) of 10 CFR Section 2.390 of the Commission's regulations.

Accordingly, this letter authorizes the utilization of the accompanying affidavit by Dominion Connecticut.

Correspondence with respect to the proprietary aspects of the application for withholding or the Westinghouse affidavit should reference this letter, CAW-09-2569, and should be addressed to J. A. Gresham, Manager, Regulatory Compliance and Plant Licensing, Westinghouse Electric Company LLC, P.O. Box 355, Pittsburgh, Pennsylvania 15230-0355.

Very truly yours,

A handwritten signature in black ink, appearing to read 'J.A. Gresham', written over a horizontal line.

J.A. Gresham, Manager
Regulatory Compliance and Plant Licensing

Enclosures

cc: G. Bacuta, (NRC OWFN 12E-1)

bcc: J. A. Gresham (ECE 4-7A) 1L
R. Bastien, 1L (Nivelles, Belgium)
C. Brinkman, 1L (Westinghouse Electric Co., 12300 Twinbrook Parkway, Suite 330, Rockville, MD 20852)
RCPL Administrative Aide (ECE 4-7A) 1L (letter and affidavit only)
G. W. Whiteman, Waltz Mill
H. O. Lagally, Waltz Mill
D. L. Rogosky, ECE 564B

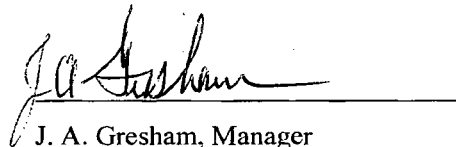
AFFIDAVIT

COMMONWEALTH OF PENNSYLVANIA:

SS

COUNTY OF ALLEGHENY:

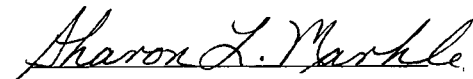
Before me, the undersigned authority, personally appeared J. A. Gresham, who, being by me duly sworn according to law, deposes and says that he is authorized to execute this Affidavit on behalf of Westinghouse Electric Company LLC (Westinghouse), and that the averments of fact set forth in this Affidavit are true and correct to the best of his knowledge, information, and belief:



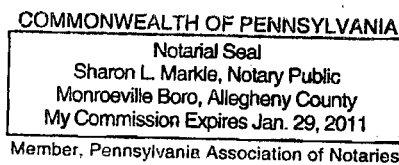
J. A. Gresham, Manager

Regulatory Compliance and Plant Licensing

Sworn to and subscribed before me
this 4th day of May, 2009



Notary Public



- (1) I am Manager, Regulatory Compliance and Plant Licensing, in Nuclear Services, Westinghouse Electric Company LLC (Westinghouse), and as such, I have been specifically delegated the function of reviewing the proprietary information sought to be withheld from public disclosure in connection with nuclear power plant licensing and rule making proceedings, and am authorized to apply for its withholding on behalf of Westinghouse.
- (2) I am making this Affidavit in conformance with the provisions of 10 CFR Section 2.390 of the Commission's regulations and in conjunction with the Westinghouse "Application for Withholding" accompanying this Affidavit.
- (3) I have personal knowledge of the criteria and procedures utilized by Westinghouse in designating information as a trade secret, privileged or as confidential commercial or financial information.
- (4) Pursuant to the provisions of paragraph (b)(4) of Section 2.390 of the Commission's regulations, the following is furnished for consideration by the Commission in determining whether the information sought to be withheld from public disclosure should be withheld.
 - (i) The information sought to be withheld from public disclosure is owned and has been held in confidence by Westinghouse.
 - (ii) The information is of a type customarily held in confidence by Westinghouse and not customarily disclosed to the public. Westinghouse has a rational basis for determining the types of information customarily held in confidence by it and, in that connection, utilizes a system to determine when and whether to hold certain types of information in confidence. The application of that system and the substance of that system constitute Westinghouse policy and provide the rational basis required.

Under that system, information is held in confidence if it falls in one or more of several types, the release of which might result in the loss of an existing or potential competitive advantage, as follows:

- (a) The information reveals the distinguishing aspects of a process (or component, structure, tool, method, etc.) where prevention of its use by any of Westinghouse's competitors without license from Westinghouse constitutes a competitive economic advantage over other companies.

- (b) It consists of supporting data, including test data, relative to a process (or component, structure, tool, method, etc.), the application of which data secures a competitive economic advantage, e.g., by optimization or improved marketability.
- (c) Its use by a competitor would reduce his expenditure of resources or improve his competitive position in the design, manufacture, shipment, installation, assurance of quality, or licensing a similar product.
- (d) It reveals cost or price information, production capacities, budget levels, or commercial strategies of Westinghouse, its customers or suppliers.
- (e) It reveals aspects of past, present, or future Westinghouse or customer funded development plans and programs of potential commercial value to Westinghouse.
- (f) It contains patentable ideas, for which patent protection may be desirable.

There are sound policy reasons behind the Westinghouse system which include the following:

- (a) The use of such information by Westinghouse gives Westinghouse a competitive advantage over its competitors. It is, therefore, withheld from disclosure to protect the Westinghouse competitive position.
- (b) It is information that is marketable in many ways. The extent to which such information is available to competitors diminishes the Westinghouse ability to sell products and services involving the use of the information.
- (c) Use by our competitor would put Westinghouse at a competitive disadvantage by reducing his expenditure of resources at our expense.
- (d) Each component of proprietary information pertinent to a particular competitive advantage is potentially as valuable as the total competitive advantage. If competitors acquire components of proprietary information, any one component may be the key to the entire puzzle, thereby depriving Westinghouse of a competitive advantage.

- (e) Unrestricted disclosure would jeopardize the position of prominence of Westinghouse in the world market, and thereby give a market advantage to the competition of those countries.
- (f) The Westinghouse capacity to invest corporate assets in research and development depends upon the success in obtaining and maintaining a competitive advantage.
- (iii) The information is being transmitted to the Commission in confidence and, under the provisions of 10 CFR Section 2.390, it is to be received in confidence by the Commission.
- (iv) The information sought to be protected is not available in public sources or available information has not been previously employed in the same original manner or method to the best of our knowledge and belief.
- (v) The proprietary information sought to be withheld in this submittal is that which is appropriately marked in WCAP-17071-P, "H*: Alternate Repair Criteria for the Tubesheet Expansion Region in Steam Generators with Hydraulically Expanded Tubes (Model F)," dated April 2009 (Proprietary), for submittal to the Commission, being transmitted by Dominion Connecticut Application for Withholding Proprietary Information from Public Disclosure to the Document Control Desk. The proprietary information as submitted for use by Westinghouse for Millstone Unit 3 is expected to be applicable to other licensee submittals in support of implementing an alternate repair criterion, called H*, that does not require an eddy current inspection and plugging of the tubes below a distance of 11.2 inches from the top of the tubesheet.

This information is part of that which will enable Westinghouse to:

- (a) Provide documentation of the analyses, methods, and testing which support the implementation of an alternate repair criterion, designated as H*, for a portion of the tubes within the tubesheet of the Millstone Unit 3 steam generators.
- (b) Assist the customer in obtaining NRC approval of the Technical Specification changes associated with the alternate repair criterion.

Further this information has substantial commercial value as follows:

- (a) Westinghouse plans to sell the use of similar information to its customers for the purposes of meeting NRC requirements for licensing documentation.
- (b) Westinghouse can sell support and defense of the technology to its customers in the licensing process.

Public disclosure of this proprietary information is likely to cause substantial harm to the competitive position of Westinghouse because it would enhance the ability of competitors to provide similar calculation, evaluation and licensing defense services for commercial power reactors without commensurate expenses. Also, public disclosure of the information would enable others to use the information to meet NRC requirements for licensing documentation without purchasing the right to use the information.

The development of the technology described in part by the information is the result of applying the results of many years of experience in an intensive Westinghouse effort and the expenditure of a considerable sum of money.

In order for competitors of Westinghouse to duplicate this information, similar technical programs would have to be performed and a significant manpower effort, having the requisite talent and experience, would have to be expended.

Further the deponent sayeth not.

PROPRIETARY INFORMATION NOTICE

Transmitted herewith are proprietary and/or non-proprietary versions of documents furnished to the NRC in connection with requests for generic and/or plant-specific review and approval.

In order to conform to the requirements of 10 CFR 2.390 of the Commission's regulations concerning the protection of proprietary information so submitted to the NRC, the information which is proprietary in the proprietary versions is contained within brackets, and where the proprietary information has been deleted in the non-proprietary versions, only the brackets remain (the information that was contained within the brackets in the proprietary versions having been deleted). The justification for claiming the information so designated as proprietary is indicated in both versions by means of lower case letters (a) through (f) located as a superscript immediately following the brackets enclosing each item of information being identified as proprietary or in the margin opposite such information. These lower case letters refer to the types of information Westinghouse customarily holds in confidence identified in Sections (4)(ii)(a) through (4)(ii)(f) of the affidavit accompanying this transmittal pursuant to 10 CFR 2.390(b)(1).

COPYRIGHT NOTICE

The reports transmitted herewith each bear a Westinghouse copyright notice. The NRC is permitted to make the number of copies of the information contained in these reports which are necessary for its internal use in connection with generic and plant-specific reviews and approvals as well as the issuance, denial, amendment, transfer, renewal, modification, suspension, revocation, or violation of a license, permit, order, or regulation subject to the requirements of 10 CFR 2.390 regarding restrictions on public disclosure to the extent such information has been identified as proprietary by Westinghouse, copyright protection notwithstanding. With respect to the non-proprietary versions of these reports, the NRC is permitted to make the number of copies beyond those necessary for its internal use which are necessary in order to have one copy available for public viewing in the appropriate docket files in the public document room in Washington, DC and in local public document rooms as may be required by NRC regulations if the number of copies submitted is insufficient for this purpose. Copies made by the NRC must include the copyright notice in all instances and the proprietary notice if the original was identified as proprietary.

Dominion Connecticut
Letter for Transmittal to the NRC

The following paragraphs should be included in your letter to the NRC:

Enclosed are:

1. 1 copy of WCAP-17071-P, "H*: Alternate Repair Criteria for the Tubesheet Expansion Region in Steam Generators with Hydraulically Expanded Tubes (Model F)," dated April 2009 (Proprietary)
2. 1 copy of WCAP-17071-NP, "H*: Alternate Repair Criteria for the Tubesheet Expansion Region in Steam Generators with Hydraulically Expanded Tubes (Model F)," dated April 2009 (Non-Proprietary).

Also enclosed is Westinghouse authorization letter CAW-09-2569 with accompanying affidavit, Proprietary Information Notice, and Copyright Notice.

As Item 1 contains information proprietary to Westinghouse Electric Company LLC, it is supported by an affidavit signed by Westinghouse, the owner of the information. The affidavit sets forth the basis on which the information may be withheld from public disclosure by the Commission and addresses with specificity the considerations listed in paragraph (b) (4) of Section 2.390 of the Commission's regulations.

Accordingly, it is respectfully requested that the information which is proprietary to Westinghouse be withheld from public disclosure in accordance with 10 CFR Section 2.390 of the Commission's regulations.

Correspondence with respect to the copyright or proprietary aspects of the items listed above or the supporting Westinghouse affidavit should reference CAW-09-2569 and should be addressed to J. A. Gresham, Manager, Regulatory Compliance and Plant Licensing, Westinghouse Electric Company LLC, P.O. Box 355, Pittsburgh, Pennsylvania 15230-0355.



Westinghouse

Westinghouse Electric Company
Nuclear Services
P.O. Box 355
Pittsburgh, Pennsylvania 15230-0355
USA

U.S. Nuclear Regulatory Commission
Document Control Desk
Washington, DC 20555-0001

Direct tel: (412) 374-4643
Direct fax: (412) 374-3846
e-mail: greshaja@westinghouse.com

Our ref: CAW-09-2659

August 27, 2009

**APPLICATION FOR WITHHOLDING PROPRIETARY
INFORMATION FROM PUBLIC DISCLOSURE**

Subject: LTR-SGMP-09-109 P-Attachment, "Response to NRC Request for Additional Information on H*; RAI # 4; Model F and Model D5 Steam Generators," dated August 2009 (Proprietary)

The proprietary information for which withholding is being requested in the above-referenced report is further identified in Affidavit CAW-09-2659 signed by the owner of the proprietary information, Westinghouse Electric Company LLC. The affidavit, which accompanies this letter, sets forth the basis on which the information may be withheld from public disclosure by the Commission and addresses with specificity the considerations listed in paragraph (b)(4) of 10 CFR Section 2.390 of the Commission's regulations.

Accordingly, this letter authorizes the utilization of the accompanying affidavit by Dominion Connecticut.

Correspondence with respect to the proprietary aspects of the application for withholding or the Westinghouse affidavit should reference this letter, CAW-09-2659, and should be addressed to J. A. Gresham, Manager, Regulatory Compliance and Plant Licensing, Westinghouse Electric Company LLC, P.O. Box 355, Pittsburgh, Pennsylvania 15230-0355.

Very truly yours,

J.A. Gresham, Manager
Regulatory Compliance and Plant Licensing

Enclosures

cc: G. Bacuta, (NRC OWFN 12E-1)

bcc: J. A. Gresham (ECE 4-7A) 1L
R. Bastien, 1L (Nivelles, Belgium)
C. Brinkman, 1L (Westinghouse Electric Co., 12300 Twinbrook Parkway, Suite 330, Rockville, MD 20852)
RCPL Administrative Aide (ECE 4-7A) 1L (letter and affidavit only)
G. W. Whiteman, Waltz Mill
H. O. Lagally, Waltz Mill
C. D. Cassino, Waltz Mill
J. T. Kandra, Waltz Mill
D. L. Rogosky, ECE 564A

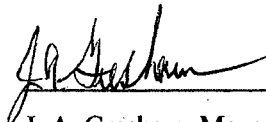
AFFIDAVIT

COMMONWEALTH OF PENNSYLVANIA:

SS

COUNTY OF ALLEGHENY:

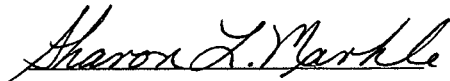
Before me, the undersigned authority, personally appeared J. A. Gresham, who, being by me duly sworn according to law, deposes and says that he is authorized to execute this Affidavit on behalf of Westinghouse Electric Company LLC (Westinghouse), and that the averments of fact set forth in this Affidavit are true and correct to the best of his knowledge, information, and belief:



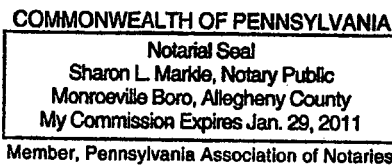
J. A. Gresham, Manager

Regulatory Compliance and Plant Licensing

Sworn to and subscribed before me
this 27th day of August, 2009



Notary Public



- (1) I am Manager, Regulatory Compliance and Plant Licensing, in Nuclear Services, Westinghouse Electric Company LLC (Westinghouse), and as such, I have been specifically delegated the function of reviewing the proprietary information sought to be withheld from public disclosure in connection with nuclear power plant licensing and rule making proceedings, and am authorized to apply for its withholding on behalf of Westinghouse.
- (2) I am making this Affidavit in conformance with the provisions of 10 CFR Section 2.390 of the Commission's regulations and in conjunction with the Westinghouse "Application for Withholding" accompanying this Affidavit.
- (3) I have personal knowledge of the criteria and procedures utilized by Westinghouse in designating information as a trade secret, privileged or as confidential commercial or financial information.
- (4) Pursuant to the provisions of paragraph (b)(4) of Section 2.390 of the Commission's regulations, the following is furnished for consideration by the Commission in determining whether the information sought to be withheld from public disclosure should be withheld.
 - (i) The information sought to be withheld from public disclosure is owned and has been held in confidence by Westinghouse.
 - (ii) The information is of a type customarily held in confidence by Westinghouse and not customarily disclosed to the public. Westinghouse has a rational basis for determining the types of information customarily held in confidence by it and, in that connection, utilizes a system to determine when and whether to hold certain types of information in confidence. The application of that system and the substance of that system constitute Westinghouse policy and provide the rational basis required.

Under that system, information is held in confidence if it falls in one or more of several types, the release of which might result in the loss of an existing or potential competitive advantage, as follows:

- (a) The information reveals the distinguishing aspects of a process (or component, structure, tool, method, etc.) where prevention of its use by any of

Westinghouse's competitors without license from Westinghouse constitutes a competitive economic advantage over other companies.

- (b) It consists of supporting data, including test data, relative to a process (or component, structure, tool, method, etc.), the application of which data secures a competitive economic advantage, e.g., by optimization or improved marketability.
- (c) Its use by a competitor would reduce his expenditure of resources or improve his competitive position in the design, manufacture, shipment, installation, assurance of quality, or licensing a similar product.
- (d) It reveals cost or price information, production capacities, budget levels, or commercial strategies of Westinghouse, its customers or suppliers.
- (e) It reveals aspects of past, present, or future Westinghouse or customer funded development plans and programs of potential commercial value to Westinghouse.
- (f) It contains patentable ideas, for which patent protection may be desirable.

There are sound policy reasons behind the Westinghouse system which include the following:

- (a) The use of such information by Westinghouse gives Westinghouse a competitive advantage over its competitors. It is, therefore, withheld from disclosure to protect the Westinghouse competitive position.
- (b) It is information that is marketable in many ways. The extent to which such information is available to competitors diminishes the Westinghouse ability to sell products and services involving the use of the information.
- (c) Use by our competitor would put Westinghouse at a competitive disadvantage by reducing his expenditure of resources at our expense.

- (d) Each component of proprietary information pertinent to a particular competitive advantage is potentially as valuable as the total competitive advantage. If competitors acquire components of proprietary information, any one component may be the key to the entire puzzle, thereby depriving Westinghouse of a competitive advantage.
 - (e) Unrestricted disclosure would jeopardize the position of prominence of Westinghouse in the world market, and thereby give a market advantage to the competition of those countries.
 - (f) The Westinghouse capacity to invest corporate assets in research and development depends upon the success in obtaining and maintaining a competitive advantage.
- (iii) The information is being transmitted to the Commission in confidence and, under the provisions of 10 CFR Section 2.390, it is to be received in confidence by the Commission.
- (iv) The information sought to be protected is not available in public sources or available information has not been previously employed in the same original manner or method to the best of our knowledge and belief.
- (v) The proprietary information sought to be withheld in this submittal is that which is appropriately marked in LTR-SGMP-09-109 P-Attachment, "Response to NRC Request for Additional Information on H*; RAI # 4; Model F and Model D5 Steam Generators," dated August 2009 (Proprietary), for submittal to the Commission, being transmitted by Dominion Connecticut letter and Application for Withholding Proprietary Information from Public Disclosure to the Document Control Desk. The proprietary information as submitted for use by Westinghouse for Millstone Unit 3 is expected to be applicable to other licensee submittals in support of implementing an alternate repair criterion, called H*, that does not require an eddy current inspection and plugging of steam generator tubes below a certain distance from the top of the tubesheet.

This information is part of that which will enable Westinghouse to:

- (a) Provide documentation of the analyses, methods, and testing which support the implementation of an alternate repair criterion, designated as H*, for a portion of the tubes within the tubesheet of the Millstone Unit 3 steam generators.
- (b) Assist the customer in obtaining NRC approval of the Technical Specification changes associated with the alternate repair criterion.

Further this information has substantial commercial value as follows:

- (a) Westinghouse plans to sell the use of similar information to its customers for the purposes of meeting NRC requirements for licensing documentation.
- (b) Westinghouse can sell support and defense of the technology to its customers in the licensing process.

Public disclosure of this proprietary information is likely to cause substantial harm to the competitive position of Westinghouse because it would enhance the ability of competitors to provide similar calculation, evaluation and licensing defense services for commercial power reactors without commensurate expenses. Also, public disclosure of the information would enable others to use the information to meet NRC requirements for licensing documentation without purchasing the right to use the information.

The development of the technology described in part by the information is the result of applying the results of many years of experience in an intensive Westinghouse effort and the expenditure of a considerable sum of money.

In order for competitors of Westinghouse to duplicate this information, similar technical programs would have to be performed and a significant manpower effort, having the requisite talent and experience, would have to be expended.

Further the deponent sayeth not.

PROPRIETARY INFORMATION NOTICE

Transmitted herewith are proprietary and/or non-proprietary versions of documents furnished to the NRC in connection with requests for generic and/or plant-specific review and approval.

In order to conform to the requirements of 10 CFR 2.390 of the Commission's regulations concerning the protection of proprietary information so submitted to the NRC, the information which is proprietary in the proprietary versions is contained within brackets, and where the proprietary information has been deleted in the non-proprietary versions, only the brackets remain (the information that was contained within the brackets in the proprietary versions having been deleted). The justification for claiming the information so designated as proprietary is indicated in both versions by means of lower case letters (a) through (f) located as a superscript immediately following the brackets enclosing each item of information being identified as proprietary or in the margin opposite such information. These lower case letters refer to the types of information Westinghouse customarily holds in confidence identified in Sections (4)(ii)(a) through (4)(ii)(f) of the affidavit accompanying this transmittal pursuant to 10 CFR 2.390(b)(1).

COPYRIGHT NOTICE

The reports transmitted herewith each bear a Westinghouse copyright notice. The NRC is permitted to make the number of copies of the information contained in these reports which are necessary for its internal use in connection with generic and plant-specific reviews and approvals as well as the issuance, denial, amendment, transfer, renewal, modification, suspension, revocation, or violation of a license, permit, order, or regulation subject to the requirements of 10 CFR 2.390 regarding restrictions on public disclosure to the extent such information has been identified as proprietary by Westinghouse, copyright protection notwithstanding. With respect to the non-proprietary versions of these reports, the NRC is permitted to make the number of copies beyond those necessary for its internal use which are necessary in order to have one copy available for public viewing in the appropriate docket files in the public document room in Washington, DC and in local public document rooms as may be required by NRC regulations if the number of copies submitted is insufficient for this purpose. Copies made by the NRC must include the copyright notice in all instances and the proprietary notice if the original was identified as proprietary.

Dominion Connecticut
Letter for Transmittal to the NRC

The following paragraphs should be included in your letter to the NRC:

Enclosed are:

1. 1 copy of LTR-SGMP-09-109 P-Attachment, "Response to NRC Request for Additional Information on H*; RAI # 4; Model F and Model D5 Steam Generators," dated August 2009 (proprietary).
2. 1 copy of LTR-SGMP-09-109 NP-Attachment, "Response to NRC Request for Additional Information on H*; RAI # 4; Model F and Model D5 Steam Generators," dated August 2009 (non-proprietary).

Also enclosed is Westinghouse authorization letter CAW-09-2659 with accompanying affidavit, Proprietary Information Notice, and Copyright Notice.

As Item 1 contains information proprietary to Westinghouse Electric Company LLC, it is supported by an affidavit signed by Westinghouse, the owner of the information. The affidavit sets forth the basis on which the information may be withheld from public disclosure by the Commission and addresses with specificity the considerations listed in paragraph (b)(4) of Section 2.390 of the Commission's regulations.

Accordingly, it is respectfully requested that the information which is proprietary to Westinghouse be withheld from public disclosure in accordance with 10 CFR Section 2.390 of the Commission's regulations.

Correspondence with respect to the copyright or proprietary aspects of the items listed above or the supporting Westinghouse affidavit should reference CAW-09-2659 and should be addressed to J. A. Gresham, Manager, Regulatory Compliance and Plant Licensing, Westinghouse Electric Company LLC, P.O. Box 355, Pittsburgh, Pennsylvania 15230-0355.